FATIGUE AND FRACTURE OF CEMENT MORTAR

by

ROBERT BENNETT TAIT

A Dissertation Submitted to the Faculty of Engineering, University of Cape Town, in fulfilment of the requirements for the Degree of Doctor of Philosophy.

Johannesburg, March 1984.

FATIGUE AND FRACTURE OF CEMENT MORTAR

ABSTRACT

This thesis sets out to contribute to the understanding of fatigue and subsequent fracture of cement mortar. Cement mortar was chosen as representative of concrete without the handling difficulties of cement paste or aggregate consistency and scale problems of concrete. A preliminary SEM study of cement hydration was undertaken as part of the literature review of the strength development of cement paste and mortar.

The initial approach was to investigate how microcracks and damage developed in mortar prisms as a result of compression fatigue and how such damage was dependent on loading range, maximum load, frequency, waveform, environmental moisture condition and temperature ($20^{o}C$ to $60^{o}C$).

The microcrack damage monitoring techniques employed incorporated measurements of lateral and longitudinal strain (including elastic and residual components), ultrasonic pulse transit time and acoustic emission associated with microcracking. Techniques were developed to utilise all three damage monitoring techniques simultaneously, even under fatigue conditions. A three dimensional "pseudo isometric plot" approach was developed and used for presenting the acoustic emission noise which added insight to the fracture process.

A brief study of the post fatigue strengthening behaviour of mortar was undertaken and a rehydration model proposed to explain the behaviour.

The damage monitoring studies of compression prisms are not readily interpreted in terms of actual crack sizes or areas, and hence from a fracture mechanics viewpoint, so the project was extended to evaluate nominal single crack growth using double torsion (DT) specimens under similar test conditions. This specimen was very powerful in that both static fatigue and cyclic fatigue tests could

readily be undertaken to obtain crack velocity-stress intensity (V-K) data. In addition, because of the constant-K characteristic of the DT specimen, changeover tests were possible in the fatigue mode, i.e. the immediate effect on crack growth rate of the change of a single parameter (e.g. water temperature, frequency, etc.) was easily observed.

The results of the DT crack growth rate and compression damage accumulation rates correlated well, for similar test conditions. It also appears that, if applied load conditions are constant (e.g. amplitude, R-ratio, mean level) then the elapsed time of fatigue testing is a controlling parameter and that fatigue is not truly strain-rate dependent. The microcracking or damage process is very dependent on the availability of environmental moisture and appears also to be thermally activated. As such the microcracking process is consistent with a stress-induced, water-dependent deterioration mechanism, which could be a form of stress corrosion, possibly dependent on hydroxyl ion attack of crack tip stressed silicate bonds. It was suggested that the mechanism of cracking is similar in both static and fatigue cases.

Since the "crack tip" in cement materials is very poorly defined, and in an effort to further understand the nature of microcracking, an in-situ DT stage was built to fracture small DT specimens inside the chamber of a conventional scanning electron microscope. Controlled cracking of mortar, cement paste and cement clinker was possible using this technique with increments in crack length controllable down to 1 micron. It is believed that such studies and allied discussion of possible microcracking models make a contribution to the understanding of the cracking nature of cement materials.

DECLARATION

I declare that this dissertation is my own, unaided work which is original, except where reference is made to the work of others. It is being submitted for a degree of Doctor of Philosophy in the University of Cape Town. It has not been submitted before for any degree or examination in any other University.

Robert Bennett Tait

th day of , 1984.

FATIGUE AND FRACTURE OF CEMENT MORTAR

TABLE OF CONTENTS

CHAPTER THREE : EXPERIMENTAL TECHNIQUES AND SYSTEMS — Page

Page

ACKNOWLEDGEMENTS

The author would like to express his sincere appreciation to his supervisor, Professor G.G. Garrett, for his continued encouragement and guidance throughout the duration of the project. I am also particularly grateful to my colleagues in the Department particularly Hamlin Jennings, Steve Akers, Tim Hughes, Graham Glover, Rick Hoare, Dave Pitman, Alan Morris and Ryan Fry for their kind assistance, discussions and encouragement.

Technical, electronic, photographic and drafting assistance is especially acknowledged from Nick Dreze, Mike Sketch, John Williams, Helgard Bohm, Isobel Clarke, Lesley Sheldon and Roy Achilles.

I would like to thank Dr. Dave Crawford of the Electron Microscope Unit and Professor A. Ball for providing laboratory and office facilities (at U.C.T.) and Professor R.P. King (at Wits).

Special thanks are due to Mrs. Thea Jarvis for typing (and retyping) the manuscript over a sustained period, and also to Mrs. G. Van der Heever.

The financial support of the Atomic Energy Corporation, ESCOM, the Portland Cement Institute and the University of Cape Town is gratefully acknowledged.

Finally, I would like to express my sincere appreciation to close friends and colleagues, too numerous to mention, for their support and understanding during this work.

> "Some books are to be Tasted, others to be Swallowed and some few to be Chewed and Digested; that is, some Books are to be read only in Parts, others to be read but not Curiously; and some few are to be read wholly, and with Diligence and Attention."
>
> Francis Bacon

CHAPTER ONE : INTRODUCTION

1.1 Introduction : World Usage, Economics and Energy

Concrete is so common and so well accepted throughout the world that we now almost tend to take it for granted. This intimate mixture of sand and aggregate, held together by a matrix of hydrated cement, has been successfully and increasingly used by engineers since Aspdin first developed modern Portland cement in 1824. It is undoubtedly the most used of the common constructional materials, with present worldwide cement production approaching a billion (i.e. 10^9) tonnes per annum (1) - far in excess, for example, of steel production.

Yet, despite its extensive usage, the fundamental behaviour of hydrated cement and concrete at a microstructural level is not yet fully understood. Recent developments in microstructural research concerning the understanding of cement hydration are particularly exciting, especially the work of Birchall (2, 3) and Double (3-5), Jennings and Pratt (6, 7) and Diamond (8, 9). Mechanisms of cement hydration are beginning to appear (9-14), although a corresponding understanding of the mechanisms of deformation and fracture of cement and concrete has yet to emerge. Indeed, cement is still regarded by many as merely the component that holds concrete together and provides the matrix to support steel reinforcing or prestressed cables.

This viewpoint, of taking cement and concrete for granted, may, however, be changing (1, 15, 16). Rather than the continued, traditional "constructional approach" to the use of concrete, questions of economics, energy optimisation and safety are being more carefully evaluated. Greater attention is being focused on the advantages of inorganic materials in general, and cement in particular, especially in view of the

present day design trends to higher live-to-dead load ratios and greater structural efficiency. Plastic design philosophies are well established (17), yet so called "safety" or design factors still tend to be large and conservative, following some early, spectacular failures. There is considerable reluctance among engineers, understandably perhaps, to reduce the safety factors despite some scientific evidence that in many cases this would be appropriate. More and more, therefore, it becomes apparent that there is a need for an increased fundamental understanding of how concrete fails at both the microscopic and macroscopic level.

Economics is also becoming an increasingly significant factor, not only in terms of money, but also in energy terms. P.C. Hewlett, speaking at the recent U.K. Concrete Society Conference, reported that cement price increases were of the order of 300 percent during 1980 and 1981, and that cement now constituted about 41% of the overall component cost of concrete (18). At this same Building Construction Conference, it was reported that shortcomings in concrete durability, and its related repair and maintenance, accounted for some 35% of the amount spent by the construction industry (18).

Yet cement is still, relatively, a cheap and abundant material. Its raw material constituents of limestone (or chalk), and clay are found in abundance worldwide and are not subject to potential strategic geographic strangleholds, in the way that oil and many metallic minerals are. It is cheap to produce in energy terms, which is becoming more important as energy costs continue spiralling and it is this criterion that may well govern material utilisation in the future (19). A comparison of the energy cost for production (per unit volume relative to the cost of cement), as given in Table 1.1, shows that cement compares very favourably with other common construction materials. In addition, the subsequent fabrication costs of cement, as cast in situ concrete, are normally very low in comparison to, for example, metals which require extensive energy costs in operations such as forging and machining(20).

Alexander, in a paper dealing with the economics of energy and materials (21), has gone even further, comparing materials from the perspective of "energy cost per unit of mechanical property". Concrete is the most important material in world usage whether considered from a tonnage or

volume aspect, with timber running second. In the past few years, cement has also exhibited the lowest price per tonne in comparison to steel, timber and plastics (by nearly an order of magnitude)(21). If cost per unit of property is considered, Table 1.2, reinforced concrete is the optimum material in terms of cost per meganewton of tensile strength, and in terms of fatigue performance.

In terms of energy consumed in production, however, the best constructional material, per unit of tensile or fatigue strength, is timber, with values about a quarter of that of reinforced concrete, Table 1.2; and indeed, Alexander (21) foresees that, with ever increasing energy shortages, future long term constructional needs will most probably be met with greater utilisation of concrete and timber.

After a consideration of these economic and energy advantages it is perhaps surprising that cement has not been utilised in more diverse ways. The major problem, however, is that cement paste and concrete, made in the normal manner, have low tensile strengths and are comparatively brittle. They are employed by civil engineers almost exclusively in compression and, possibly because of this, the understanding of their properties has been greatly under researched in comparison to metals and plastics. In materials such as metals, plastics and other ceramics, an understanding of the properties has only really come about, however, by concentrating on the microstructure and crystallography of these materials, together with the importance of internal "defects" (such as dislocations or grain boundaries); hence the likely envelope of their attainable mechanical properties is quite well appreciated.

A recent major contribution to the understanding of one aspect of cement has, however, been made. Double (22, 1) and Birchall (23) have conducted detailed investigations of the effect of microporosity during cement hydration on consequent strength development. The importance of eliminating, or at least controlling, microporosity has been recognised by others (16) and preliminary indications are that high tensile strength- so called "macro defect free" (MDF) - cements <u>can</u> be developed, with tensile strengths of the order of at least 150 MPa (23). This is comparable with nature's own mollusc shell or mother of pearl, which is 99% calcium carbonate (similar to cement), and yet has a flexural strength of 110 MPa and a fracture energy as high as 3000 J/m^2 (16).

While modifications to cement, and cement strength, by controlling porosity through an understanding of the mechanisms of cement hydration, provide a very valid and necessary approach, there is still a dearth of information as to how damage develops in hardened cement pastes and concrete, and how cracks propagate and fracture occurs. The exciting developments in MDF cements strongly suggest that notch sensitivity and fracture mechanics parameters of "toughness" are very important, but further improvements are likely to rely on more detailed mechanistic information. What, for example, are the factors controlling mechanical performance of ordinary concrete under service load conditions? What parameters control damage development in concrete and the propagation of cracks, particularly under varying cyclic loading (fatigue) conditions? What are the likely synergistic effects of environment, and what part do time-dependent processes play in damage development?

It is in an attempt to answer some of these, and related, questions that this thesis has been directed. It is thus relevant to consider, briefly at this stage, fatigue and fracture of concrete.

1.2 Fatigue and Fracture of Concrete

Fatigue in concrete is far more widespread than appears at first glance, and there has been a research interest in the subject since the turn of the century. Concrete road bridges focused attention on concrete fatigue and this attention was increased with the advent of concrete road surfaces or pavements, airport runways and more recently, railway sleepers. Most research on the fatigue behaviour of concrete was directed at concrete in bending or on the measurement of the effect on modulus of rupture, since concrete was largely being used to resist flexural tensile forces. More recently, concrete has been used in foundations for heavy vibrating plant and machinery and also in marine environments, for example in breakwater protection units like dolosse, or offshore oil rigs.

This has meant that concrete structures are often required to withstand many millions of load cycles (up to 500 million in the case of marine dolosse, for example (24)), during their normal service lives. In the

1960s some research effort was directed at reinforced concrete structures subjected to earthquakes and shock loading where the number of loading cycles is low and in any event seldom above 10^3. In this so-called "low cycle fatigue" regime, the rules and equations attempting to explain concrete degradation are different from those in the "high cycle fatigue" range (25). Many research efforts have looked at a very limited spectrum of fatigue lifetimes and studies in the range of high cycle fatigue, for example, cannot be extrapolated to low cycle fatigue, and vice versa. In particular, time-dependent and loading rate effects are reported, on the one hand, to have no effect on concrete fatigue behaviour in the high cycle regime (26-27). Whereas under low cycle conditions, fatigue strength is reportedly significantly both rate (28) and time dependent (27). Static fatigue, the phenomenon of failure with time under sustained loading below ultimate strength levels, has also been well established in this material (27, 29, 30), although an understanding of the detailed failure mechanism is far from complete. Recently Hsu (25) has put forward a useful time and rate dependent correlation theory for concrete fatigue, but its range of validity still needs extensive experimental verification.

It is clear, therefore, that there is certainly a need for a greater knowledge of concrete behaviour under both low and high cycle fatigue, and concomitantly, the development of an appreciation of how concrete fractures and fails under such conditions.

This point was emphasised by the President of the 'Federation Internationale de la Precontrainte', Professor B.C. Gerwick who highlighted recently, among the other concrete research topics, the need for more research into and understanding of both high and low cycle fatigue of concrete (31).

The objective of this thesis is thus an attempt to contribute to this understanding through experimental studies of the fatigue behaviour of cement mortar. Mortar, the principal binding matrix of concrete, has been used in the compression fatigue studies reported in this thesis and has highlighted the importance of inherent microcracks and their subsequent proliferation during fatigue. This study has been extended to specific (nominally single) crack growth in mortar utilising double

torsion specimens, and the results correlated with compression fatigue results using fracture mechanics principles. This has been undertaken in an attempt to interpret both the fracture mechanisms and the applicability of fracture mechanics to crack propagation in mortar. In particular, time dependent and environmental effects have been examined in conjunction with microstructural studies using scanning electron microscopy. Through this work, and related studies concerning the rate of damage development, outlined in the next section, an attempt is made to understand fatigue and fracture in cement mortar and hence develop models and mechanisms which explain such behaviour. Only from such a fundamental viewpoint will it be possible to make positive steps to eliminate, or at least alleviate, the deterioration of concrete due to fatigue. At the same time a fundamental appreciation of fracture of mortar and concrete, as described by fracture mechanics, may lead to a suitable means for its control in practical situations. The next section outlines the content, and explains the format, of this thesis.

1.3 Details of Thesis Format

It was considered appropriate to include a brief section explaining the philosophy and layout of the research reported in this thesis. The chapters, while consecutive, are largely self contained, following the initial descriptions of Chapters Two and Three.

Background and previous studies of cement and concrete, and how these materials respond to fatigue, are considered in Chapter Two. This includes not only sections on the general factors affecting static strength and fatigue strength of concrete, but also a section discussing hydration, hydration mechanisms and strength development of cement itself. It was considered very necessary to include this section in this chapter because of the relevance of hydration and microstructure to discussion detailed elsewhere in the thesis. This is particularly the case for Chapter Five where post-fatigue increases in strength ("fatigue hardening") are discussed, but also in view of the time dependence of some of the phenomena examined.

Chapter Three details the conventional experimental techniques and systems employed. In particular it describes the materials and

compression sample fabrication, mechanical testing facilities and damage monitoring techniques. These latter include elastic and accumulated strain methods, ultrasonic transit time techniques and acoustic emission monitoring.

Experimental compression fatigue studies are described in Chapter Four. From a general study of fatigue strength and damage development, the work is extended to look specifically at the effects of cycling frequency, waveform (and wave programme) and finally environmental and temperature effects on the fatigue of concrete mortar. Attempts to correlate the importance of these effects in multicracked mortar are described.

Chapter Five, as has been mentioned, describes experimental studies of the phenomenon of fatigue hardening and puts forward a microstructural model that is consistent with the experimental evidence.

In view of the difficulty of examining the effect of various parameters on fatigue and crack development, because of the abundantly microcracked nature of the fatigued mortar compression prism samples, it was decided to extend the research to a more "individual, or single, crack" approach that is more amenable to the application of conventional fracture mechanics principles. The literature of the experimental applicability of fracture mechanics to crack propagation within cement systems is therefore reviewed in Chapter Six, and relevant testing techniques examined.

In Chapter Seven an experimental study using the so-called "double torsion" specimen geometry was undertaken. Both static fatigue (and associated slow crack growth) and conventional fatigue were examined as a function of frequency, environment and temperature, effectively running parallel to the compression studies reported in Chapter Four. Results have been meaningfully expressed in terms of conventional fracture mechanics methods using crack velocity-stress intensity curves.

Mechanisms of crack propagation and failure are described in Chapter Eight where the compression results of Chapter Four concerning overall "damage" and the double torsion results of Chapter Seven, concerning "discrete" crack growth, are correlated and compared as a function of the

parameters examined. An "in situ" SEM microstructural study of crack development and growth in cement and mortar is described and followed by a discussion of the models of microcracking in cement systems. Chapter Nine summarises the thesis and outlines future areas of research and application.

In the Chapter to follow, therefore, a background to the thesis is provided by a literature review of previous studies in the field of concrete strength development, together with an examination of cement hydration, and a study of fatigue and fracture in this material.

TABLE 1.1

Comparison of Energy Cost for Production of Various Materials (per unit volume, relative to cost of cement)

MATERIAL		AUTHOR			
		KELLY (1)	DOUBLE (1)	BIRCHALL (15, 19)	ALEXANDER (21)
Cement		1	1	1	1
Glass		1.3	1.3		
Aluminium		52	35	32	38
Steel		22	20	19	22
Plastics	Polyethylene	5			4
	PVC	6.8		6	5
	Polystyrene	8.5	5		

TABLE 1.2

Cost Related to Material Properties. (After Alexander (21)).

Energy consumption related to material properties

Material	Tensile strength (MN/m^2)	Modulus of rigidity (MN/m^2)	Fatigue strength (MN/m^2)	Density (kg/m^3)	Specific energy (kWh/kg)	Total energy per unit of:		
						Tensile strength	Modulus of rigidity	Fatigue strength
Cast iron	400	35 000	105	7 300	16.0	293	3.34	1 112
Steels								
EN-1	250	77 000	193	7 850	16.0	502	1.63	651
EN-24	800	77 000	495	7 830	16.0	156.6	1.63	253
EN-309	300	86 000	360	7 900	16.0	421	1.47	351
EN-420	1 200	86 000	630	7 900	16.0	105	1.47	186
Copper-zinc alloys	400	37 300	140	8 360	16.5—	345	3.70	985.3
Aluminium alloys	300	26 000	90	2 700	79.0	710	8.20	2 370
Magnesium alloys	190	17 500	95	1 700	115.0	1 029	11.17	2 058
Titanium alloys	960	45 000	310	4 510	155.0	720	15.53	2 255
Polypropylene	30	0.0	7.5	900	20.0	600	0.0	2 400
Propathene	35	0.0	7.5	900	20.0	515	0.0	2 400
Polythene L.D.	13	0.0	3.25	920	15.0	1 062	0.0	4 246
Rigidex 2000	30	0.0	4.0	950	15.0	475	0.0	3 560
Nylon 66	80	0.0	20.0	1 360	50.0	850	0.0	3 400
PVC(R)	50	0.0	12.5	1 400	20.0	560	0.0	2 240
R. Concrete	38	10 000	23	2 400	2.3	145	0.55	240
Timber (Oak)	14	4 500	6	670	0.5—	24	0.07	56

"The more extensive a man's knowledge of what has been done, the greater will be his power of knowing what to do."

Benjamin Disraeli

CHAPTER TWO : BACKGROUND AND PREVIOUS STUDIES

2.1 Introduction

This chapter considers the response of cement and concrete to fatigue. A necessary prerequisite, however, is an evaluation of the present knowledge of the intrinsic character of cement and the mechanisms of cement hydration and strength development. This strength development is reviewed before the two major components of this chapter are examined, namely those factors affecting the static strength of concrete and, subsequently, the parameters that appear to control fatigue strength. While this thesis does not deal specifically with various mixes, the effect of the various components is dealt with and, subsequently, those parameters that are of more direct importance to the thesis, for example, time dependence, temperature and moisture condition, are handled in more detail. The development of strength in hydrated cement is first examined in the following sections.

2.2 Strength Development of Cement

2.2.1 Introduction

The first successful attempt to make 'modern' Portland Cement was undertaken by Joseph Aspdin in 1824 who deliberately calcined a finely divided mixture of limestone and clay. This process, after some refinements, yielded conventional clinker that, after being finely ground and hydrated with fragments of stone, produced a poorish concrete which was said to resemble Portland stone - a limestone quarried in Dorset. It is, however, beyond the scope of this thesis to review the detailed historical development of cement which is very adequately handled elsewhere (32-35); instead attention is focussed on current day knowledge concerning strength development. Fundamental concepts are introduced and particular aspects, which will be relevant in future sections and discussions, are highlighted. It is thus relevant to examine, firstly, the constituents and chemical composition of modern cement.

2.2.2 Chemical Composition

Although the chemical equilibrium achieved at the clinkering temperature is not rigorously maintained on cooling it is generally considered that the cooled clinker is in "frozen equilibrium". The four main (mineralogical compound) components of cement clinker are listed at the end of the Chapter in Table 2.1. Note that cement chemists usually make use of a shortened notation where each oxide is described by a "one letter" symbol, (33) viz:

CaO	=	C	Fe_2O_3	=	F
SiO_2	=	S	H_2O	=	H
Al_2O_3	=	A	$Ca(OH)_2$	=	$CaO.H_2O$ = CH

Minor oxides, such as magnesia (MgO), titanium oxide (TiO_2), manganese oxide (Mn_2O_3) and the oxides of alkalis (K_2O and Na_2O) are usually present in much smaller amounts. Dicalcium silicate, C_2S, usually has three forms : firstly α C_2S, which exists at high temperatures and which converts to β C_2S on cooling below 1456^oC (33). This in turn transforms to γ C_2S at 675^o, but in most commercial cements the rate of cooling is such that β C_2S is preserved in the clinker. (Generally, when C_2S is referred to, the implication is that it is the β C_2S form). The pattern of formation and hydration of cement is conveniently and schematically summarized in Fig. 2.1. It is also worth noting that the compositions given in Table 2.1 for C_3S, C_2S, and C_3A that occur in clinker are only approximate and these are often known as alite, belite and aluminate phases, respectively.

2.2.3 Cement Hydration

The term "hydration" is usually employed to imply all forms of reaction of cement with water, i.e. both true hydration and also hydrolysis. The principle reactions are between the tri- and di-calcium silicates, which, with water, form a tricalcium disilicate hydrate, ($C_3S_2H_3$), together with calcium hydroxide. This former hydration product is generally in a gel form, often referred to as a tobermorite gel (32, 36) and denoted by cement chemists as C-S-H (see equation 2.1, to follow).

The naming of C-S-H as tobermorite gel (36) is, however, of dubious value since it is based on a questionable structural analogy (37). Tobermorite is a naturally occuring calcium silicate hydrate which is distinctly crystalline and stable, while C-S-H, as it occurs in its various forms in hydrated cement, is only crystalline to a very limited extent and often metastable. Since C-S-H appears in a variety of forms (9, 32) its collective description as "tobemorite gel" is simplistic (9) and in certain cases its structure is reportedly closer to the naturally occurring alkali containing calcium silicate hydrate, jennite (37).

$$\text{Tri-, di-calcium silicate} + H_2O \rightarrow \underset{\text{"gel"}}{C_3S_2H_3} + Ca(OH)_2 + \text{Heat} \qquad (2.1).$$

The calcium hydroxide product is often referred to as "portlandite" (32, 38, 39).

C_3A and C_4AF combine with gypsum and water during hydration to yield complex calcium sulpho-aluminates and calcium sulpho-ferrites, which are susceptible to swelling, particularly in high sulphate situations. Bogue and Lerch (40), as well as other authors (33, 37, 39), have established the development of the compressive strength of the various phases with time. C_3S is the principal active hydraulic compound of the cement and the early strength is dependent almost completely on C_3S, since it develops approximately 70% of its full strength in 28 days. C_2S has a much slower rate of hydration and strength development, but catches up with and can exceed the strength of C_3S alone, with time (Fig. 2.2(a)). C_3A is rapidly hydrated with water, and is markedly exothermic. However it contributes little to the overall strength (Fig. 2.2(a)) and is generally regarded as of little value except as (a) a flux in the kiln (32) and (b) as an inhibitor in the "bleeding" process of concrete during compaction and placement. To retard the rapid hydration action of C_3A, calculated amounts (1 to 5%) of gypsum ($CaSO_4.2H_2O$) are added to cement (2). C_4AF similarly makes very little contribution to the overall strength of cement.

2.2.4 Hydration Products and Morphologies

A full understanding of the precise mechanisms of hydration and the development of strength has not yet been achieved despite some intense research activity in this area in recent years (2-4, 6, 9-14, 20, 22, 23, 32-34, 37, 38, 40-58). In this respect, studies have regarded the two main controlling factors as:

(i) the reactivity of components with water (considered mostly from a fundamentally chemical approach); and

(ii) solubilities of the hydration products and subsequent studies of structure, texture and morphology of the resulting material (a more physical approach).

The structure and morphology of hydrating cement will be considered in particular detail here, because of its relevance to some of the work described in this thesis, and is in line with the definitive paper on microstructural aspects of cement by Diamond (9). It is generally acknowledged (2-6, 9, 10, 13, 14, 22, 32, 36-38, 40, 50-53, 58) that there is a development of fibrous growth after an initial dormant period, which occurs from several minutes after mixing and can extend for up to about four hours (4, 9, 11, 13) (See Fig. 2.2(b) and also section 2.2.5).

The hydration products, as can be seen from equation 2.1, are primarily (i) calcium silicate hydrate, (C-S-H), in a variety of forms depending on conditions, and (ii) calcium hydroxide (CH) which generally forms hexagonal crystal platelets, if given sufficient time to develop (Figs. 2.3 (a,b,c)).

The amorphous, gel-like, "fibrous" structure of C-S-H is very variable and extremely small - certainly sub-micron - and with large specific surface area (of the order of 2 - 3 x 10^{16} cm^2/grm (32, 37, 59)) which is significantly larger than unhydrated cement powder itself (of the order of 3 000 cm^2/gm).

Diamond (9), among other authors (10, 37, 41, 44, 60, 61), has distinguished four varieties of morphology of calcium silicate hydrate which are described and depicted in a recent paper (9). For this review, however, typical, representative micrographs of the various morphologies are taken from the author's own studies. The relevant experimental details concerning specimen preparation for SEM (after appropriate hydration times) are given in the final part of Section 5.3.2. of Chapter 5. The various types are described below:-

Type I = Thin (< 0.2 μm) fibrous particles, up to 3 μm in length, which are often curved and branched and which have been described as tubular, lath-like solid, or rolled foils or sheets.
Typical examples are shown in Figs. 2.4(a), (b) and (c) and Fig. 2.3(c).

Type II = An interlocking, honeycomb or "reticular" structure of the same order of magnitude as Type I.
Some typical C-S-H Type II microstructures are in evidence in Fig. 2.5 (and also in Figures 2.3(a) and 2.4(a) (in the background)).

Type III = This type of C-S-H is very common and has a rather nondescript structure, but can be described as being comprised of equant or flattened grains which are often very small (< 0.5 μm) (8). It is typical of large areas of C-S-H as seen at high magnification in the SEM. Figs. 2.6 (a, b) show the form of type III C-S-H.

Type IV = Type IV consists of dense material which has formed in the space originally occupied by the cement grains which is similar to, but smaller than, type III, and is only rarely encountered (Figure 2.7).

In addition to C-S-H and CH, which are the two most important product phases, two other crystalline phases occur, but only sporadically. These are the so called "A.F.m" phase, standing for Al-Fe-mono, typified

by the monosulphate, $[Ca_2\ Al(OH)_6]_2\ SO_4.6H_2O$, and the "A.F.t." phase, standing for Al-Fe-tri and typified by ettringite, $[Ca_6(Al(OH)_6)_2.24H_2O].(SO_4)_3.2H_2O)$. (These latter phases apparently form from solution, not at an interface (7)). The so called "rosette" structure, analogous to Diamonds' A.F.m type, was first proposed as a calcium aluminate by Walsh et al. (41) and substantiated by Taylor (46) and Brevel (42). Figs. 2.8 (a,b) and 2.9 (a,b) depict typical A.F.m and ettringite phases respectively. Needles of ettringite can also be seen in Fig. 2.3(a) and Figure 2.4(a) extending from the bulk material.

The structural or morphological development of cement during hydration follows a gradual growth of predominantly fibre tubules and other hydration products in two distinct regions. These are those originally occupied by water and those areas extending from the original cement grain boundary inwards (i.e. the area originally occupied by cement grains). With time this process results in an appearance that becomes more dense and interlocking so that after considerable time an apparently "solid" amorphous, dense structure results. Typical developments in the hydration process are shown in the micrographs 2.10 (a,b,c,d).

It is interesting to note, however, that recently Pratt and Jennings (10, 11) and Dalgleish and co-workers (14) reported that even when the surface of a hydrating cement appears, in SEM, as completely intertwined with hydration product (predominantly fibrous type I C-S-H) to such an extent that it forms a solid amorphous mass of type III appearance, the subsurface - or bulk region - is still largely composed of fibrous materials of so called innerproduct. This finding was based on elegant STEM "internal" observations of identical surfaces examined by SEM (11) and substantiates earlier conjectures of its presence (39, 57). Very recently the author has observed similar features in cement paste hydrated 28 days and subsequently fractured "in situ" in the specimen chamber of the SEM (Fig. 2.11 (a, b)). (See also Chapter 8). The surface is predominantly "dense" and amorphous, reminiscent of type III morphology, but in certain sub-surface areas fibres are observed in the freshly fractured surfaces. This is further evidence in support of Dalgleish and Pratt's observation (10, 11) that within the bulk of fully hydrated material, fibrous hydration product still persists, and that hydrated product is not always "dense".

It is also relevant to comment at this stage that, despite the wide variety of morphologies and combination of hydration products that result from hydration, it is not generally useful to consider certain hydration products as "good" or "bad" from a strength or property viewpoint. Their performance is interrelated and depends on various circumstances. Calcium hydroxide is, however, regarded as being weaker and the C-S-H Types I and II, stronger. It is therefore perhaps naive to take a simplistic approach that certain hydration products are 'better' than others (37).

Having considered the various morphologies of hydrating cement, the general features of strength development during hydration can, at a basic level, be regarded as gradual filling of the space between cement grains with (mainly fibrous) hydration product, which ultimately forms a rather nondescript amorphous structure. It is of relevance to consider how this comes about by examining the mechanisms which have been proposed to model cement hydration.

2.2.5 Mechanisms of Cement Hydration

The various mechanisms proposed for the hydration of cement have recently been reviewed by Skalny, et al. (12) and Pratt and Jennings (10). While the overall picture appears to have emerged, certain areas still remain to be resolved.

The most interesting phases of the C-S-H morphology would appear to be the fibrous ones, namely types I and II, as defined by Diamond (9). These fibrous growths have also been described as "tubular" (4, 10, 13, 36, 52), "rolled foils" (14, 38) and "solid rods" (6, 38, 52, 62) and the mechanism of their formation appears to be best explained by a "membrane osmosis" model. This was first put forward by Powers (53, 57) in the early fifties but only really achieved prominence through the more recent work of Double et al. (4, 5, 22, 54, 58) and Birchall (2, 23, 38), and now appears to be valid in many circumstances (2, 3, 9, 38).

The mechanism of the membrane osmotic model as proposed by Double (4, 5, 19, 22, 58), Birchall (3, 23, 38, 51) and others (52, 55), depends on the rapid formation of a semi-permeable layer or membrane, probably consisting of C-S-H, around an hydrating cement grain, shortly after water comes into contact with the cement grain. This "fuzzy gel" layer forms subsequent to the rapid leaching of calcium ions into the solution (together with the virtual absence of silicate ions in solution) which later forms calcium hydroxide (38). The consequent calcium depleted surface areas of mass silicic acids react with dissolved hydroxylated calcium species (e.g. $Ca(OH)_2$) to form the C-S-H membrane at the hydrated grain surface (Fig. 2.12 (a)) (6). Very small amounts of aluminium and silicate also go into solution. The rate of reaction is thus slowed down because of the protective covering provided by this membrane. This behaviour would also explain the observed "dormant" or induction period in heat evolution, as determined by calorimetry studies, which occurs after an initial period of high activity (Fig. 2.2(b)). The length of time, and products formed, however, depend on various factors which include: particle size, solubilities, temperature, amount of aluminium and presence of other contaminating ions. The osmotic membrane model proposes that pressure then builds up inside the membrane as a result of water passing into the shell and calcium ions passing outwards, but at an ever decreasing rate. Osmotic pressure rises within the membrane and eventually causes it to rupture at weak points. This rupture may also possibly be assisted by precipitation of $Ca(OH)_2$ at the surface, which weakens it (6). The fluid contents are extruded into the bulk aqueous phase and C-S-H forms at the interface of the two phases. Continuous precipitation of this C-S-H at the stream periphery then gives rise to tubiform excrescences, of various types (10, 52), often with closed ends to the needles (50), Fig. 2.12(c). However the morphology is not restricted only to hollow needle forms (51, 54). Double et al. (4, 22) have drawn the analogy of this model of cement hydration to that of the tubes and needles formed in a "silica garden", and although the scale is very different, this sytem also relies on an osmotic pump action and differential diffusion.

Arguments in favour of this "membrane precipitation" process include :
(i) the observed lack of any long range order in hydrated material (except for crystalline CH or portlandite) which, presumably, would be

present if the precipitation mechanism was a "through solution" one, and where the critical nucleus size is longer than the unit cell. (Such conditions probably do not exist at the fluid interface where C-S-H is formed (2)). And

(ii) that the precipitated C-S-H morphology appears to be significantly dependent on water cement ratio, or more strictly on the space available for such "osmotic pressure bursting" and other factors, e.g. solubilities, particle size, composition, etc. (62). Indeed, it is reported that hollow tubular growths do not occur in synthetic C_3S (13), and may be closely allied to an aluminate presence (50). The strength of an hydrated cement then presumably derives from an interpenetrating mass of fibrous C-S-H which can also incorporate unhydrated grain residues, (Fig. 2.12(d)).

The action of gypsum as a retarding agent in the rapid hydration of C_3A is also consistent with the membrane osmotic mechanism above. It is considered (7, 11) that a small amount of gypsum ($CaSO_4$) preferentially reacts at the membrane thus inhibiting the rate of development and subsequent rupture, of the C-S-H membranes and thus significantly retarding any so-called "flash set".

This model of C-S-H formation has been extended by Jennings and Pratt (6, 10) and Dalgleish et al. (11) who report some shortcomings of this possibly over-simplified approach. The development of a membrane is acknowledged (10, 62) but the former authors have observed not only hollow needle formation, consistent with the Double-Birchall model, but also "crystalline" formation of ettringite needle growth emanating from pinholes in the membrane surface which can also exhibit hexagonal morphology (10). In addition, and more signficantly, they have noted the rapid formation of exfoliated sheets or foils which can then "roll up" into needles when the bulk of the silicate rich interior meets the calcium rich exterior in the latter stages of hydration (Fig. 2.12(d)). Such a "rolling up" process was first suggested by Brunauer (36) and has also been observed by other authors (14, 52). On the other hand, in the case of specimens hydrated for 1 to 2 hours and then subsequently placed in a water-rich environment, needle growth was found to be more extensive (10), consistent with the osmotic pressure model (2, 4, 5, 22, 38, 58). It was sometimes observed, however, that rolled foils forming needles can

have rounded ends (6, 50), falsely indicating an osmotic rupture formation mechanism, whereas this was apparently not the case. Further evidence in support of this is shown in studies by Dalgleish et al. (11), who report that although a membrane forms around cement grains, the growth of fibrous C-S-H hydration product is not necessarily associated with sudden rupture of this physical membrane or shell, but rather is somewhat more gradual.

Thus it can be seen that the mechanisms of cement hydration are various and complicated and far from being unequivocally resolved. It seems reasonable that a shell structure or membrane generally forms around grains and that subsequent formation of virtually all the hydration products mentioned earlier can occur by either or both of the following mechanisms:

(i) Osmotic pressure rupture yielding predominantly closed-end hollow needles, as well as other morphologies; and

(ii) formation of specific phases at this surface (once again yielding a variety of morphologies), not dependent on sudden rupture.

In addition, evidence exists, for cements of certain types, that the membrane is not always strong and protective (10, 11). It may therefore be that the concept of all C-S-H formed by an osmotic pressure rupture mechanism is too simplistic and the evidence for foils and bulk hydration, admittedly at surfaces or interfaces, as reported by Dalgleish and the Jennings and Pratt group (6, 10, 11), strongly supports this idea. Osmosis through the membrane does, however, appear to be accepted, (10, 51) especially in view of additional evidence put forward by the proponents (63, 64). Further extensive studies are reportedly in progress (10) to attempt to resolve more fully the mechanisms of cement hydration and to evaluate the effect of such other parameters as admixtures (10, 62, 65), composition (62), solubility (10, 62) and environment (66).

2.2.6 Porosity and Strength Development

The most important single factor controlling the strength of mature portland cement paste is the water - cement ratio. This is hardly surprising because the water - cement ratio is closely related to the porosity and the porosity is, in turn, apparently logarithmically related to both strength (37, 67, 68) and stiffness (69) (Figs. 2.13 (a, b & c)). (See also Alford's review (70)). There is no unique relationship between porosity and strength that is applicable for all cement based materials (and indeed, depends on the method of measurement (71)), but Feldman and Beaudoin (68) have used an interesting approach to describe the situation. They assumed that any given cement-like material could be treated as if it were a mixture of coarse, dense crystalline particles and fine, low density, poorly crystalline particles and that for any given porosity an optimum blend existed that gave the highest strength. They further assumed that the strength depended on the intrinsic strengths of the particles and of the strengths of the attractive forces between them. At high porosities the attractive forces between particles were of more importance than the intrinsic strengths of the particles so that a high proportion of low density poorly crystalline fine particles are required from the cement for high strength. At low porosities the reverse is true. Fig. 2.13(b) shows their results (68). This suggests that, for normal water cement ratios, strengths might be increased by raising the proportion of high density, large size and high crystallinity material and this appears to be borne out in practice by the increased strengths of high alumina and pozzolanic cements.

Jambor (67) essentially expressed similar ideas in reporting that not only does porosity decrease as the water cement ratio decreases but that the rate of hydration is also accelerated in the early stages. (He attributed higher specific binding capacity to the early stage hydration products for low porosity cement pastes which appears consistent with the approach of Feldman and Beaudoin (68, 69)). With decreasing water-cement ratio, and hence porosity, there is an increase in modulus and compressive strength as shown in the Fig. 2.13 (a) and (c). At the same time the average pore radius decreases together with the amount of water bound in the hydration products, as the water-cement ratio decreases.

Jambor's results, shown in Fig. 2.13(c), indicate that reductions in porosity due to reductions of water - cement ratio are more important than such porosity reductions resulting from ageing at constant water - cement ratio. The implication drawn by Jambor (67) was that such pores that exist at low water - cement ratios are more completely filled with a hydration product, which itself has a "higher binding energy" (because it contains less water). Together with this change in binding energy is a change in the morphology of the C-S-H hydration products, which generally become more fine grained. These changes in morphology and hydration reactions with dilution have been highlighted by Jennings and Pratt (62) who advise that extreme caution should be used in extrapolating observations made in dilute solution to more realistic cement systems, a point that appears to have also been made by Higgins and Bailey in their earlier studies (72).

Thus it is seen that porosity in cement paste appears to be a major limitation to its strength and recent observations on the fracture behaviour tend to confirm that such flaws control fracture strength (72, 73). Higgins and Bailey, for example, have shown that hardened cement paste is not as notch sensitive as might be expected, which they attribute to the inherent flaws or porosity in the paste, (72). Fine, stable crack propagation has been observed prior to catastrophic failure by Tait and Bohm (74) and Higgins and Bailey where crack tortuosity and cracking in the vicinity and ahead of the crack tip, has been reported, (75).

Recently, in acknowledgement of the severely limiting effect of porosity, or at least of large inherent flaws on cement paste strength, efforts have been made to produce hydrated cement pastes with very much reduced porosity and flaws - or more importantly, to reduce the absolute size of these pores and flaws (70). Such ideas were suggested by Higgins and Bailey (72) but their estimate of absolute inherent strength of cement paste (15 MPa) has proved conservative.

Very exciting advances in this field have been reported by the Birchall (2, 3, 15, 23, 38, 51, 76) and Double and Alford (1, 5, 70, 77) groups, who have shown that when cement paste is largely macro defect free (MDF) the strength of cement is substantially improved. By using very low water cement ratios, coupled with relatively small amounts of water soluble polymer

admixtures (77), reductions in macro defects have resulted in tensile strength improvements from typically 5 MPa up to 150 MPa (Fig. 2.14). The critical parameter of macro defect free (MDF) cement has recently been shown, by Alford, Groves and Double (70, 77), to be intrinsic flaw size and not total measured porosity (Fig. 2.15).

Corresponding improvements in the intrinsic toughness by the reduction of such flaws and porosity is predicted to lead to MDF cements with flexural strengths approaching 200 MPa. Very recently, flexural strengths of 150 MPa has been achieved by Birchall and his team (15).

The potential of such a material, especially when allied in composite form to 'new' strong fibres like carbon, boron and alkali resistent glass fibres, is extremely exciting and promises to provide revolutionary new materials for the future (1, 23).

In summary, in this section the constitution of cement and hydrated cement paste, together with the typical morphology of their hydration products, as reported by a number of authors, has been examined in some detail. Mechanisms of hydration, which appear to depend to a lesser or greater extent on a membrane model, have been reviewed and allied to strength development. The importance of inherent flaw size on strength has been emphasised. It is now in order to examine how this cement matrix material contributes to the static strength of concrete itself since, from an engineering viewpoint, this is the most important material. This is therefore considered in the following section.

2.3 Factors Affecting Static Strength of Concrete

2.3.1 Introduction

The widespread and ever-increasing use of concrete is probably due to several factors. It is inexpensive, easy to cast into a variety of shapes, durable and resistant to weathering, while at the same time providing nearly rock like strength - in compression at least. It is thus appropriate to examine in some detail the factors affecting strength of concrete. In particular, this section is concerned with the static strength of concrete, i.e. those situations where loading is non dynamic and loads once applied

change little throughout the life of a structure. The effect of dynamic, or fatigue, loading on concrete is considered in Section 2.4.

Concrete, of course, is comprised of a mixture of hydrated cement paste and aggregate of various types and coarseness. As observed by Walker and Bloem (78) "the strength of concrete results from (i) the strength of the mortar matrix; (ii) the bond between the mortar and the coarse aggregate; and (iii) the strength of the coarse aggregate particles themselves - i.e. their ability to resist the stresses applied."

The emphasis, at this stage of this review, on concrete, arises because it is the important practical constructional material, whose properties have been well documented. A study of mortar itself or cement paste alone, while giving an accurate picture of the behaviour of the binding matrix, does not allow for the stress concentrating effects of the aggregate, or flaw development at aggregate interfaces, even though the aggregate may simply be regarded as an "inert" composite addition. The complete study of any one of the three materials, cement paste, mortar or concrete should thus only be undertaken in the context of the other two. For comparative purposes, then, it is useful to consider cement paste, mortar and concrete separately in referring to strength and to be wary of discussing their properties collectively although they are obviously closely related.

Such a distinction has therefore been made in this thesis. For example in the preceding section the development of strength in cement paste alone has been discussed and in the following sections the discussion relates only to concrete. In chapter 6, where fracture and crack propagation are considered in some detail, the above classification into cement paste, mortar and concrete is again quite distinct.

2.3.2 Water-Cement Ratio

Perhaps the most important parameters on which the strength of concrete depends are the water-cement ratio and the degree of compaction, both of which are closely allied to the porosity of the concrete. The strength dependence on porosity or void content is discussed in more detail in section 2.3.3 to follow and therefore for this discussion it is assumed that the concrete is fully compacted in the normal way.

Changes in the water-cement ratio effectively make the concrete a new material. There is a rough, but valid, analogy in this case with the iron-carbon system where a small change in the carbon content can change a mild steel to a high yield strength steel or even to a cast iron.

Empirical "laws" relating the strength of concrete to water-cement ratio were first proposed by Feret in 1896 (see e.g. (33)) and Duff Abrams in 1918 (79). These authors effectively found an inverse relationship between the strength of concrete and the water-cement ratio (raised to some power). A typical strength versus water- cement ratio plot is shown in Fig. 2.16.

Here it can be seen that the range of validity of the water-cement ratio "law" is restricted and that at low water-cement ratios strength appears to be limited by flaws characterised by air voids and porosity of various types. This is also strongly influenced by compaction and the flaw shape, since even at high cement contents and very low water-cement ratios shrinkage may be so severe that the resulting flaws and voids severely limit the strength.

Since the form of the strength versus water-cement ratio curve appears hyperbolic (Fig. 2.16) attempts have been made to represent this information in a linear fashion suitable for interpolation (33, 80). Figs. 2.17 and 2.18 indicate respectively an inverse (33) and logarithmic (33, 81) fit to empirical data and Popovics (80) has recently developed a generalised practical form of Abrams "law" (33).

2.3.3 Air Voids and Porosity

Since porosity and void content are generally closely related to water-cement ratio, the strength dependence of concrete on these former parameters is obviously very similar to that shown in Figs. 2.16 - 2.18. Entrained air in concrete, resulting from incomplete compaction, severely limits concrete strength. A plot of normalised density ratio (a measure of the degree of compaction) against the normalised strength ratio (Fig. 2.19) indicates the very deleterious effect of such void content. The effect is most significant : a mere 5% void content can reduce the strength by 30%; even as little as 2% void content can result in a strength reduction of about 10%.

2.3.4 Effect of Aggregate on Strength

The effect coarse aggregate has on the strength of concrete is also quite significant although the influence appears to depend more on small cracks and inherent flaws at the interface of the aggregate than on the intrinsic strength of the concrete or aggregate. Thus, Jones and Kaplan have reported that the load at the onset of cracking, as distinct from ultimate load, for both compression and flexure, is independent of aggregate type or texture (82). In contrast, it has also been reported that first microcracks occur at the largest aggregates (83-86) and that concrete with small aggregates has a higher compressive strength than similar concrete with large aggregates (78, 87, 88).

Ultimate strengths do, however, depend on the properties of aggregate types, particularly surface texture and size (89, 90) (Fig. 2.20). To a lesser extent, ultimate strength is affected by the slope and grading of aggregate as well as the aggregates' intrinsic strength and stiffness (33).

The effect of aggregate content and type on strength of concrete is most marked at low water-cement ratios ($\simeq$ 0.4) where mechanically well-bonded crushed aggregates give higher strengths than gravels. The effect declines, however, and is not observed at high water-cement ratios (above 0.65) where presumably the intrinsic strength of the paste is the limiting factor.

For high strength concretes (above about 35 MPa) there is an apparent anomaly regarding the leanness of the mix on strength. Although the aggregate-cement ratio is of secondary importance to the water-cement ratio with respect to strength, it has been found that for a constant water-cement ratio a leaner mix leads to higher strengths (See Fig. 2.21 (33, 91).

This behaviour is probably associated with the absorption of water by the aggregate: the larger amount of aggregate absorbs a greater quantity of water and thus the effective water-cement ratio is reduced (91).

The influence of aggregate content on cracking resistance on the one hand and as a source or initiation of microcracks on the other - and thus an inhibitor of concrete strength - is discussed further in Chapter 6.

2.3.5 Static Stress-Strain Behaviour of Concrete

This topic has recently been excellently reviewed by Wastiels (92) and the reader is referred to this paper for further details. When concrete is loaded to failure in uniaxial tension or compression a curve which is by no means perfectly linear is obtained (Fig. 2.22). The two components of concrete, cement paste, and (coarse and fine) aggregate individually exhibit linear stress-strain curves but concrete itself exhibits a pronounced curvature from quite an early stage. The reason for this is attributed to microcracking at the interfaces between the cement paste and aggregate (93, 94). These microcracks develop at a variety of angles with respect to the applied stress and there is a progressive increase in the local stress intensity (95, 96). The magnitude of the strain increases at an increasingly faster rate and hence the material exhibits only psuedo-plastic behaviour.

Indeed, Hsu et al. (83) and Wastiel (92) describe four stages in the stress-strain curve of concrete (Fig. 2.22). Stage I, up to 30% of ultimate stress corresponds to purely linear elastic behaviour where the deflection is linearly related to the applied stress. (Removal of the stress up to this level results in completely reversible recovery of the strain with no hysteresis). Stage II, from about 30% to 50% of ultimate stress, marks the intiation of microcracking and the first departure from linearity. Microcracks develop when the local interfacial strength is exceeded, (93). This is consistent with first detectable damage monitored by acoustic emission monitoring (Section 3.5.4). Stage III, between about 55% to 90% of ultimate stress; exhibits increased curvature and slow propagation of existing microcracks together with increases in their number and width, and finally, stage IV marks the onset of catastrophic failure when cracks propagate rapidly and join up, leading to final fracture and loss of strength of the concrete.

The shape of the so called "static" stress - strain curve, and the magnitudes of the observed ultimate stress and strain, are dependent on the rate of application of stress, (Figs. 2.23 (a,b)). At very slow loading rates care must be taken to distinguish loading rate effects from creep and normally an arbitrary distinction is made that the strain that occurs subsequent to initial loading is regarded as creep (33).

At fast loading rates (or strain rates approaching 10^2 sec $^{-1}$) there is a rapid increase in strength (97 - 102), as shown in Fig. 2.23 (c and d) (taken from impact studies by Kormeling (97) and McHenry and Shideler (98)). The impact resistance of concrete depends on various parameters, particularly aggregate type and shape, casting direction, admixture addition, presence of fibre reinforcement, cement content, etc. (97, 103, 104). Despite such complex interactive effects, Zech and Wittman have recently developed a theory for interpreting impact fracture behaviour of concrete (102).

At the other end of the strain rate scale is the phenomenon of "static fatigue". This occurs at very slow loading rates, or more particularly in situations where the concrete fails after a period of time under conditions of constant stress (27, 29, 30, 105, 106). This phenomena must be distinguished from creep and leads ultimately to failure through slow crack propagation and appears to depend on environmental moisture condition (27, 30). This phenomenon, and that of conventional fatigue, are of particular interest in the work reported in this thesis and are discussed in more depth in Chapters 6 and 7.

In addition to the effect of strain rate on the stress-strain behaviour of concrete it has been suggested that failure occurs at a particular, critical strain, of the order of 0.001 to 0.003 in compression (27, 33, 103) and 2 x 10^{-4} in tension (33). Recently, critical tensile failure strains of 6 x 10^{-3} have been achieved with macrodefect free (MDF) cement pastes (23). In comparison, results of the current study indicate that, for mortars, failure occurs at a critical strain of approximately 5 x 10^{-4} to 2 x 10^{-3} (Section 4.2).

In this respect concrete can be considered as a brittle material even though it does exhibit some pseudo-plastic behaviour. The dependence of failure on a critical strain is not, however, universally accepted (33) and further studies need to be undertaken to resolve this question and if applicable, the dependence on water-cement ratio, aggregate type and content, curing conditions, etc. (107-109).

Another factor which has a bearing on the measured static strength of concrete is the moisture condition at the time of test (68, 110, 111). Generally, dry concretes are stronger than wet concretes. However, concretes kept continually moist are stronger than dry concretes at ages up to approximately six months (112). Lowest strengths are obtained with concretes that have been dried and then soaked just prior to testing and tested wet, (113) (Fig. 2.24).

2.3.6 Effect of Temperature on Static Strength of Concrete

Since many fatigue fracture situations are concerned with associated changes in temperature it is appropriate to examine how temperature affects both the fatigue and fracture behaviour of cement, mortar and concrete. Experimental studies in the present work are described in Chapter 4 (fatigue aspects in compression) and Chapter 7 ("single" crack aspects utilising double torsion methods). Accordingly, it is relevant to examine the effect of temperature on the static strength of concrete, as a useful prerequisite, and this is undertaken in this section.

Temperature can affect concrete strength in a variety of ways and its influence, from accelerated hydration of fresh concrete, through strength dependence, to testing concrete under hot conditions have been extensively reviewed elsewhere (29, 33, 106, 114-119). Here only the effect as to how temperature changes affect strength and elasticity are examined in any detail.

An increase in temperature in the vicinity of ambient temperature causes a faster rate of hydration in fresh concrete and thus an increase in the development of early strength. It has been reported that, for temperatures between ambient and about 38^{o}C, there is a linear relationship between compressive strength (and modulus) and the log of "maturity" (where maturity is the product of temperature and time in ^{o}C days) (118). Some of the hydration products are, however, reportedly of poorer physical structure, with more pores and less C-S-H gel (115); thus later strength may, in fact, be slightly reduced. High temperatures during curing (but well below 100^{o}C) can increase shrinkage cracking with consequent reductions in measured strength (120). Kleiger (116) has reported that the optimum temperature for maximum strength development is approximately 13^{o}C for

concrete made with O.P.C. and approximate 4°C for R.H.P.C. (or type III cement).

These effects of temperature on ultimate strength of concrete are, however, slight and significant decreases in strength only really begin to occur above about 250°C to 300°C (117, 121, 122), Fig. 2.25. At higher temperatures, i.e. 600°C to 800°C, the strength of concrete rapidly decreases and in many cases the concrete changes colour as indicated in Fig. 2.25.

Generally, the influence of temperature on elastic modulus parallels the effect on compressive strength. There is little change with temperature from ambient conditions up to about 90°C (33), but once water is expelled through drying at temperatures above 150°C to about 400°C there is a significant reduction in modulus (Fig. 2.26).

Similar strength dependence on moisture occurs as a function of (normal) temperatures at time of testing, but to a lesser extent (123). Comparative concrete compressive tests performed at 20°C can exhibit an approximate 10% strength change with a temperature change of plus or minus 20°C around this ambient temperature (33). Hanson and Erikson (124) report a type of "Kaiser effect" on elasticity (as measured by deflection), i.e. previously heated concrete does not exhibit significant deflection on reheating unless the previously attained temperature is exceeded (see section 3.5.4).

2.3.7 Age Effect on Concrete Strength

The increase in strength of the various components of cement paste with age during hydration has already been examined (Fig. 2.2(a) and Section 2.2.3.) Strength development in concrete is naturally very similar but does depend, for its exact form, on such parameters as mix, water-cement ratio, cement type, temperature and curing conditions (33, 116, 118).

In view of the nature of the mechanisms of hydration of cement, as discussed in section 2.2.5, where a shell of hydration product forms around cement grains, it is hardly surprising that the strength of cement and concrete continues to develop with time, although admittedly at an ever decreasing rate. Hydration and consequent strength development are reportedly still proceeding, albeit slowly, from cements and concretes in excess of two to

four years old (6, 11). The gradual full hydration of cement grains inside this shell takes a very long time and accounts for this gradual and sustained strength increase with age.

Since it is often useful in practice to establish the likely 'final' strength of concrete before 28 days (the normal engineering age criterion), the 7 day strength is often measured. The 28 day strength is typically between 1.3 to 1.7 times the 7 day strength for O.P.C., with a lower strength increase (1.3 to 1.4) being associated with higher initial ambient temperature (and hence faster curing) or lower water-cement ratios (Fig. 2.27). The codes CP 110, 114, use a value of 1.5 for prediction purposes (125).

The nature of the ever decreasing rate of strength development of concrete with age also affects the modulus, creep behaviour and impact behaviour of this material. Modulus usually increases at a faster rate than strength at greater ages (33, 118). The older the material before load application the smaller the consequent creep deformation. With regard to impact situations, impact strength generally increases with age but Green has shown (126) that the greater the static strength the less energy is absorbed per blow before cracking occurs. To some extent this is related to concrete toughness which, according to the literature either increases with age (127) up to a certain stage and then levels off (72, 128, 129), or is independent of age (130, 131).

In addition to the above parameters, others which are also affected by age include, for example, resistivity, permeability and the coefficient of expansion. However, these are not considered relevant here and for more information the reader is referred to the established texts, for example Neville (33) and Lea (32).

In this section, 2.3, the properties and static strength characteristics of concrete have been briefly examined as an introduction to the fatigue strength of concrete. The general characteristics of the present understanding of the effect of fatigue loading on concrete are briefly reviewed in the next section, but more specific aspects of particular characteristics of concrete fatigue are reviewed and discussed in Chapter 4.

2.4 General Factors Affecting Fatigue

2.4.1 Introduction

So far in this chapter we have considered static strength of both cement and concrete under various conditions. Many situations exist, however, where loading is applied repetitively and can lead to premature failure. Fatigue can be regarded as taking place when failure occurs after the repeated application of loads which in themselves are not large enough to cause failure in a single application. The problem of concrete fatigue is a common one, but is not necessarily always recognised as such, as noted in Chapter 1. This latter factor probably accounts for the absence of fatigue rules from the engineering design codes for concrete; however recognition of the more widespread nature of fatigue in concrete has stimulated a developing research interest in this area.

A brief general discussion and literature review of fatigue in concrete is given in this section, while Chapter 4 provides a report on the detailed experimental investigation of the factors affecting fatigue strength. In particular, a detailed consideration of the effect of frequency, environment, temperature, waveform and stress range is left to Chapter 4.

In discussing fatigue in concrete it is important to draw several clear distinctions. In this context, concrete fatigue can be considered as occurring in three ways: static fatigue, cyclic fatigue and impact fatigue. Static fatigue has been briefly mentioned earlier and is discussed at greater length in Chapters 6 and 7. Impact fatigue, i.e. repetitive, high strain rate loading, will only be mentioned briefly since the more common and more relevant condition - cyclic fatigue - is of most interest in this thesis.

It is also useful to bear in mind the testing methods used to investigate fatigue (and fatigue failure) in concrete and these can broadly be separated into pure compression, pure tension and flexural tests. Flexural tests (132-136) have probably been most commonly used and are the easiest to perform but because of their mixed compressive/tensile stress field are possibly less useful than pure compression fatigue tests, which have also been quite widely reported (27, 89, 96, 135-138). Pure tensile tests are very difficult to undertake in view of the brittle nature of concrete and

the difficulty of ensuring an absence of bending moment or non-uniform stresses during cycling (108). The fatigue performance of concrete under each of these testing methods is not always identical so it is important to be aware of the particular stressing mode when fatigue in concrete is discussed.

2.4.2 Cyclic Fatigue Representation : SN, or Wöhler, Curves

One of the conventional ways of representing fatigue behaviour of materials in general, and which is no less true of cement and concrete, is by means of the so-called "SN", or "Wöhler" curve. In this representation, empirical data is obtained of the fatigue "life", or number of cycles to failure, and is plotted on a log scale against the cycling level of stress amplitude, expressed as a percentage of the ultimate failure load (whether in compression, flexure or tension). Normally the minimum stress is close to zero so the full stress range is utilised. Traditionally, investigations of fatigue of concrete utilise SN curves and thus incorporate, in the number of cycles to failure, both flaw or crack initiation as well as subsequent crack propagation. A typical SN curve is shown in Fig. 2.28. This curve, although similar to other SN curves in the literature (25-27, 33, 95, 96, 133-137, 139-142) utilises data obtained by the author pertaining particularly to this thesis. It includes data for tests conducted in both "wet" and "dry" environments. (The exact details of moisture content with respect to "wet" and "dry" and the implications of these results, are discussed in more detail in Chapters 3 and 4.)

The significance of the effect of fatigue in concrete can now be seen from the form of the SN curve. Cyclic stressing at high stress levels, for example at approximately an 80% stress level or above, implies a high probability of failure after only a few hundred to a few thousand cycles. However, at stress levels of the order of 60%, the fatigue life is approximately one million cycles. This may seem adequate for many civil engineering structures where a safety factor of 2 (i.e. nominally 50% stress level) is not uncommon, although, in certain situations, it is inadequate. Consider, as an example, mass concrete breakwater dolosse subjected to a sea wave impact, where a million cycles of wave impact are achieved in only about four months. If each were causing nearly 50% of ultimate failure stress in the dolosse, this would imply that after about half a year these

dolosse structures would be in great danger of failing, even though the original safety factor of 2 would, superficially, have appeared more than adequate. (In practice, the stresses achieved during wave impact are probably far less than this 50% level.) This example, however, focuses attention on the importance of a consideration of fatigue in structures subject to repeated loading, such as pavements and bridges, and illustrates the need to accommodate the effects of fatigue in design as was first attempted by Clemmer (133).

Hsu (25) draws the further distinction, in the use of the SN curve, between "high cycle" and "low cycle" fatigue. "Low cycle fatigue" - up to approximately 2000 cycles - typically refers to reinforced concrete structures subjected to seismic activity, and "high cycle fatigue" - from approximately 2 000 to 10 million cycles - covers most bridges, pavements, runways and marine structures. Hsu argues that the results of research conducted over a very limited part of the fatigue life spectrum cannot always be extrapolated to cover fatigue behaviour at very much higher or lower number of cycles and that, indeed, the actual mechanism of fatigue failure may be different. This point is developed and discussed in more detail in Chapter 4 (Section 4.3 and 4.6).

If the upper level of cycling stress is sufficiently low (say approximately 30% of ultimate) it has been proposed that no fatigue (leading to failure) occurs (33), implying that there is a "fatigue limit" in this material. More generally, however, concrete is regarded as not exhibiting any such fatigue limit, i.e. there is no limit below which fatigue damage does not occur (25-27, 96, 132-135, 137-140, 143-147, 152).

This conclusion is based on experimental fatigue studies to high but still finite numbers of cycles, as it simply becomes exceedingly tiresome to run experimental tests to 10^8 or 10^{10} cycles at realistic frequencies. Hence a "fatigue strength" is often defined at a fixed number of cycles (usually 10^7) which for concrete is about 55% of the static strength in flexure (26, 133, 135-137, 140, 145, 148) and about 55 to 60% of the static strength in compression (132, 137). However, this level of fatigue limit appears only applicable when the cyclic loads vary from near zero to the predetermined maximum (i.e. the fatigue force ratio, Pmin/Pmax or R tends to 0) and is no longer accurate when the minimum load is a significant

percentage of the maximum (132, 135) (i.e. $R \rightarrow 1$). In reversed loading (R=-1) Murdock (135), reporting work by Hatt and Crepps, notes that for flexural tests a conventional fatigue limit was found (i.e. a levelling out of the SN curve) at about 55% stress level after only about 10^4 cycles. More recent studies by Cornelissen and Timmer (142) confirm this trend of shorter lives in tension, as they report that a considerable decrease in fatigue life was observed for the case of uniaxial tension-compression fatigue tests than for fatigue test where the minimum load was a finite proportion of the maximum load (and of the same sign). It is probable that fatigue damage in concrete, while progressive, does not accumulate linearly (135, 149).

One of the shortcomings of the SN curve representation of fatigue data for concrete is that the regression line (typically log N = 16.1 - 0.15 S (148), where S is the stress level) of the SN curve is inherently located along the 50% probability of failure line, and does not itself take into account the probability of failure or express the likely scatter in results. McCall (148) was the first to recognise this shortcoming of the SN curve representation and to introduce a third variable P, the probability of failure, thus leading the way for SN curves to become "three dimensional". McCall proposed the relationship:

$$L = 10^{-aSb} (\log N)^c$$

for flexural tests in which L = probability of survival = (1 - P);
S = stress level; and N = number of cycles; and a, b and c are empirical constants. This relation implies that the range of scatter of log N is greater at lower stress levels, which tends to be observed in practice (Fig. 2.28). This concept of including probability in fatigue SN evaluation has been elegantly extended by Hsu (25).

A characteristic of the SN curve representation is that the cyclic stress is expressed as a normalised value in terms of the static ultimate strength and thus many factors that affect the static strength tend also to affect the fatigue strength, as represented by an SN curve, in a similar way. This has been noted by various authors (26, 140, 144, 150-152), indicating that concrete mortar and cement paste have almost identical reponses to cyclic loading when expressed in terms of their static strengths (143). In other words there is no effect of some variables when the results are normalised

with respect to static strength, as there is reportedly similar percentage changes in fatigue strength as static strength.

In particular, the parameters of water-cement ratio (138), porosity (or entrained air (96, 135, 143, 150)) and age (151) of the cement, mortar or concrete are reported to have similar effects (despite some exceptions) on the fatigue strength as on static strength. Antrim (138) conducted fatigue tests on both cement paste and concrete for two water- cement ratios (0.45 and 0.7) and obtained results which indicated that the 0.7 ratio gave a slightly increased resistance to fatigue when expressed on an SN curve, which he attributed to the "less brittle" nature of 0.7 water-cement ratio concrete. Antrim also noted that, although the fatigue behaviour of air entrained concrete was similar to non air entrained concrete, the scatter was less in the former case. Raithby and Galloway, in flexural fatigue tests on concrete, noticed a substantial increase in fatigue endurance with age (151), the actual gain being dependent on the type of concrete and on the applied stress level. However, it is not clear whether the appropriately aged static tests were used for normalisation in the SN curves. These authors finally conclude that "changes in fatigue strength closely follow changes in static flexural strength under these conditions".

2.4.3 Damage Accumulation and Change in Modulus

One of the interesting phenomena relating to fatigue of concrete and related materials is the change in compliance, or shape of the compressive and flexural stress strain curves, with progressive number of fatigue cycles. For static tests there is a pronounced curvature of the stress-strain curve (Fig. 2.22). With increasing fatigue cycling, between fixed stress limits, the shape of the stress-strain curve changes from concave towards the strain axis (with hysteresis on unloading), through an approximately linear regime, to concave towards the stress axis (Fig. 2.29) (96, 132, 135, 137, 143, 145, 153, 154). This indicates that there is some softening and accumulated "damage" or so-called "irrecoverable set", which is indicative of how close the concrete is to ultimate failure. The reason for this appears to lie with the development of microcracking in the concrete, ultimately leading to final failure as this "damage" accumulates. This phenomenon, mentioned by Bennett and Raju (143) and Brown (155), has been used to advantage in this thesis since the degree of accumulated microcracking damage can be monitored

by means of both lateral and longitudinal strain measurement and also by ultrasonic methods. (For example, see Fig. 2.30 which is taken from data obtained by the author.) This damage accumulation can subsequently be used as a parameter to measure the effect of other variables (such as frequency, moisture content or temperature) on damage development. This work is described in detail in Chapters 3 and 4.

Observations of the hysteresis curves for complete loading-unloading cycles are consistent with this concept of progressive microcracking or damage development with fatigue. Apart from an initial decrease in the area of the hysteresis loop in the first few cycles, the area generally increases. This indicates progressive softening and an increase in energy absorption associated with microcracking. The variation of hysteresis loop area and increased softening is shown in Figs. 2.31 (a) and (b). (Fig. 2.31 (a) is taken form the present study: Figure 2.31(b) is from the work of Bennett and Raju (143)). This hysteresis behaviour is consistent with the compliance softening and modulus change just mentioned.

2.4.4 Strain Considerations

Since there is such extensive microcracking development during fatigue, it is hardly surprising that the observed strain at failure in fatigue is larger than in static failure (Fig. 2.32) (135, 143, 150). The total measured strain is comprised of an elastic and a plastic, or inelastic, component (96, 143, 145). In fatigue situations, due to the extensive microcracking the degree of this inelastic, accumulated or "residual" strain can be far greater than the elastic component, with failure strains approaching 4 000 microstrains. This residual strain also appears to increase with number of cycles (at constant frequency) but as mentioned subsequently (Chapter 4) it may well be that the actual time elapsed may be of more significance than simply the number of cycles (25). Bennett and Muir (96) report an increase in both the elastic and residual strains in fatigue with the maximum stress level.

Awad and Hilsdorf (27) have developed this theme further and regard damage accumulation as being comprised of a cycle dependent component coupled with a time dependent part. They have used their experimental data to establish an analytical procedure for predicting failure lives of concrete.

While the development of microcracking (or damage) in concrete during cyclic fatigue is progressive, its rate of development appears to be non linear (48, 135, 139, 140). The rate of microcracking damage development appears to be sigmoidal (Fig. 2.30) and it is also apparent that the Palmgren- Miner Rule* of damage development is not applicable (135, 144, 150, 156, 157). This progressive, but non-linear, microcracking development also results in a progressive decrease in the secant modulus of elasticity (143) (Fig. 2.33).

There is some controversy in the literature concerning whether or not there is a limiting or critical value of strain just prior to final failure in fatigue. Bennet and Raju (143) report that the onset of failure in both static and fatigue tests appears to be associated with a critical elastic strain, while Murdock (132) reports a critical ultimate strain. Raju (152) reports the existence of a critical limiting strain for both static and fatigue tests of the order of 1 500 to 2 500 microstrains.

On the other hand, Neal and Kesler (140) report that, although there is a greater scatter in measured values of final fatigue strain, there does not appear to be any limiting strain criterion for failure. Environment also appears to be an important factor since Cornelissen and Timmers (142) have observed that wet concrete specimens tested in fatigue exhibited greater tensile peak strains than corresponding dried samples, while Spooner (99) cites curing environment as a factor of major importance to fatigue life and proposes a maximum stress criterion for air cured concrete and a maximum stain criterion for water cured concrete.

---

* The Palmgren-Miner Rule states that the proportion of a fatigue life used up when n cycles of a particular load are applied, is equal to $\frac{n}{N}$, where N is the number of cycles to failure at that load. Under variable amplitude loading failure is predicted to occur when $\sum \frac{n_i}{N_i} = 1$.

2.4.5 The Effect of Variable Loading Programme and Rest Period History

Variable Loading History

The effect of variable load studies on fatigue have been examined principally by Hilsdorf and Kesler (157) and Bennett and Jinawath (156). The approach used involved one change in the maximum stress level during a fatigue test which could either be an increase or a decrease (Fig. 2.34(a)). In Hilsforf and Kesler's study (157) they maintained a constant ratio between minimum and maximum loads of 0.17. The results of both series are shown in Fig. 2.34(b). There, the cycle ratio n_2/N_2 is given as a function of n_1/N_1, if n_1 and n_2 are the number of cycles at stress levels σ_1 and σ_2, and N_1 and N_2 represent the average number of load repetitions necessary to cause failure under constant stress levels of σ_1 and σ_2, respectively.

The cycle ratio, n_2/N_2 therefore, indicates how much of the fatigue life of a specimen was used by n_1 cycles under a stress level σ_1. If the cycle ratio n_2/N_2 is equal to unity, then the repeated loads under a stress level of σ_1 had no effect on the fatigue life of the specimen. For values of $n_2/N_2 < 1$ the cycles under the stress level σ_1 decreased the fatigue life; for $n_2/N_2 > 1$ the repeated loads at a stress level σ_1 caused an increase in the fatigue strength under σ_2.

According to Fig. 2.34(b) the sequence in which repeated loads of different magnitude are applied has considerable influence on the fatigue behaviour of concrete. For $\sigma_1 < \sigma_2$ the fatigue life of concrete under stress level σ_2 is generally decreased by the repeated loads under stress level σ_1. However, for $\sigma_1 > \sigma_2$, small values of n_1/N_1 will have a beneficial effect on the fatigue life of the specimen under the second stress level σ_2.

If these results are compared to the Miner hypothesis, which assumes a linear accumulation of damage, it is apparent that when the lower stress level was applied first the Miner theory was unsafe, whilst when the higher stress level was applied first the Miner theory proved conservative. It is thus clear that the assumption of linear accumulation of damage of concrete in fatigue is false.

In contrast to the above flexural fatigue study, Bennett and Jinawath (156) conducted similar fatigue tests on compression prisms. Their test programme (carried out at a test frequency of 3 Hz cf. 7·5 Hz used by Hilsdorf and Kesler) utilised 70% and 80% stress levels as the maximum fatigue levels but the minimum stress level was kept constant, near zero. (This is in contrast to Hilsdorf and Kesler's tests and may be of considerable significance). Their results, shown in Fig. 2.34(c) indicated that when 70% level preceded the 80% level the sum $\sum \frac{n}{N}$ was greater than unity; and less than unity when the higher stress was applied first. This is in direct contradiction to the Hilsdorf and Kesler studies (157), as is also apparent from Fig. 2.34(c).

Tests by both these groups of researchers on multiple step tests revealed no significant effect on fatigue life of such alternate step tests, although Bennett and Jinawath did report the Miner hypothesis conservative for 16 of 20 such tests conducted.

Rest Periods

In engineering practice, the cyclic loading of concrete structures is very often not applied in a regular pattern over a period of a few hours or days, as in the case of conventional fatigue tests. Such loadings often occur intermittently with rest periods of varying duration and thus questions arise as to the effect of recovery between loads and loading history as well as to the effect of age and environment.

Hilsdorf and Kesler (157) conducted flexural fatigue tests which included variable rest periods of 1, 5, 10, 20 and 27 minutes and found that an improvement in fatigue strength was obtained for rest periods up to 5 minutes. Longer rest periods did not apparently lead to any further increase in fatigue strength (Fig. 2.35(a,b)). The fatigue strength was improved from 62 to 68% at 10^6 cycles.

Similar beneficial effects of rest periods have been reported by other workers, (96, 133). Bennett and Muir (96) reported that rest periods of 24 hours, after 190,000 load cycles, led to a recovery of 50% of the residual strain but the strain recovery was only 10% if the rest was applied after 3 to 4 million load cycles. This would imply that the

recovery seems to depend on the degree of initial damage. For short rest periods (of 2 seconds in 20 Hz tests) Raithby and Galloway (151) reported that such tests did not exhibit any significant difference from conventional fatigue tests.

2.4.6 Modified Goodman Diagram for Design

Graf and Brenner (158) introduced a modified "Goodman diagram" for design purposes, as a means of relating the fatigue performance to the maximum and minimum stresses to which the concrete is subjected (Fig. 2.36). The abscissa represents the ratio of the minimum, σ_ℓ, to the maximum, σ_h, cycling stress - i.e. some measure of the "cyclic amplitude" - and the ordinate the stress level (i.e. the percentage that the maximum cyclic stress is of the static strength). Thus an ordinate from a line at 45^o through the origin shows the tolerable range of stress, $(\sigma_h - \sigma_\ell)$, for a given number of cycles. Alternatively, for given upper and lower stresses, one can obtain an indication of the probable number of cycles to failure. For a given lower stress value, σ_ℓ, the number of cycles is very dependent on the range, as can be seen from the small appropriate adjustments on the diagram. Generally, the smaller the lower stress loading condition, σ_ℓ, the shorter the number of cycles a given concrete can withstand (144).

The modified Goodman diagram achieved some renown for design purposes (159, 136) and adequately illustrates the effect of maximum and minimum stress levels, and also range of stress on fatigue life (132, 135, 140, 142, 146, 150).

2.4.7 Parameters Affecting Fatigue Life

In fatigue testing of concrete and cement based material various parameters are kept constant or assumed to have no effect, in order that the effect of other specific parameters may be investigated. In this former category the parameters of frequency, waveform, loading programme and loading rate, moisture condition and temperature have been grouped by various researchers. Recently it has become more apparent that time-dependent processes do occur in the deterioration processes associated with concrete fatigue (27, 28, 99, 141). Thus such effects either need to be accommodated in the overall evaluation, or be minimised by choosing test programmes which do not make assumptions about their effects.

In view of the controversy surrounding particular time-dependent and thermally-or moisture-activated parameters, a significant portion of this thesis has been devoted to studying their effects. Three divisions have been made in dealing with the effects on fatigue of

(i) Frequency of Loading (Section 4.3)

(ii) Waveform and Stress Range (Section 4.4)

and (iii) Environment and Temperature (Section 4.5)

This section (2.4.7) serves merely to identify and define those divisions and their components which are then described in greater detail in the appropriate section, which will cover both previous studies as well as the author's own research.

A great deal of the experimental fatigue work on concrete reported in the literature has been conducted over a fairly limited range of testing frequency (or rate of loading) which then arbitrarily has been applied to a much wider regime or, indeed, different ranges altogether. The applicability, however, of such results to other frequencies is only valid if there is either no effect of frequency or if a quantitative expression exists which will facilitate the appropriate transformation to other frequencies. As the result of tests in the high cycle region it has been suggested (1, 26, 95, 144, 150, 158,) that the fatigue strength is independent of the rate or frequency of loading. In the low cycle region, some workers claim that the rate of loading has a strong effect on the fatigue performance of concrete (25, 27, 28, 141), while others say the effect is small (135, 151).

In view of this controversy the work reported in this thesis has examined some aspects of the so-called "frequency effect" and associated time dependent damage mechanisms. In addition to the frequency effect discussed in Section 4.3, Section 4.4 is concerned with allied effects of loading rate and load programme, waveform, e.g. sawtooth versus sinusoidal, and stress level. Since elapsed time in fatigue would appear to be of some significance, the investigation is concluded with an evaluation of the effects of moisture condition and temperature (over ranges on fatigue performance), in Section 4.5. The time dependent nature of recovery is also examined in Chapter 5 on Fatigue Hardening.

2.4.8 Impact Fatigue

Although the effect of loading rate or so-called "strain rate" on the response of concrete has already been mentioned (Section 2.3.5), this section on Impact Fatigue is included here for completeness and also because of its relevance to the time dependence of waveform, and frequency aspects mentioned in the previous section. Under single loading high rate (impact) conditions it is well known that the impact strength of concrete is much higher than its corresponding static strength (92, 97, 98, 100, 101) and increases rapidly with increasing strain rate (Figs. 2.23(c) and (d)). This is thought to be related to creep effects or to the crack taking a shorter path (not having the time to seek out a more tortuous path), which invariably exhibits greater load requirement and crack resistance as aggregate particles may be fractured. Thus the impact strength is higher than the (very much more slowly obtained) static strength.

In investigations of repetitive impact conditions (24, 33, 100, 101) or 'impact fatigue' Green (126) and Kormeling et al. (97) have contributed significantly to this field, which is still far from fully understood despite its importance in such situations as pile driving. Green (126) for example, measured the ability of concrete to withstand repeated blows using a ballistic pendulum to impact 100 mm cubes of concrete. Kormeling et al. (97) on the other hand, employed a split Hopkinson bar technique. If we discuss briefly their findings together, in the first instance it is evident that scatter in results tends to be greater in impact fatigue than in simple cyclic fatigue. In general the higher the compressive strength of concrete the lower its impact strength, evaluated in energy absorbed per blow before cracking. Thus curing conditions become significant and Green (126) reports that, (for a given mix) the energy absorbed per blow was usually less for water-stored specimens than for air-stored concretes, although the difference was less for rich mixes. This latter observation was confirmed by Kormeling et al. (97) who further noticed that water-cured specimens can absorb more blows between first crack and final fracture than air-dried specimens, but that changes in humidity itself do not affect impact performance (Fig. 2.37).

Komlos (100), in addition to Kormeling (97) and Green (126), noticed that a greater cement content made concrete less sensitive to the effects of impact loading (Fig. 2.38). Impact fatigue performance of concrete improves with decreasing aggregate size and surface roughness (97, 126), decreases with smaller water-cement ratios and the use of superplasticizers (103), and only improves slightly with age (126). Casting direction is apparently also of importance as Kormeling et al. (97) report that when the principal cracking plane is parallel to the casting plane, impact fatigue resistance is lower than in a transverse cracking direction. This is attributed to void formation below aggregates during casting.

Tait and Willmott (24), in conducting impact fatigue drop- weight tests on model concrete dolosse, noticed that there was both an energy threshold and a stress threshold which needed to be exceeded for failure to occur. Variations in performance could be accounted for in terms of loading rate, a factor which is of great importance. For repeated impact loading conditions they recorded that the cumulative total energy absorbed prior to failure is not constant and that only a proportion of the energy is absorbed per blow, even when the critical energy and stress thresholds are both exceeded (Fig. 2.39).

2.5 Summary of Thesis Objectives

2.5.1 Summary

(1) This chapter has examined in some detail the background studies and literature pertaining to cement and concrete strength development and fatigue behaviour. The strength development of cement, the prime constituent of concrete, has been discussed by means of a detailed examination of cement hydration and the changes in morphology and microstructure that occur. The importance of flaws, defects and porosity have been mentioned together with the exciting developments of MDF (macro-defect-free) cement developed by Double and Birchall (1-3, 5, 15, 22, 38):

(2) A discussion from a microstructural viewpoint, of cement hydration and strength development preceded the discussion on the static

strength development of concrete itself, with particular reference to the factors that affect the static strength. Prime among these, obviously, is the water-cement ratio which effectively controls the microstructure and properties of concrete and as a variable has the flexibility to make quite different materials. The significance of aggregate, porosity and curing conditions have been mentioned along with strength development as a function of age. Subsequently, factors affecting the stress-strain behaviour of concrete, such as temperature and loading rate, have also been discussed.

(3) Such a review of factors affecting static strength of concrete was a necessary prerequisite to a preliminary discussion of the behaviour of concrete in fatigue, as given in Section 2.4. The conventional SN curve method for representing fatigue data has been presented together with how such data are affected by maximum stress level and load programmes.

(4) Damage, or microcracking, appears to develop throughout the fatigue life, although whether this initiates from the first few cycles or not is still debatable. Consequent changes in strain and modulus occur and can, under appropriate conditions, be used to evaluate the extent of fatigue damage. Time spent during fatigue is of prime importance as is the loading rate, as evidenced from impact fatigue and frequency effect studies (5), although any detailed understanding of the effect of these parameters is far from complete. Allied to the controversy covering time and loading rate effects is the influence of environment- and thermally- activated deterioration processes and the susceptibility of concrete to a form of stress corrosion cracking.

This chapter is now concluded, following the above literature reviews, with an evaluation of the shortcomings in the present state of knowledge of fatigue and fracture of concrete, which provides a guideline to the objectives of this thesis.

2.5.2 Shortcomings in the Present State of Knowledge

From the foregoing literature reviews and background studies it is clear that there are still significant shortcomings in the state of knowledge and understanding of fatigue and fracture of cement based materials, despite much extensive and elegant research work.

Some of the topics requiring further, detailed attention are listed below and the work reported in this thesis attempts to answer some of these through experimental studies described in subsequent chapters.

(i) Effect of cycling frequency.
(ii) Effect of loading rate and cyclic waveform.
(iii) Effect of moisture content, humidity and also temperature on fatigue.
(iv) Assessment of microcracking or damage for concrete during fatigue - so-called "damage monitoring" and integrity assessment. Murdock (135) regards this aspect, namely "the detection and subsequent 'tracking' of cracks in the material" as one of the major shortcomings in present cement and concrete research.
(v) Damage and microcracking development in fatigue, with particular emphasis on, and understanding of, the underlying mechanisms and micromechanisms.
(vi) Post-fatigue strength increases or "fatigue hardening".
(vii) An assessment of the applicability of fracture mechanics to cement based systems, particularly in respect of material in the vicinity of a propagating crack in concrete.
(viii) Effect of cyclic stress range.
(ix) Experimental fatigue studies in uniaxial tension.
(x) Effect of stress reversal on fatigue performance.

The above list is not meant to be exhaustive but it does highlight some shortcomings in the present state of knowledge. Some of these have been addressed in this thesis and provide the objectives for the research described. These are, in particular, points (i) to (viii). Points (ix) and (x) have not been considered in the present work. Some emphasis has been placed on the importance of time dependent processes. More or less parallel experimental programmes have been conducted in fatigue on compression prisms and on double torsion specimens, utilising - nominally

- a "single" crack situation. A substantial microstructural study on crack development or "tracking" has been undertaken utilising in-situ scanning electron microscopy methods and this whole study is correlated in the Discussion Section of Chapter Eight, where the mechanisms of fracture and fatigue are considered in depth.

The next chapter describes the experimental techniques and systems developed for evaluating compression fatigue in mortar prisms. The associated damage monitoring equipment, including lateral and longitudinal elastic and residual strain measurement systems, ultrasonic pulse transit time methods and acoustic emission monitoring, are also described.

TABLE 2.1

Typical Compound Components of Cement Clinker

COMPONENT	OXIDE COMPOSITION	ABBREVIATED NOTATION	APPROXIMATE COMPOSITION IN O.P.C.
Tricalcium Silicate	$3CaO.SiO_2$	C_3S	50%
Dicalcium Silicate	$2CaO.SiO_2$	C_2S	25%
Tricalcium Aluminate	$3CaO.Al_2O_3$	C_3A	10%
Tetracalcium-aluminoferrite	$4CaO.Al_2O_3.Fe_2O_3$	C_4AF	10%

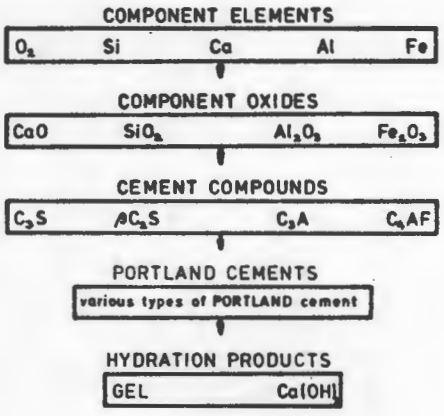

Fig. 2.1: Illustrates schematically the formation and hydration product of Portland cement, (33).

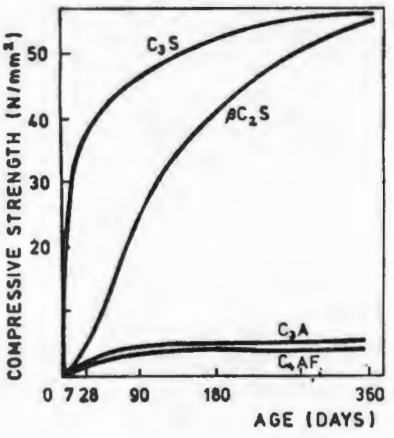

Fig. 2.2(a): Strength development with time for pastes of each of the various cement phases, C_3S, C_2S, C_3A and C_4AF, (34).

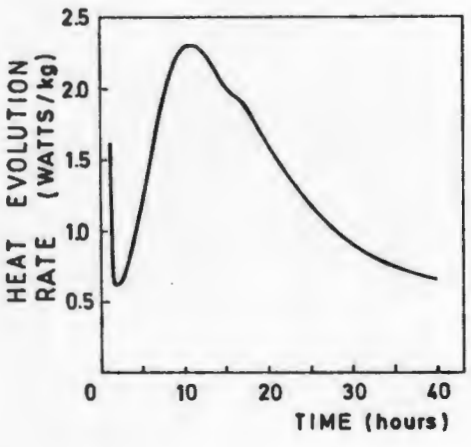

Fig. 2.2(b): The rate of heat evolution as a function of time for Portland cement, (11).

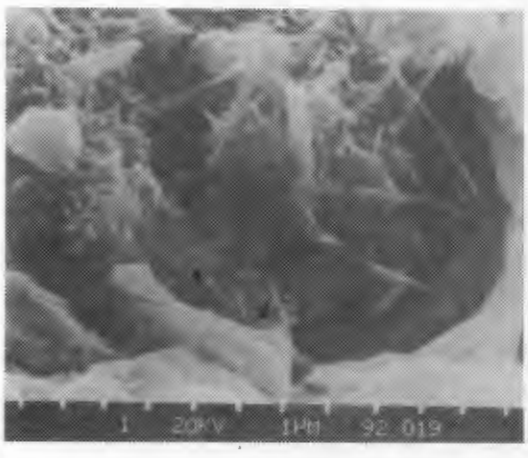

(a)

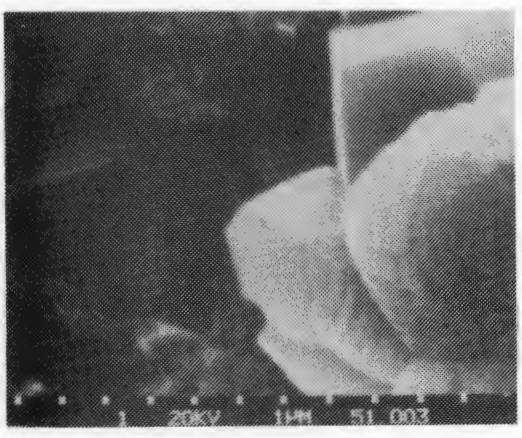

(b)

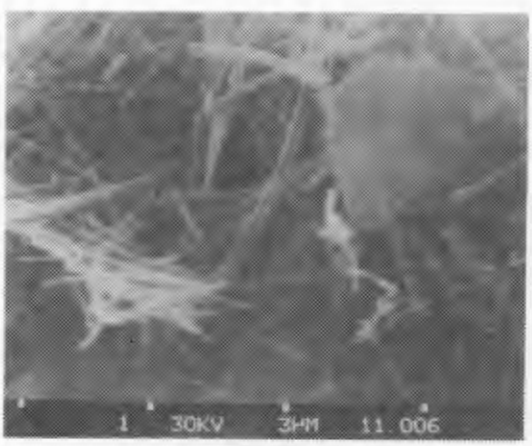

(c)

Fig. 2.3(a,b,c): SEM micrographs of hydrated cement paste indicating calcium hydroxide, $Ca(OH)_2$ platelets, together with "type I" C-S-H gel.

(a)

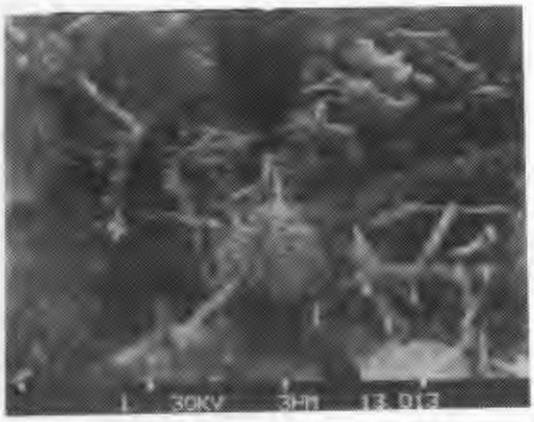

(b)

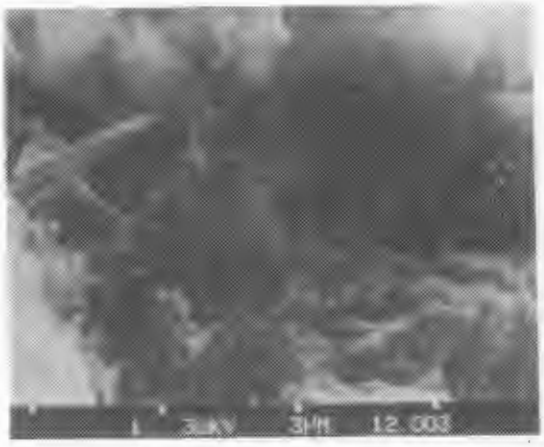

Fig. 2.4(a,b,c): SEM microgaphs of "Type I" C-S-H gel structure typified by a fibrous nature (also called tubular, lath-like solid, or rolled foils or sheets).

(c)

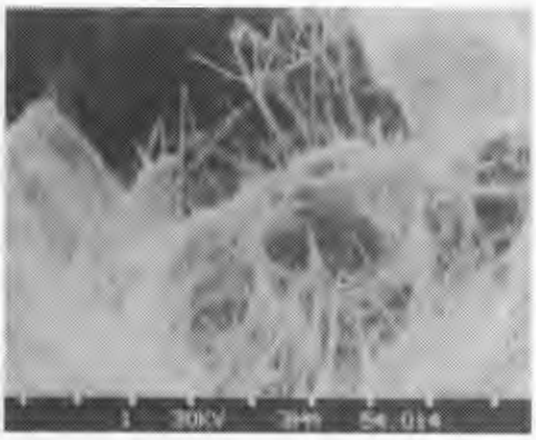

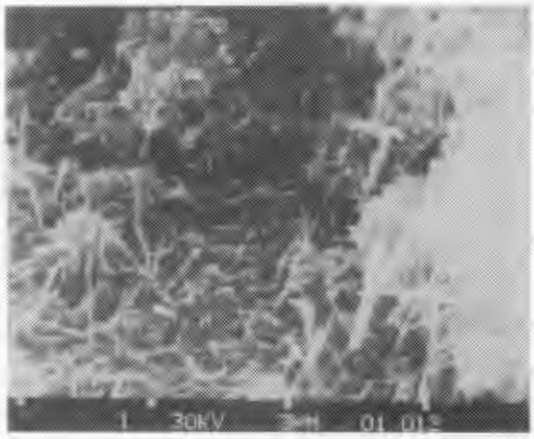

Fig. 2.5: SEM micrograph of Type II C-S-H microstructure, typified by its interlocking honeycombed nature.

(a)

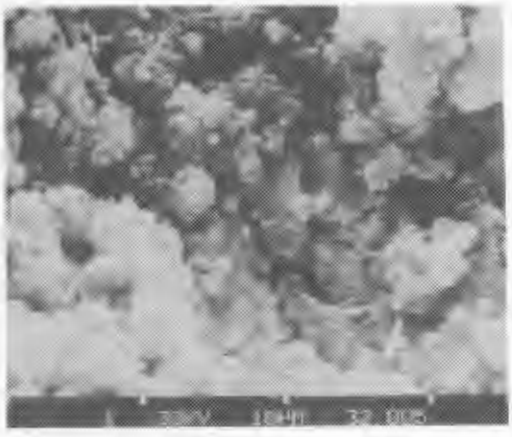

(b)

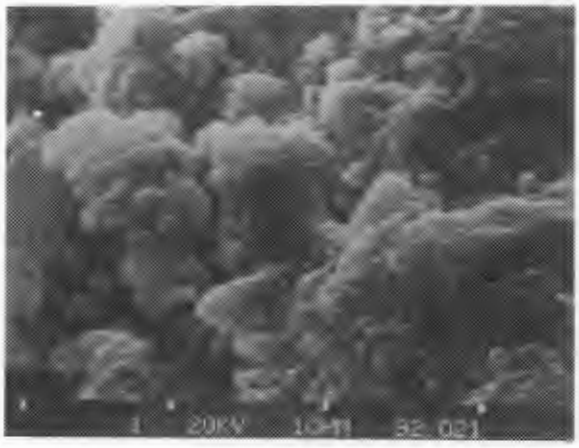

Fig. 2.6(a, b): SEM microgaphs of "Type III" C-S-H microstructure indicating that it is rather nondescript, often of small equant grains.

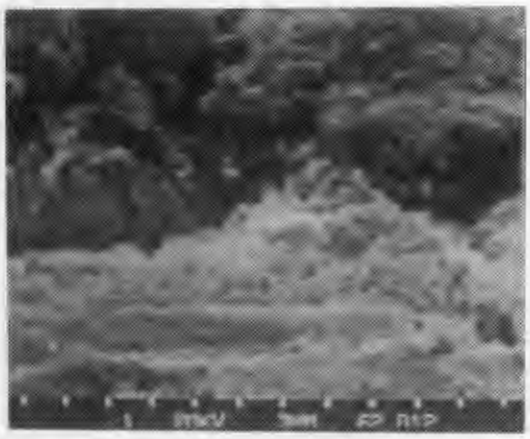

Fig. 2.7: SEM micrograph of "Type IV" C-S-H microstructure, which is rare, dimpled and dense inner product material.

(a)

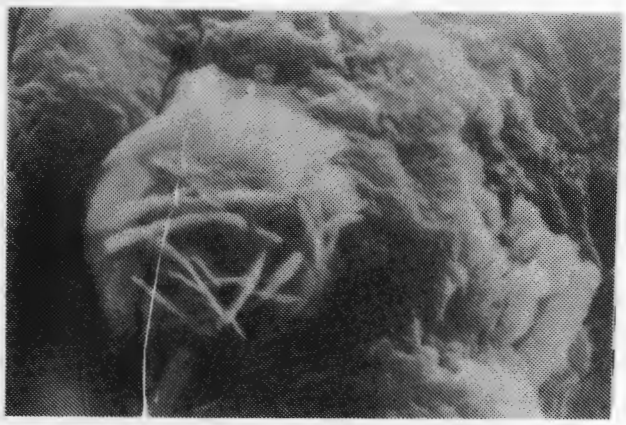

(b)

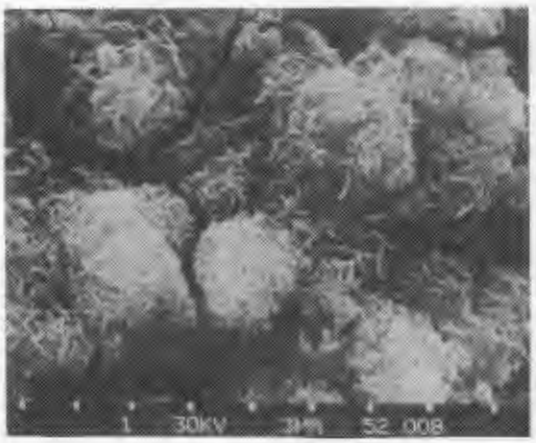

Fig. 2.8(a, b): SEM micrographs illustrating the morphology of the "A.F.m." phase which is of a "platey rossette" crystalline structure.

(a)

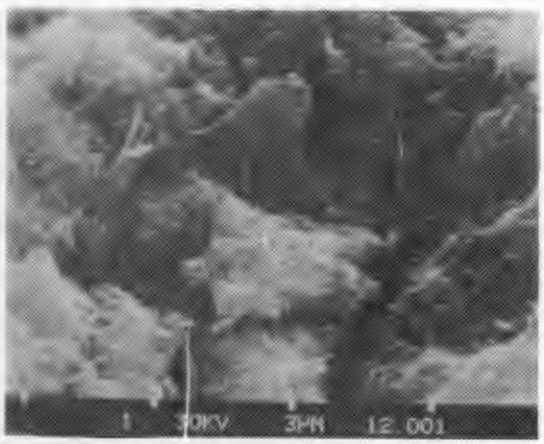

(b)

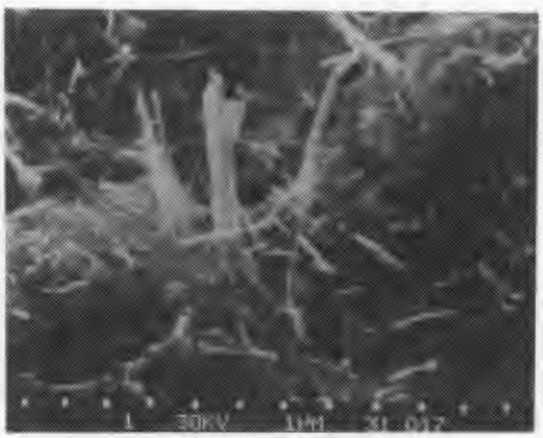

Fig. 2.9(a, b): SEM micrographs illustrating the morphology of the "A.F.t" phase typified by the rod like form of ettringite.

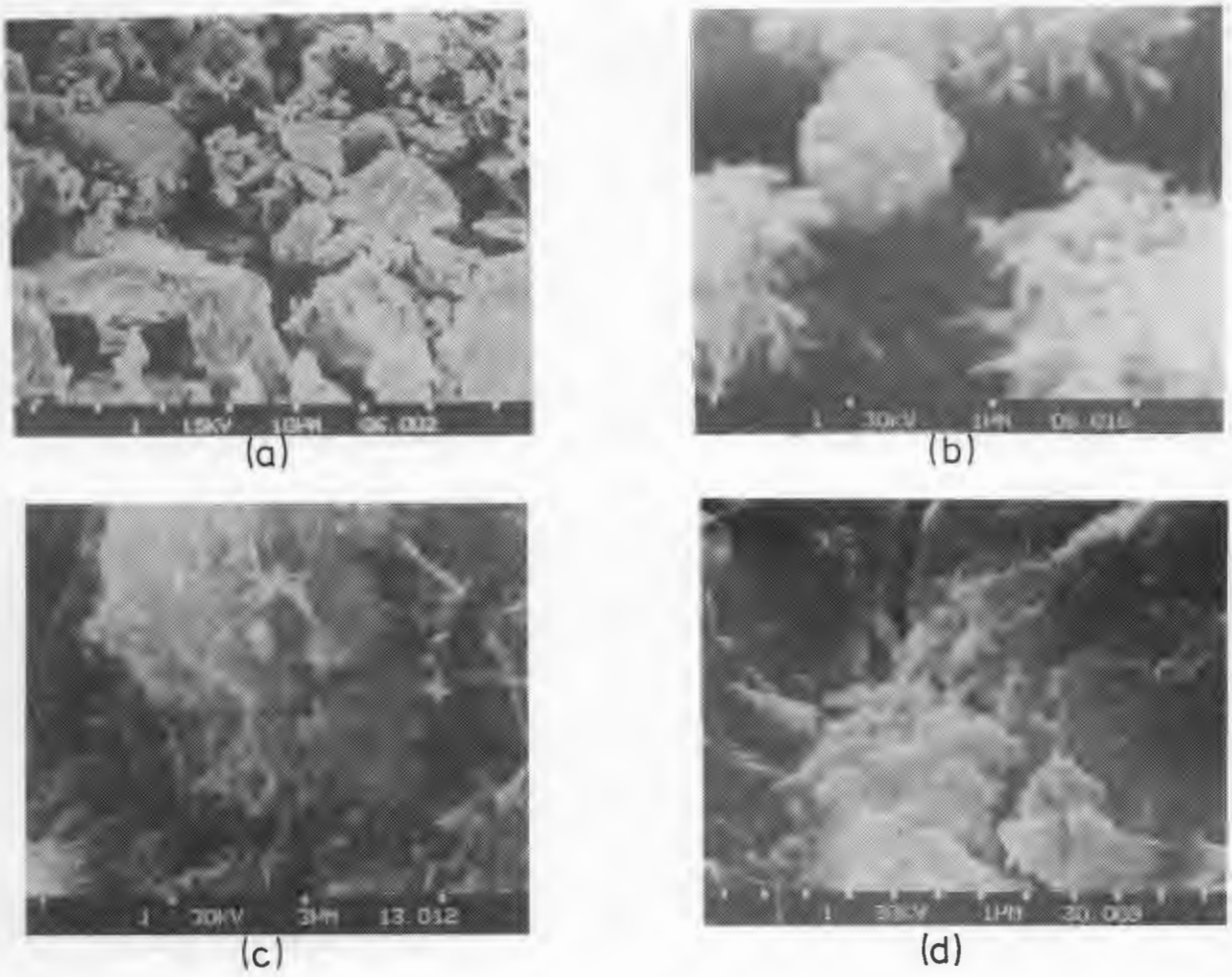

Fig. 2.10 (a,b,c,d): SEM micrographs illustrating the cement hydration sequence:
(a) cement powder before mixing with water;
(b) initiation of hydration and C-S-H product after 6 hours;
(c) increased development of hydration product at 7 days, and
(d) well-developed amorphous hydrated product at 6 months.

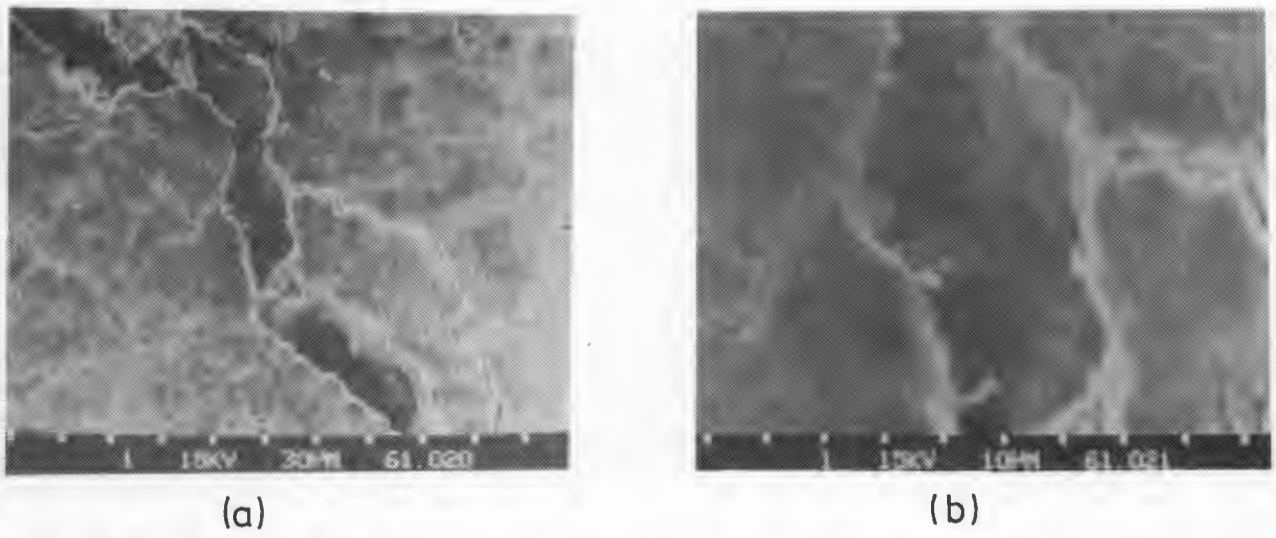

Fig. 2.11(a,b): SEM micrographs illustrating the fibrous nature of fully hydrated cement paste (aged 40 days) in the subsurface - or bulk region - even though the surface itself appears as a solid, amorphous type III mass. Fig. 2.11(b) is an enlargement of the central region of Fig. 2.11(a) and C-S-H fibres are clearly apparent.

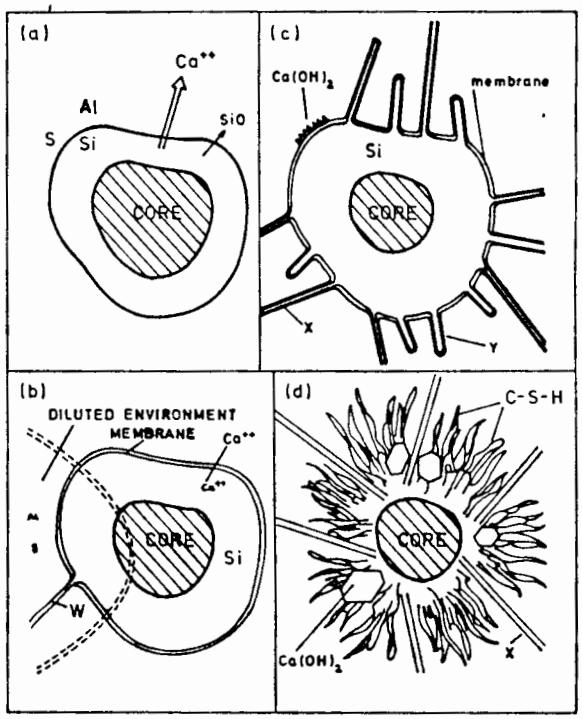

Fig. 2.12: (a) Stage 1; large quantities of Ca^{++} are leached into the aqueous environment. A very small amount of silicate is also dissolved.

(b) Stage 2; protective membrane around particle; area on left indicates fibular formation (W) when particle is placed in dilute environment.

(c) Stage 3; membrane rupture and formation of acicular products (X open ended needle, Y closed-ended needle).

(d) Stage 4; formation of CSH gel (52).

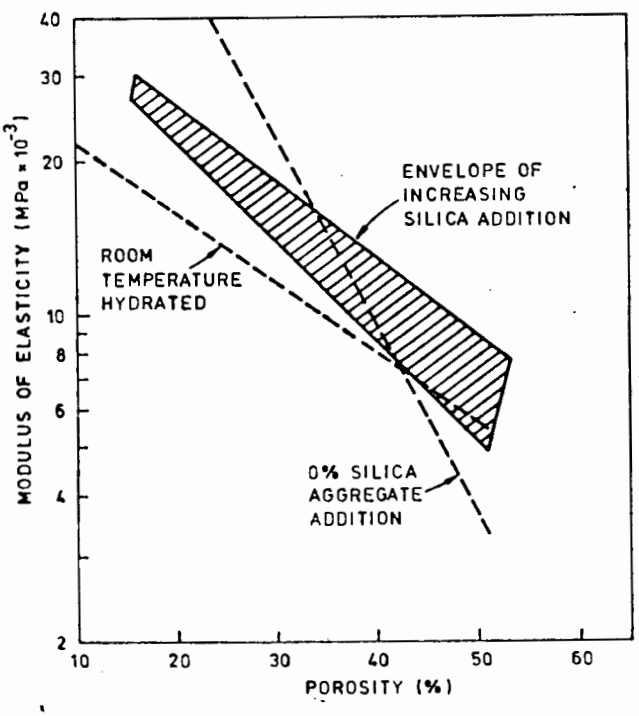

Fig. 2.13(a): Modulus of elasticity for various autoclaved and room temperature hydrated cement and cement-silica preparations (69).

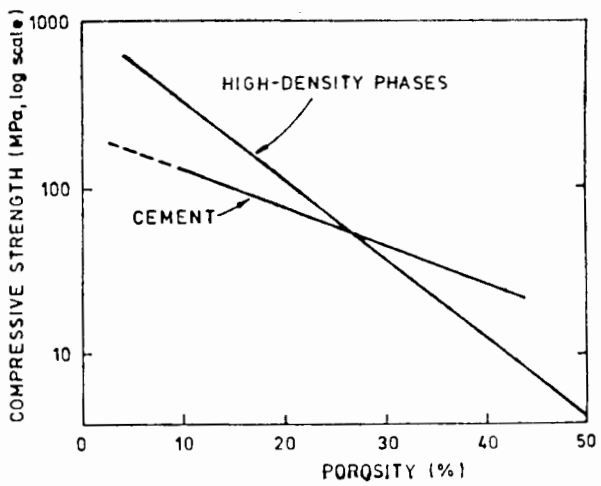

Fig. 2.13(b): Relationship between compressive strength and porosity for cement and high density cement phases (68).

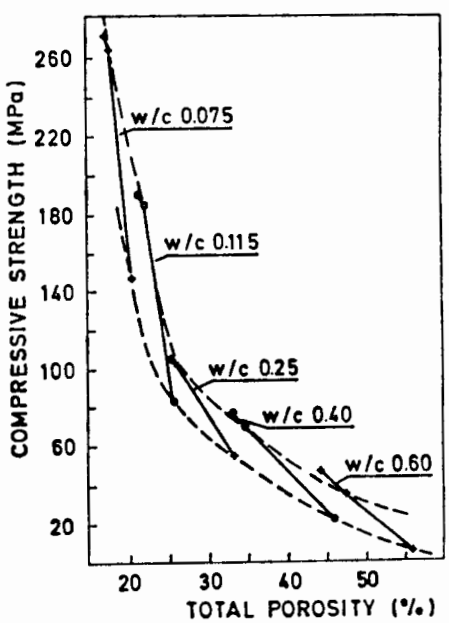

Fig. 2.13(c): Relationship between compressive strength and total porosity of hardened cement pastes with different water/cement ratios (67).

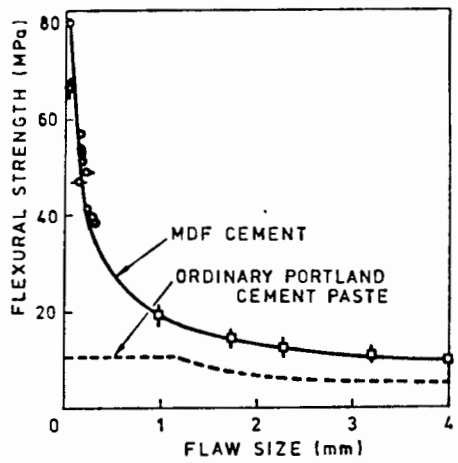

Fig. 2.14: Flexural strength of notched Macro-Defect-Free (M.D.F.) cement (solid line) compared with ordinary cement paste (dashed line) (15).

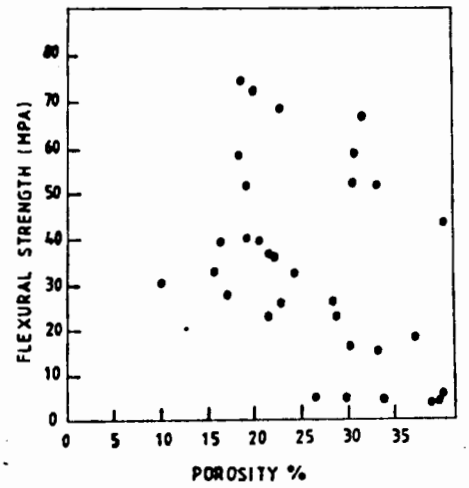

Fig. 2.15: Total porosity versus flexural strength (77).

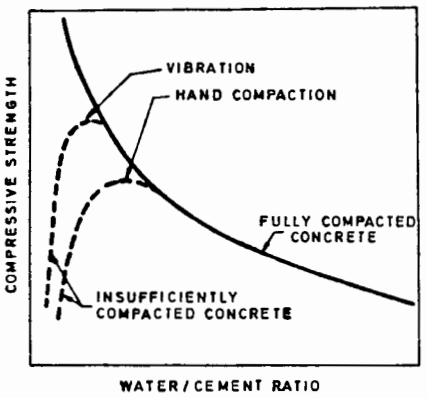

Fig. 2.16: The relation between strength and water-cement ratio of concrete (33).

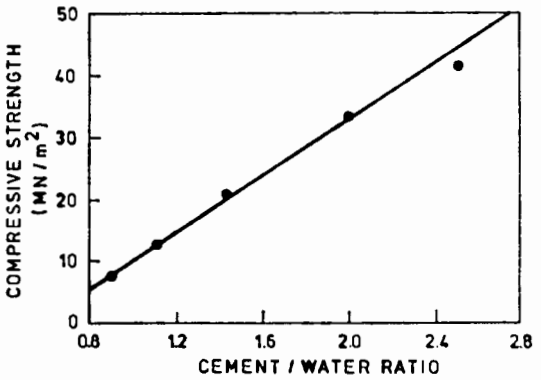

Fig. 2.17: A plot of strength against cement-water ratio for Rapid Hardening Cement at an age of 7 days (33).

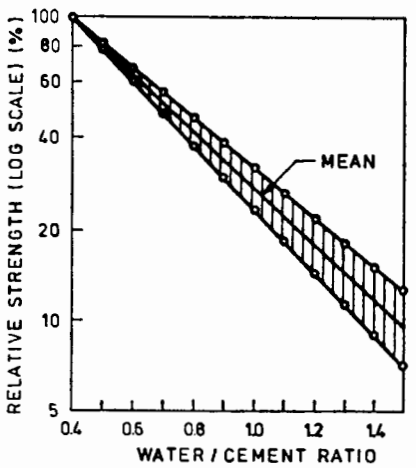

Fig. 2.18: Relation between logarithm of strength and water-cement ratio (33).

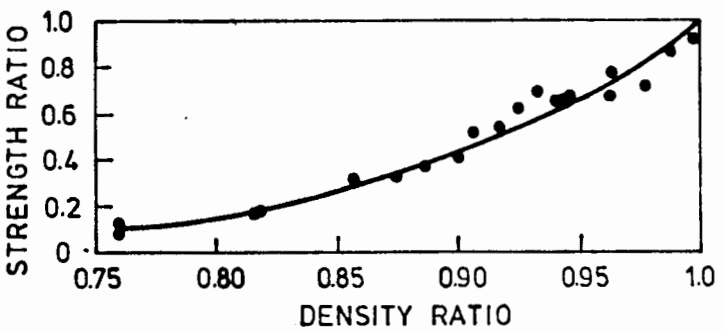

Fig. 2.19: Relation between strength ratio and density ratio (33).

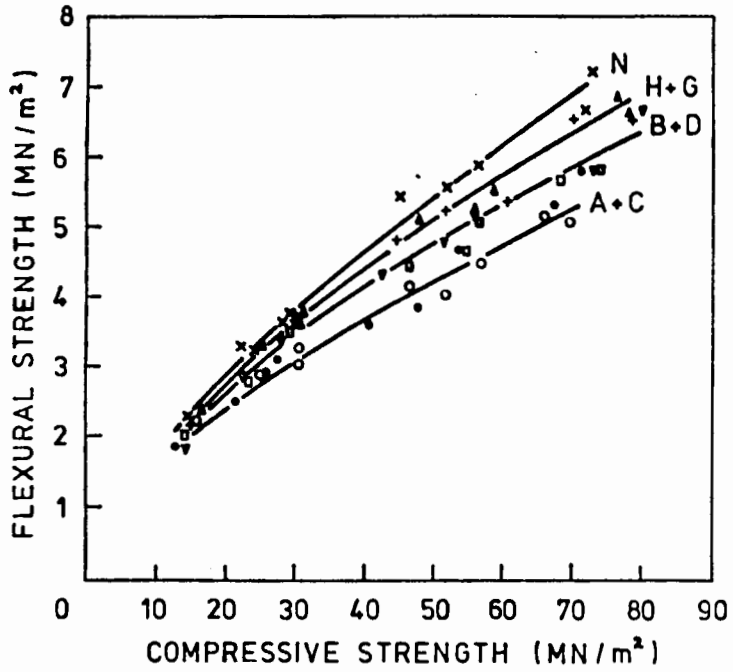

Fig. 2.20: Relation between flexural and compressive strengths for concretes made with different aggregates (82). (The abbreviations refer to various aggregate types).

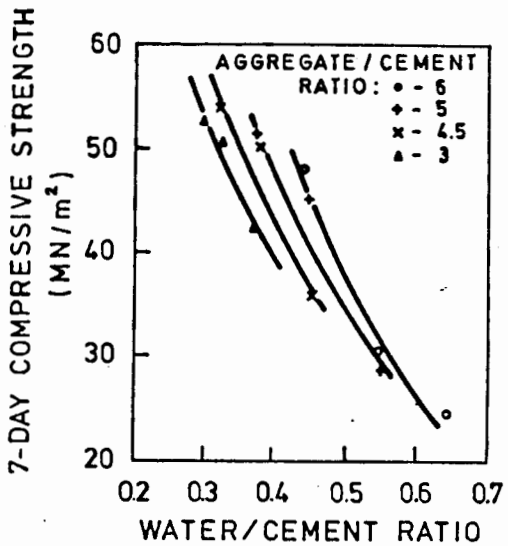

Fig. 2.21: The influence of the aggregate-cement ratio on strength of concrete (33).

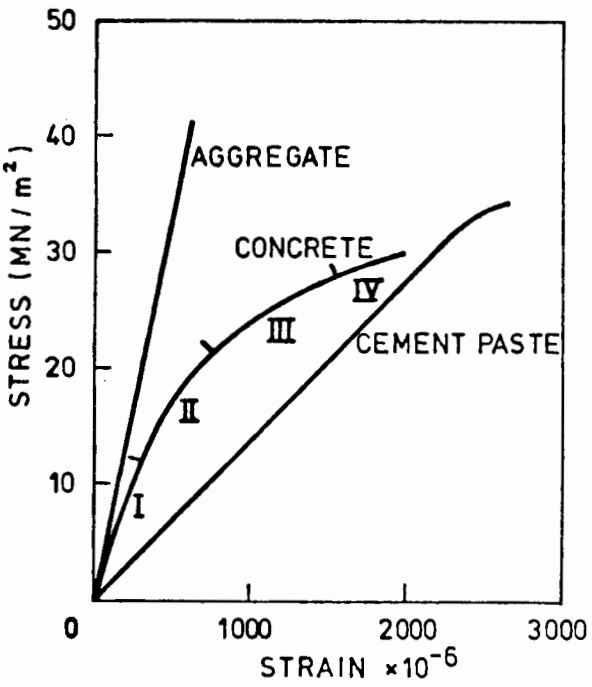

Fig. 2.22: Stress-strain relations for cement paste, aggregate and concrete.

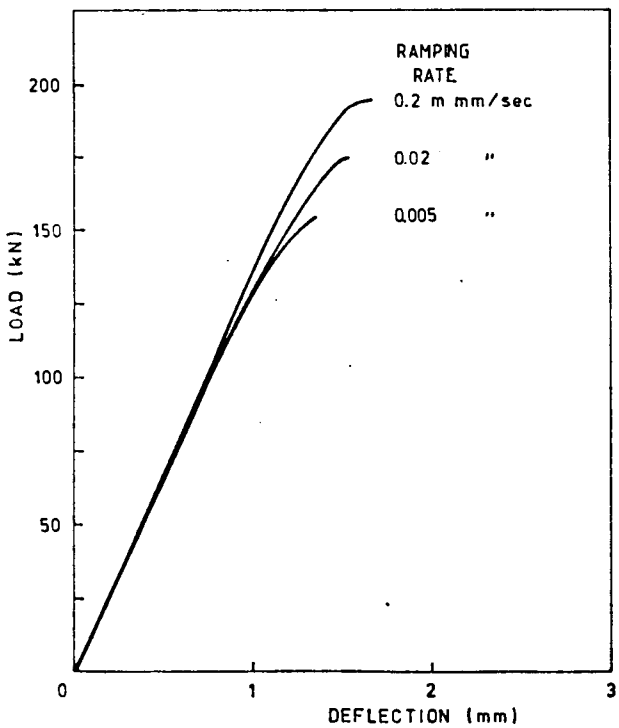

Fig. 2.23(a): Effect of ramping rate on stress strain performance of mortar used in this study.

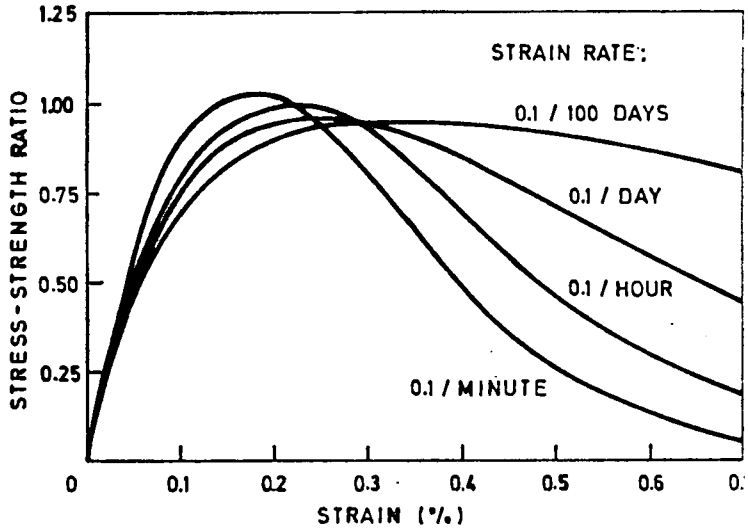

Fig. 2.23(b): Influence of the rate of application of strain on the shape of the stress-strain curve (24).

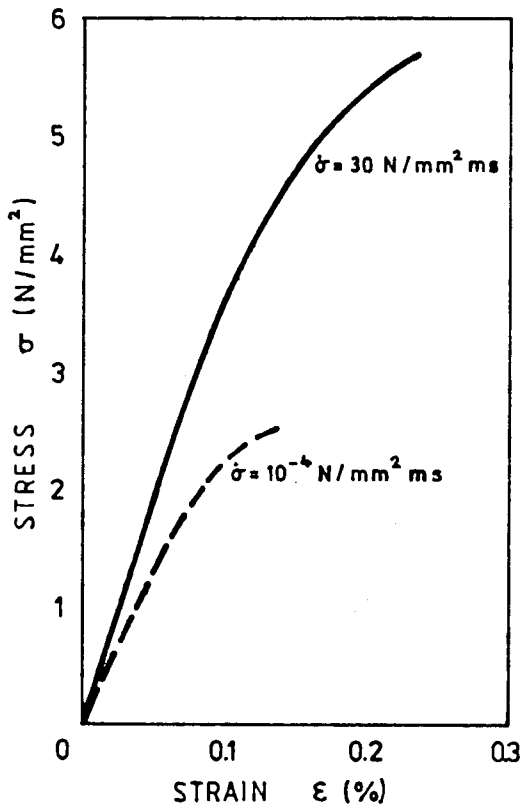

Fig. 2.23(c): The influence of a high stress rate upon the stress strain relationship for concrete in tension (97).

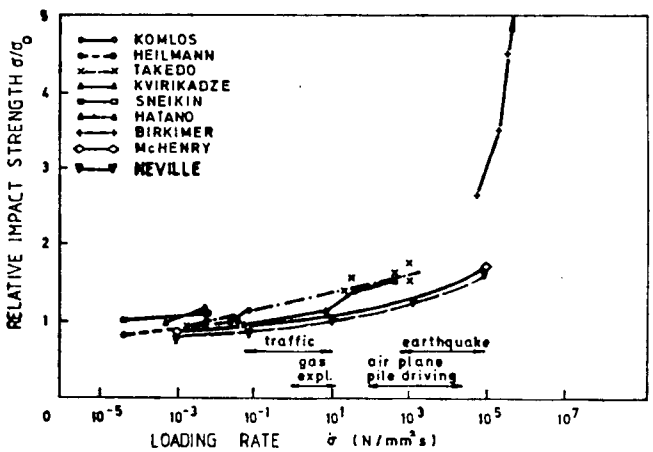

Fig. 2.23(d): Survey of results of experiments on tensile strength related to loading rate (97).

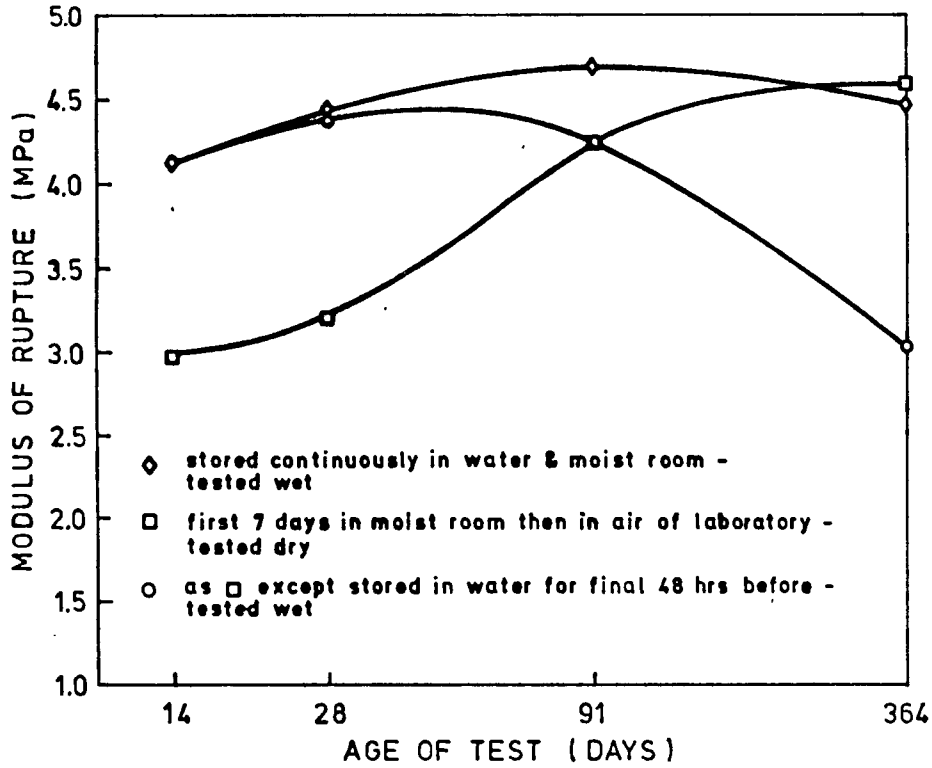

Fig. 2.24: Effect of storage and testing conditions on modulus of rupture (113).

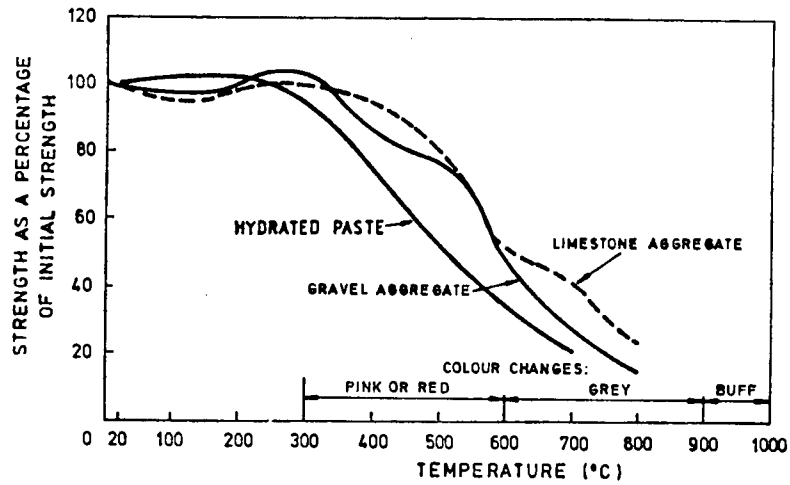

Fig. 2.25: Compressive strength of concrete (33) and hardened cement paste (121) after heating to high temperatures. (Note that above about 1200°C concrete turns yellow).

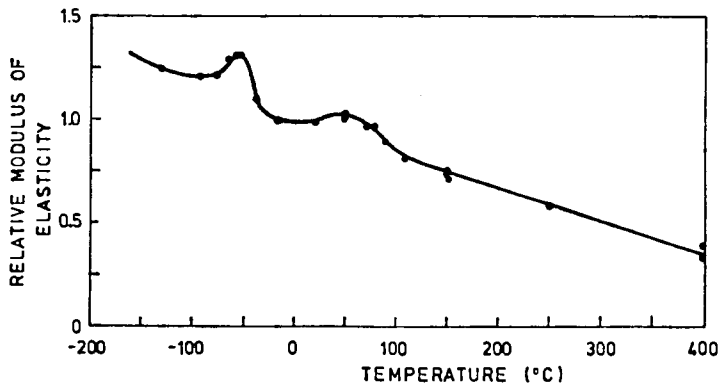

Fig. 2.26: Influence of temperature on the modulus of elasticity of concrete (33).

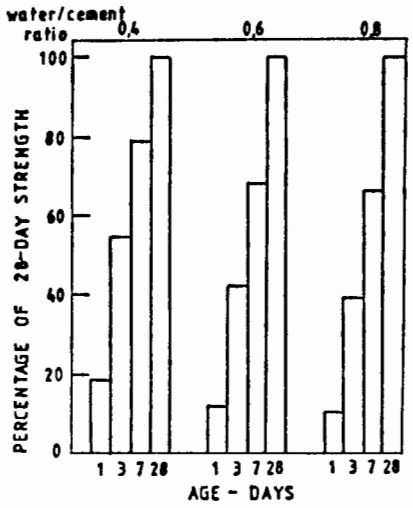

Fig. 2.27: Relative gain of strength with time of concretes with different water cement ratios, made with ordinary Portland cement (33).

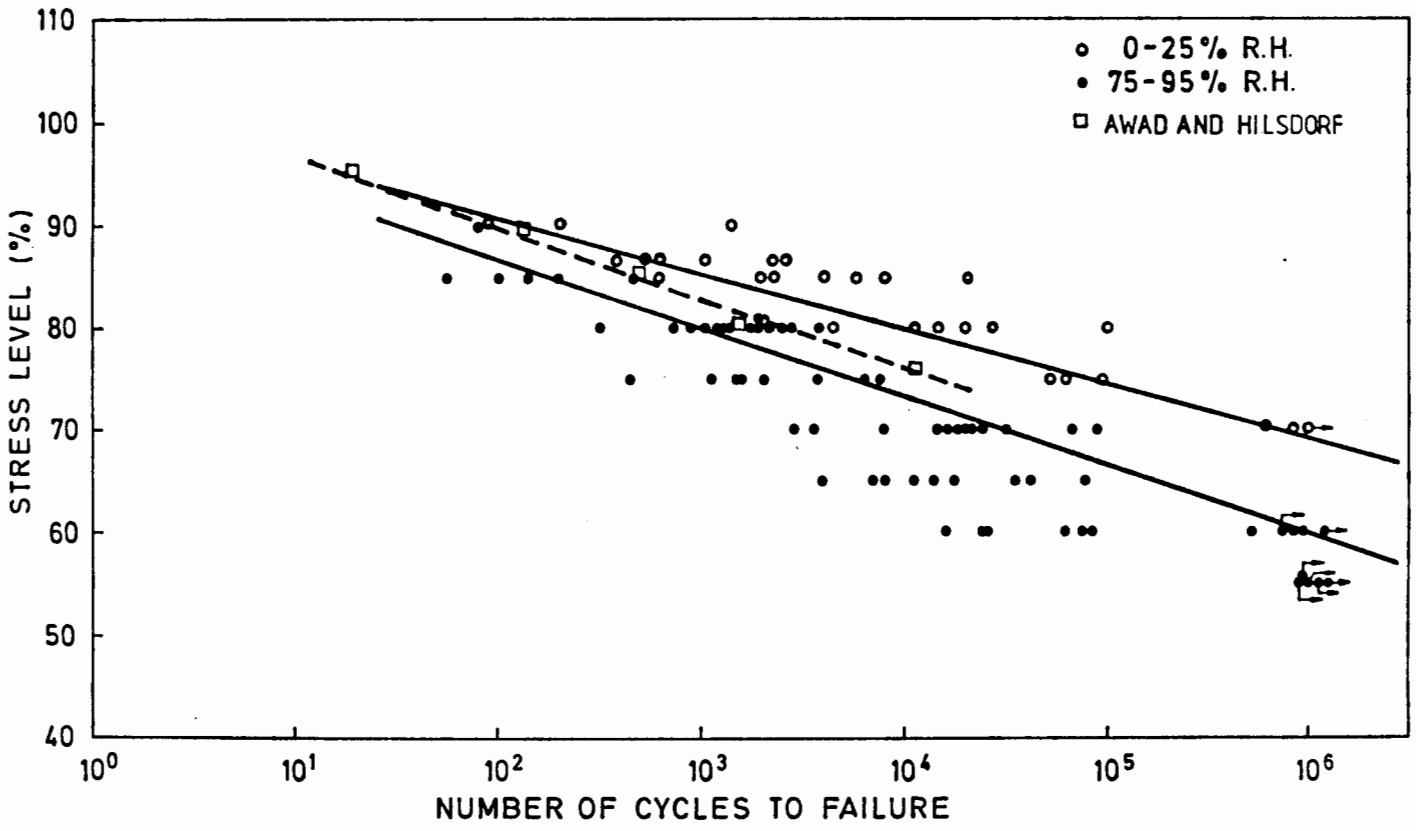

Fig. 2.28: Typical Wöhler, or SN curve illustrating the fatigue behaviour of the cement mortar used in this project.

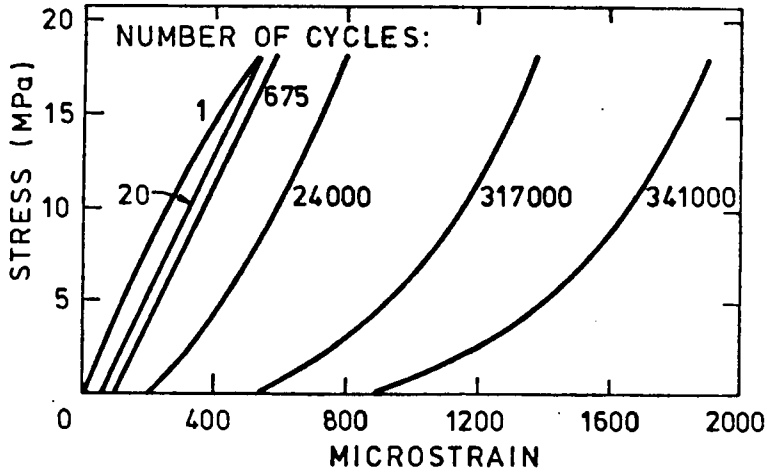

Fig. 2.29: Variation of stress strain curve with number of cycles (143).

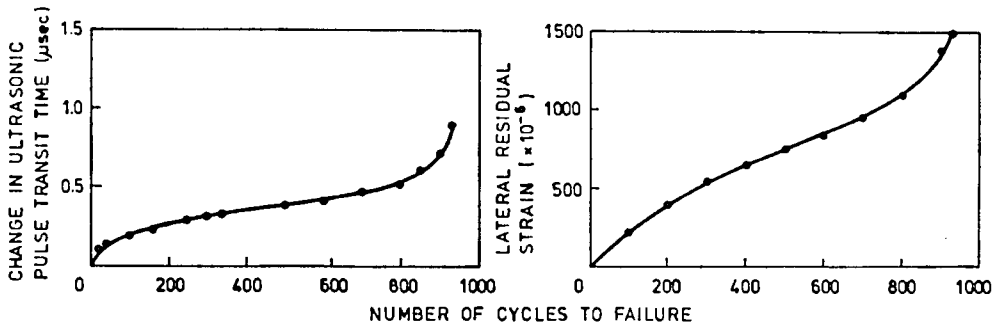

Fig. 2.30: Illustration of the variation of
(a) ultrasonic pulse transit time and
(b) residual strain with number of fatigue cycles (161).

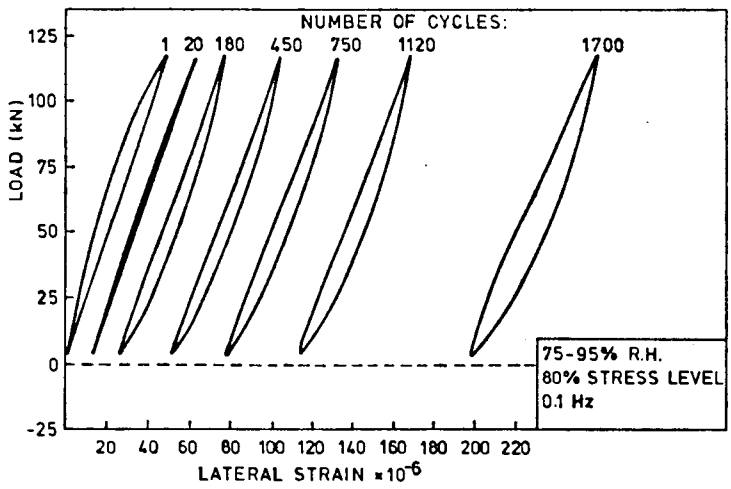

Fig. 2.31(a): Variation of the shape of the hysteresis loop of the stress strain curve with number of cycles (present work).

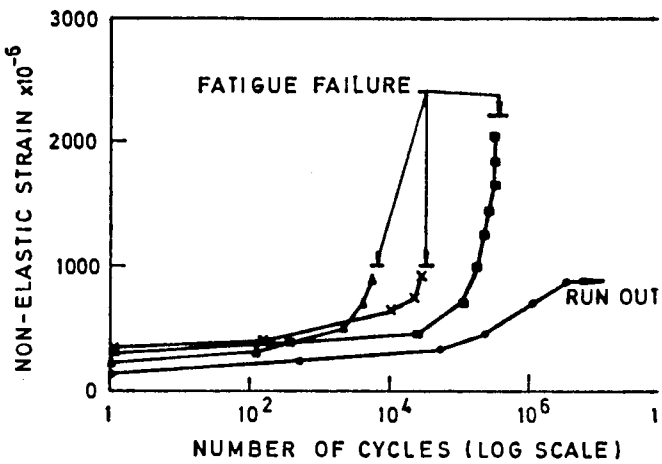

Fig. 2.31(b): Variation of non elastic strain with number of cycles (143).

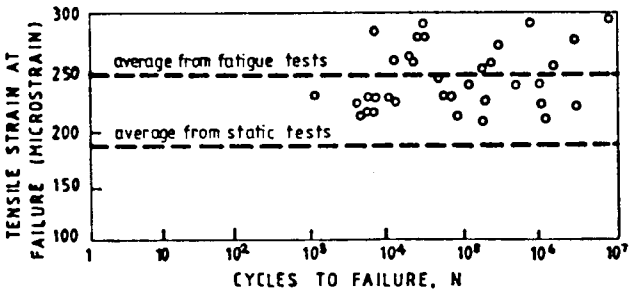

Fig. 2.32: Maximum tensile strains at failure (150).

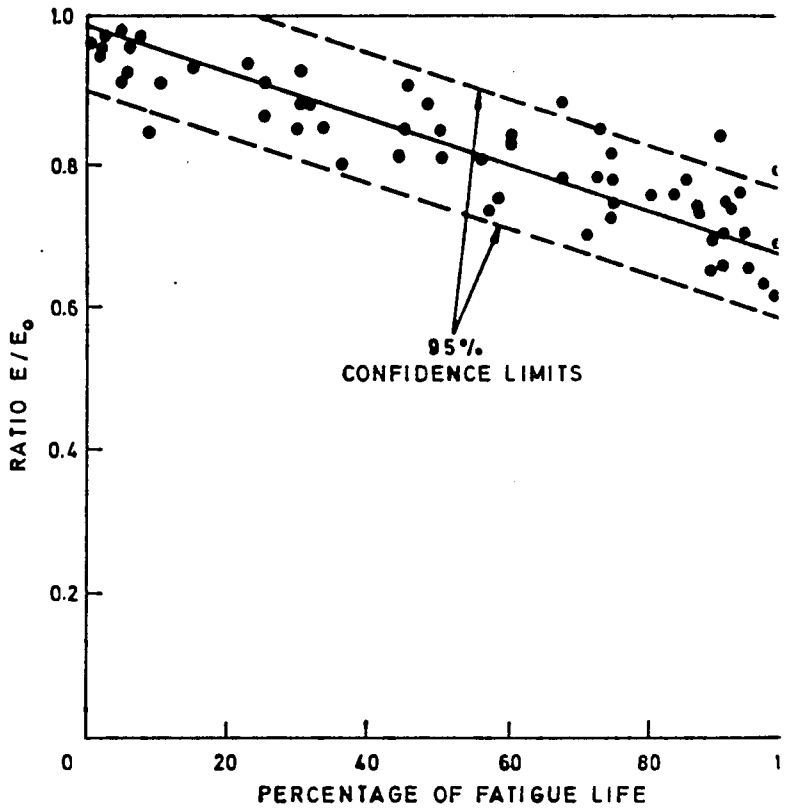

Fig. 2.33: Relationship between the ratio of secant modulus of elasticity at the given instant (E) to the modulus at the beginning of softening (E_o) and the percentage of expended fatigue life (143).

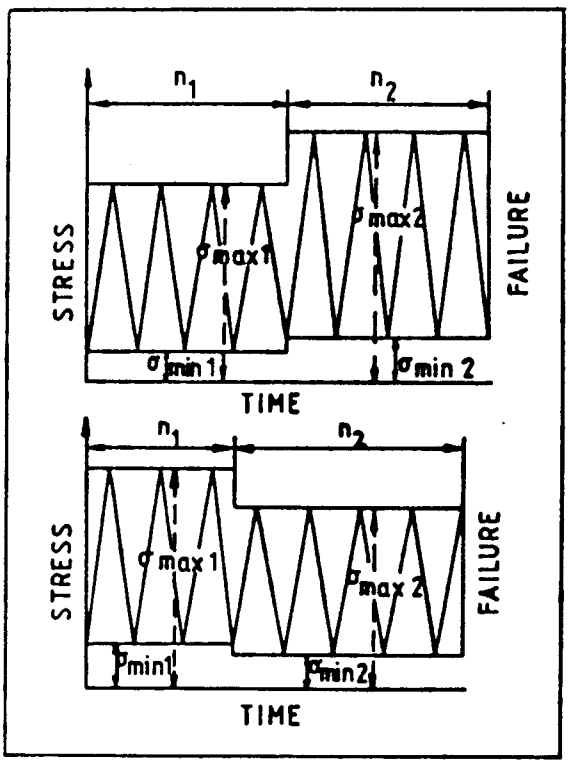

Fig. 2.34(a): Variable load programme used by Hilsdorf and Kesler (157).

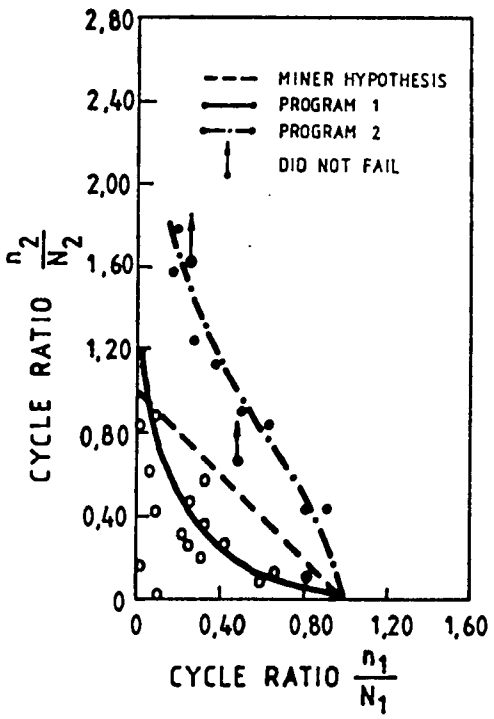

Fig. 2.34(b): Results of Hilsdorf and Kesler's variable load programme (157). Note that they obtained longer lives with the greater stress programme first.

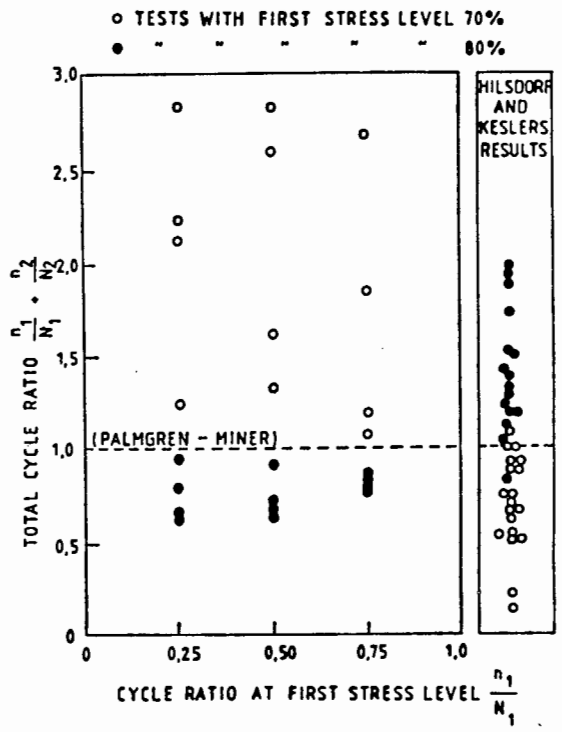

Fig. 2.34(c): Results of Bennett and Jinawath's variable load programme tests (156). Note they obtained shorter lives for first fatigue stress level of 80%, contrary to Hilsdorf and Kesler's results (157) which are also shown on this diagram.

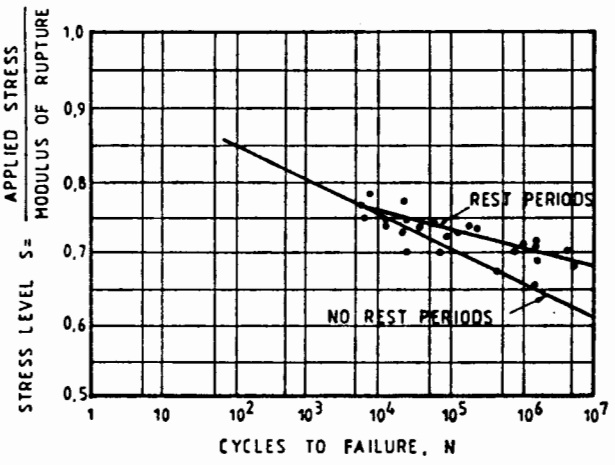

Fig. 2.35(a) Effect of Rest Periods on the Fatigue Behaviour of Plain Concrete Beams. Based on Ref. (157).

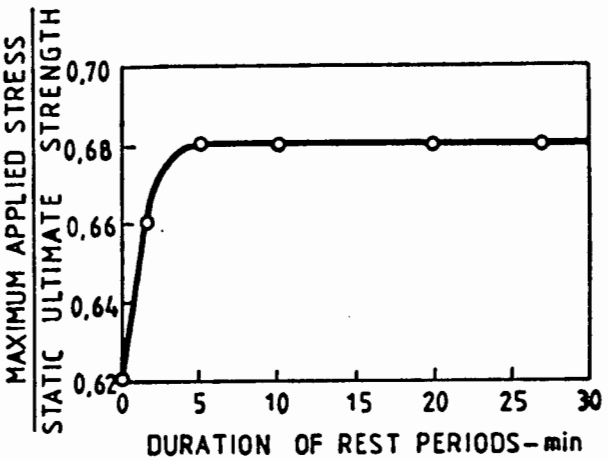

Fig. 2.35(b) Effect of rest periods on fatigue strength at ten million cycles (From Hisldorf and Kesler (157)).

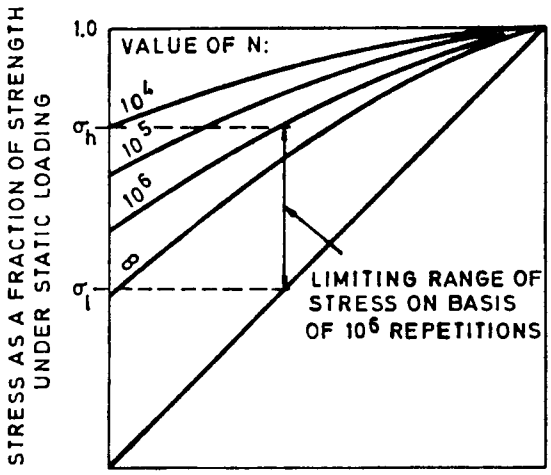

Fig. 2.36: Modified Goodman diagram for concrete in compression fatigue (σ_l and σ_h are respectively the lowest and highest stresses attained during fatigue cycling) (33).

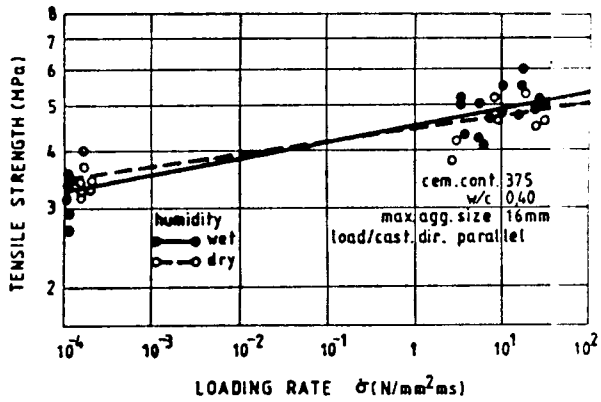

Fig. 2.37: Effect of the changes in specimen humidity upon the static tensile strength and impact tensile strength (97).

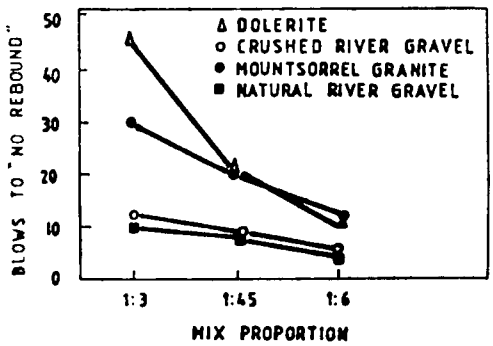

Fig. 2.38: Effect of cement-aggregate ratio on impact performance. Note that as the proportion of binding matrix is suffiently reduced, so the impact fatigue resistance declines (126).

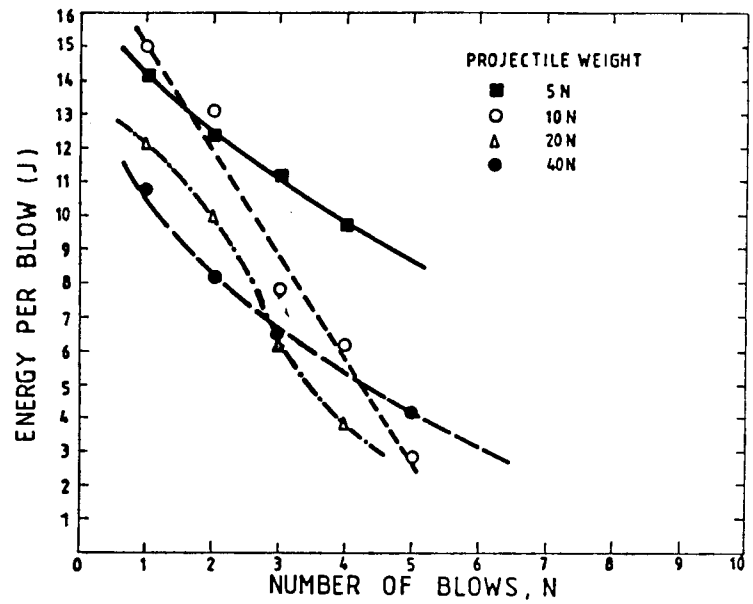

Fig. 2.39: The effect of impact fatigue on concrete dolosse. The average number of blows for projectiles of different weights (40,20,10 and 5N) is plotted against energy per blow (24).

"Man is a tool using animal."

Thomas Carlyle

CHAPTER THREE : EXPERIMENTAL TECHNIQUES AND SYSTEMS

3.1 Introduction

The previous chapter has established the need for an experimental investigation of certain factors that affect the fatigue and fracture behaviour of concrete, particularly in regard to time and rate dependence. This chapter describes the experimental techniques and systems used in the investigation.

Specifically, this chapter includes details of the compression prism specimens tested under both static and fatigue conditions. However, the subsequent development of double torsion specimens used for a more detailed examination of damage development in the vicinity of a so-called "single crack" is left to Chapter 7 (Section 7.2). This latter experimental programme builds on the results of previous chapters and may be regarded as an extension of the compression studies.

This chapter deals sequentially with the details of the materials used for, and the subsequent fabrication of, mortar compression prisms complete with the relevant curing history. The mechanical servohydraulic testing facility is described together with the standard techniques for static and fatigue testing.

In section 3.5 the nature of "damage" in terms of the degree of microcracking is discussed which forms an introduction to the description of damage monitoring techniques of both longitudinal and lateral, elastic and accumulated, strain as well as changes in ultrasonic pulse transit time. Changes in the acoustic emission behaviour of concrete are also investigated and are regarded as a powerful tool in damage monitoring. This is discussed in two sections: (i) as a standard measure of damage development in static tests, and (ii) in fatigue testing as an indication of the point of initiation of microcracking in a given loading cycle in the early stages of fatigue. This work has led directly to the development of a novel pseudo-

isometric-plot method of data representation. This development (henceforward referred to as PIP) is discussed in detail in Section 3.5.4. The chapter is summarised in section 3.6.

3.2 Materials

3.2.1 Introduction

Throughout the experimental study the emphasis has been placed on cement mortar. Although cement paste itself may be regarded as the more fundamental matrix agent, the inclusion of the fine aggregate addition (sand) more closely simulates concrete behaviour, especially on a small scale, without encountering the difficulties of grading and consistency that may be experienced with large aggregate (stone) additions. Furthermore, it has been widely reported that the mechanical behaviour of concrete and mortar are very similar and that the mortar constituent controls the primary behaviour of concrete (89, 120, 143, 162). The role of large aggregate additions appears to be one of providing stress concentrations and regions of interfacial weakness (at bond interfaces) without contributing significantly to the fundamental mechanisms responsible for failure. Thus the experimental simplification of restricting investigations to limited aggregate contents appears to be justified. The individual components of mortar are now discussed.

3.2.2 Cement

Portland cement of the so-called "rapid hardening" variety (RHPC), or type III (33) was used throughout this investigation. A large, single batch of 60 pockets (each of 50 kg.) of this RHPC cement was purchased and carefully stored in airtight containers to be used as required throughout the duration of the project.

This procedure was adopted in an attempt to remove any inconsistencies due to batch variations. Subsequently another batch of 60 pockets was purchased and analyses of the cement at the time of purchase indicated that there was no significant deterioration or difference between the batches (Table 3.1.)

As a direct result of the smaller average cement particle size in RHPC, the curing process is accelerated and higher strength is achieved in a comparatively shorter time. Thus the 28-day strength of ordinary Portland cement (OPC) is achieved at around 7 days (163). This greatly facilitates specimen preparation and testing.

3.3.3 Sand

The mortar included 34% by weight of 600 m average diameter dry sand, which was of a quartzitic nature derived originally from Table Mountain sandstone. A grading analysis of the sand used is shown in Fig. 3.1. To ensure consistency and reproducibility the sand was purchased in a "one-off" lot and air-stored until required. It was then sieved and air-dried on a tray in the laboratory before being used in the mortar mix. These precautions were implemented to ensure a reproducible "water demand" of the sand in the mix and therefore to maintain a constant water-cement ratio in the mix.

3.2.4 Water

The water used for the mortar mix was standard tap water (suitable for drinking and therefore acceptable (33) at a temperature of between 18 to 22^{o}C. The pH of the tap water used was in the range of 6 - 7. The water was of the type commonly regarded as 'soft' with less than 800 ppm of dissolved solids. No special efforts were made to use distilled water as realistic engineering situations were to be simulated. In any event the water used for mixing (and curing) was consistent throughout and it is believed that its minor variations did not contribute significantly to any scatter in the subsequent static and fatigue tests.

3.3 Sample Fabrication

3.3.1 Specimen Size and Shape

In compression testing of concrete, extensive use has traditionally been made of cubes, typically of dimension 100 X 100 X 100mm or 150 X 150 X 150 mm. Tests using prisms or cylinders are, however, better for two principal reasons. Firstly, the loading direction in cubes is parallel to possible

lines of weakness beneath aggregate particles due to moisture migration or "bleeding" or bond weakness; and secondly, and more importantly, there is no section in the cube which is subject to a pure uniaxial stress because of frictional restraint at the plattens (33, 162). Neville (120, 164) has estimated that the specimen height must be at least 3 times the lateral dimension to obtain a central region of uniform uniaxial stress, thus ensuring that the two "cones or pyramids of fracture" do not touch. It is generally regarded that the height-to-width ratio should be at least two (120, 143, 165-167) and a ratio of three or more has often been successfully employed (27, 142, 143, 168, 169). Using such prism (or cylinder) type specimens, strengths are obtained which are more representative of the actual material properties and tend to yield strengths between 10 and 20% lower than equivalent cube strengths (154, 165, 169).

The discussion so far in this section has assumed that there is, in fact, significant platten restraint, which is the common experimental situation. Various techniques have, however, been employed in an effort to eliminate, or at least minimise, the effect of platten frictional effects. These include: fluid lubrication, roller bearings, and packing of various sorts including teflon, neoprene, aluminium laminates and foils (92, 169, 170). Probably the best method, however, is that used by Kupfer (171) which employs steel brushes. For full and critical reviews on this topic, the reader is referred elsewhere (92, 169, 172).

With respect to specimen size it would appear that when a certain specimen volume is exceeded the measured mean compressive strength becomes constant (165), certainly as far as cubes are concerned (Fig. 3.2). Jayatilaka and Nanayakkara (165) also report that the standard deviation of compressive strengths is inversely proportional to the square root of the specimen volume (Fig. 3.3.)

3.3.2 Moulds

Because of the points made in the foregoing discussion, rectangular prism mortar specimens of dimensions 180 X 60 X 60 mm were used throughout. Twelve steel moulds were machined which provided for the vertical casting of specimens of this size, with faces accurately orthogonal (33, 162) (Fig. 3.4). The mould sections were milled from 22 mm thick EN8 steel plate, slotted together and held in place by means of G-clamps. These located

onto a steel base plate and were open at the top. The use of twelve moulds in a batch facilitates the static testing of four specimens to establish the batch strength, with the remaining 8 specimens used for fatigue testing. Very often 6 fatigue tests were undertaken and the remaining 2 specimens were subsequently tested under static loading to measure any variation in static strength over the duration of the fatigue testing.

The inside and mortar splash zones of the mould were coated with a thin film of oil release agent to prevent bonding of the (hardened) mortar to the mould and to facilitate removal of the specimens. A high quality "off shutter" finish was also obtained in this way.

3.3.3 Mixing

The standard mix, which was kept constant throughout the duration of the project, included 34 per cent by weight of dry sand, which was required to inhibit shrinkage and drying cracks (especially for oven-dried specimens). The mix proportions used were : water-cement ratio 0.388, sand-cement ratio 0.72. The components were dry mixed in a (consistently dried) rotary paddle mixer for 1 minute. Then the water was carefully added followed by mixing for a further 4 minutes.

3.3.4 Casting

The mix was transferred from the mixer to the twelve moulds with a bucket and carefully and uniformly poured into the moulds to minimise the possible entrainment of air bubbles causing subsequent porosity. The specimen moulds were then vibrated on a conventional vibration table for 25 seconds to remove air bubbles and the top surface of each specimen was smoothed off with a trowel.

3.3.5 Curing

After the initial gel formation or set (33) of the mortar, and within two hours from inital casting, the specimens were covered with continuously wet sacking and a polythene outer covering, which together approximates a 100% humidity curing condition for the first 24 hours (33, 116). The moulds were stripped and coded before being placed in a lime- saturated water bath which was temperature controlled to $20^{o} \pm 2^{o}C$ and provided with mild water

circulation. Here the specimens were left, fully submerged, until testing at the appropriate age. This 'normal' curing proceeded for six days, so the age at test was 7 days for these so called "wet" specimens. "Dry" samples were also wet cured for 7 days in an identical manner to the above "wet" specimens, following which they were air-dried for one day and then oven-dried progressively to 105°C for six days to remove the chemically uncombined and evaporable, or "free", water.

3.4 Mechanical Testing

3.4.1 Servo-hydraulic Testing Machine

All the static and fatigue compression tests were conducted on a 250 kN ESH servohydraulic testing machine. This machine had the capacity for accurately controlled slow ramping in stroke (or load) control as well as compressive fatigue loading in both stroke and load control modes up to 250 kN over a wide range of frequencies from .001 Hz to 10 kHz. Standard waveforms of sine and square wave together with the "saw tooth" mode, were readily available. A pre-selected mean level of load and range of applied stress in cyclic loading could be chosen, rapidly achieved and accurately monitored, by means of an amplitude measurement unit and a peak reading facility in conjunction with a built in oscilloscope. The 250 kN load cell was accurate to 0.1%.

Two linear variable differential transformers (LVDTs) with a total stroke of 10 mm and associated modular amplifiers are standard for this model of ESH machine and were used extensively for strain monitoring (described in greater detail in Section 3.5.2.).

3.4.2 Sample Preparation

The mortar prisms as cast and cured still require preparation before either static or fatigue testing can be undertaken. In particular, the prisms must be capped and various damage monitoring equipment attached. These procedures are described in turn.

3.4.2.1 Capping

The need to ensure pure axial and uniform loading (on the central portion of the prism at least), together with a freedom from stress concentration

effects, has been recognised by many researchers and consequently prisms have often been 'capped' (92, 143, 162, 168, 169, 173). (Indeed, BS1881:1970 (174) requires plane end surfaces to within 0.05mm.) Such capping, in between the machine plattens, does not eliminate the friction constraint mentioned elsewhere (Section 3.3.1 and (92)), but approximates a uniform axial loading condition. Capping has sometimes been preceded by surface preparation, for example, with a diamond saw (121, 175) to minimise stress concentrations from surface irregularities. Harmathy and Bennett (121) conducted high temperature compression tests on prisms and hence felt that capping was inappropriate, and simply trimmed off the top 25mm of the specimens with a diamond saw. Such trimming in itself was, however, insufficient to eliminate stress variations and they obtained wide scatter in their results which necessitated the use of sophisticated statistical methods.

In the present investigation, specimens were removed from the curing bath for between sixty and ninety minutes prior to capping. Although the top of each specimen was made as smooth as possible in the mould at the time of casting, by means of the trowel, small irregularities in the surface topography were still present, resulting in some stress concentrations and non uniform stresses. This face of the specimen was first ground down slightly using the face of a conventional rotary carborundum saw to remove "high spots", and subsequently a thin layer of epoxy putty (Pratleys putty) was placed on the surface. The epoxy layer was squeezed flat to a final thickness of approximately 1 to 1.5 mm. The capping itself was conducted using the ESH plattens protected by small sheets (65 X 65 X 0.1 mm) of semi-rigid polythene (overhead projector material) and duplicated the subsequent testing situation, with the same marked side of the samples always facing in a fixed direction (the control module). In this way the specimen capping was "form fitted" to the loading platten arrangement and despite any possible inequalities of platten alignment, the capping ensured that the load was still being applied uniformly and axially to the mortar. When the capped specimens were returned to the platten after appropriate curing of the epoxy at the same orientation and axial position, it was believed that there was no eccentric loading, induced bending, or non-uniform loading due to stress concentrations. This was borne out by the relatively small scatter for mortar prisms (of the order of 7%) for the static samples. After capping the specimens were placed in the water

curing bath with only the top cap (and some 2mm of mortar prism) emerging, for continued curing.

3.4.2.2 Attachment of Damage Monitoring Equipment

Damage (or microcrack) monitoring of the specimens was conducted using the attachment of LVDT strain monitors and ultrasonic probes. Subsequently acoustic emission monitoring, as a measure of damage development, was also utilised but this is described in more detail in section 3.5.4.

It is considered appropriate to include a description of the attachment of such damage monitoring equipment at this stage as part of the general sample preparation even though a detailed discussion of the justification of such damage monitoring is only considered in section 3.5.1. The standard fatigue test situation entailed the attachment of: (i) 2 LVDT's in a longitudinal and lateral manner to measure the corresponding strains (of both elastic and residual components); and (ii) the attachment of two ultrasonic probes to measure changes in ultrasonic pulse transit time (henceforward referred to as UPTT).

LVDT Attachments

Stainless steel stubs were glued onto the mortar specimens using epoxy glue (Pratleys quickset) and were used to clamp the LVDT's into position. For longitudinal strain measurement the stubs were placed 100 mm apart (centre to centre) with the lower stub being 25 mm from the bottom of the specimen. Those for the lateral strain transducer were placed laterally in the centre of the specimen on the face opposite to the longitudinal LVDT using the full specimen width, where non-uniform (non-axial) strains due to platten frictional restraint were minimal. The gauge lengths for the longitudinal and lateral transducers were thus 100 mm and 48 mm respectively. This is consistent with the published work, where gauge lengths of approximately half the specimen length have often been used (142, 168, 173, 176).

In the stub opposite each LVDT forming the strain monitoring pair a stainless steel threaded rod was located and adjusted for optimum sensitivity of the appropriate LVDT before being clamped in position with a

teflon screw. The LVDTs were similarly clamped in position using teflon screws. A photograph of the LVDTs attached to a specimen is shown in Fig. 3.5.

Ultrasonic Probes Attachment

The extent of internal damage development due to microcracking was also assessed from changes in ultrasonic pulse transit time. Two piezoelectric ultrasonic transducers were attached on opposite sides of the central portion of the specimen and were used to detect microcracking of a longitudinal (vertical) nature arising from the compressive loading, manifested as a change in transit time. The transducers were located in the central third of the specimen and an effective (ultrasonic) acoustic connection achieved by means of a high viscosity grease (Shell Barbatia). Due care was taken to minimise any air cavities between the specimen and the ultrasonic probe, thus ensuring maximum acoustic energy transfer, and the probes were held firmly in place with rubber strapping. (Fig. 3.5 shows detail of the ultrasonic probe attachments to a specimen prior to fatigue testing.)

3.4.3 Environmental Controls

The static and fatigue compression tests were conducted under three principal environmental conditions. These were namely (a) a so-called "moist" condition, (b) "dry" conditions, and (c) underwater conditions. These latter underwater tests were, in addition, conducted over a range of temperatures from 25°C to 60°C while the other tests (a) and (b) were undertaken at room temperature (20°C $\pm$ 2°C). Each of these conditions and how they were achieved are discussed in turn below.

3.4.3.1 Moist Conditions

Capped compression specimens were removed from the curing bath and allowed to dry in the laboratory atmosphere. Measurements of the laboratory relative humidity over a period of a year indicated that this fluctuated between approximately 65% and 75%.

The time that compression specimens were left in this atmosphere prior to testing was between 30 and 60 minutes. Approximately 15 minutes after

removal from the water curing bath, the compression specimens were "touch dry" and capable of having the LVDT mounting stubs glued into position using the quickset epoxy. The glue would not bond onto mortar surfaces that were "running wet". Approximtely 15 to 20 minutes elapsed to allow the glue to set and then the LVDTs themselves were attached to the stubs with the teflon screws together with the ultrasonic probes. The appropriate electrical connections were made and then the (by now, fully instrumented) specimen was placed inside a transparent polythene bag and placed on the platten. Only the electrical cable connections protruded from the bag mouth which was sealed, as mentioned above, between half an hour and one hour after emergence from the curing bath. (Neville (33) has noted that for drying periods of concrete in air less than six hours, the variation in specimen properties is less than 5%).

The humidity of the prism in its sealed bag was allowed to equilibrate and the relative humidity measured in several (but not all) instances, during both static and fatigue testing. Particular care needed to be taken of the monitoring instruments and relative humidity meter during fracture of the prism, which often tended to be "explosive" due to the stored energy in testing, particularly under high frequency (10 Hz) fatigue. The relative humidity so measured lay within the range of 75% and 95% in all the observations made, with a tendency towards the upper of these two limits. Occasionally, in long-term fatigue tests (i.e. lasting several hours or days - for example, the fatigue hardening studies in Chapter 5 or the development of SN data), it was observed that fine moisture droplets developed on the inside of the polythene bag indicating that the humidity was approaching 95% to 100%. A photograph of a test prism with its attached damage monitoring equipment inside a polythene bag ready for testing in the "moist" condition is shown in Fig. 3.6.

3.4.3.2 Dry Conditions

In the inital test series it was established that there was negligible weight loss (due to moisture extraction) after the first three days of drying; thus it is believed to be justified that the weight of the dried mortar samples had stabilised after the 6 day drying procedure.

The dried (hot) specimens were transferred to desiccators containing silica gel, allowed to cool, and stored until the various preparations for testing

were undertaken. The gluing of the LVDT stubs to the specimens were undertaken in the desiccators and any exposure to normal laboratory air was minimal. Once the LVDT's and ultrasonic probes were attached which was carried out with minimum delay, the suitably mounted specimens were transferred to the polythene bags and sealed. Two small sachets, one of non-hydrated (blue) silica gel and the other of phosphorous pentoxide, were placed inside the polythene bag just prior to sealing to further minimise the prevailing humidity. The humidity in the vicinity of the specimen was measured by the relative humidity meter to be in the range of 10 to 25% for all the tests undertaken. While this represents a relatively wide spread and also does not represent a "perfectly dry" environment, it was believed that this atmosphere was sufficiently dry to evaluate trends in the effect of moisture on crack propagation and damage development. Neville has reported (120) that atmospheres with relative humidities of less than 50% are regarded as "very dry". This environment, as far as tests are concerned, is henceforward referred to as dry.

3.4.3.3 Underwater Test Conditions and Temperature Control

Although the tests carried out under moist conditions (Section 3.4.3.1) were regarded as being undertaken in humidities above 95%, it was felt that for completeness that completely water-submerged specimens should also be tested. Such tests also facilitated the use of controlled temperature tests through water bath temperature control.

For the underwater tests an underwater container was constructed from a 300 mm long section of 400 mm OD pipe of 10 mm wall thickness (Fig. 3.7). The 15 mm thick circular base was welded into position and the edges sealed, also by welding, to make a watertight container. Handles were fitted and after stress relieving the container was coated with an appropriate sealant. A circular recess of the same size as the lower platten (diameter 180 mm) and 2 mm deep was machined concentrically into the outer surface of the base for accurate location under test conditions, as shown schematically in Fig. 3.7.

A schematic diagram of the water circuit is shown in Fig. 3.8. A temperature-controlled water reservoir was located adjacent to, and 300mm below, the testing table of the servohydraulic machine. The specimens were

placed in this reservoir just prior to test for a time of between 15 and 45 minutes to bring them up to temperature prior to testing. The temperature of the water in the reservoir was kept constant with a temperature controller accurate to $\pm$ 1°C; the reservoir also incorporated its own water circulation system using a small impellor, (Grant, type 505). This latter device proved invaluable for providing a constant flow of temperature-controlled water to the testing bath, Fig. 3.8. The reservoir (containing the temperature controller), and the test water bath were connected by two tubes. This was considered acceptable, since the linear coefficient of thermal expansion of concrete is about 10 to 15 microstrain (120) and thus variations in measured strain caused by temperature change would be no more than 50 microstrain (comparable to total micro strains of usually several thousand (Section 4.2.)

Equal flow rates to and from the bath were elegantly achieved with this system merely by controlling the total amount of water. A small cylindrical attachment to the top of the impellor housing facilitated a "pumping" of water only when water overflowed this housing from the top onto the impellor. (Fig. 3.9). Thus by having a constant depth of water in the reservoir so that overflow just occurred, a constant self regulating flow rate was achieved. For underwater tests instrumented specimens were placed inside finely perforated polythene bags which facilitated debris removal after the test without inhibiting water access to the specimen. The siphon pipe was then easily used to remove any other small pieces of mortar debris still in the test bath on a "vacuum cleaner" principle similar to the conventional swimming pool cleaning devices (e.g. Kreepy Krawly). A similar temperature control and water reticulation system was used for the double torsion tests described in detail in Chapter 7. A photograph of the complete hydraulic and temperature control system is shown in Figure 3.11.

A photograph of the complete hydraulic and temperture control system is shown in Fig. 3.9.

3.4.4 Static Testing Procedure

The prime purpose of the static testing was to obtain a measure of the static strength of a batch for subsequent fatigue work. Thus only occasional static test specimens were fully instrumented with LVDT and ultrasonic transducers to measure damage development and obtain load

deflection traces. Peak loads were recorded on every occasion, however, and those (infrequent) fully instrumented static tests served more as a quality control check on specimen fabrication and repeatability.

The static tests were removed from the water curing bath for a standard period between 15 and 20 minutes to dry (as well as to simulate the average fatigue testing during situation). The specimens were placed in a polythene bag (used for humidity standardisation and debris collection) and located on the compression platten. Great care was taken to ensure that the specimen end faces (which abutted on the plattens) were flat and free from grit or other stress concentrating particles. The specimen was located concentrically on the platten face (to better than 1/2 mm) with its coded face appropriately oriented. Care was also taken to ensure that the polythene film of the bag was smooth and flat over the bearing surface and free from creases or wrinkles. (It is interesting to note that a single fold in the 48 gauge plastic created a sufficient stress concentration to cause premature failure of the prism exactly along the line of the crease at approximately 70 to 80% of the expected ultimate load.)

The loading rate needs to be sufficiently slow to avoid dynamic effects yet sufficiently fast so that static fatigue processes do not play a part. For instance, it has been found that if the load is gradually increased up to failure over a period of 30 minutes the measured ultimate strength is less than 90% of that strength recorded when the rate of application of stress is less than 0.2 MPa/sec. (98). With extremely slow rates of loading this can reduce to less than 70%. However, practical loading rates on conventional testing machines tend to lie between 0.1 and 1.0 MPa/sec and therefore have little effect on measured strength (approximately $\pm$ 3%) (120). The code ASTM C39-71 specifies a rate between 0.1 and 0.4 MPa/sec (177), and similar values have been used by various researchers (142, 174). In the present study a ramp rate of 0.02 mm/sec. was used which was still within the codes (177, 178) but at the upper end to minimise testing time.

3.4.5 Fatigue Testing Procedure

3.4.5.1 Test Philosophy

Procedures described in the previous section on static testing provide the

basis for the fatigue testing described in this section. An estimate of the static strength of the particular batch (of 12 specimens) was obtained from the average of four, or sometimes five, static tests. SN curve data was obtained for the mortar specimens for stress levels between 50% and 90%. Test specimens which had not failed after 106 cycles were entered as "run out" results. On the basis of this SN data it appeared that an upper stress level of approximately 80% would yield a fatigue life of between 10^3 and 10^4 cycles (depending on enviromental testing conditions) (Fig. 2.28). This lifetime in number of cycles, would appear to yield suitable fatigue testing time periods even when various test frequencies from 0.1 to 10 Hz were employed. This choice of such an upper stress level is comparable with similar work (143, 89).

In all, 65 so called "wet" tests (RH 75% - 95%) were used, together with 29 "dry" tests (RH less than 25%) for the development of the SN curves.

3.4.5.2 Test Procedure

Having correctly tuned the servogain (on a dummy mortar compression specimen) the appropriate test conditions were selected. The test variables selected for study included: waveform (e.g. sinusoidal or assorted saw tooth), frequency (0.1 to 10 Hz), stress level (both upper and lower limits), temperature and environment.

A fully-instrumented test specimen, inside its polythene bag under the appropriate environmental conditions, was inserted between the plattens and accurately located in a manner identical to a static test described previously. The electrical connections of the damage monitoring apparatus were made, the bag sealed and the top platten lowered to touch the specimen. The minimum cyclic load level was set at a constant but finite low level of 5kN, representing a lower bound stress of approximately 1.4 MPa (or approximately 2.5% of peak load). This ensured that the specimen was always under compressive stress and was never fully unloaded, even during small overshoot of peaks in the setting up of cyclic amplitude, so that any impact or macroscopic movement of the specimen was prevented. Stable fatigue loading conditions were achieved to within 1% of the required levels within approximately 10 seconds of initiating cycling by using the standard ESH controls.

A full description of this damage monitoring equipment and a brief justification of its use follows in the next section (3.5).

3.5 Damage Monitoring Techniques

3.5.1 Introduction : Damage/Microcracking Equivalence

It has been widely recognised (89, 92, 107, 141, 143, 179-183) that damage development in concrete and mortar under both static and cyclic loading is associated with microcracking. Non-linear elasticity (no residual strain after unloading) does not appear to occur, nor is there evidence for true plastic microdeformation (for example by flow or cement gel), although the cumulative effect of microcracking may sometimes be regarded on a continuum level as a non-elastic "plastic" response.

Thus it is reasonable to regard the degree of microcracking in mortar or concrete, in a fatigue specimen, as a measure of the extent of accumulated damage. As mentioned previously, recent studies (184) have demonstrated that the non-linear behaviour of concrete under compressive loading is highly dependent on the non-linearity of its cement paste and mortar constituents (162, 185). Cement paste and mortar must not, however, be regarded as purely elastic (brittle) materials (93) but rather as non-linear materials that exhibit continuous damage under load (168), even after very low strains (185). There is some evidence to suggest that this non-linearity of the stress-strain behaviour and early accumulation of residual strain is associated with the matrix material itself and not simply with aggregate bond microcracks. Indeed, it is generally accepted (92, 176) that microcracks exist in concrete (from differential hydration, shrinkage, porosity, curing, etc.) even before the application of any external loads. The question of a whether there is a lower stress "threshold" above which microcracks develop is still a moot point. Spooner and Doughill (185) indicate that there is no evidence to support a lower threshold concept and contend that the increase in damage is continuous although the extent of microcracking below approximately 30% of ultimate appears to be limited (176).

At the other end of the scale final failure occurs when the damage level, or extent of microcracking, becomes so great that a significant proportion of "failed microcracks" join up to form a continuous fracture path (165). In

depth discussion of the detailed causes, models and mechanisms of damage development are, however, held over to Chapter 8 and this section (3.5) rather discusses the background and details of the damage monitoring techniques used in this project.

Assuming then that damage and microcracking may be regarded as equivalent in both compressively loaded mortar and concrete specimens, various techniques have been developed to evaluate and quantify this damage. The microcracking, as well as final failure surfaces, tend to be parallel to the direction of loading, at least in the uniformly axially-stressed region of the prism (84, 170, 179, 186). Thus measurements of lateral and longitudinal strain (including both elastic and inelastic, or "residual" components), as well as changes in ultrasonic pulse transit time, have regularly been employed as damage monitoring methods, (Fig. 3.10(a)). These are now discussed in some detail. In addition, changes in elastic modulus are also indicative of damage, as was shown, for example, in Fig. 2.33 (143, 184) and occur even at quite low stress levels. Further, a more recent method of detecting and monitoring damage is by means of acoustic emission monitoring (AEM).

In the following sections the three damage monitoring techniques of (a) strain, (b) ultrasonics and (c) acoustic emission are discussed, together with the description of the experimental details of these techniques as used in this project.

3.5.2 Damage Monitoring Using Strain Measurement Methods

3.5.2.1 Background and Recording Details

Lateral and longitudinal strain gauges were used to measure elastic and accumulated strains of the mortar under both static and fatigue loading. The application of reusable linear variable differential transformer (LVDT) transducers for damage monitoring of concrete in fatigue is not new (89, 107, 141, 168, 180-182); they are ideal for detecting both elastic and residual, or accumulated, strain which are evident on unloading (120, 168, 176, 187). The magnitudes of these total strains in compression prisms are reportedly of the order of 1000 to 2500 microstrains (27, 120) consistent with values obtained in this study (see for example section 4.2) with values

approaching 4000 microstrains or more for lower strength (15 MPa) concretes (141).

During fatigue the longitudinal dimension of the prism specimens decreased and the lateral increased (Fig. 3.10(a)). Because of inertial effects at the highest test frequency used (10 Hz) an ultra violet oscillograph galvananometer recorder was used for strain recording. Although both LVDTs could operate simultaneously it was necessary to switch from one to the other periodically to obtain full strain versus number of cycles traces as the testing machine used only had one LVDT signal output. This switching was useful, however, as it acted as periodic timing markers at specific numbers of cycles Fig. 3.10(b).

3.5.2.2 Strain Calibration

Calibration of the LVDTs output, as manifested by the horizontal axis of the photosensitive chart recorder paper (Fig. 3.10(b)) in strain terms, was effected using a 150mm jaw-width micrometer. LVDT calibraton curves are given in Figs. 3.11(a) and (b), and Table 3.2. Measurements of "width" of trace (Fig. 3.10(b)) can be regarded as proportional to the elastic strain, while a measure of the residual (or accumulated) strain is obtainable from the progressive deviation of the boundaries of the strain amplitude signal. (Note: from henceforward the term strain will be used for convenience when strictly the meaning is LVDT deflection. The strain can, however, be easily obtained simply by appropriately normalising the LVDT deflection.)

It is important to recognise that this definition for "elastic" strain does not necessarily correlate with the linear portion of the stress-strain loading curve. Generally, the "elastic" deflection defined here includes a significant portion of the non-linearity and is, in effect, a measure of the strain width of a stress-strain hysteresis loop.

3.5.2.3 LVDT Underwater Protection

It was necessary to waterproof the LVDTs up to a temperature of 60°C (Section 3.4.3.3). Ordinary long balloons either proved insufficiently robust or impinged on the easy reciprocating movement of the LVDT plunger. The problem was solved using conventional contraceptives(!) (Durex

gossamer), which were sealed at the electrical lead with a rubber sealant, (Fig. 3.11(c)). Unfortunately at high underwater temperatures ($60^{o}C$) the LVDT stubs occasionally debonded so strain recordings for these tests were somewhat limited.

3.5.3 Damage Monitoring Using Ultrasonic Techniques

3.5.3.1 Introduction and Background

The ultrasonic pulse velocity technique of non destructive testing of the quality of concrete was first used by Long, Kurtz and Sandenaw (188) and consisted of transmitting an (ultrasonic) vibrational pulse through a fixed distance of concrete. Many investigators (89, 143, 183, 179) have used a longitudinal wave velocity method for detecting the formation of microcracks inside concrete specimens and of these, Jones (179, 82) has conducted the most comprehensive study by ultrasonics of microcracking under short term loads. Shah and Chandra (89) recognised the ultrasonic technique as a means of continuous monitoring of damage in concrete under fatigue conditions and Jones and Kaplan (82) showed by means of ultrasonic techniques that internal microcracking develops predominantly parallel to the loading direction but not perpendicular to it.

Ultrasonic detection methods are also very useful for continuous monitoring of damage development as microcracking tends to occur in a predominantly parallel direction with respect to loading (Fig. 3.10(a)). Consequent transfer of sound energy across an air gap (at a crack) in a direction perpendicular to the loading direction is minimal and the stress wave takes a variety of longer paths around the microcracks to be detected by the receiving transducer. Thus there is a corresponding increase in transit time which can be regarded (178) as a measure of how damaged or microcracked the sample is. Similar techniques and frequencies have been used by other researchers (82, 120, 143, 179, 189, 190-192). Shah and Chandra (89) in using piezoelectric crystal transducers with resonant frequencies of 25, 250, 750 and 2250 kHz, found that the higher the frequency of the transmitted pulse, the more sensitive were changes in pulse velocity in detecting microcrack propagation. Measurement of the attenuation of the received ultrasonic signal is also indicative of the damage development and this technique has been quite well used (89, 179, 192, 194).

3.5.3.2 Experimental Details of the Ultrasonic Techniques

The apparatus used for the continuous damage monitoring by measurements of changes in ultrasonic pulse transit time was obtained from AERE Harwell (type 3127-1 of the 'Ultrasonic Research System').

This unit was used in conjunction with two 50 kHz barium titanate transducers which were capable of operating in either a reflected echo or a transmitter/receiver mode. These transducers were attached to opposite sides of the specimen by means of a high viscosity acoustic grease and held in place by rubber banding. Pulses were emitted at 100 millisec. intervals by the transmitter transducer and after passing through the specimen were received by the other (receiver) transducer (Fig. 3.12). Changes in the time interval between these two events were measured and displayed as a voltage which could be represented on a recorder. This was effected by having an integrating capacitor charge up from the suitably delayed end of the transmitted pulse and which was stopped when the appropriate part of the received signal pulse arrived. This was achieved by ensuring that a consistent point of the received signal was evaluated, in this case the fifth downward crossover point. This was used because the high gradient on this portion by the waveform facilitates greater accuracy.

The stabilised input current in the sampling integrator was 10 mA and this resulted in a stabilised current at the capacitor of 4mA. The choice of capacitor was such that it was large enough to ensure that the change in voltage (V) produced by this current does not exceed 5V in the time of integration (t), where

$$CV = It$$

For example, with a transit time of 30 m secs. C should be not less than 24 nF (=.024 μF). To record transit time (or more particularly variations in transit time, which was the case in this project) the dual strobe generator unit of the Harwell system selected a precise point (the next downward crossover) on the ultrasonic waveform following the first occasion when it exceeds a preset amplitude at the receiver.

This system, together with a Bryans 26000 series XYYt chart recorder, was thus capable of monitoring damage development in mortar (in both static and fatigue test conditions), by measuring changes in ultrasonic pulse transit

time (UPTT). The noise level of $\pm$1mV, in comparison to the total signal change in fatigue tests, of approximately 20-30mV due to damage development, was consistent with published data in the Harwell Manual (195) and regarded as acceptable.

3.5.3.3 Ultrasonic Pulse Calibration

The calibration of the ultrasonic pulse transit time signal, as seen by the Bryans chart recorder, was facilitated by means of the time base control of the oscilloscope (Tecktronic ENC type 5030). For example, a typical square wave (capacitor) signal was measured at 31.1 mV (using a digital voltmeter) and on the scope represented 2.33 cm on a 2 μsec/cm division. Thus 10mV is regarded as 1.498 μsec and in practice the calibration factor of 10mV equivalent to 1.5 microseconds was used throughout this project (196, 197). With this system it was thus possible to measure changes in ultrasonic pulse transit time due to damage (of the order of 1 to 4 microsecs) to within 0.02 microsec.

3.5.3.4 Underwater Protection of Ultrasonic Probes

It was sufficient to waterproof only the electrical BNC connection and electrical leads since the front face adjacent to the piezo crystal (and which abutted onto the mortar) was already sealed and water resistant. This waterproofing was achieved by sealing the leads and connections with strain gauge wax covered with silicone rubber. While this technique achieved satisfactory water protection the performance of the probes underwater was not entirely satisfactory, evidently because of the temperature dependence of the piezo crystal which precluded its use above approximately 45^{o}C. Thus only limited results were obtained which are described in Section 4.5.3.

This concludes the description of the experimental strain and ultrasonic pulse transit time methods of damage monitoring which were extensively used. The section is, however, concluded with a discussion on Acoustic Emission Monitoring and its experimental use in this project.

3.5.4 Acoustic Emission Monitoring

3.5.4.1 Introduction

Acoustic emmission is the term applied to the elastic stress waves released as a result of dynamic processes such as crack growth and plastic deformation which occur in a material, and also to the technique employed in their measurement (198). Acoustic emission has also been referred to as stress wave emission, sonic pulses, microseismic activity and seismo-acoustic activity and during the last few years the field of AE testing has grown very rapidly (199, 200). This growth has been stimulated by (i) the realization that acoustic emission can be used to characterize and monitor the processes of fracture and flow that occur during mechanical static and dynamic loading; and (ii) the availability of commercial testing equipment at reasonable cost. The subject, however, is still rather complex and the scale of acoustic emission's practical success in the field has been somewhat limited despite a large number of research publications. An excellent review of acoustic emission and its application is given by Wadley (201).

Acoustic emission is particularly valuable in that it is a passive system and is therefore the only NDT technique capable of effectively monitoring, on a continuous basis, the "health" of a component or structure. In addition, AE is reportedly the only NDT method (199, 202, 203) whose signal output can be directly correlated with the crack tip stress intensity factor, K, a parameter widely used in the description of slow crack growth rates in fatigue and reactive environments as well as for the onset of unstable crack propagation. Evans, Linzer and Russel (203) have developed this, both theoretically and experimentally, to show a correlation between the rate of occurrence of acoustic events, $\frac{dN}{dt}$, and the rate of crack growth, $\frac{da}{dt}$, for many materials.

When a structure or component deteriorates through loading and approaches failure (by, for example, plastic deformation or cracking) associated stress waves are often spontaneously generated, concomitant with stress relaxation. In concrete and mortar, in particular, there are small, localised areas of high stress and it is as a result of sudden

redistributions or relaxations of these stresses by, for example, microcracking, that stress waves originate and propagate - effectively from point sources. In addition, there will be reflection, transmission and refraction of the waves at internal surfaces and also probably vibrations, resonances and standing waves set up which severely complicate any subsequent attempts to deconvolve the signal and relate the AE to any particular mechanism or source. The stress wave is also modified as it propagates, in that different frequency components in it are attenuated at different rates within the specimen or structure.

These stress waves are detected on the surface by means of sensitive (lead zircano-titanate) transducers which convert the mechanical impulses to electrical impulses. Sensitivity is approximately 10^6 times that of electrical resistance strain gauges with pressure changes as small as 6×10^{-3} Pa readily detectable (204). The signal from the transducer output requires both pre-amplification and filtering before subsequent further amplification by a high gain/low noise type of amplifier and this requirement is discussed in more detail on the section on instrumentation (3.5.4.3).

The transducer itself modifies the stress wave signal in that it can resonate or vibrate in different modes. This can be beneficial, for sharply-tuned frequency requirements; however, it can also be disadvantageous since more generally a flat frequency response for a range of frequencies is preferred, to give uniform amplification, and resonances distort the detected characteristic stress wave.

Ringdown Counting and Event Counting

The randomly-occurring burst emission is typically characterised by a fast rise time energy burst with an exponentially decaying amplitude. Continuous emission can also occur which is normally of a much lower amplitude but is not considered further here as it is not relevant. An oscilloscope trace of a typical burst emission, i.e. one "event", is shown in Fig. 3.13. The amplified signal can be counted in two different ways, viz.: (a) ringdown counting or (b) event counting. In ringdown counting the single acoustic emission event (Fig. 3.13) does not produce a single count, but rather produces several counts associated with the number of times the signal crosses the threshold, V_t, in "ringing down" to a voltage

below the trigger level. Five counts would result from the signal shown in Fig. 3.13. Hence the number of counts can be related to the energy released in the (single) event. In event counting, by increasing the threshold level one can arrange to count just once for each event. (Alternatively, in event counting, one can arrange to have a lower threshold but then stop the counter for the typical duration of the ringing down, thereby only recording one count per event.)

Both methods have inherent advantages and disadvantages. In ringdown counting, for example, since there is a count every time the threshold is crossed, it is not clear whether there are several separate events or just a few, each with a large amplitude ringdown. Ringdown counting does, however, have the advantage that for a particular event the amount of ringdown, i.e. the number of ringdown counts, for a particular threshold, is often considered a characteristic of the material (205). By first recording an event and playing it back at different threshold levels one can obtain some idea of the amplitude distribution of the signal using ringdown counting.

In event counting one may miss certain low amplitude events by having too high a threshold level. On the other hand, if one is interested in the number of events this is the preferred counting technique. However, it is questionable whether counting alone, either ringdown or event, provides the best means of signal monitoring. Certainly a good deal of information concerning frequency, waveform and amplitude will be lost. It is both an inefficient and inexact means of monitoring what is really required, i.e. the frequency or energy spectrum and amplitude distribution. However, it should immediately be pointed out that such determinations are no easy task, and the non-uniform response of the transducers and the attenuation throughout the specimen or structure under test further complicate interpretation.

For either (or both) event counting and ring down counting the AE data events can be interpreted as a certain number of counts per time interval (rate counting) or as a monotonically increasing signal (cumulative counting). This is mentioned further in Section 3.5.4.4.

3.5.4.2 AE in Concrete and Other Materials

AE in Materials Other than Concrete

Extensive AE research has been undertaken in metals (94, 201, 206, 213), ceramics and glasses (198, 199, 202, 203, 214-218), and composites (216, 208, 219). AE is generally associated with material deformation, debonding or cracking but can arise, for example, from dislocation movement, grain boundary sliding or domain wall motion in magnetic materials. The interested reader is referred to the above and other sources (199, 200, 201) for background which are inappropriate to include here.

It is worth mentioning here, however, the Kaiser effect (220) which refers to the immediately irreversible characteristic of AE resulting from applied stress. If the Kaiser effect is present there is little or no AE until previously applied stress levels are exceeded.

In addition, for brittle materials, AE has been noted (202) at relatively low stress levels (30% of ultimate). A further interesting point that has been well studied (198, 202, 203, 209, 214-216) is the empirically-established relationship between stress intensity, K, and number of acoustic emission ringdown counts, N, for precracked specimens under monotonic loading:

$$N = DK^m$$

The index m depends on material type and specimen geometry and is reportedly 4 - 5 for steels (cf. 18 to 30 for various ceramics) (199). There is, however, a great deal of controversy and conflicting work concerning the theoretical basis of the above correlation (209, 211-214), although such correlations do suggest a relationship between microstructure and toughness (202). Tetelman and Evans (199), as well as Dalgleish et al. (202) have elegantly illustrated the relationship between acoustic emission rate and crack growth rate with stress instensity factor for ceramics (Fig. 3.14).

Acoustic Emission in Concrete

Rusch (221, 222), in 1959, made tentative, preliminary observations concerning acoustic emission produced by stressed concrete and was among the first to do so, together with L'Hermite (160) and Ruetz (223). Robinson, (194), in 1965, using transducers resonant at 100 kHz and a tape recording system, determined that the emissions were mainly of two frequency regimes 2

kHz and 13 to 14 kHz, and emissions occurred at loads well below those where the ultrasonic pulse propagation velocity and Poisson's ratio are affected. The propagation velocity and Poisson's ratio changes are usually attributed to the formation and coalescence of microcracks. Hence the important conclusion was reached that acoustic emission could indicate earlier and smaller structural changes than do the more conventional methods.

In 1970, Wells (224) devised an apparatus to record acoustic emission from concrete under stress, "listening" in the frequency range 2 kHz to 20 kHz. He reported that AE starts at a stress level of around 50% and increases as failure is approached. Similar findings were reported by Newman and Newman (192) and Terrien (225), who observed AE noise above approximately 40% of ultimate which increased progressively with load until cracks (with associated AE) were observed on the concrete surface.

Perhaps the most thorough acoustic emission work on concrete to date has been done by Green (226), who detected emissions as high as 100 kHz. Green's work is significant in that it showed that acoustic emission from concrete can be an indicator of failure processes. Early warning of total compressive failure and preliminary correlation to material modulus was indicated. AE recognition of gross cracking, onset of concrete pressure vessel failures and leakages, and prestressing rod failure was accomplished.

McCabe et al. (215), in a detailed study of acoustic emission in concrete using a transducer resonant at 140 kHz, reported various interesting characteristics including a greater number of counts, relatively, with decreasing specimen size, and a decrease in AE with specimen age. Of particular practical value were the results of creep tests, where these authors reported a linear drop off of AE with time when plotted on a log-log scale. This is significant since field testing of concrete structures require use of acoustic emission <u>rates</u>, as opposed to cumulative acoustic emission counts, to assess structural integrity.

The irreversibility of noise, i.e. the Kaiser Effect, in concrete has been reported by several researchers (e.g. 221, 215, 226) but appears from the literature to be applicable only up to 80 to 85% of the static failure stress. Nielsen and Griffin (227), using a transducer with a 100 kHz to 300 kHz pass band, report that the observed Kaiser Effect in concrete was temporary and there was recovery of noise at low stress levels, within 20

minutes to 2 hours, although the number of counts was reduced. They also reported that "dry" concrete was noisier than "wet" concrete for the same age - under static conditions. Goodman (228), who reported the Kaiser Effect in rock, also noted the partial recovery with time of the Kaiser Effect with consequent implications for proof testing applications.

In a more recent study (1980), Terrien (225) observed three principal regimes of acoustic emission noise from mortar and concrete using 1MHz resonant broadband transducers. These were broadly (a) up to 100 kHz (b) 50 - 200 kHz and (c) 100 to 300 KHz, with a large proportion of the energy in the first 0 to 40 KHz. Terrien (225) also reports "bursts of AE events" ("Salves d' evenements" (sic)) from wet mortar (but not dry) which occur approximately 200 microsecs apart, which he cites as important evidence of the role of water as a means of stress redistribution and relaxation. This results in further cracking presumably by stress corrosion or time dependent static fatigue processes ("corrosion sous tension"). The presence of water was regarded as assisting microcracking as it decreases surface energy.

3.5.4.3 Acoustic Emission Instrumentation

Introduction

Illustrations of the compression testing facility including the damage monitoring aspects, are shown in Figs. 3.15(a) and (b). Illustrations of the acoustic monitoring system specially developed for this study (which is typical of other A.E.M. systems), and how these fit into the overall system, are shown in Figs. 3.16 (a), (b).

In order to interpret and analyse the signal at the transducer output, certain processing was necessary. After detection of the stress waves by the 50kHZ P.Z.T. piezo-electric transducer and subsequent transformation, the small electrical signal, with an initial rise time of 10 - 100 μsec, was amplified by a low noise/high (but variable) gain preamplifier (Brookdeal 9453; $\simeq$ 60 dB) and filtered, or band limited, variably between 1 kHZ - 200 kHZ by cascading fourth order Bessel high and low pass filters (Kronhite, model 3500). The amplified and filtered signal, displayed at this stage on an oscilloscope, was further amplified 30 dB (precision Monolithics, OP01) to 5 V peak to peak (National Semiconductor LM361) with a 1.36 V

reference. Noise immunity of the comparison point was enhanced by incorporating a hysteresis of $\pm$ 50 mV centered symmetrically about the reference. The threshold could be chosen, by careful adjustment of gain control and threshold level, so that one count per event was obtained, i.e. event counting. The signal was used to trigger a monostable multivibrator (TTL 74121) whose output of a square pulse of 0.5 msec duration was very suitable for counting by a recycling digital counter. Components of a single acoustic emission event exceeding the comparator threshold within 0.5 ms of the initial leading edge did not retrigger the monostable, and the maximum count rate was limited to 2000/sec which was more than sufficient to monitor the AE from mortar compression.

The monostable pulses could be divided by factors 1, 10, 100, or 1000 before being counted in standard TTL circuitry (TTL 7490) either (i) as a rate count, (ii) as a certain number of counts per given time interval (typically 2 seconds, but with a range from 0.1 sec to 20 min) by using a built-in triggered pulse from a digital clock, driven by a 3.6 MHz crystal oscillator, or (iii) as a cumulative or total count. The digital count was displayed on a 3 digit light emitting diode display and could be recorded as a function of, for example, time or load, after further conversion from a digital to analogue signal (Precision Monolithics DAC.02), suitable for use with an X-Y or X-Y-T chart recorder.

Other facilities of the acoustic emission system used include (i) a "Hold" control to hold whatever number of counts has been reached; the counter however continues to count as fresh data arrives to be displayed when the "hold" button is released; (ii) a "disable count" control which prevents the counter from accepting data and was useful in setting up procedures, as were (iii) "zero" and (iv) "Full Scale" controls, which were used for scaling and calibration of recorders. Full details of the acoustic emission monitor especially built for this project are given elsewhere (229).

Noise Problems

Noise, originating for both mechanical stress and electronic interference effects, is a major problem in A.E.M. Testing machines are inherently noisy to a greater or lesser degree, and in practice it is necessary to attempt to employ a monitoring system that is responding only to the

relevant AE events and not to spurious machine or other noises. Machine noise is a very much more serious problem in fatigue testing and will be discussed later. Other background noises which occur, even in static testing, are of various types and include: (i) slippage between transducer and sample; (ii) particulate crushing between the sample and the testing machine platen; (iii) noise originating in the capping material; (iv) relative movement of the transducer on the sample surface as a result of imposed strains, or "barrelling"; (v) specimen movement on the testing plattens; and, (vi) electrical and other spurious energy waves in the vicinity of the transducer (e.g. nearby radio transmitter).

Noise from (i) and (iv) could be almost totally removed by ensuring a good acoustic bond by means of a suitable grease film and firm transducer attachment. "Seating" noise, i.e. (ii), (iii) and (v) could be all but eliminated by using accurate capping (Pratley's quickset epoxy putty) and by using suitable mechanical insulators. (Several small sheets of blotting paper were found to be very suitable (227)).

Frequency Spectra

In an attempt to discriminate between real acoustic emission and machine noise, particularly under fatigue conditions, the potential for simple "filtering out" of machine noise was evaluated. This was achieved by considering the frequency spectra of (i) a typical acoustic emission event itself from mortar and (ii) of the characteristic testing machine noise under load conditions.

A typical mortar prism specimen was acoustically monitored while being loaded to destruction in a very quiet testing machine (AMSLER; hydraulic 600 kN capacity). The amplitude-frequency spectrum of typical mortar acoustic emissions was evaluated by means of a Spectral Dynamics RTA analyser and indicated (Fig 3.17) that the bulk of the AE energy was in the frequency range 0 to 10kHz with peaks at 1 to 2 kHz, 3 - 4 kHz and 7 kHz using the 50 kHz resonant transducer. It was believed that any evidence of large AE energy bands (of frequency) coinciding with "quiet bands" of the machine noise could be sharply filtered to detect the AE and discriminate against the machine noise. However, this was not possible as the frequency spectrum of the machine showed that its noise component was more or less

continuous up to about 14 kHz under static loading and continuous up to 36 kHz under fatigue loading conditions. The frequency peaks shifted slightly as the load changed and the amplitude of the lower frequency components also increased under increasing load. The amplitude of the higher frequencies, tested right up to 200 kHz of machine noise was very low, (less than -30 to -49dB), Fig. 3.18 (a, b).

What is of particular interest, however, is that there was a small but significant energy content in the acoustic emisions from mortar between approximately 20 and 200 kHz, whereas the machine noise was almost non existent, or at least of very much lower amplitude (for the same gain conditions), above about 20 kHz (compare Figs. 3.17 and 3.18 (a, b)). This situation greatly facilitated AE detection under fatigue conditions simply through the employment of a sharp cut off filter system (the Kronhite 3500 series 4th order Butterworth filter) operating with a pass band typically between 45 kHz and 200 kHz. This is consistent with the studies by Green (226) who observed significant AE noise from concrete in the regime of 30 kHz to 80 kHz.

Employing these techniques, with a fixed threshold level, the procedure adopted was to operate at a comparatively high gain ($\simeq$80 dB total) but below the level where spurious electrical and machine noise was being amplified to above the threshold (i.e. "oscillating"), and then to reduce the lower limit of the filter passband to just above the machine noise level. Tests were then conducted with only minor subsequent adjustments to the filter and, sometimes gain controls. Under these (filtered) conditions the signal from the transducer arising from typical acoustic emissions was typically 25 to 200 μV in amplitude, rising to 700 μV near failure, whereas the background noise level was between 0.5 and 1.5 μV. (With a wider filter pass band from 1 kHz to 200 kHz this background noise level was up to 300 μV under similar amplification (gain) conditions.) Under normal operating conditions the signal to noise ratio (SNR) was evaluated at 36 dB. The gain setting was increased just to detect the background noise and then reduced approximately 2 dB for normal operation.

For setting-up purposes, calibration and checking the efficiency of the acoustic emission monitoring system it was necessary to develop a "standard simulated acoustic emission event". This was achieved by breaking a 3mm long pencil lead of diameter 0.5mm which projected from an ordinary clutch

pencil against the surface of a mortar prism at an angle of 45°. A similar technique using 0.3 mm pencil lead was used by Scruby and Wadley (230) who showed that this technique simulates very closely the theory for a point source of AE buried within a semi-infinite solid. The event in our case was highly reproducible (and corresponded to an impact force (measured using a spring balance) of approximately 3.3N. A frequency spectrum of this pencil lead fracture simulated AE event is shown in Fig. 3.18(c) and the distribution is comparable with a mortar AE event, Fig. 3.17, (except that it it of smaller amplitude).

Simultaneous Acoustic Emission and Ultrasonic Monitoring

All the initial Acoustic Emission monitoring of concrete was undertaken using a separate 50 kHz probe specifically for the task. It was soon realised, however, that since the ultrasonic probes and the AE probe were of similar dimensions, characteristics and resonant frequency, simultaneous monitoring of AE events from microcracking and ultrasonic monitoring of microcrack damage could be carried out using the same transducer and simply using a gating device. The relevant portion of the ultrasonic signal was only approximately 3 to 5 ms long in a period of 100 ms (Fig. 3.19) and it was this 5 ms section which was used for ultrasonic transit time measurement. The other 95% (95 ms) could be gated out of the ultrasonic shock system and used for "listening for" acoustic emission signals. Admittedly 5% of the AE events would be lost but this was not thought to be significant in terms of the advantages that would accrue. Obviously it was necessary to gate out the relevant part of the ultrasonic signal with respect to AE monitoring otherwise these would be registered as AE events.

The gating was achieved using a GATE CONTROL addition to the Acoustic Emission Monitor (AEM), the circuitry of which is shown in Fig. 3.20. The circuitry basically detects the first spike of the ultrasonic pulse and this then triggers three multivibrators in series in order to be able to vary both the gate position and the gate width. Also, consideration had to be given to obtain at least 90 to 95% of the duty cycle with the 74121 integrated circuit. The circuit was constructed and worked very satisfactorily. For all subsequent acoustic emission work in fatigue involving the pseudo isometric plot PIP techniques this simultaneous AE and ultrasonic signal system was used.

3.5.4.4 Acoustic Emission Studies in Mortar

Plain Mortar in Monotonic Compression - Static Tests

Static tests were conducted using the above Acoustic Emission Monitor and the (relatively) quiet AMSLER hydraulic testing machine.

With the threshold level fixed and with a total gain of 80 dB, the AE signals emitted during a rising load test were event counted and recorded either as a rate count (typically sampling every 2 seconds) or on a cumulative (total) count basis.

Rate counting methods are generally regarded as the more informative (compared to cumulative counting) (199, 227), although both techniques are displayed in Figs. 3.21 (a, b). In these figures the load record and associated acoustic emission are plotted vertically against real time on the horizontal axis. The tests in these figures are all comparable, being conducted on moist 7 day old specimens on the Amsler machine with a pass band width of 20 kHz to 200 kHz. The count rate was two seconds. It is apparent from these static tests that measurable acoustic noise occurs from first loading but only becomes really significant above approximately 50 to 80% of full load, with a large increase in AE activity just prior to failure.

Bearing in mind the nature of the detection and recording A.E.M. system responding, as it does, to all types of stress waves, the detected acoustic emission from concrete in this experimental set-up (i.e. short-time load duration) can realistically be associated with damage, presumably in the form of microcracking. Such damage can also be monitored using established ultrasonic pulse velocity techniques, and it is useful to compare the AE signals (Fig. 3.21 (a, b) say, during static ramping to failure) with those of corresponding ultrasonic pulse transit time (UPTT) measurements Fig. 3.22. It is evident that these are of the same general form, but an important observation is that acoustic emission can detect small changes associated with the initiation microcracking and therefore provides earlier damage information than the more conventional ultrasonic methods.

3.5.4.5 Kaiser Effect

A series of tests was performed on both the wet and dry plain mortar specimens to observe the immediate hysteresis behaviour of the acoustic emissions. Fig. 3.23 indicates that for successively applied loads, and for a controlled strain-rate, the Kaiser Effect is entirely valid (for this high cement mortar) in that acoustic emissions do not occur until stress levels exceed those previously experienced by the specimen. In Fig. 3.23 AE is displayed as a 2-second rate count. It can also be seen that above about 85% of failure load application of the Kaiser Effect is limited because of the comparatively high level of emission.

The implications of the Kaiser Effect as a proof testing aid are readily apparent. In addition, this phenomenon provides, under some situations, a technique whereby one can determine the magnitude of the previous stress (e.g. due to overload) to which a structure has been subjected. However, it remains to clarify the effect of moisture content on emission irreversibility, particularly in the high stress regions and also over extended time periods. There is some evidence (227) to suggest that the Kaiser effect phenomenon in mortar is short lived. This was not specifically investigated in this project but some recovery was observed three days after initial testing.

3.5.4.6 Acoustic Emission Monitoring During Fatigue

It is well established that fatigue in concrete and mortar is associated with microcracking and damage development (see for example section 3.5.1) and that such microcracking damage is continuous and progressive. Acoustic emission monitoring is a very sensitive means of observing and detecting damage and hence it follows that efforts to investigate and interpret acoustic emission behaviour under fatigue conditions may well contribute to an understanding of how such microcracking occurs at a microstructural level. In particular, if it were possible to discriminate between real acoustic emission events and background (machine induced) noise, then distinction of where and when the AE occurred, with respect to position on the load cycle, should be obtainable and may add to the understanding of the origins of microcracking. Such AE monitoring is not without difficulties, however, because of the high and overlapping machine noise levels. The

following paragraphs describe how reliable AE data in fatigue was obtained together, ultimately, with ultrasonic data.

Using the filtering technique it became possible to obtain AE data during fatigue. Fig. 3.24 shows a typical plot of AE events on a 2 second rate counted basis with (rate counted) number of events on the y axis and number of cycles, or time, on the x axis. From this (typical) trace it is apparent that for a specimen under fatigue conditions (0.05Hz, sine wave, moist) acoustic noise occurs from virtually the first cycle and activity increases significantly near failure.

It was also apparent that AE noise occurred at various portions of both the loading and unloading cycle, but the method of data acquisition shown in Fig. 3.24 did not facilitate distinction of where on the load cycle these acoustic events actually occurred.

In an attempt to resolve this situation, to obtain more data than simply the "number of counts in a certain time interval", a pseudo-isometric plot technique was developed (henceforward referred to as PIP). Various researchers (199, 206, 209, 214) have used amplitude sorting and frequency analysis to attempt to classify, or "fingerprint", acoustic emission events and, by deconvolution, to identify their sources, but with limited success. One technique employed by Carlyle and Scott (204) effectively used the rate counted AE signal to modulate the intensity control of an oscilloscope (i.e. "Z modding"), with the horizontal axis as number of cycles and y axis as load, and taking a time exposure of the resultant "trace". While successful, this technique was limited because ideally a prior knowledge of the number of cycles to failure was required and also the amplitude of the AE output was not easily quantified simply from degrees of light intensity on the final photograph.

In the pseudo isometric plot technique developed here, ("pseudo" because the presentation was not truly isometric because there were no hidden surfaces), the rising load and falling load were displayed separately by connecting the sinusoidal load signal to both the two Y inputs of a two channel time base chart recorder (Bryans 26000 series). The rate counted acoustic emission events were led to the x input which responded with a total shift of the 2 y pen carriage when the AE event occurred. With the chart recorder time base drive unit switched on, and by alternately tracing rising load and falling

load traces, a pseudo isometric plot could be obtained (Fig. 3.25 (a, b)). When the time base speed is reduced the individual load cycles are compressed almost to straight lines and the effect is as shown in Fig. 3.25 (b) with an isolated AE event also shown. A more realistic section of an actual AE PIP plot is shown in Fig. 3.25(c).

The alternating Y_1 and Y_2 pen up/down remote switching unit of the Bryans chart recorder was activiated from the peaks overshoot facility of the ESH serohydraulic machine. This peaks overshoot was typically of 50 mV amplitude (Fig. 3.26) and was ideal for signalling the start of the decreasing load cycle or increasing load cycle. It is worth noting that no PIP acoustic emission was recorded during the first few cycles of a fatigue test because the PIP system relied on the full and accurate development of the "peaks" load overshoot facility to operate the pen lift switch system (See Fig. 3.26(b)). Thus in each of the PIP traces presented the first five cycles have been considered noise free and presented as such.

The automatic pen control circuitry, developed for this project and shown in Fig. 3.27 (a, b), was basically a zero crossing detector using two LM 319 comparators. These comparators trigger the R and S inputs respectively, of an R, S Flip Flop made out of the two NAND gates. The transistors trigger the remote pen relay switch of the chart recorder resulting in the trace as shown in Fig. 3.25 (a, b. c). All this development was undertaken using the standard 50 kHz probe attached to the mortar specimen, and the results were quite successful (Fig. 3.28 a, b, c). For clarity the AE PIP traces have been photoreduced and traced omitting all the load lines except the acoustic emission noise itself. In addition, to allow for convention, this information has been inverted so that as one reads from bottom to top the load increases. Thus 3.28 (c) data is finally presented as Fig. 3.28 (b)

It is apparent from Fig. 3.28 that there are various characteristics of these PIP traces. These are discussed in detail in Chapter Four and here only certain points are highlighted. The AE noise develops from start to finish of the test, increasing markedly near failure, and can be used for failure prediction. The noise is unquestionably real AE and not a spurious signal as was evidenced by its "random", or sporadic, occurrence (and not on every cycle which would be the case if it were related to some machine phenomenon). Of particular interest is that for certain tests (for

example, moist and wet tests) there is substantially more acoustic noise at a particular point on the unloading portion of the loading curve, near minimum load, often forming a "mountain chain" appearance, Fig. 3,28 (b, c). This very interesting and reproducible result is discussed in Chapter 4.

3.6 Summary

(1) This chapter has described the experimental details of sample preparation and damage monitoring techniques. The sample preparations have been restricted to mortar compression prisms (excluding double torsion specimens which are covered in Chapter 7) and their constituent materials, fabrication and curing history. The physical testing facility, constituting the ESH fatigue testing machine together with various environmental controls, has also been described and standard static and fatigue test methods mentioned.

(2) The other major topics covered in this chapter include damage monitoring by means of strain transducers, ultrasonic pulse transit measurements and acoustic emission monitoring.

(3) This latter topic has been covered in some detail to explain standard AE testing, static test results and the Kaiser effect.

(4) The AE monitoring is extended to describe methods of detecting AE under fatigue conditions by simple frequency filtering based on spectral analysis. A simultaneous ultrasonic pulse transit time and AE damage detection method has been described which facilitates a three dimensional pseudo isometric means of data representation. Some results have been included as evidence of its capability.

With this extensive experimental background it is now in order to examine the results of mortar fatigue under particular frequency, waveform and environmental conditions and this is covered in the following chapter.

	Analytical Composition		Bogue Composition			Physical Tests		
	1st Batch %	2nd Batch %		1st Batch %	2nd Batch %	Test	1st Batch	2nd Batch
SiO_2	21.7	22.5	C_3S	49.7	54.6			
Fe_2O_3	2.4	2.3	C_2S	19.6	18.5	Setting Times		
Al_2O_3	5.6	4.9	C_3A	12.1	9.1	initial	100 min	80 min
						final	2h 45m	3h 05m
P_2O_5	0.4	1.0	C_4AF	7.3	7.0	Fineness		
CaO	64.1	63.6	$CaSO_4$	3.2	3.1	Blaine SS	5020 $\frac{cm^2}{gm}$	5050 $\frac{cm^2}{gm}$
MgO	1.3	1.6	Free CaO	2.2	1.2			
SO_3	2.3	1.8	MgO	1.5	1.8	Compressive Strength (to SABS 749)		
Ignitionloss	1.7	1.7				3 day cure	41.5 MPa	44.5 MPa
						7 day cure	52.0 MPa	55.0 MPa
TOTAL	99.5%	99.4%	TOTAL	95.6	95.3			

LVDT Probe	Range (mm)	Calibration Slope Deflection (mm)/mm unit of chart paper	Strain Scale Factor x 10^{-6} 100 mm Gauge Length	48 mm Gauge Length
A	± 5.0	0.00558	55.8	
A	± 0.5	0.00054		11.25
B	± 5.0	0.00565	56.5	
B	± 0.5	0.000568		11.83

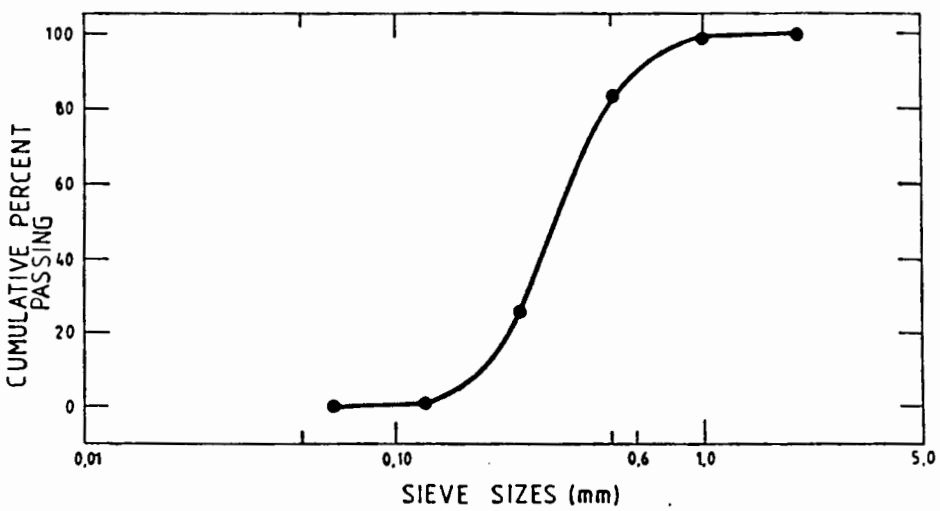

Fig. 3.1 Sand aggregate - sieve analysis

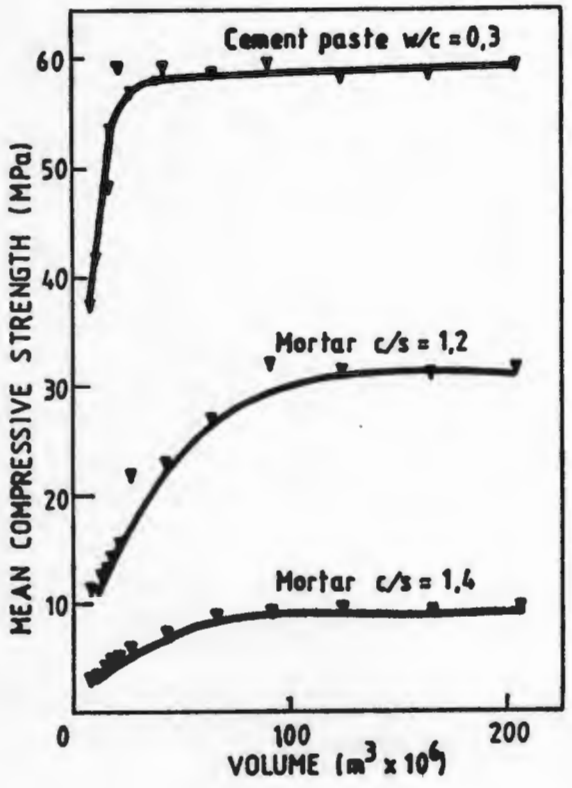

Fig. 3.2 A plot of mean compressive strength against the volume for cubic samples. (From Jayatilaka and Nanayakara (165).

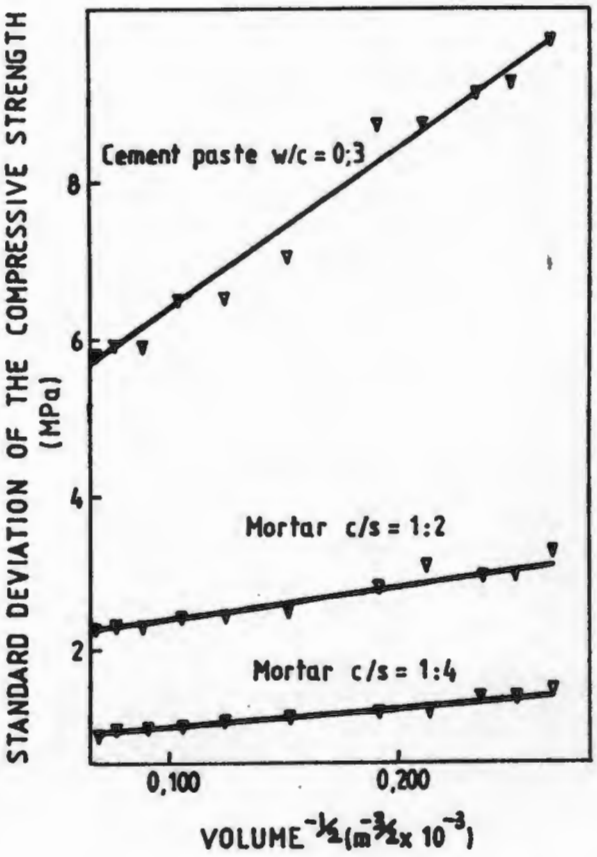

Fig. 3.3 Standard deviation of compressive strengths for a given composition and size shows linear behaviour. (From Jayatilaka and Nanayahara (165).

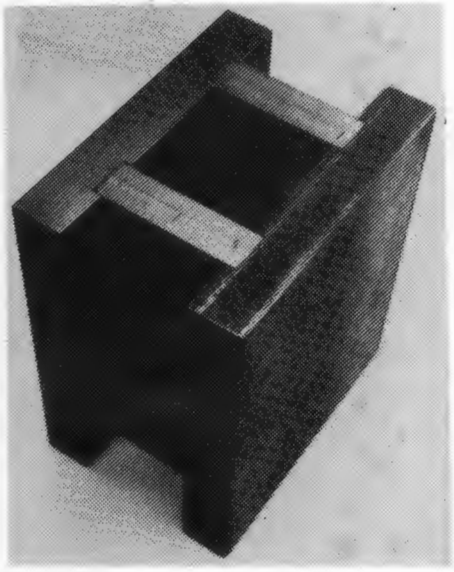

Fig. 3.4 Photograph of a prism mould.

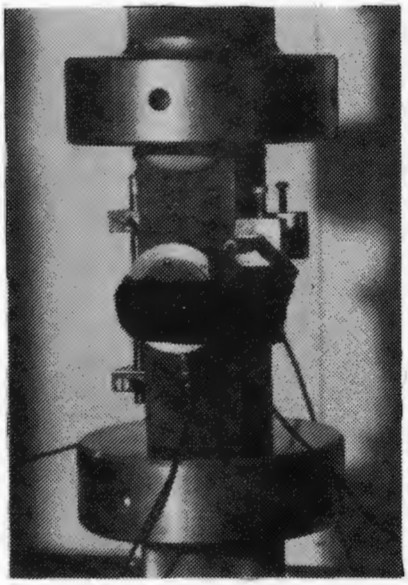

Fig. 3.5 Compression Specimen illustrating LVDT and ultrasonic probe attachments.

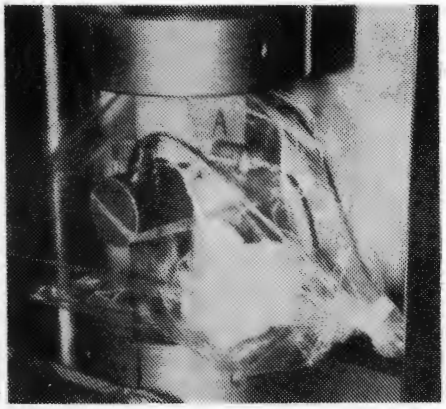

Fig. 3.6 Instrumented compression specimen inside its polythene container.

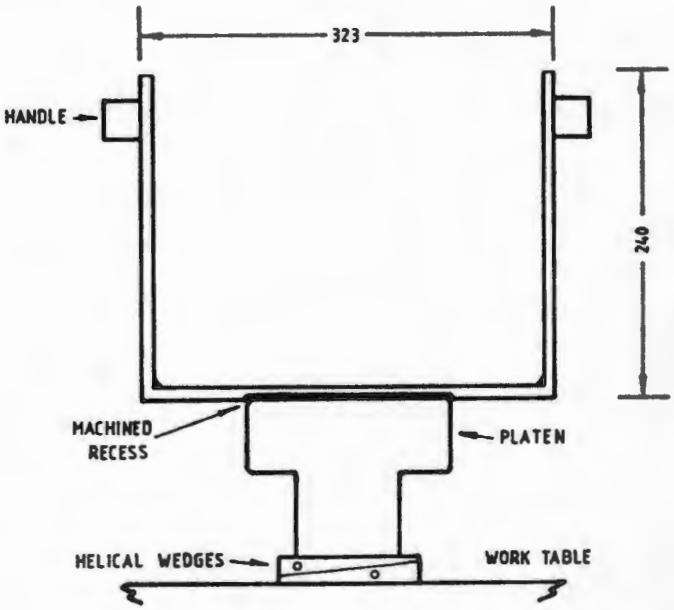

Fig. 3.7 Test chamber for underwater and temperature controlled compression tests. (Note recess for platten location).

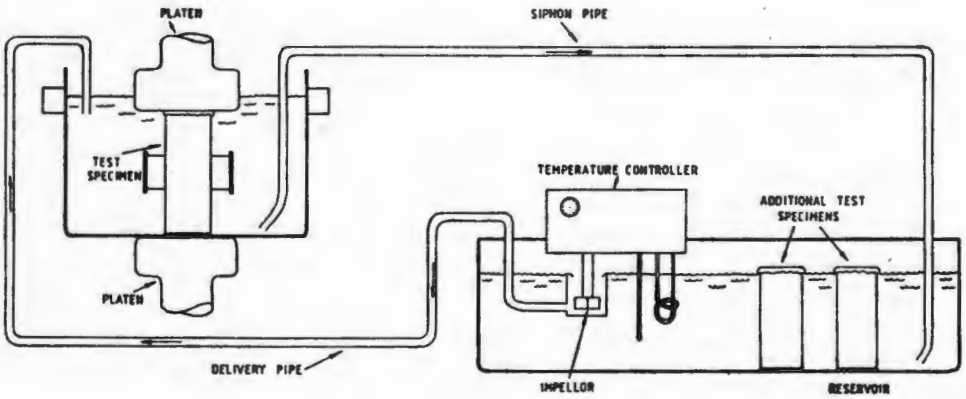

Fig. 3.8 Diagram showing hot water reticulation system for underwater and temperature controlled compression tests.

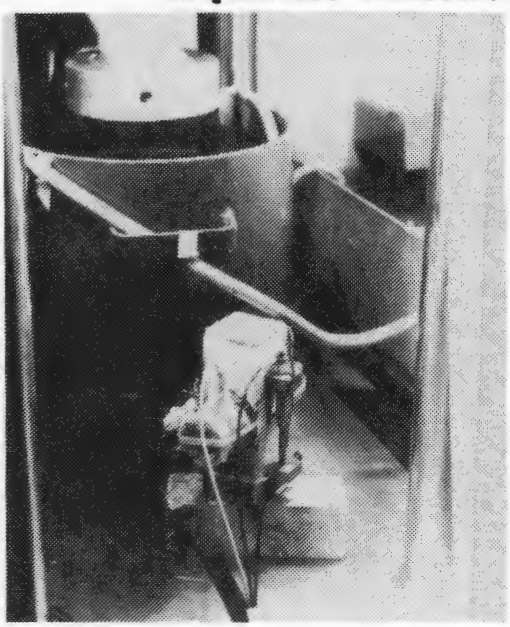

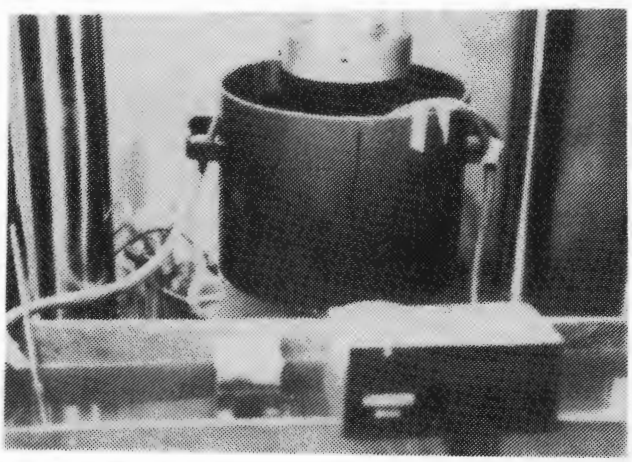

Fig. 3.9 Photographs of the general layout of the water reticulation and temperature control system for compression specimens.

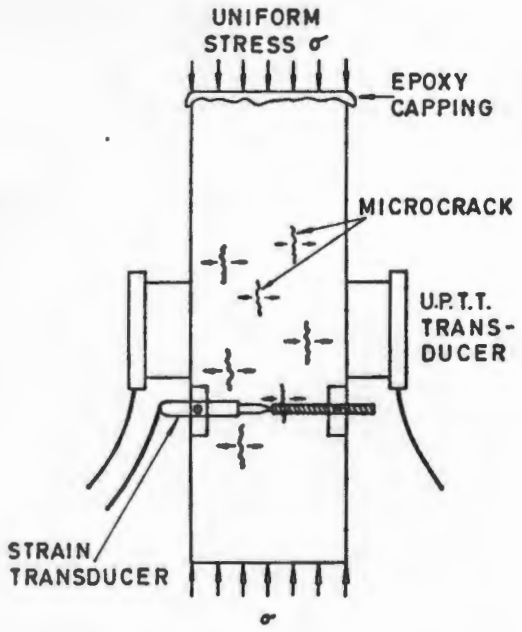

Fig. 3.10(a) Diagram of an instrumented compression prism. (Note the epoxy capping at the top and the vertical nature of the microcracks.)

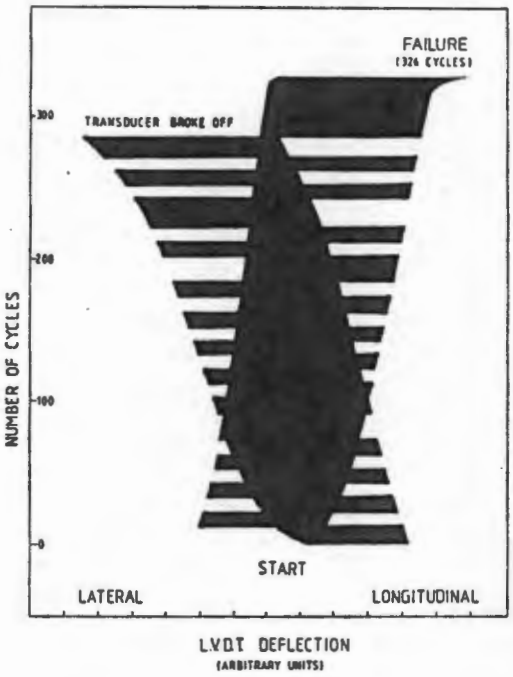

Fig. 3.10(b) Typical LVDT deflection trace for lateral and longitudinal "strains" during fatigue.

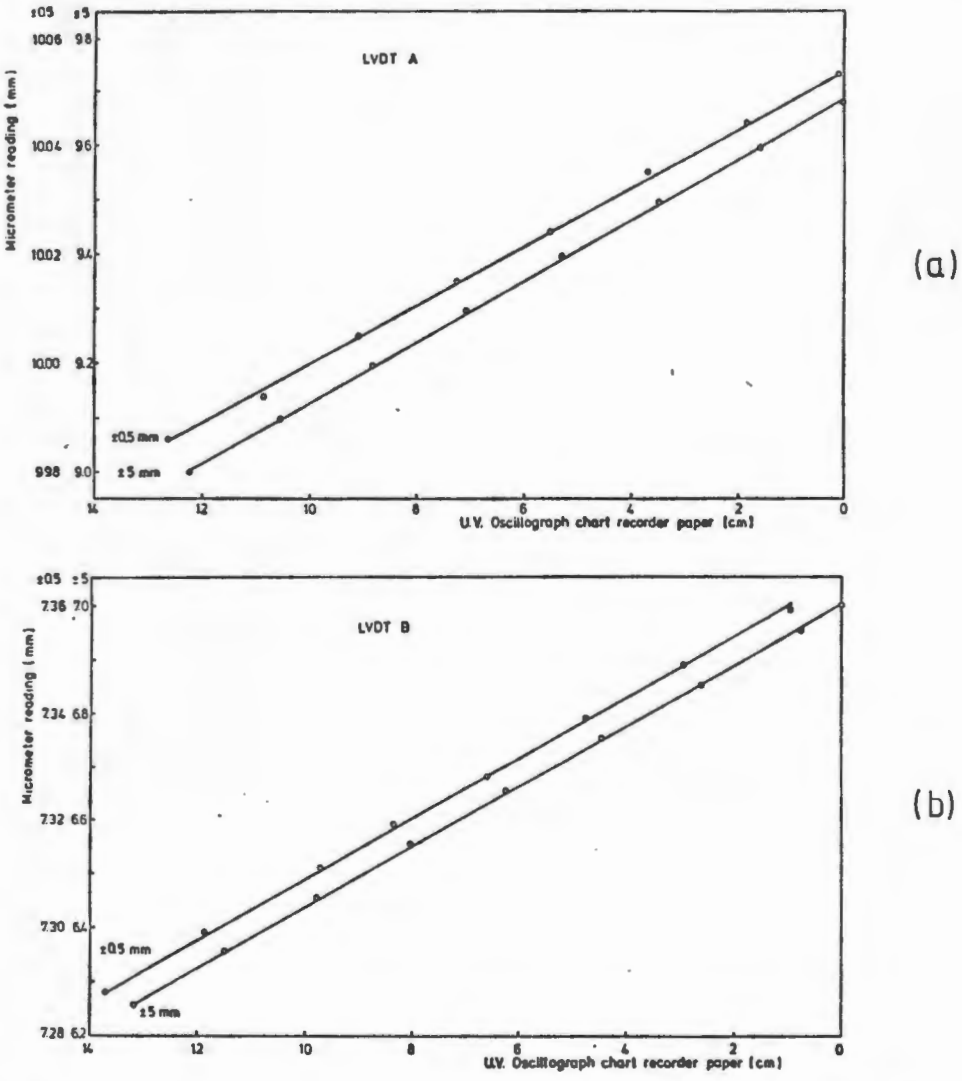

Fig. 3.11 LVDT strain calibration curve relating LVDT displacements to movements on the U.V. chart recorder "pen", (a) for LVDT 'A', and (b) for LVDT "B".

Fig. 3.11(c) Photograph of a waterproofed LVDT.

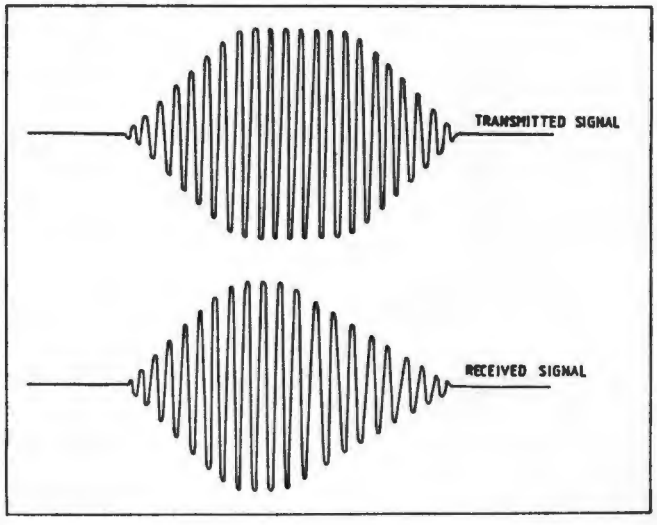

Fig. 3.12 Diagrammatic representations of the transmitted and received ultrasonic pulse signal.

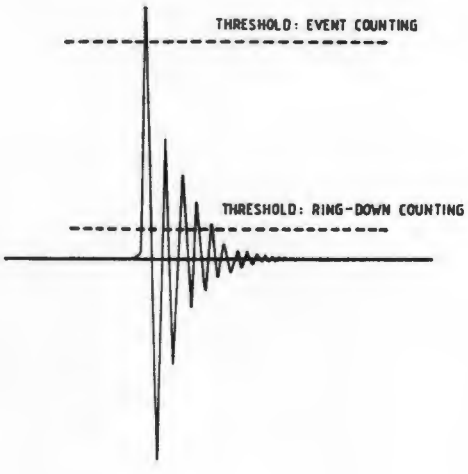

Fig. 3.13 Schematic oscilloscope trace of a typical single acoustic emission (or burst) event, illustrating the damped sinusoidal signal and how selection of the relative threshold level may affect counting mode.

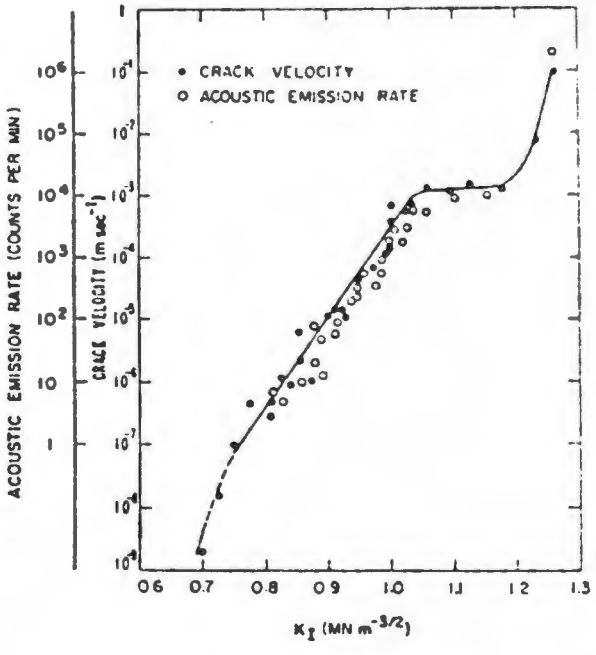

Fig 3.14 The variation of acoustic emission rate and crack growth rate with stress intensity factor for porcelain. (From Tetelman and Evans, (199).

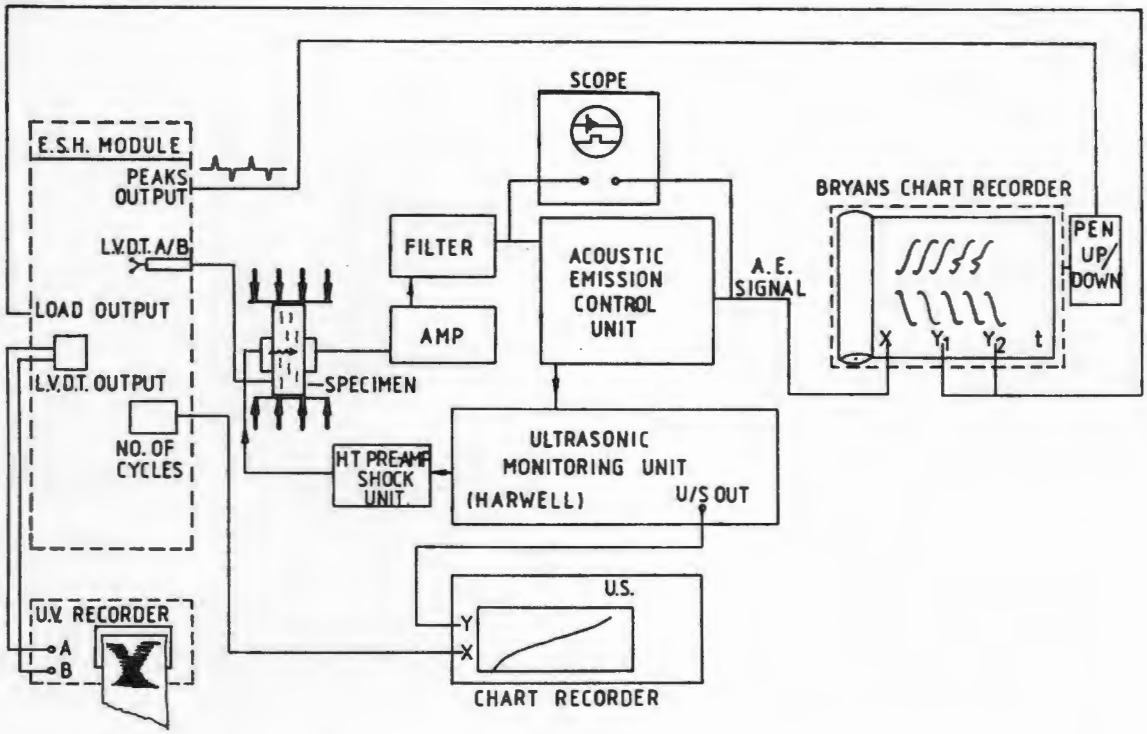

Fig. 3.15(a) Block diagram of the general layout of the whole compression testing facility, including damage monitoring.

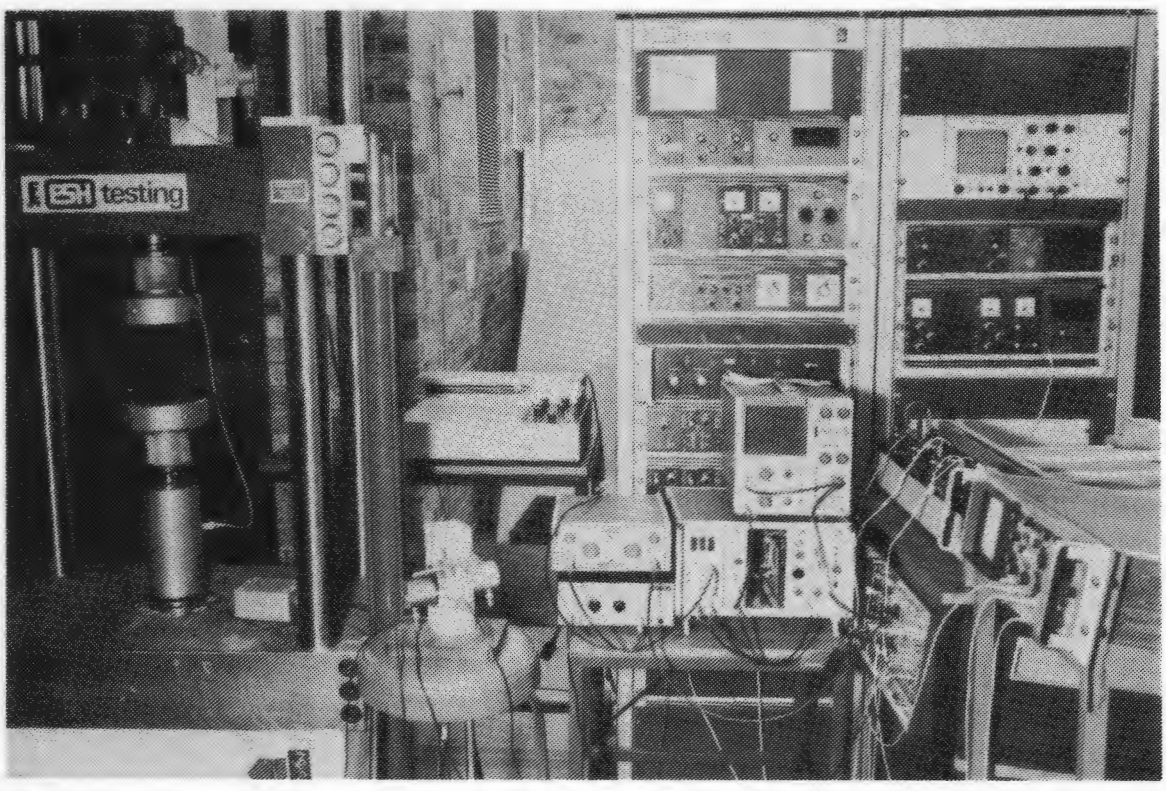

Fig. 3.15(b) Photograph showing general layout of compression testing system and associated 'strain', ultrasonic and acoustic emission damage monitoring systems.

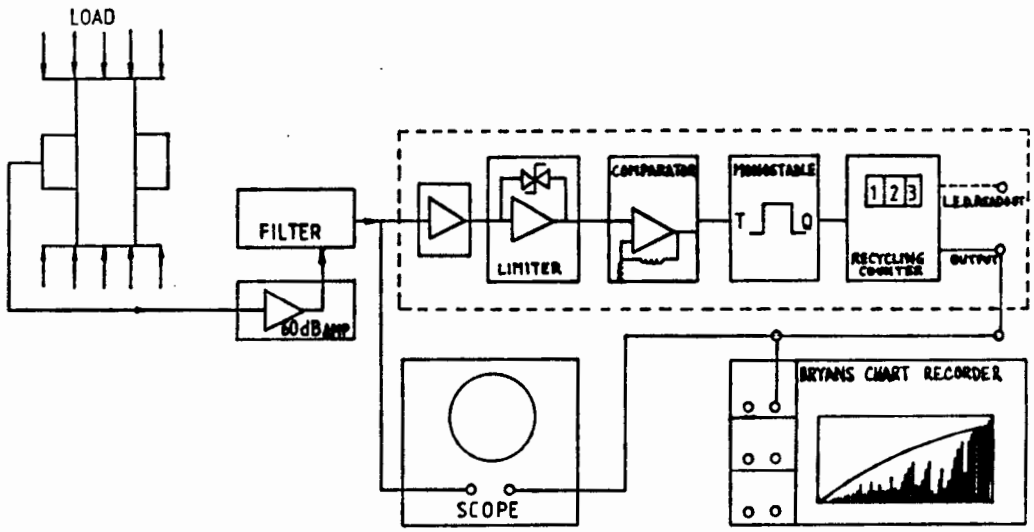

Fig. 3.16(a) Block diagram of A.E. monitoring system.

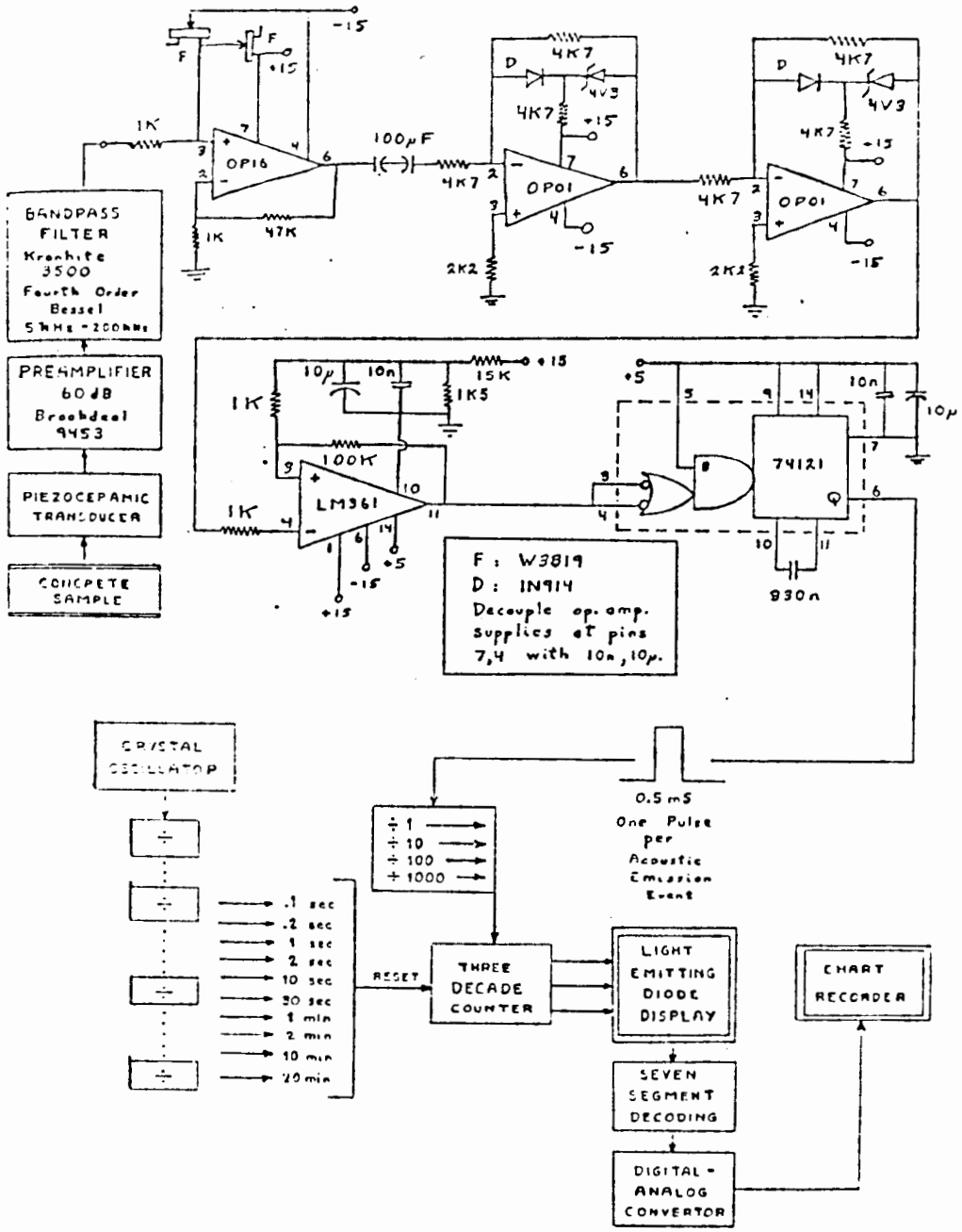

Fig. 3.16(b) Circuit diagram of the Acoustic Emission Monitor developed

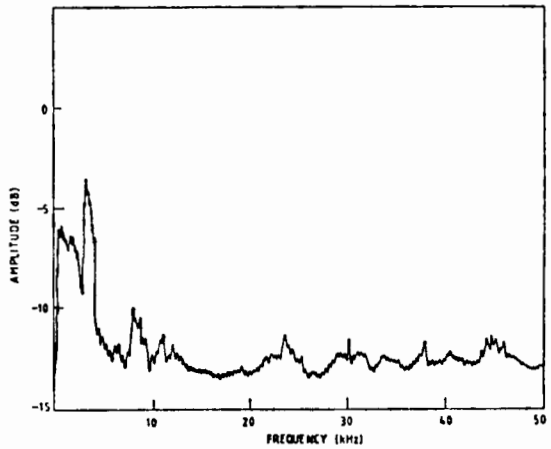

Fig. 3.17 Frequency spectrum of a typical captured AE event from mortar. (Note the small but definite energy content at frequencies between 20 kHz and 50 kHz.)

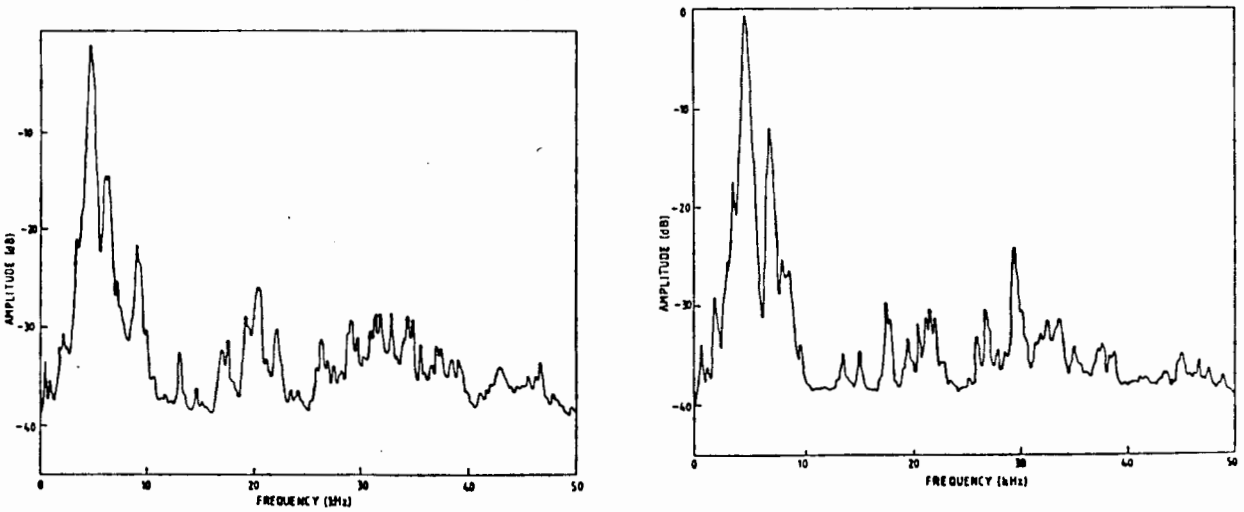

Fig. 3.18(a) and (b) Two frequency spectra of the ESH testing machine noise under two different load conditions. (Note that the amplitude of the signal above 25 kHz is very small).

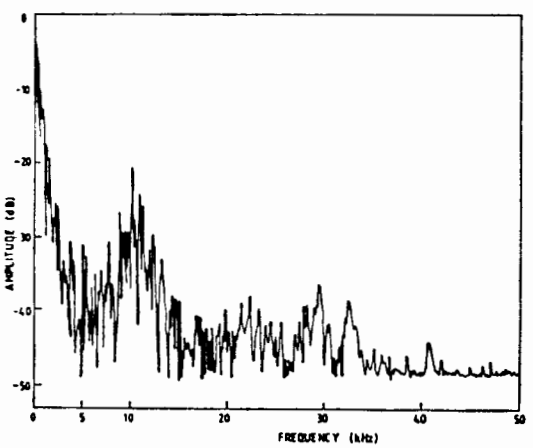

Fig. 3.18(c) Frequency spectrum of simulated AE from pencil lead fracture on a mortar prism surface.

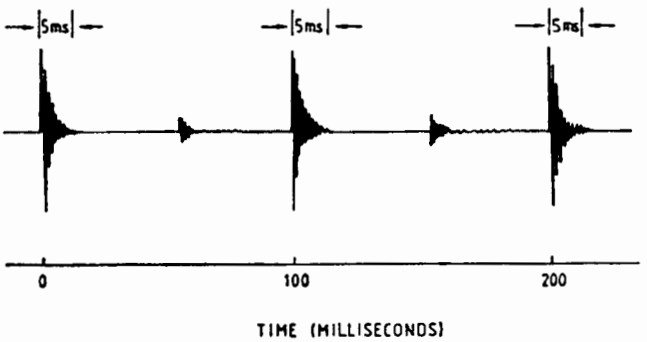

Fig. 3.19 Schematic illustration of burst nature of ultrasonic signal used in gating for simultaneous UPTT and AE (PIP) monitoring. (Not to scale).

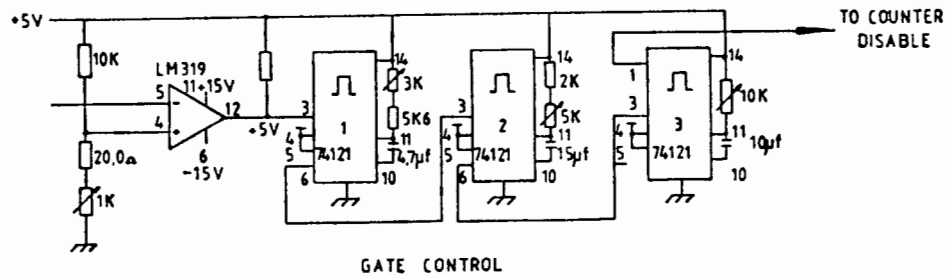

Fig. 3.20 **Circuit diagram for gate control to facilitate simultaneous ultrasonic and acoustic emission monitoring.**

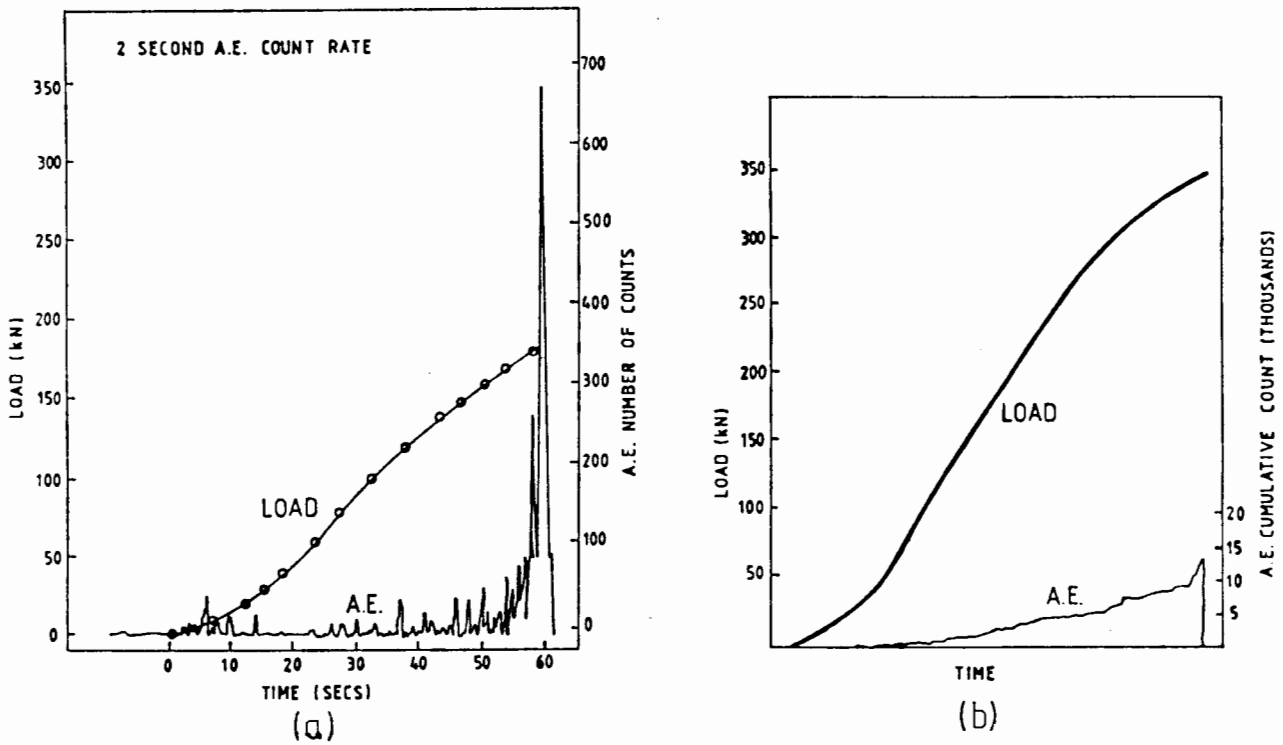

Fig. 3.21 Typical acoustic emission damage curves for static mortar compression tests, (a) rate counted and (b) cumulative counted.

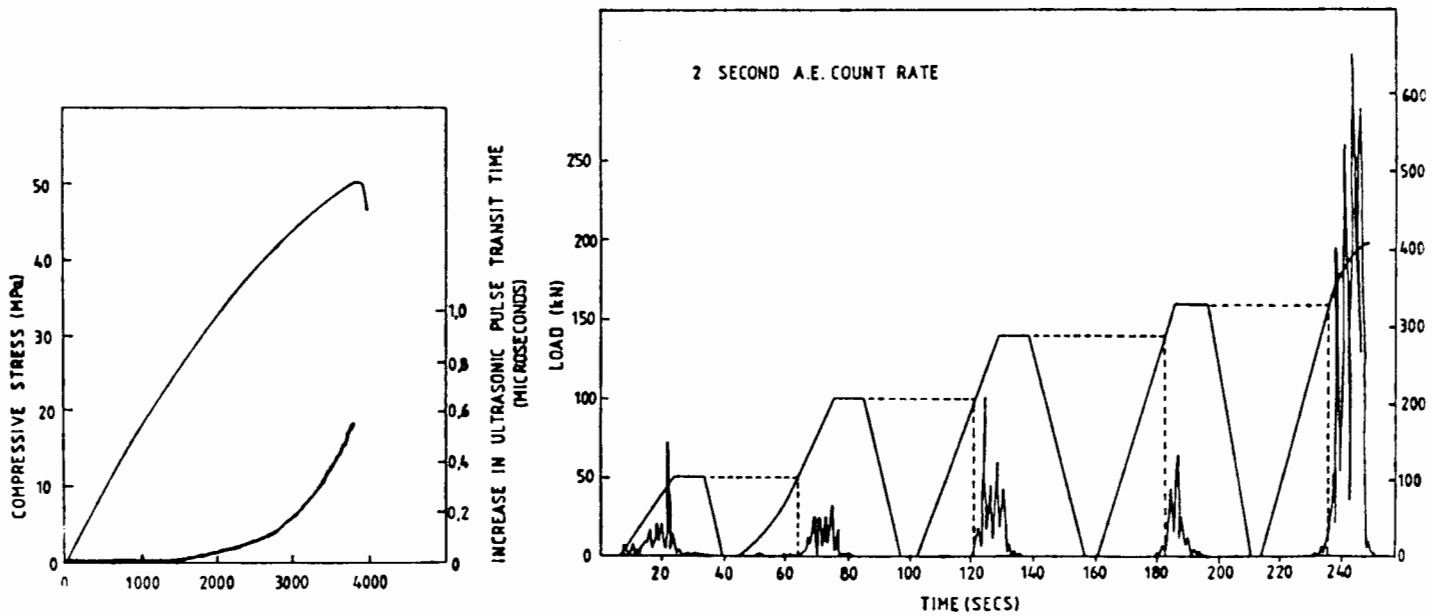

Fig. 3.22 Typical change in UPTT during a static compression test. The response is similar to, though less sensitive than, the corresponding AE monitoring (see Fig. 3.21 (a, b)).

Fig. 3.23 Illustrating the Kaiser Effect in cement materials (at loads less than 85% of ultimate). Note that no AE occurs until stress levels in excess of those previously experienced by the specimen are exceeded.

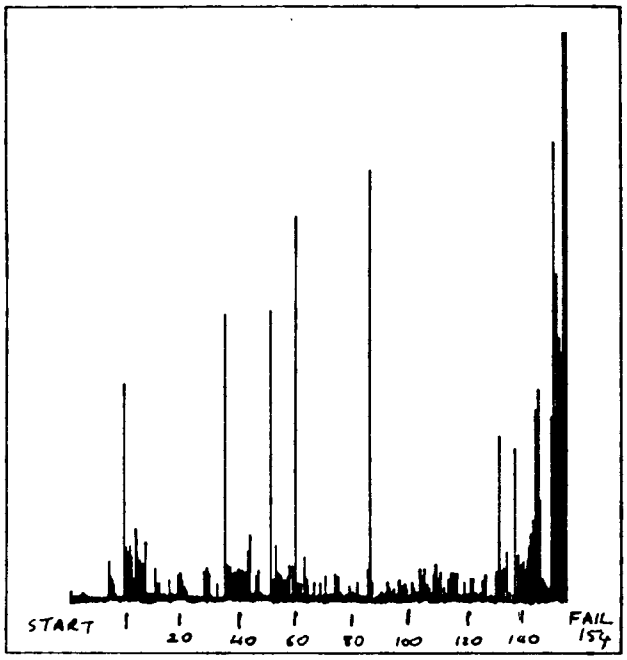

Fig. 3.24 Rate counted AE in a typical fatigue test. Note the large bursts of emission at approximately 60 and 85 cycles, as well as just prior to failure.

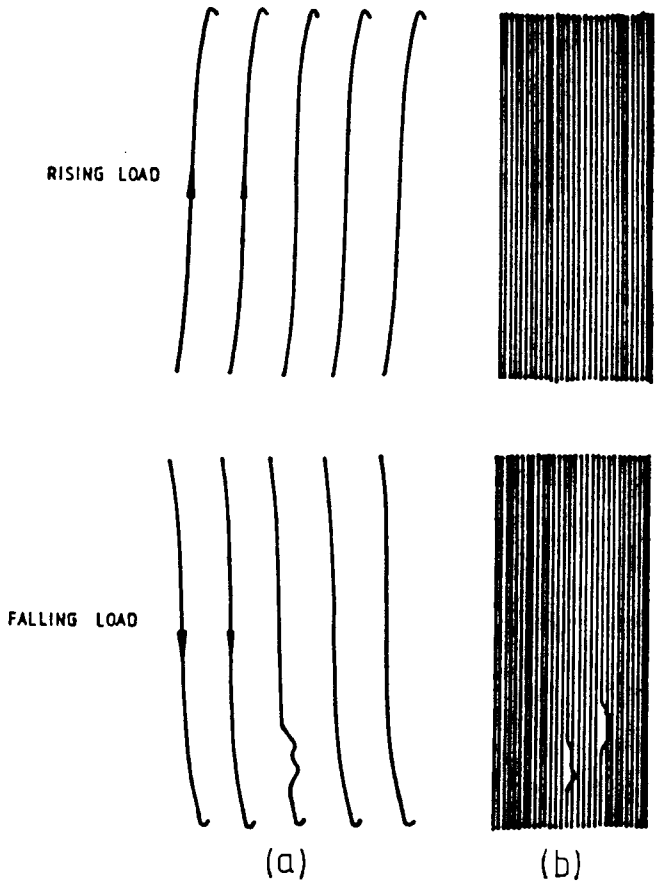

Fig. 3.25 Typical load versus time traces using the two pen pseudo isometric plot system, (a) at fast paper speed and (b) at slow paper speed. The lower signals in each case have AE.

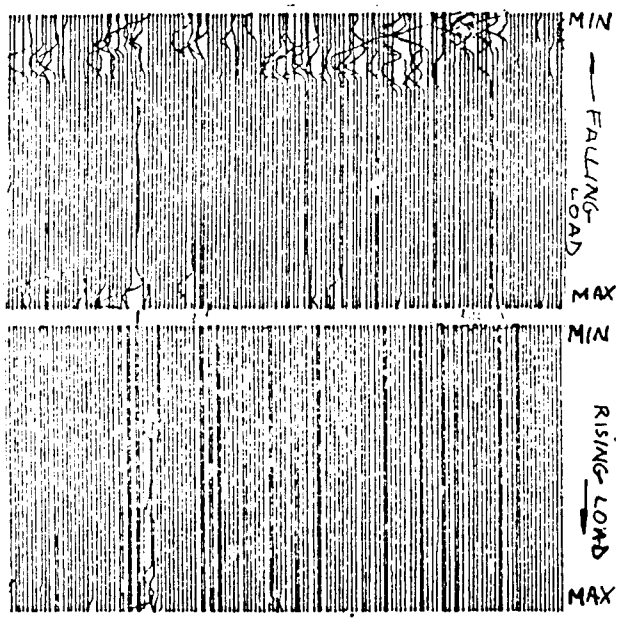

Fig. 3.25(c) Typical acoustic emission PIP trace showing noise on the unloading portion of the cyclic wave.

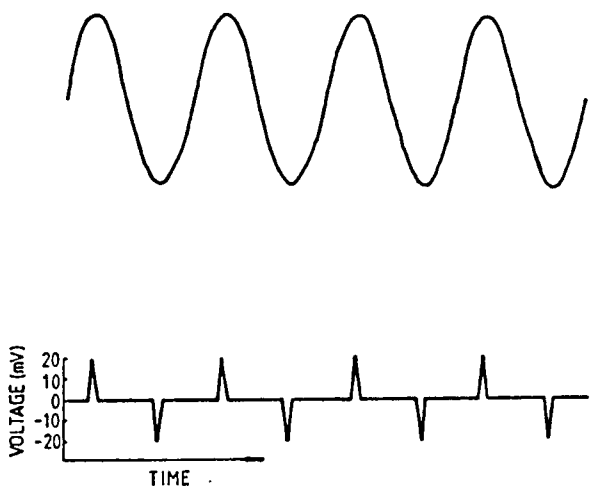

Fig. 3.26 Peaks overshoot facility (b) derived from (a) ordinary sinusoidal load waveform and used to trigger the alternating pen up/down facility of the PIP system.

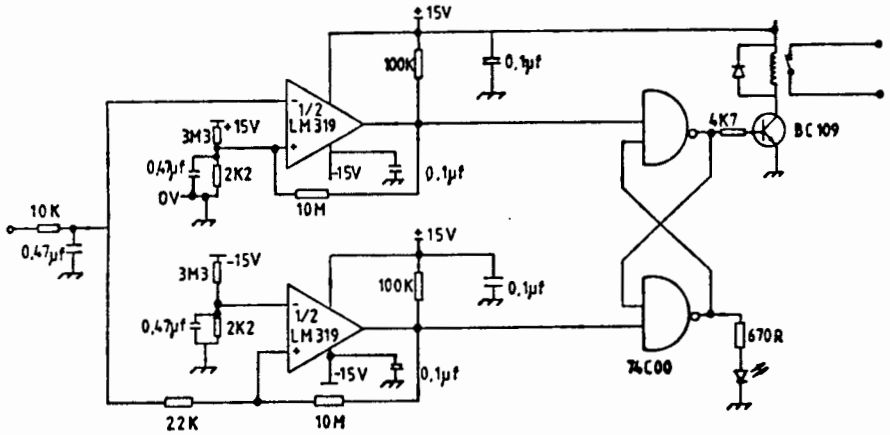

(a)

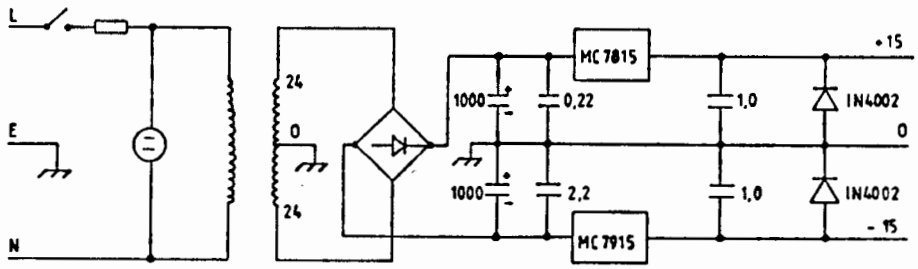

(b)

Fig. 3.27 Circuit diagrams for (a) the automatic pen control system and (b) its associated power supply unit.

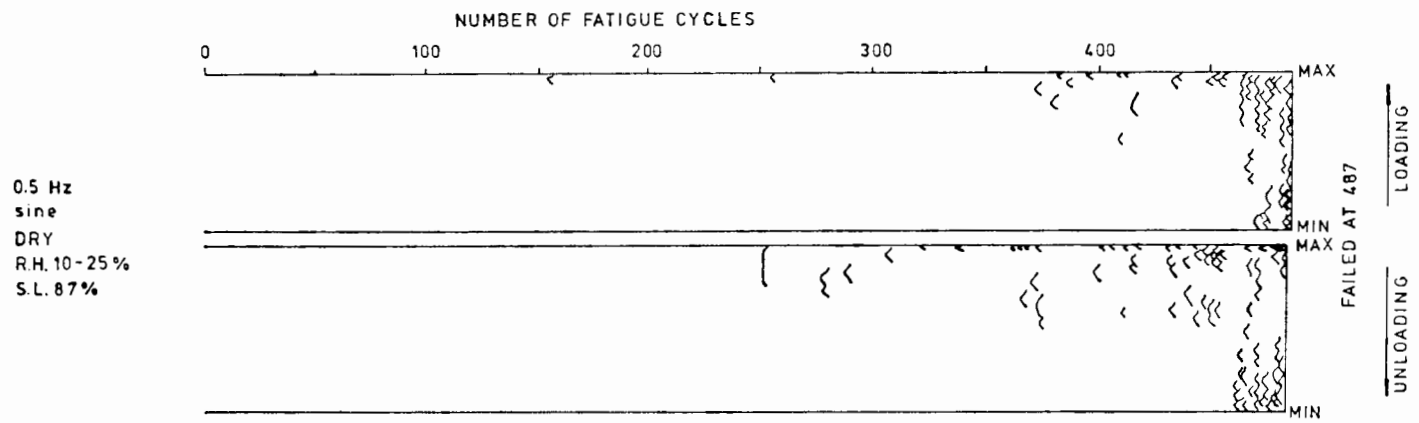

Fig. 3.28(a) Typical AE PIP trace after processing for a dry fatigue test.

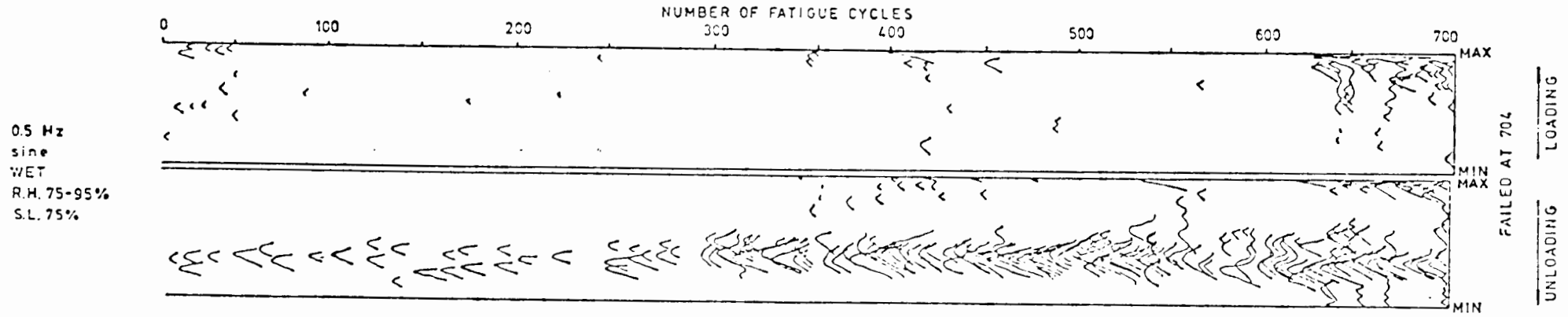

Fig. 3.28(b) Typical AE PIP trace of a 'moist' concrete fatigue test after "processing".

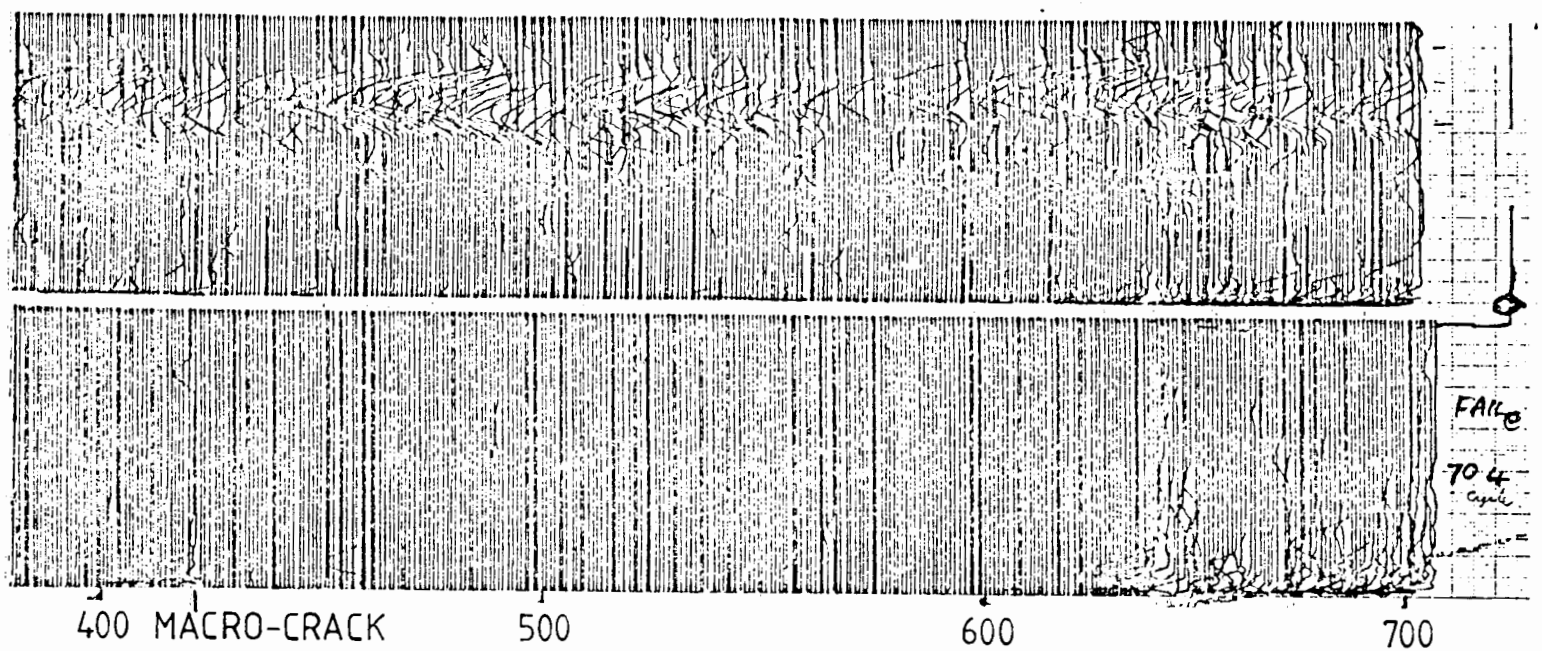

Fig. 3.28(c) Typical AE PIP trace of the moist fatigue specimen of Fig. 3.28(b) before processing.

"A veil 'twixt us and Thee, dread Lord
A veil 'twixt us and Thee:
Lest we should hear too clear, too clear
And unto madness see"

R. Kipling, Many Inventors, 1915.

CHAPTER FOUR : STUDIES OF COMPRESSION FATIGUE BEHAVIOUR

4.1 Introduction

Chapter 2 highlighted some of the shortcomings in the state of knowledge of fatigue in concrete under compression. In particular, from a review of the literature, it would appear that time or rate dependent parameters may have a significant effect on the assessment of fatigue damage. This chapter, then, reports on the results of experimental programmes conducted on over 280 compression fatigue specimens in an attempt to identify the role of time and its related parameters on fatigue behaviour. Some emphasis is obviously given to damage monitoring studies, the details and techniques of which have been described in the previous chapter, as it is believed that these techniques provide valuable insight into the mechanisms of damage development during fatigue.

The layout of the compression fatigue results presented in this chapter is as follows, with the influence of time dependent processes providing a unifying theme. Firstly, in Section 4.2, following a brief literature review of fatigue pertinent to this section, the general i.e. "standard" results of compression fatigue are reported together with the corresponding damage monitoring behaviour. This forms the data base from which one can better evaluate subsequent special cases of fatigue.

In Section 4.3 the subject of the effect of cycling frequency on the compression fatigue behaviour of mortar is discussed by first reporting previous studies on this topic and then presenting the results of tests performed at 0.1Hz, 1 Hz and 10 Hz.

The effects of waveform and load programme on fatigue behaviour are examined in section 4.4 with the emphasis again being placed on time dependent and damage accumulation processes. In particular, two sawtooth waveforms (fast loading versus fast unloading) are compared as well as the effect of cyclic range with a constant maximum load.

Since it was believed that time dependent processes must be important in fatigue and damage development, it is reasonable to consider that damage mechanisms may also be environmentally dependent and/or thermally activated. Section 4.5 reports on limited fatigue tests conducted underwater and at various (realistic) operating temperatures. Full damage monitoring under these environmental conditions presented considerable experimental difficulties, so this section is less comprehensive than the others.

The results and implications of the preceding four sections are discussed and summarised in section 4.6 but full mechanistic discussions are held over to Chapter 8.

4.2 General Fatigue Strength Behaviour

4.2.1 Introduction

As a precursor to the information presented in this Chapter, it is appropriate just to restate certain important aspects mentioned in the review of Chapter 7.

(i) 'SN' data is widely used to describe fatigue behaviour in cement-based materials, and typically there is no fatigue 'limit'.

(ii) The prevailing stress level in fatigue is conventionally 'normalised' through the test sample's corresponding static strength. Many variables have been shown to affect static and fatigue strength in the same way, therefore.

(iii) Time dependent effects in fatigue are controversial;

(iv) Damage accumulation in fatigue does not occur linearly, or even uniformly.

4.2.2 Standard Static and Fatigue Results

4.2.2.1 Typical Static Results

There was a significant difference in the measured static strength between 'wet' and 'dry' specimens. Batch strengths were typically 46 MPa and 67 MPa respectively with the standard deviation in the results less than 5%. Such reproducibility greatly facilitated the generation of subsequent reliable fatigue test data which depends on a knowledge of the batch strength and stress level. The development of damage during a standard static test was also recorded on several occasions, using ultrasonic techniques. A typical trace of the development of such ultrasonically-detected damage is shown in Fig. 3.22. Evaluation of 41 wet tests indicated that the change in transit time was 0.36 ± 0.08 μsecs while for 21 dry static tests the change was 0.75 ± 0.15 μsecs. An interesting aspect of the damage development in static testing, as monitored by ultrasonic methods, is that the trace of UPTT develops very gradually, only becoming noticeable above approximately 50 to 60% of maximum failure stress (see Fig. 3.22). Allied to this is the shape of the load deflection curve in this (typical) figure which shows extensive non-linearity near failure - again indicative of microcracking prior to failure.

4.2.2.2 Typical Fatigue Results

The fatigue test programme yielded the SN curve data as shown in Fig. 2.28. It is apparent from this SN curve that 'dry' test specimens exhibit a longer fatigue life than corresponding 'wet' specimens. (Similar behaviour for the rate of growth of individual cracks as opposed to bulk damage, was observed in the double torsion test programme - see Chapter 7).

The present SN curve results indicate that mortar does not appear to have a conventional fatigue limit. The fatigue strength at 10^7 cycles, from the present data is approximately 54% for the 'wet' specimens and 64% for the 'dry' specimens. These results are comparable to variously reported fatigue strengths in the range 50% to 55% at 10^7 cycles (26, 132, 133, 135, 137, 140, 145, 148).

It was noticed that there was a distinct increase in temperature of wet specimens during fatigue tests performed at 10 Hz. An investigation of this phenomenon was undertaken using conventional thermocouples inserted into 2mm diameter and 10 mm deep holes in the central portion of compression specimens. Three fatigue tests on "wet" specimens in their polythene containers at 50% stress level, yielded temperature increases of 21°C, 24°C and 19°C, after between 4 and 6 hours of fatiguing (by which stage the temperature had equilibrated). Such a temperature increase was presumably due to the relatively large energy input at 10Hz, bearing in mind the hysteresis nature of the stress strain curve, and was specific to wet specimens. The corresponding temperature increases on two dry 10Hz fatigue specimens was only 1.5 and 2°C. The effect of such temperature increases during fatigue, especially with respect to accelerated curing, are discussed in Chapter 5.

4.2.3 Damage Development in Fatigue

The development of damage or microcracking that occurs in mortar as a result of fatigue was monitored continuously using the strain, ultrasonic and acoustic emission methods already mentioned. Damage development is progressive but non-linear, and typical results for each technique, and the implications thereof, are discussed in turn.

4.2.3.1 Strain Monitoring

For each fatigue specimen both lateral and longitudinal strains, for both elastic and residual cases, were measured as described in section 3.5.2. Typical results are shown in Figs. 4.1 (a), (b), for 1 Hz tests at 80% stress level in a "moist" condition (RH.$>$ 75%). Various characteristics are apparent from these typical results. The elastic strains tend to increase approximately linearly at this stress level, although at lower stress levels (e.g. for 'run out' tests) the elastic strains tend to stabilise and not increase. Longitudinal and lateral strains vary similarly although the magnitude of the elastic strains for the longitudinal case tend to be larger than the lateral case (approximately 2000 microstrains cf. about 700 microstrains).

Since the fatigue tests were conducted under load control conditions between fixed load limits, the increase in elastic strain (as defined) implies a softening or decrease in modulus, consistent with the available literature on this topic (See, for example, Figs. 2.29 and 2.33).

With regard to the residual strains the longitudinal and lateral values are again similar as might be anticipated. These results closely parallel those obtained by both Bennett and Muir (96) and Shah and Chandra (89). The shape of the traces tend to vary between approximately linear to slightly sigmoidal. In this latter case, which was by far the most common, this sigmoidal shape of the residual strain curves is interpreted as follows: (i) there is an initial rapid development in damage or microcracking in the first few cycles; (ii) this is followed by an approximately linear increase in damage and gradual slow crack development until just before failure, where (iii) the strains increase rapidly as cracks coalesce and the structure can no longer support the fatigue loading, and failure ensues.

Such changes in the residual strain may be regarded as an accumulation of damage or microcracking with fatigue (27, 89, 96, 139, 143). This was reported by Williams as far back as 1943 (139) when he noted a progressive increase in strain with fatigue with a marked increase near failure. Similar findings have been reported by Bennett and Raju (143), Bennett and Muir (96), and Awad and Hilsdorf (27). Elastic and residual strain results for prisms of different mixes are shown in Fig. 4.2(a). Bennett and Muir (96) also conclude that aggregate size does not appear to affect residual strain. Awad and Hilsdorf (27) and others (173) also report an increase in both lateral and longitudinal residual strain with number of cycles (Fig. 4.2(b)). They further report that the strains at failure are longer as the stress level is reduced or (more significantly) as the time to failure is increased.

Comparison of the author's present static and fatigue ultimate strain results indicate that the fatigue strains, of the order of 1 000 to 2 000 microstrains, are somewhat larger than the corresponding static strains, found to be in the range 400 to 1 000 microstrains. These results are comparable to similar results in the literature (27, 89), although Bennett and Raju (143) found cracking was developing at tensile strains as low as 200 microstrains.

The longitudinal and lateral strains yield similar information as far as damage development is concerned, although the residual strains in both cases tend to be more informative than the elastic strains. Although the longitudinal strains are greater than the lateral strains (Fig. 4.1), these latter (i.e. lateral) are more sensitive to detecting changes (see section 4.3.3.1). Thus the lateral residual strain measure of damage accumulation has been used in all future discussion except where longitudinal and elastic strains lend added insight to the understanding of the fracture process.

4.2.3.2 Ultrasonic Pulse Transit Time (UPTT) Monitoring

The UPTT changes in a manner similar to that of the residual strains exhibiting a 3 stage process (Fig. 2.30). For relatively high stress levels (i.e. above approximately 70%) there is an initial rapid increase followed by an approximately linear change in transit time. The third stage of rapid increase occurs as microcracking increases significantly and failure occurs. A typical trace of ultrasonic change (UPTT) in a fatigue test is shown in Fig. 4.3 which was obtained from an 80% stress level, high humidity (R.H. $\geq$75%), 10Hz tests.

It is of value to confirm that the UPTT measurements and changes are related to damage and microcrack development and are not due to some other phenomena, such as changing moisture content. Accordingly, ultrasonic probes were attached to a specimen immediately after removal from the curing bath and the specimen left to equilibrate in its polythene container. A typical result is shown in Fig. 4.4, which indicates that the transit time increases as the mortar equilibrates by approximately 0.1 to 0.15 microseconds, during the initial 40 minutes (approximately) but remains constant for at least the following 24 hours, as long as no load is applied.

Since all the 'wet' fatigue tests required between 30 minutes and an hour to affix the strain gauge stubs and generally set up the damage monitoring equipment, it was believed that during fatigue there was no change in UPTT due to phenomena other than microcracking.

Similarly, arrest of the fatigue cycling and removal of the load leads to a reduction in the UPTT as the specimen relaxes and any cracks and microcracks

partially close up in an anelastic manner (Figs. 4.5, a, b, c). The recovery apparently depends on the stress level and percentage life (i.e. on the amount of microcracking) but is typically of the order of 0.1 to 0.3 microseconds. The results of the fatigue tests shown in Figs. 4.5(b) and (c) are on an expanded vertical scale and contracted horizontal scale. These fatigue tests (10 Hz, 80% stress level, moist) illustrate the rapid initial microcracking increase, as monitored by UPTT, in the first few cycles.

The rate of this UPTT change rapidly decreases to become approximately linear and is dependent on stress level and, apparently, frequency. This further highlights the difference between static and fatigue tests since for static tests the UPTT change develops gradually as the load is increased. In the fatigue case there is significant internal damage and microcracking even after the first few cycles.

During load removal and rest periods from one minute to 25 minutes there is partial recovery of the transit time up to approximately 0.3 microseconds. On restarting the fatigue cycling, however, the UPTT signal returns to its original (pre-rest period) value and fatigue proceeds as if the rest had not occurred. It can be concluded, then, that significant microcracking damage occurs in the first few cycles and there is no discernible crack initiation period. Residual strain traces exhibit, as may be expected, a similar recovery, and the LVDT traces also restart at the same value when cycling is recommenced.

It is also interesting to compare the difference in absolute changes in UPTT, between static and fatigue tests: this typical change in UPTT in fatigue is typically 2 to 4 microseconds. The transit time change during a static test is, however, approximately 0.36 microseconds for wet tests and 0.75 for dry tests. This would again seem to indicate that there is extensively more damage - leading to changes in UPTT - in fatigue tests than in static tests. Similar results were reported by Raju (193), Fig. 4.6(a), which are comparable with the results of Fig. 2.32 for strain tests. The characteristic increase in transit time as failure is approached is evident in Fig. 4.3 and 4.5 (b) and (c).

Such changes in ultrasonic transit time behaviour have also been noted by other workers (89, 143, 193), particularly Shah and Chandra (89), whose compression results at 80% stress level (but for larger specimens) are shown in Fig. 4.6(b). Studies by Raju (193) and Bennett and Raju (143) on the decrease in pulse velocity transverse to the direction of loading, indicated that such decrease depended only on the percentage life. They obtained ultimate decreases in velocity of between 25 and 35% (Fig. 4.7). The author's results are comparable in that, for one test series, the UPTT average change was 3.1 microseconds in a total of 11.3 (i.e. 27%) for wet tests and 4.6 microseconds in a total of 12.2 (i.e. 38%) for dry tests. The apparently longer UPTT change in 'dry' tests presumably arises from the greater propensity of drying and shrinkage cracks which can open up and proliferate, in comparison to wet tests. A larger increase in UPTT was also reported by Bennett and Raju (143), with increasing time to failure as opposed to, simply, stress level or number of cycles. Corresponding increases in residual strain with time were also noticed and the concept of a form of stress corrosion cracking in concrete, proposed (89).

4.2.3.3 Acoustic Emission Monitoring in Fatigue and Pseudo Isometric Plots

The general results of acoustic emission monitoring have already been mentioned in section 3.5.4. In that section the acoustic emission associated with static tests was described together with the Kaiser Effect studies. With regard to acoustic emission in fatigue, the discussion so far of results has noted that simple rate counting of events as a function of number of cycles (see, for example Fig. 3.24), gave little further information as to the microcracking process. Efforts to determine where (on the load cycle) these acoustic events occurred led to the development of the pseudo-isometric plot (PIP) technique.

This was shown to be successful in the previous chapter, (Figs. 3.25 and 3.28). This section describes typical PIP results and their characteristics, from which certain information about microcracking in fatigue may be described. It should be borne in mind throughout, however, that these results were obtained using a high cut-off band pass filter with a passband between 45 kHz and 200 kHz. It is possible (although unlikely), that events occur which have a low frequency spectrum, which would thus be missed by this technique. The studies so far, however, would seem to

indicate that AE events have sufficient energy at frequency components in excess of 45 kHz for successful detection. All the tests were also conducted under identical gain setting thresholds and A.E.M. equipment conditions.

Pseudo Isometric Plot Results

The PIP technique in effect adds a third dimension to damage monitoring and there are several more characteristics derived from the application of this method which can be identified. In particular, these may be described as:

(i) Correlations - of particular AE events (from, for example, a macro crack) with the other damage monitoring techniques of ultrasonic pulse transit time and strain monitoring (as well as audio recognition of such a major event);
(ii) "Chains" - frequently the occurrence of noise on, or near, the same loading portion of a test over several cycles led to a "mountain chain" or topographic appearance;
(iii) Warnings - of impending cracking or damage on the one hand, and impending failure on the other, had an associated characteristic acoustic signal (which was normally large, near the maximum load portion, and led to increased acoustic activity);
(iv) Other Characteristics are also mentioned in turn which relate, for example, to frequency, environmental conditions or temperature.

These identifying characteristics are discussed consecutively together with some interpretation of their significance. An attempt is also made to distinguish between qualitative and quantitative interpretation of the data. The PIP traces included here have been carefully selected from 159 valid PIP tests to illustrate the various observations and should be regarded as representative.

Perhaps the most significant general characteristic of the pseudo isometric plots is that the noise occurs sporadically or intermittently, or may be described, at first glance, as being "random" in nature. In particular, the AE noise as recorded does not occur on every cyle or even after a particluar set of cycles. It is also intermittent with respect to number of cycles or load, although there are certain definite trends which are described below. The inference from this sporadic occurrence of recorded noise is that it

corresponds to real acoustic emission arising from stress waves associated with microcracking. That the recorded signals are real and not spurious is without doubt and is further confirmed by other correlations, to follow. This sporadic or intermittent occurrence is evident in all the subsequent PIP traces (see, for example, Figs. 3.25 and 3.28 in Chapter Three and, indeed, any PIP trace reported in this chapter).

Another general characteristic of the PIP traces is that the amount of noise increases with fatigue life and there is generally most noise just before failure (Fig. 3.24). Some specimen types are particularly quiet but these are discussed subsequently as exceptions, and this general observation, of noise increasing near failure, is almost universally valid, in the observations made. The sporadic nature of the AE events is still maintained despite the increased activity: (Figs. 3.28 (b) (c); 3.25 (c), and Fig. 4.8(a), (b)). The amplitude of the AE signal often increases near failure, (Figs. 3.24, 3.25(c), 3.28(b), 4.8(a), (b)). it might be expected that such cracking noises get "louder" near failure as stress wave emission increases from increasingly large cracks. Otherwise, remote from failure, the amplitude of the ordinary sporadic AE events tends to be approximately constant. The other general characteristic of the PIP tests is that acoustic noise often occurs from early on in the fatigue test, i.e. from an early stage in its life. This is evident from the PIP figures mentioned so far, but it should be noted that this characteristic, while present in most cases, is not as universal as, say, its sporadic nature, depending on other circumstances.

(i) Correlations

One of the more exciting observations of PIP acoustic emission studies is its correlation with other (ultrasonic and strain) damage monitoring methods on the occasion of a particular event. This "event" or occurrence is usually something unique and large scale such as, for example, the development of a large crack, or so called "macrocrack". Such a crack can sometimes develop at a corner of the prism, resulting in the small (pyramidal) corner chip falling off, or beneath an LVDT stub which may also subsequently break off. By far the most common, however, are large longitudinal cracks which develop in the specimen as the result of fatigue.

It is, firstly, relevant to note the 'standard' behaviour of damage development and how the various monitoring methods correlate in a specimen before so called 'anomalies' are examined, (although these latter are often equally informative). Fig. 3.28(a) shows the normal development of AE noise with fatigue life for a dry specimen (RH 25%, sine wave, 0.5Hz, S.L. 87%). The corresponding ultrasonic pulse transit time trace for this test is shown in Fig. 4.9, which is also completely conventional and well behaved. (Fig. 4.3 shows another standard ultrasonic fatigue result). The trace, (photocopied from the original) indicates the elapsed number of cycles and also the change in UPTT, in microseconds (from an arbitrary offset timebase).

Deviations from this standard behaviour of slow microcrack development are shown up graphically by the damage monitoring systems. Figs. 4.10(a), (b), (c), show respectively the AE, PIP, change in UPTT and lateral LVDT strain results for a 0.1Hz dry test which lasted for 84 cycles. (Note: for clarity, the amplitude of the AE signal has been amplified 5 times, in this particular case only). The ultrasonic (UPTT) trace is approximately well behaved except for two macrocracks which developed; one after 42 cycles and the other at 77 cycles. Both cracks were also heard by the author. The ultrasonic trace correspondingly has major deviations at these numbers of cycles. The lateral LVDT strain signal, Fig. 4.10(c), also exhibits deviations and increases at approximately 42 and 77 cycles if the trace is examined carefully. The AE PIP trace (Fig. 4.10(a)) also exhibits major noise at 42 and 77 cycles in correlation with the strain and UPTT results, but it is interesting to note that there is more warning of the first crack (at 42 cycles) developing by the large amount of acoustic activity, prior to the actual macrocrack's appearance. This appearance of a macrocrack thus "relaxes" the noise sources associated with the crack's prior development and consequently there is almost no noise immediately afterwards. Near failure (i.e. at 77 cycles) the amplitude of the noise is much greater, and so is the crack much larger, with little warning and final failure follows soon after. The value of the PIP technique is now apparent in that it can provide further, more detailed evidence of microcracking than conventional ultrasonic or strain monitoring methods, and also give warning of major cracking or impending failure.

A similar correlation between UPTT and AE PIP is apparent in Fig. 4.11(a) and (b), for a 'dry' slow test (RH 25%, 87% SL, Sine, 0.1Hz life 252).

Significant cracking, developing from approximately 130 cycles led to an audio crack at approximately 144 cycles and a macro crack occurred at peak load at 165 cycles. As might be expected this was followed by a comparatively quiet spell. Since dry tests do not normally exhibit much acoustic noise this unexpectedly noisy behaviour implied that a crack was developing which was undetectable by other means, only manifesting itself on the UPTT signal at approximately 143 cycles.

In the ensuing cracking and noise up to 165 cycles the lateral LVDT transducer partially broke away, as its mortar footing became fatigued. Having thus become inoperative, this LVDT was gently removed by the author at approximately 175 cycles which resulted in some "noise" on the PIP trace. The AE-PIP technique could thus be used reliably to predict some macrocracking event, such as a corner chip failure, from an apparently sound fatiguing specimen, and provided many interesting demonstrations.

Further correlations of audio macrocracks with PIP were evident on test 704 (Fig. 3.28(b)) at about 420 cycles and test 1050 (Fig. 3.25(c)), at approximately 830 cycles. Other acoustic emission (but not PIP) results for this latter test further supports such macro cracks at approximately 505 and 830 cycles respectively (Fig. 4.12).

(ii) Chains

It was mentioned earlier that a characteristic which was often, but not always, observed (depending on test conditions), was that of so called "mountain chains". The sporadic or intermittent nature of the AE noise is, however, maintained, even in a chain. Examples of such chains have already appeared in Figs. 3.25(c) 3.28(b), (c) and 4.8(a), (b). With reference to such figures, it is particularly interesting and perhaps surprising to note that such chains only appear to occur on the unloading portion of the PIP trace, an often near the minimum load. Further evidence of this phenomenon is shown in Fig. 4.13, which also exhibits the characteristic of increased noise near failure.

Examination of the chains and their occurrence indicated that they occurred only under wet or moist conditions (relative humidity $> 75\%$), but that fatigue tests under such conditions did not necessarily imply that chains

would always occur. A quantitative estimate of tests conducted under such moist conditions revealed that chains occurred in approximately 3 out of 4 tests (i.e. 39 out of 53 tests). When chains did occur, however, they were almost always on the unloading portion of the load curve near the minimum load. A quantitative measure of this was obtained by plotting a histogram of occurrence against load (Fig. 4.14(a)). This figure clearly indicates the predominance of chains near the lowest unloading load. As the specimen approaches failure there tends to be more noise at all load values; although the chain is maintained. Figs. 4.13 and 4.8 indicate this but no quantification was attempted.

The length of the chains, and at what stage during the fatigue life they occurred, as a function of the percentage of the fatigue life of the specimen, was also quantified. Fig. 4.14(b) shows a histogram plot of the number of times a chain of a certain length occurred. The probability of chains became more numerous and tended to build up towards failure, as is evident from Fig. 4.14(b). This figure also shows more occurrence of chains in the latter 40% of fatigue life than in the first 60%. Some tests, however, exhibited chains throughout their life, indicating that microcracking often occurs from very early on in the fatigue life of a sample, as previously mentioned.

Of particular interest is that there appeared to be no instance of chains occurring in fatigue tests of dry mortar (i.e. relative humidity less than 25%) which were otherwise tested in similar conditions to moist mortar. Figs. 3.28(a) and 4.11(a) illustrate this point: such acoustic noise as is present (which is less than in wet tests) tends to be more widespread on both the loading and unloading portions of the PIP trace.

Fully submerged underwater tests at 25°C also exhibited chain behaviour, (Fig. 4.15), and this is discussed in more detail in section 4.5 on environmental effects.

An interesting point is the apparent occurrence of a chain in the AE PIP signal, of a dry fatigue test which lasted 924 cycles, Fig. 4.16 which would be most uncharacteristic for such dry specimens (< 25% RH, Sine, 87% SL, life 924 cycles). In fact this chain is only associated with grinding or attrition noise of the LVDT stub mounting before it fell away at about 780

cycles as the chain is promptly arrested, and does not continue after this had occurred. Hence the chain in this case is not of the same nature as others mentioned elsewhere, and indeed the shape of the AE signal can be seen to be different (See, for example, Figs. 4.8, 3.25 and 3.28).

(iii) Warnings

Warning events refer, in this context, to impending failure in particular, and less to macrocracking or transducers falling off, which have already been discussed. Green (226) reports that similar warnings of impending failure of model concrete reactor vessel materials was possible once the AE characteristics of failure had been recognised. For the present work, the noise associated with such warning cracks, which occurred on most of the present tests, tended to be large (i.e. of large amplitude), near the peak load during a fatigue cycle and near the end of the fatigue life. Subsequent to such a warning event there was generally increased acoustic activity leading to failure. A trace of such a typical warning event is shown in Fig. 4.17 (0.5Hz sine, 80% SL, moist) at approximately 755 cycles at the peak load. The noise is predominantly on the loading cycle at the peak load, although there is also some evidence on the unloading cycle. Similar warning events are clearly apparent in Fig. 4.16(a) at approximately 855 cycles and Fig. 3.28(c) at approximately 425, 560 and 650 cycles. Other, less clear, but nonetheless warning, events are apparent in Fig. 4.13 at approximately 1460 cycles and Fig. 4.10(a) at approximately 61 cycles (both on the loading portion at maximum load) and Fig. 3.25(c) at 840 cycles at maximum load on the unloading portion. Warnings are also apparent at about 800 cycles and 1200 cycles at maximum loads for Figs. 4.8(a) and (b) respectively.

Certain common characteristics of these warning events can be noted. They tend to occur in the last 25% of the fatigue life, or last 150 cycles before failure, at or near peak load and tend to be of a sudden nature (i.e. little prior build up) with large amplitude. Subsequently there is often more AE on the rising load half of the signal (e.g. Fig. 3.28(c) and Fig. 4.8) which develops to final failure, often with a trend of more noise at higher loads as failure is approached, (Fig. 4.13).

The occurrence of warning events can be plotted as a function of, either number of cycles prior to failure, or as a percentage of the life, (Figs. 4.18(a) and (b)). From these figures it is apparent that warnings occur in the last 50% of life, although generally predominantly in the last 20% of life. There appeared to be no distinction in the AE warning behaviour as a function of frequency, waveform, environment or temperature. Histogram plots of the warnings as a function of the above parameters showed no significant difference, i.e. almost all tests exhibit some warning in the last 20 to 25% of the fatigue lines, and warning, per se, could not be used to distinguish test conditions or behaviour.

This concludes the section on the general results and characteristics of acoustic emission in fatigue and in particular typical results of Pseudo Isometric Plots. Further discussion of PIP results as applied to fatigue tests of various frequencies, waveforms and environments follow in section 4.3 to 4.5. This section 4.2 is, however, first concluded with a brief discussion of the general fatigue, and associated damage monitoring, results.

4.2.4 Discussion and Summary

This section, 4.2, has presented the results of standard fatigue tests in mortar and has shown how damage accumulates in such tests. The results of static tests, as the basis for fatigue tests, were briefly examined and then the compression fatigue results presented conventionally as SN curves (in Fig. 2.28) were then discussed. The results of these test series indicated that the fatigue strengths, at 10^7 cycles for wet and dry mortar, were approximately 54% and 64% respectively, comparable with other results in the literature. It is worth re-emphasising that fatigue and damage results presented here refer to the integrated or cumulative effect of a series of microcracks growing in a tensile manner in the central portion of a compression specimen and do not refer to so called "nominal single crack" situations. These latter crack types are discussed in Chapter 7. From the SN curves obtained it was possible to choose the appropriate stress level to obtain satisfactory fatigue lives for subsequent tests. For example, for fatigue tests to last approximately 1000 cycles and thus be both representative of true fatigue conditions while still being sufficiently brief to conduct several tests in one day, the appropriate stress level was approximately 80% for wet tests and 87% for dry tests. This formed the basis of the subsequent frequency (section 4.3) waveform (section 4.4) and temperature (section 4.5) studies.

The damage monitoring results presented for standard fatigue conditions are most interesting. They show unequivocally that damage, in the form of microcracking, can be reliably evaluated by strain, UPTT and acoustic emission methods, which also show strong correlations between the various techniques. In fatigue tests, in contrast to static tests, damage appears to develop sigmoidally in a three stage manner (Figs. 4.1, 4.3, 4.9). Thus there appears to be significant cracking just after starting fatigue which rapidly settles down to an almost linear rate of damage accumulation (Fig. 4.9). Just prior to failure, however, (in the last 20% of life) macrocracks tend to develop and the damage monitoring techniques all indicate impending failure. The results of the pseudo isometric plots (PIP) have been particularly informative and have indicated that the cracking was of a sporadic nature but that it builds up as failure is approached. Warning events were also manifest for each testing regime and, often (for moist and wet tests at 0.5Hz) significant noise occurred on the unloading portion of the fatigue test close to the minimum load, often near failure, resulting in so called PIP "chains".

It is thus apparent from the discussion in this section (4.2) that mortar is susceptible to fatigue and results in non linear damage accumulation that can be monitored using the techniques described. To add further insight to this process of damage accumulation, and of the effect of time, fatigue tests at different frequencies were undertaken and the results described in the following section.

4.3 Effect of Cycling Frequency on Fatigue

4.3.1 Introduction and Literature Survey

The importance of the time aspect in fatigue testing of cement based materials has been mentioned on several occasions already in this thesis. In this section its effect, expressed in terms of cycling frequency, is examined in detail. It is very necessary and important to evaluate such a frequency effect (if any) on fatigue performance, since fatigue testing takes considerable time, especially in view of the large number of parameters to be investigated. More specifically it is of prime importance to establish what the effect of time involved in testing individual specimens has on their fatigue performance and damage accumulation behaviour.

Examination of the literature reveals that the effect of cycling frequency on fatigue strength and damage development has been variously reported as being independent of cycling frequency and rate of loading (26, 95, 96, 135, 144, 150, 157, 158, 237) through to having a measurable effect (25, 27, 28, 231). Hsu (25) draws the distinction between low cycle fatigue (10^3 - 10^4 cycles) and high cycle fatigue. He proposes that, in the latter case, time dependence is small whereas in the former, low cycle case, rate of loading is a strong variable affecting the fatigue strength of concrete.

Pioneering studies on the effect of frequency on fatigue performance were undertaken by Kesler in 1953 (26) who conducted flexural fatigue tests on 150mm deep beams at 1 and 6Hz. The concrete was 7 day wet cured and then aged for 3 months before fatigue testing, tests which in themselves could take 3 months! He presented his results in SN curve form, which is not, however, the most discerning technique for distinguishing frequency effects. His range of frequency testing was also not particularly great and the experimental scatter was large. Careful examination of his results indicated that, for example, at 80% stress level, the lower frequency tests had slightly shorter lives, but because of the large scatter he felt that this difference was not significant. He concluded that, over the range tested, the cycling frequency had no effect on fatigue behaviour.

In work similar to Kesler's (26), Raithby and Galloway (151) observed a slight increase in fatigue strength of dry flexural beams tested at 20Hz (compared to 4Hz), but concluded that the effect was not significant. They did not detect any frequency effect for saturated beams.

Murdock, in a review published in 1965, (135), regarded the speed of fatigue testing as not very significant although tests at low frequencies were generally associated with somewhat low fatigue strengths, shorter lives and greater cumulative strain. Murdock concludes, however, by saying that "the fatigue response, as a proportion of the ultimate strength, is independent of frequency". Arthur et al. (232) report that, for large concrete beams containing steel reinforcing, fatigue tests in sea water exhibited no frequency dependence.

By contrast, however, Spooner (99) in studies on stress-strain-time relationships for concrete, noticed a decrease in static strength of 12% as the time to failure increased from 5 minutes to 15 hours, for water cured specimens tested under moist conditions. He suggested therefore, that in fatigue tests, the frequency of loading could indeed affect fatigue strength.

Similar behaviour has been observed by various workers (25, 27, 28, 141, 176, 231) of which the work of Awad and Hilsdorf (27) and Sparks and Menzies (28) are particularly interesting and therefore discussed at some length subsequently. Stroeven (141) conducted fatigue tests over the range 0.175Hz to 17.5Hz and examined the development of microcracking. He reported (unfortunately without detailed data or figures to substantiate his arguments) that "at low frequency, high transverse strains were observed together with a drastically reduced lifetime". He attributed this to prolonged effects of "time dependent processes" (141).

Jordan (176), in an investigation of the damping of concrete, noted that "over the range 0.2Hz to 1Hz the damping was lower at the higher frequency. This suggests that there was a decrease in the time dependent strains at the higher frequency reducing the viscous component of damping". The effect was also more marked in wet concrete compared to dry concrete which tends to have more inherent microcracks.

Perhaps the best study of the frequency effect in fatigue to date is that undertaken by Awad and Hilsdorf (27). They tested concrete prisms in compression over a range of stress levels (from 80% to 95%) and frequencies (0.068 MPa/sec to 6.8MPa/sec) and reported that an increase in frequency (or stress rate) by one order of magnitude led to a corresponding increase in the number of cycles to failure by almost an equivalent order of magnitude, (Fig. 4.19). They add that this frequency effect is likely to diminish with decreasing maximum stress level, as was also noted by Kesler (26), whose tests involved maximum stress levels from 65 to 85%. This contention, of reduced frequency effect with decreasing stress level, was also expanded upon by Hsu (25). Awad and Hilsdorf (27) further conclude that damage caused by high repeated loads depends both on the number of applied cycles and the total time that the concrete has to sustain high cyclic stresses, in excess of the "sustained strength" (typically 75% of the static strength (25)). Thus strains at failure are reportedly greater the longer the time to failure, (27).

Recently, Hsu (25) introduced the concept of time, in the form of the period, T, between repetitive loading and the fatigue force ratio, R, to conventional SN curves (or f-N curves as he calls them) to develop a so-called f-N-T-R relationship. In this form of presentation (Fig. 4.20), the normalised stress, f/fsus, the number of cycles, N, and period, T, are represented on log scale orthogonal axes and covers the whole range from fatigue loading to sustained loading. A 45^{o} line joining the two horizontal axes can be regarded as the duration of time of repetitive loading; (this is discussed in greater detail in the evaluation of the results of this frequency effect, section 4.3).

Hsu then uses a linear approximation of Fig. 4.20 (See equations (9) and (20) of his paper (25)) to evaluate existing data in the literature. Returning to Awad and Hilsdorf results (27) for concrete at 90% stress level as evaluated by Hsu (25), it is apparent from Fig. 4.21(a) that there is a distinct frequency effect. Similar frequency effect behaviour is apparent from Sparks and Menzies studies (28), Fig. 4.21(b), and those of Assimacopoulos et al. (231) (Fig. 4.21(c)), which indicate a reduction in fatigue life at lower frequencies. While the quality of fit to Hsu's equations 9 and 20 is somewhat debateable because of the relatively large scatter in the results (Figs. 4.21(a), (b) and (c)), the distinct frequency effect is nevertheless quite evident.

Hsu (25) concludes that the effect of cycling period, T, (or frequency) on fatique strength is real, but because of the large scatter of results inherent in fatigue testing the effect is not always clearly discerned by experiment unless the difference in T is two orders of magnitude.

The effect on the so-called frequency effect of moisture content does not appear to be fully understood, nor indeed does the nature of frequency effect itself (176, 25). Hsu's paper (25) only postulated a theory to describe existing data and did not himself undertake specific experimental verification. In view of this and certain controversies concerning the frequency effect mentioned in this brief review, an experimental programme was undertaken to examine this question in more detail. An attempt was also made to obtain a greater understanding of the mechanisms of damage development in mortar under such conditions. The following sections describe the specific experimental programme and the results obtained.

4.3.2 Experimental Procedures

Full experimental details concerning materials and sample fabrication for compression specimens have been given in Chapter 3, sections 3.1 and 3.2, together with the standard procedure for fatigue testing (section 3.4.5). In this section, only the programme of tests to investigate the frequency effect itself is described.

To obtain a wide, yet realistic, range of cyclic test frequencies over two orders of magnitude, compression fatigue tests were conducted at 0.1Hz, 1Hz and 10Hz. The stress level chosen was based on the previous fatigue work as shown in the SN curve, Fig. 2.28. A stress level of 80% indicates that for moist specimens the fatigue life may expected to be approximately a few thousand cycles. At 10Hz this would imply that the real time duration of tests would be of the order of a few minutes, while 0.1HZ tests (if they exhibited the same lifetime in number of cycles) may be expected to last up to 3 to 4 hours. It was considered that these test duration times were satisfactory from a test time viewpoint and facilitated testing of a complete batch within one working day, while at the same time being truly representative of fatigue behaviour.

The tests were conducted on 7 day wet cured compression prism specimens in the "moist" condition in the first instance, because it was believed that any time dependent process that might affect performance may be moisture dependent. It is, for example, well known that fully dried specimens do not creep (233). Subsequently some frequency tests were conducted on dry specimens; however, it was necessary to use a stress level of 87% to obtain approximately the same predicted fatigue lives. This in itself led to other problems of greater scatter in the results since small errors in assessing the static strength had a relatively more marked effect on fatigue life. If, in reality, the cycling stress was very close to the failure stress the fatigue life was very short. Conversely, if the static strength had been underestimated, disproportionately long fatigue lives were obtained. Because of this difficulty, and consequent increased scatter on damage monitoring results as well (particularly LVDT "strain" measurements), these results are somewhat limited.

The frequency effect on individual crack growth rates for both moist and dry double torsion specimens (single crack growth) is examined in more detail in Chapter 7.

The prism specimens were fully instrumented for damage monitoring so that changing strains and microcracking could be monitored during testing using the LVDT and ultrasonic systems already described in section 3.5.2 and 3.5.3. In addition, and where appropriate (i.e. not at 10Hz where the AE PIP system does not respond due to inertial constraints), acoustic emission pseudo isometric plots were also obtained. The results are given in the next section.

4.3.3 Results

4.3.3.1 Moist Frequency Effect Tests

The results of the frequency effect tests at 0.1Hz, 1Hz and 10Hz on mortar compression prisms under moist conditions are best presented by means of the strain and UPTT damage monitoring techniques (Figs. 4.22 and 4.23 respectively). It is immediately obvious that the form of these damage curves is progressively increasing and sigmoidal as would be expected for gradual damage accumulation (see Figs. 2.30, 2.31, 4.1, 4.2 and 4.3).

Careful examination of these damage accumulation traces indicates that there is a distinct separation into three regimes corresponding to the three frequencies examined. This is particularly apparent for the case of the UPTT results (Fig. 4.22). For the residual strain results, for both lateral and longitudinal cases, the scatter is somewhat larger. This seems to be because of the LVDT system's greater susceptibility to individual cracks; and as a surface measurement it is also less effective than the ultrasonic method at measuring the "integrated" microcracking damage. Nevertheless, the three regime distinction is still quite apparent.

For completeness, the "damage curves" for both lateral and longitudinal elastic strains are shown in Fig. 4.23(c). The three regime distinction, while still present, is not as obvious as in the earlier residual strain cases, but this is hardly surprising as it is residual microcracking (and hence residual strain) which is more indicative of damage development than the elastic measure of how much the cracks open. It is interesting to compare the magnitude of the lateral and longitudinal elastic strains. At first glance, because the microcracking runs in a predominantly longitudinal direction, it might seem that the lateral strain may be expected to be relatively "greater" than the longitudinal strain. One needs to take account, however, of the nature of the loading (longitudinal compressive) and of the effect of Poisson's ratio (typically 0.2 in this case), which causes the lateral strains in the first place. From such loading and Poisson's ratio effect it is thus to be expected that the lateral strain would, in the absence of any microcracking anisotropy, be about one fifth of the longitudinal strain.

In actual fact, (see both Fig. 4.23(c) and the envelopes of these results replotted as a percentage of life, Fig. 4.23(d)), the lateral elastic and residual strains are about 1/2 to 1/3 of the longitudinal strains (and not one fifth) indicating that there is a predominance of microcracking in a longitudinal, as opposed to lateral orientation. Thus, in effect, the lateral strain is indeed "greater" and a more sensitive measure of damage development. Such cracking and microcracking is also noted by direct observation.

Also apparent from Figs. 4.23(c) and (d) is the increase in elastic strain with fatigue life, consistent with a gradual increase in compliance, as noted previously (Figs. 2.29, 2.33).

For clarity the results of the UPTT and lateral residual strain damage traces, together with others, are incorporated in an envelope to show more graphically the division into the three frequency regimes, Figs. 4.24(a) and (b). From the frequency test results the following points can be made:

(i) at this 80% stress level, the fatigue life increases with frequency:

(ii) the rate of damage accumulation, as monitored by both ultrasonic pulse transit time and residual strain techniques, increases with decreasing frequency, and

(iii) the ultimate amount of microcrack damage that can be sustained before catastrophic failure appears to be greater the lower the frequency. (However, this contention is not as unequivocal as points (i) and (ii)).

Point (i) is evident from simple inspection of the results. A representative, quantitative estimate of the rate of damage accumulation (point (ii) above) can be obtained by measuring the slope of the UPTT and lateral residual strain curves at half the fatigue life. These were believed to be approximately in the central region of the sigmoidal damage accumulation trace and considered to be representative damage monitoring rate parameters. For convenience these rates are referred to on the graphs as $\frac{d(u/s)}{dn}$ and $\frac{d(\varepsilon_{lat})}{dn}$ respectively. If these results are plotted as a function of frequency on a log-log scale, there appears to be a clear frequency dependence, Figs. 4.25 (a) and (b). The extent of microcracking damage at failure, point (iii), as indicated by the limitating change in UPTT value and the limiting lateral residual strain, seems to be less sharply defined although it is possible that such a trend exists. Such behaviour, of high failure strains at lower cyclic test frequencies, have in fact been noted before by Murdock (135) and Awad and Hilsdorf (27).

4.3.3.2 Dry Frequency Effect Tests

As mentioned earlier, the scatter in the dry tests was larger, in part because of the higher stress level used to obtain realistic fatigue life durations and also possibly because of the intrinsic nature of the dried mortar. Damage monitoring measurements consequently also exhibited

significant scatter, particularly in the strain measurements. These results have thererfore been excluded in this presentation as they make no significant contribution; for the change in UPTT traces, on the other hand, there was some distinction into the three frequency regimes, comparable to Fig. 4.24(a). This distinction was not, however, as clear and measurement of the damage accumulation rate at half life, $\frac{d(u/s)}{dn}$, better represents this distinction in the manner comparable to Fig. 4.25(a). This is shown in Fig. 4.26. For comparative purposes the corresponding line for the moist specimens (from Fig. 4.25(a)) also shows the relative difference, (Note, however, that these data have been obtained at two different stress levels.)

4.3.4 Discussion

From the results presented in Figs. 4.24 to 4.26 it would appear that there is certainly a distinct "frequency effect" which is more pronounced for moist than dry samples. Inspection of the log scale presentation of the results in Fig. 4.25 for moist specimens leads to the conclusion that damage accumulation rates as a function of time should be plotted: i.e. damage accumulation per second $\frac{d(u/s)}{dt}$ and $\frac{d(\varepsilon_{lat})}{dt}$, as opposed to per cycle, $\frac{d(u/s)}{dn}$ and $\frac{d(\varepsilon_{lat})}{dn}$. One is led to this conclusion because an order of magnitude change in frequency, and hence cycling period, appears to lead to almost an order of magnitude change in damage accumulation rate. Plots of these damage accumulation rates at half life (as a function of time) for moist specimens versus frequency for the UPTT and lateral residual strain cases are shown in Figs. 4.27(a) and (b) respectively. From these results it would appear that the frequency dependence has been all but removed and that the damage accumulation rate is a function of elapsed time as opposed to being truly frequency dependent. In other words, when normalised with respect to time the rate of damage accumulation is almost constant. It can be argued that there still appears to be some slight frequency dependence as the 10Hz tests show slightly less extreme damage accumulation rates. The two damage monitoring techniques of Figs. 4.27(a) and (b) are combined in Fig. 4.27(c) to illustrate further the virtual absence of frequency dependence. A similar reduction of ultrasonic damage rate per cycle to damage rate per second, for dry specimens, is shown in Fig. 4.28. The dependence on frequency appears again to have been reduced to a predominant time dependence although there is still a slight but real frequency effect. Note that the damage accumulation rates in dry specimens are less than for

moist specimens even though the dry specimens were tested at a high stress level, 87% (cf 80% for moist specimens.)

A plot of the actual times to failure also tends to show this time dependent trend although there does appear to be a slight reduction in duration at higher frequencies (Fig. 4.29(a) for most specimens and Fig. 4.29(b) for dry specimens).

From the foregoing discussion of the results it seems that, for mortar fatigue tested under both moist and dry conditions at high stress levels, the fatigue life is principally controlled by time dependent, as opposed to frequency (i.e. strain rate) dependent, mechanisms. The time dependence is greater for wet compared with dry samples.

These conclusions suggest the contribution of a creep mechanism affecting, or controlling, life, although this cannot be the complete answer because of the slight remanent frequency dependence at higher test frequencies, (Figs. 4.27(c) and 4.29(a)), and because of the absence of creep in dry specimens (233). Efforts to evaluate the effect of true loading rate (by means of varied waveform tests) and moisture and temperature contributions thus become particularly significant and are discussed in section 4.4.

Examination of the acoustic emission pseudo isometric plots, AE PIP, provide little extra information on the mechanism of damage accumulation. Because of the inertial nature of the PIP system it was only possible to obtain AE PIP traces at frequencies of 1Hz or lower. Much data in the mid frequency range at 1.Hz (and 0.5 Hz) have already shown a preponderance of AE noise on the unloading cycle for moist specimens (Figs. 3.28(a), 4.8 (a), (b), 3.25(c)), sometimes in "chain" form with increased noise near failure. At lower frequencies, 0.1 Hz and 0.05Hz, the noise appears to occur at all load values and does not predominate on the unloading side (for example Figs. 4.30(a) and (b)). In a dry condition at low frequencies, the noise still occurs at all loads, Fig. 4.10(a).

Once again AE noise is of a sporadic nature and increases towards failure. In addition warnings are apparent at approximately 62 and 85 cycles in Fig. 4.30(a) which corresponds to large AE events as shown in Fig. 3.24 (for the same test). Note also that the life in both cases, Figs. 4.30 (a), (b), is

short and that there is significant AE noise concomitant with greater damage, consistent with points (i) and (iii) mentioned (section 4.3.3.1). One interesting point is that in acoustic emission studies of loaded ceramics, Dalgleish, Pratt and Rawlings (198) noticed that the AE was of a more low-amplitude-nature at low strain rates (comparable to the low frequency cases here). Comparison of Figs. 3.28 and 4.8, for mid frequencies, and Fig. 4.30, for low frequencies, would seem to be in accordance with this observation. This, together with the apparent difference in PIP signal between these two frequency regimes suggests that there may after all be a small rate dependent mechanism in the microcracking.

For brittle ceramic materials, silicate glass and tungsten carbide cobalt, Evans and Linzer (234) observe no frequency effect in glass but a distinct frequency effect for the WC/Co system. They conclude that crack tip plasticity is a necessary condition for such a frequency effect. Such a plasticity model would presumably be inappropriate with the present materials system. A further excellent paper by Evans and Fuller (235) develops an analysis which enables damage (and crack) development rates under cyclic loading conditions to be predicted.

For various ceramic materials, including glass, porcelain and alumina, they (Evans and Fuller) suggest that "there is no significant enhancement of the slow crack growth rate due to cycling", i.e. the crack growth rate in the low frequency regime (< 20Hz) occurs by the same mechanism as the quasi-static slow crack growth process. Single cracks and their growth rate, evaluated under both wet and dry conditions by the double torsion technique, is discussed at some length in Chapters 6 and 7.

With respect to concrete, Hsu's presentation (225) of Awad and Hilsdorf's (27), and Sparks and Menzies results (28), indicates the presence of a frequency effect when plotted on an SN type format (Figs. 4.21(a) and (b)). However, these results reduce to a time dependence, and a frequency independence, in a manner similar to the author's own work presented in Section 4.3.3. This is more apparent from the data points, than from Hsu equations [9] and [20], which show an approximate two order of magnitude change in life for a hundred fold change in frequency. Hsu does, however, recognise the importance of the test duration, NT, i.e. elapsed time as mentioned earlier in section 4.3.1.

4.3.5 Conclusions

This section on the frequency effect in fatigue, was introduced by a review of the literature, before details of the tests at 0.1, 1 and 10Hz were given. Results of these tests, particularly as represented by damage monitoring techniques, have indicated a distinction of the sigmoidal damage trace parameters into the three frequency regimes, particularly for moist specimens. These results suggest (i) an increase in fatigue life with frequency, (ii) an increase with rate of damage accumulation as the frequency is reduced, and (iii) (but less distinctly), an increase in damage at lower frequency. This apparent dependence on frequency is, however, all but removed for moist tests when the results are replotted as a function of time and the controlling factor becomes test duration. In effect the results show true time dependence.

There remains a slight "real" frequency dependence, however, especially at 10Hz (Fig. 4.27(c) and Fig. 4.29) suggesting that there may in fact be rate dependent mechanisms contributing to fatigue. This is more marked from the dry specimen tests. Pseudo isometric plots of AE data also indicate noise at all load levels at low frequency (compared to predominantly on the unloading cycle at 1.Hz) suggesting that there is a different (rate dependent) cracking mechanism at low frequencies. In addition, since time dependence seems to be the major life governing parameter, it is reasonable to consider static processes of crack propagation as controlling the cracking process, and thus creep, a form of stress corrosion cracking or chemically- or thermally- activated mechanisms may be of importance. Indeed, such dependence of the frequency effect on free moisture from the environment has already been noted (176). Thus it is in order to evaluate, in the following sections, the effect on rate dependence on the one hand (Section 4.4), and moisture and temperature on the other (Section 4.5).

4.4 Effect of Stress Level, Stress Range and Waveform on Fatigue

4.4.1 Introduction and Literature Survey

The previous section has highlighted the importance of rate dependent and time dependent processes in the fatigue of mortar. Since time dependence seems to be of importance, it is reasonable to consider that the maximum level of stress, as well as the cyclic stress range, has a significant bearing on the duration of fatigue life and damage accumulation behaviour. In addition, some dependence on loading rate, especially at higher frequency, is also apparent from previous investigations. This section [4.4] is therefore concerned with an investigation of the effect of (i) cyclic stress level and stress range, and (ii) waveform (as a convenient means of obtaining different loading rates without otherwise altering the time to failure) on the fatigue behaviour of mortar.

Stress Level and Stress Range

For large stress ranges, i.e. where the minimum load is very near zero, the influence of maximum stress level is effectively given by conventional SN curves, where the ordinate stress level ratio refers to the maximum cyclic load. (See for example, Fig. 2.28.) Further detailed discussion of this effect is well documented and can be found, for example, in Awad and Hilsdorf's paper (27).

Awad and Hilsdorf (27) also conducted sustained load tests (i.e. where there was no range of cyclic stress) and noticed that for high stress levels older concrete is more resistant to sustained load than young concretes. However, for low stress levels the trend is reversed: the time to failure for young concretes is larger than for older concretes. This is attributed to the effects of continued hydration (222) which is discussed in more detail in Chapter 5.

The effect of the range of stress, R, is clearly shown in Figures 4.31 (a) and (b). (Here R is defined as the ratio of minimum stress to maximum stress.) It is apparent that as the lower cyclic fatigue stress level approaches the maximum fatigue level the fatigue life of the concrete increases (25, 27, 132, 136, 142, 146, 231, 232, 236) and greater fatigue

strengths are obtained. An alternative, but graphic representation is given by Awad and Hilsdorf (27) and reproduced as Fig. 4.31(c), where their stress range, R*, is plotted against number of cycles to failure. (In this case, Awad and Hilsdorf defined R* as the difference between the maximum and minimum cyclic leads and not, as is more conventional, as the ratio of minimum to maximum stress levels.)

Awad and Hilsdorf (27) conclude that, for concrete subjected to high repeated compressive stress, a decrease in either the maximum stress level, or the stress range, results in an increase in the number of cycles to failure. (The increase in failure cycles with decreasing stress range becomes insignificant at high maximum stress levels and small stress ranges).

This apparent decrease in fatigue life with increased cyclic stress range, also reported by Maher and Darwin (184), is consistent with a more modern linear elastic fracture mechanics approach to fatigue, based on the Paris equation concept as commonly used for metals (237).

Shah and Chandra (89) conducted a particularly interesting microcrack development study on the effects of cyclic stress level and range, and sustained load, on concrete in compression fatigue. Their sustained load tests were performed at 60, 70 and 85% of ultimate stress and their fatigue tests from 60% to 70% stress level (to zero loading in each case). They noted that the strains for sustained loading were less than for cyclic loading cases, at the same stress level, i.e. cycling causes more damage than simple sustained loading. They also note that (for the same stress) there was a significant increase in microcracking with increasing time to failure. Measurements of microcrack area, comparable to the author's own damage measurements, for their sustained and fatigue tests (with varied maximum stress level) are shown in Fig. 4.31(d).

Waveform

The effect of frequency of loading on fatigue life was examined in the previous section and life was shown to be almost completely time dependent. There was, however, still some apparently real but small "pure" frequency dependent component (Figs. 4.27, 4.28). It is also well known, (28, 92, 97

- 100, 102), as has been discussed earlier (section 2.3.5), that there is an increase in measured (static) strength at fast loading rates. It was thus of interest to establish to what extent the actual loading rate (or unloading rate for that matter) in a fatigue test was of importance in fatigue life and damage terms. Awad and Hilsdorf (27) used triangular waveforms of various frequencies, and noticed a frequency dependence which reduces to time dependence in a manner similar to that discussed in the previous section. This waveform did not, however, distinguish between loading rates for the same time duration. In addition, the phenomenon of acoustic emission on unloading for wet, medium frequency tests, as shown by PIP, was thought to be rate dependent. Consequently, it was felt that fatigue tests subject to two types of sawtooth loading may give further insight into the processes and mechanisms controlling fatigue failure in mortar. The detailed experimental programme to evaluate this effect of waveform and the effect of stress level and range, mentioned earlier, are described in the next section.

4.4.2 Experimental Programme

Two experimental programmes were undertaken in this section in the light of the foregoing discussion of previous work.

4.4.2.1 Stress Level and Range Programme

The tests conducted in the present programme consisted of a constant upper (or maximum) stress level (of 80%) and variable lower (or minimum) stress level of respectively 2.4%, 30% and 60% (all tests being performed at 1 Hz). From such tests it was hoped to distinguish the relative importance of loading range in comparison to maximum stress level on fatigue life. (Dependence on the latter only would be consistent with a purely time dependent failure mechanism, like stress corrosion.)

4.4.2.2 Waveform Test Programme

To obtain nominally comparable durations of fatigue life, but with different loading rates on loading and unloading, two test series using two types of sawtooth loading were employed. In all other respects, except for the waveform, the test conditions were identical. The sawtooth waveforms were

generated by a standard signal generator: on the one hand with a fast unloading signal (F.U.) and on the other with a fast loading signal (F.L.). The tests were all conducted at 1Hz and a representation of the load traces is given in Fig. 4.32. (Note that since the test system is compressive, the convention for the direction of increasing load is downwards, i.e. negative.) The minimum cyclic load was again 5kN and the maximum stress level selected again 80%, to be comparable with earlier studies, and to obtain realistic testing durations. The specimens were instrumented for damage monitoring using strain transducers (LVDTs) and ultrasonic probes, but AE was not employed because of the inertial limitation of the PIP system on the fast portion of the loading/unloading signal.

4.4.3. Results

4.4.3.1 Stress Level and Range Programme Results

The results of this test programme, where the maximum cyclic stress level was maintained at 80%, and the minimum successively at 2.4%, 20% and 60%, are best represented by the UPTT and strain monitoring traces, Figs. 4.33 and 4.34.

It is apparent from the results that the fatigue lifetime is very strongly dependent on range of loading for a constant maximum stress level. The lives recorded in this test series are given in Table 4.1 and indicate the marked dependence of lifetime on cyclic stress range. The rate of damage accumulation is also greater per cycle, at larger ranges as is evident from Figs. 4.33 and 4.34, where each of the test ranges separate into three regions. The final failure values of "damage", monitored by UPTT and residual strain measurements (both lateral and longitudinal), also appeared larger at greater ranges, although this contention is not as marked.

4.4.3.2 Waveform Test Programme Results

The results obtained for this programme, Figs. 4.35 and 4.36 showed there to be no significant difference between the two loading modes, fast loading (FL) and fast unloading (FU) Measurement of the rate of (strain) damage accumulation at half life is given in Fig. 4.37(a), and the elastic strain amplitude at 20% and 80% of life in Fig. 4.37(b), for the two loading

modes. Once again there is evidently no significant difference, in the damage accumulation behaviour, between the fast loading and fast unloading cases.

The damage as evaluated by changes in ultrasonic pulse transit time (UPTT) also indicated no signficant difference between the loading modes, Figs. 4.38(a) and (b). Measurements of the rate of (ultrasonic) damage accumulation at half life is shown in Fig. 4.38(c) which again shows no difference between FU and FL loading modes, within the range of scatter.

It should be noted, of course, that this "no effect" conclusion is strictly only applicable for 1Hz compression tests at 80% in a moist condition. Under other test conditions, variations could obviously emerge, although this current test programme is clearly representative. The indications are, therefore, that the rate of loading or unloading does not affect fatigue behaviour in this materials system.

4.4.4 Discussion

It is evident from the stress level and range test programme that one of the prime parameters adversely affecting fatigue life is large cyclic stress range coupled with high stress levels. This has been extensively examined in SN type presentations of data (see for example section 2.4), and seems to be broadly applicable. Further insight may, however, be gained from a linear elastic fracture mechanics approach to fatigue, but this is discussed in more detail subsequently (Chapter 8).

The lifetimes of the stress level and range tests are broadly consistent with a modified Goodman diagram approach to fatigue and cyclic stress range. Reference can be made to, for example, Fig. 2.35 (from Neville (33), which is schematic only and does not apply quantitatively to the experimental materials or test system used here). The expected lifetimes, using the Goodman diagram approach for relative upper and lower percentage stress level (σ_h-σ_ℓ) values of (80-2.4), (80-30) and (80-60) - are respectively: (very approximately) 800, 1.1 x 10^4 and 10^5 cycles (multiplied by a constant). These values are approximately consistent with the lifetime obtained in the present test series (Table 4.1).

The damage monitoring results, Figs. 4.33 and 4.34 are qualitatively comparable to the microcrack damage area accumulation as a function of time, presented by Shah and Chandra (59) and shown in Fig. 4.31(d). Although they used sustained load (of 85%) and different cyclic load ranges, increases in the rate of damage accumulation with increasing range and increased upper stress level, are apparent in both their results and the present ones.

It may be concluded from the literature, augmented by the present studies, that the principal fatigue life controlling parameter is cyclic stress amplitude. As this increases so fatigue life decreases. However, upper stress level is also important since, at a constant stress range, increases in mean level lead to reductions in fatigue life. Both these findings are reasonably well explained by conventional SN curves and the (appropriate) modified Goodman diagram. It is only when these parameters of stress level and stress range are kept constant that other parameters become of importance. For example, only at constant upper and lower fatigue stress levels, does the duration of loading (for example by varying the frequency) become important and where, for example, microcracking damage increases with time. Similar conclusions were drawn by Shah and Chandra (89). The absence of any affect of sawtooth waveform, within the frequency and loading rate tested, is also consistent with this, since the stress levels and approximate fatigue life durations were effectively unchanged.

A major shift in all these results occurs if the specimens are tested in a dry condition, when they apparently become more resistant to damage and fatigue. At a frequency of 1Hz it would appear that if such a strain rate effect were to exist, it doesn't have any effect on fatigue life or damage accumulation. At other frequencies this may not be the case. It was also to some extent unfortunate that no AE PIP data could be obtained for the sawtooth waveform tests as these may have given further insight into the mechanisms of microcracking.

It would appear then that there isn't any true strain rate effect, at least at 1 Hz. The processing of the original damage accumulation results (Figs. 4.22 - 4.26) in terms of damage per unit time as opposed to damage per cycle (Figs. 4.27, 4.28) suggested that any frequency effect was all, but not quite, removed. It was thought that any remanent frequency effect might have been due to strain rate mechanisms, but the absence of any effect due

to different waveforms (FU and FL), in a study specifically undertaken to investigate this, suggests that strain rate effects play only a small, if any, part. Thus any small remaining fatigue lifetime, or damage accumulation, variations may still depend on elapsed time under fatigue. Here, competing processes of a form of creep or stress corrosion on the one hand or rehydration and strengthening on the other (See Chapter 5), are suggested, and may affect the fatigue damage accumulation situation. To evaluate this further, a limited extension of the waveform studies was undertaken using a test batch involving four fatigue tests to evaluate the effect of rest periods, or so called "dwell" times, at (i) the maximum and (ii) the minimum load, in an otherwise triangular waveform (Fig. 4.39). The tests were comparable to earlier work in other respects (80% stress level, moist compression specimens) but the frequency was 0.33Hz, as this was the fastest that could reasonably be obtained using the ramp generator and programmer units of the testing machine. The fatigue lives for dwell (of 1.6 secs) at minimum load was 1116 and 895 cycles, while for dwell (also of 1.6 secs) at maximum load, the lives were 432 and 109 cycles. The damage accumulation data were not significantly different, as is evident from the AE PIP plots of Fig. 4.40(a) and (b), except for the different life times. Despite the very limited number of these tests the trend suggested is that when all other test parameters are constant including stress level, frequency, loading rate etc., then the effect of sustained load can affect fatigue duration. These tests should be regarded as preliminary only, however, and further work is required to validate the effect.

4.4.5 Conclusions

This section, 4.4, has examined the effect of (a) stress level and cyclic loading range and (b) waveform, on the fatigue performance and damage accumulation of mortar under moist conditions. Compression fatigue tests at 10Hz at a constant upper stress level of 80% and variable lower stress levels of 2.4, 30 and 60%, led respectively to increases in fatigue life and reduced rate of damage accumulation. The prime fatigue life controlling factors for mortar appear to be stress level and cyclic range, as covered by conventional SN curves and the modified Goodman diagram.

Fatigue tests using two sawtooth waveforms incorporating (a) fast loading and (b) fast unloading characteristics indicated no difference in fatigue performance or damage accumulation in the frequency range tested (1Hz). Preliminary tests incorporating a dwell period at either maximum or minimum load during the fatigue cycle did, however, indicate a shortening of fatigue life due to sustained load effects. This effect may be attributable to a form of time dependent stress assisted environmental attack, and it is clearly evident that the effect of free moisture plays a significant role (89, 27). Allied to this moisture dependence is presumably the effect of temperature, and these parameters are discussed in the following sections.

4.5 Effect of Aqueous Environment and Temperature on Fatigue

4.5.1 Introduction and Literature Survey

4.5.1.1 Introduction

The apparent importance in fatigue of the presence of free moisture or water has been mentioned several times so far. Since it is apparent that moisture dependent processes can control fatigue duration (assuming other parameters like stress levels, range, etc., remain unchanged) it is also reasonable to contend that a form of environmental and stress dependent degradation may be taking place. This has been suggested previously as a form of "stress corrosion" (29, 30, 89). If the processes at the crack tip(s) were to be controlled by the rate of mechanico-chemical reaction, then the process would presumably also be dependent on temperature. This section reviews the effect of moisture on fatigue performance, both from previous studies and the present work, and also describes some results of fatigue tests conducted underwater at temperatures of $25^{o}C$, $45^{o}C$ and $60^{o}C$.

4.5.1.2 Previous "Wet versus Dry" Fatigue Studies

The difference in both static and fatigue behaviour between so called "wet" and "dry" specimens has been often noted by previous workers (68, 89, 110, 111, 138, 140, 232, 238, 239). Dry specimens have been shown to exhibit substantially greater strengths and longer fatigue lives than moist or wet specimens. This is the case even when the fatigue data is normalised by the appropriate static strength in the same moisture conditions (140, 238).

Antrim (138) reports that the difference in SN behaviour between wet and dry tests is more pronounced at low water cement ratios (approximately 0.4) than at higher ratios (0.7). Shah and Chandra (89) noticed that for sustained load (static fatigue) tests, failure of their moist concrete specimens occurred in approximately 6 minutes, whereas dry specimens, under similar load conditions, did not fail even after 4 hours. Probst (145) reports similar results. Wet concrete prisms sealed in polythene containers exhibit shorter fatigue lives than dried specimens by about half an order of magnitude according to work reported by Cornelissen et al. (142).

Raithby and Galloway (151) conducted flexural fatigue tests on concrete beams of various moisture contents and found that the highest strength, (and longest lives) were obtained for oven dried specimens. The lowest strengths and fatigue lives were obtained with specimens which had been partially dried in the laboratory before test. The fully saturated specimens gave intermediate strengths and endurance values. Specimens which had been oven dried and then soaked for 3 weeks prior to testing in a wet condition, had a "static" strength midway between the oven dried and the fully saturated specimens, but both types had similar fatigue performances.

4.5.1.3 Previous Fatigue/Temperature Studies

While there have been some studies (32, 33, 117, 121 - 123) on the effect of temperature on the static strength of cement based materials, there does not appear, in the general literature, to be any specific studies that have investigated the effect of temperature on fatigue strength, particularly in underwater conditions. The strength of concrete reportedly (33, 121, 117) decreases with temperature, but only above approximately 250°C, as is evidenced by Fig. 2.25 of Chapter 2. Barrick and Krokosky (29) report, somewhat surprisingly, that static fatigue reduces with increases in temperature (within their testing range); i.e. static fatigue life is greater at 60°C than 25°C. This they attribute to the dependence on cracking of hydroxyl ions derived from inherent calcium hydroxide (in the hydrated cement), whose solubility decreases with temperature (29).

In view of this controversial finding and the dearth of information on cyclic fatigue in underwater conditions at different temperatures, such an investigation was undertaken here and is described in detail below.

4.5.2 Experimental Programme

4.5.2.1 Wet versus Dry Tests

A substantial number of both wet and dry tests have already been conducted in the development of the SN curve data (section 4.2) and in the course of the investigation of the frequency effect (section 4.3). Included in this latter section is damage accumulation data, which provides some comparison between wet and dry fatigue behaviour, although admittedly only at high stress levels.

The results of these tests and discussion of the earlier wet versus dry tests is given in section 4.5.3.

4.5.2.2 Underwater Temperature Test Programme

To investigate the effect of water and temperature on fatigue, the proposed test programme consisted of three test temperatures, 25°C, 45°C and 60°C. The tests were to be conducted at the 80% stress level and at a frequency of 1Hz.

Certain difficulties arose, however, in these underwater tests right from the first static tests. The scatter obtained in the static tests was larger than normal, which might have been related to the duration of time the static specimens spent at test temperature prior to test. In an effort to standardise this, the static test sequence involved removing the sample from its (ambient temperature) curing bath, and placing it in the water reservoir that feeds the test chamber, for an approximately standard time. In this way static specimens experienced between 10 and 20 minutes at test temperature prior to ramping.

Fatigue specimens were similarly "prepared", but even more care was taken to ensure that the time the specimens spent at temperature in the test bath, was between 15 and 20 minutes prior to commencement of fatigue testing.

It was also soon established in preliminary tests that the fatigue life was shorter under (hot) water than under cooler moist conditions. Thus the preselected stress level of 80% led to unreasonably short testing lives and times. Thus it was decided to conducted the fatigue tests (for all three temperatures) at a 76% stress level and at 1Hz. Unfortunately this inhibits direct comparison with already obtained fatigue data at 80% stress level but, within this temperature series, the results and the effect of temperature are comparable.

Damage monitoring of underwater specimens also posed problems. Continuous and successful waterproofing of all damage monitoring components was necessary throughout testing, and any perturbations that did occur - necessitating repair - led to delays and restarting of the "time at temperature" sequence of the specimens. At the higher test temperatures ($45^{o}C$ and $60^{o}C$) the LVDT holder stubs frequently debonded, particularly under fatigue situations, and consequently the amount of valid strain data obtained was somewhat limited. With regard to the waterproofing technique of the LVDTs utilising contraceptives, great care had to be taken to ensure that the waterproofing membrane only touched the plunger portion of the LVDT at its tip and did not impinge on its sides (by, for example, water pressure) and interfere with the free in-and-out movement of the LVDT plunger into its transformer coil housing. This was not always possible, especially on re-use of the LVDT from one specimen to the next.

Generally the ultrasonic probes system behaved rather better than the strain system although there is some temperature dependence of the piezo electric crystal especially at the higher temperatures. In addition, any modifications to the damage monitoring equipment, once under water at the highest temperatures of 45^{o} and $60^{o}C$ (for example, for LVDT zeroing or ensuring complete acoustic bond of the ultrasonic probes) was uncomfortable and necessitated the wearing of cumbersome insulating gloves.

From the above it is hardly surprising that the number of successful and reliable damage monitoring traces was limited; these are, however, presented in the following section, together with some relevant PIP traces.

4.5.3 Results

4.5.3.1 Wet versus Dry Fatigue

Fully dried specimens exhibit a greater resistance to fatigue than wet specimens in agreement with other published work (89, 138, 140, 232, 238). The author's present results, represented in an SN curve form (Fig. 2.28), indicate that the dry specimens have greater fatigue lives than wet by about an order of magnitude (section 4.2.5) (at 80% stress level).

From the frequency effect studies, section 4.3, the rate of damage accumulation is slower for dry than wet specimens (Fig. 4.26). It should be borne in mind, however, that the dry specimens were tested at 87% stress level, with the wet at 80%, so that the damage rates are not quantitatively comparable. However, from the SN curve (Fig. 2.28) and the trend suggested by, for example, Fig. 4.34, it could be considered that the rate of damage accumulation at 87% (for dry specimens) would be very much greater than (or at least comparable to) the damage rate for wet specimens at 80% stress level. Despite this, the damage accumulation rate per cycle for dry specimens is less than for moist specimens (Fig. 4.26), by a factor of between 2 and 6. This is also the case when other parameters of wet and dry specimen tests are compared, (Figs. 4.27(c), 4.28).

With respect to fatigue damage, monitored by means of acoustic emission pseudo-isometric plots, it was evident that for moist specimens, (RH: 75%) the AE noise predominated on the unloading portion of the loading traces (at mid range frequencies). This is clear from Figs. 3.28(b), 4.8(a) and (b), 4.13, 4.17 and also from the probability plot, Fig. 4.14(a). Dry specimens on the other hand, (RH < 25%) exhibit noise on both loading and unloading portions of the sign wave loading, (Figs. 3.28(a), 4.10(a), 4.11(a) and 4.16(a)) and generally the level of acoustic noise for dry specimens was lower than for wet specimens (Figs. 4.11(a) ad 4.16(a)). "Warnings", as discussed in Section 4.2.4.3, occurred in both wet and dry tests.

4.5.3.2 Underwater Temperature Test Results

The scatter in static strengths and fatigue lives in underwater tests is illustrated in Table 4.2, and indicates primarily that the fatigue lives decrease as the temperature is increased. In view of the experimental difficulties just mentioned more tests were conducted at 25°C (which is a more tolerable working temperature) in establishing the appropriate experimental procedures. From Table 4.2 the scatter in static results is evident but it is also interesting to note that this static strength appears to decrease with temperature. The fatigue lives also show a decrease, even though the 76% cyclic stress level used in the fatigue test was based on static strengths measured at the appropriate temperature. The mean fatigue lives at 25°C, 45°C and 60°C were respectively 1002, 409 and 257 cycles.

Damage monitoring trace results were limited in view of the difficulties and no reliable strain traces were obtained at 60°C. However, changes in ultrasonic pulse transit time, Fig. 4.41(a), indicate extensively more damage at 60°C, than 25°C or 45°C tests. The magnitude of change in UPTT was, in this former case, as much as 6 microsecs as opposed to typically 1 to 2 microsecs for all the other types of fatigue tests mentioned so far. The exact temperature dependence of the piezoelectric probes was not, however, determined so these results should perhaps be regarded more as semi-quantitative.

Lateral residual strain damage results, plotted in Fig. 4.41(b), again indicate the sigmoidal form of damage accumulation, but futher interpretation is not really feasible because of the large scatter and paucity of results.

Acoustic emission PIP plots obtained from underwater tests at various temperatures indicate that "chains" are still present (at 25°C) on the unloading portion near minimum load (Fig. 4.15). On PIP traces typical of tests at 45° and 60°C Figs. 4.42(a) and (b), the A.E. noise tends to occur at all load stages with most noise at 60°C, consistent with the greater damage evidence in Fig. 4.41(a) at 60°C.

4.5.4 Discussion

From the foregoing results for wet versus dry fatigue tests, and for underwater fatigue tests, it is clear that dry mortar at a curing age of up to 2 weeks is more resistent to fatigue than equivalent wet or moist mortar. This is the case not only as far as lifetime is concerned, but also in terms of damage accumulation rate, clearly defining the role of internal water in any mechanism of fatigue in this material. Although not as clearly distinguished, the present experimental results indicate that the fatigue lifetime is also reduced at higher temperatures (in the temperature range $25^{o}C$ to $60^{o}C$), and that the damage is more extreme at the higher temperature. The data for the $45^{o}C$ tests, particularly the damage monitoring information, does not, however, appear to be approximately midway between the $25^{o}C$ and the $60^{o}C$ cases, but rather does not differ very much from the lower temperature case.

The results of this section are, however, somewhat sparse as substantial experimental difficulties were encountered. Although these were individually overcome, occasions arose when the difficulties were not all solved simultaneously. In addition, only fully reliable results have been presented. One of the significant difficulties appeared to arise from the dependence of measured strength (both static and fatigue) on the period of time spent at "high" temperature underwater. Since accurate information of this behaviour is germane to the subsequent fatigue study this aspect was investigated somewhat further.

Five nominally identical batches of mortar prisms (i.e. 60 specimens) cured under (ambient temperature) conditions for seven days, were statically ramped to failure underwater at $60^{o}C$ after sustaining different periods under these conditions. The results are shown in Fig. 4.43 which indicates a marked decrease in measured static strength for up to two hours immersion, with approximately little change after this period. Such behaviour is contrary to what was expected from the literature (33, 117, 121 and Fig. 2.25) which reports a strength decrease only above temperatures of approximately $250^{o}C$. Reported tests, however, were not conducted underwater but rather in moist air conditions. The slow strength increase after approximately two hours (at $60^{o}C$) may be associated with accelerated curing (120) but the initial rapid decrease apparently occurs before any of

the beneficial effects of accelerated curing can occur. Weakening of the bonding in the numerous inherent pre-existing cracks in mortar may occur in the first stages of exposure to 60°C water and the ramp tests may be sufficiently slow (at about 2 minutes) to exploit this weakening effect. Further work is, however, required to obtain a better understanding of this strength decrease with time at temperature.

We return now to Barrick's studies which are most interesting (29, 106). He conducted flexural tests on mortar at different temperatures and controlled relative humidities and monitored time to failure at high stress levels. After application of sophisticated statistical methods he produced graphs relating time to failure to relative humidity and temperature, Figs. 4.44(a) and (b). These results indicate that not only does static fatigue increase (and hence time to failure decrease) with increasing relative humidity, but that increasing temperature results in less static fatigue, (longer times to failure). This is further borne out by Table 4.3, which indicates that static temperature is almost non-existent. Barrick attributes this interesting behaviour, not to the attack of the silicate bonds by water as proposed by Charles for glass (259), but to attack simply by the hydroxyl ion, OH^-. From Charles' theory (259) of the simple water attack of silicate bonds, it might be expected that at high temperatures because of the higher thermal energy, the attack would be faster. However, if the hydroxyl ion alone is the prime driving force in the static fatigue, as proposed by Barrick, and because there is a high proportion of hydroxyl ions present from the dissociation of $Ca(OH)_2$ (one of the major products of cement hydration), significantly different behaviour is observed with temperature. The solubility of $Ca(OH)_2$, unlike almost all other hydroxides, decreases with temperature and so there is a lower concentration of hydroxyl ion to act on the cement paste in static fatigue (See Fig. 4.45). Barrick (29) proposes this mechanism of hydroxl ion attack to explain the observed behaviour of his results - namely an increase in static fatigue with increasing relative humidity but a decrease with temperature. This is consistent with Charles' theory if one only considers the latter two stages. However, Cook and Haque (112, 119) report significantly two to

three times longer tensile and compressive strength reductions for concrete and cement mortar exposed to water absorption, as opposed to methanol absorption, in apparent contradiction to Barrick's proposal. Mills (260) measured the strength of dried concrete on resoaking and obtained greater strength reduction for water than alcohol.

An alternative possible explanation of Barrick's findings, that time to failure increases with temperature even in high humidity situations, (i.e. decreased static fatigue), may be the effect of accelerated curing at the higher temperatures. Barrick's samples were relatively young ($\simeq$ 14 days) and despite their specific curing history, the strength increases as the mortar hydrates. This may appear to account for the decreased static fatigue with temperature.

Barrick and Krokosky's (29, 106) suggestion, that the nature of the stress corrosion is one of hydroxyl ion attack deriving from inherent calcium hydroxide, is at odds with the present findings. Shorter lives and greater damage were observed at the highest temperatures of $60^{o}C$ and thus the damage mechanism would appear to be thermally activated, in contrast to Barrick and Krokosky's results. Their results, however, involved some questionable truncation of very short lifetime data, (together with some debatable statistical methods), which may well not have been insignificant - so their results may have been biased. The controversy thus appears to remain, if one examines only damage development in compression prism specimens.

Prior to any detailed consideration of the mechanisms of fatigue in cement based materials, there thus appears to be a requirement to examine the development of a single crack in terms of fatigue crack growth rate and the factors affecting it, rather than the accumulated effect of many microcracks heretofore called damage, which has so far been investigated. A more quantitative response for crack growth rate should be possible under a variety of test conditions similar to the foregoing. This may be more successful than damage accumulation rates in leading to an understanding of the mechanism of fatigue failure under such conditions. Such an investigation of single cracks and their growth rate under tight environmental controls, is undertaken in Chapter 7.

4.5.5 Conclusions

This section has examined the effect of moisture and temperature on the fatigue behaviour of cement mortar. Previous studies were first reviewed, and proved to be very limited, particularly with regard to submerged hot water fatigue tests. An experimental programme consisting of underwater fatigue tests at 25°C, 45°C and 60°C was developed. Although undertaken in full, the number of results obtained, particularly with regard to damage monitoring, were limited because of certain experimental difficulties. Increased scatter in both static and fatigue results occurred which may, as was subsequently suggested, be due to the duration of time the specimen spent at the test temperature prior to test.

Despite these difficulties it was apparent that dry specimens have a greater fatigue life than moist, or wet, specimens and that fatigue tests at 60°C have shorter lives, and sustain more damage, than tests at lower temperatures. There was evidence to suggest that some form of "accelerated curing" or "fatigue strengthening" occurred in heated, cooled and subsequently fatigued tests. This latter aspect forms the subject of the following chapter.

4.6 General Discussion and Conclusions

Discussion has already been presented in each of the sections of this chapter and it is not intended to reproduce this here. This section, 4.6, is concerned in summarising those effects which interact between the sections considered and which add to the greater understanding of the nature of fatigue of cement mortar.

The factors that primarily affect the fatigue of cement mortar, based on the findings of the present study, are given below in order of importance. In addition distinction is made, in this section of the chapter, between (i) duplicaton and confirmation of previously reported studies on the one hand and (ii) new and original work on the other.

1. The principal factors in controlling the fatigue life are the cyclic stress range and maximum cyclic stress level, assuming, of course, constant environment, for example high humidity conditions. The stress

range programme results supplement and confirm these effects which have previously been well documented. Fatigue behaviour of cement based materials can, to a large extent, be described in terms of a conventional SN curve and by the use of the appropriately modified Goodman diagram.

2. If the cyclic stress levels and range are kept constant, then variations in other parameters, such as frequency, appear to affect fatigue life, at the high cyclic stress level of 80%, at least. This finding, although noted before (25, 27, 28, 89), appears to be the subject of some controversy as the majority of the literature suggests there is no dependence of fatigue life on frequency. In the present programme tests at three frequencies of 10, 1 and 0.1 Hz, particularly when evaluated in terms of a damage accumulation viewpoint, yielded a separation into three frequency regimes, suggestive of a very definite frequency effect. As the frequency was reduced it appeared that fatigue life became shorter, the rate of damage accumulation increased and that (to a less clearly defined extent) the final degree of damage also increased. The two former conclusions were based on the number of cycles, but if the results were re-evaluated from a time dependence viewpoint, i.e., damage rate per unit of time, as opposed to per cycle, it turns out that there was very little real frequency dependence, only a time dependence.

3. There does appear to remain a small but real frequency effect, however, especially with respect to fatigue test duration, at 10Hz, which gave slightly shorter (real time) lives. This was perhaps thought to be related to the increased temperature arising from cycling, of approximately $20^{o}C$ - a factor which needs further study; or perhaps from strain rate dependent loading of water being trapped inside open cracks at 10Hz. This is discussed in more detail in Chapter 7.

4. At 1 Hz, however, there does not appear to be any strain rate dependence, since fatigue with two sawtooth loading forms, including fast loading and fast unloading, did not produce any difference in fatigue life or damage accumulation behaviour. However, since the fatigue duration for both sawtooth waveforms was approximately constant, in the absence of any rate dependent mechanism, it is perhaps not surprising that the life and damage behaviour is very similar.

5. Fatigue tests with a dwell period at the high stress level or the low stress level yielded shorter and longer lives respectively. This is again consistent with the importance of time dependence, all other parameters being constant.

6. When the specimens are fully dried (to below 25% RH and probably closer to 10%) the fatigue strength increased from 54% to 64%, in this case, confirming behaviour reported in the literature. Fatigue lifetimes increased by about an order of magnitude and the damage accumulation rates were similarly reduced. Behaviour in other respects was apparently similar (at least for those parameters tested).

7. It was clear despite certain experimental difficulties, that underwater tests at $60^{o}C$ had a shorter life and sustained more damage than tests performed at lower temperatures of $45^{o}C$ and $25^{o}C$. The decrease in life (from $25^{o}C$ to $60^{o}C$) was of the order of about 3 times (compared to about 10 times for dry to wet tests just mentioned), although these measures should be regarded perhaps only semi-quantitatively. The strength appears to decrease with time at temperature and may be related to creep effects (which increase with temperature). Alternatively stress-assisted environmental attack may be operating, assuming significant residual stresses in the mortar matrix in the vicinity of the numerous inherent cracks in dried and cured mortar. This is discussed in more detail in Chapters 7 and 8 together with Barrick's hydroxyl ion temperature dependent solubility postulate (29, 106).

8. The damage accumulation investigations mentioned in this chapter have been particularly successful. Ultrasonic transit time detection methods allied to longitudinal and lateral strain measurements have reliably measured the degree of microcracking in a specimen during fatigue. This was supplemented by acoustic emission monitoring using both simple rate counted data and the pseudo isometric plot technique. These damage monitoring methods, UPTT, strain and AE, correlated very well with one another.

9. It is of value to highlight the importance of the acoustic emission damage monitoring, and in particular the PIP technique. The frequency bandwidth was restricted to between 45kHz to 200kHz to filter out machine noise, but was shown by AE spectral analysis to detect reliably real

acoustic events. From the PIP results, it is clear that the AE is discrete, intermittent and unquestionably arises from cracking and microcracking. It develops and becomes more pronounced near failure; indeed, characteristic AE signals near peak load can be used as warnings of impending failure or of some major cracking event. It is possible, knowing the PIP AE characteristics, to correlate AE.PIP traces with the appropriate testing parameters, for example, high or low frequency, or wet versus dry conditions.

10. Considering only the phenomenology, damage development appeared to be of a sigmoidal three phase character. Shortly after commencement of fatigue there was a rapid increase in measured "damage" while existing cracks achieved stable conditions and the matrix took the cycle load. In the second stage there was an approximately linear increase of damage until, near failure, the third (rapid) stage was reached where there was substantially more microcracking and coalescence of cracks leading to failure.

It might seem appropriate to discuss mechanisms of cracking at this stage, but this is held over to Chapter 8. This is done because it was believed that fatigue crack growth for single cracks (under similar experimental conditions to Chapter 4, as investigated in Chapter 7), may add to the mechanistic understanding of crack behaviour.

A discussion of the AE PIP noise, particularly on the unloading cycle for wet tests is also held over to Chapter 7, where a hydrowedge postulate is proposed together with associated possible mechanistic implications.

This Chapter, then, has examined in some detail the fatigue and damage behaviour in compression prisms under a variety of testing environments and investigating parameters.

Only two of the items (1) and (6) of this section 4.6 effectively supplement existing knowledge; the others can be regarded as new contributions to the phenomenology of mortar behaviour. (The frequency effect is included in this latter group in view of the controversy surrounding it). Before moving onto the investigation of single cracks the phenomenon of strength increase following fatigue, mentioned earlier in this chapter, is investigated. This forms the basis of Chapter 5, to follow.

TABLE 4.1

Fatigue lifetimes of compression prisms at various stress ranges but with a constant maximum stress level of 80%.

LOADING RANGE STRESS LEVEL (PERCENT)		
80 - 2.4	80 - 30	80 - 60
750	12 500	59 140
420	13 310	25 940
1 750	7 700	60 000
665		53 500

TABLE 4.2

Underwater fatigue lives at various temperatures.

FATIGUE TEST TEMPERATURE					
25°C		45°C		60°C	
Static Strength (MPa)	Fatigue Lives	Static Strength (MPa)	Fatigue Lives	Static Strength (MPa)	Fatigue Lives
53,8	720	48,2	252	53,2	137
51,5	2 089	51,0	522	41,5	414
58,2	1 391	30,2	359	33,9	19
56,7	-	40,3	377	45,3	363
60,6	332		533		317
54,8	1 088				374
51,6	505				174
53,0					
53,1	518				
61,2	1 626				
52,3	503				
51,6	1 243				
54,8	1 002	44,7	409	43,5	257

TABLE 4.3

BARRICKS STATIC FATIGUE TIMES

(HOURS)

RH	25°C	35°C	60°C
10%	2.505	114.700	...
55%	0.105	2.879	...
96%	0.016	0.664	237 400

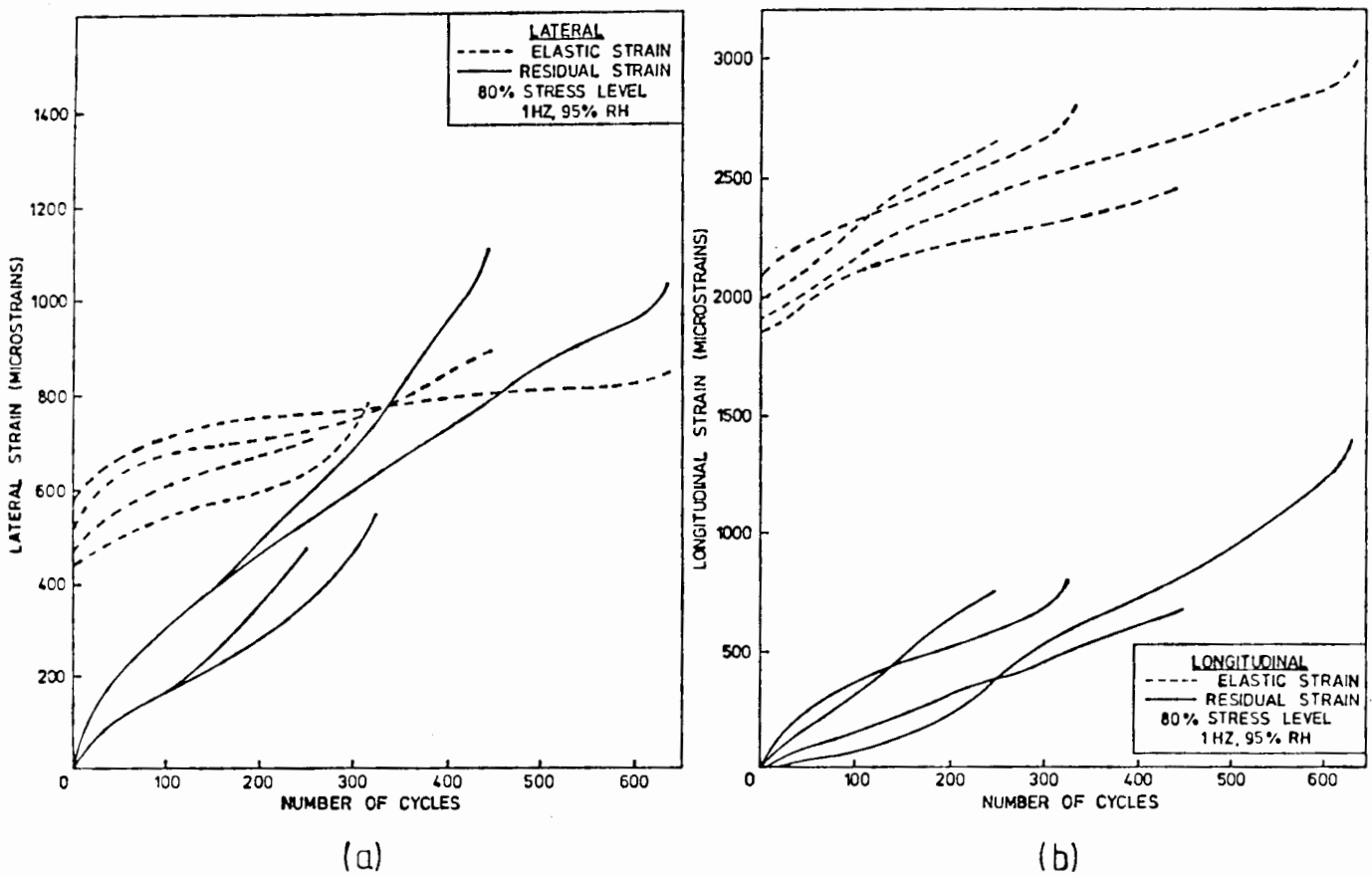

Fig. 4.1 : Typical fatigue strains for both elastic and residual strains for four fatigue tests (1Hz, 80% stress level, moist) showing (a) lateral and (b) longitudinal strains as a function of number of cycles.

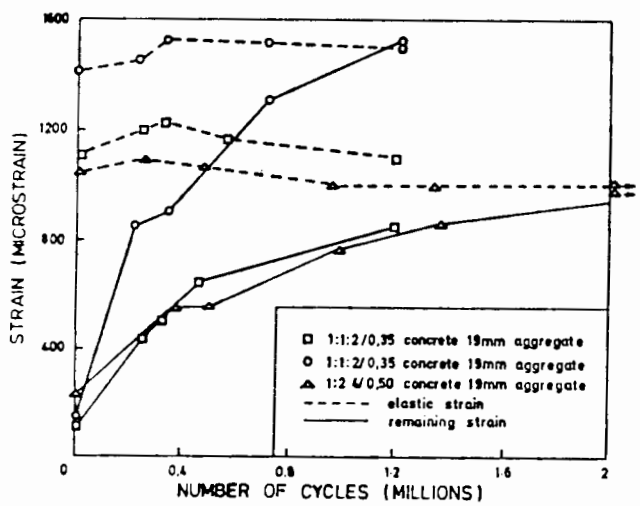

Fig. 4.2(a) : The development of residual and elastic strains with repeated loading for three specimens. (After Bennett and Muir (96)).

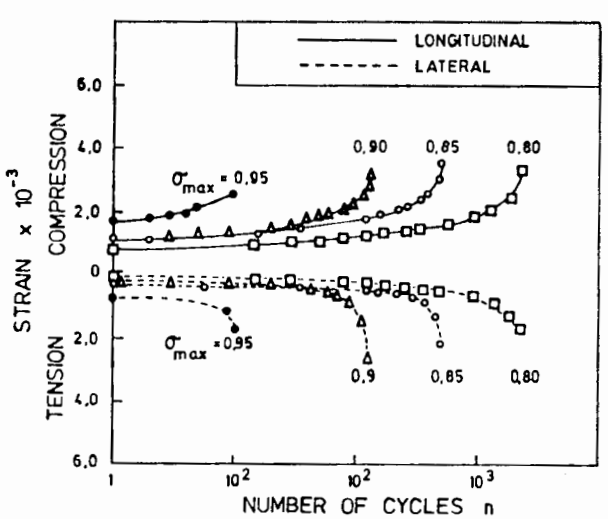

Fig. 4.2(b) : The effect of age at loading on the time and strain to failure of concrete subjected to different level of sustained stress. (After Awad and Hilsdorf, (27)).

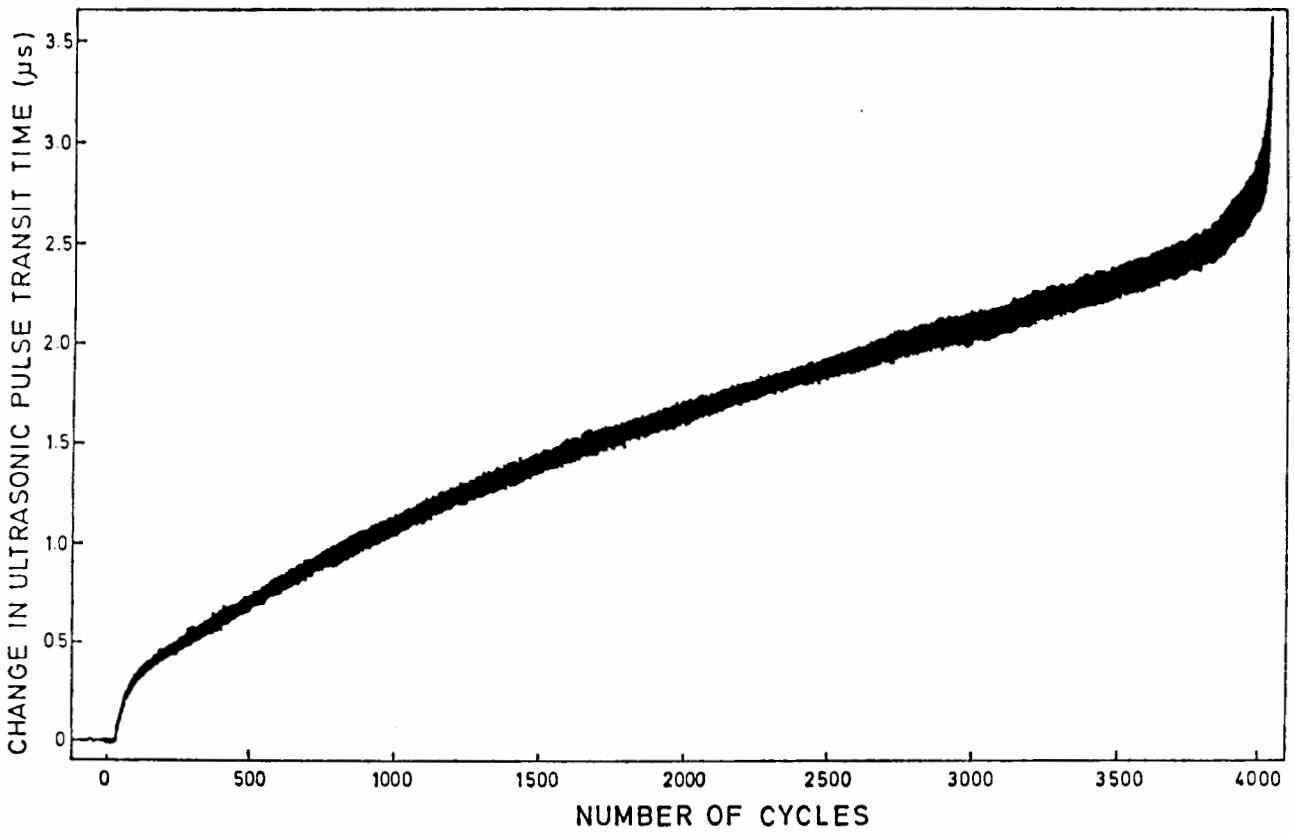

Fig. 4.3 : Typical trace of changes in ultrasonic pulse transit time (UPTT) associated with fatigue. (10Hz, 80% SL, moist).

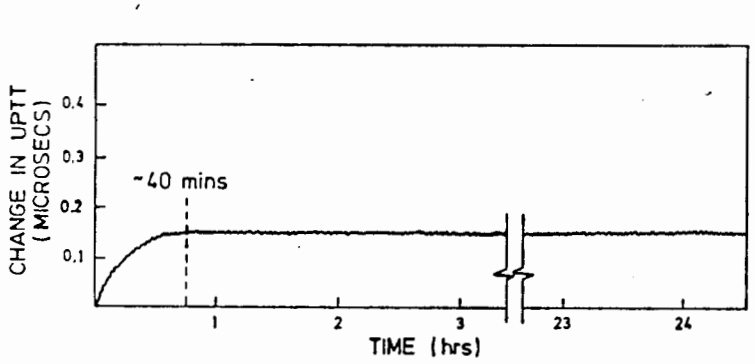

Fig. 4.4 : Typical UPTT base line test illustrating the small effect of specimen humidity equilibration. The transit time was measured from the instant the probes were attached immediatly after specimen removal from the curing bath. There appeared to be no further change in UPTT after approximately 40 minutes.

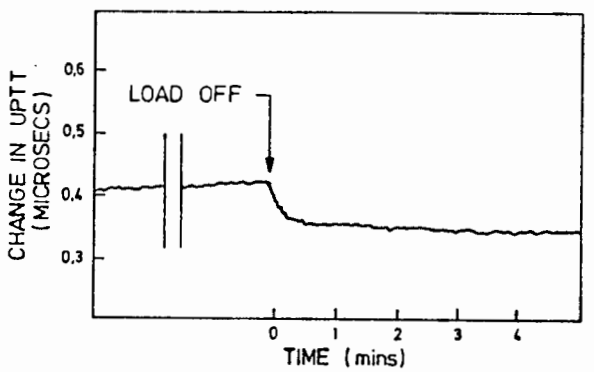

Fig. 4.5(a) : Illustrating the small decrease in UPTT when the load is removed.

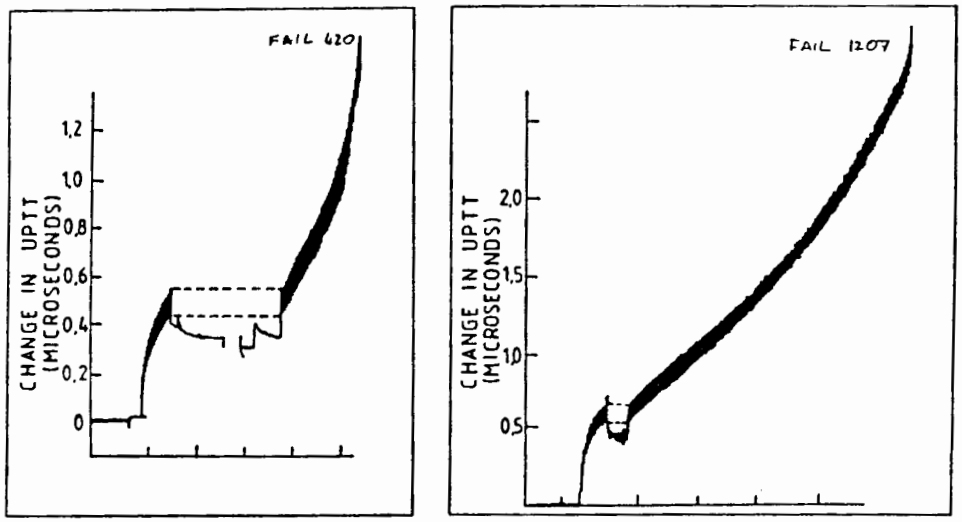

Fig. 4.5(b) and (c) : Interrupted fatigue tests with load removal from (a) 25 minute rest period and (b) 1 minute rest period, illustrating recovery of microcracking and decrease in UPTT during unloading. Note that where fatigue recommences the previous UPTT value is re-established.

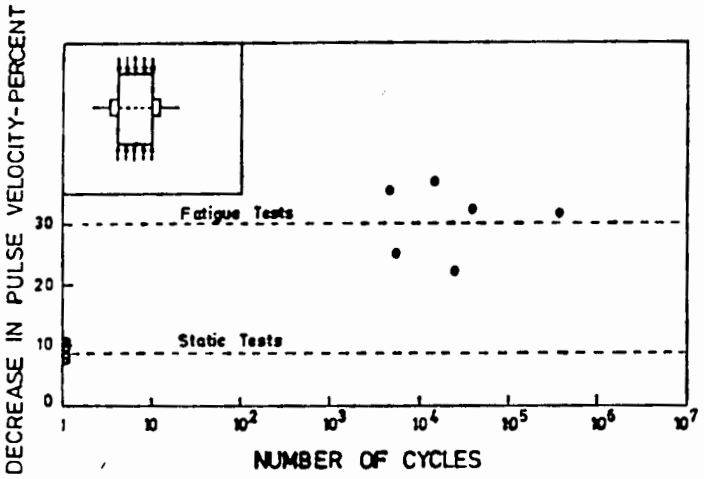

Fig. 4.6(a) : Reduction in pulse velocity near failure in static and fatigue tests. (After Raju (193)).

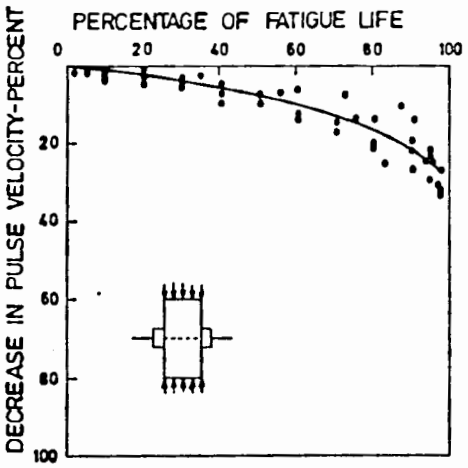

Fig. 4.6(b) : Decrease in transverse pulse velocity under repeated loading (After Bennett and Raju (143)).

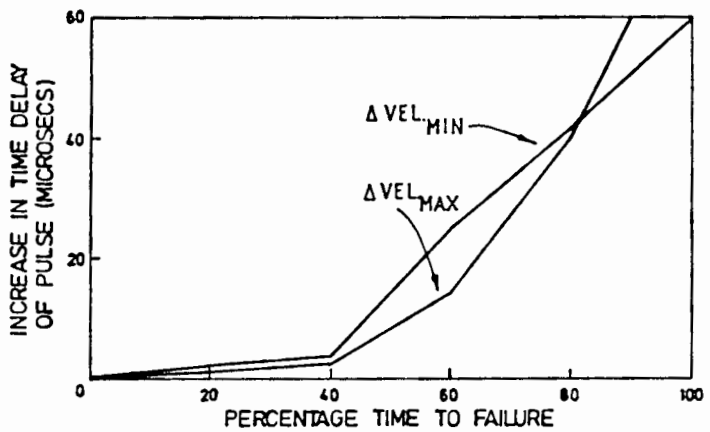

Fig. 4.7 : Ultrasonic measurements for cyclic tests. (after Shah and Chandra (89)).

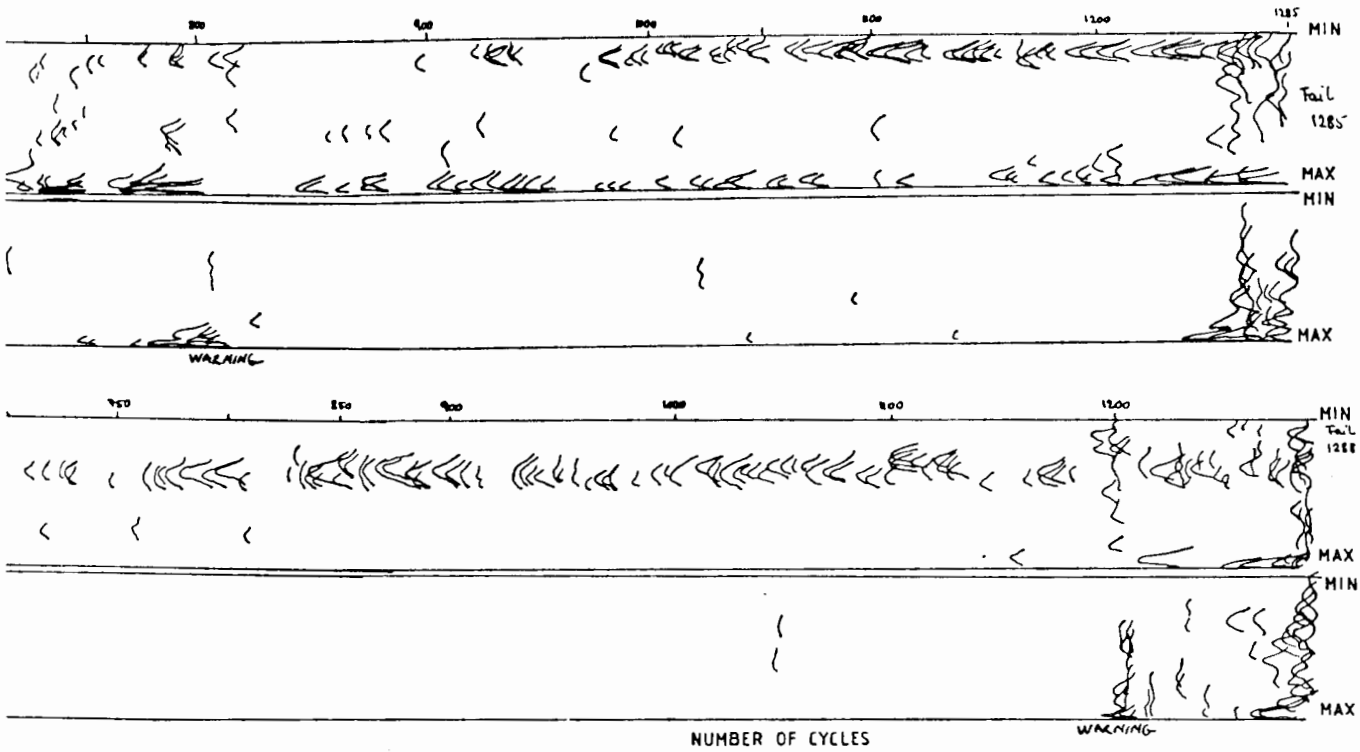

Fig. 4.8 : PIP trace of the last 600 cycles of two fatigue tests (80% SL, sine wave, 0.5Hz moist). For both tests note the increase in acoustic noise as failure is approached, the sporadic or intermittent nature of the events, and that for these ("moist") tests there is more noise on the unloading cycle near minimum load forming a so called "chain". "Warning" events are also apparent at approximately (a) 800 cycles and (b) 1 205 cycles respectively.

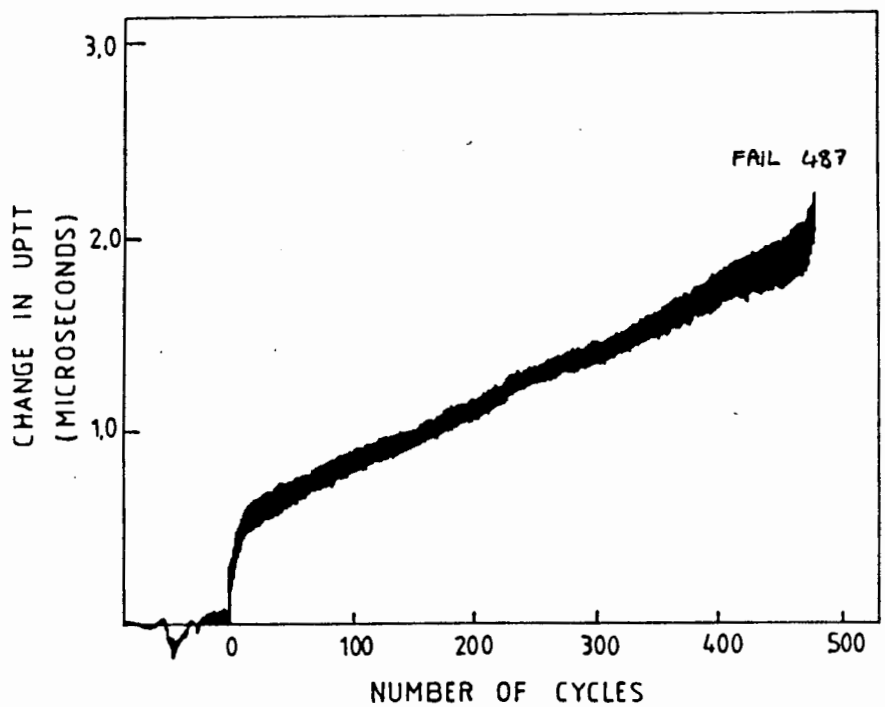

Fig. 4.9 : UPTT trace associated with the AE PIP result shown in Fig. 3.28(a), (Dry, 87% SL, 0.5HZ, life 487 cycles). This UPTT trace is very typical and also shows the development of the number of cycles and the change in UPTT.

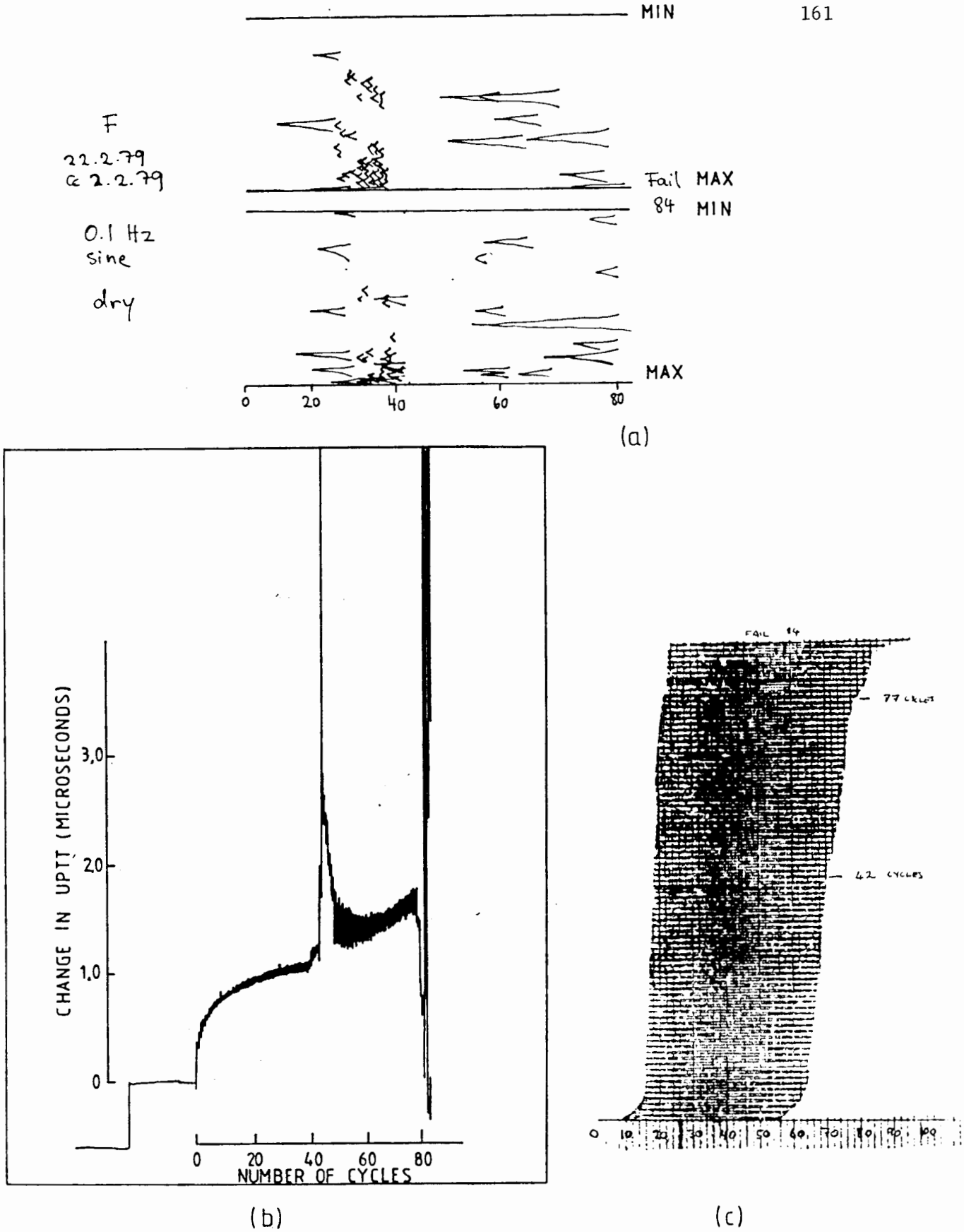

Fig. 4.10 : Damage monitoring results of a dry fatigue test, (0.1Hz, sine dry, 87% SL, life 84 cycles, also AE amplitude was amplified 5 times compared to other tests), showing correlation between (a) the PIP result, (b) the UPTT signal and (c) the lateral LVDT "strain" trace. Note the effect of macrocracks at approximately 42 and 77 cycles on the damage monitoring signals, particularly PIP and UPTT methods.

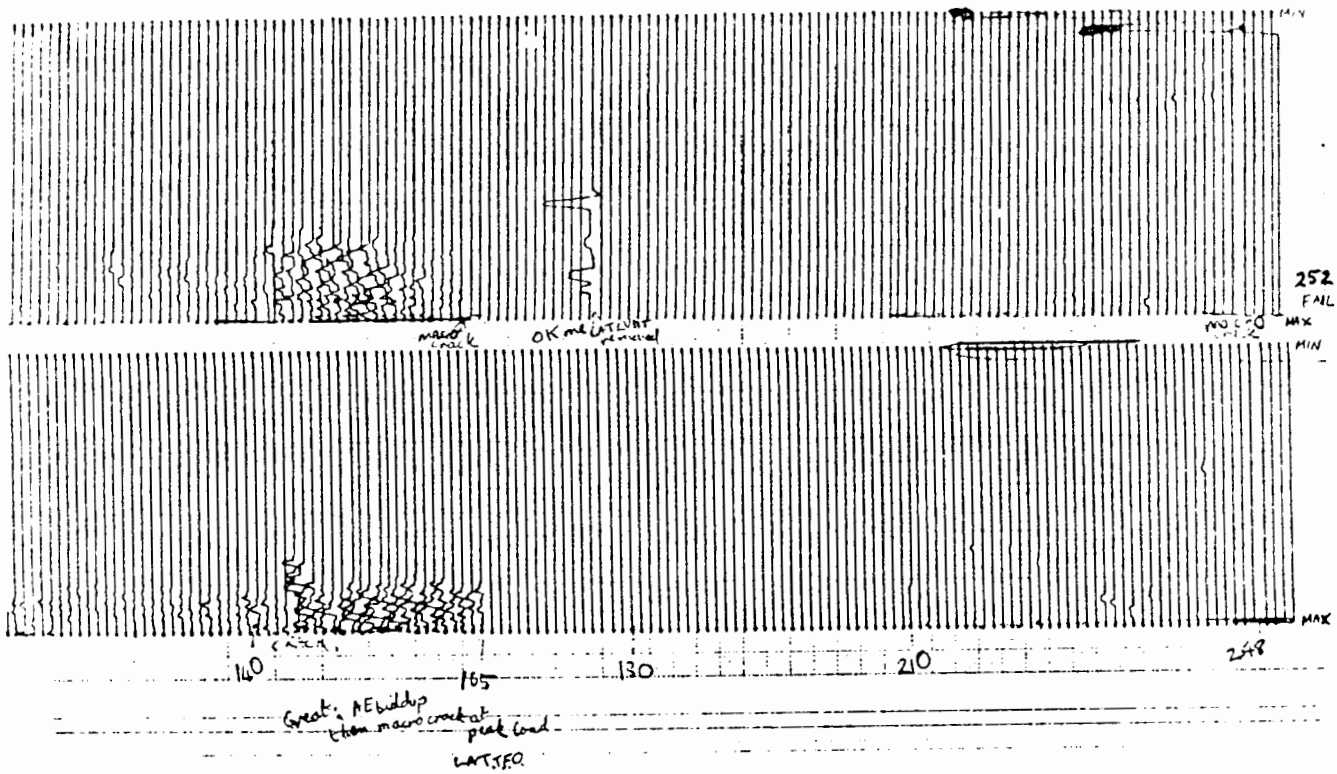

(a)

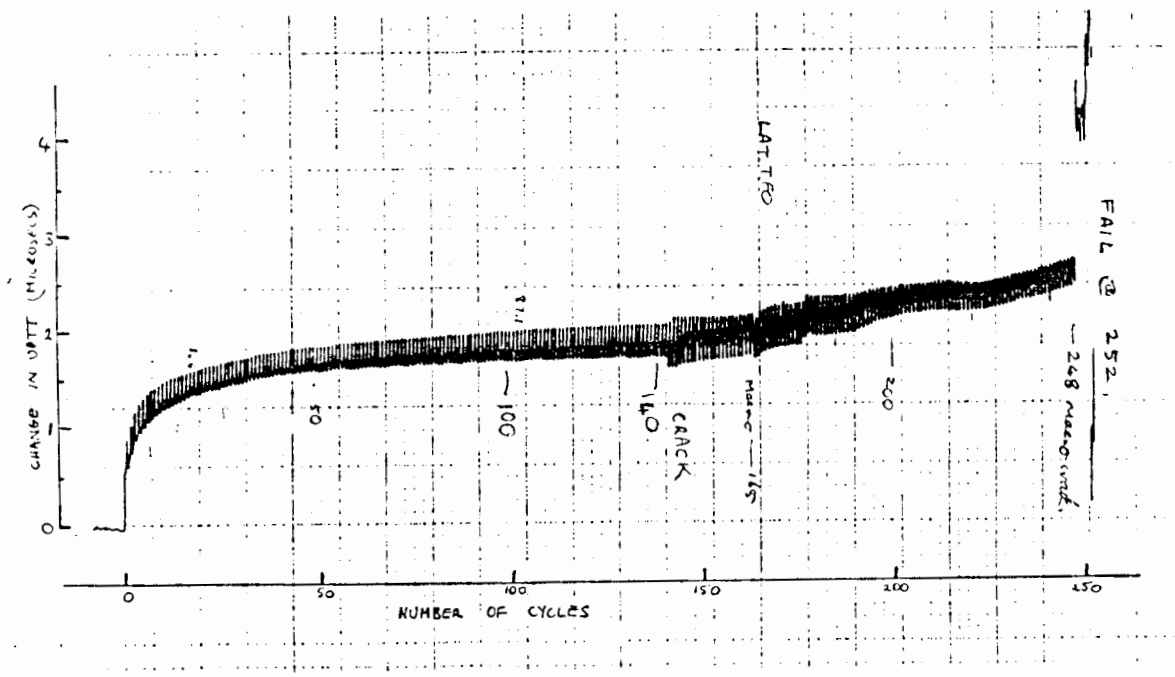

(b)

Fig. 4.11 : Part of an (a) pseudo isometric plot and (b) corresponding ultrasonic (UPTT) trace of a dry 0.1Hz fatigue test, (87% SL, RH 25%, sine, 0.1Hz, life 252 cycles). Note that at approximately 143 cycles microcracking developed and resulted in a macrocrack at 165 cycles. This led to the lateral transducer breaking away and falling off (LAT T.F.O.). A further "warning" macrocrack occurred at peak load, at 248 cycles and final failure soon followed.

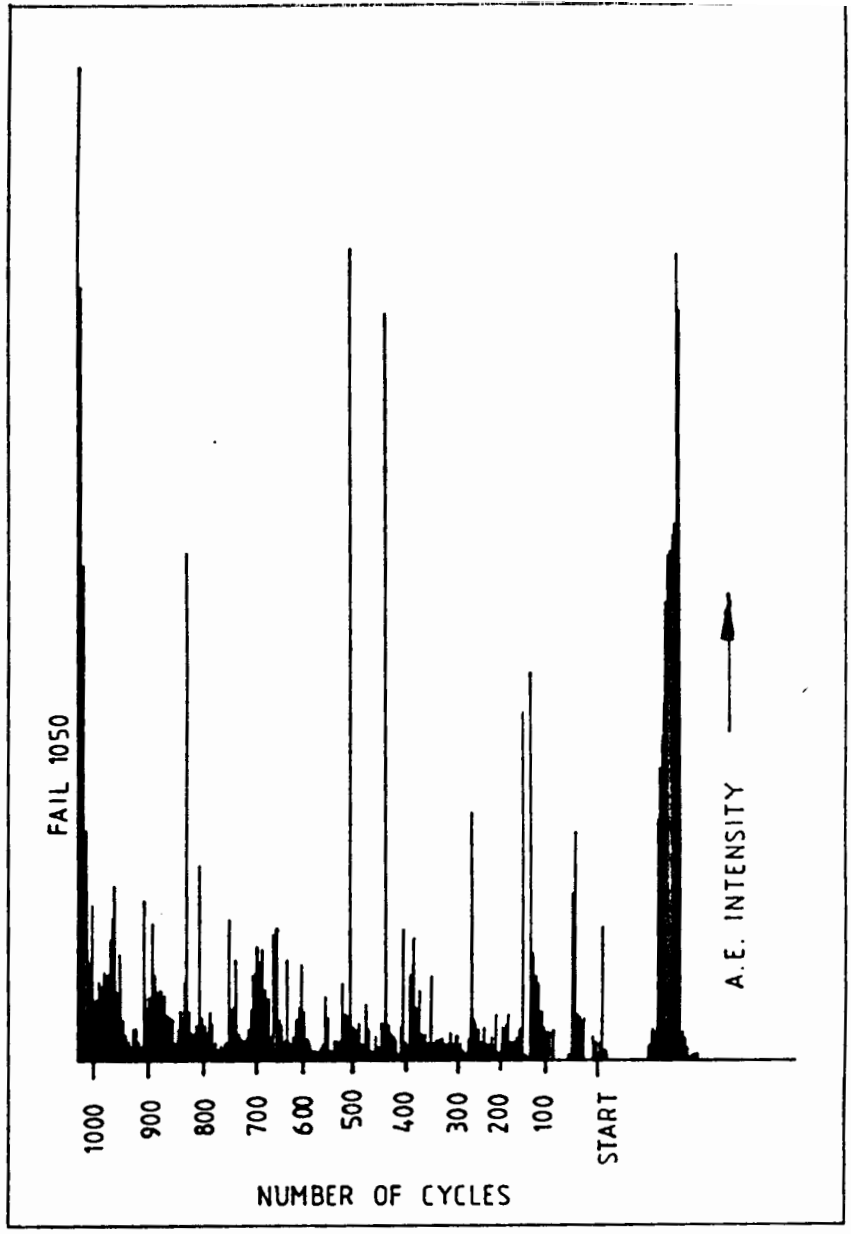

Fig. 4.12 : Non PIP acoustic emission results indicating macrocracks at approximately 505 and 830 cycles for the 1 050 cycle fatigue test, (80%, sine, 0,5Hz, moist.)

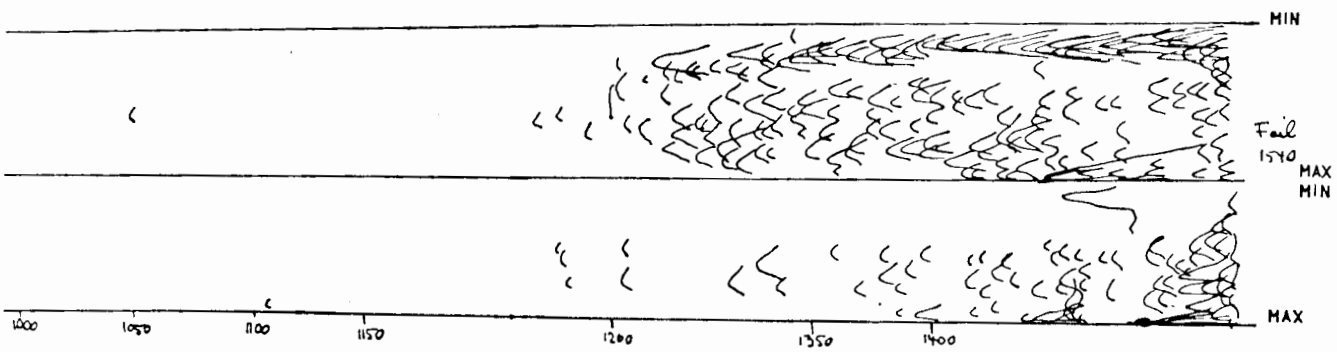

Fig. 4.13 : Illustrating "chain" occurence for moist mortar with increased noise near failure. (80% SL, sine, 0.5Hz, life 1540 cycles).

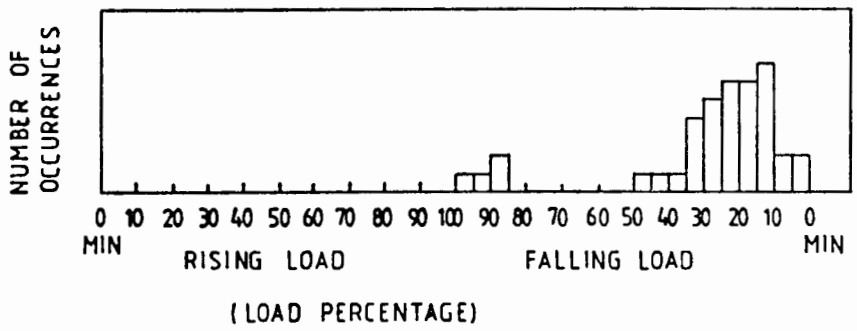

Fig. 4.14(a): Occurrence of AE "chains" as a function of load. Note that when chains occur (under moist conditions) they are almost always near the lowest load on the unloading portion.

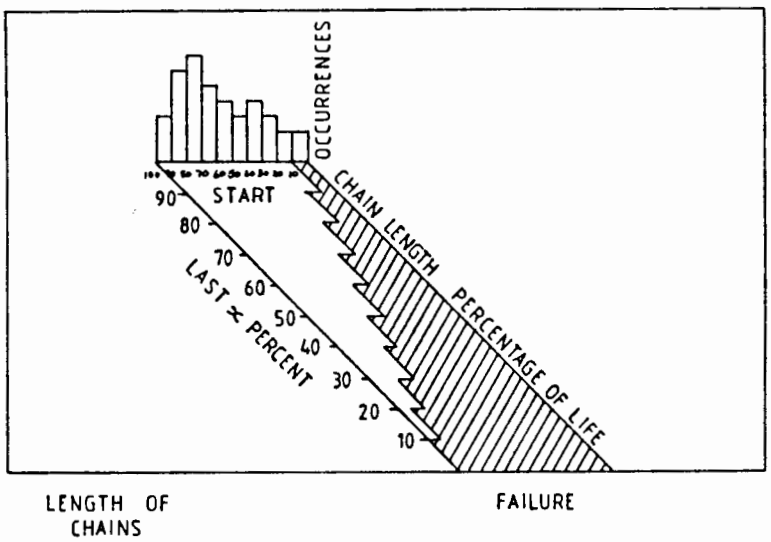

Fig. 4.14(b): Histogram of chain length and its location as a percentage of fatigue life. While some tests exhibited chains for 100% of life, most chains occurred only in the last 40% of life.

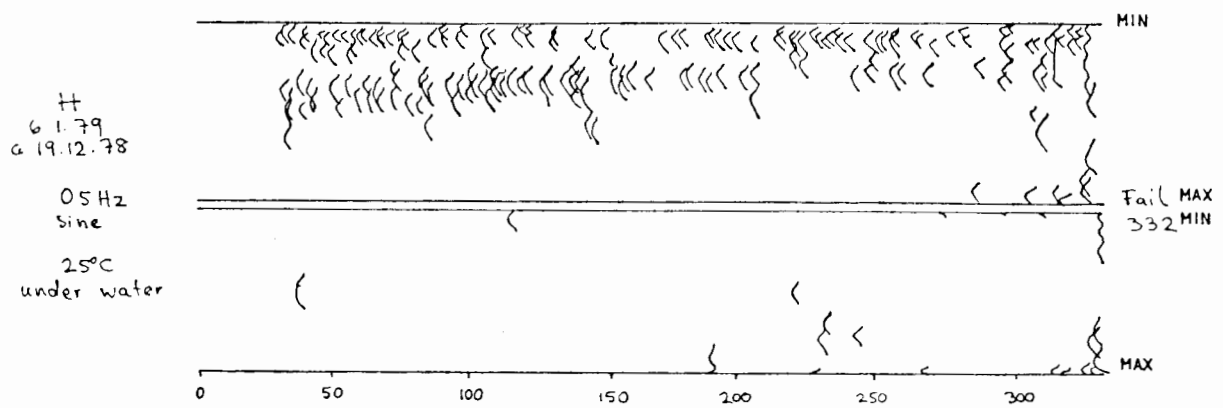

Fig. 4.15 : Illustrating AE "chain" occurence for underwater tests at 25°C on the unloading portion near minimum load. (76% SL, 0.5Hz, sine, 25°C under water, life 332 cycles).

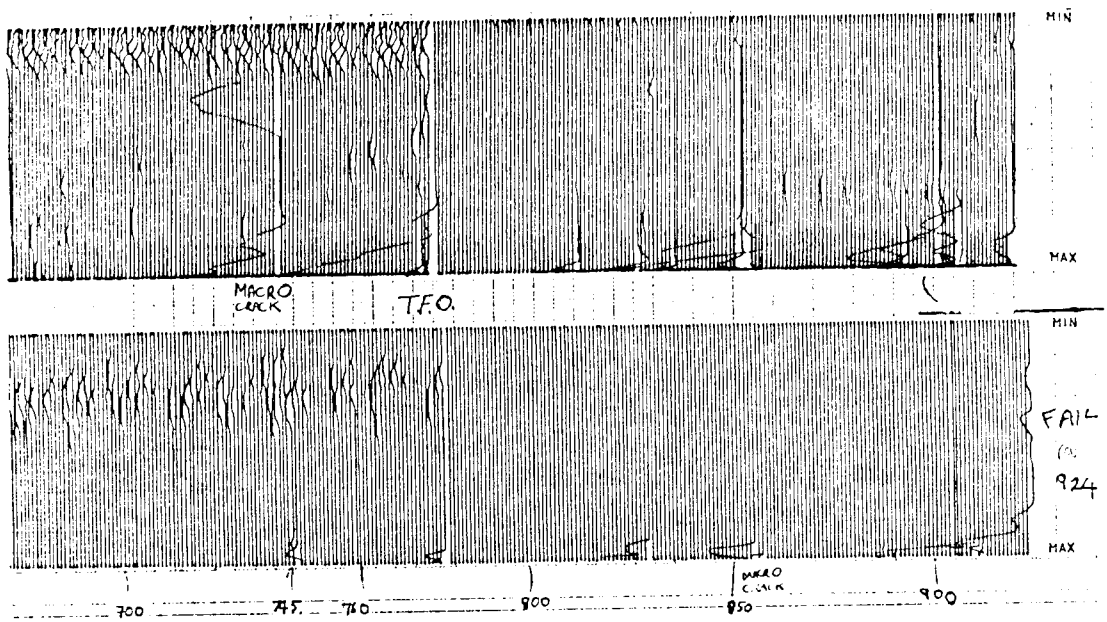

Fig. 4.16 : Damage monitoring results for a dry fatigue test. (87% SL, 0.5Hz, Dry, Life 924 cycles), illustrating the PIP signal for the latter part of the fatigue life. Macrocrack occurrences at 745 cycles (resulting in the transducer falling off at 789 cycles) and 836 cycles are evident.

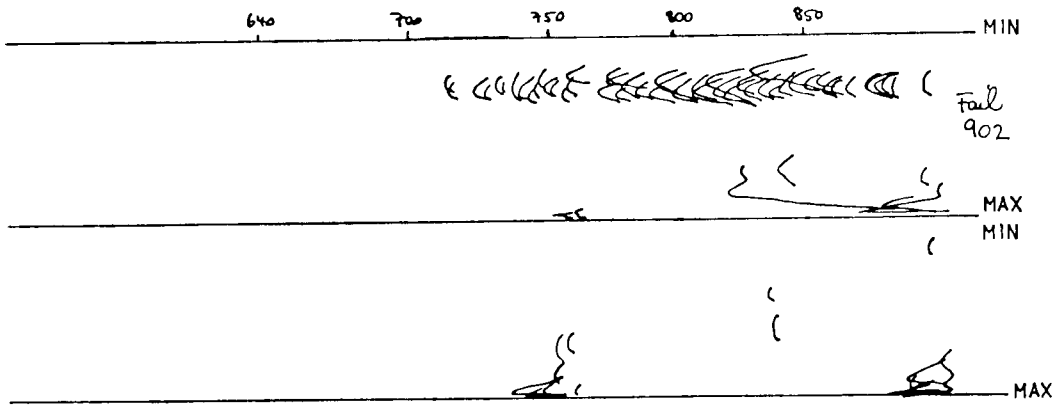

Fig. 4.17 : PIP trace illustrating a typical "warning" event at 755 cycles. The warnings tend to be larger at or near peak load and in the last 25% of the fatigue life (80% SL, 0.5Hz, moist, sine, life 902 cycles).

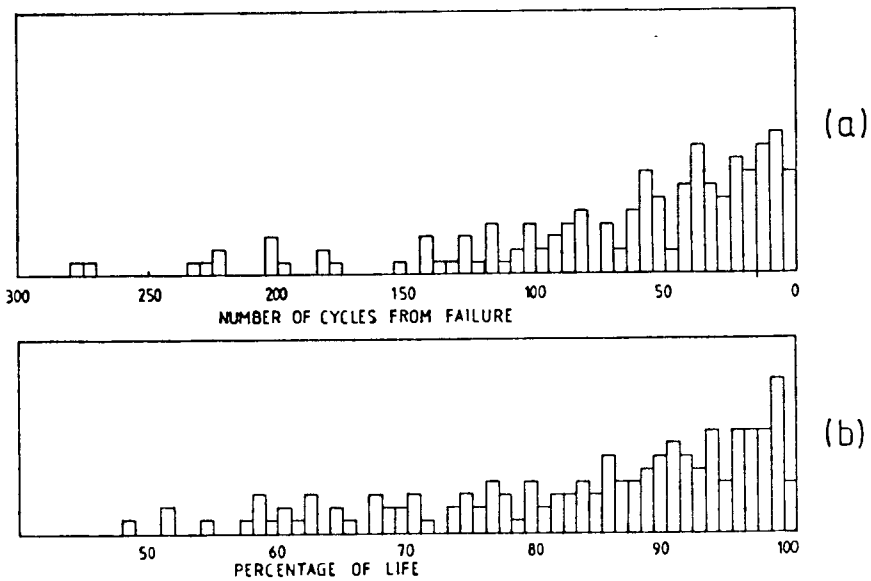

Fig. 4.18 : Histogram of the AE warning events as a function of (a) number of cyles or (b) percentage life.

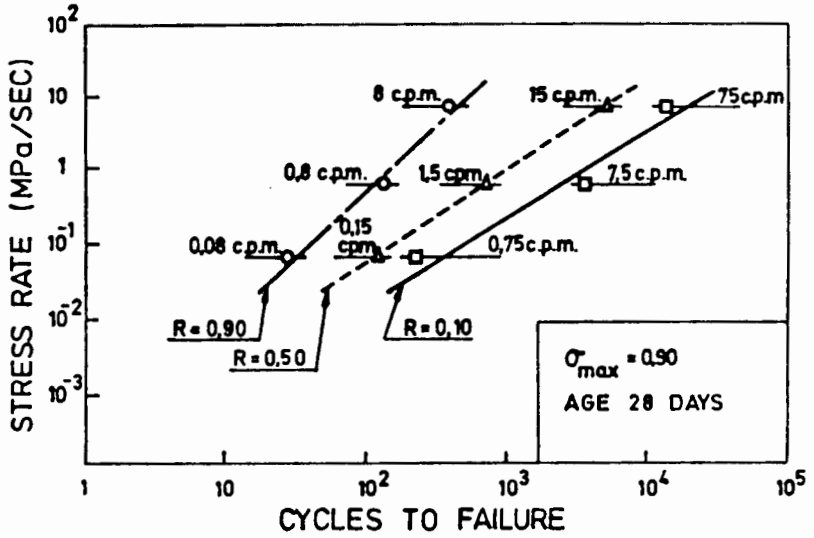

Fig. 4.19 : Influence of stress rate and frequencing of testing on the fatigue life of concrete, (SL = 90%, loading of 28 days, moist (After Awad and Hilsdorf (27)).

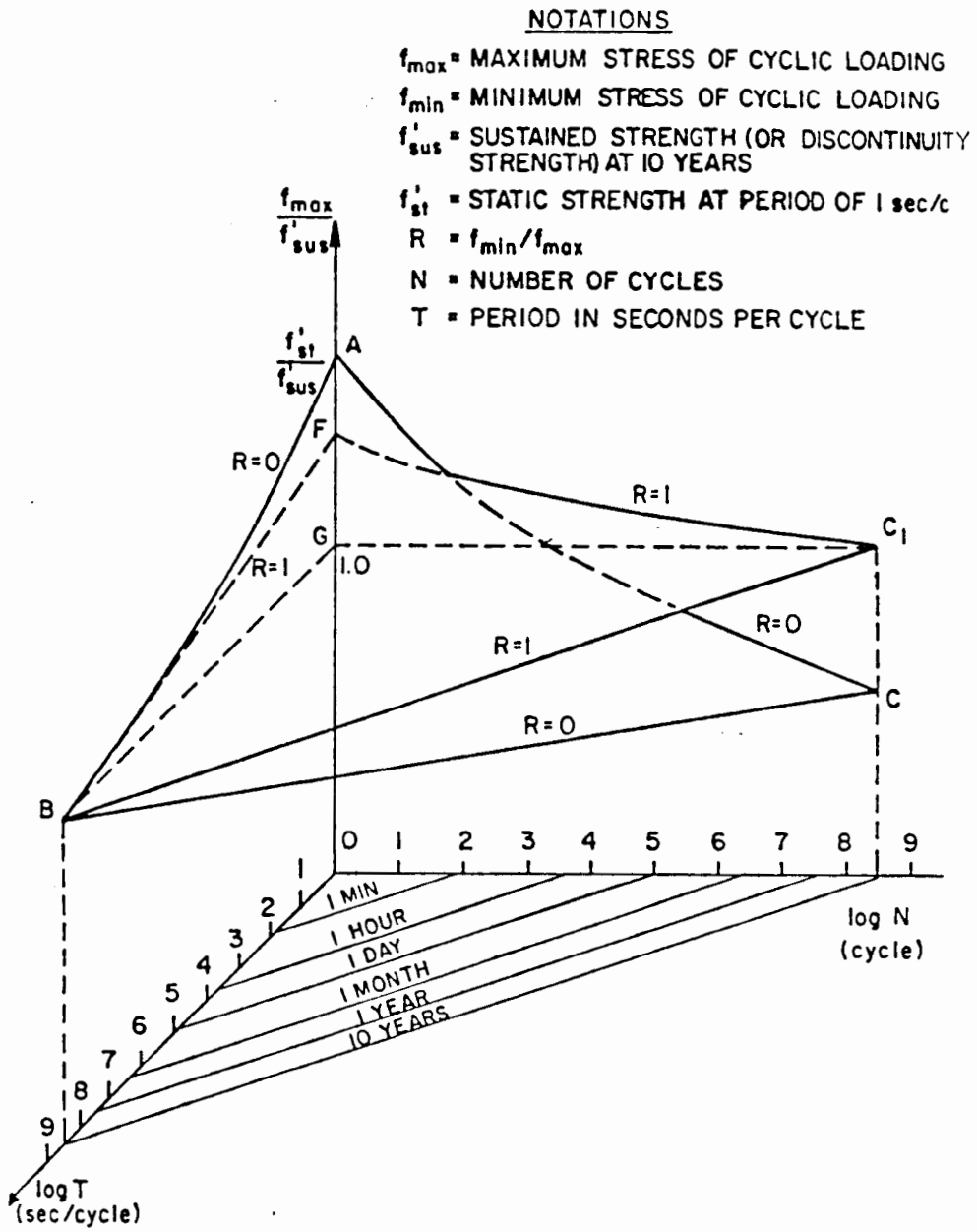

Fig. 4.20 : Hsu's graphical representation of the f-N-T-R relationship (25).

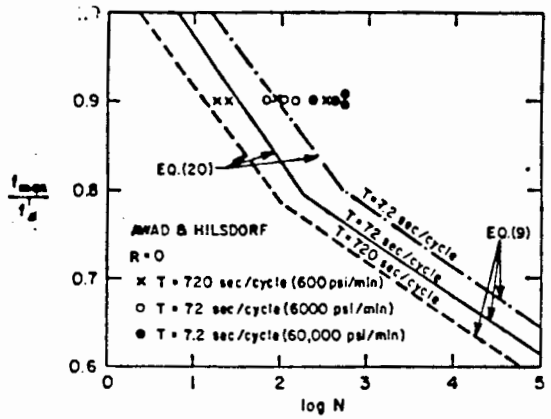

Fig. 4.21(a): Hsu's (25) presentation of Awad and Hilsdorf's results (27). Note the effect of reduced frequency (i.e. increased period) is to shorten life.

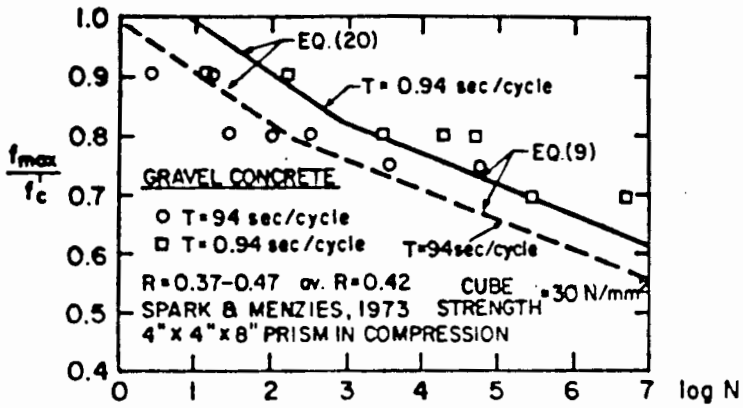

Fig. 4.21(b): Hsu's (25) presentation of Sparks and Menzies results (28). Note the effect of reduced frequency is to shorten life.

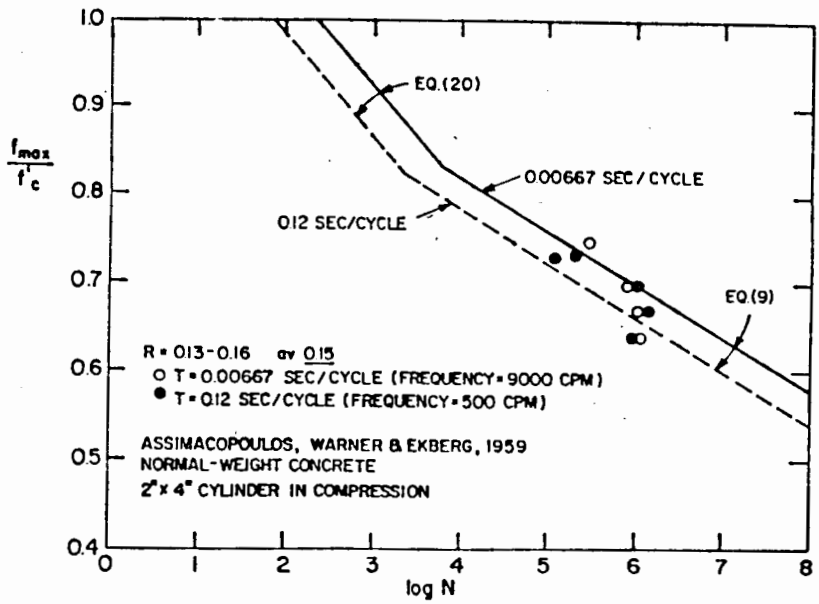

Fig. 4.21(c): Hsu's (25) presentation of Assimacopoulos et al. results (231) for two rates of loading.

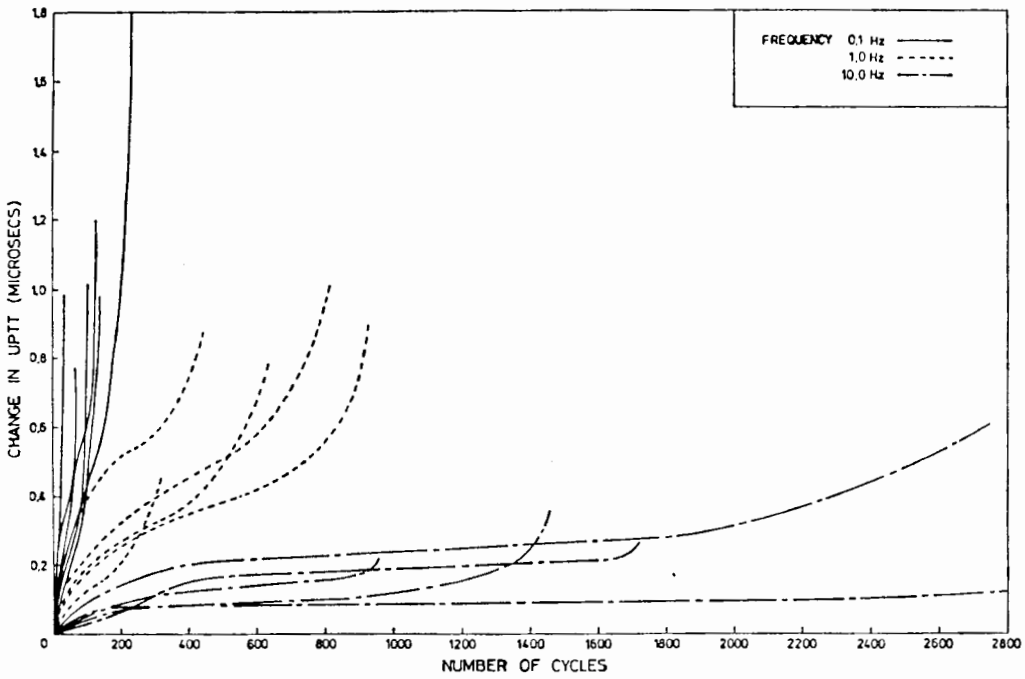

Fig. 4.22 : Change in ultrasonic pulse transit time for various frequencies. (Moist specimens, 80% SL, sine).

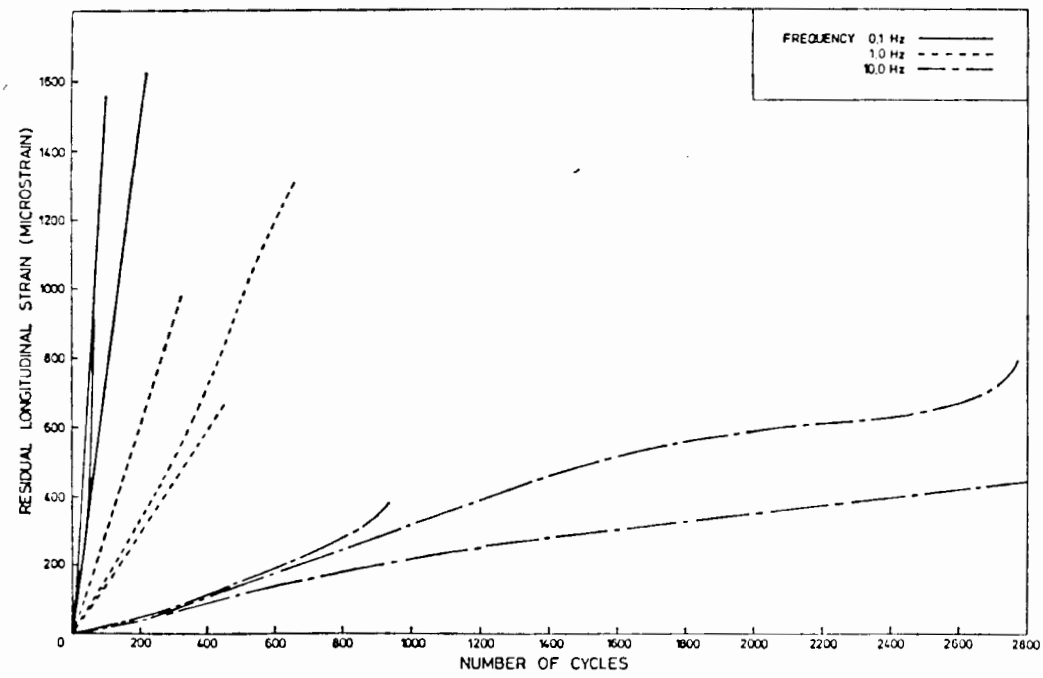

Fig. 4.23(a): Longitudinal residual strain versus number of cycles for various frequencies. (Moist specimens, 80% SL, sine).

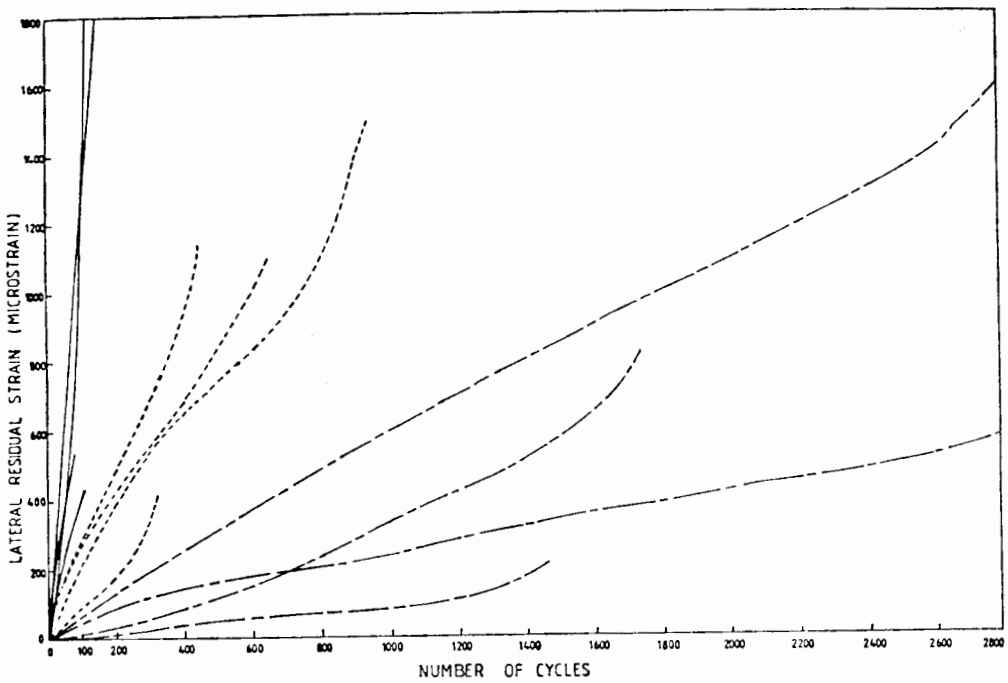

Fig. 4.23(b): Lateral residual strain versus number of cycles for various frequencies (Moist specimens, 80% SL, sine).

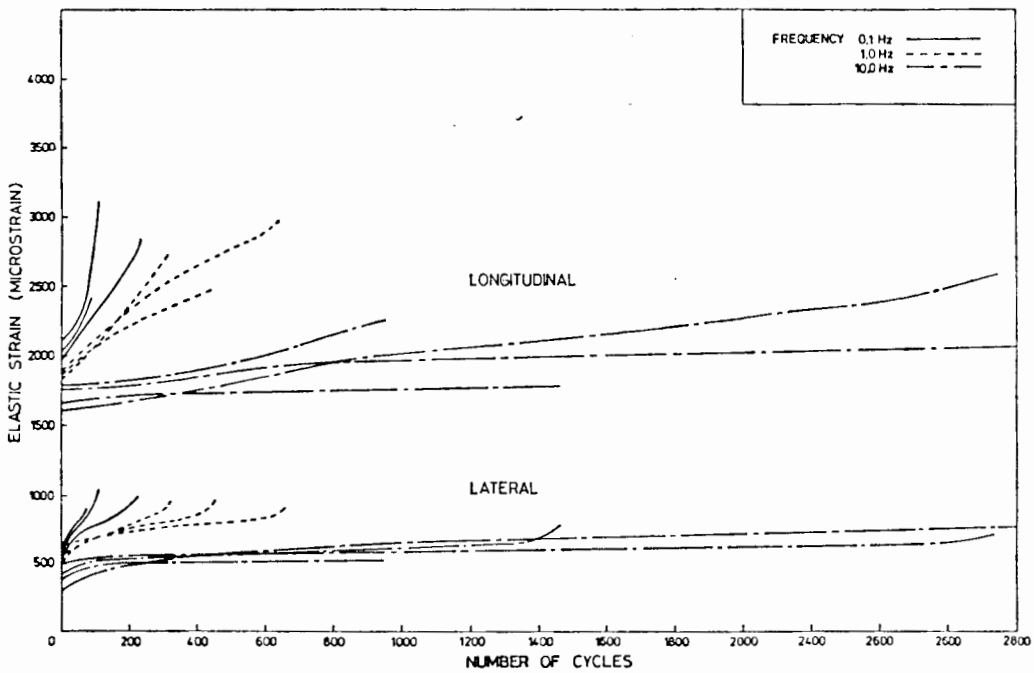

Fig. 4.23(c): Elastic strains for both longitudinal and lateral cases for various frequencies (Moist specimens, 80% SL, sine).

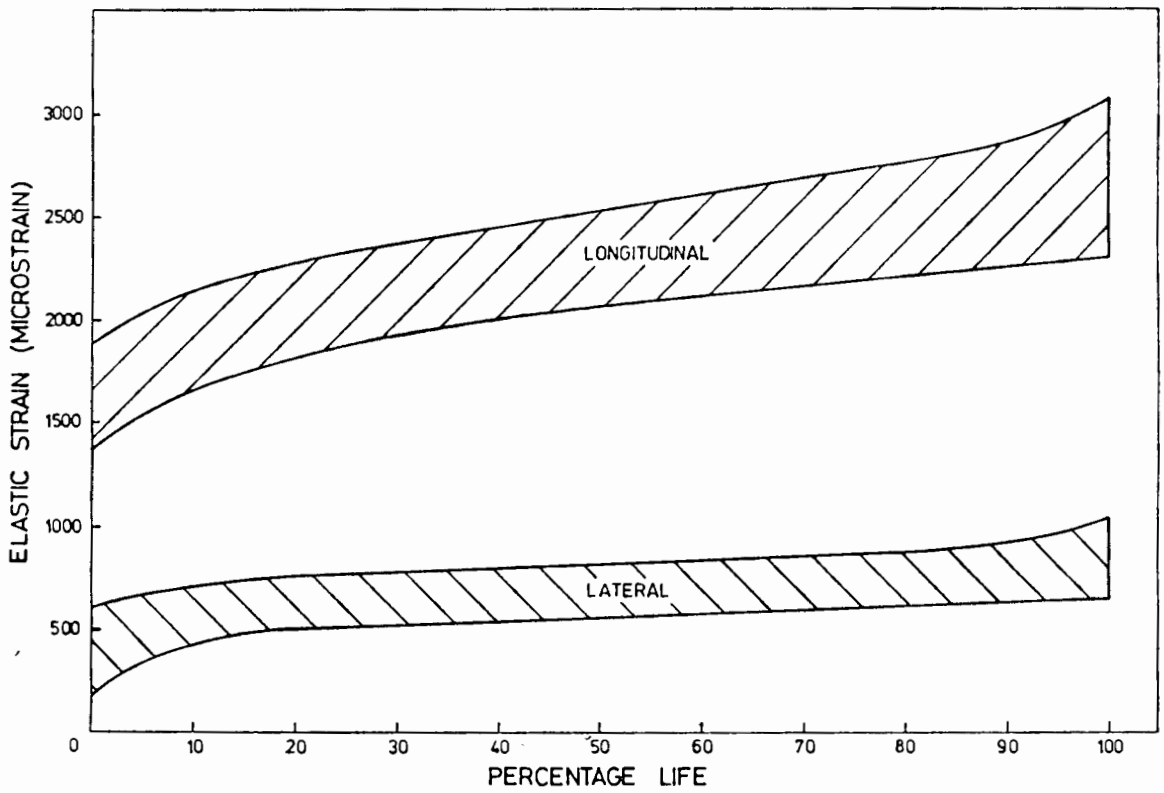

Fig. 4.23(d): Envelopes of elastic strains for various frequencies as a percentage of fatigue life, (Moist specimens, 80% SL, sine).

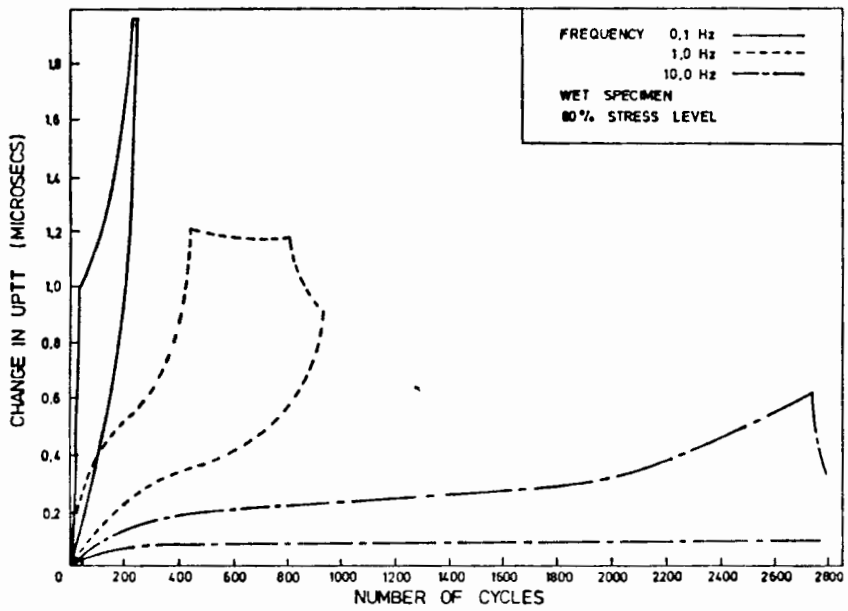

Fig. 4.24(a): Envelopes of UPTT detected damage versus number of cycles for various frequencies.

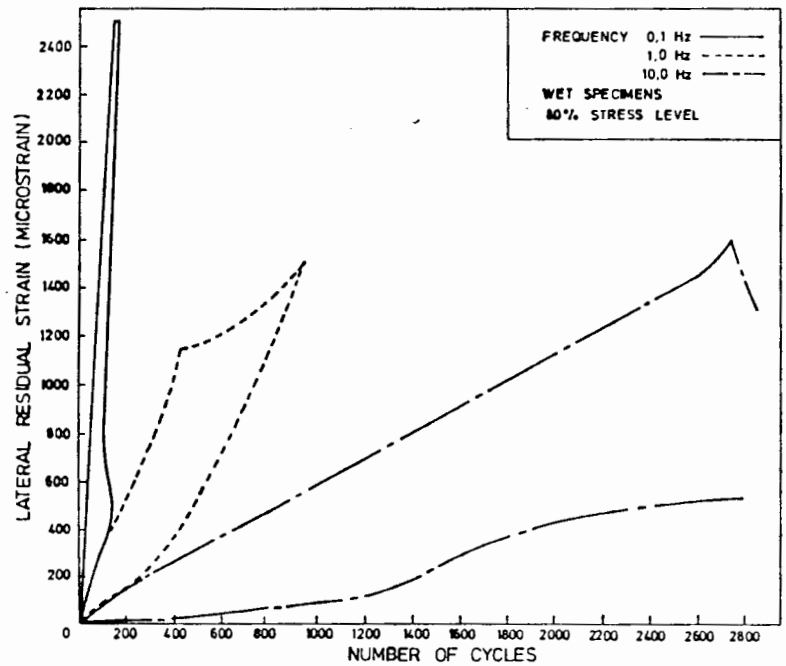

Fig. 4.24(b): Envelopes of lateral residual strain damage versus number of cycles for various frequencies.

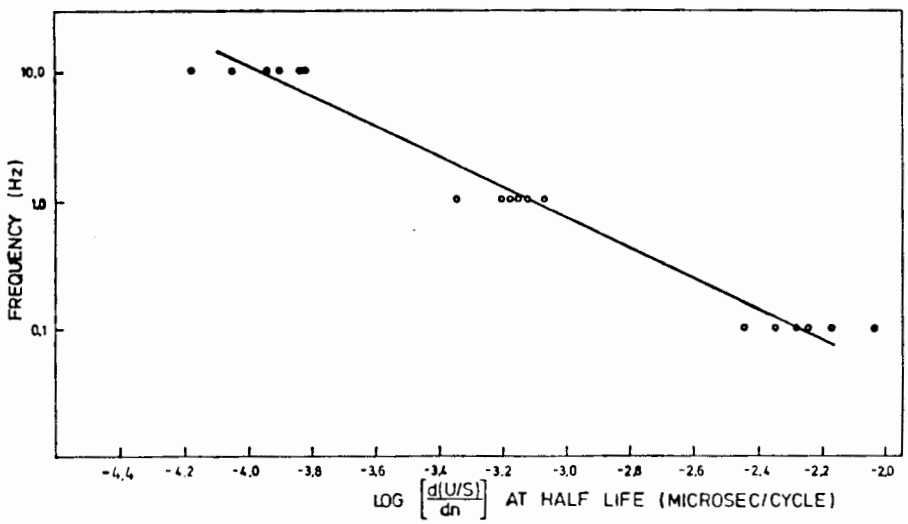

Fig. 4.25(a): Rate of ultrasonically detected damage accumulation per cycle at half life for moist specimens as a function of frequency.

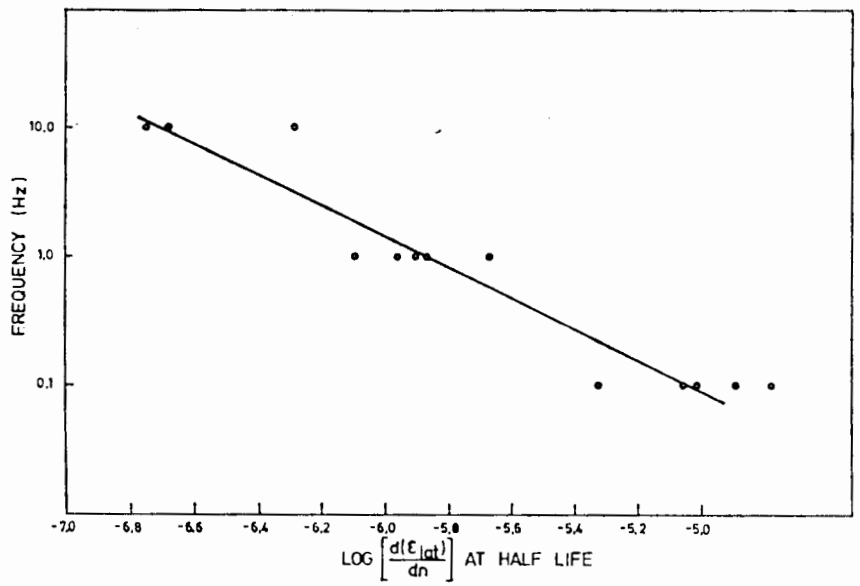

Fig. 4.25(b): Rate of lateral residual strain damage accumulation per cycle at half life for moist specimens as a functon of frequency.

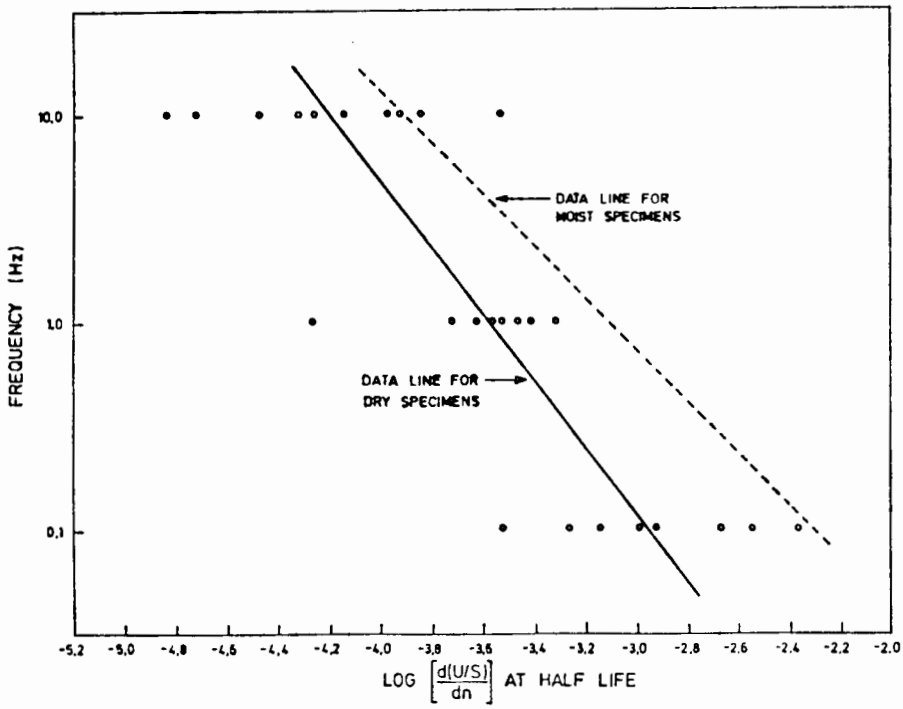

Fig. 4.26 : Rate of ultrasonically detected damage accumulation per cycle at half life for dry specimens as a function of frequency. (Note that the data line for moist specimens Fig. 4.25(a) has been included for comparison).

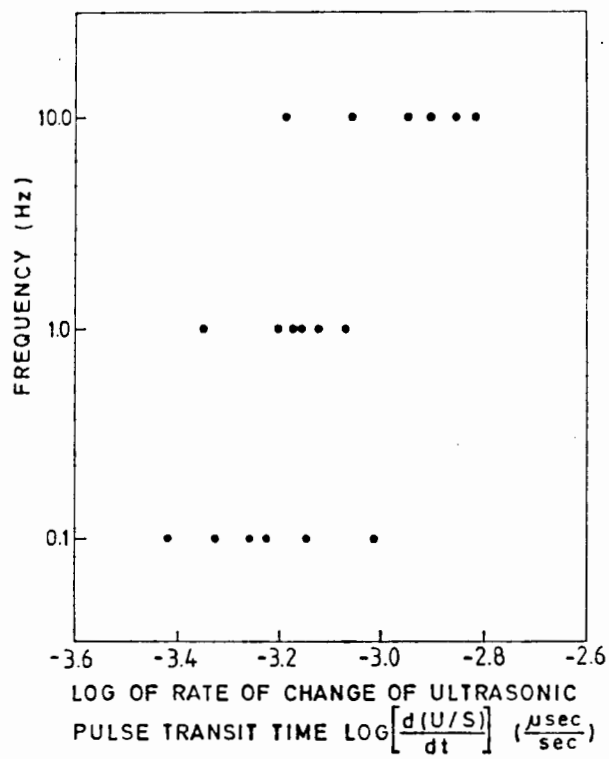

Fig. 4.27(a): Ultrasonically detected damage accumulation rate (per second) assessed at half life for moist specimens.

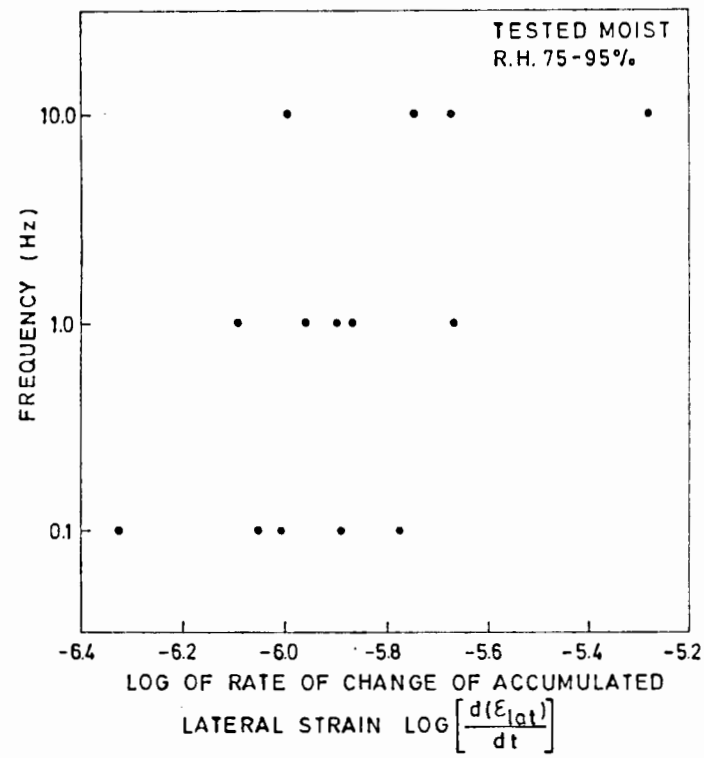

Fig. 4.27(b) Residual strain damage accumulation rate (per second) assessed at half life for moist specimens.

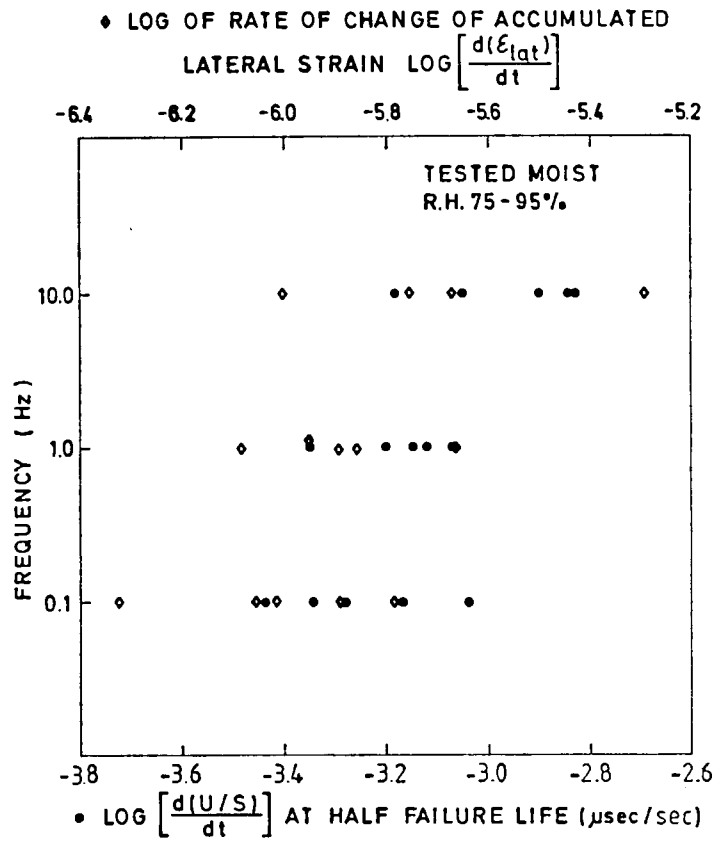

Fig. 4.27(c): Damage accumulation rate (per second) at half life for both ultrasonic and strain detection techniques for moist specimens.

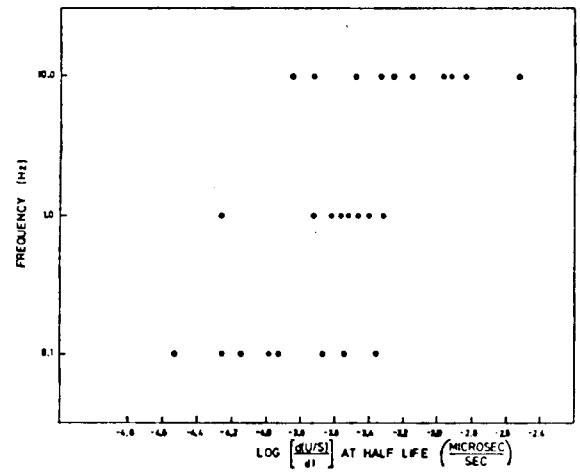

Fig. 4.28 : Ultrasonically detected damage accumulation rate (per second) assessed at half life for dry specimens.

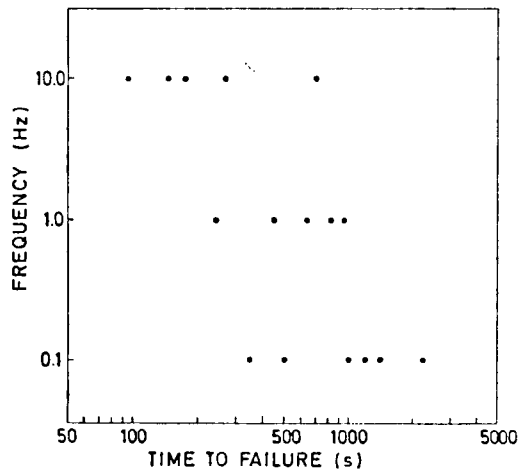

Fig. 4.29(a): Time to failure as a function of frequency for moist specimens.

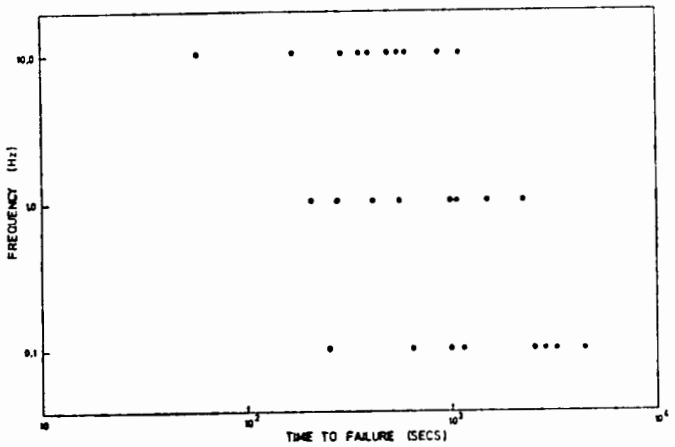

Fig. 4.29(b): Time to failure as a function of frequency for dry specimens.

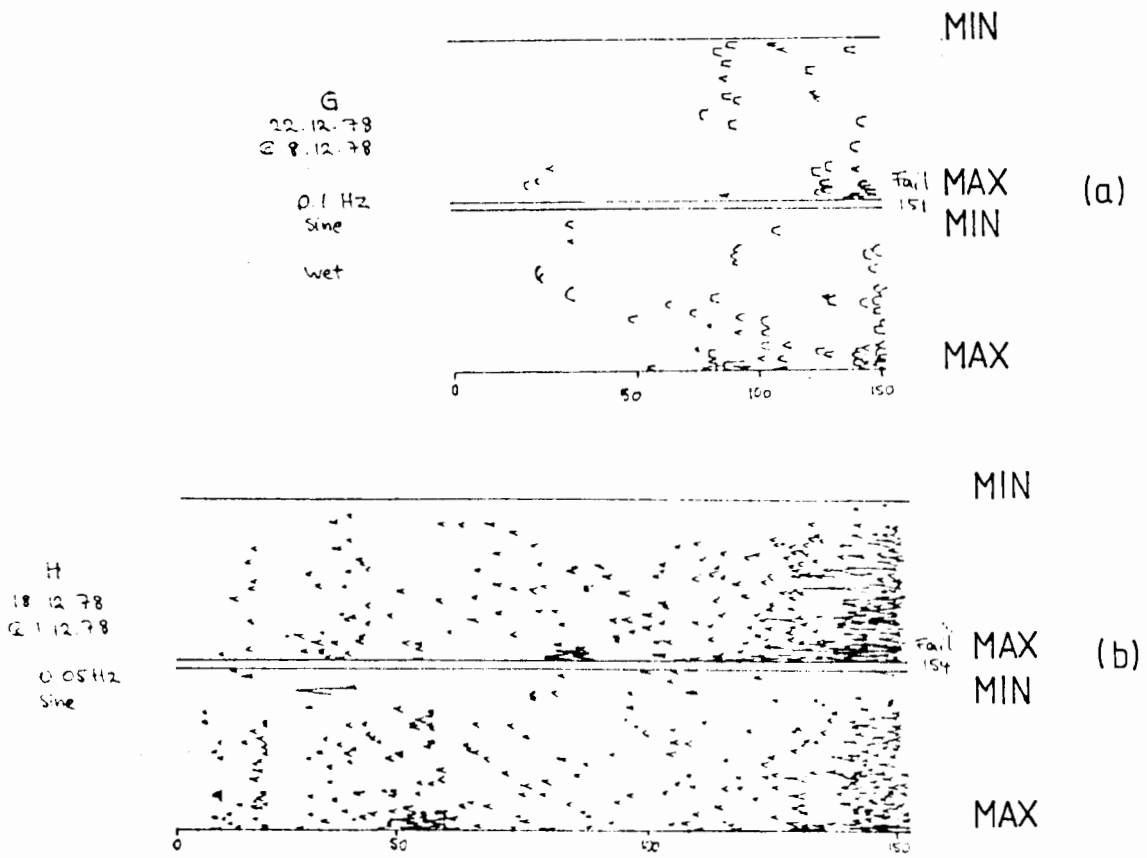

Fig. 4.30 : PIP traces of moist low frequency tests (a) at 0.05Hz and (b) at 0.1Hz at 80% SL illustrating the widespread distribution of acoustic noise on both loading and unloading portions of the cycle. Also note the greater amount of noise compared to other tests consistent with more microcracking damage at lower frequencies.

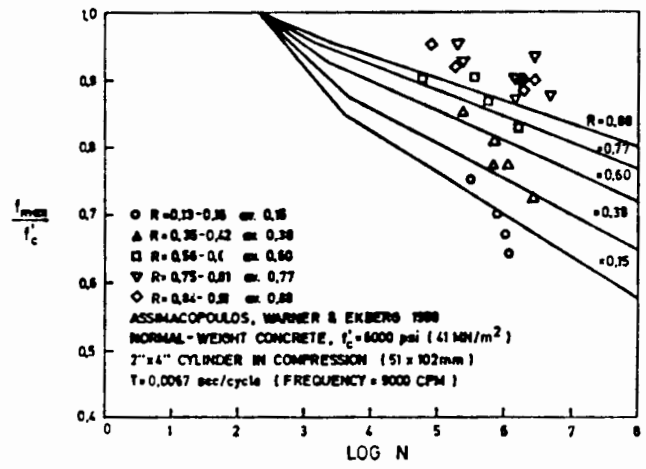

Fig. 4.31(a): Effect of range of stress on SN fatigue curve behaviour of concrete from Assimacopoulos' tests (231).

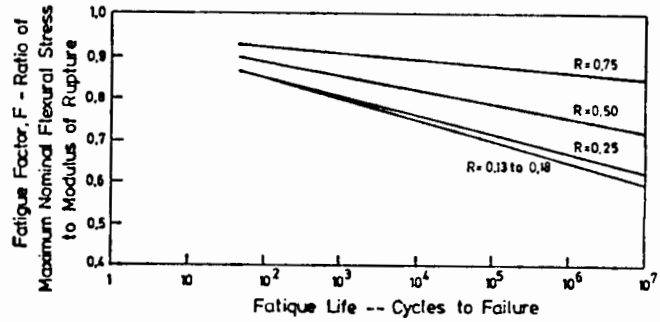

Fig. 4.31(b): Effect of range of stress on SN fatigue of concrete from Murdock and Kesler's tests (146).

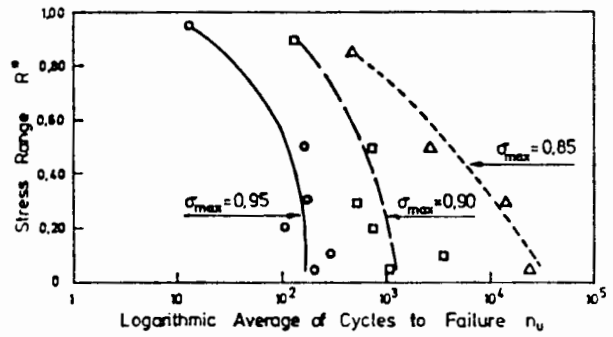

Fig. 4.31(c): Relation between stress range and number of cycles to failure for different maximum stress levels. (Note that in this case the stress range R* refers to Smax-Smin and not the more conventional $\frac{Smin}{Smax}$ - (27).)

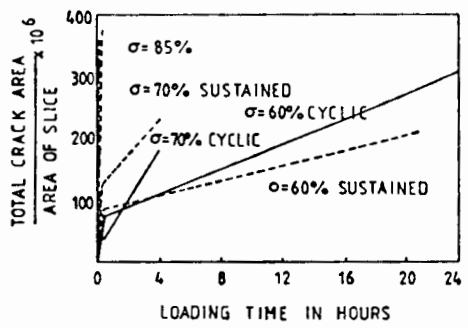

Fig. 4.31(d): Microcrack development under sustained and cyclic loading (From Shah and Chandra (89)).

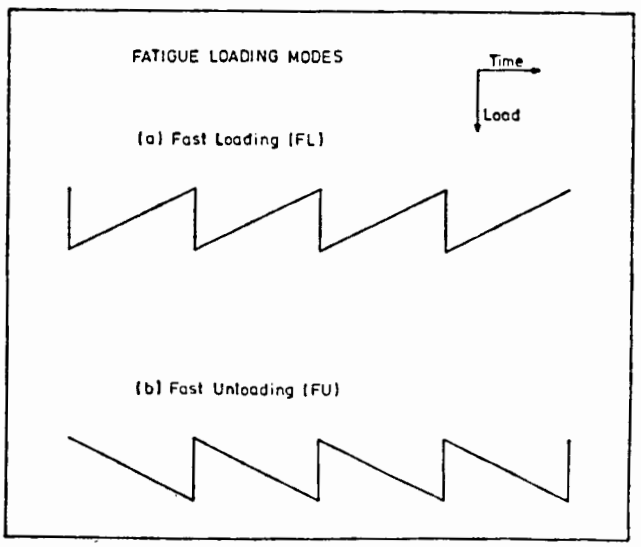

Fig. 4.32 : A representation of the sawtooth loading employed in the waveform tests. (Note that the convention is for compressive load increasing in the negative direction.

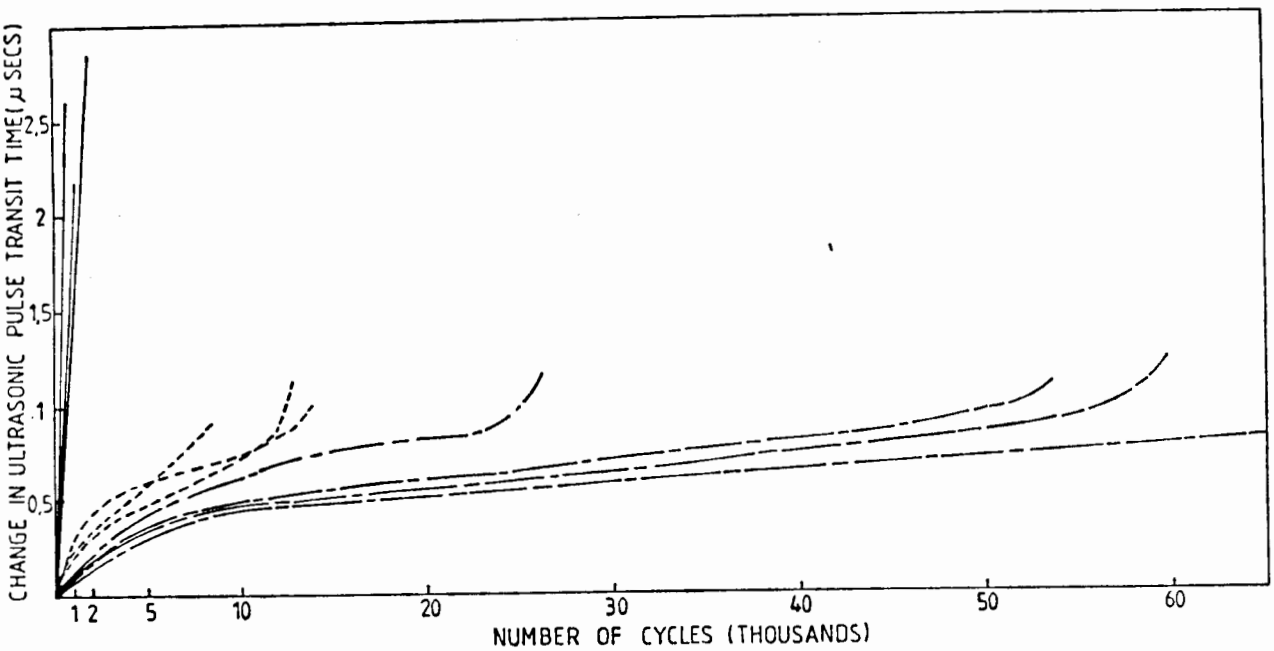

Fig. 4.33 : UPTT damage monitoring results of fatigue tests conducted at stress levels of (i) 80-2.4% (ii) 80-30% and (iii) 80-60% for moist specimens.

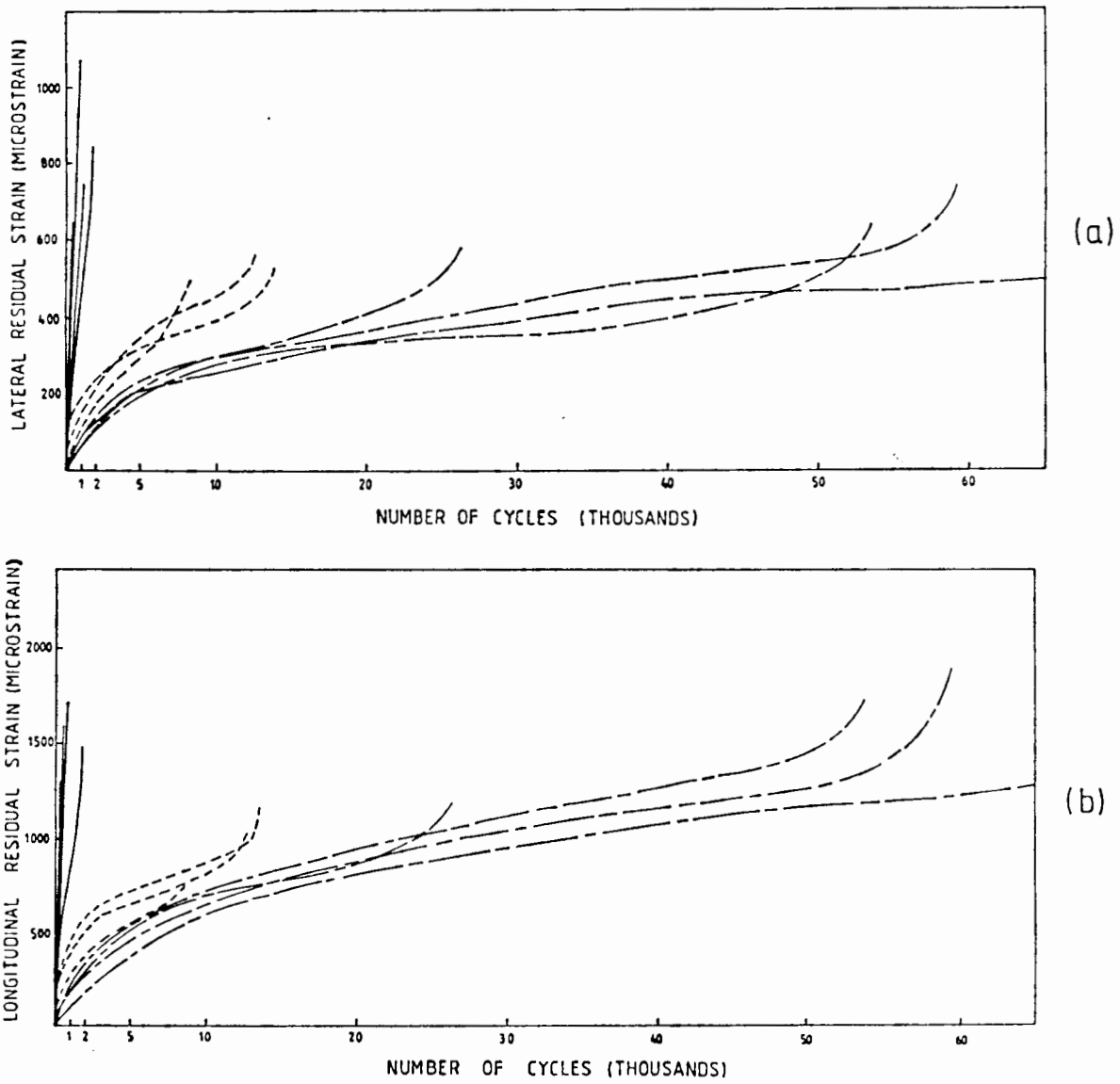

Fig. 4.34(a) and (b): Residual strain monitoring damage results for variable range tests for (a) lateral and (b) longitudinal directions.

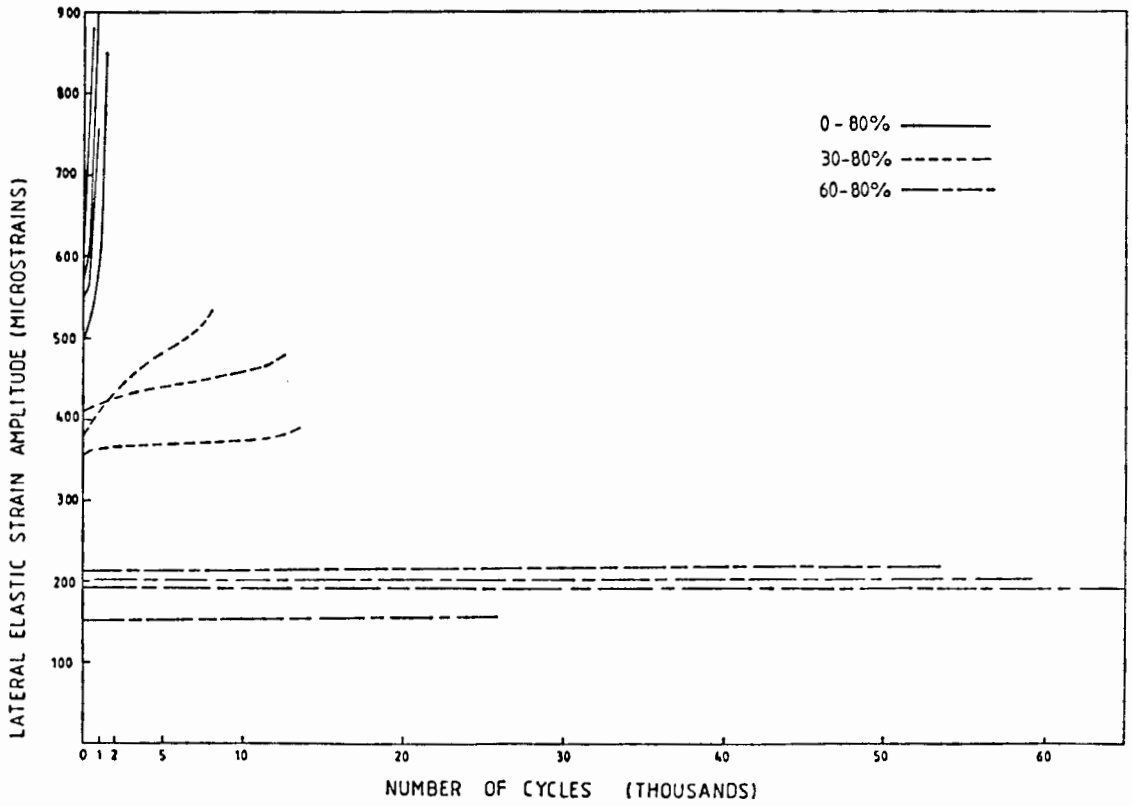

(c)

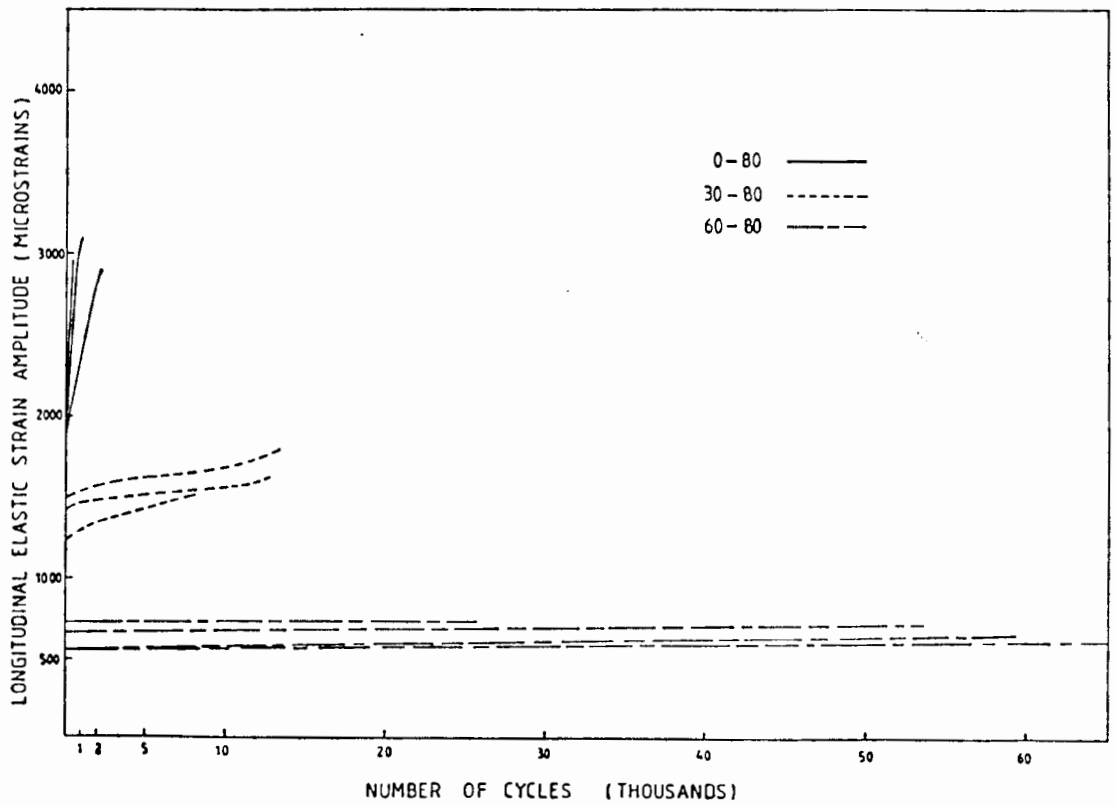

(d)

Fig. 4.34(c) and (d): Elastic strain monitoring damage results for variable range tests for (a) lateral and (b) longitudinal directions.

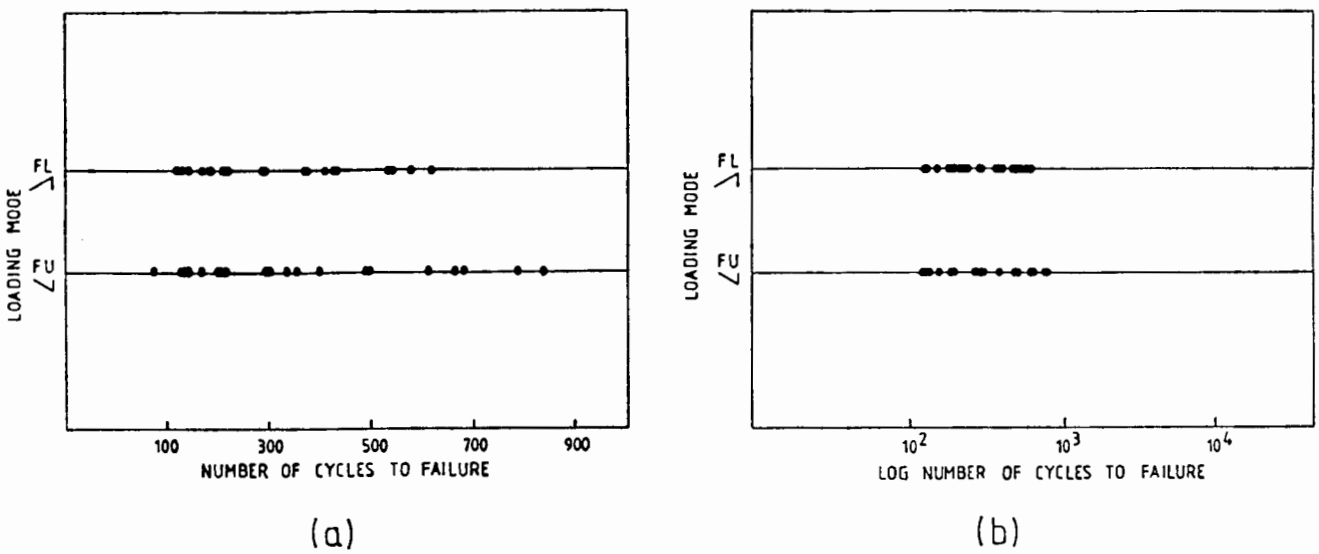

Fig. 4.35 : Fatigue lifetimes of the two loading modes fast loading (FL) and fast unloading (FU) on (a) a linear scale and (b) a log scale.

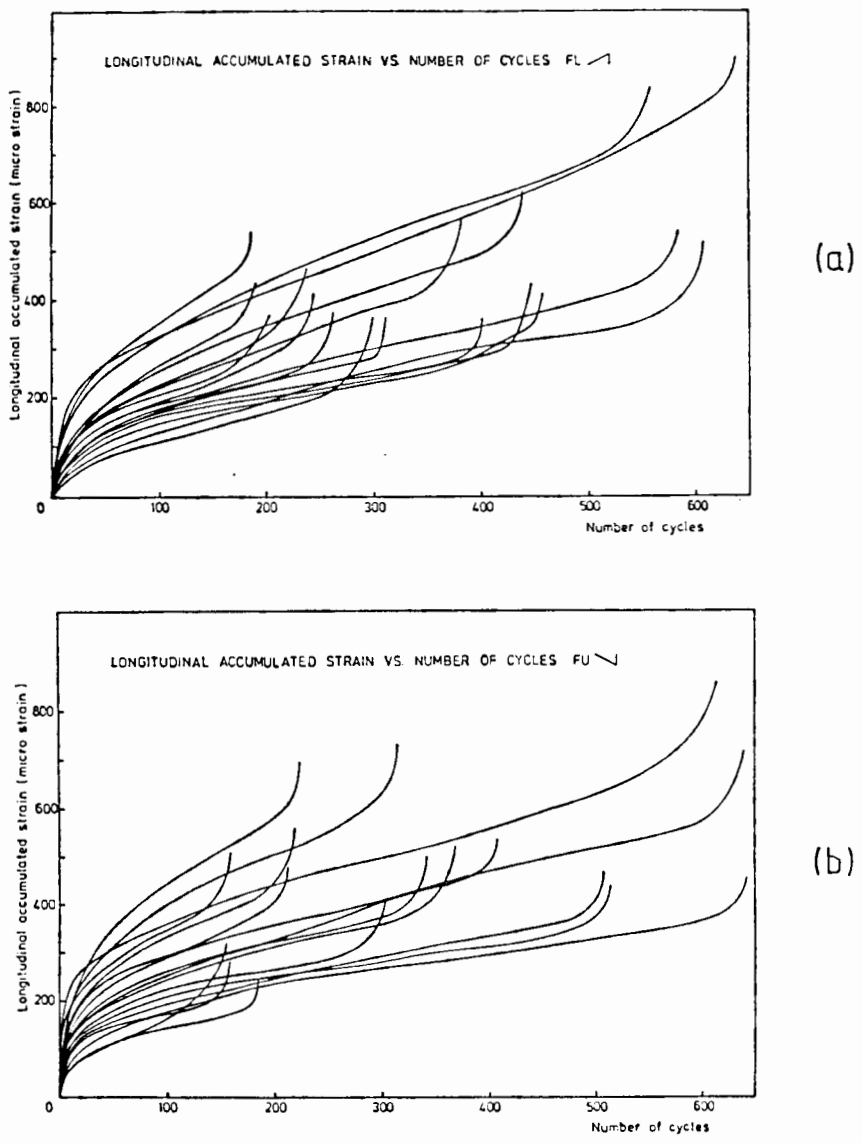

Fig. 4.36 : Longitudinal residual (or accumulated) strain damage traces for the (a) fast loading (FL) and (b) fast unlaoding (FU), sawtooth waveforms.

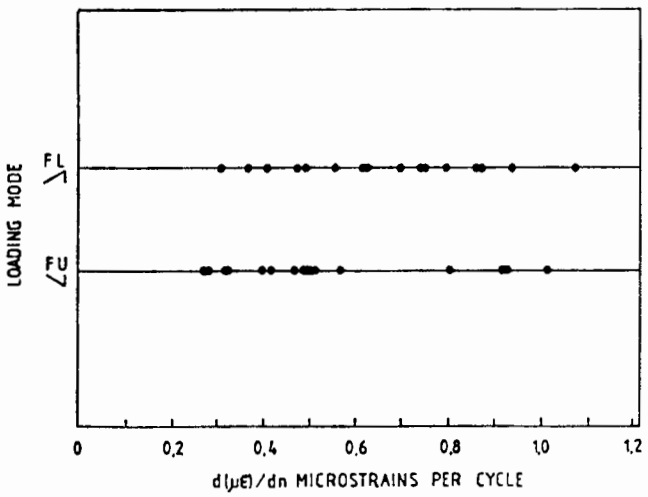

Fig. 4.37(a): Rate of longitudinal residual strain damage accumulation per cycle at half life for the two sawtooth loading waveforms.

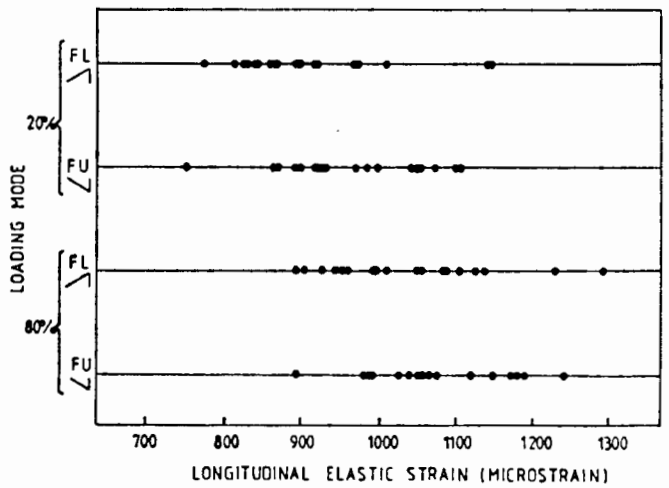

Fig. 4.37(b): Longitudinal elastic strain at 20% and 80% of the fatigue lifetimes for the two sawtooth loading waveforms.

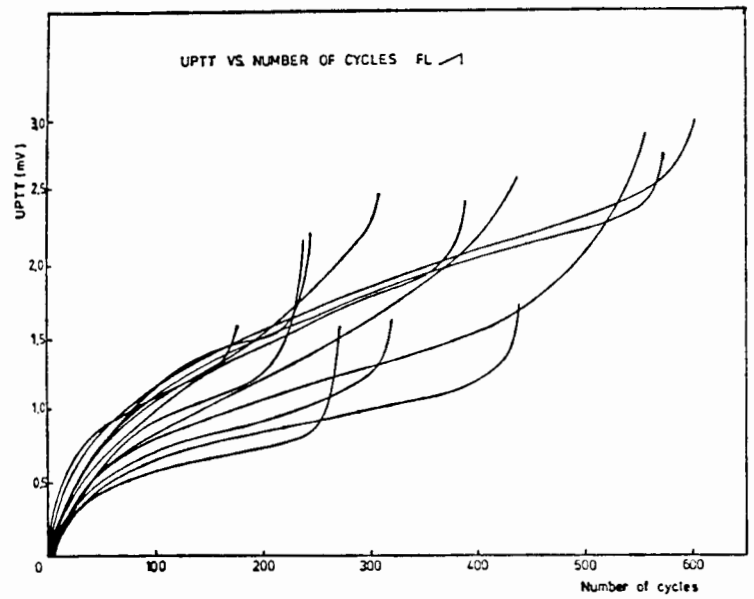

(a)

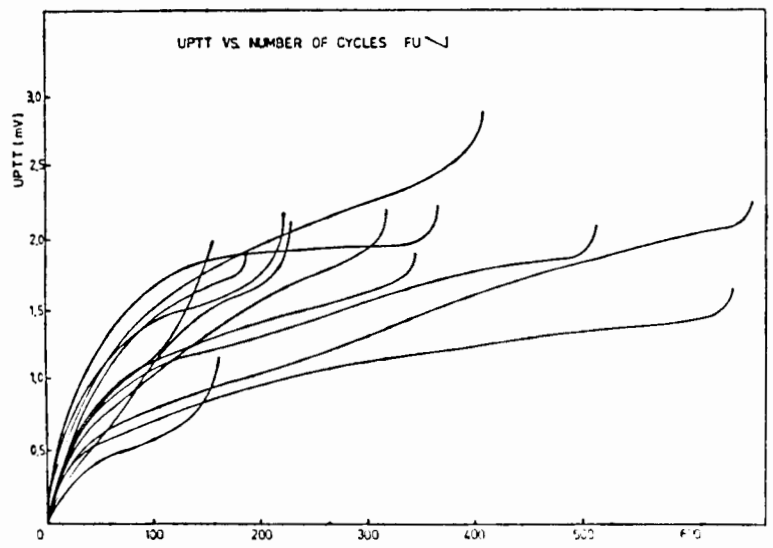

(b)

Fig. 4.38(a) and (b): UPTT damage monitoring traces for (a) the fast loading (FL) and (b) fast unloading (FU), sawtooth waveforms.

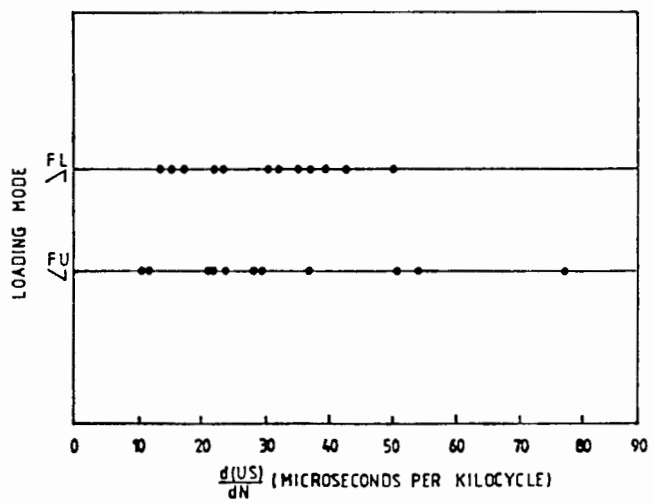

Fig. 4.38(c): Rate of UPTT detected damage accumulation per cycle of half life for FL and FU sawtooth loading modes.

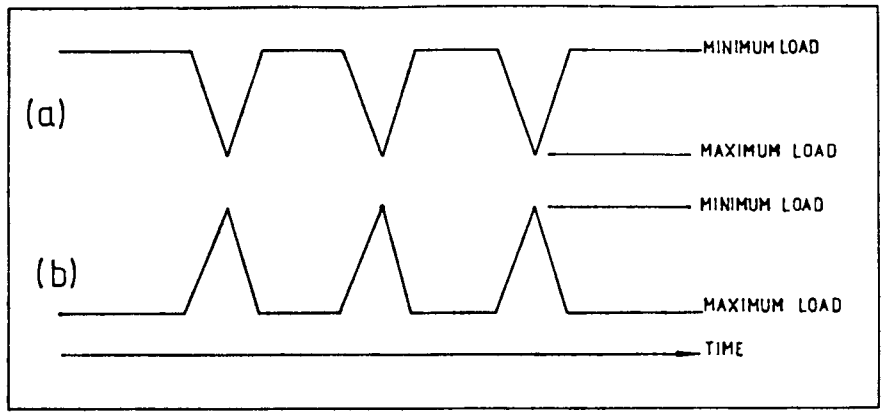

Fig. 4.39 : Test waveforms containing a dwell period (of 1.6 sec) at either (a) minimum load or (b) maximum load.

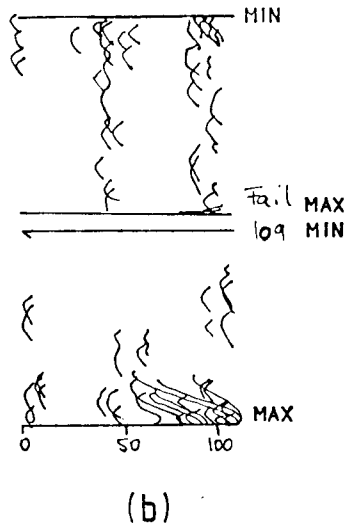

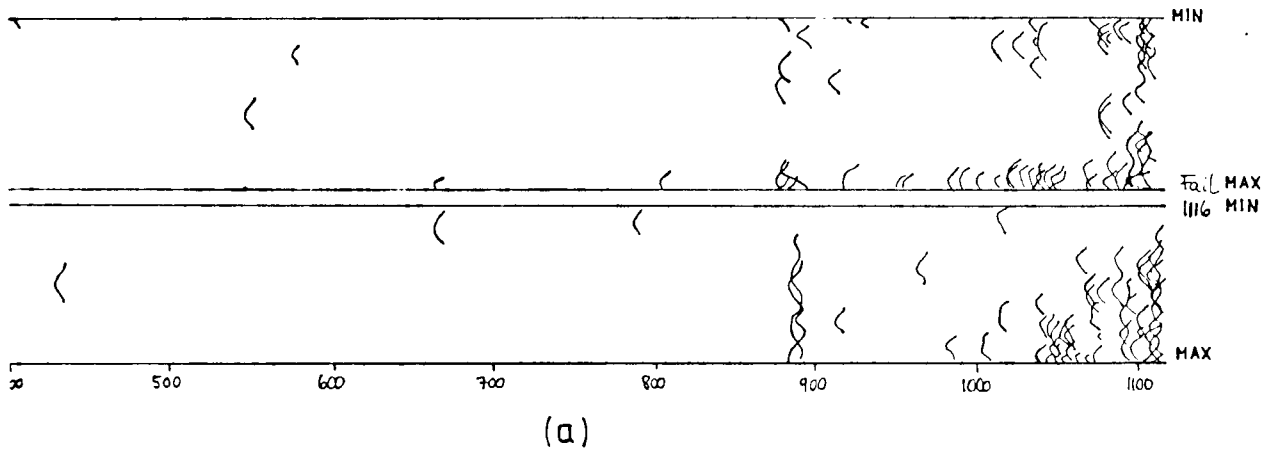

Fig. 4.40 : Acoustic emission pseudo isometric plots for dwell periods at (a) minimum load and (b) maximum load, for an otherwise triangular waveform, (Moist specimens, 80% SL, 0.33 Hz).

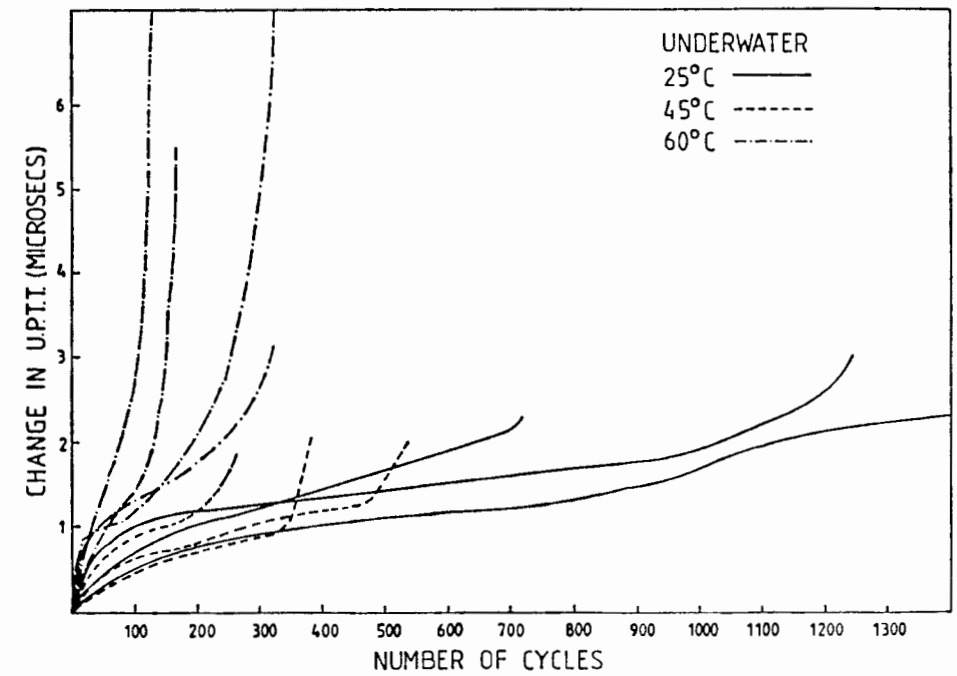

(a)

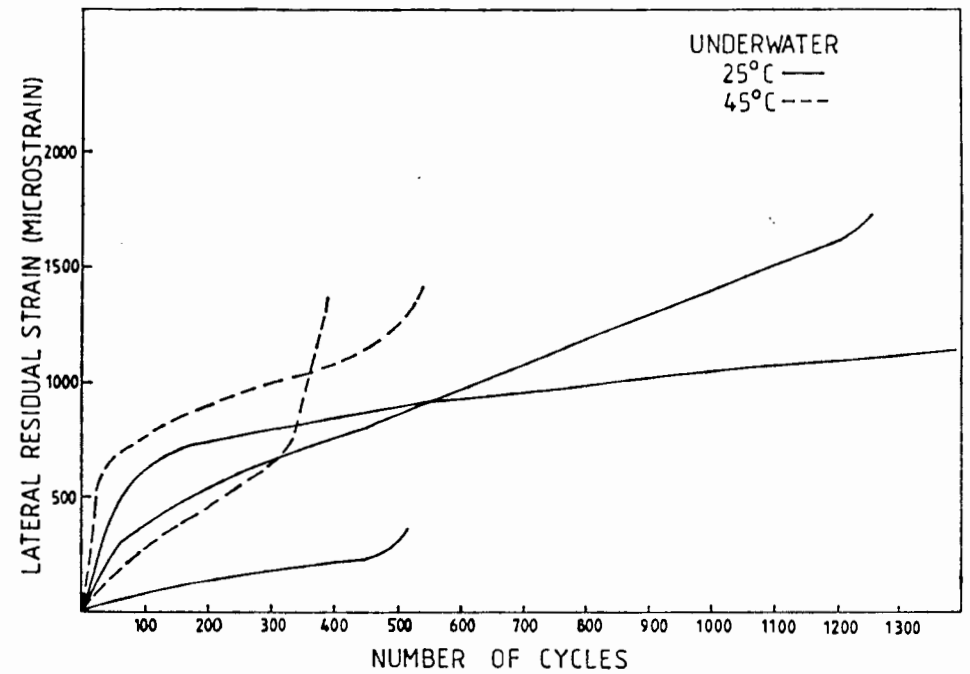

(b)

Fig. 4.41(a) and (b): (a) UPTT and (b) lateral residual strain damage traces versus number of cycles for underwater fatigue tests at various temperatures.

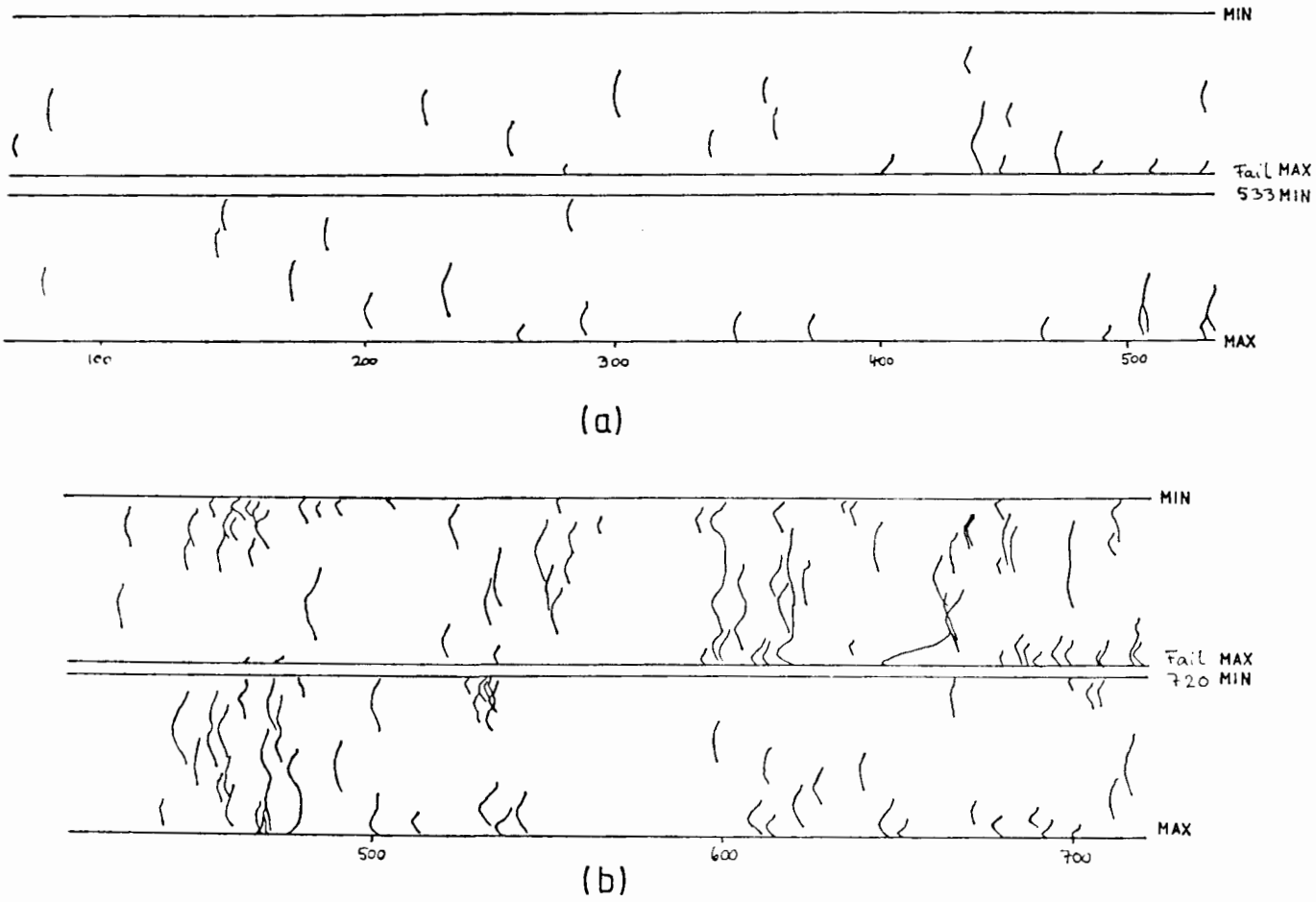

Fig. 4.42 : Typical acoustic emission PIP traces for (a) 45°C and (b) 60°C underwater tests indicating damage and noise on both loading and unloading, as well as greater noise at 60°C than 45°C.

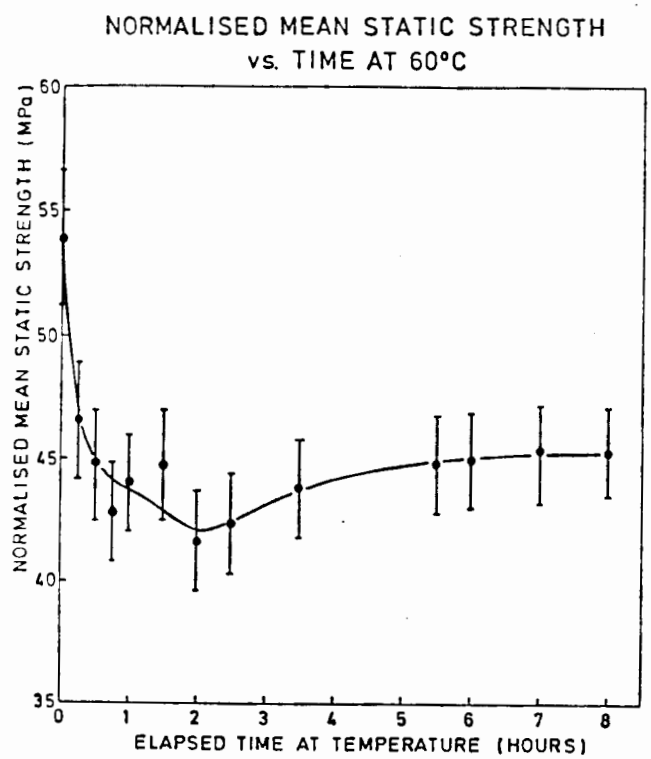

Fig. 4.43 : Mean static strength of mortar specimens which were kept at 60°C for varying times prior to testing.

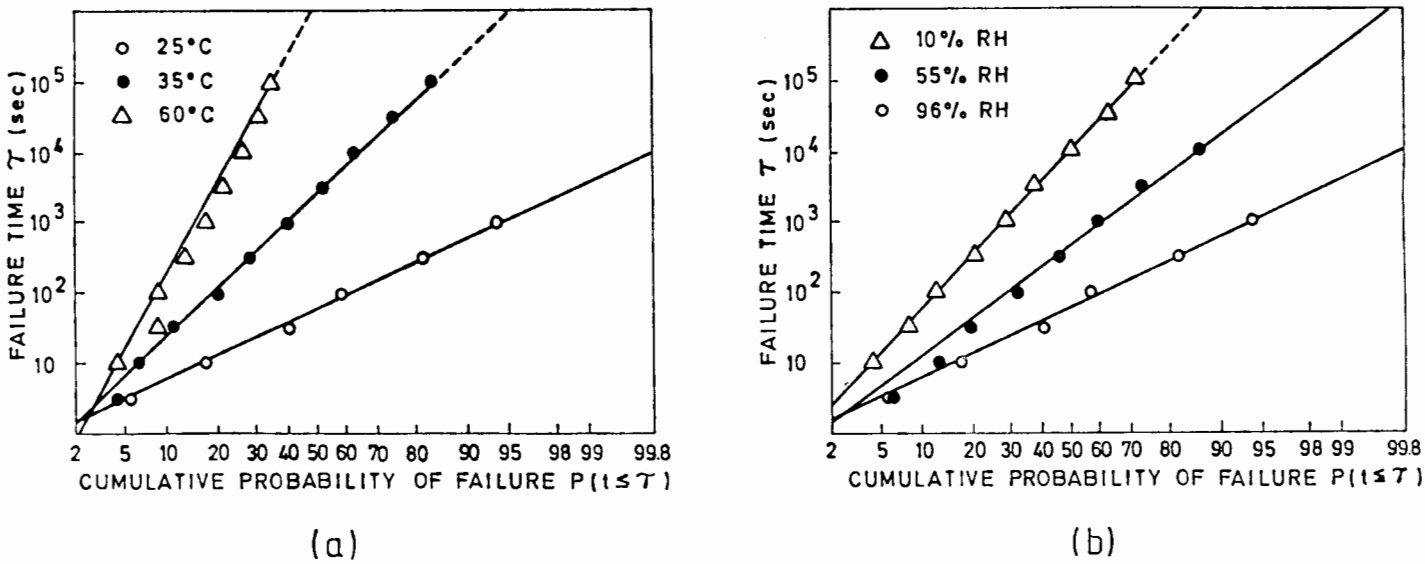

Fig. 4.44(a) and (b): Barrick's (29) static fatigue tests indicating time to failure dependence on both (a) temperature and (b) relative humidity.

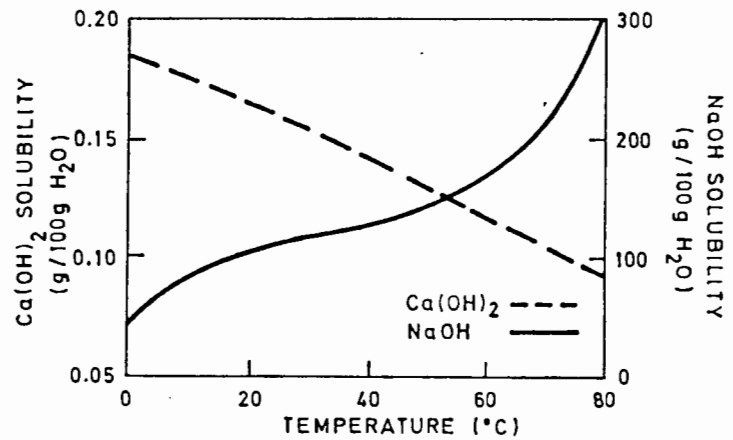

Fig. 4.45 : Hydroxide solubilities as a function of temperature used to explain Barricks results (29).

"All would live long, but none would be old"
Benjamin Disraeli, 1749

CHAPTER FIVE : FATIGUE HARDENING

5.1 Introduction

Although many aspects of the phenomenon of fatigue in cement based materials have been extensively researched for over seventy years (137), there still remain many aspects which are by no means fully understood. This is particularly so from a mechanistic point of view, and it is this area of cement research that needs (and is receiving) attention if projected improvements in controlling microstructure and upgrading physical and mechanical properties of cement and concrete, are to become a reality.

One of the more interesting effects observed in cement-based materials, widely reported in the literature (27, 89, 96, 120, 133, 134, 144, 145, 150, 140-244), and ostensibly having an analogue in metallic systems, is the phenomenon of "fatigue hardening". Thus, specimens fatigued at a relatively low stress level frequently exhibit an increase in static strength when tested after fatigue. In metals such hardening arises from dislocation interactions during cyclic deformation; however, no simple analogy is possible with cement-based materials, and an acceptable mechanistic explanation for the phenomenon has never really been put forward. Indeed, it would be advantageous to be in a position to predict the residual strengths of a concrete structure that had been subject to fatigue or micro-damage inducing loads by way of the extent, and likely effect, of such damage.

This chapter reports on experiments designed to investigate the origins of this behaviour in a cement system, and in particular (i) to quantify the extent of the strengthening which occurs; (ii) to establish at what stage of fatigue life it occurs and its dependence on applied stress level; (iii) to investigate its dependence on environment and moisture content; and (iv) to propose, from the results of the experiments, a possible mechanism to explain the observed behaviour.

5.2 Previous Studies

The phenomenon of fatigue hardening following low level fatigue has been recognised for over sixty years.

Clemmer first documented (133) the effect in 1922, (although Abrams apparently "noticed" it in 1913) by reporting that cantilevered beams subject to extensive fatigue cycling ($>10^6$ cycles), could subsequently "withstand fatigue at a higher load better than if they had not been fatigued." In the following year, Crepps (134) inadvertently noticed that concrete beam specimens subject to many cycles of complete stress reversal fatigue - and seemingly on the point of collapse - recovered completely during a five week rest period necessitated by repairs to the equipment. Further early observations of fatigue hardening were reported by Probst (145) and Bogue (40). Unfortunately, in these early reports, the degree of strengthening, or a quantitative measure of improvement, does not appear to have been recorded, nor any mechanism to explain the effect put forward.

By the late sixties quantitative measures of the fatigue hardening effect began to appear, together with theories to explain the behaviour. Bennett and Muir (96), for "run out" fatigue tests ($>10^6$ cycles) on moist prism specimens, observed a consistent increase in strength over control specimens by up to 23%, with a mean of 11% but suggested no explanation. Subsequent fatigue tests by Bennett and Raju (143) at low stress levels (30 - 53%) on moist 28 day old specimens at 3Hz produced strength increases of up to 15%, with a mean of 5%. They also observed (but did not report measurements of) an increase in temperature with fatigue, and felt that the strengthening may be due to accelerated curing (i.e. greater "maturity") or to "loss of gel moisture".

Kesler (144), Neville (120) and Cornelissen and Timmers (142) (this latter work being carried out in pure tension) also report fatigue hardening increases of up to 15% which was attributed by Neville to "probably (be) due to the densification of the concrete" (120). Similar increases of up to 12% (observed by Shah and Chandra (34), which applied to sustained loading as well as to dynamic fatigue) were attributed to "consolidation" (89).

It was alleged (89) that the secondary bonding strength between gel particles improved because of the "decrease in interparticle distance resulting from consolidation". Van der Waal's bonding forces, as put forward by Wittman (245), are strongly 'separation distance dependent' and were cited in this secondary bonding strength improvement. This contention is questioned by the author, however, in that compressive stresses on concrete prisms would set up large lateral tensile forces, through Poisson's expansion. Indeed the nature of failure of concrete prisms is by the development of longitudinal tensile cracks - and thus there would be an expansion, and not a consolidation, in the lateral direction, which is exactly where strength increases would be required to explain the observed strength increase behaviour.

Hilsdorf and Kesler (157) observed improvements in SN fatigue performance (i.e. longer fatigue lives by about an order of magnitude at 70% stress level, see Fig. 2.35(a)) following rest periods of 1 to 25 minutes during moist fatigue tests. This strengthening they attribute to relaxation of residual stresses, which arise from shrinkage and drying (which are located at or near inherent cracks). Through fatigue the stresses supposedly become relaxed and the structure effectively "stress relieved" thus resulting in greater resistance to fatigue. The action of autogenous healing (40, 240) in strength improvement was considered but felt to be untenable in times as short as 5 minutes.

The concept of autogenous healing suggested by Bogue (40) in 1934 was first seriously investigated by Lauer and Slate (240) in 1956. Their study was not concerned with dynamic fatigue in any way but is mentioned here because of its subsequent relevance. Their study consisted of measuring the initial tensile strength of tension briquettes as well as the "rehealed strength" after the two halves were held together under water, or in high humidity conditions (RH 95%), for periods up to 90 days. They obtained 10 to 25% of the original tensile strengths and most of this developed early during the "healing" process. Such facilities for microscopic investigation that were available at that time, indicated the bonding material of the healed joint to be predominantly calcium carbonate and calcium hydroxide, and no C-S-H material species, for example, needles of type I, were observed. It is also interesting to note that Lauer and Slate report that the degree of autogenous healing of cement paste is independent of cement composition or type (240).

Jordan (176) noticed an improvement (i.e. reduction) in damping of concrete specimens which had been fatigued and then left (in a moist condition) overnight. In view of this change he simply excluded these results from his analysis, but noted at the same time that the effect might have been caused by autogenous healing, (173).

The effect of age also appears to be important, in that Awad and Hilsdorf (27) report that 90 day old concrete is more resistant to high stress level fatigue than 7 day old concrete. At low stress levels, however, the trend is reversed - the time to failure of concrete statically loaded at an age of seven days to failure is greater than for older concrete. This phenomenon they attribute to continued hydration under loading which was not manifest under short term loading. Similar conclusions are drawn by Rusch (222).

Another interesting point arising out of Awad and Hilsdorf's study (27) is an attempt to determine at what stage in the fatigue life fatigue hardening occurs. They interrupted some of their moist (albeit high stress level) fatigue tests on prism specimens at 30%, 60% and 90% of the predicted life and undertook post fatigue static tests. The results are shown in Fig. 5.1 and indicate an initial strength increase of about 5%.

This is followed by an ultimate overall decrease, only after between 30 and 70% of the total life had been consumed. These tests were undertaken for high (or sustained) stress levels and no work appears to have been done on low stress levels. Verna and Stelson (246) obtain similar results to Fig. 5.1 but with decreases occurring from 20% of life onwards. Such results imply that there is some form of strengthening mechanism operating during the initial portion of the fatigue life, and that fatigue failure does not merely arise due to a progressive degradation of the material's structural integrity by damage accumulation, but rather involves two opposing mechanisms, one beneficial to strength and the other destructive.

It would thus appear that some controversy still remains as to the magnitude and source of the fatigue hardening effect, as well as at what stage in its fatigue life it occurs and whether it is affected by stress level. The following experimental programme was undertaken in an attempt to document the effect more closely and to understand the mechanisms leading to it.

5.3 Experimental

5.3.1 Materials, Testing Methods and Programmes

The test materials and methods used have been appropriately detailed in Chapter 3.

The actual test programme involved conducting fatigue run out tests, at stress levels in the range 55 to 60%, on both moist and dried out samples, at 10Hz, for approximately 10^6 cycles. Following a fatigue test, the (fatigued) sample was ramp tested statically to measure any change in strength over static control samples, four of which were tested before, and two just after, the post fatigue test. The majority of the tests were conducted inside the environmental control system of sealed plastic containers with a humidity of greater than 90%. Several fatigue tests were also conducted under water in a temperature controlled ($20^{o}C$) water bath. The fatigue hardening results from the two test systems were not significantly different and are therefore considered together in discussions as follows.

To investigate the effect of stress level on fatigue hardening, and to obtain some indication of the stage at which strengthening develops, a further series of fatigue tests was conducted. This consisted of conventional fatigue tests as described above, but at higher stress levels, namely 55, 60, 65, 70 and 75%, which were interrupted at approximately 20% of the predicted fatigue life, appropriate to that level. These fatigued specimens were "post fatigue statically ramped" to failure, to obtain strength comparisons with static controls, some of which were tested after fatiguing as mentioned above.

The testing programme was fairly limited, at least in a statistical sense, in view of some of the existing and extensive studies in the literature on fatigue hardening. The prime objectives of the experimental programme were to test, experimentally, existing theories of fatigue hardening and to provide specimens suitable for fractography, described in the following section.

5.3.2 Scanning Electron Microscopy

It was necessary to obtain specimens for scanning electron microscopy that were truly representative of fatigue fracture and which were not produced in the final catastrophic failure of the specimen in compression. Fracture specimens taken from this latter case, for example from a normally failed specimen, may well have been subject to abrasion or attrition or just static fracture at the time of collapse.

This requirement was achieved by making use of the damage monitoring systems of change in strain and UPTT. Very near failure, in a medium to high stress level fatigue test, the rate of damage accumulation increases rapidly as evidenced by, for example, Figs. (2.30, 4.1, 4.3, 4.22 and 4.36). With experience of the form of these damage accumulation traces it was possible to stop the fatigue test on the point of failure and thus arrest the fatigue process. The resultant specimen, still ostensibly intact from a macroscopic standpoint (and still able to maintain the full stress level load appropriate to the load level of the test), was however extensively microcracked through fatigue and was thus readily "taken apart", in tension, by hand. This was not an entirely easy task, especially initially, where six specimens were destroyed, before two fatigue fracture halves could be obtained. These resulting portions, however, showed no macroscopic evidence of catastrophic damage, and small specimens from the true fatigued fracture surface were readily selected. Numerous samples were taken from several fatigued specimens so that a wide and hopefully representative selection of microstructures was obtained. No specific statiscal count of the surface types was made, however, and the following micrographs should be regarded as qualitatively indicative of the surface characteristics.

Small specimens from the fatigue fracture surface were immediately placed in a vacuum dessicator or re-hydrated in water for times which varied from 1 hour to 48 hours. Preliminary fractographic observations, of suitably prepared but otherwise simple non-re-hydrated fracture surfaces, were disappointing in as much as little information could be gained from the surfaces. In order to study in more detail the mode of microcrack propagation through the cement, a technique of "re-hydration" of the fracture surface was developed.

The structure of cement paste, already discussed in some detail in Chapter 2, can, in simplistic terms, be considered as a matrix of unhydrated particles, each surrounded by an interlinking hydrate gel coating, arising from the hydration reaction between the cement and water. This coating effects the bond between the adjacent particles, as well as inhibiting further hydration because of the relatively impermeable layer which builds up between the unhydrated particles and the water present in the various pores, capillaries and interparticle spaces. It is as a result of this sort of process that concrete goes on hardening, at a much reduced rate, for months, and even years, after it is originally cast.

Thus, on exposing a fractured surface to water, already hydrated regions would be relatively unaffected, whereas unhydrated areas would readily hydrate and therefore become distinguishable by the hydration products so produced.

The procedure adopted was that the samples were exposed to water for a particular re-hydration time: they were then dried in a vacuum to ensure that the re-hydration process had stopped. Although drying can have a disruptive effect on the microstructure, the effect is sufficiently small to enable realistic observations to be made (4). The specimens were then coated with carbon, followed by a layer of 60/40 gold palladium approximately 100A thick. The fracture surfaces were subsequently examined using a Cambridge Stereoscan 180 operating at either 20, 25 or 30kV.

5.4 Results

Fig. 5.2 shows the results obtained for fatigue run out tests on moist and wet samples indicating a hardening effect of approximately 20% following fatigue.

Results obtained for tests carried out at higher stress levels, and at fractions of the life to failure, are shown in Fig. 5.3. This data suggests that fatigue hardening is definitely not restricted to long-life/low-stress tests. Strength increases at high alternating stresses can be obtained, provided these tests are not continued beyond a certain limit when progressive damage outweighs the effect of hardening; certainly, the mechanism leading to hardening appears to occur within the first 20% of the

life. The results shown in Fig. 5.3 are consistent with those of Awad and Hilsdorf (27) (Fig. 5.1). Note that the stress levels in the two cases are very different but the contention that applies, for both cases, is that there are two opposing mechanisms operating, one beneficial to strength and the other destructive.

For dry specimens, however, there seems to be no such corresponding increase in post-fatigue strength (Fig 5.4). It is also of interest to note that the temperature increase during fatigue of dry specimens was less than $2^{o}C$, while for moist specimens the temperature increase associated with fatigue was approximately $20^{o}C$.

It would thus appear that fatigue hardening depends on the degree of environmental or inherent moisture in the specimen, and also it appears to occur relatively early in the fatigue life of the specimen and only in lower stress level fatigue tests, although the effect is probably present also at higher stress levels. Further insight into this strengthening effect, of typically 10 to 25% (of prior static strength), can be gained by scanning electron microscopy studies, described in the next section.

5.5 S.E.M. Studies

5.5.1 S.E.M. Fractography and Rehydration Observations

A study of the plain, fractured surfaces showed that fatigue samples exhibited a significantly greater abundance of microcracks than corresponding, statically-failed samples. A typical example of the former is shown in Fig. 5.5. The observation of greater microcracking damage in fatigue, as compared to static tests has been mentioned before, see, for example, Figs. 3.22, 4.3, 4.6(a) and 2.32. Typical changes in ultrasonic transit time for moist specimens tested statically or in fatigue were typically 0.5 and 2.0 microseconds respectively.

Following a re-hydration treatment the growth of hydration product, in particular needle like type I calcium silicate hydrate, from the fatigue surfaces was prolific, Figs. 5.6 and 5.7. These figures show predominantly Type I C-S-H as discussed in Chapter 2, although in the lower right hand corner of Fig. 5.7 some calcium hydroxide platelets are in evidence.

Statically failed specimens, by contrast, show much less hydration product for the same re-hydration duration (Fig. 5.8(a) and (b)). In broadly quantitative terms based on observations of a number of different surfaces, exposed cement hydration products (from previously unhydrated material) covered approximately 60 to 90% of the fracture surface for the fatigued specimens, compared with only 5 to 10% for statically failed surfaces, subjected to identical re-hydration treatments. The re-hydration treatments involved the use of tap water and were comparable for both static and fatigue samples. Recent studies, however (10, 247, 248) suggest that solution chemistry in the vicinity of the fracture surface is also of major importance, implying that local solution chemistry plays a more important role than bulk water solution chemistry.

5.5.2 Cement Hydration and Microstructure

The understanding of cement chemistry in general, and cement hydration in particular, is far from complete despite the significant amount of relevant published literature, especially in the last five years. See, for example extensive discussion in Chapter 2, or recent competent reviews (4, 39, 247.) It is not intended here to recapitulate this discussion of Chapter 2, but rather to highlight certain aspects relevant to the subsequent model proposed for fatigue hardening.

When cement is hydrated there appears to be a rapid initial formation of highly impermeable, gelatinous hydrate coating around the cement grain and consequent reaction rates are slowed down as assorted microchemistry changes and migration of ions occur; the "inner" product is laid down within this coating or shell and is generally fine-grained. The "outer" product develops in the surrounding interparticle space or original water filled void beyond the grain geometry, at a faster rate than the inner hydrate. This outer product, as has been mentioned in Chapter 2, often includes a fibrous or needle-like C-S-H microstructure but can include hexagonal crystals of calcium hydroxide. The C-S-H hydration products ultimately develop to fill the interparticle space with a nominally amorphous, consolidated mass. In effect, shells of (largely) impermeable calcium silicate hydrate gel surround pockets, or kernels, of uncombined (or at least incompletely hydrated) cement grains, with the intervening volume filled with needles of hydrating C-S-H radiating outwards in a "porcupine"

fashion from the individual cement grains. Fig. 5.9 (after Double, 4, 5) illustrates schematically the sequence of events in the hydration of ordinary Portland cement. The "shell concept", in fact, is not only restricted to C_3S and C_2S, since Brevel (42) mentions in a study of the hydration of C_3A, that a tight layer of C_3AH_6 forms around the C_3A grains, impeding further intrusion of liquid, a view also noted by Lea (32) and Ramachandran and Feldman (48).

Double et al. (4), as mentioned in Chapter 2, have proposed a viable model for the formation and growth of the needles based on an osmotic mechanism and originally drew an analogy with silicate "gardens". The C-S-H fibres which grow radially from the original cement grains appear to be needle-like and hollow (4). This is a view which has been substantiated by the author, although it must be noted that composition and water chemistry can substantially affect the needle morphology. (247). Indeed, it appears that the morphology of C-S-H and the other cement hydration products is strongly dependent on various factors including water content, pH and local cement chemistry (44, 45, 247), age (41), mix proportions (44, 30) particle size and admixtures (247), presence of carbon dioxide (44, 32, 46) and temperature (47, 247). The development of the strongly interlocking fibrous microstructure into a amorphous mass does, however, appear to be responsible for the materials strength, particularly in compression (4, 41).

5.6 Discussion

5.6.1 Models for Fatigue Hardening

It is appropriate first to review various models to explain fatigue hardening. These include:-

(i) Accelerated curing due to observed temperature increases (95, 96, 143);

(ii) loss of gel moisture under load, or "drying hardening" (143, 242); and

(iii) redistribution of internal stresses (caused by shrinkage and curing) during fatigue, or "stress annealing" (144, 241, 244).

Taking these in turn, fatigue hardening has been observed in samples at least a year old, where accelerated curing at elevated temperatures could reasonably be expected to have little effect. In addition, tests carried out under constant temperature conditions in the present investigation, using a large capacity water bath as a heat sink, also produced increases in strength comparable to specimens fatigue tested in moist air.

These latter tests, by providing a continuous supply of free water through the capillary network, also suggest that specimen drying-out during fatigue cannot account for the observed strength increases.

Finally, a "shakedown" mechanism would have some appeal, having as it does a general similarity with such effects occurring in metals. (Although this typically gives rise to fatigue softening by dislocation re-arrangement in a previously highly dislocated, or strain-hardened, structure.) However, if this were the major cause of the effect, one would anticipate that the internal stresses set up during the drying process would provide a significantly greater potential for stress redistribution, and therefore fatigue hardening, in "dry" samples. This is not found to be the case (Fig. 5.4).

The fact that dry tests do not show fatigue hardening indicates that free water plays a significant role in the process. Furthermore, wet samples tested in air produce substantially more heat than dried ones. Bearing in mind, then, the heat evolution associated with the curing process, it would seem that the basis of the hardening phenomenon involves the rapid hydration of previously unhydrated particles.

5.6.2 Modes of Microcrack Propagation

It is of considerable interest to determine the mode of fracture in the cement composite, for a given testing situation, i.e. whether cracking occurs through the cement hydrate region, or through the unhydrated cement cores. In addition it would obviously be of value if it could be established how this fracture mode varied with certain factors, such as cement particle size, age of curing, water cement ratio and nature of the applied stress (for example: static, long or short term; or fluctuating).

The re-hydration technique described in a previous section represents a convenient, rapid and unequivocal way of distinguishing between the two possible alternatives. Thus, fatigue appears to produce a largely "intragranular" mode (exposing fresh, unhydrated surfaces), compared with primarily "intergranular", or interparticle, fracture observed under static loading (by cracking through hydrate regions). However, it remains to be established whether fatigue loading, per se, results in a predominantly different fracture path, or whether the unhydrated surfaces are produced subsequent to the major fatigue damage.

Previous studies on the mode of cracking in cement appear to be in some disagreement; certainly, the age of the test sample and the water-cement ratio do seem to exert an effect. Thus, Williamson (39), in tests on 60, 100 and 171 day old samples (water-cement ratio = 0.5) reports that the fracture path largely follows the water-filled spaces which, initially at least, separates the grains; however, he goes on to show micrographs illustrating the fracture of unhydrated cores, exposing uncombined C_2S. Walsh et al. (41), on the other hand, suggest that the failure mode is dependent on the amount of hydration: at curing times longer than 21 days, fracture reportedly changes from essentially intergranular to increasingly transgranular. (These authors carried out tests with a water-cement ratio of 0.5 on samples cured between 1 hour and 2 years.)

Contrary to this work, Higgins and Bailey put up an argument that static fracture is predominantly intergranular (72, 75). In addition to scanning electron fractography, albeit on samples having the very high water-cement ratio of 3:1 (and therefore more amenable to free fibrillar growth), their direct, surface observations (water-cement ratio = 0.3) using optical microscopy incorporating diffuse illumination (75) suggests that the fracture path skirts around unhydrated particles, which on occasions can also act as "crack stoppers".

Higgins and Bailey's approach (72, 75) is most interesting but appears to be only part of the explanation. Recent studies by the author (74), involving in situ S.E.M. studies of crack propagation in mortar and pure cement paste (including relatively large cement clinker grains), indicate that there is a "process zone" of microcracks ahead of the "major" propagating microcrack.

This is discussed in more detail in Chapters 6 and 8 (see Figs. 6.18 and 8(a)) and it is sufficient at this stage to mention simply that observations of microcracking fracture under slow controlled conditions in the S.E.M. (albeit under vacuum dry conditions) led to some microcracking through cement grains or at least their shells (Fig. 8(b)), as well as around cement grains.

The development of a large number of microcracks in the "process zone" at the so-called crack tip is also consistent with greater probability of cracking into or through cement grain shells. The cracking development in fatigue is a relatively long term procedure compared to static fracture and is thus probably greatly assisted by moisture and time dependent processes, as discussed in Chapter 4. Conventional static fractures have less (real) time to develop this microcracking (and the associated process zone) to the same degree and thus exhibit less overall damage, as indicated by both the damage monitors of changes in strain (Fig. 2.32) and ultrasonic pulse transit time (Fig. 4.6(a)). The fracture surfaces in static failures would thus be consistent with the interpretation of predominantly intergranular failure since the fractographic information obtained from re-hydrated static fracture surfaces yield less prolific hydration product (Fig. 5.8(a) and Fig. 5.8(b).)

At this point in time it is not possible to determine unarguably whether fatigue does in fact result in a change in fracture mode. It seems more likely that general damage and microcracking are more extensive in fatigue especially in view of the large number of very small associated microcracks of the process zone after passage of the main (micro) crack fronts through predominantly intergranular, or hydrate gel regions, and thus one obtains greater exposure of intragranular material. It is also possible that intragranular surfaces result from progressive attrition during cycling. It cannot be specified at this stage, however, whether such an assumed attrition process involves progressive grinding away of the, relatively, soft hydrate coatings surrounding each unhydrated particle, or an abrasion process, the stresses due to which induce intraparticle cracking.

It is also interesting to observe, in Chapter 4, that much of the acoustic noise, shown by the AE PIP method, occurred on the unloading cycle near minimum load (Figs. 4.14(a) and (b)). The concept of attrition of microcrack

fracture surfaces is consistent with this AE PIP noise if it is interpreted that the AE arises from some grinding process of the crack sides, since it would predominate on the unloading cycle and approach a maximum at minimum applied load.

5.6.3 Proposed Mechanism of Fatigue Hardening

Experiments described in preceeding sections indicate that the fatigue process results in the exposure of significant numbers of unhydrated cement particle cores. If sufficient "free", i.e. chemically uncombined, water is available, (normally present in capillaries, interlayer spaces and microgel pores) it will combine with freshly exposed unhydrated material to form new hydration products (197). The reaction is strongly exothermic, contributing to the increased temperature of the sample under test. The reaction is likely to be rapid because of the finely divided nature of the fractured, unhydrated cement particles, and the fine, C-S-H needles can readily bridge the cracks, typically 0.5-5 m wide (Figs. 5.8 and 5.10(a) and (b)).

The point must be raised as to why such a microstructural repair process should result in a material that has a strength exceeding that of the original product, particularly in view of the preceeding discussion which suggests that the hydrate is weaker than the unhydrated cement. The answer would appear to lie with the effect that such "repair" has on the total pore volume within the matrix. It is well known that porosity is a major factor affecting the strength of cement products (for example, see Jambor (67) and Double (1)), and for a wide range of water-cement ratios the compressive strength increases inversely with the porosity. Thus, during fatigue, by reducing the total volume of water-filled, or partially filled, pores through the hydration of previously unreacted cement, a resultant increase in strength would be expected.

Lea (32) also reports a resetting strength for a cement paste which has been allowed to hydrate and strengthen for periods between 3 and 28 days, and then subseuqnetly reground and its strength remeasured. Strengths of between 27 and 35% of the original were obtained. This is consistent with the present results, where it is assumed that just sufficient microcracking is introduced to release unhydrated cement but that little damage is done to the load bearing structure of the prism: thus consequent strength increases of approximately 20% are obtained.

Studies have shown that needles of Type I calcium silicate hydrate appear in the fatigue crack after as little as one hour of rehydration (Fig. 5.11). (It is just possible, but unlikely, that such needle-like C-S-H microstructure, as shown in the microcrack of Fig. 5.11, already existed in the crack as a subsurface characteristic of incomplete hydration. This was reported by Jennings (10, 11) and Dalgleish (14) and substantiated in the present work as mentioned in Chapter 2 (Figs. 2.11(a), (b)).

Assuming the C-S-H fibrous morphology is not pre-existing and is indeed associated with rehydrated material, it is apparent that re-hydration and therefore strengthening can begin to take place from the point when cracks first form, and certainly throughout the test. Longer (re)hydration periods result in more extensive growth of hydration products: Figs. 5.10a, 5.10b and 5.6 show surfaces which have been fatigued and rehydrated for, respectively, 7, 24 and 48 hours. These observations are consistent with the results shown in Fig. 5.3: damage introduced in the first few cycles, or at any rate in the first stage of the fatigue life ($\simeq 0{,}2\ N_f$) is repaired by hydration, either during the test or while the specimen is left to stand, and bigger increases over the static control samples are observed the longer the period which has elapsed after damage has occurred.

One assumption fundamental to this relatively simple mechanism is that hydration, and therefore fatigue hardening, can continue uninhibited during fatigue cycling, i.e. the microcracks, once formed, remain sufficiently open to allow the growth of fresh hydrate. This, at first, seems unrealistic when one considers the loading/unloading nature of the fatigue cycle.

The applied longitudinal compressive stress results in lateral tensile stresses within the sample, opening up (approximately) vertical microcracks (Fig. 3.10), which might reasonably be expected to close during the unloading portion of the cycle. However, measurements of UPTT and residual (permanent) lateral strain during a fatigue test show that there is a progressive, and quite similar, increase in both parameters (Figs. 2.30, 4,1, 4.22, 4.36). (Note that acoustic emission studies, 4.10, 4.11 confirm that change in UPTT is indeed a measure of the extent of microcracking within a test sample.) Similarly, simply unloading during a fatigue test does not produce any significant recovery of the UPTT, (Fig. 4.5(a, b, c)) : were the cracks to close completely, it would be expected that UPTT would

revert to its original value at the start of the test. It can therefore reasonably be concluded that microcracks formed during fatigue remain open, or at least partially open, at all points of the loading cycle, facilitating the formation and growth of fresh hydrate and therefore fatigue hardening.

An immediate implication of the observations described and interpreted in the preceding paragraphs is that, provided a wet environment is available, in-situ, microstructural self-repair can take place in any cement or concrete structure. In addition, fatigue loading results in increased strengths (and therefore, for example, improved long-term creep resistance), provided a certain fraction of the fatigue life is not exceeded.

5.7 Conclusions

(1) Strength increases of up to 20% following fatigue can be observed in tests carried out for moist or wet specimens over a wide range of applied stress level, and result directly from damage introduced in the form of microcracks in the early part of the life. These microcracks remain at least partially open even at the minimum in the loading cycle, and therefore facilitate microstructural repair.

(2) A scanning electron microscopy, fractographic study indicates that static fracture appears to result in a largely intergranular fracture path, i.e. through the hydrate gel regions; fatigue, on the other hand, produced extensive regions of exposed, unhydrated cement particles, presumably by the more extensive process zone cracking associated with greater microcracking in fatigue.

(3) Consideration of the mode and origins of stable microcracking during fatigue suggests that such unhydrated particles are exposed by an attrition process which takes place subsequent to the passage of the main (micro-) crack fronts, and the associated process zone cracks.

(4) Fatigue hardening requires the presence of free, i.e. chemically uncombined, water within the matrix; samples dried at $105^{o}C$ do not exhibit the effect. The likely mechanism involves microstructural repair and the hydration of freshly exposed, previously unhydrated surfaces in fatigue microcracks, with strength increases resulting from a decrease in the overall porosity of the composite, in conjunction with reductions in localized stress concentrations.

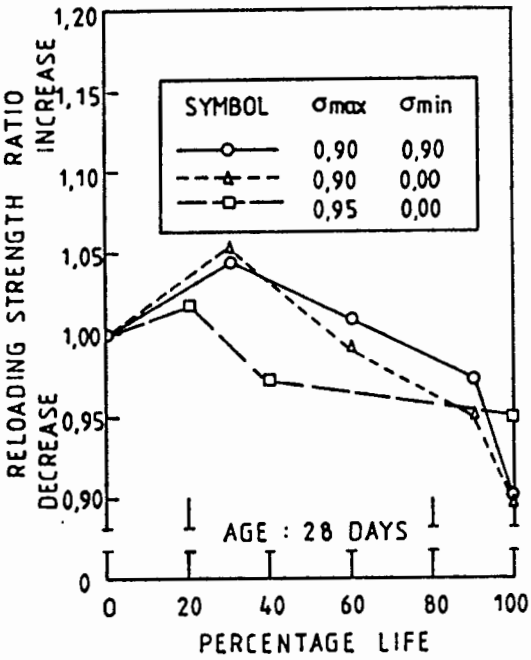

Fig. 5.1 Change of static strength of concrete during repeated or sustained load tests. (From Awad and Hilsdorf (27).

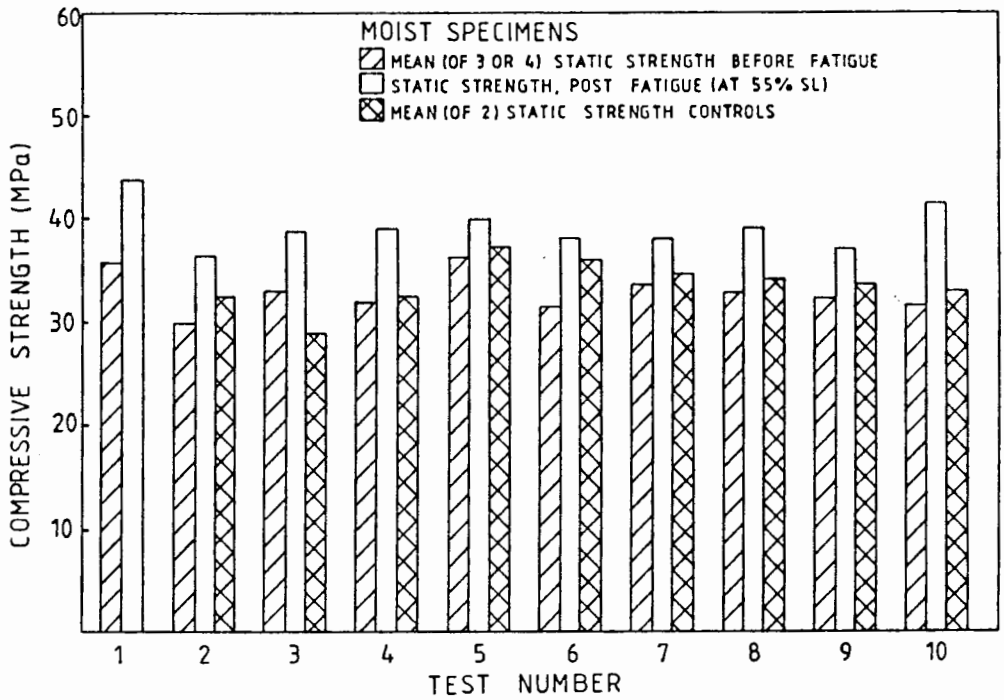

Fig. 5.2 Histogram illustrating the fatigue hardening effect for moist and wet specimens.

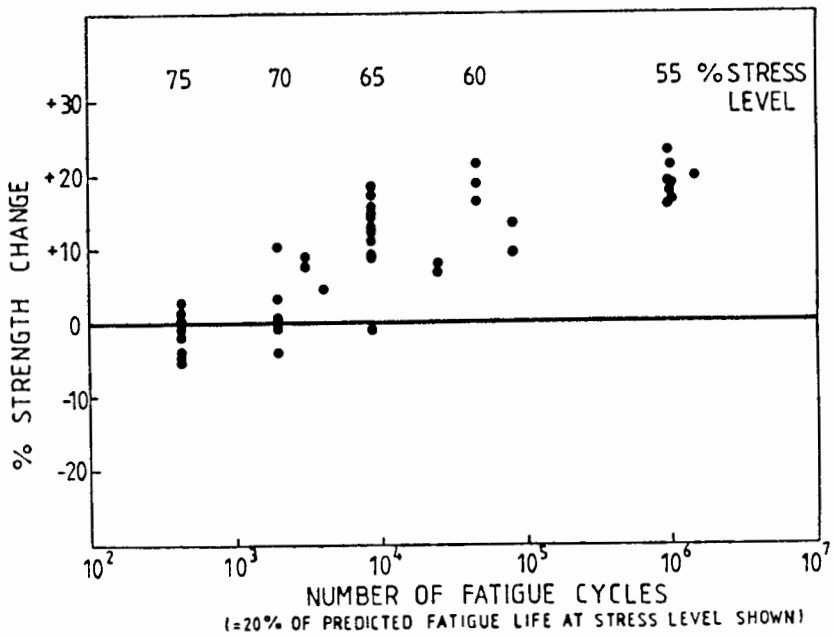

Fig. 5.3 Fatigue hardening as a function of applied stress level, for moist and wet specimens. Tests at the stress levels indicated were interrupted at 20 per cent of their predicted fatigue lives, estimated from Fig. 2.28. Fig. 5.3 plots the percentage static strength change = (post-fatigue strength - original static strength)/ original static strength X 100, against the respective number of fatigue cycles.

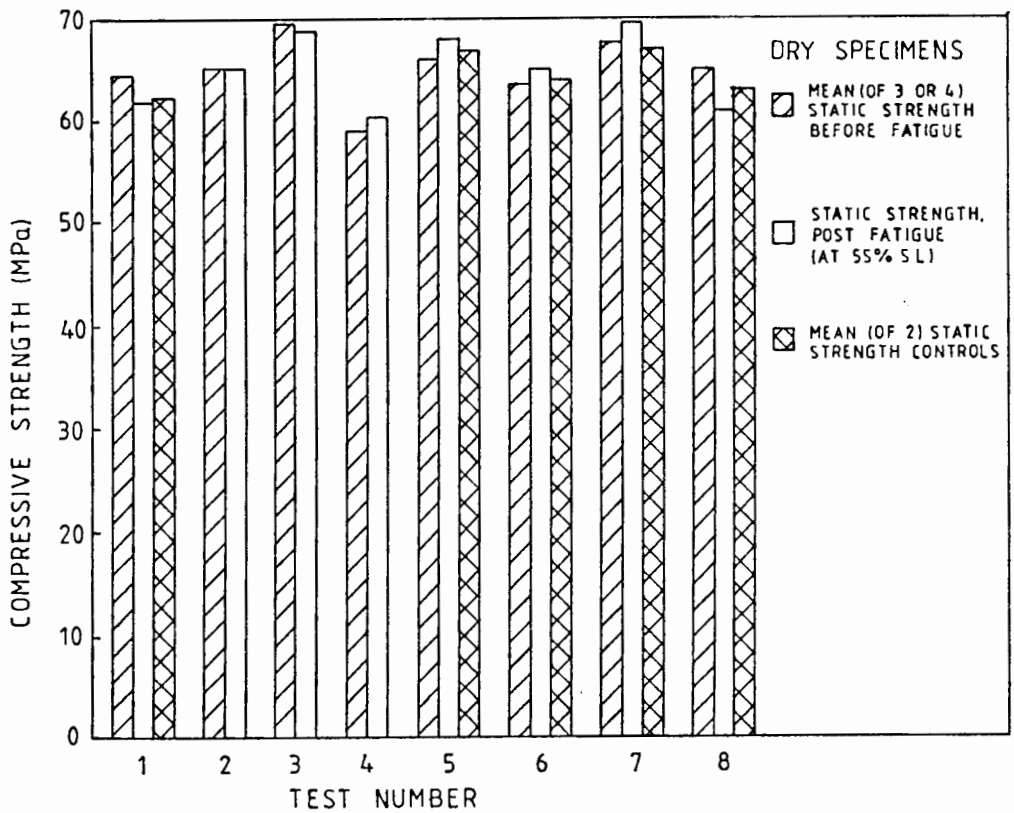

Fig. 5.4 Histogram illustrating the absence of fatigue hardening for dry specimens.

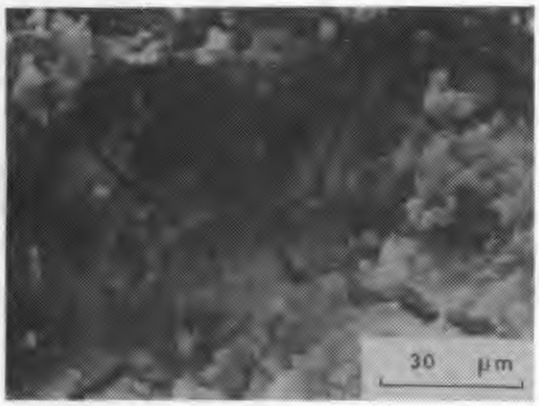

Fig. 5.5 Typical fatigue surface showing extensive microcracking which is significantly more widespread compared with its corresponding static failure.

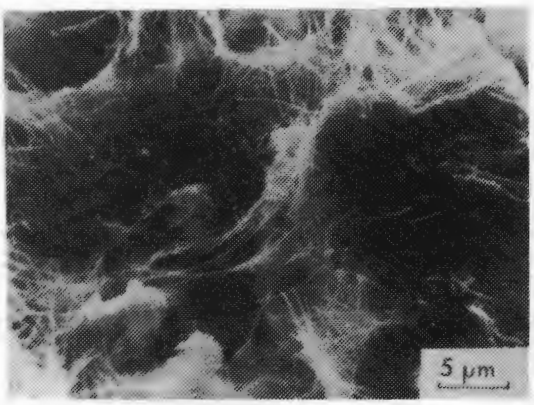

Fig. 5.6 Fatigue fracture surface, re-hydrated for 48 h by exposing the surface to an aqueous envrionment, showing extensive fibrillar growth of calcium silicate hydrate from unhydrated surfaces produced during the fatigue process.

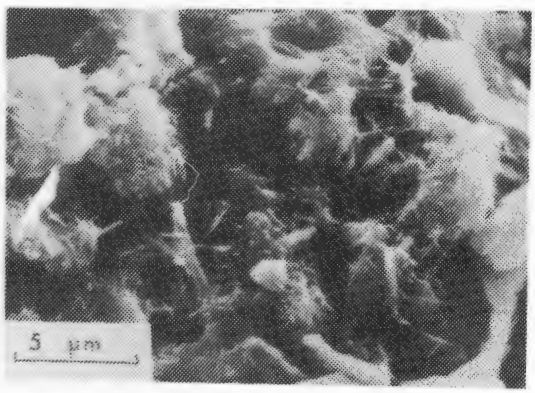

Fig. 5.7 Sample fatigued and re-hydrated for 24 hours.

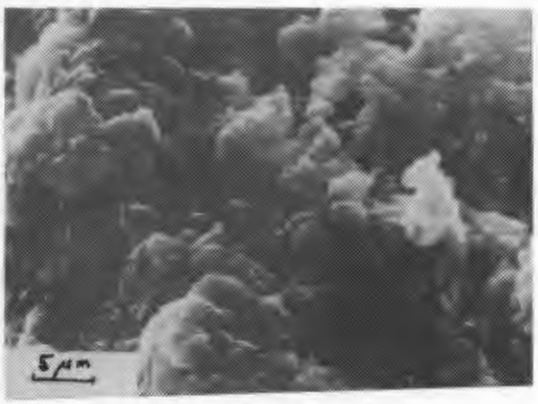

(a)

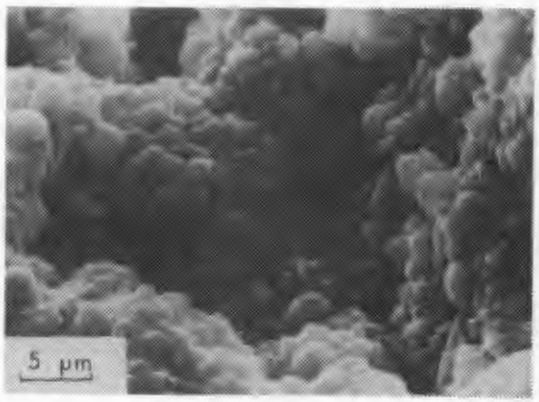

(b)

Fig. 5.8(a) and (b) Static fracture surface, monotonically loaded to fracture and re-hydrated for 48 h. Minimal formation of fresh hydrate, indicating that fracture is probably largely intergranular, i.e. through the interparticle hydrate gel network formed during curing.

Fig. 5.9 Schematic illustration of the stages involved in the hydration of Portland cement (Courtesy of D.D. Double). On adding water (a) gel coating (the "inner" product) quickly forms around the grains, (b), and hexagonal crystals of calcium hydroxide form as a by-product of the silicate hydrate reaction. As the curing process proceeds, (c), fibres and needles (or other hydrate morphologies) develop and interlink to bind the product together. (after Double, 4,5).

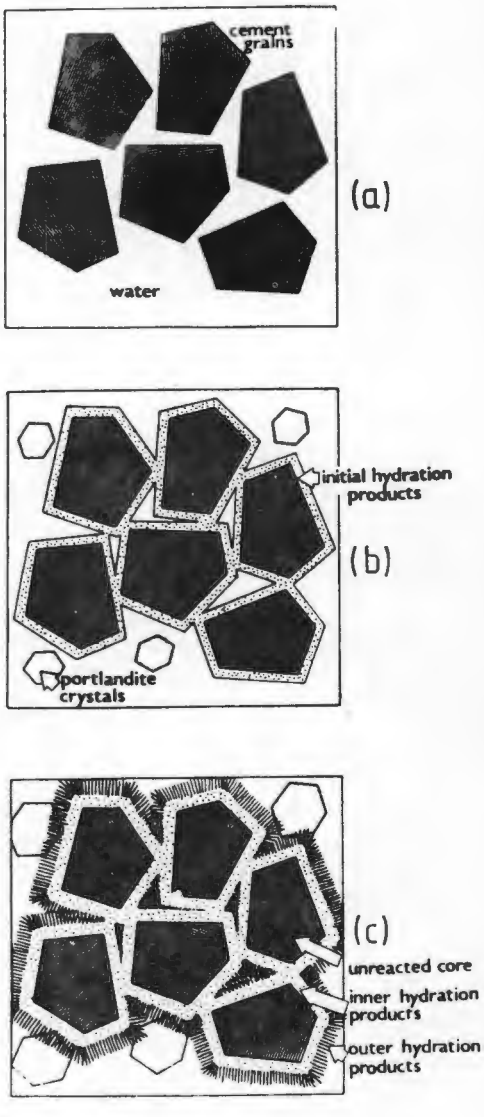

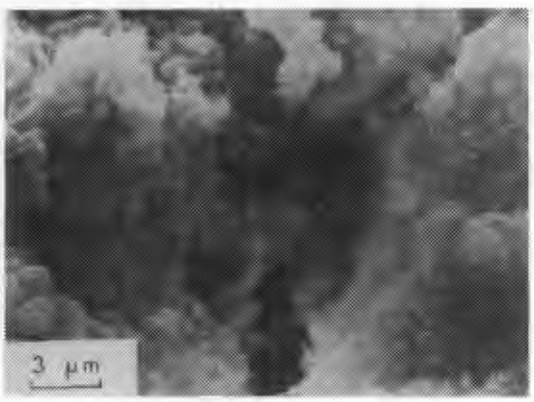

(a)

Fig. 5.10 Fatigue fracture surfaces re-hydrated for (a) 7 h, and (b) 24 h illustrating hydrate bridging of microcracks as the basis of the "microstructural repair" process.

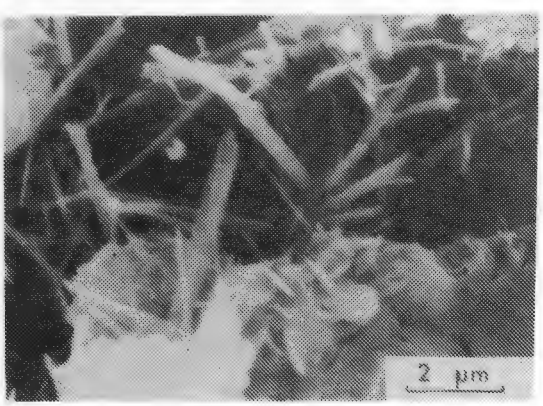

5.10 (b)

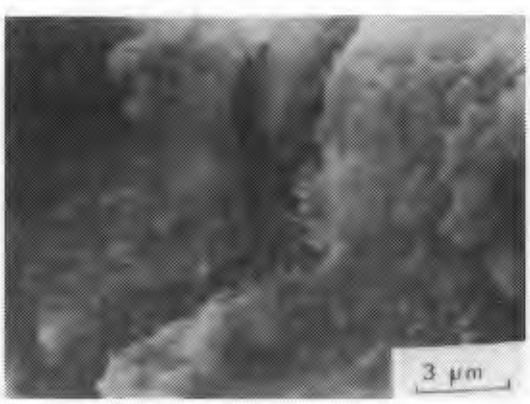

Fig. 5.11 Fatigued and re-hydrated for 1 h only: C-S-H needles form in the microcracks after very short times, provided free water is available.

"Truth is never pure, and rarely simple"

Oscar Wilde.

CHAPTER SIX : A REVIEW OF THE EXPERIMENTAL APPLICATION OF FRACTURE MECHANICS TO CRACK PROPAGATION IN CEMENT BASED MATERIALS

6.1 Introduction

Previous chapters (and in particular Chapters 2 and 4) have highlighted the importance of the need for an understanding of the cracking behaviour of concrete and other cement based materials, based largely on observations of damage. It appears (19) that the strength limiting characteristic of cement, mortar and concrete is one of "flaw" size within the material. It is the behaviour of these flaws in concrete that is of interest in the present survey - how do they initiate? - under what conditions will they propagate? - where and to what extent can they be tolerated? - how does fracture occur? - is stress intensity a meaningful parameter? - these and other questions become all important in highly stressed civil engineering structures. It is only through a better understanding of the crack resisting - or toughness - as well as crack propagation characteristics of concrete that such questions can be answered. Indeed efforts directed at more efficient design and better use of concrete materials have now reached the stage where a detailed knowledge of the applicability of fracture mechanics to concrete may be crucial. Such understanding may also contribute to ways of improving concrete's main shortcoming - its low tensile strength. Indeed, such efforts in producing macro defect free (MDF) cement have recently led to tensile strengths of cement of up to 150 MPa (19). Concrete is, however, a very heterogeneous material and fracture mechanics models, which normally assume that the material is continuous, homogeneous and isotropic, have to be modified to account for the heterogeneity and stress concentrations associated with aggregate inclusions.

Local variations in stress would result in a low observed strength, and for an isotropic medium failure occurs when a flaw increases to a critical size under a particular stress. The determination of the flaw size/stress distribution relationship and the potential for crack

propagation can be considered from two points of view. Firstly, by means of analysing the stress and displacement fields in the vicinity of crack tips, where local stresses exceed local intrinsic material strength, or secondly, from an energy point of view, which is usually more reasonable for a brittle material like concrete which exhibits multiple cracking (155, 219). The optimum method for implementing such a study is by way of the approach where the strain energy released (as a result of the fracture) is more than sufficient for the surface energy requirement of the new fracture surfaces for crack propagation to occur, on which the methodology of fracture mechanics is based.

The motivation for a fracture mechanics approach for conrete, in addition to the crack propagation briefly mentioned, is further justified by the following phenomena (249):-

(i) Fracture is generally of a brittle nature;
(ii) Strength increases with loading rate (104) and both cement and concrete are subject to static fatigue (106 250). Both of these phenomena can be attributed to subcritical crack growth;
(iii) Cement is highly notch sensitive (251 - 253). To a lesser and decreasing degree, are mortar and concrete (respectively) although there is much conflicting evidence on this point (254 - 256).
(iv) Stress concentrations are reported (257) to exist near the cement aggregate interfaces and could easily be of such a magnitude as to exceed the local theoretical strength.
(v) Tensile strengths are approximately $^{1}/10$ of the compressive strengths which is close to the value of $^{1}/8$ predicted by Griffith (258) for brittle materials.

This chapter is hence concerned with a review of the applicability of quantitative fracture mechanics, particularly with regard to crack propagation, to these cement materials. The LEFM application is reviewed with some discussion of the meaning of toughness for such materials (Section 6.2). It is, however, beyond the scope of this thesis (which is more concerned with fatigue and subsequent fracture) to examine the factors affecting toughness in any great detail. This has in any case been handled elsewhere (261). Rather, the recent widespread

attempts to apply fracture mechanics to cement systems through toughness measurements which are summarised here (Section 6.2), provide some justification for its application to crack growth studies to follow (Section 6.5). The measuring systems employed for toughness investigations can, however, also be used for crack propagation studies. These experimental techniques, are discussed (in Section 6.3) and the particular single crack growth method selected for this study (i.e. double torsion) is critically examined (Section 6.4) as its use is contentious. This is followed by an evaluation of the techniques and previous studies of velocity-stress intensity (V-K) information (Section 6.5) and, together with the summary (Section 6.6), provides the background for the experimental single crack growth studies of Chapter 7.

6.2 Application of LEFM to Cement Systems

6.2.1 Introduction

Cement based materials, and concrete in particular, contain flaws which can arise from various sources, for example, shrinkage cracking porosities, aggregate debonding as well as section changes and construction joints. These can affect the macroscopic strength of the material either directly or after some crack growth.

The discrepancy between the theoretical and actual fracture strength, as a result of flaws, and the associated objective of describing the ability of a homogeneous brittle material to resist crack propagation, was first discussed by Griffith (262) in 1921 using an energy balance approach, and this has since developed into the discipline of Fracture Mechanics. Griffith showed that it was possible, through a consideration of the relationship between the stress and strain distribution and flaw size in the vicinity of that flaw, to determine the likelihood of rapid fracture of the structure, and hence relate actual measured strengths to theoretical predictions.

The origins and fundamentals of fracture mechanics are now so well known and established that a review of the basic principles is certainly not required here. Any standard text (for example J.F. Knott (263), Broek (264) or others (265, 266,)) should be consulted for introductory details.

6.2.2 The Application of Fracture Mechanics

6.2.2.1 Introduction

Linear elastic fracture mechanics, in general, is most applicable to purely brittle materials, and a number of studies have been undertaken on cement based materials, even though these materials are far from homogeneous, isotropic and ideally elastic; (19, 72, 73, 77,130, 149, 153-155, 180, 251, 155, 267-275). Furthermore, concrete failure is generally controlled by the propagation of interacting cracks, rather than by a single crack, (276).

Various assumptions are normally made to provide for the application of the Griffith-Irwin theory. In the first instance, it is generally assumed that concrete is homogeneous and continuous as far as the application of the laws of elasticity are concerned. In practical terms this implies that both the scale of the microstructure, or "grain size", and flaw size must be small in relation to specimen dimensions - usually by at least one or two orders of magnitude. However, in reality when concrete is considered at a microscopic level it is heterogenous and cracking apparently occurs discontinuously. This implies that the fracture mechanics concepts as applied to metals are not directly applicable to cement based materials, and other models are required. In addition, for the application of linear elastic fracture mechanics the "inelastic" region in the vicinity of the crack tip is assumed to be small in comparison with both the specimen and flaw dimensions.

Hilleborg (276) and Petersson (129, 278) expand on this concept in the "fictitious crack model" (F.C.M.), where they relate acceptable specimen dimensions and crack lengths in the material to a "characteristic length", l_{ch}. In Hilleborg's notation this characteristic length is given by

$$l_{ch} = \frac{EG_F}{f_t^2} = \frac{K_{Ic}^2}{f_t^2} \qquad 6.1$$

where E is the Young's modulus, G_F the fracture energy at total separation, K_{Ic} the fracture toughness and f_t the tensile strength. For cement paste, mortar and concrete, the characteristic lengths, according to Hilleborg, are approximately 10, 150 and 300 mm respectively, and the so called "process zone" of microcrack interaction or "stress perturbation" at the tip of a macrocrack has a length of the order of 0.3 to 0.5 times l_{ch}. Thus specimen sizes would need to be of the order of 200 mm deep for mortar, for example. [Recent studies by the author, however, using direct measurements of microcracking in an SEM (see Chapter 8), indicate that, for paste and mortar, the process zone radius is more of the order of 0.4 to 2 mm, with a consequent decrease in acceptable specimen size.]

Higgins and Bailey (72) and others (277) similarly report that for cement paste beams in flexure over a range of depths from 5 to 110 mm, LEFM is not directly applicable because, although K_{Ic} is independent of crack length, it does depend on overall specimen size. They also related this to the size of the "process zone" and said that this was not small with respect to the specimen size, even though the macrocracking was stable.

Using this characteristic length approach it is proposed that so called "valid" estimates of toughness are only obtainable when the specimen and crack dimensions are comparable to, or greater than, the characteristic length. (Perhaps the best contention is that of Alford, Groves and Double (77) who infer that the inherent flaw in the material must be small compared to the notch size and beam depth, for meaningful application of linear elastic procedures).

Another assumption to be made is that the values of elastic modulus, E, and Poisson's ratio, ν, are constant throughout the material, and are normally regarded as average values, representative of the material.

While these assumptions are not rigorously applicable at a microscopic level, it is reasonable to regard concrete, from a statistical viewpoint, as behaving as such an isotropic, homogenous continuum. This has been the approach of pioneer investigators as well as subsequent workers in this field.

6.2.2.2 Variables Measured: G_c, γ_c, K_c

Fracture mechanics studies in this material system have, to date, defined three parameters of a materials resistance to cracking, as having meaning in cement systems. These are the critical strain energy release rate G_c, the fracture surface energy γ_c, and the critical stress intensity factor K_{Ic}. The following sections briefly consider such questions as whether these parameters represent fundamental properties for cement-based materials and, if so, how they depend on such variables as concrete age, degree of hydration, water cement ratio, mix, environmental moisture, specimen size and shape, aggregate (volume, angularity and surface roughness) and porosity. In addition, the question of the applicability of LEFM to cement based systems, a question not yet fully resolved, is examined. Certainly this would appear to depend to a large extent on some of the variables mentioned above, but is relevant for consideration because of the employment of such a methodology - to advantage - in subsequent sections.

Popular methods for investigating the application of fracture mechanics principles to concrete have included the use of notches in simply supported 3 or 4 point beams, (77, 105, 127, 130, 131, 155, 249, 252, 253, 255, 256, 267, 268, 275, 278-283) and more recently in double cantilever beams (DCB) (130, 155) and double torsion (DT) (73, 104, 105, 284, 285) configurations, as well as some other specimen geometries (108, 128, 251, 254, 269, 274, 286-289). The notch, or initial crack, represents a flaw of known size (nominally at least) where fracture initiates preferentially. A review of fracture toughness techniques for ceramics is given by Shih and Opoku (291).

Early measurements of concrete's and mortar's resistance to cracking were made by Kaplan (267) and Irwin and Kies (292) using single edge notched beams (SEN) and dimensional stress analysis and compliance relationships. They expressed results in terms of G_c, the critical strain energy release rate.

Kaplan's results suggested that the critical strain energy release rate (G_c) concept, as a criterion for rapid fracture, was applicable to concrete but that G_c may be influenced by such variables as mix

proportions, specimen dimensions and loading mode. Glucklich (154) obtained similar results which led him to believe that G_c was a material constant but one which has different values in tension and compression. In recent years strain energy release rate G has become almost redundant as an index for fracture resistance and has largely been superseded by the initial stress intensity factor, or fracture toughness, K_{Ic}.

An alternative approach is to consider the fracture surface energy γ, where, from the Griffith equation,

$$\sigma = \sqrt{\frac{2E\gamma}{\pi a(1-\nu^2)}} \qquad (6.2)$$

Here σ = applied fracture stress, γ is the specific surface energy, E = Young's Modulus, ν = Poisson's ratio and a is the half crack length (see for example, Knott, (263)). It can be seen that the tensile fracture strength of a material depends on its surface energy, γ, and that this parameter may be used directly as a measure of a material's resistance to the initiation and propagation of cracks. Fracture energy, and hence surface energy (equal to fracture energy per unit area) is applicable to stable and semi-stable fracutre, Fig. 6.1, and is comparatively easy to measure from load deflection plots as $-\frac{\delta U}{\delta A} = \gamma$. Here U is the total elastic energy stored in the system, A is the area of the fracture face and γ is the surface energy. Nakayama (293) assumed that the energy expended to induce stable fracture is equal to the surface energy of the newly formed surface, that is

$$U = 2A\gamma$$

This applies quite adequately for ideally brittle materials where the fracture area is equal to the single crack cross sectional area of the specimen. However, for concrete the fracture surface area may be significantly larger than the geometrical cross section area because of the irregular fracture path and extensive secondary fracture or microcracking of the "deformation zone" or process zone in the vicinity of the crack tip (131, 74). This may well result from the heterogeneity of concrete (154) and in this case (for larger actual values of surface area), the surface energy calculated would be excessive. The "effective" surface energy γ_{eff} may be computed as $\gamma_{eff} = \frac{U}{2A_o}$ where A_o is the cross sectional area of the specimen. In effect, since the real crack area is

Void Content and Porosity

The effect of porosity or void content on the fracture toughness of concretes, mortars and cement paste has not been widely reported possibly because of the relatively small effect it exerts. However, recent studies, particularly by Alford, Groves and Double (77) have highlighted the importance of intrinsic flaw size in cement and mortar as being the strength limiting factor. This is often, but not always, related to porosity as is seen subsequently. A cement material exhibiting very small flaw size but relatively large porosity can still have quite large strength and toughness (77).

6.2.3.3 Effect of Testing and Environmental Conditions

The measured toughness of cement materials is apparently dependent on the specimen's size and shape (72, 105, 127-129, 155), e.g., 4 point bend tests reportedly yield toughness values about 15% lower than equivalent 3 point bend tests (267). As a result there have been some attempts to employ other test methods which are less susceptible to such dependencies, for example, double triangle/triangular web flexural tests (128), double torsion (104, 198, 249, 284, 291, 294) and double cantilever beam methods (155, 130, 294).

Localised environmental moisture or even humidity has been recognised as affecting track resistance by reducing toughness measurements (29, 89, 105, 106, 149, 155, 250, 268) and also conversely that toughness decreases with increased drying out (72).

As regards the effect of temperature on toughness there does not appear to have been any test programmes that have specifically examined this aspect - although the effect on strength has been reported earlier (section 4.5).

6.2.4 Summary

This section (6.2) has briefly examined the applicability of fracture mechanics to cement materials, identifying first the types of crack resisting parameters and the importance of the relative sizes of the

specimen and process zone. The problem of premature crack growth in most fracture mechanics type measurements has been mentioned and the section concluded with the brief examination of those factors that affect measured toughness. From the above summary it is apparent that several researchers have regarded the application of fracture mechanics to cement materials as meaningful and have measured the corresponding toughness and factors on which it depends.

The applicability of linear elastic fracture mechanics to concrete mortar and cement paste is still, however, questionable and further studies are needed before this matter is resolved. Assuming, however, that it is meaningful to refer to a fracture toughness, values that have been reported for cement paste lie in the range of 0.1 to 0.6 MPa $\sqrt{m}$, and for concrete (including mortar) in the range 0.4 to 2.0 MPa $\sqrt{m}$.

This provides the background for the following section which discusses the experimental methods for slow crack growth (V-K) studies in mortar.

6.3 Experimental Methods

6.3.1 Introduction

One of the most useful ways of representing slow crack growth behaviour in brittle materials is by means of the so-called "V-K curve" (285) (Fig. 6.8). Here K is the (mode 1) stress intensity factor and V, the crack velocity. The particular value of the V-K curve is that it is possible, at least in principle, to estimate the time dependent fracture properties and times to failure of cement mortar and concrete, once the stresses and other appropriate material characteristics are established.

Methods of obtaining such V-K data (and also toughness data) are complicated because of the premature crack growth that usually occurs at the tip of the prepared notch in typical fracture toughness type specimens before maximum load is reached (see section 6.2.2.3). Hence techniques and loading configurations have been developed in which the stress intensity is independent of crack length. In particular, these are the double cantilever beam (DCB) and double torsion (DT) techniques which are discussed in more detail below.

6.3.2 The Double Cantilever Beam Technique

Brown (130, 155) in 1972, appears to have been the first to make use of a double cantilever beam technique as a method for obviating the problem of accurately monitoring slow crack growth in concrete. In its simplest form the DCB specimen can be regarded as a 'long' compact tension (CT) specimen (Fig. 6.9). However, the most useful DCB form is the "constant K specimen" configuration which results in crack length independence for K_I. For the DCB these are of two forms: the tapered DCB (Fig. 6.10(a) (294) and the tapered or profiled web DCB (Fig. 6.10(b)) as used by Brown (130, 155) on concrete. These latter specimens comprised two rectangular beams linked by an approximately triangular fillet or web, Fig. 6.10(b). This was shaped so that as a crack was developed from the apex of the triangle by mechanical separation of the ends of the cantilever; the increase in width of the crack front exactly compensated for the increase in bending moment at constant load, thus ensuring a constant stress intensity system - provided that there was no change in effective fracture toughness with crack growth.

Brown (155) reports that, even though tapered web (DCB) specimens (Fig. 6.10(b) are more difficult to construct than simple tapered DCB specimens (Fig. 6.10(a)), a higher degree of success was generally possible.

If the specimen is regular and of uniform web width, the load necessary to propagate the crack will decrease as the crack length increases. However, if the web width is not uniform but made to conform to the specified profile (155) then the stress intensity parameter, K_I, becomes independent of the crack length. The effect of increasing crack length on the reduction of applied load, F_c, is exactly balanced by the increasing web width and K_{Ic} can be determined without determining crack length. K_{Ic} is thus directly proportional to F_c and if K_c is thus constant the crack can propagate at a constant load.

Brown's results indicated that the fracture toughness of cement paste was independent of crack growth, while for mortars the toughness increased slightly with increasing crack length in the range 10 to 100 mm.

Sok, Baron and Francois (301) have used large (2m) DCB specimens and measure the toughness of concrete as 3 to 4 MPa. They conclude that the characteristic lengths is about 200 mm.

The DCB technique has also been used successfully by other authors in the fracture study of brittle materials (130, 291).

6.3.3 The Double Torsion Technique

6.3.3.1 Introduction

A further toughness testing technique which avoids problems of crack length determination, since K is independent of crack length, is afforded by the Double Torsion (DT) test method. This is discussed in some detail here because it is the method that has been selected and extensively used in this thesis.

The choice of the double torsion specimen was fairly evident. A specimen type which facilitated slow crack growth studies in brittle material was required. The specimen also needed to be suitable for so-called "change over" tests - i.e. where only one parameter is changed during the test on a single specimen, so graphically illustrating the effect such change has on crack growth rate. The 'constant K' type of specimen was thus essential. Examination of the techniques available (294), Table 6.2, reduced the choice to Double Torsion (DT), tapered Double Cantilever Beam (DCB) or constant moment techniques. The former was chosen, for reasons of ease of manufacture and testing in a variety of environments.

DT Specimens are also both economical in test material and simple to prepare and analyse. In contrast, the DCB technique is extravagant in material terms and can (in mortar) require relatively skilled preparation procedures. Experimental DT techniques, once established, are no more difficult than the double cantilever beam.

The specimen is loaded and failed in "double torsion" by flexural loading of one end, in such a way that a single crack is driven down the centre of a thin rectangular specimen, Fig. 6.11. The energetics of the system of failure are such that the load causing the crack remains constant as

the crack propagates, and the load can be related directly to the fracture toughness. The crack length does not enter into the equation for the derivation of stress intensity or fracture toughness and so difficulties with its measurement or that of specimen compliance are no longer important. Since the stress intensity is constant for a large range of crack lengths, (perturbations only becoming significant for the beginning and end 15 to 20% of the specimen length) it is possible to use the testing configuration in a variety of ways. These include: static tests to provide valuable information on the stress intensity for the material under (i) constant load or (ii) constant position control as well as (iii) steady ramping at known deflection rates. Alternatively tests in a fatigue mode coupled with measurements of the actual observed crack length can be undertaken. This readily facilitates investigation of the effect of other parameters on crack growth rate such as stress level, frequency, temperature and environmental conditions. A brief summary of the theoretical basis of the double torsion technique follows as it adds understanding to the subsequent critical evaluation of the DT technique (section 6.4) and the use of this method throughout Chapter 7.

6.3.3.2 Theoretical Analysis of the Double Torsion Technique

The double torsion test specimen was first reported by Outwater et. al (305) and Kies and Clarke (306). However, these references contained an error in the final mathematical derivation for fracture toughness so the complete and correct analysis is given in Appendix A. This technique has been used extensively by many investigators for subcritical crack growth studies of ceramic and brittle materials (73, 77, 104, 190, 198, 203, 235, 249, 284, 285, 291, 294, 295, 305-321). The essence of the double torsion system is shown in Fig. 6.11 and can be considered as two elastic torsion bars each with rectangular cross sections and loaded as shown in Fig. 6.11.

The relation between stress intensity K, specimen dimensions and load P is given by

$$K = Pw_m \left[\frac{3}{t^3 t_n W(1 - \frac{5}{4}\frac{t}{W})(1-\nu)} \right]^{\frac{1}{2}} \qquad 6.3$$

for the plane strain condition

where
- w_m = moment arm
- W = specimen width
- t = plate thickness
- t_n = web thickness in plate
- ν = Poissons ratio
- P = Applied load
- K = stress intensity

See Fig. 6.11 for location of these parameters.

The stress intensity K, is thus independent of crack length and is a function only of applied load, specimen dimensions and Poisson's ratio. It is this feature of independence of crack length which makes this specimen configuration particularly useful for certain types of subcritical crack growth studies.

The analysis described in appendix A for the double torsion specimen is based on the assumption that the specimen can be treated as two independent torsion bars and that all displacements are related to torsional deflections of these bars. This, of course, neglects the possibility of either shear strains in the individual bars or flexure of the uncracked portion of the specimen or, indeed, interaction between the cracked arms. This latter assumption imposes the constraint that the analysis only applies at relatively large crack lengths where the deflections are substantially larger than the deflections in an uncracked specimen. The validity of these assumptions is best checked experimentally by performing a compliance calibration on a specimen and comparing this empirical relationship with that which would result from the analytical expression

$$C = \frac{y}{P} = \frac{3w_m^2 a}{Wt^3 G\psi} \qquad 6.4$$

(See Appendix A, equation A.4) The results of experimental compliance data by the author for the cement mortar used in this thesis is shown in Fig. 6.12. There is a small departure of the data from the analytical

expression but this is probably associated with the limitations at small crack lengths.

6.3.4 Summary

Of the slow controlled crack growth methods available for obtaining crack velocity and stress intensity data, the DCB and DT methods have been highlighted. The theoretical basis of the method selected (double torsion) has been examined but since many of the details of its application are contentious, the practical use of the DT method is critically evaluated in the following section.

6.4 An Evaluation of the Practicality of the Double Torsion Technique

6.4.1 Introduction

This evaluation will take the form of a discussion of the pros and cons of the double torsion technique from an experimental and practical viewpoint. Excellent reviews of the DT technique from both an analytical (323) and experimental (322) viewpoint are already available and can be supplemented with finite element studies (324, 325).

The double torsion specimen provides a particularly elegant, and ostensibly simple, technique for evaluating quantitative fracture parameters. Over a large portion of its length, (approximately the central half - see section 6.4.5), the stress intensity, K, is independent of crack length, so that crack length measurement is not specifically required. This is particularly useful for cement based materials, composites, and some ceramics, where definition of the "crack tip" is often difficult. The geometry is simple and relatively easy to fabricate although optimum dimensions are still the subject of debate. Specimen loading is also straightforward: four point loading (or more rarely, three point loading) in compression. This facet of the test method, together with its crack length independence, makes it suitable for use in hostile or aggressive environments and it has often been used in high temperature studies (316, 321, 326, 327). In the present investigation it is therefore most suitable for the controlled temperature underwater tests.

Since it does not increase with crack length increases, the DT technique is ideal for brittle materials which require very careful control of stress intensity and applied loads to facilitate precracking.

Once the specimen is correctly aligned, experiments are relatively easy to perform and the analysis nominally straightforward. However, in practice, the application of the double torsion technique is rather more complicated and requires "special techniques and specimen and experimental conditions" to obtain truly valid data, (322). The most important of these special conditions are discussed below.

6.4.2 Specimen Geometry and Dimensions

The double torsion specimen can be regarded as a thin plate with typically the proportions - and often the dimensions - of a microscope slide. There does not appear to be a standard specimen size or proportion and hence a review of the sizes of D.T. specimens reported in the literature was undertaken. The results are shown in Table 6.3 and Fig. 6.13. In addition to the actual dimensions, Table 6.3 also shows the relative proportions of D.T. specimens normalised with respect to the width, and whether they have incorporated (either single or double) side grooving. The proportions, as determined in Table 6.3 are plotted in Fig. 6.13. From this survey it is apparent that length is popularly three times the width. The thickness is more variable but appears to lie broadly between 1/6 and 1/15 of the specimen width. Indeed, recommendations by authorities in the field suggest the following specimen proportions.

Reference	Length (L)	Width (W)	Thickness Full (t)	Thickness Web (t_n)
(322) Pletka et al.	2W	W	$\frac{1}{12}$ W	1/2t
(328) Evans	3W	W	1/8W to 1/10W	2/3t
(310) Atkinson	2W	W	1/15W	0.8t

These recommendations follow from good correlation (328) of such DT results with DCB specimens for a variety of materials. Atkinson's recommendation (310) that plates should be less that 1/15W thick may have been prejudiced by his relatively short DT specimens (only 1.75 to 2W); Trantina's finite element study (324) used a thickness of 1/10W. The general conclusion is that specimen proportions should be of the order of 3W:W: 1/8 to 1/10W, as suggested, and used on several separate instances, by Evans (203, 234, 235, 294, 307, 309, 315, 316, 322, 328, 329).

In order to obtain the actual dimensions of the DT specimen, it is generally considered that the non linear zone near the crack tip should be small with respect of the thickness of the specimen.

For metallic materials this condition for plane strain is presented as follows:

$$B > 2.5 \left(\frac{K_{Ic}}{\sigma_y}\right)^2 \qquad 6.5$$

Its restrictive use for ostensibly brittle materials is questionable as fracture in these materials is generally regarded to be of a plane strain nature, even when quite thin. However, use of equation 6.5 has been made by eminent researchers (e.g. Fuller (323)) when referring to brittle materials. Many DT investigations conducted on specimens between one quarter and half this minimum thickness requirement, still, however, yielded valid data comparable with other (CTS, DCB) results (305, 314). It would thus appear that plane strain conditions do exist, at least for the tensile section of the mode I opening of the crack tip.

6.4.3 Side Grooves

Grooves have frequently been cut (or cast) into the surfaces of the double torsion specimen to ensure that the crack propagates down the centre line, where the stress intensity can be accurately calculated. However, "the centre slot causes certain intellectual discomfort because its effects, other than guiding the crack, are not well understood" (330).

Almost every conceivable combination of grooves has been used in the past, for example:

(i) grooves in both surfaces, equal depths (305, 331) and unequal depths (73, 297, 314, 332)

(ii) grooves in the tension surface only (285, 307, 310-312, 316, 317, 326, 329)

(iii) grooves in the compression surface only (104, 105, 284, 318, 322, 327, 328, 334)

(iv) no grooves at all (198, 306, 319, 321, 330, 335, 336).

As with the overall dimensions there appears to be no mathematical or analytical base for selecting a particular groove geometry. There are several uncertainties relating to the effect of grooves, and a test piece with no centre grooves appears ideal.

The effect of groove geometry in stabilising the crack into the longitudinal axial direction is not fully understood. Murray and Perrot (317) report that a sharp groove, and thus significant stress concentration, is what is necessary rather than the reduced section provided by a groove. Conversely, Pletka, Fuller and Koepke (322) recommend the use of wide grooves with minimum stress concentrating effects, which would otherwise tend to attract the crack to the stress concentrating edge and keep it there (323). The author's experiences support this contention. By the use of wide grooves it is believed (322, 327) that the crack is turned within the minimum section to maintain an axial path. Recent studies by Pabst and Weick (337), utilising several groove geometries, revealed greater scatter in V-K results with the use of grooves compared to non-grooved specimens.

The contention that grooving provides better experimental control is questionable and the overriding factor for straight crack growth seems to be specimen alignment (322, 330, 336). This ideal alignment is only achieved with great care, however, requiring a well finished surface, an extremely well balanced loading system, ideal dimensions (321) and homogenous material (307) but is apparently the best solution (307, 322, 336). Allied to these alignment and experimental details is the

contention, borne out by the author, that loading through ball bearings (or spherical load points) is preferable to rod loading (322, 328). Support at the rear end of the specimen is nominal and simply supported and does not play any part once the DT specimen is under load (73, 322). Despite reports (307), that grooving is probably unnecessary and has no effect on n values (of V-K curves) (104), their use has been extensive as shown previously.

There does not seem to be consensus either on whether, in the case of a single groove, the groove should be on the tensile or compression face. Of the two principal proponents of this DT method, Evans and co-workers (203, 234, 285, 307, 316, 328, 329, 333) have favoured the tensile face and Mindess and co-workers the compressive face (104, 105, 284, 318, 334). As will be discussed (Chapter 7), the author found that either unequal double grooves, with the deeper groove in the compression face, or a single groove in the compression face, proved the most satisfactory. This experience is in agreement with the work of Mindess - whose work has been predominantly concerned with cement materials - in contrast to, say Evans, whose investigations have covered a variety, of usually ceramic, materials.

6.4.4 Mode of Failure

One of the difficulties associated with the double torsion technique is whether it is appropriate to describe the mode of failure as Mode I, i.e. the opening mode of fracture. Fuller (323) believes the fracture mode is indeed mode I since the loading configuration and specimen geometry are symmetric about the crack plane. The contention that there is a mode III (shear) component (309) appears to depend on the relative amount of axial to through-thickness crack driving force. Comparative results with other techniques, however, indicate (307, 309) that the opening mode is in fact applicable, at least for materials which have much larger K_{IIIc} than K_{Ic} values.

An additional consideration is that of the interaction of the two sides of the cracked specimen, especially for thick specimens. The four point loading applies equal torques to the side beams (338, 339). It has been shown by Fuller (323) that, if possible, the two separate beams would

interpenetrate each other (Fig. 6.14). Contact stresses would be generated by this action but are normally ignored for analysis, which is probably a good approximation for thin beams. (No indication is given of the thickness-to-width ratio which is considered thin.) These contact stresses may, however, be significant for thicker specimens, thus affecting the stress intensity acting at the crack tip. It has been suggested in an analysis by Fuller (323) that these stresses could explain why values of K_{Ic} for polycrystalline alumina were underestimated using specimens with a thinness ratio, t, defined as $t = \frac{2d}{W} \simeq \frac{1}{4}$, but were in good agreement with other methods of measurement for $t \simeq \frac{1}{6}$ (203). A groove in the compression face reduces these interaction effects, but as discussed in section 7.2.3, the stress concentrations due to grooves are not fully understood.

The outcome of Fuller's analysis (323) yields a thickness correction factor, by which thick specimen test results should be multiplied, and is given (to within 0.1%) by Fuller as

$$\psi = 1 - 0.6302t + 1.20t\, e^{-\frac{\pi}{t}} \qquad 6.6$$

or (less accurately) as

$$\psi = 1 - 0.63t\, [1 - (\frac{t}{12})^4] \qquad 6.7$$

where t is the thinness ratio, $t = \frac{2d}{W}$.

6.4.5 Dependence of Stress Intensity, K, on Crack Length

A simple analysis of the double torsion specimen reveals that it is a so-called "constant K" test - i.e. the stress intensity is constant with crack length. However, this finding is only applicable in the central region remote from end effects. The range of this validity has been a debatable issue and has been reported on by various researchers (297, 305, 307, 314, 321-324, 332, 335). The range of validity of crack length, a, is best summarised in terms of the DT specimen length, L, and width, W, as shown in Table 6.4.

From the data shown in Table 6.4 it appears that the crack experiences constant K conditions over at least the middle third (and possibly as much as the middle half) of the specimen (for L/W = 3). The trend of K_{Ic} with crack length is graphically illustrated in Fig. 6.15(a) for glass, and Fig. 6.15(b) for Trantina's finite element analysis (324).

In Fig. 6.15(b) the stress intensity for a given load is shown as a function of the value calculated by a conventional approach. The implication of this is that in order to obtain the critical stress intensity, K_{Ic}, for a material, higher loads (and hence higher apparent K_{Ic} calculated) will have to be applied at the start of cracking (and lower at the end) than in the middle 'valid' region of the specimen. This is possibly one reason why catastrophic failure of specimens can be difficult to prevent in slow crack growth tests.

These end effects alter the compliance calibration curve so that it is not linear for short and long crack lengths (323). Shetty and Virkar (335), however, report that toughness is a more sensitive measure than compliance of the crack length validity criteria. In addition, they add that the valid region decreases as the length-to-width ratio decreases (335).

6.4.6 Measurement of Crack Length by Crack Tip Observation

One of the primary advantages of the double torsion technique is that crack length can be determined from the compliance of the specimen, once the compliance - crack length correlation has been obtained (Fig. 6.12). This means that the crack length can be measured without direction observation (328, 329, 332). It is, however, useful to check that the compliance is affording accurate crack length measurements by performing direct measurements at representative stages during the test, for example, at the end, (328).

In view of this need, and also more especially for so called "change-over" tests, where the effect on crack growth rate of one parameter is investigated (and thereby necessitating measurement of change in crack length with time), various techniques have been developed. Most of these depend on visual observation of the crack tip which may be highlighted in some way. Direct observation in transparent materials, like glass and perspex, is readily achieved (322, 340) but for opaque materials techniques are required to show up the crack tip itself.

Crack propagation gauges, in various forms, have been used but can be somewhat coarse; an extension of this technique measuring change in resistance as a potential drop, has been employed using silver evaporated onto the surface (332), but is expensive.

Dye penetrants have been extensively used, (316, 322, 327) but Pletka et al. (322) have expressed concern over whether the dye actually penetrates to the crack tip. Evans et al. have employed fluorescent dye penetrants in both static and fatigue applications (316).

For fatigue crack growth rate studies, a technique has been developed and used in this present study (336), but which has not been mentioned elsewhere in the literature. The dye penetrant is carefully placed in the crack, remote from the tip, and with the combination of capillary action and the opening and closing of the crack, the liquid is drawn to the crack tip. On the unloading portions of the fatigue cycle it is squeezed out - seen under magnification as a "pumping" action - and thus the crack tip is clearly indicated. Accurate measurement to a fraction of a millimetre is facilitated using a travelling microscope. It is, however, arguable that the presence of the dye penetrant at the crack tip may cause an environmental or pressure effect on the crack growth rate, even though specifications require that dye penetrants are non corrosive.

6.4.7 Crack Front Profile

The analysis of the double torsion technique (see, for example, Appendix A) assumes a crack front perpendicular to the surfaces of the test specimen, but practical observations show that the shape is curved, extending further along the tension than the compression faces (Fig. 6.16(a)). Part of this analysis requires the determination of rate of change of crack surface area, A, with increasing crack length, a. Fuller (323), Evans (307, 309) and several others (320, 324) have assumed that the crack profile is independent of crack length at constant load (in the valid region), i.e. $\left(\frac{\delta A}{\delta a}\right)_P = t$. In other words the shape of the crack front doesn't change as it propagates, Fig. 6.16(b). Since the local direction of crack propagation is perpendicular to the crack front the velocity clearly varies along the crack front.

Since the crack velocity is invariably related to stress intensity (or stress intensity amplitude, in fatigue) through V-K (or Paris type) relationships, it is apparent that the stress intensity varies along the crack front. It may thus be expected that the crack front shape depends on the material and the exponent, (320). Virkar and Gordon (320) thus contend that accurate velocity measurements cannot be obtained simply using a crack front shape correction factor.

Trantina (324), by contrast, using a finite element method, finds that K is effectively constant over half the plate thickness, for crack front inclinations of 30 to 50 degrees, (which are typical). No exponent dependence was thus considered. From Trantina's finite element study (324) it appears that equation 6.3 (equivalent to appendix equation A.12(b)) is entirely valid and is indeed the assumption that is often made (322, 323).

Attempts to accommodate a crack profile correction factor have, however, been put forward by Evans (309, 307) and, more recently, by Leevers (331). Evans suggests that the measured velocities on the torsion surface, be reduced by a factor ϕ, where ϕ is given by

$$\phi = \frac{t_n}{\sqrt{\Delta a^2 + t_n^2}} \qquad 6.8$$

(see also Fig. 6.17), or by the factor sin α, where α is the angle at the surface of the incidence. However, the use of such correction factors seems questionable (324) in view of the foregoing discussion of changes in stress intensity along the crack profile.

A recent (1982) study by Leevers (331) examined DT crack profile effects in detail for various polyester resins. He develops the concept of a crack front shape factor S, where $S = 1.5h/t_n$ where h is the axial distance between the crack front at $1/2t_n$ and $3/4t_n$ from the tensile face. The crack front shape figure, S, is essentially a multiplication factor based on the axial distance between the crack tip and the fulcrum plane, about which torsional rotation occurs, where this distance is given by St_n. Leevers suggests that, despite large elastic displacement effects, S may be related to a COD-type of parameter for double torsion tests. His conclusion, however, is that the only rational

crack velocity to use, in the V-K presentation, is that based on the intersection of the crack with the tensile surface. Although the crack front shape is markedly curved it merely translates axially in the valid region as suggested by Fuller (151) and others.

The conclusion to this section on crack profiles is basically summarised earlier, i.e. that the stress intensity is given by the simple analytical solution (equations 6.3 or A12(b)). With regard to measured crack velocities, no correction factor was applied in the present project because of the uncertainty of its valid application and also because the exact form of such a correction factor, if relevant, has not been established beyond doubt. Certainly, this question of crack profiles and their dependence on materials, specimen geometries and loading is recognised as requiring further study (320, 322-324).

6.4.8 Pre-cracking

It is generally recognised (317, 322, 323, 327) that a sharp precrack is required for reliable measurements of stress intensity using the DT technique, although it has been suggested that this requirement is not essential (291). Values obtained from blunt cracks from DT specimens, however, are apparently too high (317, 322), by up to 10 to 15% (309).

The double torsion technique is readily amenable to precracking, however, because of the high stress intensity at the crack tip, (323). In view of the observed increase in stress intensity at short crack lengths (e.g., see Fig. 6.15(a)) prior to the crack entering the stable constant K region, it is sometimes necessary to apply high initiating loads. Without careful control these can lead to complete fracture of the specimen.

The problem is overcome using a slightly tapered web for intitiation of the sharp crack. From equation 6.3 it is clear that stress intensity, K, is inversely proportional to $t_n^{\frac{1}{2}}$. Hence a reduction of the web thickness by linear taper from "full web" thickness to zero results in very high stress intensities at first loading, which facilitates the formation of a sharp crack in the brittle material (see also Section 6.5.3). An analogy exists here with the accepted practice of using a

chevron starter notch in fatigue precracking of conventional metal fracture toughness specimens (341). The crack can thus initiate at loads well below those required to cause fast fracture of the full web thickness.

6.4.9 Summary

In this section, 6.4, an attempt has been made to evaluate and examine the Double Torsion technique, primarily from an experimental viewpoint. The DT technique has numerous advantages stemming from its independence of crack length based on an elementary compliance analysis. This leads to a "constant K" type of specimen with a stable crack which is ideal for brittle materials. The specimen geometry is relatively simple and thus easily and cheaply manufactured, but this must be done within certain tolerances so that, combined with careful alignment, straight cracks are grown. The loading is four point in compression, and thus very suitable for difficult environments of assorted liquids or temperatures. In this respect it is preferable to the DCB techniques which, for reliable use, needs a particularly stiff testing machine, otherwise catastophic fracture can result from stored strain energy.

There are, however, some shortcomings which have not yet been fully overcome. Interaction effects, due to what would be interpenetration from torsional rotation of the two torsion bars from thick specimens, may be accommodated by a thickness correction factor (323). The size of specimens for concrete materials appears to be almost prohibitively large (276, 325) but the approximate proportions of the DT specimen appear to be accepted together with the useful range of validity of the crack length in the specimen. The question of mode of cracking (apparently predominantly mode I based on comparison and DCB results) is less contentious than the effect of the crack profile on measured values of crack velocity and stress intensity. This profile question still remains unresolved, along with the applicability of some correction factor. There are inherent load relaxation errors in measuring crack velocity but these can largely be overcome using data acquisition systems. The only other major difficulty is the effect of side grooving on performance. This aspect, together with that of crack profile, remain perhaps the two largest problem areas with the DT technique at present. Results of

tests, however, for a variety of materials, show that the DT technique is generally quite acceptable and is gaining in popularity.

The double torsion technique is particularly beneficial in fatigue tests, for so called "changeover" tests, in investigating the effect of other parameters on crack growth rate.

6.5 Velocity-Stress Intensity (V-K) Curves

6.5.1 Introduction and Background

A typical V-K curve for a brittle material is shown in Fig. 6.8 plotted conventionally as log V vs. log K. There are three principal regions, viz.: region I, in which the rate of the reaction of the crack tip controls crack motion; region I often commences at a certain minimum K_o value (the so-called stress corrosion cracking limit); region II in which the crack velocity is essentially constant and crack motion is controlled by corrosion of the corrosive species, and region III, where the crack velocity increases very rapidly with increase in K. At the onset of region III, K is generally very close to K_{Ic} and very often, for brittle and ceramic materials, regions II and III are relatively small. For brittle materials then, the region I is often the controlling one as far as time to failure is concerned, and can be described by $V=AK^n$, where A and n are constants. An alternative description of the crack growth velocity relationship is

$$V = V_o \left(\frac{K_I}{K_a} \right)^n \qquad 6.9$$

reported by Pletka, Fuller and Koepke (322) and is often more useful because otherwise very large values are generally obtained for log A. It is thus often possible (312) to obtain an estimate of the time to failure of a brittle material (under stress, containing a flaw, and in a particular environment), from a single V-K curve, and thus the importance of the determination of the V-K curves and constants n and A is evident. For optimum time dependent fracture resistance n and A^{-1} should be maximised. It is possible to obtain the crack growth parameters in three ways (249, 285, 312): (i) by direct measurement of crack growth, (ii) by measuring the time to failure under constant load, and (iii) by measuring the effect of the strain rate on strength. The time dependent, slow crack growth function can be converted directly for use with the latter two cases (see for example (309, 312, 342).

The first study to evaluate VK curves for cement paste was undertaken by Mindess, Nadeau and Hay (105, 284) using double torsion specimens (Fig. 6.18(a)). They determined the V-K relationship as log V = 36 log K -200. Evans, Clifton and Anderson (285) obtained similar V-K curves for mortar using double torsion specimens (Fig. 6.18(b)) and obtained a value for n of approximately 30. In addition they found no systematic dependence of the V-K curves on curing time or water-cement ratio in the range 0.4 to 0.6. Similar work by the author reported elsewhere (161) on time to failure studies indicates an exponent n for mortar of approximately 19 to 30. Values of n from strain rate type tests on cement mortar and concrete are shown in Table 6.5. Actual V-K studies on mortar by the author, which are discussed in detail in Chapter 7 yield n values of approximately 26.

More recently studies by Yam and Mindess (334) on cement paste (as a preliminary aspect of an investigation of fibre reinforced cements) have yielded n values of 37 and 38, comparable to earlier work for cement paste. The recent study on large double torsion mortar specimens by Wecharatana and Shah (73) yielded a V-K curve but no value of n was quoted. Analysis of their data for mortar reveals that their value of n would be approximately n = 16, which is comparable to the values for mortar (n = 14.7, n = 17.8) obtained by Mindess and Nadeau (104).

The various experimental techniques of obtaining V-K data using DT type specimens are now considered and include: static methods (load relaxation at constant position, and rate of change of displacement at constant load) as well as a novel cyclic fatigue approach.

6.5.2 V-K Determination Using the Load Relaxation Procedure

A typical test procedure for DT specimens involved the following steps:

(i) growth of a sharp crack beyond the sawn notch, usually under conditions of stroke (or sometimes load) control.

(ii) Measurement of the compliance of the specimen with two different notch lengths (sharpened as in (i) above).

(iii) Rapid loading of the specimen to some preselected load, and fixed position, under conditions of - ideally - controlled displacement rate. (This preselected load was determined by experience (using the sharpened crack length), as being just sufficient to cause measureable crack propagation and significant load relaxation.)

(iv) The load, at constant displacement, was then recorded as a function of time as the crack propagated, to obtain a measure of the load relaxation. It was necessary to subtract off, from this "measured" curve, the background relaxation of the non cracked specimen, in order to obtain the "true" load relaxation curve (322, 328). The two curves were sufficiently different for approximately 200 seconds (see Chapter 7). From this corrected load relaxation curve it was then possible to measure the compliance (from the slope) at various points and the corresponding load at each point for the stress intensity calculation. Computerised data acquisition systems have proved useful for this data processing of trace subtraction and slope determination (322, 328).

(v) From compliance measurements (of the specimen containing this sharp propagated crack) the crack length was determined from the compliance curve. The consequent data points for crack velocity V at particular stress intensities, could thus be determined.

(vi) Subsequent reloadings of the specimen were possible (usually at least once) leading to other load relaxation curves.

(vii) Rapid loading of the specimen (while the crack was still in the valid region of the specimen) could also lead to an approximate estimate of K_{Ic} for the material.

A load relaxation procedure for double torsion specimens quite similar to this has recently been reported by Yam and Mindess (334). A typical load relaxation curve with the background relaxation trace from their work is shown in Fig. 6.19, (334).

greater than A_o, the specimen cross sectional area, the value of γ_f will give a larger value than a "true" measure of the materials surface energy. In addition, for catastrophic fracture the calculated surface energy is again excessive because some of the energy supplied by the external force would be consumed in other forms of energy, for example potential energy (128), acoustic energy (285), local deformation of the loading points and kinetic energy of the fragments (294). For such situations the value of using a fracture energy measurement of toughness is questionable, and it becomes necessary to control the amount of crack growth. This control can be achieved by limiting the amount of stored energy in the specimen and machine at the time of fracture by (i) using a very hard (stiff) machine or (ii) shaping the specimen and notch so that only a small load is required to initiate crack growth. The crack may then arrest and a small portion of stable crack growth occur (294). The fracture energy technique is particularly suited to materials where a significant amount of energy is absorbed in crack propagation during stable fracture. This has more application for composites and fibre reinforced ceramic materials (219, 295) than for very brittle materials where the additional energy component (kinetic, AE, deformation, etc) is relatively more significant and from a practical viewpoint, more difficult to eliminate. However, successful estimates for cement paste have been made (128, 276). The use of the work of fracture technique is thus limited, although the technique has some attraction for easily estimating approximate or comparative values and is also becoming more popular with the use of J-integral applications to concrete (282, 128, 276).

The advantages of the use of the stress intensity factors K and K_c over the strain energy release rate, G and G_c, is that superposition is valid and the application of different stress systems to a component or specimen can easily be assessed since the stress intensity factor K is additive.

6.2.2.3 The Problem of Premature Crack Growth

The majority of work on the application of fracture mechanics and the measurement fracture toughness of cement based materials reported in the literature (104, 127, 131, 180, 252, 254, 267, 280, 287) suffers from the

shortcoming that the influence of slow crack growth, which occurs from the tip of the (usually sawn) notch or crack before maximum fracture load is reached, has been ignored. The assumption that is generally made is that at the onset of crack instability the "real" crack length is the sawn notch depth. However, this is now generally regarded as incorrect (72, 149, 155, 251, 252, 267, 294) Slow crack growth has often been neglected in calculations even though various authors (127, 131, 251, 255, 254) were aware of its occurrence. The effect would be to raise the calculated G_c values and this then would be regarded as the so called "effective" fracture toughness parameter. The relative extent of slow crack growth for the three materials, paste mortar and concrete, is still in dispute (72, 149, 155, 251, 252, 293, 296) together with the variables on which it depends, (such as: relative notch depth and shape, specimen size (72, 251, 252, 255, 267, 276), loading rate (267, 297) mix proportions, aggregate volume and type and environmental moisture condition (29, 72, 109, 112).

The recognition of the subcritical slow crack growth problem has led to quantitative attempts to measure and compensate for it. These entail either entirely different specimen configurations and stress intensity situations or the use of compliance techniques (151, 153, 155, 255, 273) first suggested by Kaplan (267).

6.2.2.4 Summary

It would thus appear from the literature that fracture mechanics may indeed by applicable to cement systems - despite the shortcomings mentioned above. It was considered that perhaps an improved evaluation of its applicability could be obtained from examination of the main dependencies of the crack resisting parameter (e.g. G, γ, or K - but in this case for convenience reduced to stress intensity, K, terms), and this is summarised in the following section.

6.2.3 Factors Affecting Fracture Toughness and the Applicability of LEFM to Cement Materials

6.2.3.1 Introduction

This summary is taken from an earlier report (261) and provides a background for the meaningful application of the stress intensity parameter, K, in subsequent experimental fatigue crack propagation rate (i.e. V-K) studies.

Several researchers report that fracture mechanics can be applied directly to cement paste (77, 130, 251-253), mortar (251, 267, 290) and concrete (251, 255, 267, 274, 290). There are numerous other authors, however, who report that fracture mechanics is not directly applicable (254), or only applicable under certain conditions (72, 77, 249) and this latter view is being increasingly recognised.

Often the requirement for the application of fracture mechanics has been that the materials be notch sensitive, i.e. the net failure stress at the notched beam section decreases with increasing crack length (277). Generally cement paste is regarded as notch sensitive, mortar only slightly notch sensitive while concrete appears to be notch insensitive (147, 251-254, 267) (Fig. 6.2). Size and dimensional considerations apparently also affect toughness response, (72, 73, 77, 128-130, 249, 253, 255, 256, 267, 268, 276-278, 287, 290, 298-300) (Fig. 6.3 a, b). Notch shape and acuity can also apparently affect measured toughness values (72, 127, 155, 251, 273)

It may, however, still be valid to employ fracture mechanics as a discipline to such materials, if one compensates for microcracking and relative sizes as proposed by Ziegeldorf (277), Petersson (129, 278) and others (276), and mentioned in Section 6.2.2.1. The recommendations for a standard test specimen and particularly a valid specimen size have yet to be resolved although once again it may be possible to compensate quantitatively for any shortcomings of specimen size. This is related to the microcracking zone and the general belief that LEFM is applicable to concrete may be valid if beams are thick enough.

An alternative, and possibly more useful, way of representing the toughness characteristics of cement paste, mortar and concrete as a function of normalised crack length is shown in Fig. 6.4 (a,b) where the fracture toughness, as opposed to the net section stress, is plotted against normalised crack length. These figures summarise extensive research by several authors.

The data appears to be of two forms, Fig. 6.4 (a) and 6.4 (b). In both cases the fracture toughness of cement paste appears to be independent of normalised starter crack length, within a range of at least half the specimen depth. Mortar and concrete by contrast, however, have been reported as exhibiting a dependence of toughness on crack length. However, the form of this dependence appears contradictory with both an increase with crack length reported (for example, Brown (130, 155), Romualdi and Batson (274), and others, (180) as well as a decrease, e.g. Shah and McGarry (252), Naus and Lott (127) and Gjorv et. al (253) and others (251, 254). In both cases, however, mortar exhibits this dependence less strongly and predictably lies between the concrete and cement paste curves (Figs. 6.4 a, b).

The very question, however, of the validity of the assumption of a plane strain stress condition has yet to be answered: many workers (122, 249) have obtained satisfactory results using this assumption, while others have assumed a plane stress condition (129, 276) and others say it is not relevant because the concrete does not develop shear lip ductility (276).

6.2.3.2 Specimen Parameters

Water-Cement Ratio

Probably the most important factor affecting strength of concrete is that of water-cement ratio, where increases in water-cement ratio lead to weaker concretes. The trend for fracture toughness is similar, with an increased water content reducing the fracture toughness - certainly for cement paste (72, 105, 127, 130, 149) and mortar (127, 149). The trends are summarised in Fig. 6.5(a) and (b) which shows a plot of fracture toughness versus water-cement ratio, taken from several sources. Watson (128) has similarly reviewed the literature and correlated K_{Ic} with water-cement ratio for a range of testing methods for cement paste, mortar and concrete (Tables 6.1 (a) (b) and (c).

Recent studies on the effect of water-cement ratio on cement paste toughness by Alford, Groves and Double (77) and Beaudoin (268), reveal a fluctuating behaviour depending possibly on porosity or humidity, Fig. 6.5(b).

Other studies by Birchall and Double and their groups (1 - 4, 15, 19, 23, 76) as reported by, for example, Alford (77), have shown that the most important strength limiting factor of cement materials is the size of the inherent flaws in the cement (or composite). By reducing these to a few microns, by various techniques, in macro defect free (MDF) cements, strengths of 160 MPa have been obtained with estimated increases in toughness.

Aggregate Content

It is generally recognised that the inclusion of aggregate or particulate particles to an otherwise brittle matrix in a composite can significantly increase the toughness (302). This appears to be particularly true for concrete, with the toughness reportedly increasing with aggregate content (45, 127, 130, 149, 155, 251, 275, 278, 299, 303) and quality often with an approximate linear relationship assuming, of course, that the aggregate is stronger than the matrix (See Fig. 6.6). Fines content is also important, however.

It would seem that the increased toughness with aggregate content is associated with the crack arresting nature of the concrete aggregate and the increased energy demand since the degree of cracking is more extensive (153, 154, 186).

Age and Curing Conditions

With strength of cement paste and concrete increasing with age or curing time - but at an ever decreasing rate, it is reasonable to suppose that toughness increases in a similar manner. This is reportedly the case as can be seen from Fig. 6.7 for paste, mortar and concrete. Fig. 6.7 also shows a range of water-cement ratios where several mixes were used by one author. The increase after the first few days is generally very slight, however, and after approximately 14 to 28 days toughness can be considered independent of curing age (72, 127, 128, 130, 131, 251, 278, 283, 304).

6.5.3 V-K Determination Employing the Rate of Change of Displacement at Fixed Load

From Appendix B.2 one can obtain a relationship between crack growth rate and displacement rate (both at fixed load) using either the differential of equation 6.4 (i.e. Appendix equation B.7) or (less easily) a compliance approach (i.e. equation B.11). The normal procedure adopted (317, 343) was to apply the load in stroke (or position) control and ramp at a very low rate, typically 0.0003 mm/sec. Typical load versus time curves from the literature (309, 317), and the present work, are shown in Figs. 6.20(a) (b) and 6.20(c) respectively. These exhibit an initial load peak followed by a more or less level plateau. The average load in the plateau region is regarded as that required to propagate sharp cracks of stable shape in the central part of the specimen, and is the value of P used in equation 6.3 for K determination. A more gradual transition onto the plateau region of the load time curves is reportedly obtainable (317) using a triangular shaped intial web shape with the apex in the tensile zone, (Figs. 6.21(a) and (b)). This technique was not, however, employed in the present series for reasons of consistency of crack front. The corresponding crack velocity was determined using equation B.7, where $\left(\frac{\delta y}{\delta t}\right)_P$ was the stroke control ramp rate, and the load P is the same "plateau" value used previously for K determination.

6.5.4 Fatigue in Double Torsion Specimens

One of the particular advantages of using the double torsion system for toughness measurement in brittle, and particularly cement-based, materials is that since the stress intensity is constant with crack length over a large proportion of the specimen length, there is no need to measure such crack length, or crack growth rate explicitly. However, it is nonetheless still possible to measure the crack length under constant cyclic loading conditions, for example by visual observation of the crack tip. This direct measure of crack growth rate may be used as an indicator of the specific effects of other parameters, for example, loading amplitude and frequency, level of stress, environmental conditions or temperature. The particular elegance of such a testing procedure is that on the very same DT specimen it is possible to change one single particular variable, keeping all other parameters constant,

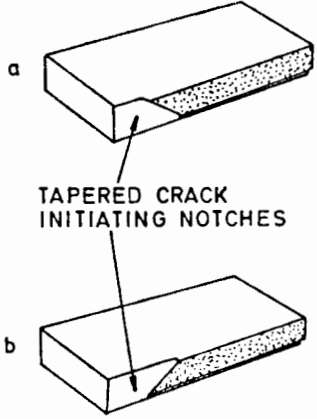

Fig. 6.21(a) Schematic diagrams showing the two types of tapered crack initiating notch used by Murray and Perrott for sintered carbide, (317): (i) Notch tapered 30° to the tension face to lower the stress at crack initiation (ii) Notch tapered 30° to compression face to give a high stress condition for crack initiation.

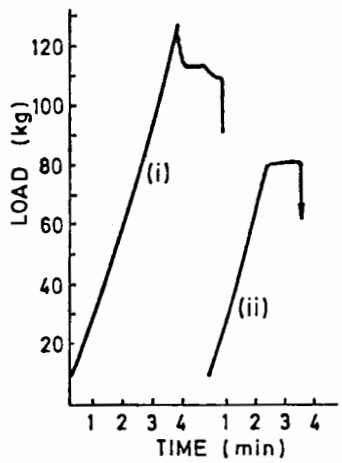

Fig. 6.21(b) Load time curves showing the effects of notch geometry. Curve (i) corresponding to the geometry of Fig. 6.13(a)(i) shows a well defined initiation peak. Curve (ii) corresponding to Fig. 6.13(a)(ii) shows the initiation peak has been eliminated (from Murray and Perrot (317)).

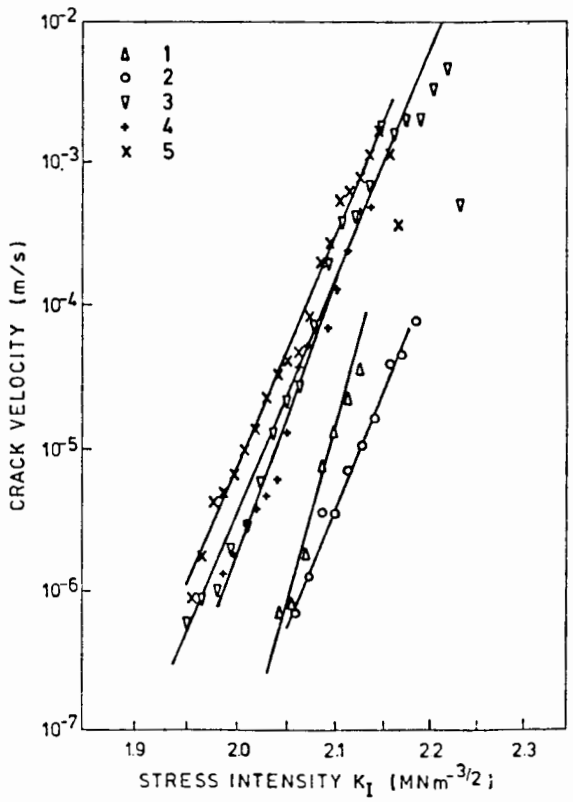

Figure 6.22 Crack velocity as a function of applied stress intensity factor for five consecutive stress relaxation experiments on the same glass ceramic specimen. (From Pletka et al. (322)).

"Where order in variety we see, and where,
though all things differ, all agree."
Alexander Pope.

CHAPTER SEVEN: EXPERIMENTAL INVESTIGATION OF CRACK PROPAGATION

7.1 Introduction

The studies on the fatigue behaviour of cement based materials tested in compression, detailed in the previous chapters, have produced some most interesting results, particularly with regard to the rate of damage accumulation in cement mortar, under a variety of testing conditions. Unfortunately it is difficult to interpret the damage studies quantitatively from a mechanistic viewpoint and thus an experimental "single crack" approach was considered. The applicability of conventional fracture mechanics to such an approach was discussed in detail in the previous chapter.

While recent published evidence (73, 334) on large specimens suggests that only large specimens are appropriate for "valid" fracture toughness evaluation, at the time that some of the present tests were undertaken this view had not emerged. In addition, because of the potential correction that could be made for small specimens (129, 278), and because changes in crack velocity performance as a result of another parameter (e.g. temperature or moisture) were of more interest in this thesis than absolute values of crack resistance, it was decided to undertake an experimental investigation of cracks in mortar using (relatively small) Double Torsion (DT) specimens. By means of such tests it was hoped to evaluate the effect of these various parameters on (nominally) single crack growth rates, in contrast to the compression "damage accumulation" rates, to which the single crack behaviour can presumably be allied.

Some discussion of the theory of the double torsion technique has already been presented in Chapter 6 and Appendix A, together with techniques of crack velocity - stress intensity, V-K curve data generation. This chapter presents the details and results of an experimental study on (nominal) single crack propagation rates in cement mortar double torsion specimens.

The experimental details of the DT test as used here are described in section 7.2. Particular techniques for observation of the crack tip region for fatigue tests are mentioned and the test programme covers similar topics to the compression tests already conducted (Chapter 4) with the exception of waveform and variable range tests, (which, based on that experience seemed of less importance). The DT technique was initially used in a static testing mode, (i.e. load relaxation at constant position, or constant load at constant ramp rate) to generate V-K data for various moisture and temperature environments. Subsequently the DT tests were extended to cyclic fatigue, which was an apparently entirely new application. Testing covered the effects of frequency and time on crack propagation rate, in addition to the environmental and temperature tests mentioned above. The results of this work are presented in section 7.3.

Discussion of the results is presented in section 7.4 and a technique - the so-called "g factor" due to Evans and Fuller (235) - of predicting cyclic crack growth rates from static crack growth (assuming similar cracking mechanims) has been used to great effect. This technique is discussed in detail in Appendix C. From the variable temperature studies on crack growth rate, the estimation of an activation energy is possible. This is followed by a discussion of cracking on closure (i.e. on the unloading cycle) first mentioned in Chapter 4, to explain acoustic emission during compression unloading cycles, in view of the increased fracture mechanics knowledge of the mortar material. The chapter is summarised in Section 7.5.

7.2 Experimental Systems and Techniques

This experimental section is concerned with the detail of the test apparatus and equipment employed in the performance of the double torsion tests on mortar specimens, as well as the techniques and procedures developed for obtaining V-K data using both static and fatigue testing. Several of the preparation, and other, techniques are similar to those used for the compression prisms, described in Chapter 3, so where relevant, reference is simply made to these sections in Chapter 3. Additional specimen preparation factors are, however, described here.

The mechanical testing system and details of the techniques used to observe the crack tip in fatigue are mentioned prior to an outline of the experimental procedures and specific test programme.

7.2.1 Specimen Fabrication

The DT specimens were made from mortar nominally identical to that used for the compression prisms. That is, the DT specimens were made from the same materials of the same batch. The full details of the cement, sand and water as given in Chapter 3 are applicable to these DT specimens, together with the mixing and casting techniques. Hence the water-cement ratio of the mortar was 0.39 and the (600 micron) sand content 34%.

With regard to the specimen size and dimensions it is apparent from the discussion of section 6.4 that a length-to-width ratio of 3 would be appropriate. At the time that the initial DT tests were undertaken not all the references discussed in section 6.4 were available. Thus it was thought, for the decision on specimen thickness, that the specimens needed to be sufficiently thick to be macroscopically representative of the material and also be unaffected by individual microstructural components. At the same time the specimen was required to be sufficiently thin to comply with the double torsion theory and analysis. The choice of thickness to width was hence taken near the thicker limit of the published specimen dimensions and proportions, shown in Fig. 6.13, to be approximately one eighth to one sixth.

For convenience, in the pilot study tests, mould inserts in the existing compression moulds, were used in casting the double torsion specimens, and the associated loading equipment and test system duly developed. These pilot tests were largely successful and the loading system was thereby refined. To remain in keeping with this refined loading system the tolerances on the DT specimens themselves needed to be tighter and thus new perspex (PMMA) moulds were constructed. The finished double torsion specimen dimensions included a length of 180mm a width of 60mm and two thicknesses of either 8mm or 10mm. A photograph of the DT moulds system is shown in Fig. 7.1(a).

Specimens cast using these latter moulds exhibited fine dimensional tolerance which proved themselves with the reduced experimental scatter. The perspex moulds were lightly oiled with release agent prior to each cast, and this method, coupled with the PMMA surface, gave an excellent off shutter finish for the DT specimens.

Pilot study tests were conducted on DT spcimens containing a cast in groove on both faces, as shown in Fig. 7.1(b). These, however, tended to result in a shrinkage crack in the groove which prejudiced the subsequent cracking performance and results. In the light of this pilot study only plane flat DT specimens were subsequently cast and grooves cut into them after curing. (The groove cutting procedure is described below).

In the light of the discussion of section 6.4 it is arguable that the DT specimens used may have been somewhat small, and proportionately too thick. However, it must be remembered that the material used was high strength mortar (rich in cement), and thus the "process zone" size was more comparable with cement than conventional mortars (276, 325). The choice of thickness-to-width ratio, while on the large side, had been successfully used previously in this range for cements, mortars and concretes (73, 104, 105, 284, 318, 334) as well as other materials (332). In any case, grooves were cut in the compression face (as recommended by Mindess for cement materials (104, 105, 284, 318)), which tends to minimise the thickness interaction effect mentioned by Fuller (232). It is possible, however, that in view of the larger thickness it may be necessary to multiply existing results by between 12% (with no groove) and 4% for the grooves actually used. Perhaps the best vindication of the use of this size and thickness of DT specimen lies in the results themselves, which tended to show relatively little scatter (for DT specimens of this material) in the V-K curves, and to be comparable to other published results (see later). The other major consideration is that, at the very least, since the effect of other parameters of temperature moisture and time on crack growth rate was examined, the results can be regarded as good comparative, if not absolute, measures of behavioural trends.

7.2.2 Specimen Preparation

The double torsion specimens, after casting and appropriate curing, required further preparation before they could be tested. In particular, grooves or slots were cut into the plate surfaces to assist in crack location and a starter slit, or notch, was also introduced. The specimens were also inspected carefully and those (few) specimens containing imperfections or visible porosity were rejected, prior to the grooving and slitting process. The groove and slit cutting are described in turn, as follows.

7.2.2.1 Groove Cutting

A prerequisite for the groove and slit cutting was the accurate measurement and marking of the double torsion specimen. The grooves were centrally located axially along the length of the specimen. The very end of the DT specimen which had been the cast surface was ground off to a depth of approximately 2mm prior to cutting of the grooves. This was achieved using a conventional carborundum rotary concrete saw (Clipper) and a special locating rig arrangement. This latter unit ensured accurate and parallel location of the grooves which were cut to a depth of 4.2 mm on one side (the compression face) and to 0.8 mm on the other. (The rationale for this is discussed further in section 7.2.6). The groove width was 3.5mm and the groove shape was approximately semicircular. This groove shape was believed to be preferable to a very sharp groove configuration which would provide a greater stress concentration. The groove depths were measured using a special underwater vernier caliper device, as all the cutting was undertaken beneath a copious flow of water. Grooves were flat and parallel and the depth consistent to within 0.1mm, although much operator expertise and practise was required to achieve these tolerances.

In this way it was possible to obtain different groove depths for evaluation of the effect of the thickness parameter, t_n. However, in view of possible dependencies on the groove depth, as discussed in section 6.4 and which is not yet fully understood, efforts were made to maintain the groove depths to 4.2 and 0.8mm respectively for the 10mm thick specimens and 3.4mm and 0.6mm for the 8mm thick specimens (Fig.

7.1(c)). Subsequently, since no significant effect on toughness behaviour for thinner (8mm) as opposed to the thicker (10mm) specimens was obtained (except for the obvious lower fracture loads) the thicker specimens were maintained for all subsequent testing because of their greater handleability.

All the groove cutting was undertaken 3 to 4 days after casting under wet conditions and the specimens returned to the curing tank for completion of their wet cure, before either further wet curing or drying as required (as described in Chapter 3).

7.2.2.2 Notch (Slit) Cutting

A starter notch, or slit, was cut into the specimen centrally and axially in the groove using a 0.8mm DISCOPLAN diamond saw.

The notch (or slit) length was 35mm and then the slit was cut partly through in the form of a taper for a further 5mm. (The effective slit length was thus 35mm on the tension side and 40mm on the compression side of the web in the groove.) This starter slit thus readily facilitated the development of an atomically sharp crack on initial loading.

7.2.3 Mechanical Test System

The double torsion load system needed to be capable of precise loading of the specimens under both static and fatigue loading; and also under conditions consistent with the theoretical analysis (see, for example, Appendix A). In particular, this implies that the loading system is very well made, colinear, square and parallel with equal loads being applied to the two outermost arms of the torsion bars. This was achieved using the apparatus shown in Figs. 7.2(a) and (b). The (upper and) outer loading ball bearing points (5mm diameter) were connected to a bracket which was centrally located and furnished with a bearing, as shown, and was thus capable of free rotation about a clevis system which connected to the 5kN load cell of the 50 kN ESH loading machine. In this way the loading system may be considered self aligning and self equilibrating. The (lower) inner loading points were two identical ball bearings (also 5mm diameter), which were located through a special mounting onto the

lower base plate of the water bath. This water bath unit could be screwed onto the actuator arm of the testing machine and carefully aligned. It provides a facility for maintaining a constant environment around the DT specimen; either dry or moist, using the polythene bag concept described in Chapter 3, or by providing a test bath for fully submerged and temperature controlled tests.

The water bath unit also included additional ball bearings for temporary simple support of the DT specimen at the end remote from loading. This loading was of a simply supporting nature, and was trivial and of little consequence, since the specimen was lifted very slightly, free of these supports, once the loading was applied and a test in progress.

In order to obtain reliable V-K data from the DT tests, accurate position control was required of the testing machine and loading train system, since some of the V-K data was obtained by load relaxation techniques, i.e. rate of change of load with time at constant position, $\left(\frac{\delta P}{\delta t}\right)_y$ (see Appendix B). Such control was achieved using the 50kN actuator together with an LVDT abutting onto a glass slide at the corner of the water bath system (Fig. 7.3). The load and load relaxation was accurately monitored using a 5kN load cell set on a high sensitivity scale. The inherent noise of the system was not insignificant but did not inhibit reliable measurement of background relaxation or V-K data.

The loading system and ESH testing machine were also very suitable for the other quasi-static technique of obtaining V-K data mentioned in Appendix B. This involved constant, accurate but very slow ramp rates which resulted in a "slow" running crack at constant load, i.e. $\left(\frac{\delta y}{\delta t}\right)_P$. With the facilities mentioned, accurately controllable ramp rates of 0.0002 to 0.0005 mm/sec were readily achieved and facilitated acquisition of such single point V-K data.

Finally, with respect to fatigue, the loading system was also very suitable for applying fatigue loading under a variety of environmental conditions. Periodic checks were made of alignment and the state of the bearing to ensure that no lateral movements, fretting or other perturbations from ideal testing conditions, were occurring as a result of the fatiguing process.

TABLE 6.4

Range of Validity of Crack Length in a Double Torsion Specimen for Constant K Conditions (From literature, 305, 307, 321, 322, 324, 332, 335)

Lower Limit	Crack length a	Upper Limit	Comments
0.55W	a	L - 0.65W	
1.0W	a	L - 1.0W	for L/W = 4
0.5W	a	L - 1.0W	for L/W = 2.5
0.4W	a	L - 0.8W	for L/W = 1.5
0.05L	a	0.85L	for L/W = 3.0
0.33L	a	0.83L	for L/W = 3.5
0.20L	a	0.7	L/W = 3.0 (mortar)

TABLE 6.5

VALUES OF DETERMINED FROM VARIABLE

STRAIN RATE TESTS

Reference	Type of Material	Type of Test	n
Watstein (346)	Concrete	Compression	26.1
Takeda and Tachikawa (347)	Concrete	Compression	43.4
Katsuta (348)	Concrete	Compression	39.2
Jones and Richart (349)	7 day concrete	Compression	29.9
Jones and Richart (349)	7 day concrete	Compression	40.1
Jones and Richart (349)	28 day concrete	Compression	30.0
Wright (350)	7 day concrete	Flexure	28.2
Wright (350)	28 day concrete	Flexure	23.0
McNeely and Lash (351)	7 day concrete	Flexure	21.0
Takeda and Tachihawa (347)	Concrete	Tension	21.9
Mindess and Nadeau (104)	Mortar	Flexure	14.9
Mindess and Nadeau (104)	Cement Paste	Flexure	17.7

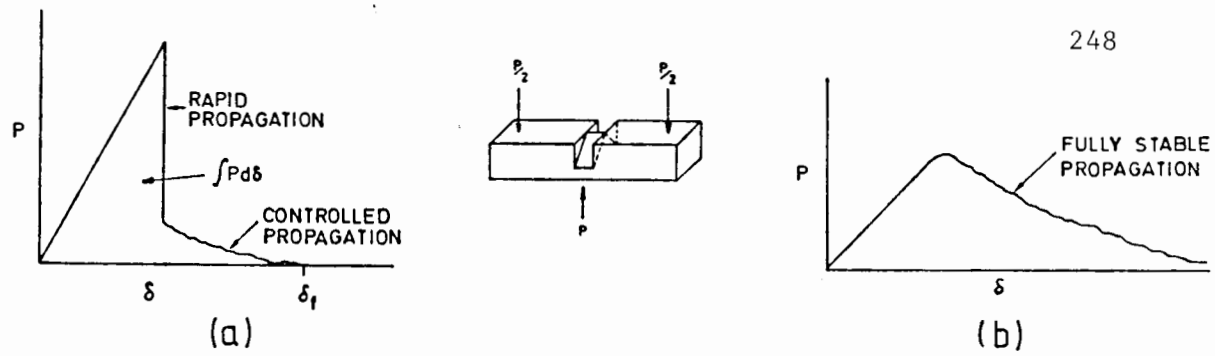

Fig. 6.1 Load-deflection behaviour for (a) semi-stable and (b) stable fracture. The work of fracture is the area under the curve (From Evans, 294).

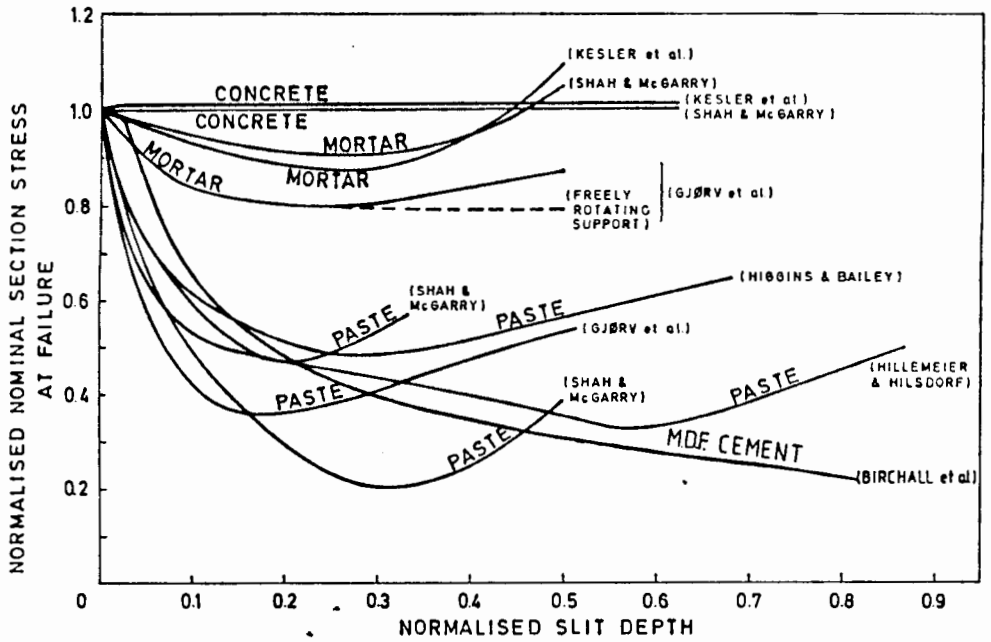

Fig. 6.2 Notch sensitivity of flexural tests for cement paste, mortar and concrete, from a variety of sources.

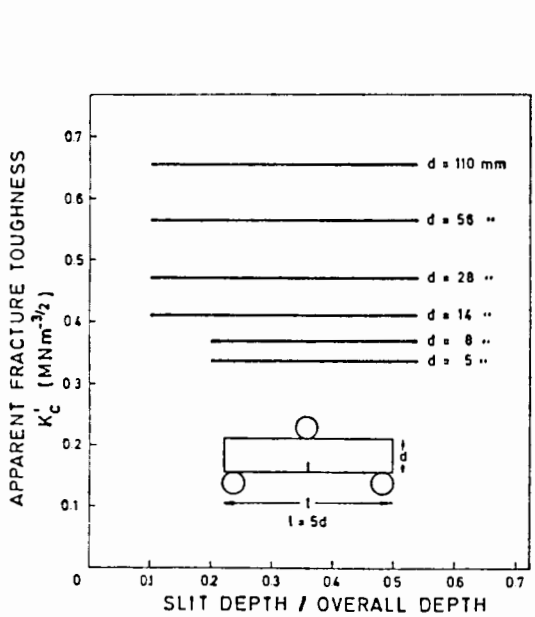

Fig. 6.3 (a) Apparent fracture toughness dependence of cement paste or specimen depth, from Higgins and Bailey's study (72).

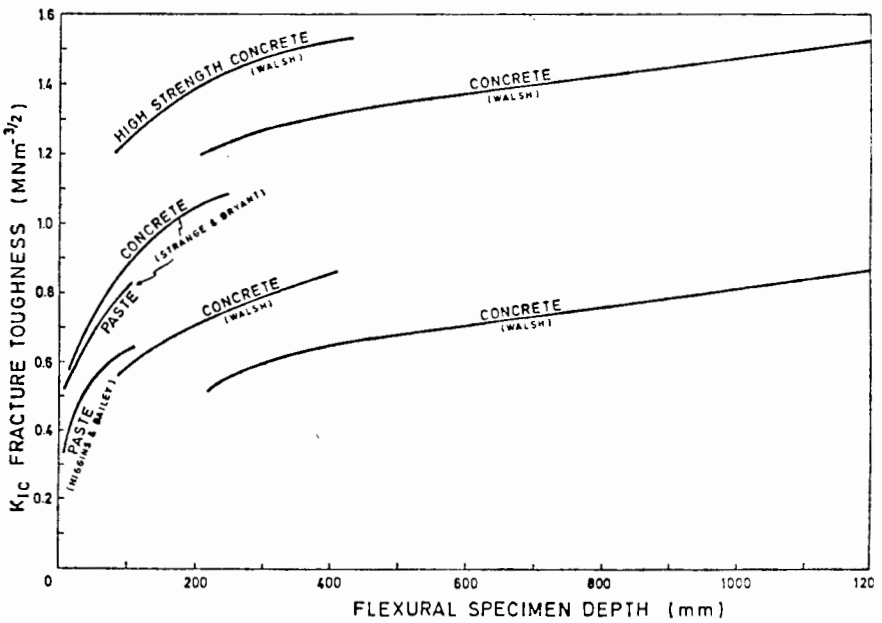

Fig. 6.3(b) Fracture toughness dependence on specimen size for cement paste and concrete from various sources.

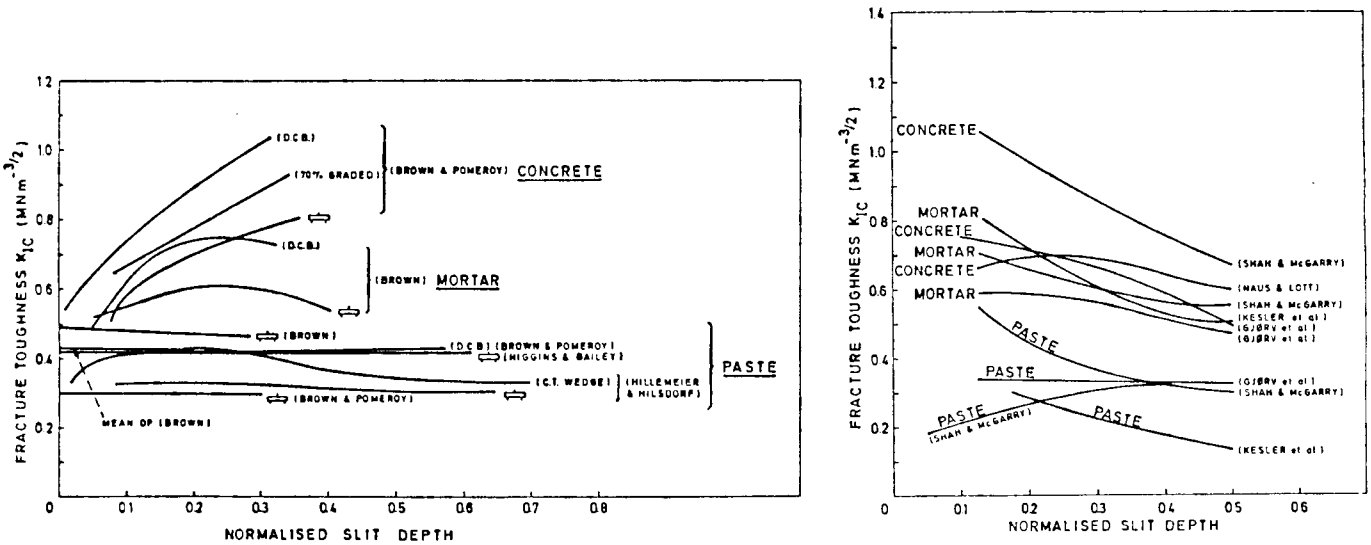

Fig. 6.4 (a) and (b) Fracture toughness versus normalised notch depth, for cement paste, mortar and concrete from a variety of sources.

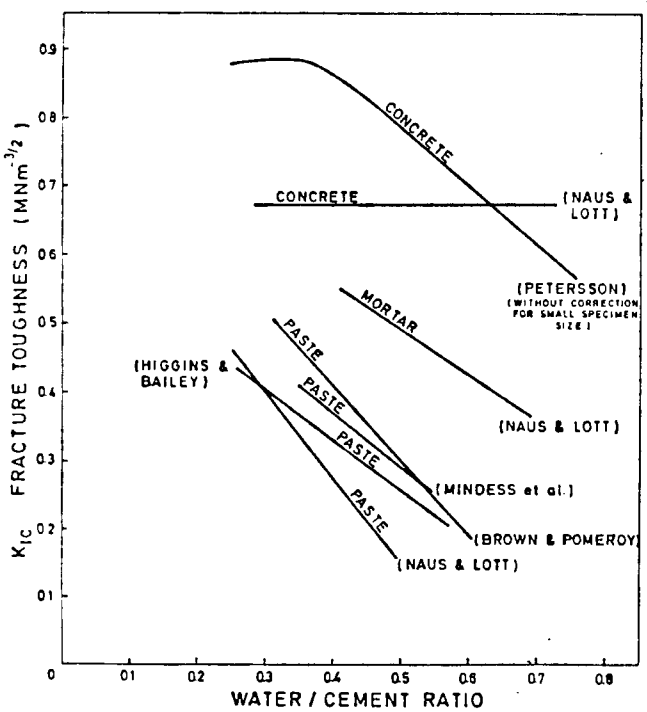

Fig. 6.5(a) Dependence of fracture toughness on water cement ratio for cement paste, mortar and concrete, from various sources.

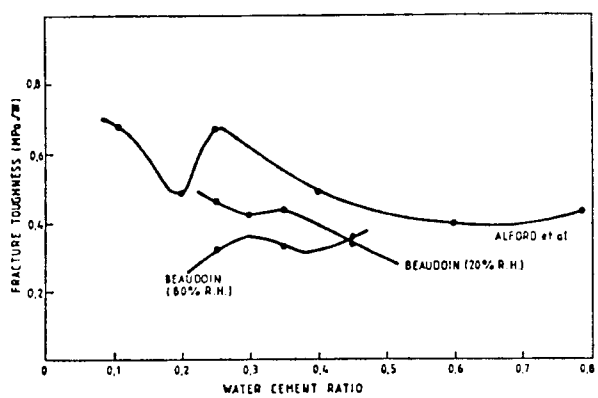

Fig. 6.5(b) Fracture toughness dependence on water cement ratio for cement paste for studies by Beaudoin (268) and Alford et al (77).

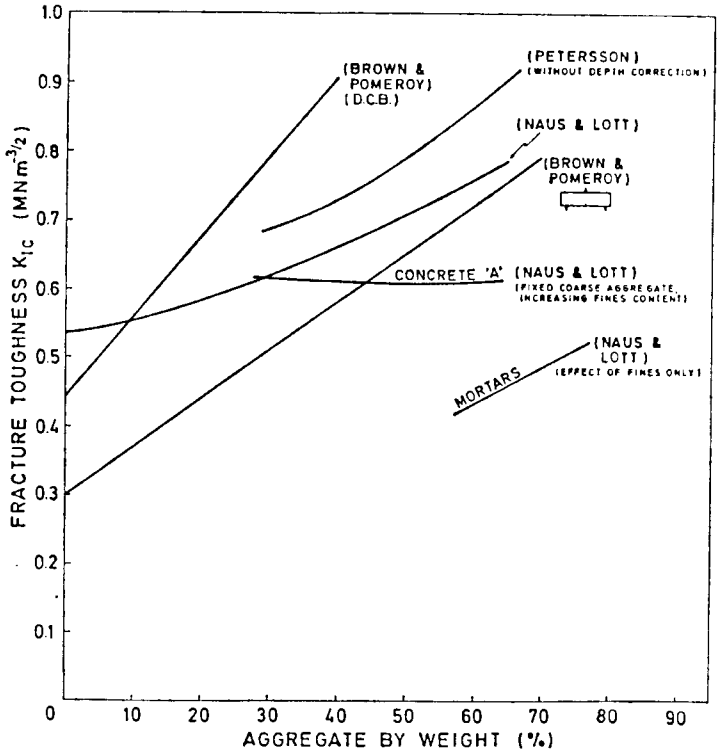

Fig. 6.6 Fracture toughness dependence on aggregate content (from assorted sources).

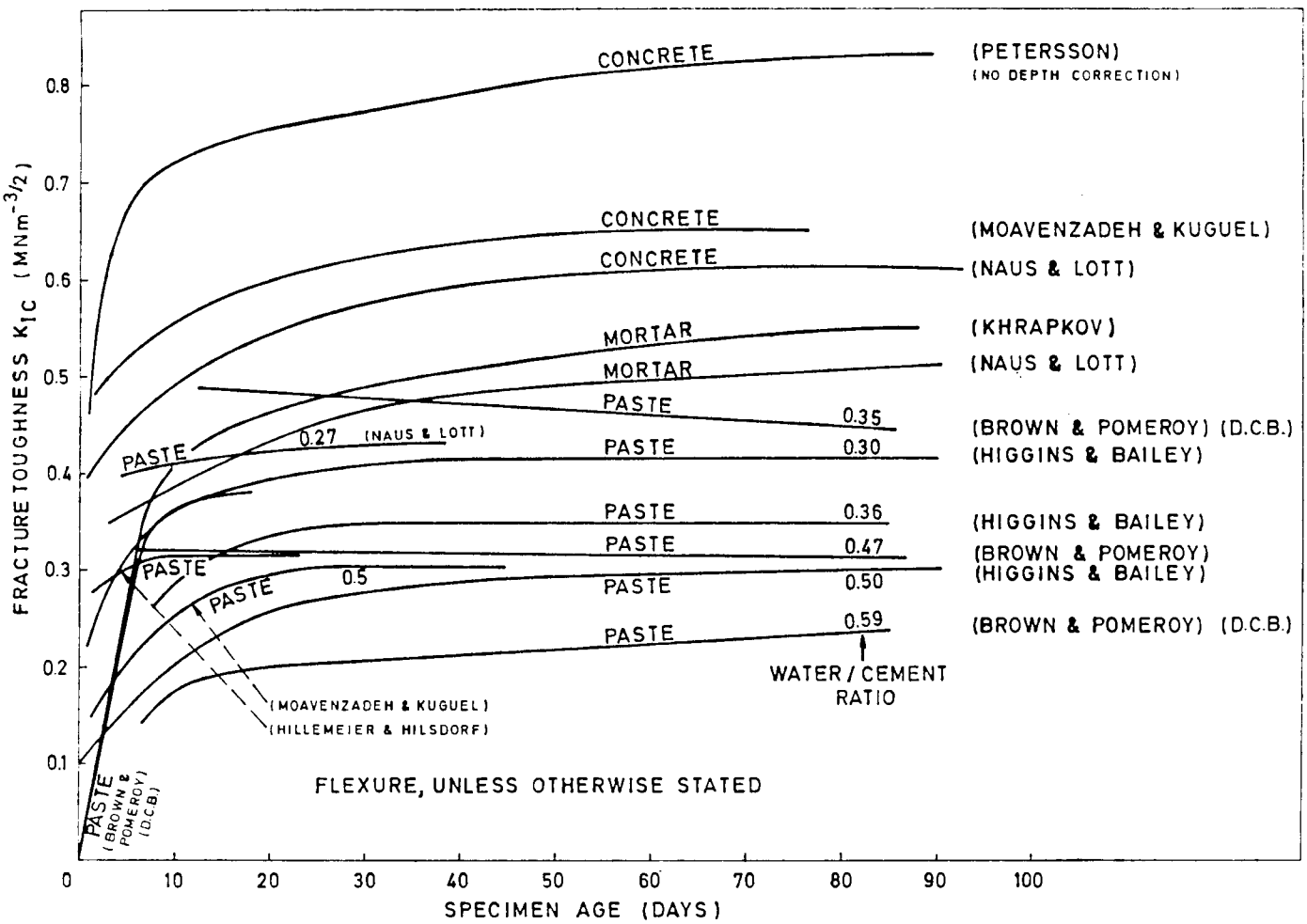

Fig. 6.7 Fracture toughness of cement paste, mortar and concrete dependence on curing age.

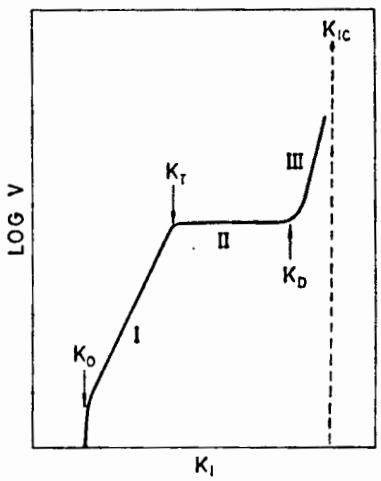

Fig. 6.8 The variation of stress intensity factor, K_I, with crack velocity V, for a material subjected to a stress corrosive environment.

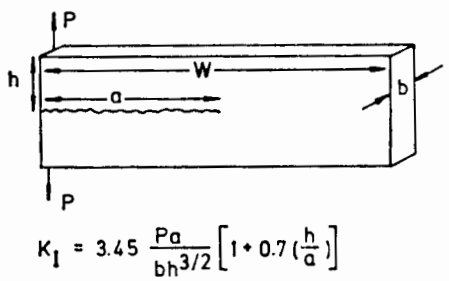

Fig. 6.9 The simple double cantilever beam specimen.

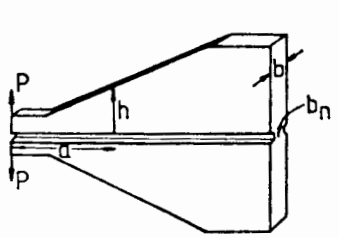

$$K_I = 2P\left(\frac{m}{b b_n}\right)^{1/2} \qquad m = \frac{1}{h} + 3\frac{a^2}{h^3}$$

Fig. 6.10(a) The tapered double cantilever beam specimen. Constant K conditions are obtained by shaping the specimen to give constant m.

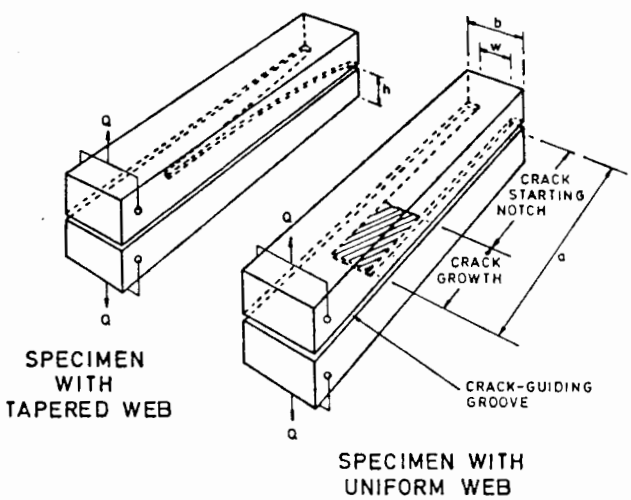

Fig. 6.10(b) The tapered web double cantilever beam.

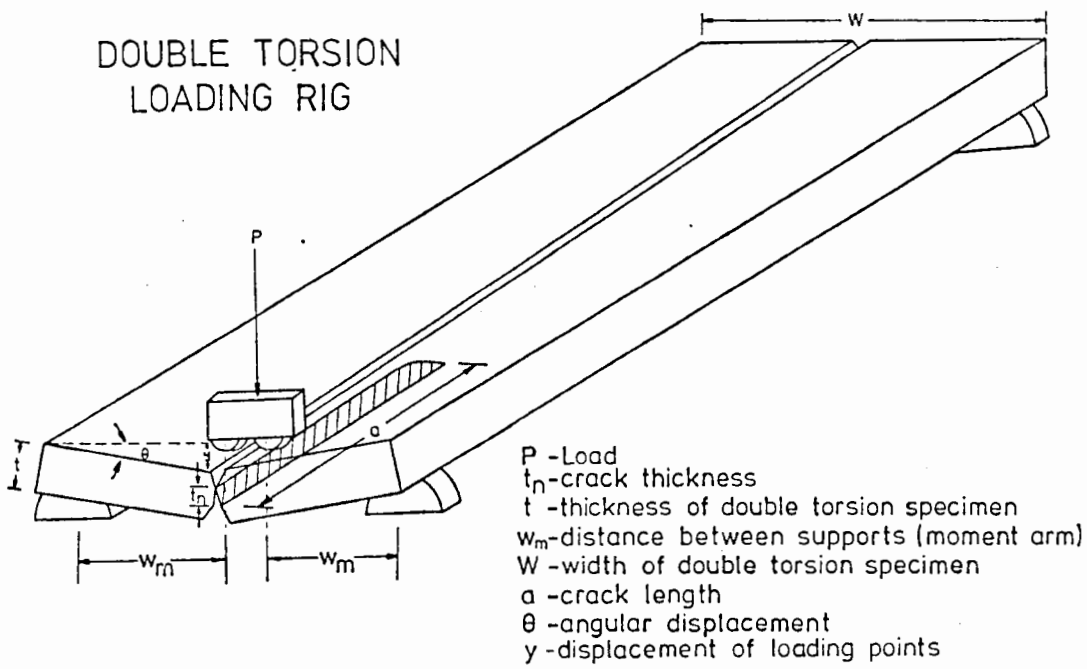

Fig. 6.11 The double torsion test specimen showing dimensional parameters and mode of deformation.

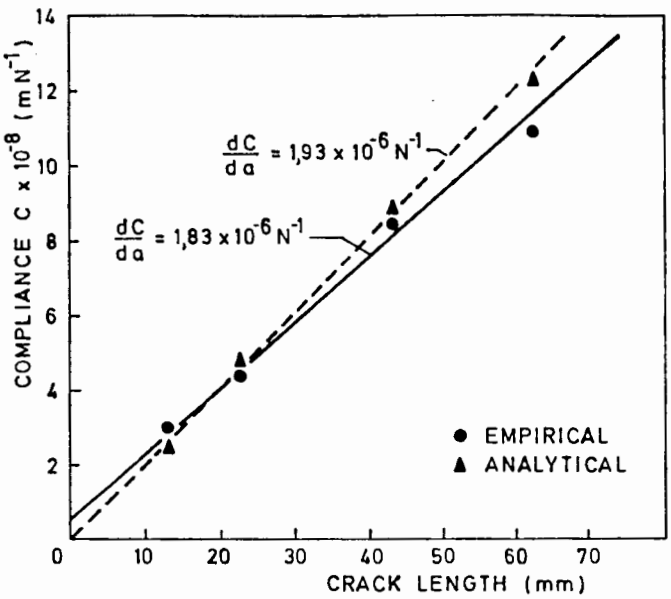

Fig. 6.12 Theoretical and experimental compliance curves for the cracked double torsion specimens used in this project.

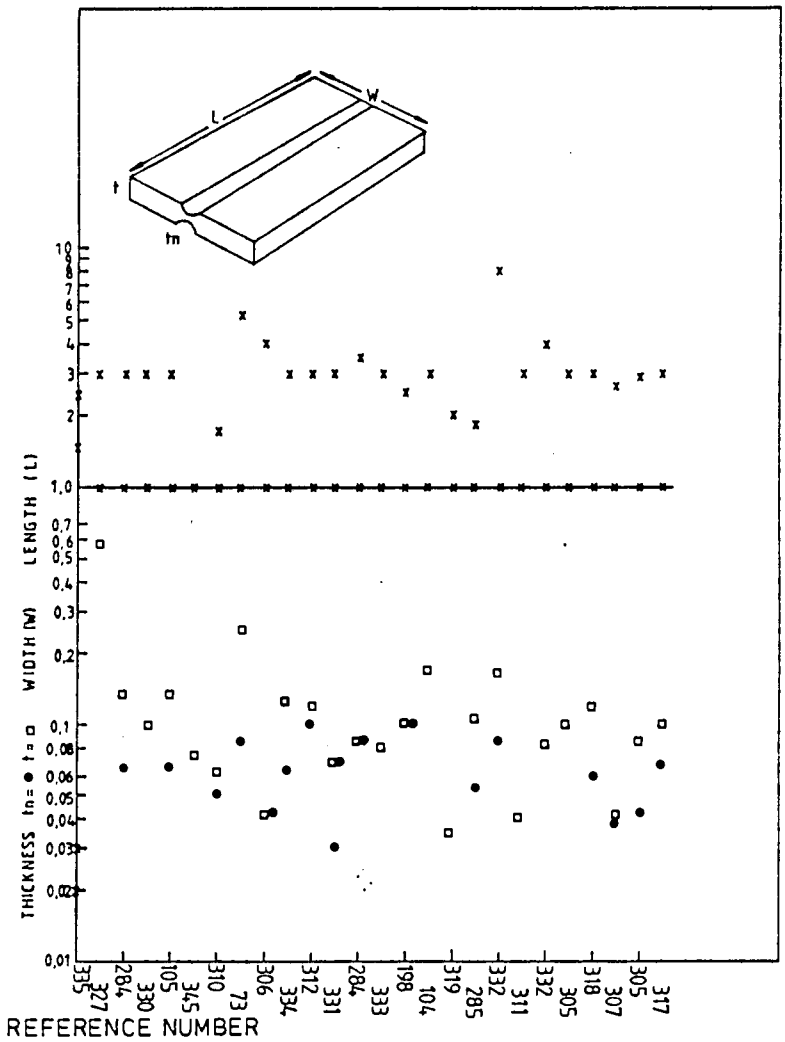

Figure 6.13 Double torsion specimen proportions, from the literature, normalised with respect to width.

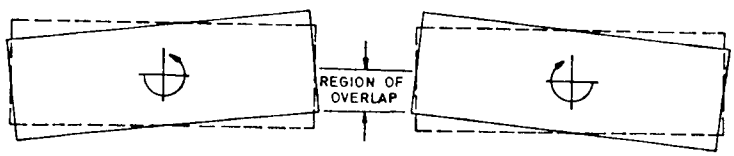

Figure 6.14 Schematic illustration of the relative rotation of the two torsion beams (separated for clarity) and of their region of overlap, used by Fuller (151) in his analysis of the effect of beam thickness.

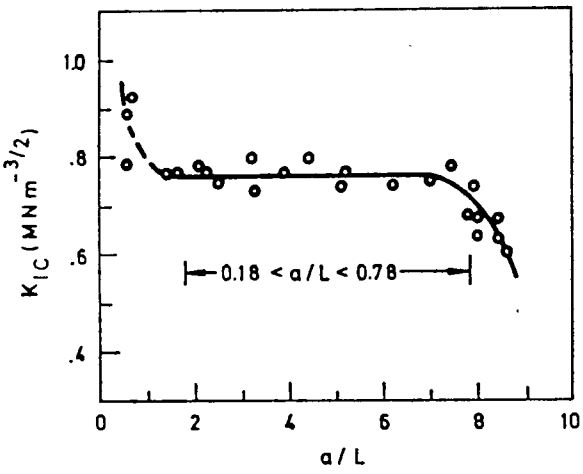

Figure 6.15(a) K_{IC} measured in toluene on soda lime silicate glass slides as a function of crack length. (From Pletka et al. (322)).

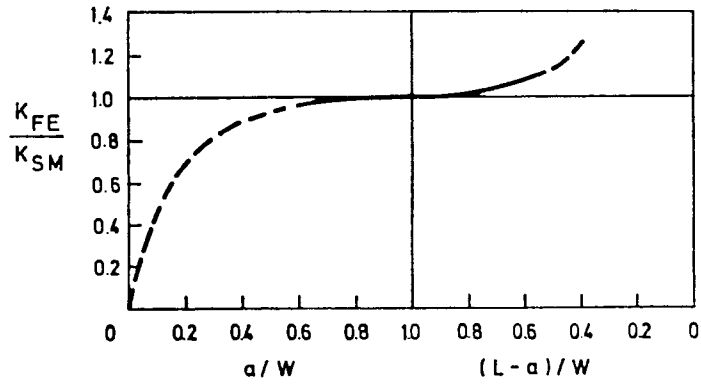

Figure 6.15(b) Relative stress intensity as a function of crack length and ligament length. (From Trantina's finite element analysis (324).

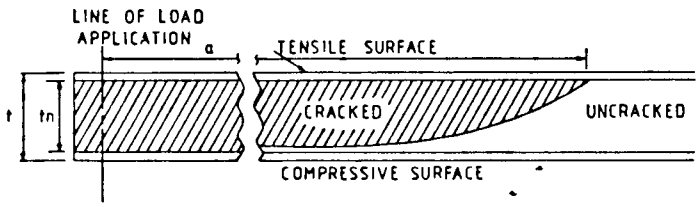

Figure 6.16(a) Schematic view of a typical curved crack front profile for the double torsion specimen.

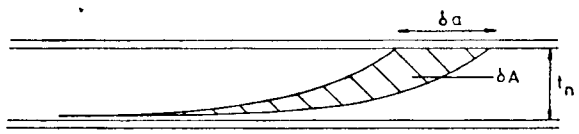

Figure 6.16(b) Schematic view of the unchanging profile of the crack front as it propagates in the valid region (336, 323).

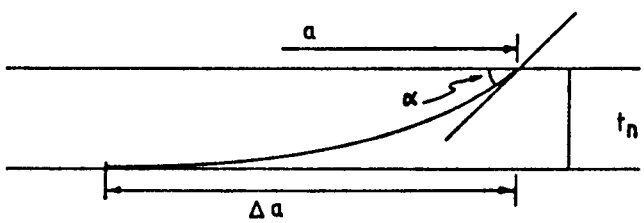

Figure 6.17 Illustrating parameters for Evans (309) evaluation of the correction factor for crack velocities, due to the crack profile.

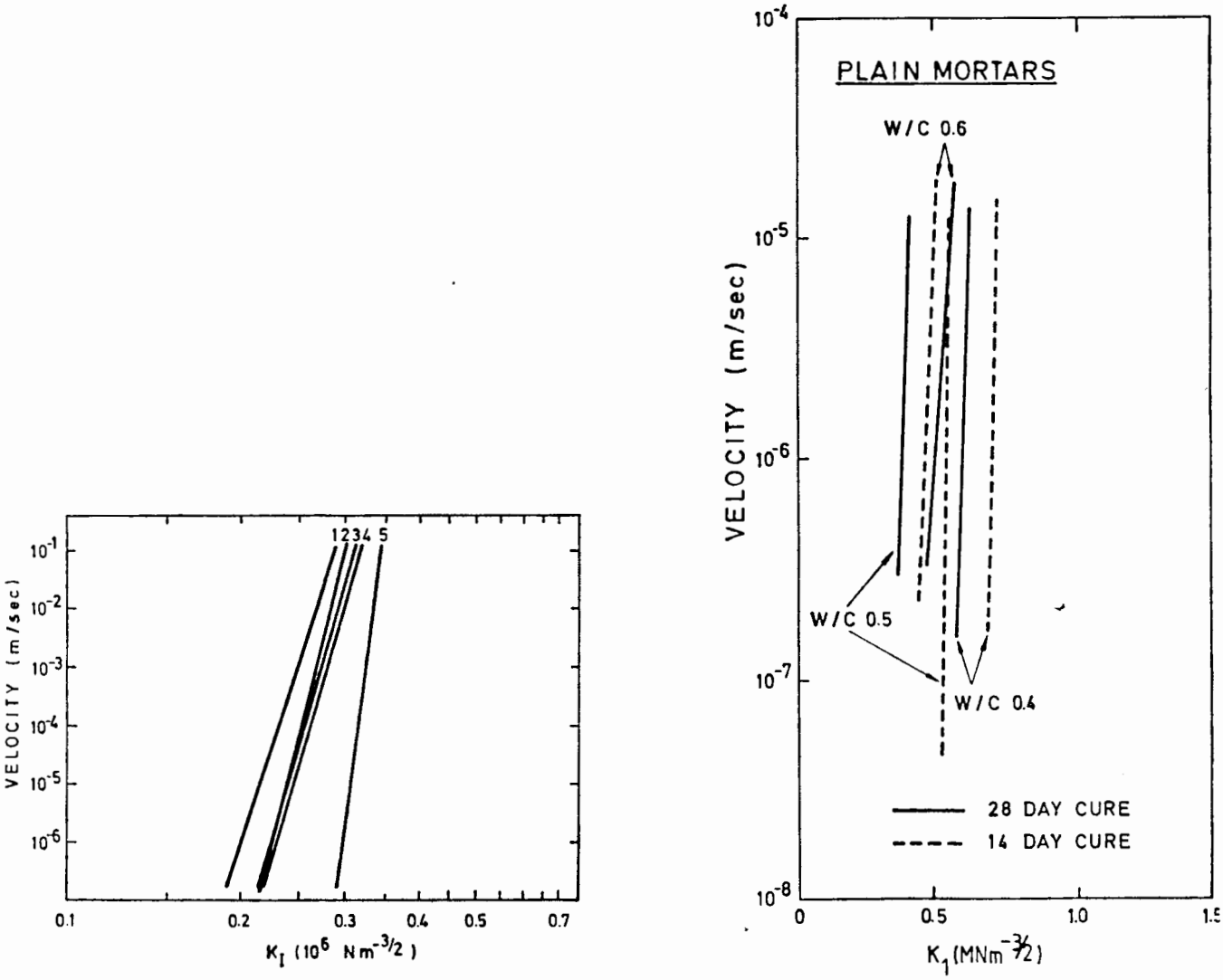

Fig. 6.18 Velocity-stress intensity (V-K) curves for cement paste from (a) Nadeau Mindess and Hay (284) for various mixes and (b) Evans, Clifton and Anderson (285).

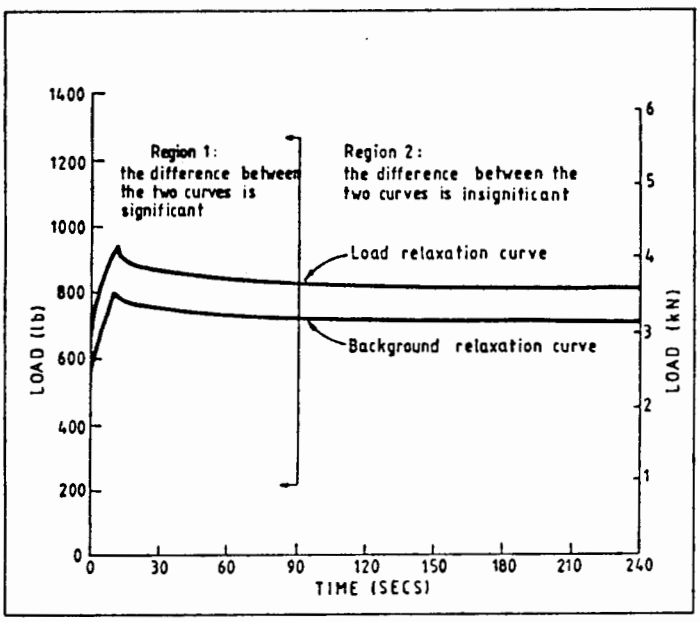

Fig. 6.19 Typical load relaxation curves from double torsion tests (From Yain and Mindess (334)).

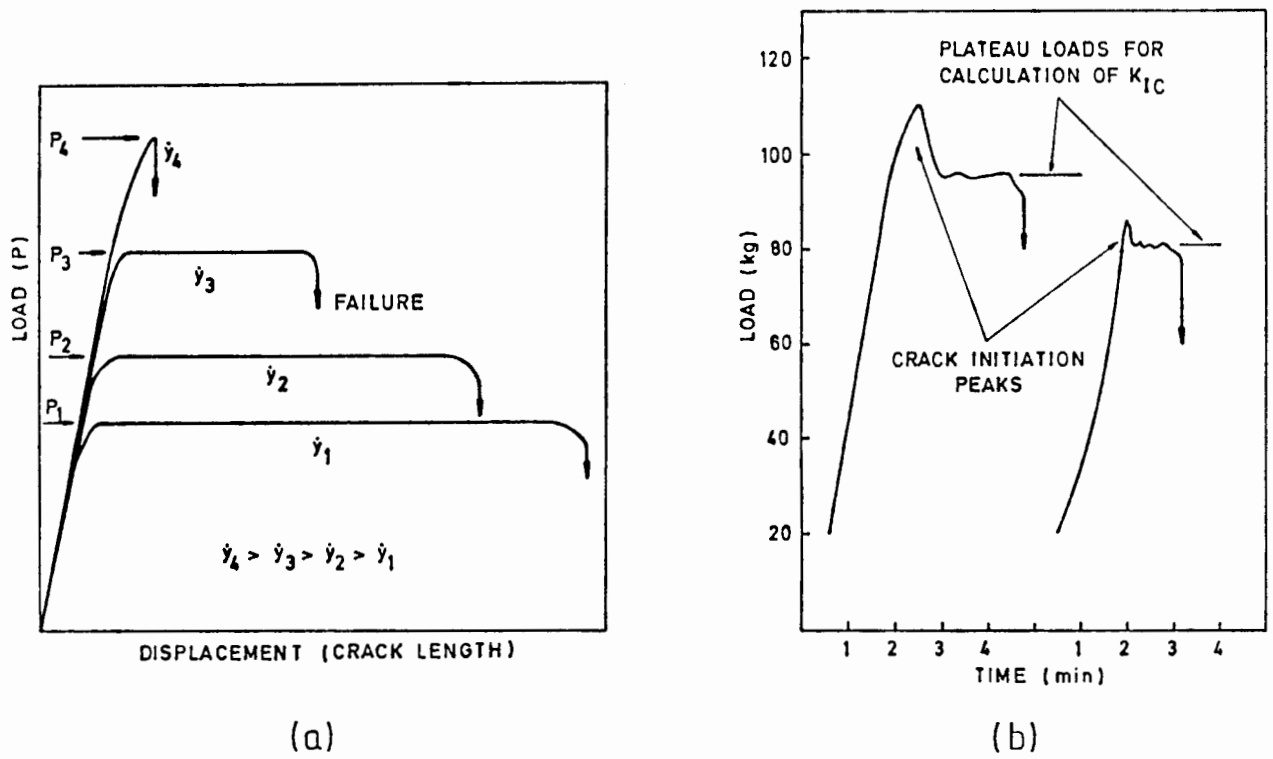

Fig. 6.20(a) and (b) Double Torsion load-time curves for constant ramp rate and (nominally) constant load tests: (a) idealisation and (b) typical results (from Evans (309) and Murray and Perrott (317) respectively).

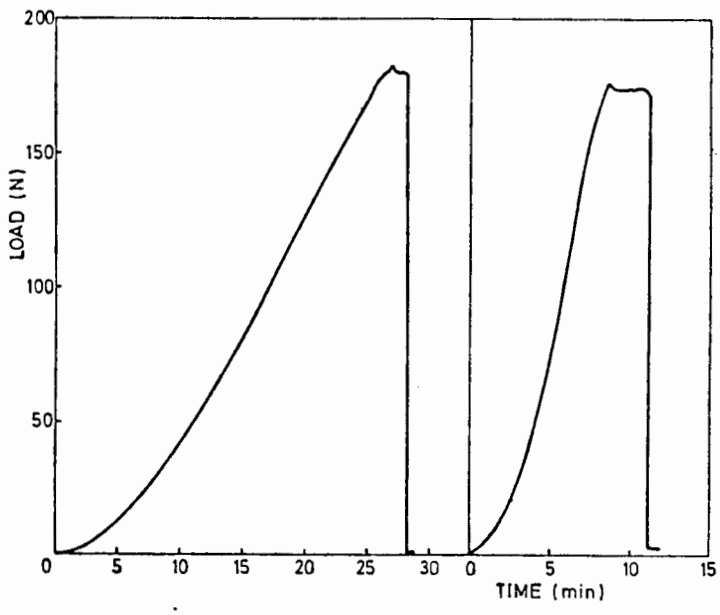

Fig. 6.20(c) Load time curves for constant ramp rate (and constant load) for mortar, (from the present work).

and to observe directly what effect this has on crack growth rate. For constant peak load, average load, load range and other operating conditions the crack growth rate is constant (see Appendix C), so the effect of changes in other parameters is immediately manifested as a change - or not, as the case may be - in the crack growth rate.

The other special advantage of using the double torsion specimen configuration in mechanical fatigue testing is that it is most suitable for distinguishing, by means of, for example, V-K curves, whether a true cyclic crack propagation effect exists in the range of frequencies and environments of practical interest. In this regard the effect of cycling frequency, in particular, can be relatively easily examined. The method is based on a comparison of the cyclic crack velocities predicted from the quasi-static crack growth parameters with direct cyclic crack velocity measurements, using the double torsion technique which is especially suitable since it combines both constant K and high stiffness requirements. A full theoretical development, based on work by Evans, with Fuller (235) and Linzer (313, 234) and others (316) is included in the Appendix C, because of its relevance here.

6.5.4.1 Load Control Fatigue : Average Displacement Rate

From Appendix C, (equation C.12) the crack length increment per cycle, δa, is given by

$$\left(\frac{\delta a}{\lambda}\right) = A\left(K_{Ia}\right)^{n} g \qquad 6.10$$

and this can be used to determine whether the cyclic slow crack growth mechanism is the same as the static one, for any given material. Use is made of the compliance relationship to determine the average displacement rate $\dot{y}_{av}$ for operation of the static mechanism (234). (See Appendix C, equation C.15.) This gives:

$$\dot{y}_{av} = gA\alpha P_{av}^{n+1} \beta^{n} \qquad 6.11$$

where α and β are constants. Since this testing is in load control we can impose the condition that ΔP and P (and hence ΔK), are constant, then g is constant (235) and all the terms on the right hand side of equation 6.11 are constant; hence $\dot{y}_{av}$ must be constant. By performing experiments at a few widely varying frequencies, all tests being carried out at the

same ΔP and P_{av}, the average displacement rate provides a very sensitive measure of a cyclic slow crack growth effect, especially, as has been mentioned, since the comparisons can all be performed on the same specimen.

6.5.4.2 Load Control Fatigue : Average Crack Growth Rate

A very similar but alternative approach to monitoring the average displacement rate $\dot{y}_{av}$, in load control cyclic fatigue is to measure, instead, the average crack growth rate $\left(\frac{da}{dt}\right)_{av}$. From equation C.5, $y = Pa\alpha$. By differentiating with respect to time

$$\dot{y}_{av} = P_{av}\,\alpha\left(\frac{da}{dt}\right)_{av} \qquad 6.12$$

and from equation 6.11 the average crack growth rate, assuming a static growth mechanism is

$$\left(\frac{da}{dt}\right)_{av} = gA\beta^{n} P_{av}^{n} \qquad 6.13$$

Once again, under load control conditions, at constant P and ΔP (and hence ΔK), all the terms on the right hand side of equation 6.12 are constant and so too must be $\left(\frac{da}{dt}\right)_{av}$. The above arguments for $\dot{y}_{av}$ apply in an analogous manner.

Specifically, if $\dot{y}_{av}$ or $\left(\frac{da}{dt}\right)_{av}$ is the same at all frequencies the cyclic and static growth mechanism must be identical, whereas significant effects of frequency on $\dot{y}_{av}$ or $\left(\frac{da}{dt}\right)_{av}$ would indicate the existence of a true cyclic fatigue process.

6.5.4.3 Stroke Control and Load Monitoring

The experiments can also be performed in displacment control where $\frac{\Delta y}{y_{av}}$ is kept constant and measurements are performed for small increments in crack length. The crack propagation load then becomes (see Appendix C):

$$P_{av}^{n+1} = \frac{a_i P_i^{n+1}}{\left[a_i + g\lambda(n+1)A\beta^{n}P_i^{n}\right]} \qquad 6.14$$

where a_i is the initial crack length and P_i is the initial load. Using this, the form of load relaxation curve should be the same for all frequencies, when all other parameters are maintained constant on the same specimen, and if the cyclic and static growth mechanisms are

equivalent. Such a technique has been employed by Evans, Russel and Richerson (316) for silicon nitride at 1400°C.

The above approaches have been used successfully, particularly by Evans and co-workers (234, 235, 313, 316) who have reported the absence of a cyclic fatigue process for porcelain and silicate glass and no frequency effect, even up to high frequencies. However, they do report a strong cyclic effect in tungsten carbide (234). Corresponding studies on the lack of a true frequency effect are reported in this thesis (Chapters 4 and 7).

6.5.5 Experimental Considerations and the V-K Curve

An interesting but disturbing phenomenon sometimes reported in DT-obtained V-K data is that reproducibility is sometimes dependent on the crack length position (321, 333). Alternatively successive loadings, resulting in several load relaxation 'runs' on a single specimen, can result in a transverse "shift" of the V-K data lines both to the left (i.e. faster, less safe region), (322, 333) Fig. 8.22, and also the right (slower, more conservative end) (284, 322). This less conservative shift is reportedly the case for some ceramics (322, 333) but does not occur for glass in distilled water (322), where reproducibility between successive loadings is apparently good (322). Similar small shifts in the V-K data lines (but without an effective change in slope, exponent n) were observed in this present study and are discussed in Chapter 7.

The phenomenon of shifts in V-K data lines with multiple load relaxation is not fully understood at this stage (322) but has been attributed to interactions of the crack with the groove edges (284) or with the microstructure (333, 322), possibly through process zone effects (276).

Generally, however, the use of the double torsion specimens to obtain V-K data is well accepted (309, 317, 323, 328, 344), particularly when the effect of other parameters (e.g. temperature, moisture) are of interest. V-K data obtained by both DCB and DT techniques (181, 317, 344) are sufficiently close for acceptance of the DT V-K techniques. Further work still remains, however, to resolve both this (minor) reproducibility difficulty (which may be more a function of groove characteristics (337)

and that of applicability of a crack profile correction factor to the crack velocity, V.

6.5.6 Summary

This section has described the velocity - stress intensity V-K curve approach which is particularly useful for analysing the effect of various parameters on crack growth rates, and in effect is what the rest of this chapter has been working towards.

The literature on the application of V-K curves to cement materials has been reviewed together with particular experimental considerations.

The various techniques of using DT specimens to obtain V-K data have been described including both static methods (rate of change of load at constant position and rate of change of position at constant load).

The use of double torsion specimens in the mechanical fatigue mode, have been described in some detail incorporating, in the appendices, a technique of predicting fatigue crack velocity from static data assuming the cracking mechanisms are similar. This is a powerful technique (235) which has been extensively used in this thesis.

6.6 Conclusions

This chapter has examined the application of fracture mechanics to cement materials with particular emphasis on experimental crack propagation. The relative size of the process zone has been highlighted together with the problems of unwarranted slow crack growth that can affect the measured crack resisting, or 'toughness' characteristics, G, γ and K.

Assuming, however, that these toughness parameters have meaning for cement materials, the factors which affect such toughness have been briefly summarised, as a further means of evaluating the applicability of fracture mechanics to cement materials.

Despite the extensive literature on this subject, it would appear that excessive pseudo plastic behaviour invalidates the applicability of LEFM

in its classical usage, and from this various conclusions may be drawn. Either (a) that the stress intensity factor is not a valid index for concrete fracture; or (b) fracture mechanics may only be applicable if the plastic cracking zone is either (i) relatively small or (ii) accounted for by some means; or (c) the mechanism of failure is independent of the geometry (or other factors mentioned above). In this particular study, however, relative differences in cracking behaviour as a function of other parameters (for example, frequency, moisture condition, temperature, etc.) are of more importance than absolute numerical factors, that may, in any case, be subsequently corrected by the appropriate correction factor.

Experimental methods that exhibit relatively stable cracking and which yield stress intensities that are independent of crack length, namely DCB and DT techniques, have been discussed. Particular emphasis has been placed on the theory and background of the DT system as this was the method used in this thesis.

This has been followed by a critical evaluation of this application of the double torsion specimen from a practical and experimental viewpoint and the chapter concluded with a discussion of the background and various techniques for obtaining valid V-K data.

This chapter thus provides the background for the experimental investigation of single cracks propagation studies, the details and results of which constitute the following chapter.

TABLE 6.1(a)

PUBLISHED VALUES OF FRACTURE TOUGHNESS, K_C, FOR CEMENT PASTE

Test Type	Reference	Water Cement Ratio	Curing Time	Toughness, Kc (MPa m)
NB	Alford et al. (77)	0.15	2 w	0.68
NB	Alford et al. (77)	0.2	2 w	0.48
NB	Alford et al. (77)	0.25	2 w	0.67
NB	Mindess et al. (279)	0.3	5 - 13 w	0.5 - 0.66
CPB	Grudemo (285)	0.32	120d	0.45
NB	Brown (155)	0.35	84d	0.43
NB	Brown, Pomeroy (130)	0.35	14-84d	0.4 - 0.5
NB	Watson et al. (280)	0.35	16 - 35d	0.43 - 0.45
DTNB	Watson (128)	0.4	Auto claved	0.65
NB	Alford et al. (77)	0.4	2 w	0.49
DTM	Yam and Mindess (334)	0.4	90 d	0.75
NB	Mindess et al. (105)	0.4	4 - 6 m	0.46
DTNB	Watson (128)	0.4	10d	0.37 - 0.47
DTS	Mindess et al. (105)	0.4	4 - 6 m	0.36
NB	Watson et al. (280)	0.4	16 - 35d	0.38
CTWOL	Hillemeir et al. (251)	0.4	50 - 130d	0.3
NB	Watson et al. (280)	0.45	16 - 35d	0.36
NB	Brown (155)	0.47	14d	0.30
DCB	Brown (155)	0.47	14d	0.45
NB	Brown, Pomeroy (130)	0.47	14d - 84d	0.3
DCB	Brown, Pomeroy (130)	0.47	7 - 14d	0.3 - 0.4
DTS	Mindess et al. (105)	0.5	Dried	0.31
DTM	Nadeau et al. (284)	0.5	78 - 99d	0.34
DTS	Nadeau et al. (284)	0.5	78 - 99d	0.29
NB	Nadeau et al. (284)	0.5	78 - 99d	0.32
NB	Gjorv et al. (253)	0.5	21d(40°C cure)	0.11
NB	Moavenzadeh (131)	0.5	7 - 28d	0.14 - 0.17
NB	Brown Pomeroy (130)	0.59	14 - 84d	0.2
NB	Alford et al. (77)	0.6	2 w	0.41
CPB	Grudemo (288)	0.64	120d	0.15
NB	Alford et al. (77)	0.8	2 w	0.42

TABLE 6.1(b) and (c)

PUBLISHED VALUES OF FRACTURE TOUGHNESS, K_c, FOR (b) MORTAR and (c) CONCRETE

(b)

Test Type	Reference	Water Cement Ratio	Curing Time	Toughness K_c MPa m
WOL	Hillemeir et al (251)	0.4	7d	0.4
DTM	Evans et al (285)	0.4	14d	0.6 - 0.7
NB	Naus & Lott (127)	0.45	28d	0.45 - 0.58
NB	Brown (155)	0.47	14d	0.55 - 0.65
DCB	Brown (155)	0.47	14d	0.75
DTM	Wecharatana (73)	0.5	7d(large specimens)	1.32
NB	Kaplan (267)	0.5	28d	0.65 - 0.9
NB	Strange, Bryant (256)	0.53	28d	0.58 - 0.71*
NB	Shah, McGarry (252)	0.54	7d	0.54 - 0.85
DC	Kitagawa (290)	0.60	28d	0.45
CNP	Kesler, Naus, Lott (254)	-	-	0.45 - 1.0*

LEGEND

NB - Notched beam
CT - Compact tension
CPB - Circular Plate Bending
SEN - Single edge notch
CNP - Centrally notched plate
DCB - Double cantilever Beam
DTS - Double Torsion (Sharp Crack)
WOL - Wedge opening loading
DTNB - Double Triangle notched beam
DC - Diametral Compression
CNRBB - Circumferentially notched round par under bending
DTM - Double torsion (machined Notch)

* - Dependent on notch depth/specimen size
** - Dependent on aggregate content/type

(c)

Test Type	Reference	Water Cement Ratio	Curing Time	Toughness K_c MPa m
NB	Strange, Bryant (256)	0.33	28	0.65 - 1.06*
NB	Alford, Poole (275)	0.4	6 months	0.45 - 0.7**
NB	Halvorsen (282)	0.4	-	0.75 - 1.2
CNP	Romualdi (274)	0.45	-	0.4 - 0.6
DCB	Brown, Pomeroy (130)	0.47	14d	0.6 - 0.9*
NB	Kaplan (267)	0.5	28d	0.6 - 1.1
NB	Naus, Lott (127)	0.5	28d	0.6 - 0.75
NB	Moavenzadeh (131)	0.5	28d	0.46
NB	Khrapkov (283)	0.5	90d (unstable cracking)	0.6 - 0.75
NB	Khrapkov (283)	0.5	90d (unstable cracking)	1.9
NB	Khrapkov (283)	0.5	90d	0.56 - 1.0**
NB	Petersson (278)	0.5	28d	0.6 - 0.9
NB	Petersson (278)	0.5	28d (using depth correction)	1.3 - 2.0
CNP, SEN	Mazars (289)	0.5	28d	0.55
NB	Swamy (281)	0.5	10d	0.5 - 0.6
NB	Shah, McGarry (252)	0.6	6d	0.65 - 1.03
DC	Kitagawa (290)	0.6	28d	0.58
SEN	Walsh (287)	-	28d	0.8 - 1.5**
CNP	Kesler, Naus, Lott (254)	-	-	0.6 - 1.3
CNRBB	Javan, Dury (269)	-	-	0.7 - 1.1
DCB	Sok, Baron, Francois (301)	-	-	1.5 - 3.5

TABLE 6.2

FRACTURE MECHANICS GEOMETRIES SUITABLE FOR TESTING BRITTLE MATERIALS

Data Required	Critical Stress Intensity Factor, K_{IC}					Crack Growth Rate vs. K_I or K_I	
	Slow Loading Rate				Fast Loading Rate		
	Ambient Temperature		High Temperature			Ambient Temp.	High Temp.
	Porous Material	Non-Porous Material	Porous Material	Non-Porous Material			
Specimen Configurations	Tapered Cantilever Beam Double Torsion Constant Moment	Double Cantilever Beam Three (Four) Point Bend Compact Tension Double Torsion	Double Torsion	Three (Four) Point Bend Double Torsion	Three Point Bend	Tapered Cantilever Beam Double Torsion Constant Moment Double Cantilever Beam	Double Torsion

TABLE 6.3

SURVEY OF PUBLISHED DOUBLE TORSION SPECIMEN GEOMETRIES

REF. NO.	REFERENCE	DATE	LENGTH (L)	WIDTH (W)	THICKNESS FULL t	THICKNESS WEB t_n	GROOVED SINGLE	GROOVED DOUBLE	RATIOS L	RATIOS W	w.r.t. W t	w.r.t. W t_n	MATERIAL
306	Kies, Clark	1969	300	75	3.18	3.18	-	-	4	1	.042	0.042	glass
311	Beecham, Kies, Brown	1970	225	75	3.1	2.8	*	-	3	1	0.04	0.039	4340 sc
312	Davidge et al.	1973	75	25	3	2.5	*	-	3	1	0.12	0.10	ceramics
332	McKinney and	1973	600	75	12.5	6.2	-	*	8	1	0.16	0.083	PMMA
332	Smith	1973	300	75	6.2	6.0	*	-	4	1	0.083	0.08	glass
307	Williams, Evans	1973	200	76	3.17	2.92	*	-	2.63	1	0.042	0.038	alumina
314	Murphy et al.	1973	203	71	9.14 -	7.6	*	*	2.88	1	0.10	?	aluminium
284	Naudeau et al.	1974	228	76	10	5	*	-	3	1	0.132	0.066	cement
105	Mindess et al.	1974	228	76	10	5	*	-	3	1	0.132	0.066	cement
318	Nadeau	1974	75	25	3	1.5	*	-	3	1	0.12	0.06	carbon epoxy
305	Outwater et al.	1974	200	71	12.7 -	6.3	*	*	2.9	1	0.084	0.042	aluminium
317	Murray, Perrot	1976	90	30	3	2	*	-	3	1	0.1	0.067	WC
285	Evans et al.	1976	105	57	6	3	*	-	1.84	1	0.105	0.053	polymer
104	Mindess, Nadeau	1977	228	76	13	8	*	-	3.0	1	0.17	0.11	cement
335	Shetty, Virkar	1978	152	63	2	-	-	-	2.5	1	0.23	-	glass
335	Shetty, Virkar	1978	152	102	2	-	-	-	1.5	1	0.02	-	glass
327	Bruce et al.	1978	76	25	15 to 23	7 to 11	*	-	3	1	0.59	0.92	PZT
330	Annis, Cargill	1978	75	25	3	-	-	-	3	1	0.10	-	Si_3N_4
310	Atkinson	1979	70	40	2.5	2	*	-	1.75	1	0.063	0.5	rock
319	French, Raj	1979	152	73	2.5	2.5	-	-	2	1	0.035	0.035	epoxy adhesive
345	Hakeen, Philips	1979	-?	80	6	-	?	?	-	1	0.075		PMMA
322	Pletka, Fuller	1979	75	25	2	-	*	-	3	1	.08		glass & other
321	Li Shing Li et al.	1980	80	23	2	2	-	-	3.5	1	.087	.087	Zirconia
198	Dalgleish et al.	1980	50	20	2	2	-	-	2.5	1	0.1	0.1	Ceramic
073	Wecharatana	1980	813	152	38	12.7	*	*	5.3	1	0.25	0.083	Cement and Concrete
334	Yam, Mindess	1982	1220	406	51	25	*	-	3.0	1	0.126	0.062	composite
331	Leevers	1982	270	90	6	3	-	*	3	1	0.07	0.03	polyester
333	Pletka et al.	1982	75	25	2	1	*	-	3	1	0.08	0.04	ceramics

Note: All dimensions in mm.

7.2.4 Environmental Controls

Double torsion tests were undertaken under very similar environmental conditions as the original compression tests. These were namely (a) so-called "moist" conditions; (b) "dry" conditions and (c) underwater conditions; (at temperatures of 25°C and 55°C). Since trends in behaviour were of particular interest, the middle temperature (previously 45°C) was not investigated as it was felt it would not contribute significantly to mechanistic understanding. In addition, because of the greater potential for heat loss in the smaller water test bath, the test temperature was 55°C (compared to 60°C earlier). The DT specimens were still, however, stored in the large storage reservoir at 65°C prior to testing and no special effort was made to change this temperature in view of the apparent dependence of strength on time at temperature (Fig. 4.43).

7.2.4.1 Moist Conditions

The humidity history for the double torsion specimens was very similar to that experienced by the compression specimens and described in Chapter 3. The empty (but moist) water bath containing the DT specimen and the upper loading arm system were contained in polythene "tube" bags in an attempt to achieve high moisture conditions. These "tubes" were sealed around the load cell at the top and the water bath at the bottom but provided negligible constraint.

The DT specimens themselves, after removal from the curing bath, were placed in this environment and equilibrated for up to 60 minutes prior to testing. Measurements of the humidity inside this bag was typically 80 to 90%, as measured by the PNI hair hygrometer. It was still quite possible to observe the crack and crack tip with the travelling microscope up against the polythene covering. Both static and fatigue tests were conducted in such an environment.

7.2.4.2 Dry Conditions

The "dry" testing condition was also very similar to that used in the compression prism specimens, and many of the details of section 3.4.3.2 are relevant here. The specimens, after the appropriate wet curing period, were air dried and then oven dried progressively to 105°C for four days. The hot dried specimens were transferred to dessicators prior to testing.

The testing was conducted inside polythene tube bags, fixed as described in the previous section, which also contained two de-hydrating sachets in the (empty) water test bath. Using such a process of drying and environmental control, relative humidities were measured to be typically less than 10% (and in any case certainly less than 25% RH). Both the moist and dry tests were conducted at ambient temperatures of 20°C $\pm$ 2°C.

7.2.4.3 Underwater Test Conditions and Temperature Control

The underwater system used in the double torsion testing for both static and fatigue cases was very similar to that used in the compression testing (Section 3.4.3.3). The water test bath has already been mentioned and formed part of the DT loading support facility (Fig. 7.2(a)).

The same reservoir and temperature control unit was employed as in the compression case (section 3.4.3.3 and Figs. 3.8 and 3.9) and only the test bath unit and specimen were different (Fig. 7.4). In this case, since firstly the depth of the test bath was much shallower and secondly that the DT specimen tended to fracture into only two portions, mortar debris was no longer a problem.

An additional characteristic, however, of the double torsion over the compression water system was the need for even more careful water level control. This was occasioned by the need to keep the DT specimen (which lay in a horizontal plane) just submerged, but not deeply inundated, so facilitating observation of the crack tip. This was achieved using a small air jet technique to be described in the following section, which was only effective for very shallow water coverings of the specimen.

Temperature control was achieved using the Grant temperature controller in the reservoir, but two additional conventional thermometers were also employed - one in the reservoir and one in the test bath to monitor the temperature. Using this system, and despite temperature losses, temperatures could be controlled to within $2^{o}C$ of the required temperature.

Since no damage monitoring apparatus was needed for the DT specimens, the "high" temperature induced difficulties described in Chapter 3 fell away and even the highest temperature DT tests were performed relatively easily. The only consideration requiring particular care being that of alignment, which needed to be ideal throughout the testing.

7.2.5 Crack Monitoring Systems

As mentioned earlier, monitoring of the length of the crack by observation of the crack tip was required for fatigue tests, and, in particular, for changeover tests. In this way it was envisaged that direct crack velocity measurements could be made under fatigue conditions and used in the generation of fatigue V-K curves. In both dry and wet tests the feature of the crack that was exploited was that, under fatigue, it exhibited minute opening and closing. Thus, a very thin film of fluid in the vicinity of the crack tip would exhibit a "pumping" action which was utilised in identifying the crack tip position.

7.2.5.1 Dried Double Torsion Specimens

To utilise the"pumping" mechanism to manifest the crack tip under ostensibly dry conditions, the choice of fluid was critical. A conventional red dye penetrant was very sparingly used as it was intended that the tests be conducted under truly dry conditions.

It can be argued that introduction of the dye in the vicinity of the tip caused changes in the rate of crack growth. However, the dye penetrant was nominally non-corrosive and was in any case only very sparingly used. Since the specimen was dry, the dye-pen, introduced by the tip of a very fine needle and syringe, soaked away at the crack tip and

dispersed within a couple of seconds leaving a small (≃ 1 mm) red dot. Such dispersion behaviour for dry specimens has also been recognised by Yam and Mindess (334). During this time the crack tip was observed and the travelling microscope adjusted so that the crack length measurement could be read at leisure, before the next measurement sequence.

Subsequently, because of the concern about the effect of conventional dye penetrant on otherwise dry crack propagation, a dyed benzine was used for locating the crack tip. It has been reported (33) that benzine has no interactive effect on mortar strength or crack propagation behaviour. The crack velocity results obtained using dyed benzine for crack tip observation did not differ significantly from those obtained using dye penetrant, so this latter technique was maintained throughout. Scatter was, however, larger for dry than underwater DT tests.

7.2.5.2 Moist Crack Tip Observation

Fatigue crack tip observation was facilitated by the use of the red dye penetrant liquid already mentioned. The dye was introduced into the crack behind the crack tip (i.e. in the already cracked region) and was assisted to the tip by capillary action and pumping.

7.2.5.3 Underwater Crack Tip Observation

Observation of the crack tip underwater, under fatigue conditions, proved to be somewhat more difficult.

Generally, from the literature, very little research effort appears to have baeen devoted to the observation of the crack tip in unpolished opaque materials. The techniques investigated here, for the observation of the crack tip underwater, included a diffuse light spot method, a variety of brittle coatings and liquid "pumping" methods.

An attempt was made to utilise the technique of diffuse illumination as used by Higgins and Bailey (75). In this technique the region immediately adjacent to a crack was sharply illuminated by an intense spot of light. Since cement and mortar, even at low magnification, are partially translucent, the area around the bright spot becomes visible by

diffuse illumination. If there was a crack in this diffuse illumination zone it would be seen as a discontinuity in the diffuse light crack (Fig. 7.5).

Apparatus was developed to utilise this technique which consisted of a focussed, slide projector 100 watt light source. Experimental difficulties of heat dissipation from the light source and sharp focussing were ultimately overcome. However, while it was possible to observe the crack (and hence the crack tip) this was only achieved with difficulty, and at high magnification, in the present investigation. The technique was thus unsuitable for use as a practical crack tip monitoring technique as simultaneous high magnification travelling microscope observation and spot location was required on a fatiguing, and thus slightly moving, specimen. Hence, other techniques of underwater crack tip observation were examined.

Various brittle coatings were investigated, including conventional brittle coatings used on steels to detect strains; others included canada balsam, various patent varnishes and resin. These all proved to be unsuitable as they tended to remain flexible at the strains necessary to cause cracking in the mortar. The conventional steel brittle coating material and resin were successful but in coatings which were too thick to be of use or at large strains (above about 800 micro strains). As thick coatings they may also have an inhibitive effect on the truly "wet" nature of the material at the crack tip as well as detracting from the ideal analytical case by forming, in effect, "composite beam" material. It thus appeared that brittle coatings were unsuitable for crack tip identification.

Various liquids, common to a chemical laboratory, were evaluated as indicators, but no suitable ones could be found which preferentially adhered to the mortar or the crack, rather than the water itself. Thus it also appeared that crack indication, by pumping methods, would present an intractable problem.

The utlimate solution however, did utilise the pumping concept and was in itself very simple. The water level in the test bath was adjusted so that the DT specimen lay just below the water surface. In this way the

depth of water in the upper (tension) groove was typically 0.8 to 1.0mm. Any apparent drying out by the top specimen surface was obviated by gentle turbulence from the water reticulation system and occasional splashing onto the DT specimen. The specimen was thus regarded as fully wet and submerged throughout the test.

When a crack measurement was to be made, a fine jet of air (from a low pressure pipe, via ordinary tubing and a slender taper-drawn glass tube) was played into the groove at the appropriate locality. This air pressure jet effectively kept out the surrounding water (which had negligible pressure head and was retained by surface tension menisci), and the specimen surface started to dry. However, in the crack itself and at the crack tip, the water was retained and a clear pumping action was seen at the boundary of the thin film, which could be used to localise the crack tip. This technique was particularly sharp if the crack tip was approached, first from one direction (the cracked end, say) and then the other (the remote, uncracked end). The whole procedure, although requiring skill and experience, seldom took more than about fifteen seconds and immediately the crack tip was observed and "fixed" (by the travelling microscope), the air jet was removed, and the groove naturally flooded again. The zone of drying was approximately 2mm across and was maintained for so brief a period that it was believed that no deleterious drying effects took place. The specimen could thus still be regarded as 100% wet, even locally at the crack tip observation points (Fig. 7.6).

It is apparent from this discussion that this underwater crack tip monitoring technique was "operator dependent", but with practice readings could be taken consistently. Any errors in reading are not cumulative and in any case with the large number of readings it was believed that realistic V-K fatigue information was obtained.

7.2.6 Crack Profiles and Groove Specification

One of the difficulties with the double torsion specimen is the appropriate choice of groove geometry and what effect such grooves have on performance. An investigation of this effect in the mortar used in this project was undertaken, because of the conflicting research results mentioned in section 6.4 and Table 6.3.

This present investigation examined the effect of groove depth, location (tension or compression face) and the advisability of single or double grooves, on subsequent test performance. One of the performance criteria was the shape of the crack profile which is generally considered, from an analytical viewpoint, to be straight through the specimen. As mentioned in section 6.4, this was not, however, the case. Rather it was of a curved nature with the crack meeting the tension surface at some, typically non-orthogonal, angle (see for example Fig. 6.17). However, since groove geometry was a parameter which could be varied slightly, it makes sense that it should be chosen in order to meet the analytical requirements as closely as possible. In particular, the crack should be as nearly straight through as possible with the crack front meeting the tension surface at right angles.

It has already been mentioned that cast in grooves were unsuitable because of the development of shrinkage cracks and this is borne out by the crack profiles. Because of shrinkage cracks at the stress concentrations in the corners of the grooves, the dye penetrant indication of typical cracking for such cast in groove DT specimens, showed very shallow crack fronts, (Figs. 7.7(a) and (b)).

Consequently, machined-in grooves were investigated. Evans' approach (section 6.4.3) was to locate such a single groove in the tension face. However, tests on successively deeper cut tension face grooves gave progressively worse performance and crack profiles. Indeed, there was tendency for the specimen not to behave as a DT specimen at all, but to fracture in a purely tensile bending manner, especially if the web was thin.

In view of the poor performance of tensile face grooves, grooves in the compressive face were examined. This is the approach taken by Mindess (104, 105, 318, 334) and Nadeau (284) particularly for cement based materials, and proved applicable. Grooves were cut into the compression face to a depth of 4 to 5mm, with a shallow tension groove of up to 0.8mm. Such a groove geometry, from a strength of materials analysis, would have the maximum crack opening effect and tendency to DT fracture (in contrast to a deep tensile face groove). This groove geometry

produced the best crack front shape and additionally the crack was ideally centrally located in the top groove. Typical examples of the crack profiles are shown in Figures 7.8(a), (b) and (c). This groove geometry (Fig. 7.1(c) was hence used for all the subsequent DT tests, and it is believed that further improvements could only be gained by going to thinner specimens or specimens with no grooving, but with very rigorous alignment.

A few additional tests were conducted on relatively thick specimens (but of the same length and width) but these resulted in a shear mode of failure rather than DT type of failure.

7.2.7 Experimental Procedures and Programmes

7.2.7.1 Introduction

The experimental procedures were developed to obtain V-K data for a variety of testing conditions. In particular, these include both static and fatigue modes for the environmental situations of dry, moist and underwater conditions. These latter tests also incorporated tests at 25°C and 55°C to investigate the effect of temperature on crack growth rates. For the quasi-static tests, crack velocity measurements were inferred from load relaxation or constant ramp rate tests (see Appendix B), but for the fatigue tests velocities were directly measured, for all environmental conditions. Additional tests series were conducted at various frequencies to investigate the frequency and time dependence in a manner analogous to the compression prism tests.

7.2.7.2 Thickness Effects in Static Testing

In the preliminary stages of the double torsion testing it was soon established that the load to cause fracture of a DT specimen depended critically on both the web and overall thickness, t_n and t. Measurements of "static strength" (ramped at 0.005 mm/sec) were also required in a manner analogous to the compression testing (Chapter 3) to facilitate subsequent fatigue testing at the appropriate level. Consequently, static tests were conducted for a variety of web and total thicknesses for both wet (underwater) and dry DT specimens.

The DT analysis (Appendix A) relates the stress intensity K to the relation $P/(t^3 t_n)^{\frac{1}{2}}$ (equation A 12). If it is assumed that the specimen fractures at a constant, critical "thickness-independent toughness" K_{Ic}, then a plot of fracture load P against $(t^3 t_n)^{\frac{1}{2}}$ may be expected to be a straight horizontal line. Normalising P by $(t^3 t_n)^{\frac{1}{2}}$ so that it is proportional to K (but for a constant) it may be supposed that a plot of K versus $(t^3 t_n)^{\frac{1}{2}}$ would also yield a horizontal line. This was not the case as is shown in Figure 7.9. The reason for this behaviour can be attributed to an element of bending in the fracture of the DT specimen. Once again, simple analysis would indicate that if the crack propagation is not purely axial but has a component through the thickness (which it must have in almost all DT tests), then the failure stress will not be thickness independent. This failure stress, σ, will be related to the applied bending moment, M, (in the simple case of pure bending) to the reciprocal of the square of the thickness, d (say), through the equation.

$$\sigma = \frac{6M}{bd^2} \qquad 7.1$$

where b is the beam width.

Since there is this inverse "thickness squared" dependence it seems reasonable to believe that there is some pure bending contribution, and the validity of the DT analysis for these size double torsion mortar specimens is therefore brought into question.

To circumvent this problem, efforts were made in all subsequent testing to make specimens as nearly identical as possible, especially with regard to grooving and the thickness values, t and t_n. In addition, periodic static test checks were made on each new batch to see if they fell within the scatter band of the results of the so-called "calibration curves" of the form of Figure 7.9, appropriate to each curing and test condition. Where relevant, small adjustments in the appropriate load level, particularly for fatigue testing, were made utilising these "calibration curves".

This whole usage of "calibration curves" did not arise in conventional static DT test methods of obtaining V-K data, which relied on either load relaxation at constant position, $\left(\frac{\delta P}{\delta t}\right)_y$, or slow ramping, $\left(\frac{\delta y}{\delta t}\right)_P$. It was sufficient merely to measure the appropriate dimensions.

7.2.7.3 Static Techniques of Obtaining V-K Data

Load Relaxation at Constant Position

To obtain meaningful V-K curves the specific requirements and parameters for each of the techniques described in Appendix B needed to be met. Thus for the two load relaxation approaches to obtain crack growth rate at constant position, $\left(\frac{\delta a}{\delta t}\right)_y$, Appendix equations B1 and B6 needed to be used. The corresponding value of stress intensity K is obtainable from (appendix) equation A12 (or equation 6.3 Chapter 6). The various parameters employed in these equations needed to be measured, including specimen dimensions and material properties, as well as initial and final crack lengths and loads. Examination of the two equations B1 and B6 facilitated comparison of the two techniques. Results of the two techniques were comparable but the greatest error was in measuring the load displacement, y, of equation B.1 (see also Fig. 6.11). For this reason the subsequent load relaxation based crack velocity evaluations made use of the compliance approach (equation B.6) together with the initial load and crack length.

The crack was initially grown by fatigue (to sharpen it) into the relevant constant K region of the DT specimen. The crack length and compliance were measured and then a small fixed constant displacement applied. This resulted in the crack propagating over a relatively short period of time with a corresponding load relaxation (Figs. 7.10(a)(b)(c)). It was often possible to produce several load relaxation plots from one specimen as long as the crack remained in the relevant, constant K region (Fig. 6.15(a) and (b)). It was also necessary to subtract from these load relaxation traces the background relaxation of the loading train, i.e. the relaxation due to effects other than crack growth, and a typical example is shown in Fig. 7.11(a). The resultant corrected load relaxation, for example for the test shown in Fig. 7.10(b), is shown by the dotted line in Figure 7.11(b).

Slow Ramp Rate Tests

To obtain crack growth rates at constant load, $\left(\frac{\delta a}{\delta t}\right)_P$, equation B7 of Appendix B was used which relates crack growth rate to ramp rate $\left(\frac{\delta y}{\delta t}\right)_P$. The ramp rates which were used to obtain the traces shown in Fig. 6.20(c) and others of similar form were typically 0.002 to 0.00025 mm/sec. It was also occasionally possible to monitor the crack growth rates optically using the travelling microscope system (but without dye penetrant) during the slow ramping tests. These optically-obtained crack growth rates correlated well with the data obtained conventionally (using equation B.7).

One of the drawbacks of the slow ramp rate/constant load tests was that only one V-K data point pair was obtained from each test and invariably the test could only be conducted once on each specimen. This follows since there is one ramp rate (giving $\frac{da}{dt}$) and one load P (giving K_I). This is in contrast to the load relaxation method where several data point pairs, typically 5 to 7, could realistically be obtained from each relaxation trace and often 3 to 5 such relaxations could be conducted on each specimen. It was observed, however, that V-K data obtained by the load relaxation (constant position) method and the slow ramp rate (constant load) method gave similar results (Fig. 7.12 (a) and (b)). The length of the "plateau" region in these ramp tests was typically between 2 and 4 minutes and superficially appear different in form from, for example, Fig. 6.20(a), from the literature Evans (309). However, further communication with Evans himself (328) revealed that such plateau "lengths" or strictly - times, are quite acceptable (see also Murray and Perrot (317)).

Statically Derived V-K Curves

The question of reproducibility of the two statically derived V-K techniques was considered. It has already been mentioned in section 6.4 that various researchers have observed shifts to either lower (322, 330) Fig. 6.22, or higher (284, 322) K values (at constant crack velocity) on successive load relaxations. Similar behaviour was observed in the present studies, where successive load relaxations, on the same specimen,

resulted in shifts to higher K values, (Fig. 7.13(a)). In view of this scatter effect, comparable relaxation cycles on different samples were used for comparison, Fig. 7.13(b), and, in addition the crack lengths were approximately equal.

For stress intensity calculation, a value of Poisson's ratio is required. This was discussed in Chapters 2 and 4 and a value of 0.2 was taken as being generally acceptable (33, 34 125)

7.2.7.4 Fatigue Testing

Prior to fatigue testing, two or three specimens were statically failed to confirm that the batch was consistent with the calibration curve for that curing and test condition. For subsequent fatigue tests the thicknesses t and t_n were measured and the parameter $(t^3 t_n)^{\frac{1}{2}}$ determined, from which the appropriate static strength could be estimated from the calibration curve. The upper level of fatigue loading was conducted at some fraction of this value, under load control.

The lower fatigue load level was in the vicinity of 40N and was chosen to be compatible with both the g factor requirement mentioned in Appendix C, and also with the requirement that the loading points were not to be fully unloaded during testing. Were such complete unloading to occur, impacting of the specimen or its misalignment could occur, thus altering the test conditions.

Various fatigue test series were conducted utilising the powerful changeover technique. Comparative wet and dry tests were undertaken where oven dried samples, with a fatigue crack partially grown, were flooded and the change in crack velocity noted. Temperature change tests were undertaken by utilising two reservoirs at different temperatures and switching the test bath water from one to the other very promptly. The test bath water was rapidly changed, and the reticulation converted from one reservoir to the other.

Changeover frequency tests at test frequencies of 0.1, 1 and 10 Hz were also conducted using a sine wave throughout.

7.2.8 Summary

This section, 7.2, has examined in some detail the experimental aspects of the investigation of crack propagation in mortar double torsion specimens. Specimen fabrication and preparation details have been described. The loading system includes a large bearing to ensure equal loading and the alignment of this loading system and the specimen are critical. The environmental controls of moist, dry and underwater conditions are very similar to those used for the compression prism tests, although an additional advantage of the temperature tests is that changeover tests from 25°C to 55°C could be undertaken by rapid changing of the (relatively small amount of) water in the test bath. Test programmes have been outlined which include investigation of environmental effects on crack growth rate as well as frequency and time dependent effects. These test programmes are broadly analogous to those conducted on compression prisms and described in Chapters 3 and 4. In this case, however, crack growth rate becomes a more sensitive and reliable fracture mechanics parameter than damage accumulation rates (Chapter 4) although they may presumably be related. This inter-relation and all the DT test results are described in the following section.

7.3 Results

7.3.1 Static V-K Test Results

Typical V-K curves derived from static load relaxation curves are shown in Figs. 7.12(a) and (b), for mortar which had been oven dried at an age of seven days. The slopes of these V-K lines tended to be approximately equal for all the DT V-K tests undertaken. These included some 38 successful load relaxation tests, 10 static slow ramp tests, and 120 fatigue tests under a variety of environments and test conditions. The average slope or n value of these V-K lines, where the data can be described by the equation:

$$\frac{da}{dt} = V = AK^n \qquad 7.2$$

with $n = 26 \pm 4$. There was, however, significant difference in the absolute position or intercept of these lines depending on the specific test conditions.

This value of slope is comparable to other results in the literature as discussed in section 6.5 (and shown in Table 6.5) for strain rate derived data).

It was possible to obtain an average position, or intercept, of V-K curves for each particular test condition, despite the scatter due to successive load relaxations or other effects. Thus, for example, for the static V-K data lines shown in Fig. 7.12(a) for 7-day oven dried samples, the "average" V-K line can be obtained from all the data and is replotted in Fig. 7.12(b) by means of the least squares analysis. This "average" V-K line for this data (and all other oven dried data relevant to this condition) is also shown in Fig. 7.12(b).

For the analysis of the fatigue V-K data described in the next section, use is made of a theory due to Evans and Fuller (235), and discussed in Appendix C, which leads to a "g factor" of multiplication. The g factor is a function of ($\Delta K/K_{AV}$), exponent n, and the shape of the cycle. The analysis makes use of the statically derived V-K data to predict the fatigue V-K behaviour, assuming the mechanisms of failure are similar. Thus, comparison of predicted fatigue V-K behaviour with actual fatigue crack growth rate behaviour can provide a means of evaluating the validity of such predictions and the acceptability of using the same mechanism to describe static and fatigue cracking.

Practical application of the g factor approach to the prediction of cyclic crack growth rates based on static data have been undertaken by Evans, Russel and Richerson (316) and Bruce, Gerberich and Koepke (327). Evans et al. (316) conducted both static and fatigue DT tests on silicon nitride at 1400°C and obtained good correlation between cyclic V-K data and statically based g factor predictions.

The following static double torsion test series were conducted.

(i) "Young" (7 day old) oven dried samples tested in a dry environment, the results of which have already been presented (Figs. 7.12(a) and (b)).

(ii) Young (7 day old) oven dried samples subsequently thoroughly wetted and tested under water at 25°C, (Fig. 7.14)

(iii) Fully dehydrated "old" samples cured for 100 to 120 days and tested under water at (a) 25°C and (b) 55°C, (Fig. 7.15)

(iv) A limited number of tests on intermediate age samples (typically 14 - 56 days) tested under "moist" conditions (of 75% to 95% relative humidity), Fig. 7.13 (a) and (b).

(Note that Fig. 7.14 also includes some fatigue V-K data. This is referred to subsequently and the presentation of both static and fatigue V-K data on one graph was adopted as it facilitates later discussion). Despite the scatter of data shown in Figs. 7.12 to 7.15 it is apparent that the slope of the V-K curves, determined as $n = 26 \pm 4$, does not appear to depend on the nature of the test, at least for the environment and temperatures mentioned above. This independence of n on test condition is in itself an interesting phenomenon.

It is particularly interesting to note the effect of three parameters on the intercepts (or locations) of these V-K curves, as follows.

(a) The effect of environmental moisture The tests covered a range of conditions, from oven dried specimens tested in a dry (< 10-25%RH) environment, through moist tests (at RH 75%), to underwater tests. The effect of increasing environmental moisture is apparently to increase the crack velocity V, for a given stress intensity K, (or alternatively it may be considered as reducing significantly the stress intensity necessary to give a certain crack growth rate.) Changes from dry to very wet (underwater) conditions results in an increase in growth rate (at constant stress intensity) of approximately 4.4 orders of magnitude. These results are comparable with those of Mindess, Nadeau and Hay (105), who have reported a time to failure increase, of dry over wet specimens, of approximately five orders of magnitude.

(b) The effect of temperature Increases in temperature also shift the V-K curves to faster growth rates. At constant stress intensity and in underwater conditions, this shift is approximately 1.4 to 1.5 orders of magnitude (i.e. 10 to 35 times) in crack velocity, for a temperature change from 25°C to 55°C. This result is consistent with other published work on increased deflection and accelerated failure in static tests (124), but seemingly at odds with time to failure studies by

Barrick and Krokosky (29) who reported increased static lives with increasing temperature over this range.

(c) The effect of age and degree of hydration

The average V-K line results in Figs. 7.12 to 7.15 have been replotted in Fig. 7.16 (but for reasons of clarity without the data themselves). In this presentation it is apparent that oven dried specimens were the most resistant to crack propagation. These were followed successively by specimens cured for a long period (100 days) and tested at firstly 25°C and secondly 55°C. The specimen series that exhibited the greatest crack velocity for a given stress intensity was that which included specimens which were wet cured for seven days, subsequently fully dried but tested under fully wet conditions.

It is also interesting, at this stage, to compare the static fracture strength and associated stress intensity at failure, K_{If}, of young (7 day old) oven dried DT specimens tested under both dry and wet (underwater) conditions, at 25°C. The static fracture strength results are shown in Fig. 7.9 as a function of the specimen "section area", or thickness factor $(t^3 t_n)^{\frac{1}{2}}$, on which they depend. The ratio of dry-to-wet strength at any particular value of $(t^3 t_n)^{\frac{1}{2}}$, varies approximately between 1.49 to 1.58. This is of the same order as the K_I shift, at constant crack growth rate, in static load relaxation V-K curves of 1.47, and cyclic tests of 1.49, which is apparent from Figs. 7.14 and 7.17 (a) and (b). This lateral shift in K of approximately 1.47 to 1.49 (at constant crack velocity), for dry to wet tests, corresponds to a velocity shift of 4.35 to 4.5 orders of magnitude. (This is arrived at by making use of equation 7.2 and an n value of 26, i.e. 26 log 1.47 yields 4.35) These results of fracture strength and V-K curve "shifts", at constant stress intensity, for changes from dry to wet conditions, thus appear to be self consistent.

To summarise, it would appear that the following three parameters have the most significant effect on the value of the intercept, (or in essence, the "location") of the V-K curves.

(i) Increasing humidity or environmental moisture shifts the V-K lines progressively to values of higher crack velocities (at constant stress intensity).

(ii) Temperature increases also result in similar shifts in the V-K curves but to a lesser extent.

(iii) Increased hydration, interpreted as greater curing age, shifts the V-K curves to reduced crack velocities at constant K.

Similar behaviour is observed in the fatigue test series which are dicussed in the next section.

7.3.2 Fatigue Test Results

7.3.2.1 Introduction

In Appendix C the paper by Evans and Fuller (235) was discussed and was further mentioned in section 7.1. This paper put forward a means of predicting the cyclic crack velocity based on static crack velocity data assuming that the mechanisms of cracking and crack growth are the same for both static and fatigue conditions. They determined a relationship between the cyclic and static crack velocities for the same average stress intensity value, K_{Iav}, as differing by the factor g (235). This g factor for sinusoidal loading is given by

$$g(n,\xi) = \sum_{\ell=0}^{\left[\frac{n}{2}\right]_T} \left[\frac{n!}{(n-2\ell)!(\ell!)^2}\right] \left(\frac{\xi}{2}\right)^{2\ell} \qquad 7.3$$

where $\left[\frac{n}{2}\right]_T$ is the truncated value of $\left[\frac{n}{2}\right]$, ℓ is an integer, and ξ is a measure of the amplitude of the cyclic loading. That is,

$$\left(\frac{\sigma}{\sigma_a}\right) = (1 + \xi \sin\omega t) \qquad 7.4$$

A sketch of the form of this g function, for the relevant range of stress amplitude to average stress, ratio ξ, was given in Appendix C (Figure C.4) but because of its relevance is reproduced here (Fig. 7.18). For the material used in this thesis n was determined as 26, so a g^{-1} factor line was calculated and included in Fig. 7.18. This figure was extensively used in subsequent prediction of cyclic crack velocity, for various curing regimes and environmental conditions.

Actual typical values of ξ were determined from the load amplitude used during cycling. For example, one of the points in Fig. 7.17(a) has a measured crack velocity of 1.45 X 10^{-5} m/sec when cycled at 1 Hz between a maximum compressive load of 307.3N an a minimum load of 40.2N. The mean load was thus 173.7N, the amplitude 133.6 and the parameter $\xi = \frac{\sigma}{\sigma_{av}}$ = $\frac{133.6}{173.7}$ = 0.77. The corresponding value for K_{Iav} was determined from equation A.12, and in this case was K_{Iav} = 0.368 MPa $\sqrt{m}$. The V-K results are now discussed with particular reference to (a) environmental moisture conditions and curing history, (b) temperature changes and (c) frequency.

7.3.2.2 The Effect of Environmental Curing History on V-K Data

The double torsion test system in a fatigue mode is particularly suitable, for dry to wet changeover tests. With the sample in an initial dry controlled environment, it is possible to flood it and the test bath in a matter of seconds, while monitoring the corresponding crack growth rates. A typical result is shown in Fig. 7.19, where the change in crack velocity with increased moisture present is clearly in evidence (Note, however, that the average stress intensity has been significantly reduced when the water was added to maintain the same relative level of stress intensity (Fig. 7.9), and to obtain measurable crack velocities. (Were this reduction not made crack velocities would be too fast to measure at the applied loads). The combined effect of these two changes, i.e. water addition and lowering K_{av}, in real terms means an increase in crack velocity, due to the water addition, of some 4.4 orders of magnitude (at constant stress intensity) when considered on a V-K graphical presentation (Fig. 7.17(b).

The fatigue crack growth rate data for oven dried specimens, and using an amplitude parameter of ξ = 0.77, are shown in Fig. 7.17. The best straight line through this data using a least squares analysis is shown by a solid line. Use can now be made on the g factor prediction due to Evans and Fuller (107). Based on the static V-K line, also shown in Fig. 7.17(a), and for a zeta value of ξ = 0.77, the predicted cyclic V-K line is also shown (dotted) in Fig. 7.17(a). In addition to fully dried specimens some tests were also conducted, in a dry environment, on some old specimens (cured for 18 months) as well as some 28 day old samples

dried for 24 hours. The V-K behaviour of such tests was similar (Figs. 7.17(a) and (b)) indicating that the fully cured and dried specimens show very similar cracking behaviour to the young-dried samples. Evidently then, moisture plays a key role in the cracking process.

The standard deviation, considered in terms of a change in stress intensity, was of the order of 8%, so it would appear that the statically based predicted V-K fatigue line (dotted) would accommodate the actual measured fatigue data points. The implication, consequently, is that the mechanism of crack propagation or local failure is basically the same for both fatigue and static test conditions. This is presumably of a moisture assisted stress dependent form or even of a stress corrosion nature involving so called static fatigue processes.

It is arguable whether it is meaningful to refer to "stress corrosion" in cement based materials. Attack of silicate bonding in glass by water and assisted by stress is well established even at relative humidities as low as 0.02%. This is referred to by Wiederhorn as a "stress dependent chemical reaction" (340, 353). In the case of cement materials, it is also reasonable to regard attack as occurring due to hydroxyl ion attack of highly stressed calcium silicate bonds at the crack tip, and has been suggested before, (29, 30, 106, 250). An alternative description, for the time dependent cracking that is occurring, is that of "creep" which traditionally leads to failure and in which an environmental moisture contribution may be negligible. However, for cement materials creep does not occur in "completely" dry environments (233) and since moisture appears to play a major part in the present cracking behaviour the term "stress corrosion" is used from henceforward even though this is not yet proven. Full justification of its use appears in Chapter 8.

It is interesting to note in addition in Fig. 7.17 (a) and (b) that all the cyclic data points are to the left (i.e. faster crack growth) side of the predicted line and such a deviation may well be signficant. This is discussed more fully in section 7.4.5 to follow.

Similar, but more pronounced behaviour is shown in Fig. 7.14, for 7 day old oven dried samples subsequently wetted and tested wet, where the deviation of the data from the predicted line is more pronounced. This

predicted line was based on the static line shown in Fig. 7.14 for wet (underwater) specimens and a fatigue amplitude ratio, = 0.66 for these specimens. An additional series of data at greater cyclic amplitude = 0.8 for similar underwater specimens was obtained and is also shown in Fig. 7.14.

Since the cyclic data is not too far from the predicted line it would appear that the same type of crack growth mechanisms that were applicable for the static case were largely applicable in the cyclic case. However, the difference between actual fatigue data and the predicted V-K line is now somewhat larger and would appear to be significantly outside the limits of standard deviation for both the predicted line and cyclic data. The implication is that, although the major cause of cyclic crack propagation in a wet environment is of the same nature as in static fatigue (e.g. stress corrosion) there is an additional mechanism responsible for the further increases in the underwater cyclic crack growth rate, which results in the shift of the line to the left (faster velocity). Comparing this shift (of the deviation of the cyclic data from the predicted line) for the oven dried case and the oven dried and rewetted case, the interpretation is that this additional mechanism was dependent on the available water or, at least, on the relative humidity. Although the cyclic amplitude was slightly different for the dry and wet cases (ξ = 0.66 and 0.8 versus 0.77), it was still possible to obtain a comparable measure of the shift in the cyclic V-K line from dry to wet conditions. In effect, this was achieved by comparing the left hand side V-K data line of Fig. 7.17(a) (with ξ =0.77) with the V-K data line on the left of Fig. 7.14 (albeit with ξ = 0.8). The relative shift in, say, crack velocity, at constant stress intensity, is approximately 5.4 orders of magnitude which is comparable with the corresponding static shift of 4.4 orders of magnitude reported earlier in section 7.3.2. This corresponds to a lateral shift, or ratio between $\frac{K_{Idry}}{K_{Iwet}}$ of 1.5 for the static case to 1.6 for the cyclic case. These results are also comparable with the static fracture strength ratios of dry to wet as discussed in section 7.3.1.3 and Figure 7.9.

7.3.2.3 The Effect of Temperature on Cyclic V-K Data

The effect of increased temperature of a water environment on the crack velocity under cyclic testing conditions is similar to the effect in static tests.

Cyclic V-K curve results, for a similar change in temperature from 25°C to 55°C, on specimens which had been conventionally cured for between 90 and 120 days (i.e. very similar to the static tests) were derived from observations of traces of crack length versus number of cycles. Typical results of such temperature changeover tests are shown in Fig. 7.20(a) using a zeta amplitude ratio of $\xi = 0.74 \pm 0.01$, for various average stress intensities, K_{av}. The V-K curve derived from such data is shown in Fig. 7.16.

From the results it is again apparent, as in the static temperature tests, that there is a significant increase in crack velocity with this temperature change, of approximately 1.3 ± 0.1 orders of magnitude, (at constant stress intensity), (cf. approximately 1.4 ± 0.1 for static tests), (i.e. 20 to 30 times). The results of the crack velocity increases due to temperature change for the cyclic data is depicted in a bar chart in Fig. 7.20(b).

Also included on the V-K graph Fig. 7.16 is the predicted crack growth velocity for stress ratio $\xi = 0.74$ based on the static V-K data lines for 25°C and 55°C. In both cases the predicted velocity line is very close to (but slightly to the right, i.e. lower velocity side, of) the experimental data. This would again suggest that the predominant mechanism of fatigue crack propagation is the same as the static mechanism and probably of a moisture assisted stress dependent nature. In addition, the rate at which this takes place is dependent on the temperature. This is discussed more fully in section 7.4, and is consistent with an Arrhenius type dependence of the rate of chemical reaction on temperature.

7.3.2.4 Effect of Cycling Frequency on Crack Growth Rate

(A) Moist Specimens This section parallels the frequency effect studies on compression prisms described in Chapter 4. The DT specimen changeover technique, in regions of constant K, is very suitable for investigating the effect of frequency on crack growth rate. The test frequencies used were 0.1, and 10 Hz.

Typical changeover results showing crack length as a function of number of cycles for these frequency tests are shown in Figs. 7.21(a) and (b). It is clear that under constant conditions (of environmental moisture, load amplitude, and frequency) the crack growth rate is constant and linear. If the cycling frequency is changed from, say, 1Hz to 10 Hz, the crack growth rate, (measured as a distance per cycle), immediately changes. This is quite distinctly a very real effect since changing the frequency back (to 1Hz in this case) results in crack growth rates comparable with the first regime of 1Hz testing. Such results are shown in Fig. 7.21 for wet cured mortar specimens tested in a moist (RH-75-95%) condition for frequencies from 0.1 to 10Hz. Great care was taken to ensure that the region over which these frequency changes were made and corresponding crack velocities measured, was in the central constant K portion of the specimen, i.e. the central 80mm for these specimens.

Several of these crack growth versus number of cycles traces, similar to Fig. 7.21 were obtained and from their slopes a plot was made of crack propagation rate, $\frac{da}{dN}$, against frequency, Fig. 7.22(a). The scatter appears to be large, but when the standard deviation is plotted this scatter is significantly reduced Fig. 7.22(b). The scatter may also have resulted from the (small) range of average stress intensities K_{av} used. This is discussed in more detail subsequently.

Consideration of these results (plotted on a log scale) suggests that crack propagation rates as a function of time should be plotted, i.e. crack growth rate per second, $\frac{da}{dt}$, as opposed to per cycle, to test for any true frequency dependence. Replotting the lower trace of Fig. 7.21(b) as a function of time one obtains Fig. 7.23(a) and the time dependent equivalent of Fig. 7.22(a) is shown in Figure 7.23(b). These latter results would seem to indicate that the crack propagation is not,

as would first appear from Fig. 7.22(b), strongly frequency dependent, but rather more dependent simply on elapsed testing time. This is corroborated by Figs. 7.23(a) and (b).

Any change in crack velocity (as a function of time) due to change in cycling frequency can thus be regarded as relatively small. It is, however, arguable that there may be some small remaining frequency dependence of crack velocity on frequency.

If the data used to plot the previous figures, and in particular Fig. 7.23(b), is replotted as a V-K curve to investigate any frequency dependence, it is apparent that there is no frequency distinction (Fig. 7.24). The data was obtained over a small range of average stress intensity, K_{av}, since the specimen dimensions, particularly web thickness, showed some very slight changes. Attempts to accommodate the variations to maintain constant stress resulted in a small range of K_{av} and also stress amplitude, ξ . The range of the stress amplitude ratio, ξ, for this data was from $\xi = 0.85$ to $\xi = 0.64$ and the predicted cyclic crack velocity lines based on the static V-K data line for such moist specimens are also shown in Fig. 7.24 (as full lines). The data appears to be contained within the prediction lines. From the data in Fig. 7.24 there is no clear separation of crack velocities as a function of frequency, although it could be argued that there is a greater preponderance of low frequency results yielding lower velocities and higher frequencies yielding higher velocities. This small, true "frequency effect" is discussed in more detail in section 7.4.5.

(B) Dry Specimens Similar results were obtained for mortar which had been cured for 35 to 56 days and then oven dried. Crack length versus number of cycles traces (similar to Figure 7.21) were used to plot crack velocity (per cycle, $\frac{da}{dN}$) against frequency, in a manner analogous to Figures 7.22 and are shown in Figure 7.25(a). Once again, plotting true crack veolocity, as a function of time, $\frac{da}{dt}$, for this data against frequency one obtains virtual frequency independence (Fig. 7.25(b)), or strictly pure time dependence.

It must, however, be borne in mind that these "dry" tests actually may have a humidity up to 25% (although it was probably closer to 10%) and so

a mechanism of a form of stress dependent moisture assisted attack or stress corrosion could still be valid. For example, Wiederhorn (353, 340) reports only major reductions in stress corrosion below approximately 1 to 8% relative humidity, for ceramic materials. The actual crack veolocities/stress intensity curves have not, however, been included as these are simply consistent with the data shown in Fig. 7.25 and similar to Fig. 7.22.

7.3.2.5 Other Results

Finally, before leaving this results section it is worth noting that many of the cyclic fatigue crack propagation traces (crack length versus number of cycles) exhibited a type of intermittent crack growth behaviour. The characteristic is essentially one of temporary arrest. The crack appears to grow linearly for a period, then is arrested, then subsequently moves on again, at the same growth rate, (See Figs. 7.26 and 7.20(a)). This is discussed more fully in the following section.

This concludes the section on crack growth results. Tests of waveform and stress range effects were not considered based on the results of the compression tests. Discussion and interpretation of all these crack growth results follows in the next section.

7.4 Discussion

7.4.1 Introduction

The previous section has described the V-K curve results for various conditions of curing history, environmental moisture and temperature. In this section the signficiance of these results is discussed.

All the V-K results appear to indicate a linear dependence when plotted on log-log axes, i.e. the relationship between crack velocity and stress intensity does indeed seem to be covered by equation 7.2 mentioned earlier.

Implicitly this assumes that the data refer only to region I of the full characteristic V-K curve, Fig. 6.8, which is consistent with stress corrosion, or chemical rate dependent, behaviour.

In all the V-K curves derived from the available data the stress corrosion index n was measured as n = 26 $\pm$ 4. This compares with other values in the literature for cement paste (see Table 6.5) and in particular those obtained by Nadeau, Mindess and Hay (284) of 36, and for mortar, by Evans (285) of 30. In addition, it is of interest to note that the index n reported by Atkinson (326) for a fine grained quartzite rock was n=25.1 $\pm$ 1.5; while for glasses n was reportedly 17 to 24, (354, 353).

It is particularly interesting to examine the effects of environmental moisture content and temperature, as well as other parameters on the V-K curves and these are discussed below.

7.4.2 Effect of Moisture

From the analysis due to Evans and Fuller (235) it was possible to derive predicted intercepts and in effect "positions" for cyclic V-K lines from the static crack propagation data, once the waveform and ratio of cyclic stress amplitude to mean stress level, ξ, was known. This assumes, fundamentally, that if the mechanism of failure is the same in fatigue as in static conditions the cyclic data will fit the predicted cyclic line. Correlation between experimental cyclic data and the predicted cyclic V-K line was seen to be very good, for example see Figs. 7.17 and 7.16. However, there was in addition an indication of a small deviation of the cyclic data from the predicted line in Fig. 7.14. This is interesting and appears to be significant despite the fact that the scatter is not small. The curing and testing situation referred to in Fig. 7.14 was one of young samples oven dried at 7 days and tested in a wet condition. In this respect they are not fully hydrated and may exhibit this deviation from predicted behaviour as a result of these two parameters, aqueous environment and degree of hydration. By contrast, young (7 day old oven dried) specimens tested in a dry environment (RH $<$ 25-10%) exhibited only very small deviations from the normal predicted "stress corrosion" line, Fig. 7.17. In addition, fully wetted specimens (tested under water) which had been well cured (age 90 - 120 days) appeared not to exhibit significant deviation from the predicted cyclic lines (Fig. 7.16).

The implication of these observations is that, if the mortar is relatively well cured, the crack propagation behaviour in a cyclic mode can be predicted from static data and so is presumably occurring by the same mechanism as the static failure, (235), i.e. a type of stress corrosion. On the other hand, for mortar that is, relatively, uncured (e.g. seven days) the deviation from the predicted line is larger (Fig. 7.14), suggesting that for poorly cured mortar there is an additional cracking mechanism in fatigue. This may well be present in well cured mortar but is not as noticeable as the magnitude of its effect is less. Also, the deviation from the predicted line may also possibly depend on the available water present (or relative humidity) as evidenced by Figs. 7.14 and 7.17. This influence of water-assisted cracking over and above the predicted stress assisted environmental attack or stress corrosion is of particular interest and is discussed further in section 7.4.5.

7.4.3 Failure Mechanisms

Returning to the mechanisms of failure in mortar, for both static and cyclic modes, in high water content environments, it is recognised that a mechanism of stress assisted environmental attack or stress corrosion may be largely responsible. Indeed, the analysis of Evans and Fuller (235) is germane to the predicted cyclic crack propagation lines fitting the cyclic data.

The postulate of a stress corrosion mechanism for cracking in rock which may be applicable to our system (326), is that crack propagation in region I of Fig. 6.8 where V is proportionate to K_I is controlled by the rate of reaction between the corrosive environment and the material at the crack tip; in region II it is controlled by the rate of transport of corrosive species to the crack tip and V is virtually constant and in region III by some mixture of fast mechanical failure and fracture facilitated by the corrosive action of the environment. It would appear, in the case of cement materials, that there are no transport difficulties of corrosion species to the crack tip as the environment is contained in the material. Thus we might only expect to observe region I behaviour and this is indeed the case.

The question of whether conventional V-K curve behaviour may be expected to occur in very dry environments, arises, especially in view of the stress corrosion mechanism proposed here. The so called "dry" environmental regime used in the present tests was not completely dry, with a relative humidity of between 10 and 25%. It was mentioned earlier that Wiederhorn (340, 353) observed that water presence as low as 0.017% relative humidity can readily lead to conventional SCC attack of silicate bonds (for glass at least) and standard stage I V-K behaviour (Fig. 7.27). Thus it seems reasonable that stress corrosion cracking may indeed be a viable cracking mechanism in the present dry test programmes. Reduced water content (or reduced humidity) simply result in a reduction in the crack velocity which is seen as a shift (to the right) of the V-K curves, analogous to Wiederhorn's results (Fig. 7.27).

7.4.3.1 Crack Propagation Activation Energy

It is beneficial first to consider the general sequence of events for stress corrosion cracking in a material before appropriate application is made to cement systems. Considering, then the general case and region I and following the argument developed by Wiederhorn for glass (340, 853), it is reasonable to assume that crack advancement depends on a heterogeneous reaction between the material bonds and the environment at the tip of the crack. The reaction at the crack tip presumably occurs by 5 sequential steps, the slowest of which determines the rate of the overall process. The successive stages are (i) transport of the reactants to the tip (ii) adsorption (iii) reaction at the tip (iv) desorption of the products and (v) transport of the liberated products away from the surface.

In the case of cement material stage (iii) would appear to be the limiting rate controlling one because fresh fracture surface is continually being exposed, there is ample supply of corrosive reactant species (water) and adsorption can readily occur. It is also worth bearing in mind that for cement mortar, although a "one crack" situation is envisaged for the DT specimen, the so-called crack "tip" actually probably constitutes a small multiple cracking process zone. This is localised near the boundary of the single crack because of the notch or single crack stress concentration, and for discussion purposes here is regarded as the crack tip.

It is recognised (309, 310, 326, 327, 353, 355-357) that the large body of results from subcritical cracking studies for a variety of materials, including cement and mortar, can be described by the equation

$$V = V_o \exp\left(-\frac{\Delta H}{RT}\right) K_I^n \qquad 7.5$$

where V_o and n are experimentally determined constants. ΔH is the activation enthalpy, R is the gas constant and T the absolute temperature. A means of obtaining activation enthalpy from constant strain rate constant load DT tests has been described by Evans (309) and Atkinson (326). This chemically-assisted mechanism of fracture depends on an Arrhenius type of equation (354) equation 7.5, and is in competition with other diffusion and plastic flow mechanisms. For glass these mechanisms have been very adequately reviewed by Wiederhorn (353). However, it is reasonable to disregard these latter mechanisms (i.e. diffusion and plastic flow) and consider chemically assisted stress corrosion fracture as the most plausible. The motivation for this is that efforts at quantifying the diffusion concept yield processes that are too slow (353) and plastic flow processes have only been observed to occur at unreasonably high stresses (353).

From the data presented in Fig. 7.15 and 7.16, for static and cyclic data, it is possible to determine the stress corrosion activation energy for crack initiation and propagation in these mortar specimens using the Arrhenius equation above (equation 7.5).

Substitution of data from Figs. 7.15 and 7.16 into equation 7.5 yields values of 20 to 24 kcal/mol (i.e. 83 to 99 kJ/mol). These compare with a chemisorption activation energy of approximately 20kcal/mol (202) for concrete and stress corrosion crack propagation activation energies for (a) a fine grained quartz (201) of 70 kJ/mol and (b) for glass (353, 356) of 24 to 33 kcal/mol (i.e. 100 to 140 kJ/mol). For cracking in PZT and silicon nitride (both much tougher materials) activation energies have been found to be 100 kcal/mol (327) and 170 kcal/mol (144) respectively. No other comparative crack propagation activation energy data are apparently currently available for cement or mortar. This activation energy does, however, appear to be of the right order of magnitude and reinforces the belief that the mechanism of crack propagation of mortar

in high humidity environments, under both static and cyclic conditions is one of stress-assisted environmental attack or stress corrosion.

It was shown in section 7.3.2.3 that the increase in crack growth rate due to temperature increase from 25°C to 55°C was 1.3 $\pm$ 0.1 orders of magnitude (i.e. about 20 $\pm$ 4 times). Substitution into equation 7.5 of the above value for activation energy of 83 kJ/mol and absolute temperatures of 298 and 328 °K (equivalent to 25 and 55°C respectively) and with the gas constant of 8.314 J K^{-1}, a crack growth rate increase of about 22 times is arrived at which is completely consistent with Figs. 7.15, 7.16 and 7.20 (a).

7.4.3.2 Long Term Time-Temperature Effects

The actual mechanism of attack is not yet resolved. Barrick and Krokosky (29), Husak (250) and Husak and Krokosky (30) regard static fatigue in Portland cement as the result of chemical attack on highly stressed Si-O bonds. They see the behaviour of water on cement as similar to that of water on other silicate materials, in line with theories by Charles (259) and Charles and Hillig (358) for glasses. The former authors propose that hydroxyl ion attack on the silicate network is the dominant mechanism and this is discussed in more detail subsequently.

Another possible mechanism that may account for the stress corrosion of cement is the type of Rebinder Westwood effect described by Cuthrell (205, 359), as being dependent on the embrittling effect of hydrogen present in the aqueous solution (in this case, water). Cuthrell observed such hydrogen embrittlement in aqueous environments for a vast range of materials including ceramics, granitic rocks, glasses, silicon as well as various steels.

The results discussed so far regarding the increased rate of crack propagation with temperature (see for example Fig. 7.20(a), have been restricted to relatively short time durations. Temperature changes from 25°C to 55°C on the very same specimen undoubtedly resulted in an accelerated crack velocity in cyclic fatigue, and also static conditions, (Figs. 7.20(a), 7.15, 7.16). However, it was also observed that this rate of crack propagation at the higher temperature was not always maintained. In several cases the rate of crack propagation, initially

faster at the higher temperature, slowed down even to levels below the original low temperature crack propagation rate. Such behaviour is shown in Figs. 7.28 (a) and (b) for underwater conditions and temperatures of 25^{o} to $55^{o}C$.

There does not appear to be a simple explanation for this behaviour. Care was taken to ensure that it was not the result of non linear specimen conditions with the crack moving outside the region of constant stress intensity K. The following discussion is, however, put forward to explain this phenomenon of crack growth rate slowing down, but far more detailed experimental studies will need to be conducted at a future stage to confirm both the results and the implications of the results, before the argument proposed can be fully accepted.

Barrick (106) and Barrick and Krokosky (29) report an increase in static fatigue life with temperature for flexural mortar specimens tested at various relative humidities and temperatures. Their findings of increased static fatigue life, see Figure 4.44(a), with temperature increases from $25^{o}C$ to $60^{o}C$, appear at first to be in direct contradiction to the present results reported here, where an increase of approximately 30 - 40 times in crack velocity is noted. For his results, Barrick attributes the increased static fatigue life with temperature to a reduction in the hydroxyl ion content. This he regards as being principally supplied by the $Ca(OH)_2$ in the mortar and the prime driving force in the stress assisted cracking of the calcium silicate of his samples.

The origin of Barricks (106, 29) hydroxyl ion attack is based on the last two stages of Charles three stage theory for this attack of silicate bonds (259). In this case the Barrick modified Charles mechanism is as follows:

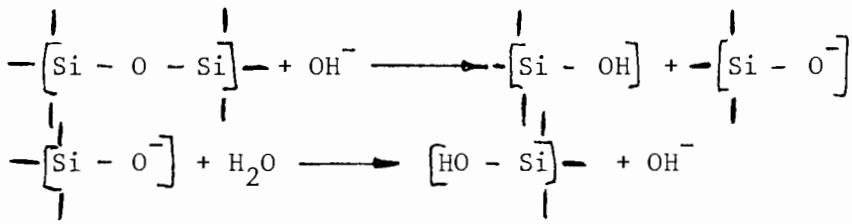

The hydroxyl ion attacks the silicate network, leaving a chain terminated by silicon hydroxide and an ion of silicon oxide. This latter is unstable and readily combines with water. The reaction is autocatalytic: the complete reaction results in the formation of reactants for the continuation of the process. If Barrick's proposal is correct, and there is some controversy over its validity (112), it is possible that the above (present) data can explain both effects. (Certainly if the mechanism is one of OH^- diffusion similar to that in quartz, where White (360) reports an activation energy of 63 kJ/mol, there appears to be approximately sufficient energy for this process to occur).

The effect of a temperature increase in the present tests is to increase the crack velocity as indicated by the V-K curves, Figure 7.16. However, this increase is only observed to be maintained for a relatively short time, of the order of 500 - 1000 seconds, before subsequently decreasing (Figures 7.28(a) and (b)). The long term effect of a temperature increase from 25°C to 55/60°C may well be a reduction in crack velocity and a consequent increase in failure time as reported by Barrick. Data for the rate of velocity decrease after temperature change is limited and more extensive experimental studies need to be conducted before this aspect of the long term effects of temperature increases is confirmed. Nevertheless, such data is plotted in Fig. 7.29 and although the scatter is large the velocity is seen to decrease approximately exponentially with time, i.e. $\log v = -bt$ where b is a constant. Such dependence is consistent with a time dependent change in solubility of $Ca(OH)_2$ with temperature as suggested by Barrick (Fig. 4.45). In essence, what this implies is that immediately the temperature is changed there is an increase in crack propagation rate due to stress corrosion, as mentioned above i.e. in accordance with equation 7.5. However, with time (within 10 to 30) minutes the rate of crack propagation decreases because the proportion of active hydroxyl ions, which presumably attack the bonds of the crack tip, is significantly reduced because the solubility of $Ca(OH)_2$ decreases, (29), Fig. 4.45.

An alternative approach is to regard the decrease in crack propagation rate at 55°C as a recovery process, since the material ahead of the crack tip is exposed to the higher temperature for longer and has

sufficient time to exhibit increased strengthening similar to the mechanism outlined in Chapter 5 of accelerated curing and hardening. No attempts, however, were made to verify this. An attempt could be made in the future to evaluate any accelerated curing at high temperature ($55^{o}C$) by testing DT specimens which had been differently "heat treated". Comparative crack propagation studies could be undertaken on DT specimens which had had the first half (or the second half) of the DT specimen heated to $55^{o}C$ for varying periods. Tests then conducted in cold water ($25^{o}C$) would reveal any change in crack growth rate at the transition where the material had been heated. Such tests provide in a sense a "double check" since crack propagation direction could be undertaken on the very same specimen from hot cured to cold cured, or from cold cured to hot cured.

7.4.4 Effect of Frequency

The above discussion has been limited to data obtained at a single frequency (of 1Hz), for different temperatures), and not various frequencies. It was shown in Figs. 7.22 and 7.23 that the effect of cycling frequency had a very small effect (if any), on the crack propagation rates when these were expressed as a function of time. Such behaviour is consistent once again with a stress corrosion (time dependent) mechanism and so appears to vindicate further the discussion concerning stress-assisted, water-dependent environmental attack at the crack with the associated activation energies. However, it could be argued from Fig. 7.24 that there was, in fact, a slight polarisation of lower cycling frequencies yielding lower crack velocities, and higher frequencies higher velocities. This would suggest that, in addition to the crack propagation mechanism being predominantly one of stress assisted environmental attack or stress corrosion, as had been established, there is possibly some other crack assisting effect which is frequency dependent. Such a mechanism involving water pressure assistance i.e. a "hydrowedge" effect, is discussed more fully in the following section where it is related to compression and acoustic emission data.

7.4.5 Hydrowedging: Mechanically Assisted Fatigue Crack Propagation due to Water

It is suggested that an acceleration in the rate of crack propagation can occur due to water or debris being trapped in a closing fatigue crack, the so called "hydrowedge concept". Evidence in support of such a contention includes the following: substantial acoustic emission on unloading of compression specimens, under moist conditions, of the formation of so called "chains" (Figs. 3.25(c), 3.28(b), 3.28(c), 4.8(a)(b) and 4.13); AE chains occurred predominantly in the last 20% of the unloading cycle (Fig. 4.14(a)); AE chains only in wet (or underwater tests (Fig. 4.15) and not in dry tests (Figs. 3.28(a), 4.11(a); and a small but real frequency dependence that could not all be explained by pure time duration considerations (Fig. 7.24), i.e. higher frequencies gave slightly shorter times to failure, (Fig. 4.29).

The waveform tests (section 4.4) indicated that there was no significant difference in the fatigue life as the result of fast or slow fatigue loading, which might militate against the hydrowedge concept. It may well be, however, that the rate differences were not sufficiently great at 1 Hz to show any distinction, i.e. 1Hz is already sufficiently fast for "hydrowedging" to occur. It may be instructive to conduct slow sawtooth tests, i.e. with a period of say 5 seconds but still with a fast unloading (or loading) portion, for comparison.

Williams regards the fluid as not being completely expelled when the crack closes during the unloading half cycle and thus work is done on closing - even if only a monolayer of water remains (352). The most probable manifestation of this work is in deformation of the material around the crack depth in compression of the fluid. This fluid may not penetrate to the crack tip, as the crack is tight and probably wedge shaped. Thus the closing crack acts like lever arms about a fulcrum, leading to high stresses at the crack tip sufficient to cause local failure and thus propagate the crack. This would result in acoustic noise near the minimum load of the unloading cycle of compression fatigue tests, as observed.

Such a proposal is surprisingly not without precedent. Shah and Chandra (89) noticed in moist fatigue tests that the localised strain (and volume dilation) was greater at the minimum stress than the maximum stress. They also reported "an increase in (ultrasonic pulse) attenuation and decrease in velocity at the minimum rather than the maximum stress". This, they say, "would mean that during unloading there was either additional cracking or crack widening". Williams, in a discussion of sintered alumina, glass and oxide, has proposed that when a fluid within a crack is sufficiently compressed during crack closure, large enough stresses may be developed at the crack tip to lead to increments in crack length. Similar proposals were put forward by Evans and Linzer (324) to account for accelerated fatigue in glass but not for tungsten carbide cobalt.

In view of the relative success of the use of fracture mechanics to observe trends in cracking behaviour as described in this chapter it remains only to attempt to quantify this "hydrowedge effect" in the light of appropriate toughness and velocity values.

There does not appear to be, anywhere in the literature, a rigorous analysis of pressure or stress intensity changes due to hydraulic effects in a closing crack, the hydrowedge effect. Plumbridge (361) however, has referred to the hydrowedge concept without giving any detailed analysis. Such an analysis would presumably need to take into account flow velocity v, local toughness K_{Ic} shear modulus G, dynamic viscosity μ, crack dimensions and distance x, from the crack tip, crack angle α, and also the angular rate at which it closes ω.

For a closing crack considered in the form of a wedge, an analysis by the author based on Ireland's book (362) (Appendix D) gives the pressure differences ΔP, due to viscous effects (but ignoring inertial and turblence considerations) as

$$\Delta P = \left\{\frac{6\omega\mu}{\alpha^3}\right\} \ln\left(\frac{x}{a}\right) \qquad 7.6$$

where x is the distance from crack tip of length a and the other symbols have the meanings shown above.

Wiederhorn (353) considered an opening running crack with a parabolic shaped tip and obtained the following expression for pressure difference:

$$\Delta P = 6\pi v\mu \left(\frac{G}{K_I}\right)^2 \ell n\left(\frac{x}{a}\right) \qquad 7.7$$

where G is the material shear modulus and K_I the applied stress intensity factor.

The corresponding change in stress intensity ΔK due to the moving liquid he calculated (in SI units) as

$$\Delta K = 13.1\ v\mu\left(\frac{G}{K_1}\right) \qquad 7.8$$

Now Wiederhorn's approach (353) has been for an opening propagating crack (which does not close). However, if a closing crack produces similar pressure differences, but of a different sign, it may be possible to compare the author's above estimates for a closing wedge with Wiederhorn's equations and use them as an approximate guide as to whether the hydrowedge concept is a plausible mechanism of increasing crack rate.

The following values of the physical parameters were used for substitution into equations 7.6 to 7.8: viscosity, $\mu = 1.2 \times 10^{-2}$ Ns/m^2, crack thickness $t = 10^{-2}m$, $\theta = 1.75 \times 10^{-3}$ radians, $\omega =$ 0.002 rads/sec, crack length a = 1mm, distance from crack tip, $x = 1$ $10^{-6}m$, $G = 1.75 \times 10^3$MPa, stress intesity toughness K = 0.5 MPa $\sqrt{m}$, fluid velocity v, 2×10^{-3} m/sec. Using these values, equations 7.6 and 7.7 yield respectively pressure difference values of 0.18 and 2.8 MPa, and the stress intensity difference (of equation 7.8) is $\Delta K = -0.016$ MPa $\sqrt{m}$.

These values are not insignificant, as for example, the deviation of fatigue crack growth data from that predicted by the Evans and Fuller g factor analysis (235) is of this order ($\Delta K \simeq$ 0.01 to 0.02 MPa $\sqrt{m}$) for wet specimens (Figs. 7.14 and 7.16). This suggests that the hydrowedge concept may be meaningful but is only so if the parameters and equations chosen above are valid, and in particular that the water velocity is relatively high ($\simeq 2 \times 10^{-3}$ m/sec). If the angular velocity and the water velocity locally were low, say less than 10^{-4} m/sec (more in

keeping with the actual crack velocity) then such viscous (and inertial) contributions would be negligible.

It would appear from the above analysis that the hydrowedge concept may indeed be viable and would explain many of the observed phenomena listed at the start of this section, 7.4.5. Extensive further investigation is required, however, before the concept may be considered as a major contributory cause to fatigue cracking in moist or wet environments.

7.5 Conclusions

(i) A detailed experimental fracture mechanics programme has been employed using the double torsion system to evaluate the fracture of mortar specimens under various conditions. The values and limitations of the double torsion system have been reviewed and the experimental techniques by which data was obtained have been described.

(ii) Methods of observing the crack tip in dry, moist and underwater conditions have been developed and utilised for the generation of V-K data.

(iii) Crack velocity stress intensity V-K curves were obtained using the techniques of load relaxation at constant position, and to a lesser extent, by using constant ramp rate/ constant load static methods, and found to be comparable.

(iv) Extensive tests were also done in a cyclic fatigue mode for a variety of parameters including frequency (0.1, 1 and 10 Hz), moisture environment (relative humidity from 10-25% to underwater RH 100% tests), temperature ($25^{o}C$, $55^{o}C$), and curing history (seven day oven dried to 18 month old wet specimens).

(v) V-K curves have been obtained from both static and cyclic fatigue test programmes under various test conditions and appears to be the first work of its kind. The static and fatigue V-K results are similar in that:

(a) changing from a dry (< 25% RH) to a wet condition results in an increase in crack growth rate of about 4.5 orders of magnitude,

(b) temperature increases from 25°C to 55°C indicate an increase in crack growth rate of about 1.4 orders of magnitude (i.e. about 25 times), and

(c) increased curing or hydration result in slower crack growth rates (See Figs. 7.14 to 7.17). In addition changeover fatigue tests from 25°C to 55°C resulted in an initial rapid increase in crack growth rate followed by an apparent slowing down of the crack growth rate.

(vi) The crack growth rate appears to be explained by an equation (7.5) which includes an Arrhenius type term viz:

$$V = V_o \exp\left(-\frac{\Delta H}{RT}\right) K_I^n \qquad 7.5$$

Here ΔH is the activation energy for crack propagation and is 20 to 24 kcal/mol (83 to 99 kJ/mol). The so-called "stress corrosion index", n, in this case was $n = 26 \pm 4$.

(vii) The outcome of these various tests would seem to indicate that the mechanism of failure and crack propagation in mortar is possibly one of stress corrosion, or stress assisted water attack at the crack tip. Cyclic prediction V-K lines based on static V-K data which depend on this mechanism appear to fit the empirical cyclic data quite well, particularly for low humidity and well cured specimen situations. The g factor prediction does, however, appear valid for all the variable moisture, temperature and frequency fatigue tests conducted.

(viii) In addition to the stress corrosion (time dependent) mechanism, there appears to be a small additional crack assisting mechanism particularly for (a) incompletely hydrated specimens (b) high humidity (or underwater) situations which (c) increases with cycling frequency. Such a behaviour is consistent with a pressure development or "hydrowedge" associated with trapped water on closure.

(ix) All the above studies on fatigue V-K methods applied to cement materials may be regarded as new and original work. Most of the static V-K studies complement scanty earlier studies in the literature by, for example, Mindess, Nadeau and Hay (105), but the treatment and range of test parameters is far wider here. Application of the g factor approach (235) to correlate static and fatigue mechanisms is new in its use to cement mortar as is the suggestion of an Arrhenius type of equation for cracking with corresponding activation energy.

Comparison of the double torsion (single crack) results and the compression tests is given in Chapter 8, together with a more detailed discussion of the nature of microcracking-including some in situ crack observation in a scanning electron microscope.

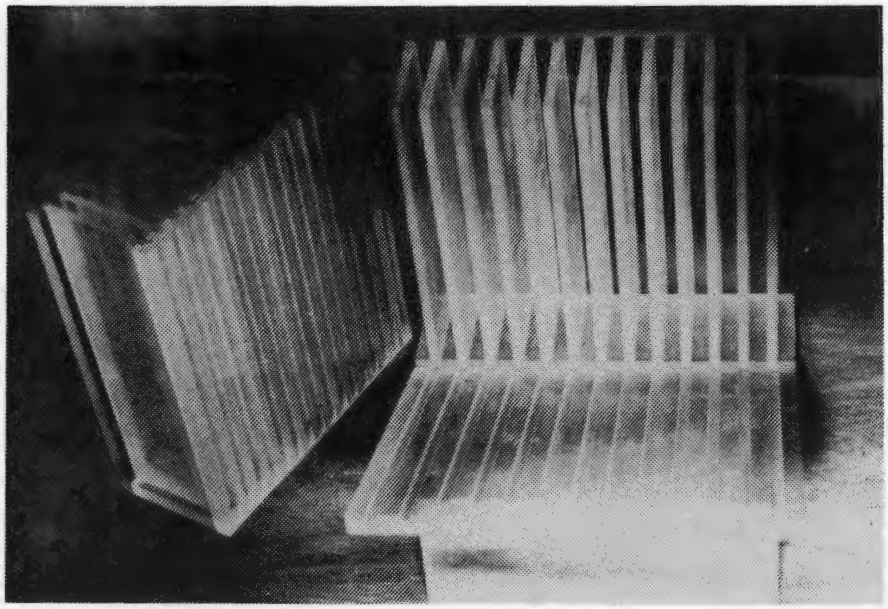

Figure 7,1(a) Photograph showing PMMA double torsion moulds.

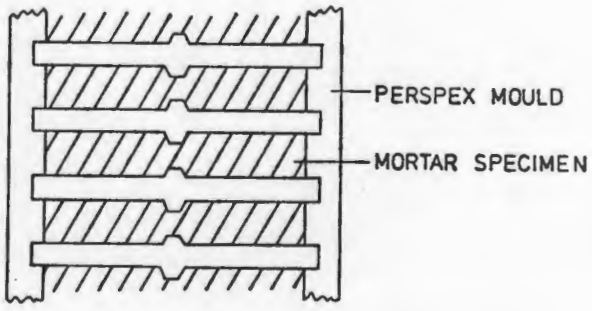

Figure 7.1(b) Moulds used in the DT pilot study showing the form of the "cast in" groove. The groove "bead" units were subsequently removed because of shrinkage cracks developing in the grooves, and only flat DT specimens cast.

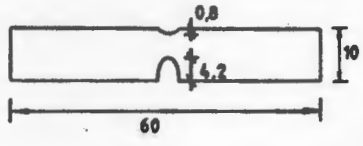

Figure 7.1(c) Diagram of the grooves used in the DT specimens.

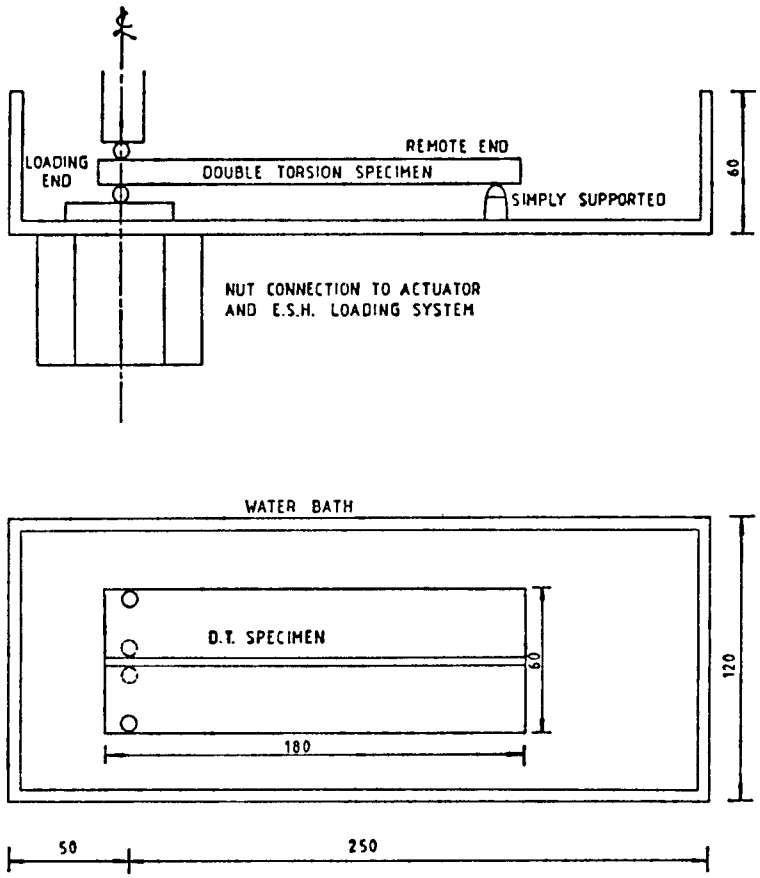

Figure 7.2(a) Diagram of double torsion loading system and test bath.

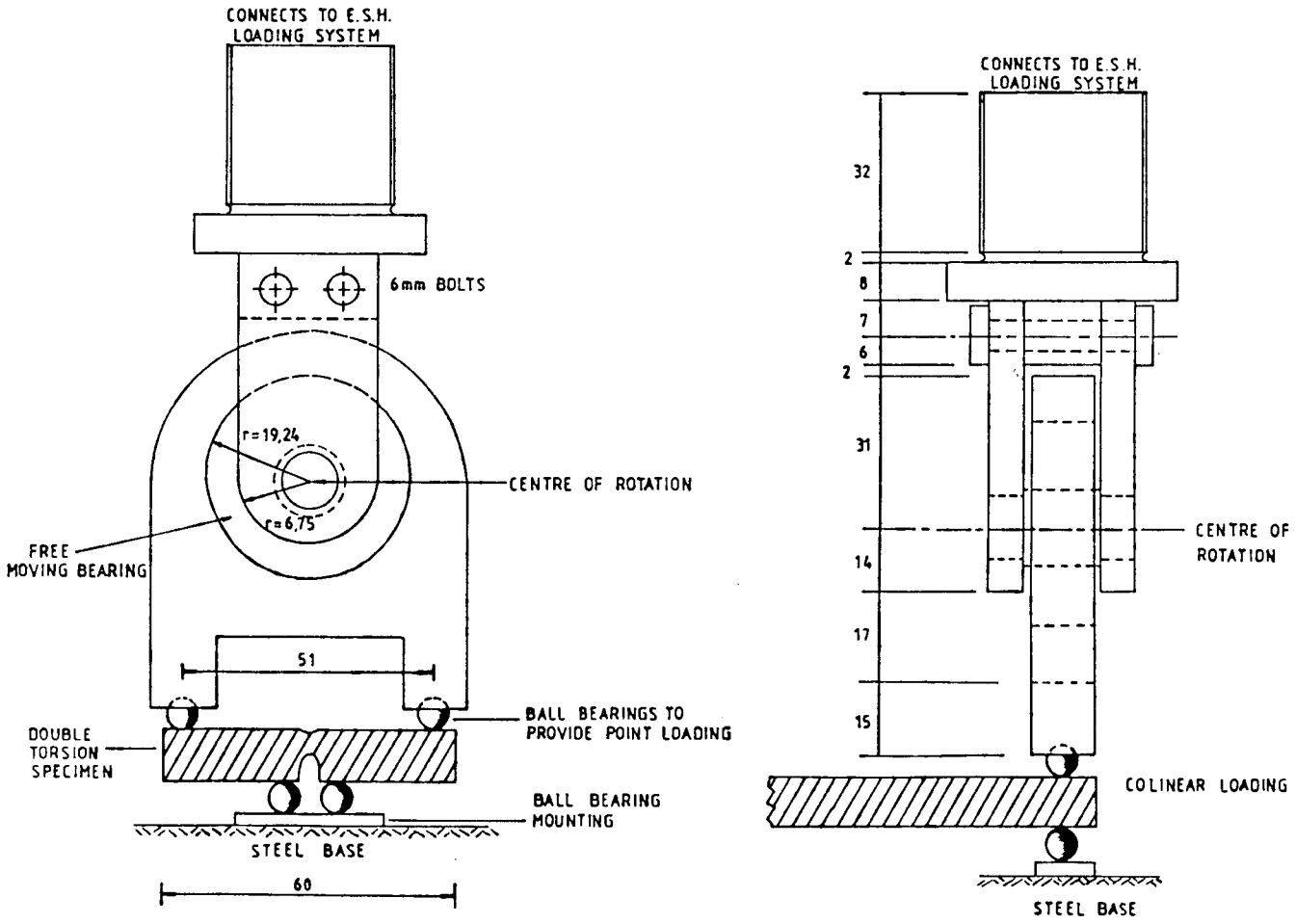

Figure 7.2(b) Drawing of the self aligning double torsion loading rig.

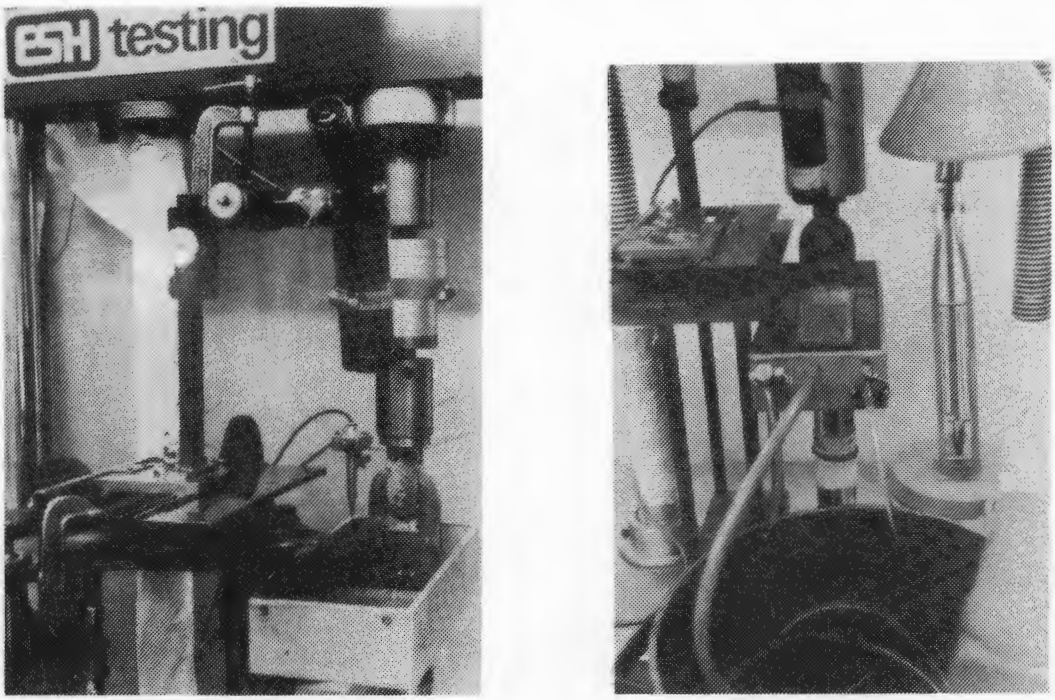

Figure 7.3 Photographs showing the double torsion loading systems together with LVDT position control, water bath unit and travelling microscope facility.

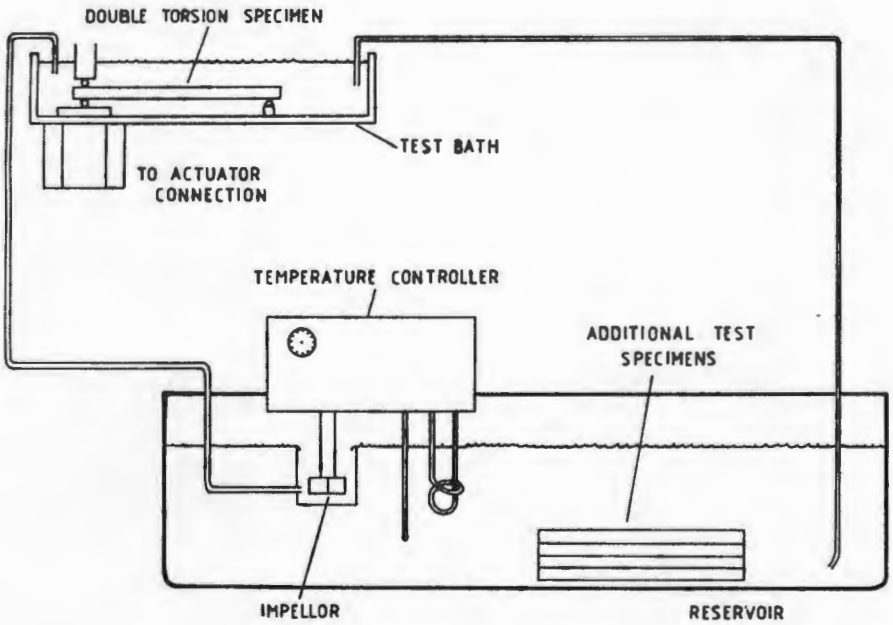

Figure 7.4 Diagram of the hot water reticulation system for temperature controlled static and fatigue double torsion tests.

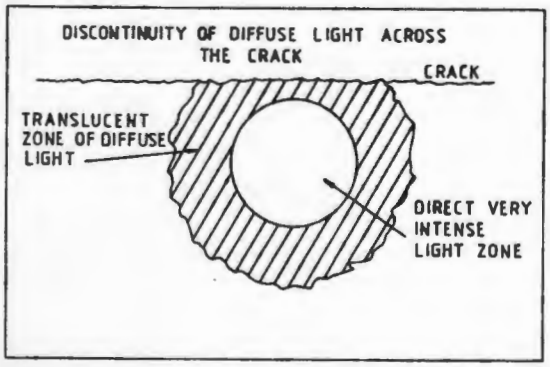

Figure 7.5 Diffuse illumination technique of crack observation. (From Higgins and Bailey 75).

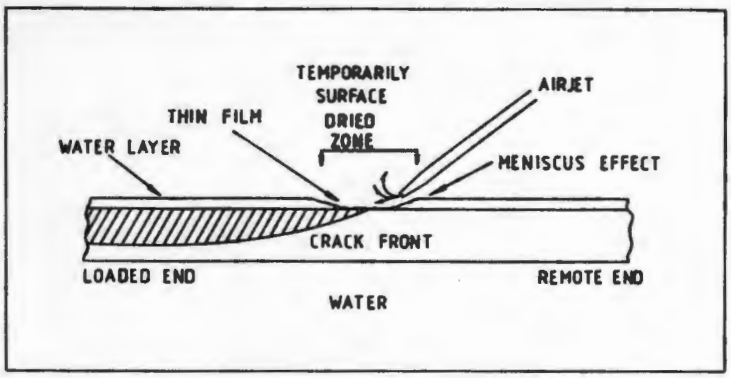

Figure 7.6 Schematic illustration of the air jet technique of manifesting underwater fatigue cracking by "pumping".

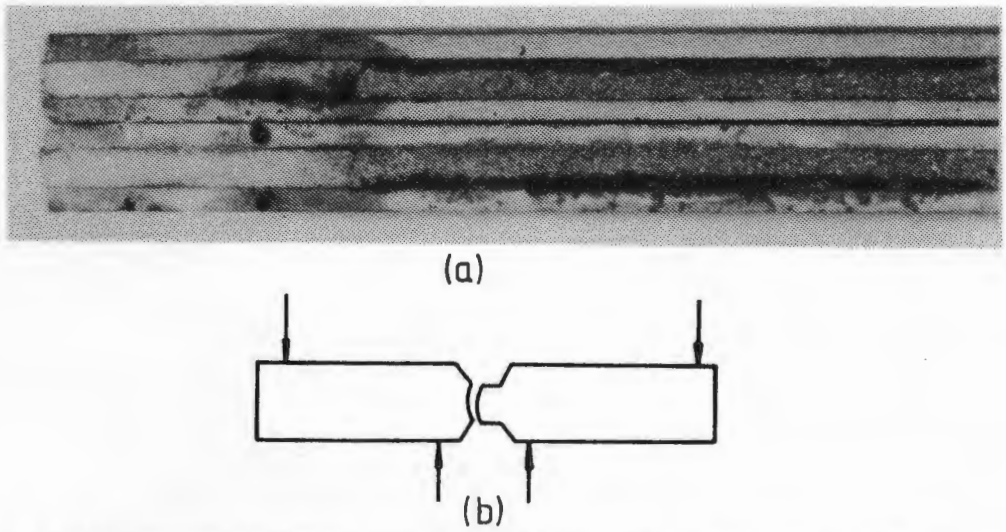

Figure 7.7(a) and (b) Crack profile for a typical cast in groove in a DT specimen. The crack front (as shown by the dye penetrant) is very shallow. The sample exhibited such surface cracking (b) in the corner of the groove at the stress concentration.

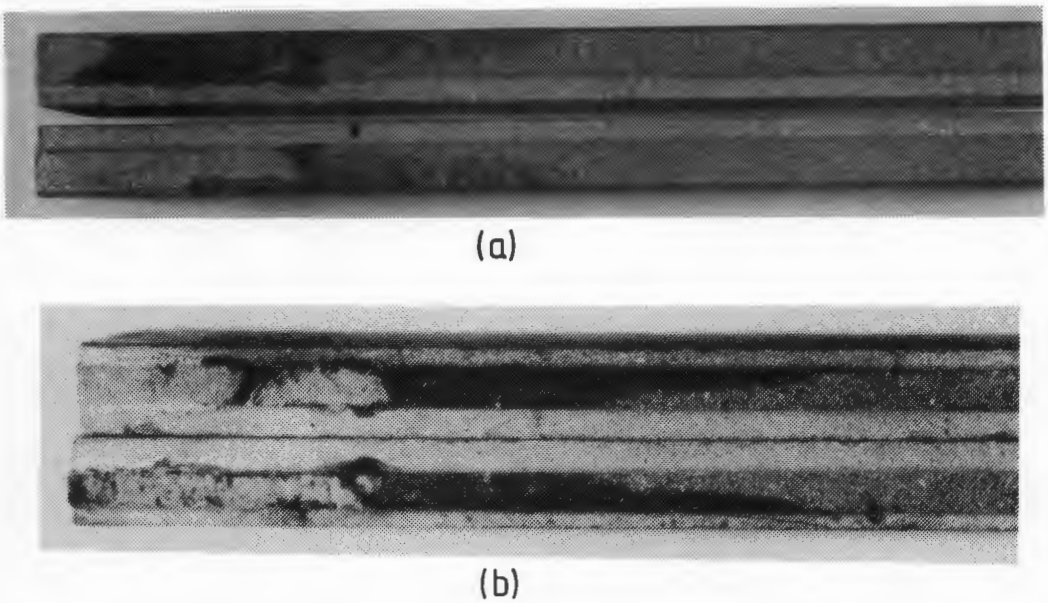

Figure 7.8 (a), (b) & (c) Crack profiles for deep compression grooves with only a small tension groove. This groove dimension with the deep groove on the compression face yielded the most suitable groove profiles of the investigation.

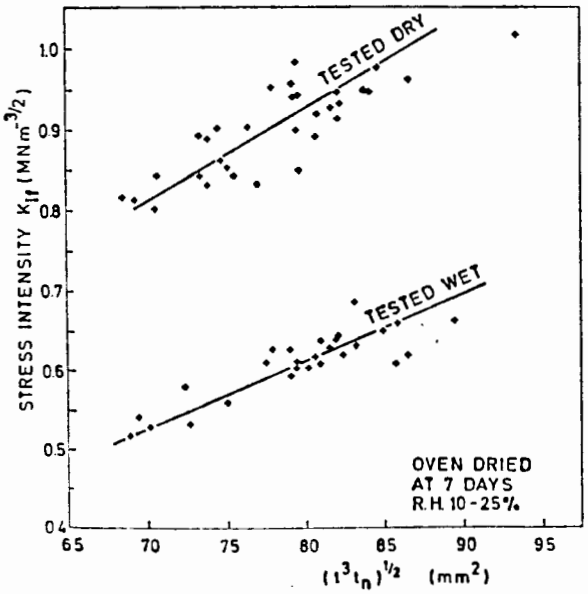

Figure 7.9 Variation of static stress intensity with specimen thickness parameters for dried and also dried and subsequently welted double torsion specimens.

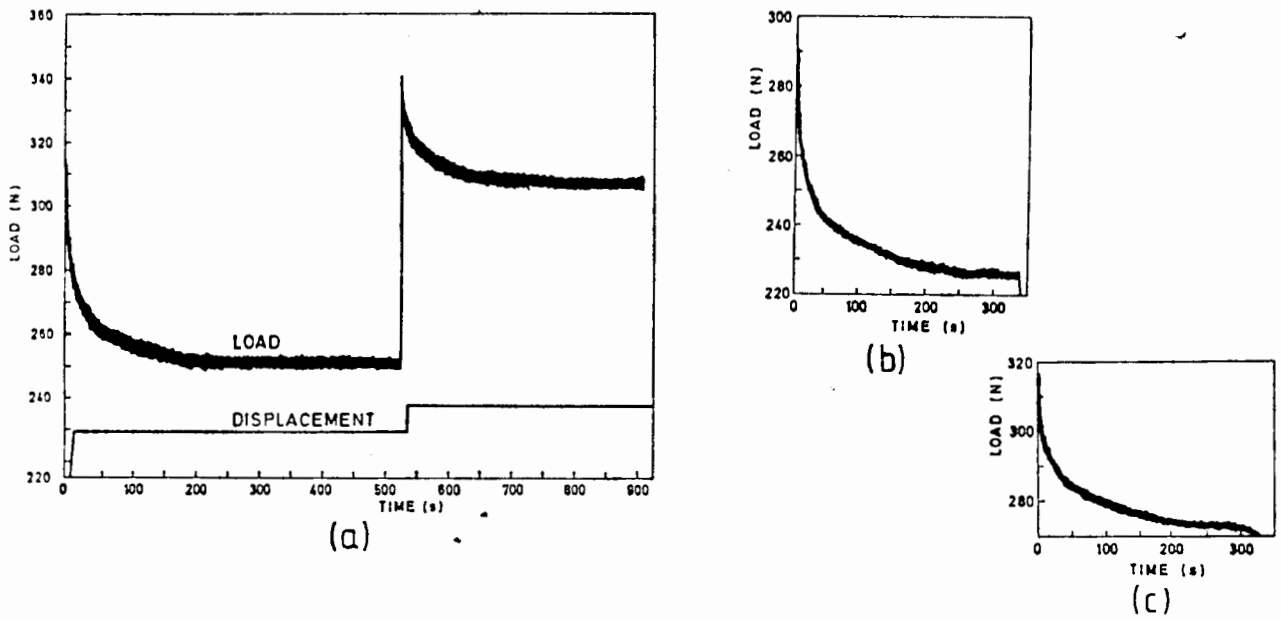

Figure 7.10 Typical quasi static, double torsion load relaxation curves (a), (b) & (c) at constant displacement.

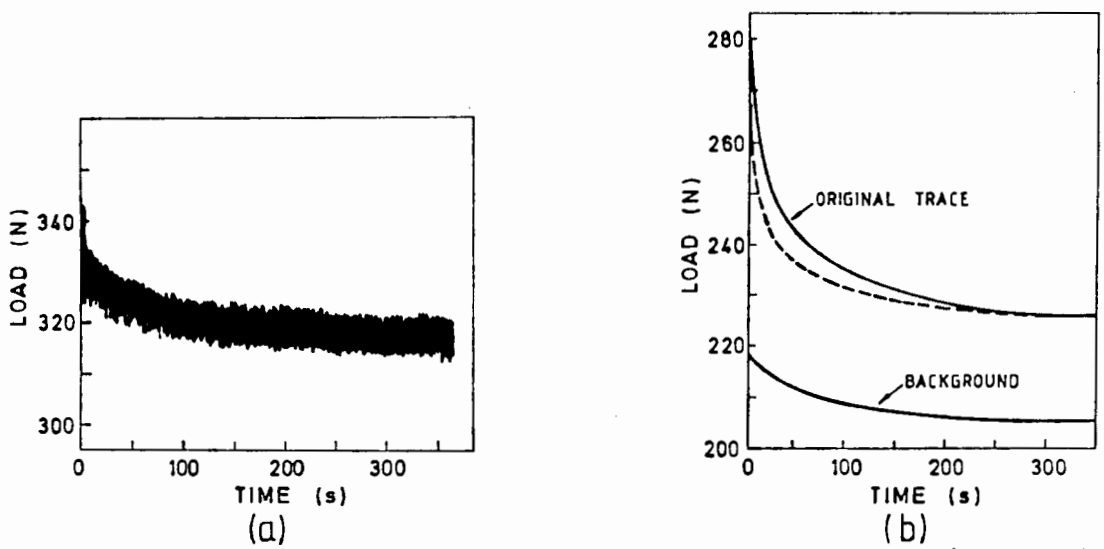

Figure 7.11(a) Background load relaxation for the quasi static, constant displacement DT tests. This background relaxation replotted in (b) is subtracted from a typical trace (e.g. Fig. 7.10(b) to provide the true load relaxation due to crack propagation, (shown dotted in Figure 7.11(b).

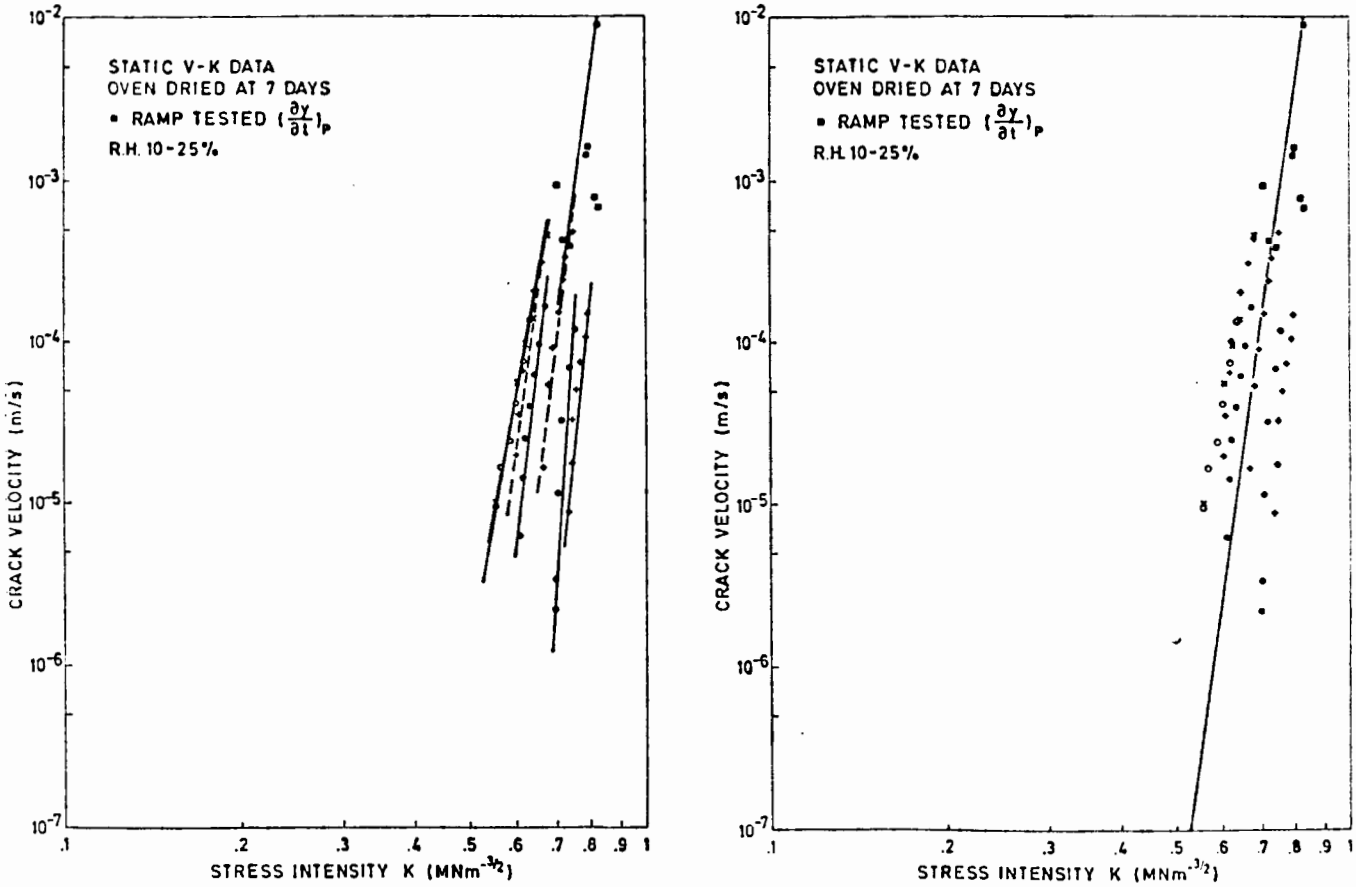

Figure 7.12 V-K data obtained from quasi static data for dry specimens, using predominantly load relaxation methods. Notice, however, the good correlation of ramp rate derived data (at constant load) with these load relaxation data.

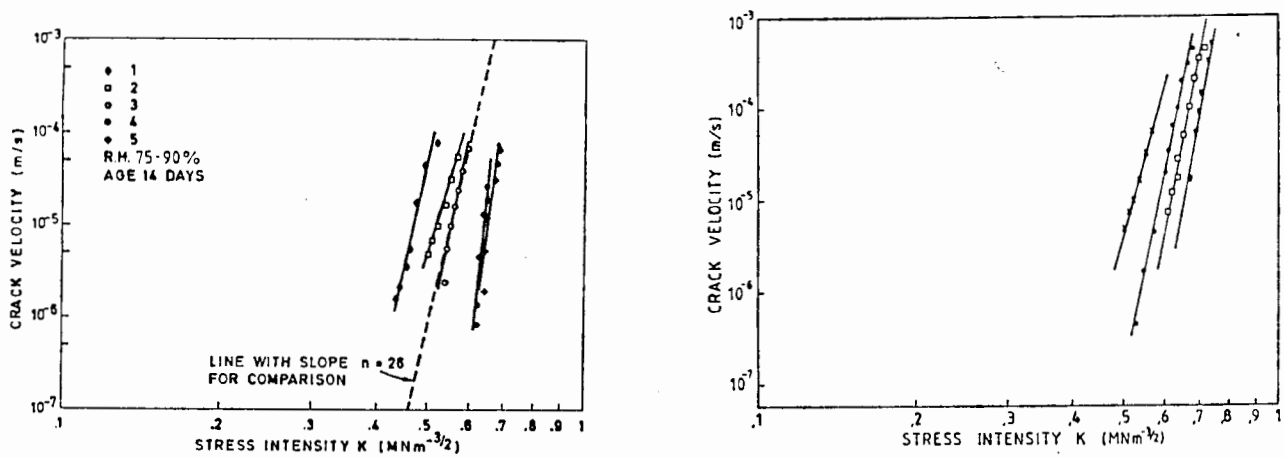

Figure 7.13(a) VK curves obtained from static DT load relaxation tests at 20°C under moist conditions. (a) The legend numbers refer to successive relaxations on the same specimen which indicates a shift to higher K values (at constant crack velocity). (b) Test results for four specimens aged 28-56 days at 20°C under moist conditions for first relaxations only.

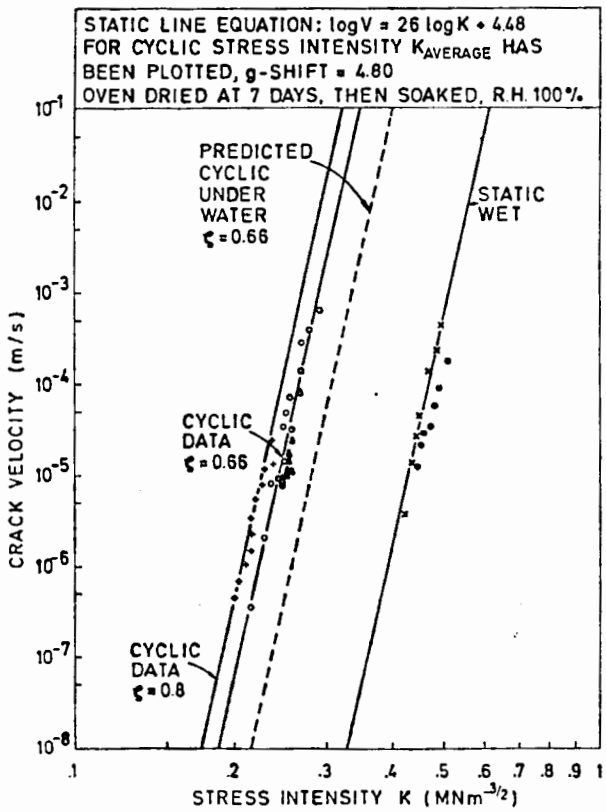

Figure 7.14 V-K curves for dried and then subsequently wetted DT tests, and including both static and fatigue results.

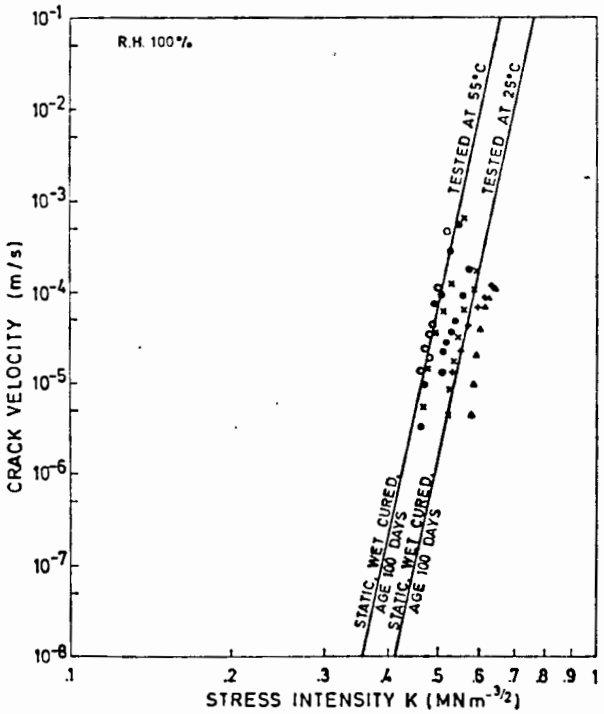

Figure 7.15 Static load relaxation based V-K curves for "old" DT specimens tested underwater at 25°C and 55°C.

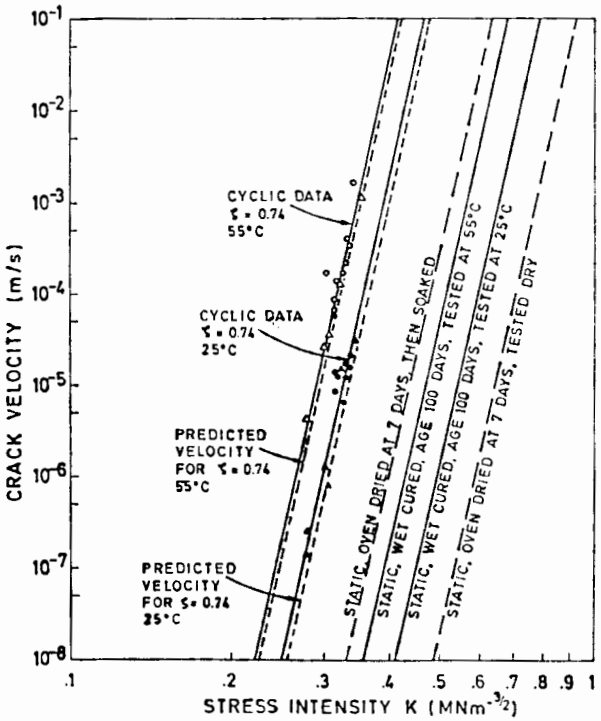

Figure 7.16 Summarised V-K data showing relative effect of curing age and test condition for static tests. (Data has been omitted for clarity and only the lines are drawn). Fatigue V-K lines and data are also shown, together with the g factor predictions.

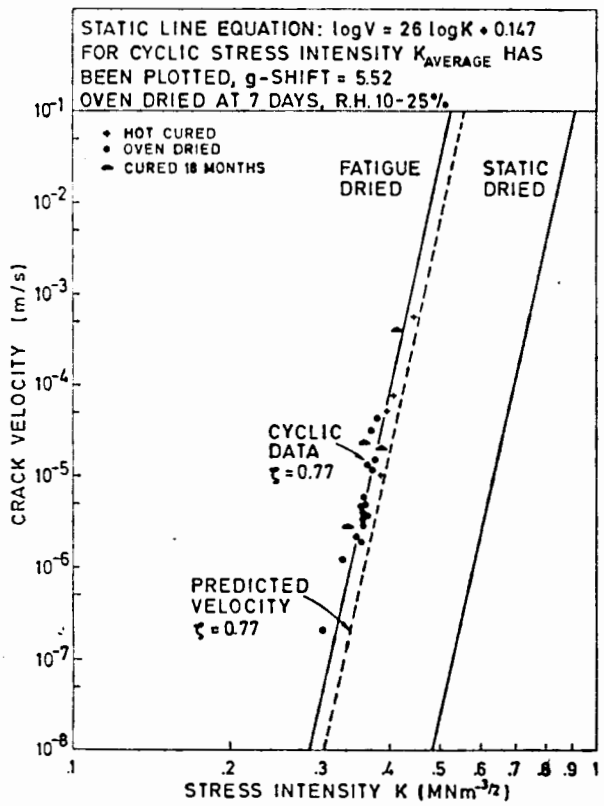

Figure 7.17(a) Comparison of static and fatigue V-K curves for dried specimens.

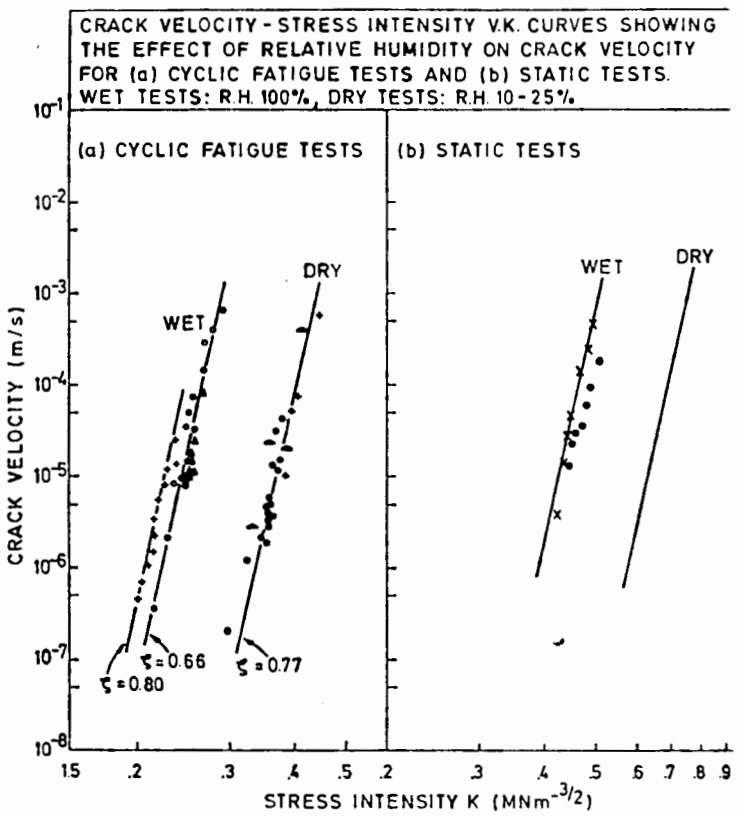

Figure 7.17(b) Effect of environmental moisture of V-K curves for both static and fatigue tests.

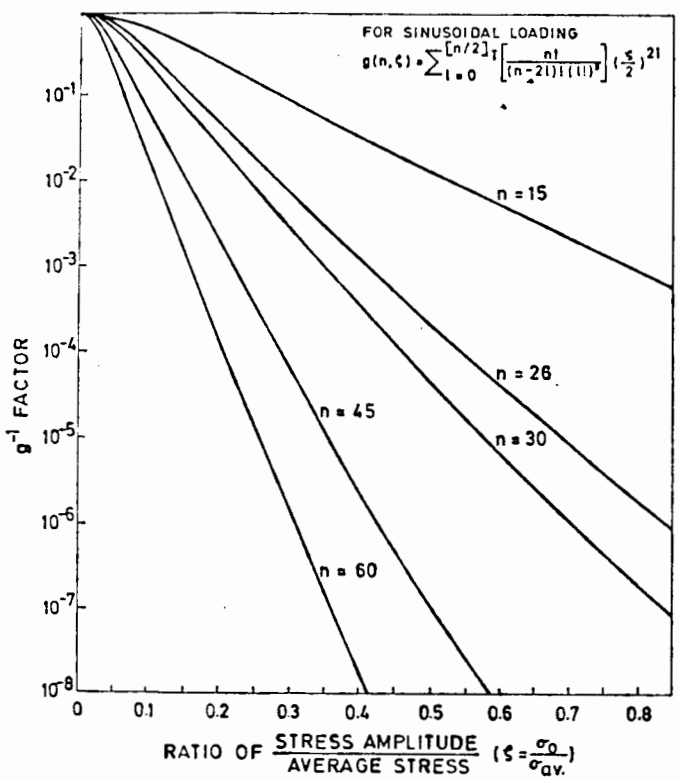

Figure 7.18 Evans and Fuller's (235) g factor for prediction of cyclic crack velocity from static data for various n values (including n=26) as a function of normalised cyclic stress amplitude,

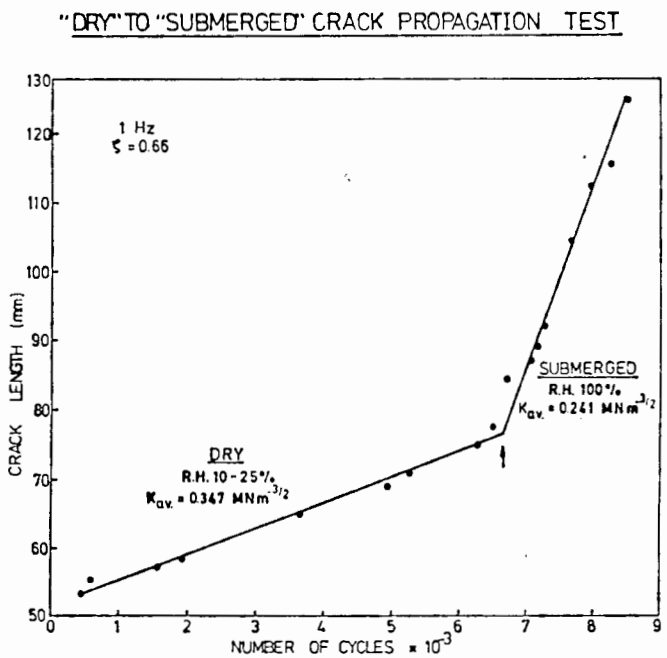

Figure 7.19 A typical "dry" to "submerged" crack growth change over test. Note that the average stress intensity has also been changed to obtain measureable crack growth rates.

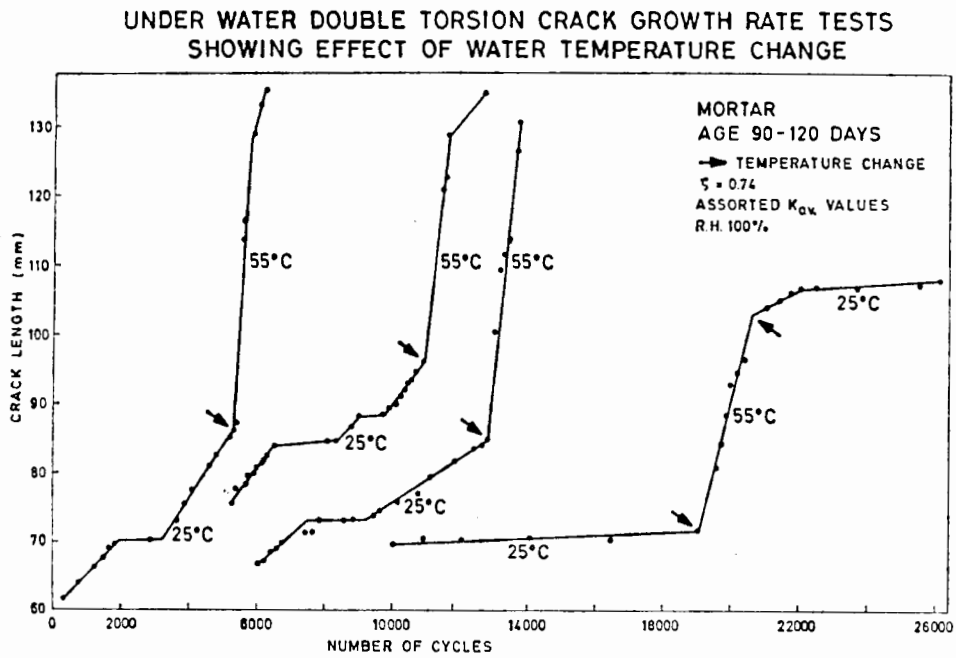

Figure 7.20(a) Underwater double torsion crack growth rate tests showing the effect of water temperature change on growth rate. The arrow indicates the stage at which the temperature change was made.

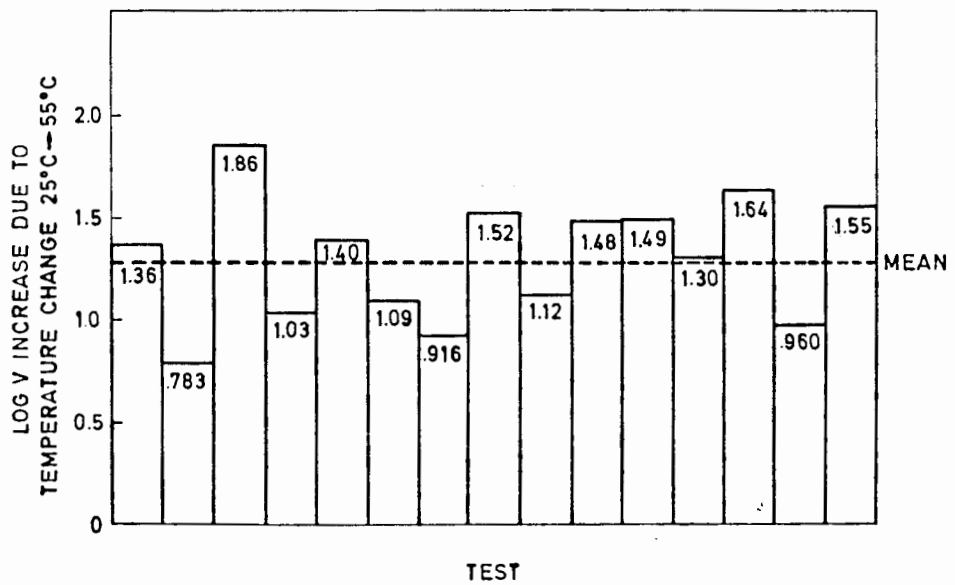

Figure 7.20(b) Bar chart of changes in crack velocity due to a water temperature increase from 25°C to 55°C.

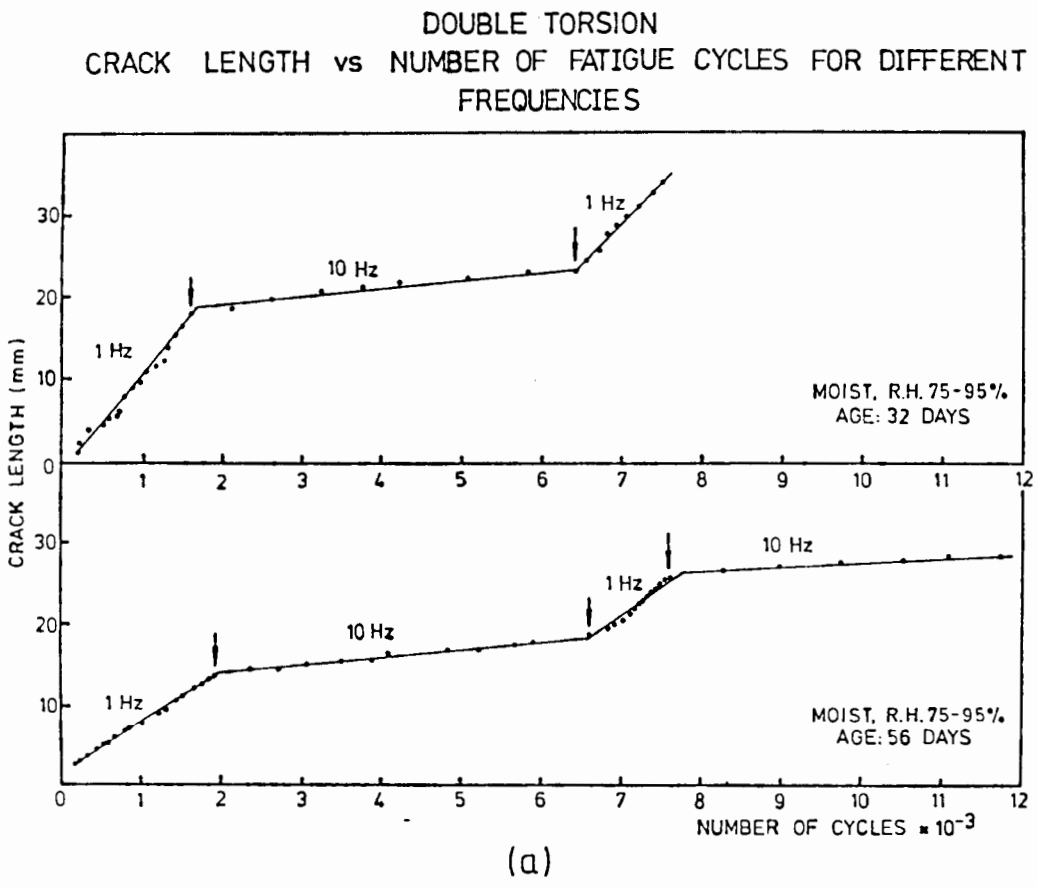

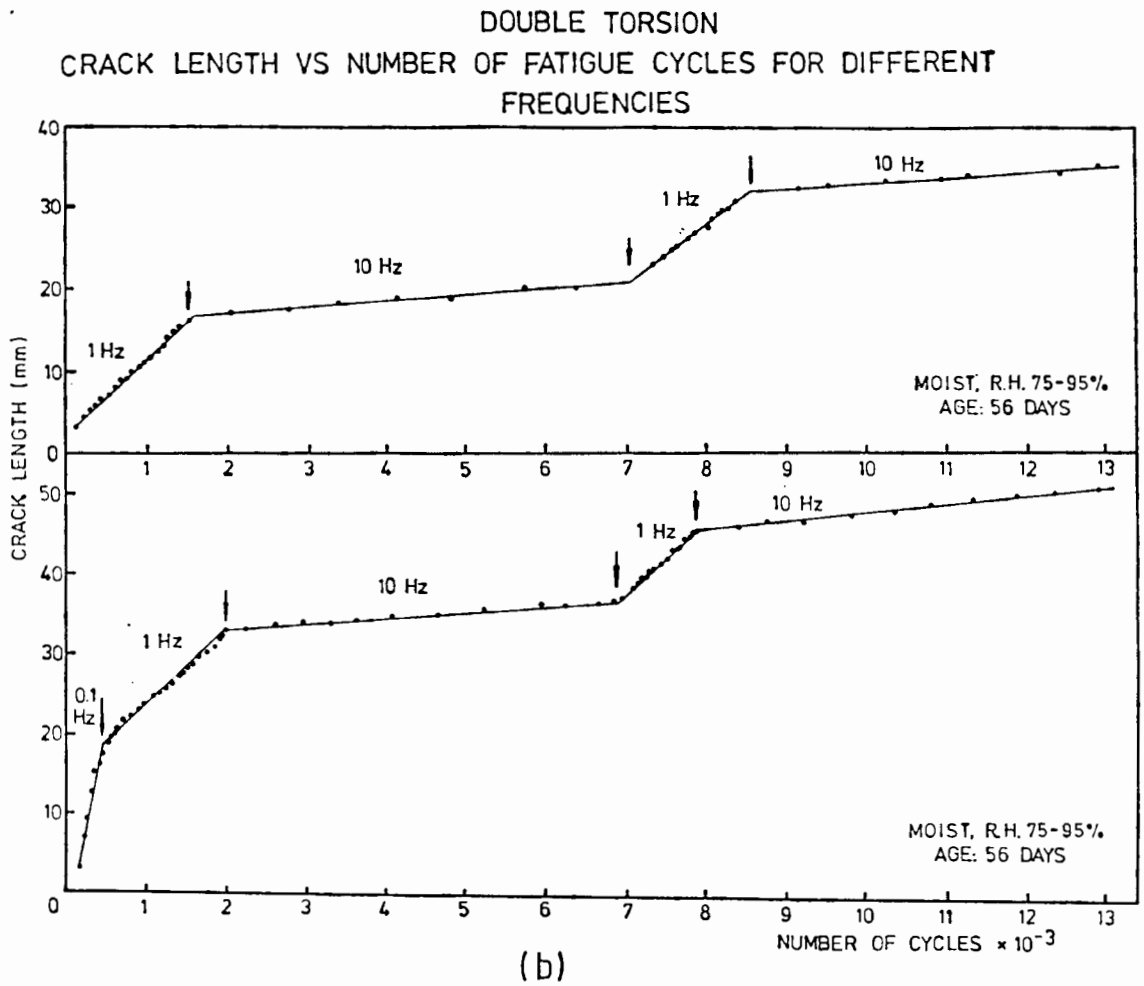

Figure 7.21 (a) & (b) Crack growth versus number of cycles changeover tests as a function of cycling frequency for moist DT specimens.

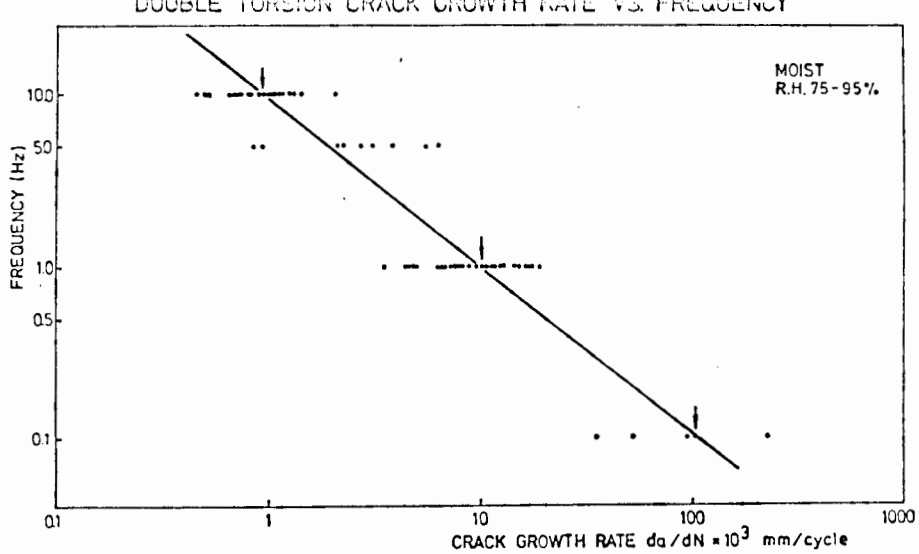

(a)

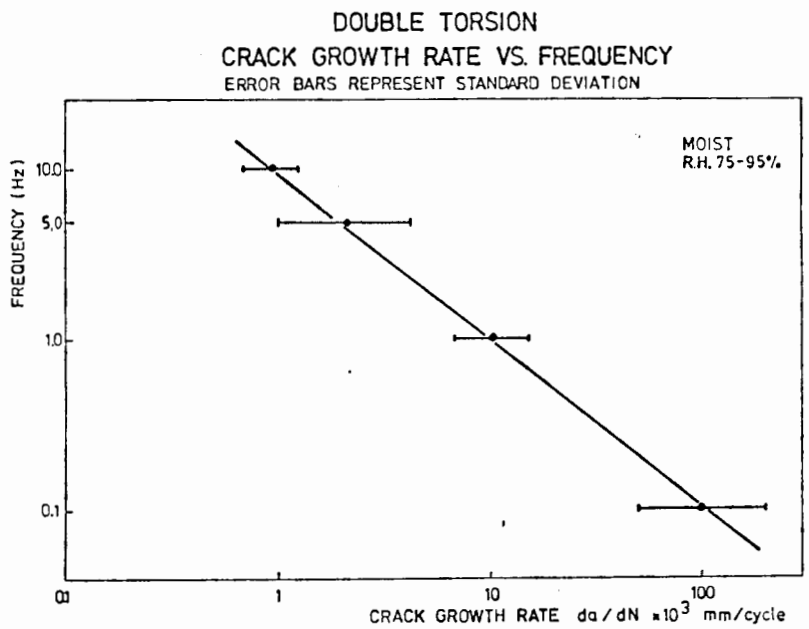

(b)

Figure 7.22 Fatigue crack growth rates as a funcion of frequency for moist (RH 75-95%) test conditions. All the crack growth rate data is shown in (a) and only the standard deviation of this data in (b).

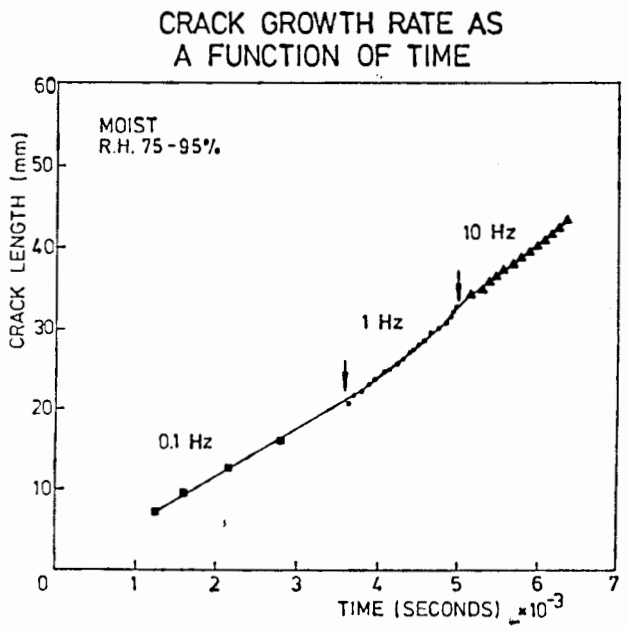

Figure 7.23(a) Crack growth versus time for three frequencies (replotted from Figure 7.21(b)).

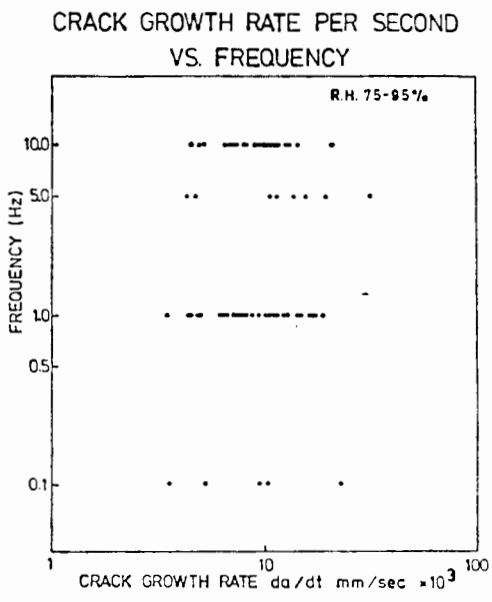

Figure 7.23(b) Crack growth rate per second versus frequency for moist DT fatigue tests.

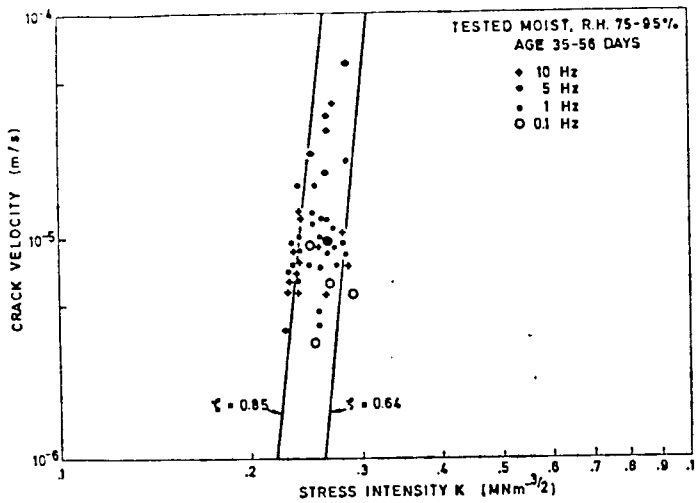

Figure 7.24 V-K data for the variable frequency tests indicating little, if any, effect due to frequency. The data also appears to be contained within the g factor prediction lines (solid lines) based on similar moist static tests and using the zeta amplitude ratios of the fatigue tests.

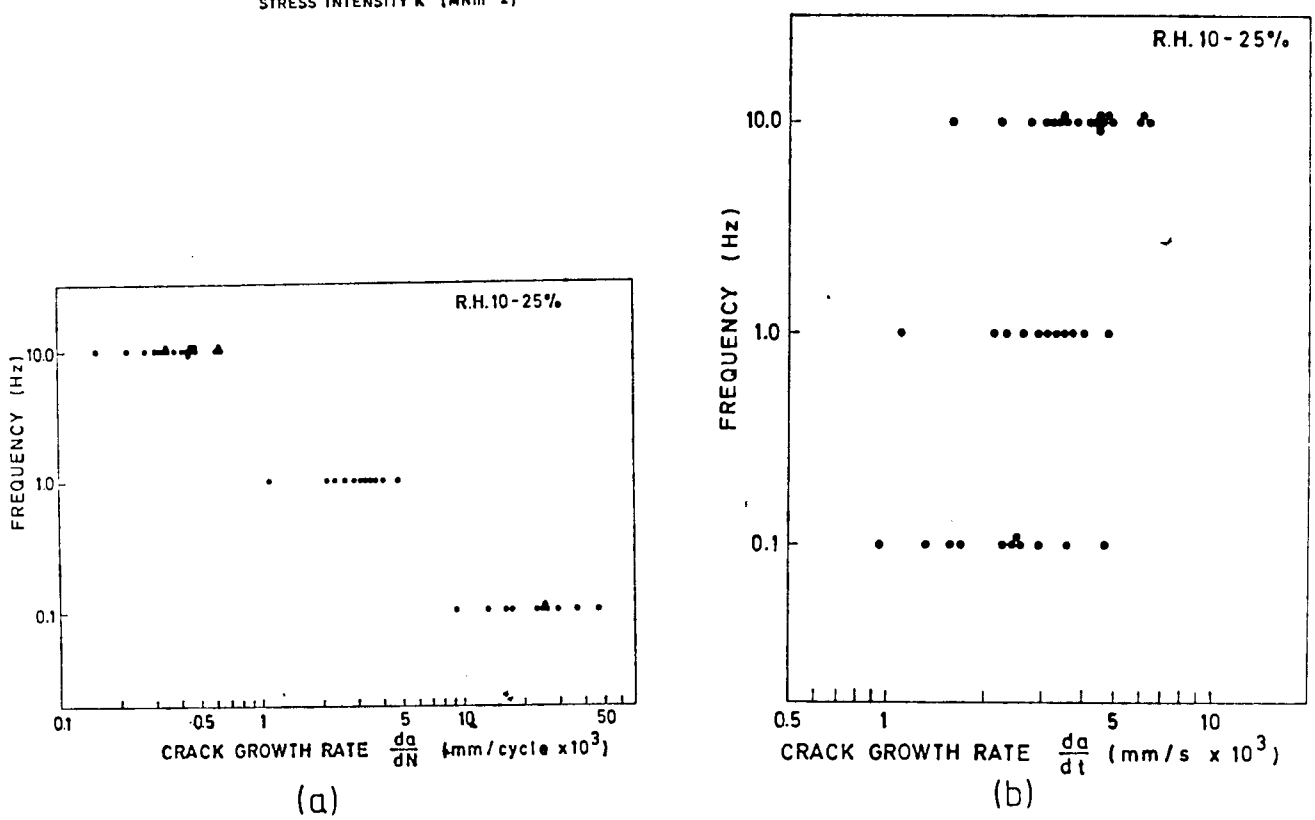

Figure 7.25 Fatigue crack growth rates versus cycling frequency for dried DT specimens (a) as a function of number of cycles and (b) as a function of time.

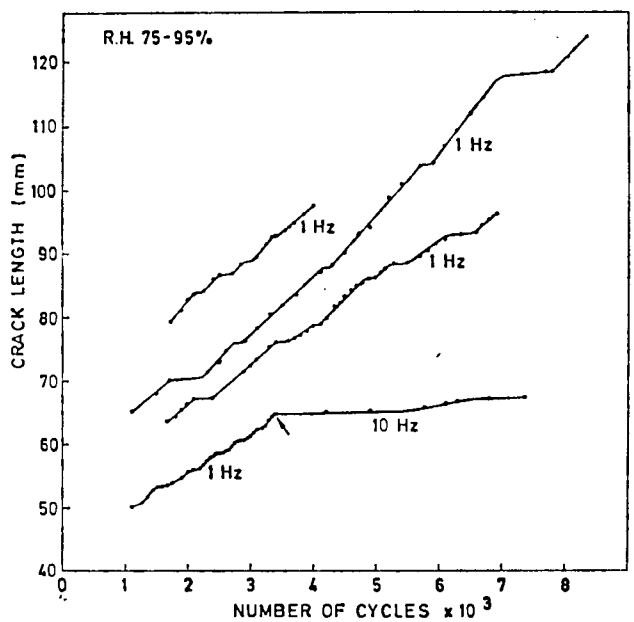

Figure 7.26 Crack growth tests versus number of cycles for moist specimens illustrating the intermittent arrest of crack growth rate. (The different lines correspond to different specimens.)

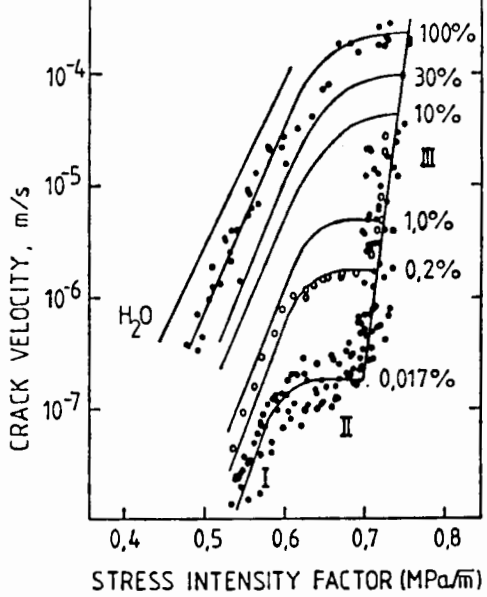

Figure 7.27 Wiederhorn's (340, 353) V-K curves for glass as a function of relative humidity. (Note: Stage I behaviour is observed even for RH = 0,017%.

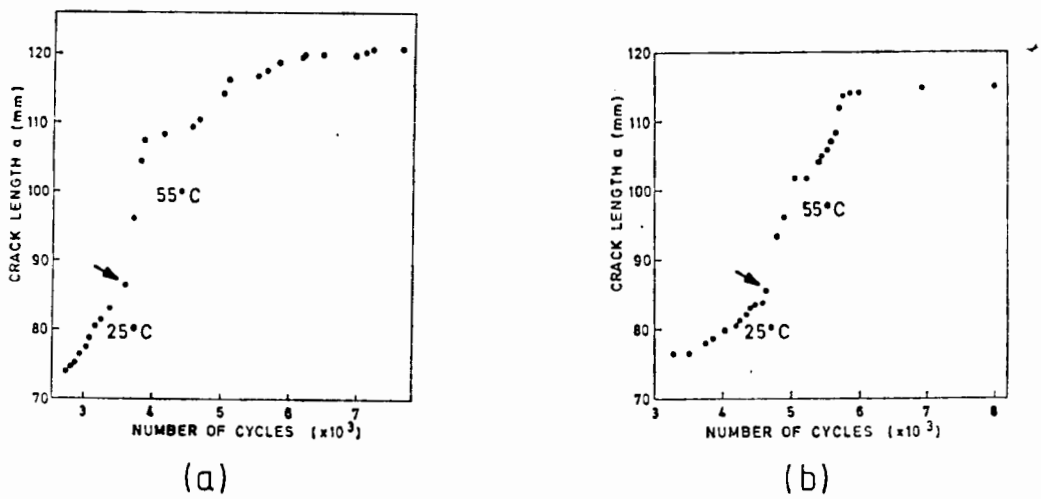

Figure 7.28 (a) and (b) Crack growth versus number of cycles for temperature changeover tests, illustrating the slowing down (or "levelling off") of crack growth rate with time at the higher temperature.

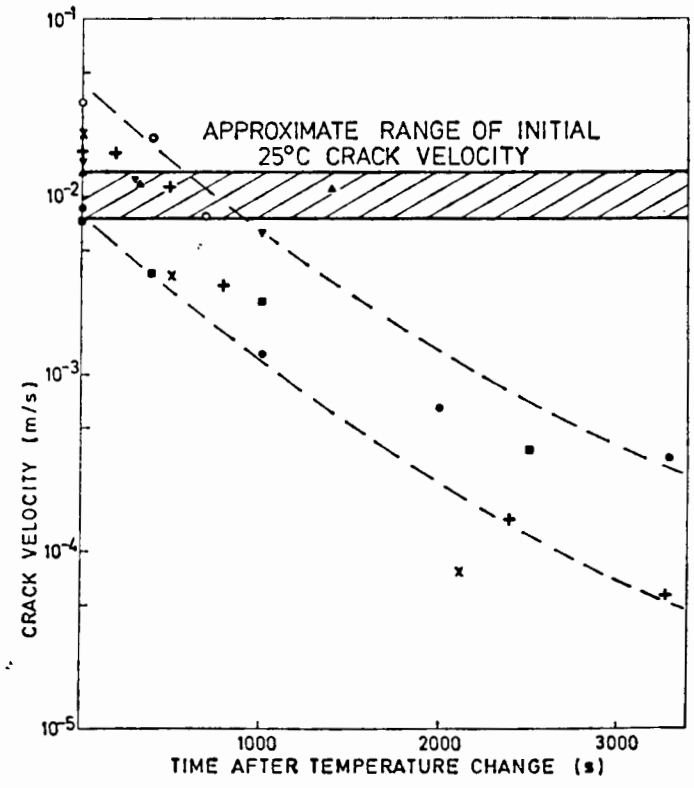

Fig. 7.29 Crack Velocity at 55°C as a function of time after changing the temperature from 25° to 55°C. Note the approximate range of the initial 25°C crack velocity is also shown.

"What do you suppose is the good of research?"
"God knows," Lofty replied, devouring the illustrations,
"Only - only it looks - sometimes - as if He were going to tell."
"That's all we want," Harries coaxed him, "Keep your eye on Him, and if He seems inclined to split about anything, put it down."

Limits and Renewals
Rudyard Kipling

CHAPTER EIGHT : MECHANISMS OF CRACK PROPAGATION AND FAILURE

8.1 Introduction

This thesis has examined fatigue behaviour and associated microcracking or damage development in cement mortar under a variety of conditions, without as yet considering in any detail the mechanisms behind such microcracking. This section sets out to discuss these mechanisms in the light of the experimental data reported earlier.

There does not yet appear, in the literature, to be a unified theory for explaining the development of microcracking, under the various conditions investigated. The questions of why certain crack growth (or damage) rates, are faster than others, or indeed why one type of cracking behaviour stops and another starts, still need to be addressed. Such a shortcoming in the mechanistic understanding of cement mortar fracture has been recognised before (249, 320, 363) and was highlighted at the end of Chapter 2.

There has been, in addition, a need to understand the development of microcracking from the tip of a so-called "single crack", as the crack at this location is often somewhat diffuse or hidden in a "process zone". It has been recognised (74, 75, 320, 364) that the ability to track a propagating single crack would probably add much to the understanding of its cracking mechanism. Such an approach has been employed in this work utilising a small, in-situ DT stage located inside a scanning electron microscope, and these studies are described in section 8.3.

Comparison between the two principal testing methods used in this study (compression and double torsion) for similar test conditions, are also discussed in this chapter. Appropriate correlations as well as variances are highlighted.

The sequence of the chapter is thus as follows:

Firstly, a review of crack growth, process zones and fracture mechanisms precedes the experimental in situ SEM study of Section 8.3. Comparison of the DT and compression results is given in Section 8.4 with a discussion of microcracking and suggested mechanistic theories of fracture pertinent to this thesis given in Section 8.5. The discussion is summarised in Section 8.6.

8.2 Crack Growth and Fracture Mechanisms

8.2.1 Introduction

It is appropriate to examine briefly previous studies on crack growth at the crack tip, the so-called "process zone", (in view of its bearing on fracture models) and associated fracture mechanisms at a microcrack level. Such theories would need to accommodate fracture phenomena in all the various conditions and environments investigated (e.g. effect on moisture, time, temperature, etc.)

8.2.2 Crack Growth and Fracture

Cracking of cement mortar and concrete has been investigated by a number of researchers and the detection and monitoring of such cracking has utilised various techniques ranging from simple visual and microscopic observations, through strain and ultrasonic monitoring (179, 196, 197) to more complex acoustic emission (160, 161, 285), scanning electron microscopy (41, 74, 197) and X-ray methods (108). It is well known that initial cracks or flaws exist in concrete even before any load is applied (83, 181, 267, 365). The nature of these pre-existing cracks is predominantly of an interface bond type between the paste and aggregate (366) and they often arise from shrinkage (249) due to volume changes in the cement during hydration and curing. Flaws in this region are also

known as "contact" zone microcracks (92) or bond microcracks (131, 367). However, these flaws may also originate from cast-in inclusions, porosity or relatively large microcracks. Kaplan (182) observed larger compressive strains with increasing aggregate content and has intepreted this as arising from increased inherent stress concentrations and microcracks at the aggregate before loading.

The stress-strain relationship for cementitious materials loaded in compression is fairly well understood following several investigations, (for example, 82, 92, 131, 181, 249). The results of such investigations have been mentioned in Section 2.3.5 (Fig. 2.22)where the stress strain curve was considered in four stages. In the initial elastic stage (up to approximately 30% of ultimate) the concrete behaves in a nearly elastic manner. Microcracks appear at stress concentrations in the aggregate-paste contact zone by exceeding the local interface strength (92). Accumulated strain is neglible, however, because the interface still carries loads by friction (92) and there is minimal increase in the length of existing bond cracks (131). With further load, cracking increases significantly, both in extent and degree and begins to form continuous crack patterns in the contact zone, with associated permanent strain (92, 192). At about 60 to 70% of ultimate the bond cracks develop into the mortar to form continuous cross linked complex crack patterns (89, 131, 366) but they are still less numerous than the bond cracks (83, 89). At this critical stage the volume of the concrete no longer decreases but begins to increase (83, 89, 170, 171, 181), and is associated with progressive slow crack growth (131). Cement paste, however, does not exhibit this volume increase, and simply continues consolidating, to failure (89). With maintained load the slow crack growth leads on to fast crack propagation and final fracture.

This transition from slow to rapid crack propagation is an area of particular interest as slow crack growth is considered to arise as a direct consequence of the heterogeneity of concrete, whereby excess energy can be absorbed without catastrophic failure (154). Such behaviour is not as common in more homogeneous materials (154). Zaitsev and Wittman (368) have developed a theoretical model using a statistical finite element approach to simulate this experimentally-observed process (83), which gives tolerable correlation, for two dimensions, at least.

On a more detailed microstructural level the cracking of concrete and cement paste is not as well understood. At early ages of curing there is some evidence that fracture propagates through the high porosity C-S-H phase (41, 60, 249, 365, 369) since $Ca(OH)_2$ corresponds to a low porosity region and acts as a rigid inclusion. For older samples the more mature concrete is considerably more dense and the fracture path is more direct (60, 370). It has been proposed, however, that fracture occurs across weakly-bonded basal planes of the $Ca(OH)_2$ (41, 288), and may be affected by environmental moisture content (89, 245).

An approach based on the Griffith criterion (262) can possibly be used to describe microcrack development. For existing inherent flaws, crack propagation can be shown to occur (82) when the rate of energy release due to external forces reaches the rate of energy requirement of surfaces formed by an infinitesimally small crack extension. Strictly speaking, the latter is the energy of the newly-formed surfaces plus the energy required for plastic deformation near the crack tip (120, 149). For cement materials this is complicated because of the formation of a microcracked "process zone" near the crack tip. Thus the total crack surface is greater than the surface of the main crack and the process zone size can increase with main crack growth until the critical strain energy release rate is reached and the crack grows spontaneously (154). The form and size of this process zone is contentious and is thus considered in more detail below.

8.2.3 The Process Zone : Microcracking in the Vicinity of the Crack Tip

The existence of a zone of microcracking, or "pseudo-plastic zone" (281), or "process zone" (120, 276) is well established, both by visual observation and from non-linearities in the stress strain curves for concrete, mortar and cement paste, and has been widely reported (75, 105, 120, 127, 129, 131, 149, 155, 203, 254, 255, 267, 273, 276, 281, 285, 288, 301, 345, 363, 371).

The form and size of this process zone, however, is still open to debate. Hilleborg (276) refers to a process zone of the form shown in Fig. 8.1(a). He regards an opening propagating crack as having a limit where the fracture surface sides of the crack no longer interfere, and

regards this point as the end of stress transfer for his "fictitious crack" model. The crack is still visible beyond this point (to the naked eye and under the microscope), beyond which stage microcracking in the process zone predominates. According to Hilleborg, the tensile stresses are greatest in this region (Fig. 8.1(a)).

At higher magnification Swamy (281) reports similar observations, with the "tip" of the crack appearing further along than supposed from naked eye observation. The crack ultimately blends into the process zone with no well defined crack tip (276, 281, 345). Swamy describes the character of the cracking as "complex, satellite microcracking in the pseudo plastic zone ahead of the obvious crack tip which is very complicated and meandering, and exhibits crack branching and crack jumping (with crushing of trapped material) and a broad general zone of microcracking" (281). Grudemo (288) regards Higgins and Bailey's (27) conventional microscopy observations of process zone cracking in cement paste in the form shown in Fig. 8.1(b). The zone from a (relatively) blunt notch is longer and narrower, and often develops in discrete steps accompanied by load relaxation.

At a finer, microscopic level, Mindess and Diamond (345, 363) carried out wedge opening tests, loading compact tension specimens of cement mortar, and noted that the crack geometry was very complicated. The crack path preferentially progressed along cement paste/aggregate interfaces but was not limited solely to these regions. They also observed sudden and discrete jumps in the length of the crack, although their loading mechanism was not really amenable to very small increases in stress intensity. Similar cracking behaviour, but with better control, was reported Tait and Bohm (74) and is discussed further Section 8.3.

With regard to the effect of the process zone on toughness, Kaplan, in his classical study of concrete toughness (182, 267) noted the existence of precracking or microcracking in the vicinity of the crack tip but did not make any allowance for it, acknowledging that his values of calculated toughness were consequently probably slightly low. He also pre-empted later studies by suggesting that some measure of the extent of subcritical microcrack growth may be obtained from compliance measurements. Brown (155) observed more extensive subcritical crack

growth, and hence lower values of K_{Ic} in toughness tests on concrete, when using a 3-point flexural bend test in comparison to the double cantilever beam technique. He used compliance techniques to allow for such crack growth, as an extension of studies first undertaken by Welch and Haisman (273) and which have been used extensively since (see, for example, 251, 255, 284, 313).

The degree of precritical microcracking in the vicinity of the crack tip (often ahead of or alongside it (Fig. 8.1)) appears to increase with aggregate content and aggregate size (339) and is more extensive in concrete than in mortar or cement paste (130, 131). This, in part, explains the corresponding increased toughness with crack length that is observed, for example, in Fig. 6.4(a), as arising from the increase in energy demand with extent of microcracking (131). Similarly, Evans, Clifton and Anderson (285) report that the existence of a microcracked zone can result in the crack propagation resistance of small cracks being significantly less than that for a fully developed macrocrack. Their explanation is that the microcrack zones interact with one another or with the specimen boundaries and effectively redistribute the stress.

In complete contrast to the above comments, Kesler, Naus and Lott (254) and Hillemeir and Hilsdorf (251) use a similar argument to explain the downward trend of toughness of concrete and mortars with normalised crack length, as illustrated in Fig. 6.4(b). They claim that, initially, with microcracking predominant in mortars, there is a correspondingly high energy demand, in comparison to a single crack, but at longer crack lengths (as the test continues) a single crack predominates and K_{Ic} decreases.

Petersson (129) describes a model for fracture by microcracking of concrete based on the gradual formation of a crack. When the stress in the vicinity of a (so-called) "macrocrack tip" is increased under tensile loading, the microcrack zone starts developing and growing until a macrocrack forms by some of the microcracks joining up (see Fig. 8.1(a,b)). This model of micro- and macrocrack growth is very similar to models already mentioned by Grudemo (288) and Higgins and Bailey (72).

It remains only to estimate the size of the process zone. This varies

with material type and is reportedly in the following range: cement paste 2 to 5 mm (129, 276), mortar 30 to 75 mm (129, 131, 276, 281, 372), and concrete 75 to 150 mm (129, 131, 276, 287).

However, smaller values for cement, $<$ 1mm, (75, 288) and mortar, $\simeq$ 10 mm, (285) have been reported, while Sok et al. (301) suggest that for concrete the process zone size is in the range 200 to 400 mm.

A characteristic length, ℓ_{ch}, parameter for cement materials, defined as

$$\ell_{ch} = 0.25\left(\frac{K_{Ic}}{\sigma_t}\right)^2 \qquad 8.1$$

has been suggested previously (129, 276, 287, 372) where K_{Ic} is the fracture toughness and σ_t the tensile strength, and specimen dimensions apparently need to be large with respect to this characteristic length for valid fracture mechanics applicability.

The range of sizes for the process zone indicated above are consistent with equation 8.1, with the substitution of appropriate values. If the above size criterion is not met, however, Petersson (129) has estimated, based on the size of the microcracked zone, the degree by which estimations of toughness will be too low and this is shown in Fig. 8.2. Also included in Fig. 8.2 is a curve based on Dugdale's assumption of the size of the microcracking zone (see Ref. 129). The curves shown in Fig. 8.2 encompass some most interesting implications - primarily that a large portion of many of the fast-fracture flexural tests on toughness of concrete reported in the literature will be numerically invalid by the factor shown in Fig. 8.2. However, corrections of previously published results of crack resistance due to this relative size effect using the Dugdale correction, indicate that specimen size effects (72) almost disappear.

8.2.4 Mechanisms of Stable Microcracking (Static and Fatigue Loading)

The phenomenon of stable crack growth is well established in cement materials as evidenced by, for example, the ultrasonic studies under both static (179, 183, 185, 188) and fatigue (82, 89, 143) conditions, as well as acoustic emission studies (185, 194, 221, 222, 226). Why such stable, as opposed to rapid, cracking occurs, is considered in this Section.

8.2.4.1 Microcracking and Crack Tip Stress Interaction

A Griffith approach (262) is meaningful for cement based materials, despite, or perhaps because of, the very heterogeneity of concrete with its associated flaws, stress concentrations and regions of local residual stress, which all arise during manufacture and curing. There are consequently considerable fluctuations in the local stress fields within the material which sometimes enable small cracks to arrest after initiation, or at least allows them to propagate in a non-unstable manner. Thus, cracks which form in a region of highest stress concentration (and therefore produce stresses which exceed the local fracture strength) at a given applied stress, can cease to propagate if they enter an adjacent region in which the local stress is lower or the local crack resistance, or toughness is higher. Such cracks will only start to move again when the applied stress is increased.

This general concept has recently been extended by Kotsovos and Newman (367), who considered, for a mortar under stress, that the stress and strain fields in the vicinity of a microcrack are significantly disturbed by the microcrack. The result is high tensile stresses and strain energy concentrations within small regions near the microcrack tips. The strain energy capacity of these regions must have a limit, depending on local material properties, which if exceeded results in spontaneous crack extension (262). Crack extension occurs in the compressive loading direction in a manner to release the excessive stored strain energy due to applied loading.

As a result of such small crack extension the localised strain energy is released to a level below the localised fracture energy requirement at the crack tips and the crack ceases to extend. This arrest may also be associated with the crack encountering locally tougher regions like cement or sand grains. Crack extension is resumed when energy supplied to the material by external loading again tends to increase the strain energy concentrations to values above the capacity of the local energy storing regions. The fracture process, therefore occurs in discrete steps and is stable, since crack extension ceases when the load is maintained constant.

However, further increases in load eventually lead to the stage when no more energy can be stored within the material. Any additional energy induced by the applied load is immediately released by crack extension which can lead to a state of instability.

The Kaiser effect results of acoustic emission also support this contention since AE noise (and hence microcracking) only occurs when previously attained local stress levels are exceeded.

The energy release which occurs during the above fracture processes results in a reduction of the stress and strain concentrations which exist near the crack tips orthogonal to the path of crack extension. Furthermore, these fracture processes can create voids within the material (see Fig. 8.3). The reduction of these high tensile stress and strain concentrations tends to cause a contraction of the material in the direction normal to the crack extension path, whereas void formation tends to cause an expansion. The overall effect upon deformation, therefore, will be a contraction in the longitudinal (compressive) direction and an expansion in the lateral direction, as observed. The cracking processes occur mainly in the direction of principal compressive stress.

Although this line of argument adequately explains stable microcracking during a static test, it is more difficult to see how it can account for similar cracking processes in a fatigue situation, when the maximum applied stress does not increase. Thus, microcracks which either do not propagate or cease to propagate after entering a lower stress region at a maximum stress in a fatigue cycle would not be expected to start again.

However, although the fatigue process does involve repetitive loading to the same stress but it is unlikely that all the small micro-cracking and stress redistribution would occur on the very first cycle. It is more realistic to consider that some microcracking interaction or stress redistribution is already going on during the first load cycle, thus altering the stress state of flaws in the vicinity. It is then reasonable to consider that several cycles are required for all the initial possible crack growth and associated microcrack interaction and stress redistribution to occur and an equilibrium state to be achieved.

Indeed successive identical loadings would result in progressive variable localised stress concentrations as a consequence of the continual process of microcracking interaction and stress alteration. On a microscopic level each loading cycle would be seen as a different localised stress with potential for small crack extension (and thus microcrack interaction and stress relaxation). This does not imply, however, that there is a cycle dependent aspect to fatigue, comparable to metals; rather that it simply takes several cycles for stable fatigue conditions to be established locally within the material.

Such behaviour is perfectly consistent with damage observations in fatigue since there is a rapid increase in damage after initiation of fatiguing, followed by a more gradual, almost linear, increase (see, for example, Figs. 4.3, 4.5, 4.9, 4.24 which illustrate the well established sigmoidal behaviour). The rapid increase in damage following fatigue initiation is clearly apparent from the figures just mentioned. For low frequencies (0.1, 0.5 Hz) stable conditions appear to be established within 10 to 20 cycles (Figs. 4.9-4.11) while at higher frequencies (10 Hz) the stable condition is reached after approximately 50 to 150 cycles (Figs. 4.3, 4.5).

The final fast fracture stage of this sigmoidal damage development is consistent with this model as it is regarded as the stage at which any further increases in microcrack length imply cracks join up to form long continuous complex cracks with high stress concentrations. These have less capability for complete strain energy absorption, microcrack interaction and stress redistribution since the stresses (to be redistributed) from a large interconnecting crack system are higher and less easily accommodated by the surrounding material, which has already sustained substantial microcrack interaction. These long cracks interlink and final fracture soon follows.

The evidence of increased microcracking in fatigue, as compared to static tests, as mentioned above, is consistent with the development of the process zone in the vicinity of the driving micro- and macrocracks. In a static test, although such process zones would exist they do not have the time to develop as extensively through successive loading as would be the case in a fatigue test. In a static test the macrocracks develop and propagate under the ever increasing stress as mentioned above until

failure occurs, pre-empting any possible widespread process zone microcrack development through successive loadings. Zielinski and Reinhardt (373) also suggest, for their impact studies on concrete and mortar, that the degree of microcracking depends on the time available for it to develop.

8.2.4.2 Mechanisms and Models for Microcracking

Models and mechanisms of microcracking have been suggested including plastic flow (120, 92), creep (33, 120, 284) and a form of stress-assisted environmentally-controlled stable crack growth or "stress corrosion cracking" (29, 39, 89, 268, 340). These former mechanisms are discussed in turn and having been shown to be unsuitable a return to the stress-assisted environmentally controlled crack growth mechanism is made in section 8.2.4.3.

There is ample evidence that cement mortar and concrete are susceptible to static fatigue and that this is accelerated by environmental moisture (27, 29, 30, 105, 106) in a manner similar to that which occurs in other ostensibly brittle materials (235, 326, 342, 374). Nadeau, Mindess and Hay (284) have regarded it as "unlikely that a stress enhanced corrosion process" would be active in microcracking of cement and mortar but do not elaborate or justify this contention. They rather suggest that creep, accelerated by stress induced internal redistribution of capillary water, may be the main mechanism of microcrack growth. It is, however, interesting to note that Neville, an acknowledged authority on cement and concrete, regards creep "as resulting in changes in displacements and stresses while not adversely affecting the strength of the structure (120). This is clearly not the case here (Chapters 4 and 7) where extensive damage is observed. It is generally acknowledged (e.g. 89, 120, 355) that microcracking is not associated with creep and thus does not affect the cement or concrete's strength.

The mechanism of creep is generally attributed to internal movement of adsorbed or intracrystalline water and can occur purely internally. Movement of water is relocated in voids as a result of the creep stresses which results in consequent creep strain. It is interesting to note, however, that as long as the material has not been oven dried, creep is independent of environmental relative humidity. This follows from the

internal movement of water, discussed above. Creep also produces no significant loss of water from the concrete to the surrounding atmosphere.

Such independence of relative humidity behaviour is at variance with the present results where microcracking increases with increased environmental relative humidity. This suggests that a creep mechanism is perhaps not useful to describe the present microcracking behaviour. It has been reported that creep does not occur (33, 120, 186, 233) for oven dried concretes and mortars, yet cracking and microcracking of oven dried mortar was still seen to occur in the present test programme, suggesting that whereas oven drying may remove the water associated with the creep mechanism, it does not provide a sufficiently dry atmosphere to preclude microcracking.

The dependence of creep on temperature also requires examination. The creep rate reportedly increases with temperature by 3.5 times between 21°C and 70°C (33, 120), whereas the crack growth rate increases by approximately 30 times for the smaller temperature range (25°C to 55°C) in the present tests. The implication once again is that a creep mechanism does not provide a satisfactory explanation of present observations. Finally, the magnitude of creep strains, typically 200 to 400 microstrains, and the time for these to develop (approximately 20 days), is inconsistent with the present damage observations. For example, typical fatigue microcracking strains from the present study are approximately 600 to 2 000 microstrains (See Figs. 4.1, 4.24) and can, in the shortest case, develop in a matter of minutes, but in the average case, certainly develop over a couple of hours.

The conclusion from the above discussion of creep is that its contribution as a mechanism of microcracking in the present study is probably very small and thus it will not be considered further.

The concepts of plastic or viscous flow mechanisms at the crack tip, although considered, are not regarded as viable (89, 375). There are probably, however, high concentrations of dislocations in the crystalline phases in the vicinity of the crack tip (120). No plasticity is observed in the vicinity of the crack tip even at high SEM magnification, and flow of hardened cement gel is not considered realistic in the present testing

times. Non-linearity of the concrete and mortar stress-strain curve can not arise from non linear elasticity, because of the residual strain on unloading; nor is it due to true plasticity as this is not observed. Rather the stress-strain non-linearity is due to microcracking as mentioned earlier in this thesis.

Hilleborg, Modeer and Petersson (129, 276, 298, 300, 372) have suggested a tied-crack model, i.e. their "fictitious crack model" which is similar to the Dugdale model in which there is a stress transfer across a crack as long as it is only narrowly opened. They have used a finite element model of this concept to try to explain crack propagation. Higgins and Bailey (72, 75) have suggested a similar model, whereby the microcracking process zone is in the form of a "line" ahead of the crack tip rather than in a circular region immediately around the tip itself. They then regard the two faces of a newly formed crack to be 'tied', i.e. to exhibit a net attractive force between them. As the stress on the body increases the length of the tied crack increases until a position of unstable equilibrium is reached when sudden crack advance occurs. The exact attractive force would be very difficult to predict but an estimate based on a Dugdale model gave a critical separation of about 1 micron. Such behaviour is consistent with Higgins and Bailey's observations (75), (even though they could not actually see cracks this small!) and is consistent with later studies by the author (see section 8.3, Fig. 8.16).

8.2.4.3 Stress Corrosion Cracking

The concept of a form of stress corrosion cracking (SCC) mechanism being involved in promoting microcracking has been mentioned in Chapter 7 and is returned to here since it appears to be consistent with the data and observations included there.

The action of stress corrosion promoting microcracking in glass is well established by Charles and Hillig (259) and Wiederhorn (340, 353). Krohn and Hasselman (375) have also employed SCC to explain microcracking in alumina. With regard to cement paste, Beaudoin (268) reports that it (cement paste) is a moisture sensitive, microporous system containing micro-crystalline, poorly crystalline and amorphous phases. The state of water in hydrated cement (as interlayer, absorbed or bulk water) appears to play a significant role in determining mechanical behaviour with

increased water promoting crack growth (30, 29, 89, 149, 155, 250). Cook and Haque (109, 112) observed similar effects for sustained loading of specimens that were first completely dried and then subject to resaturation.

The chemical equation of the form of stress corrosion cracking of silicate bonds in basic environments was given in Chapter 7 by Barrick (29, 106) as a modification of the Charles-Wiederhorn equations (250, 353). Wiederhorn further reports that attack of silicate bonds may also be dependent on pH. Direct attack of the silicate structure could occur if the pH was to exceed 9 in water, because of ion exchange of alkali ions in the glass with hydrogen ions in the solution.

In the case of alumina, Krohn and Hasselman (375) report that cyclic fatigue accelerates the SCC mechanism by generating lattice defects at or near the crack tip thereby raising the energy state and thus lowering the activation energy for cracking. It is difficult to see how such a mechanism could contribute significantly in the materials under consideration here, however.

It is hardly surprising, therefore, in view of its silicate structure, that SCC should have been proposed as a viable microcracking mechanism for cement paste, mortar and concrete (29, 30, 89, 106, 120, 249, 268, 340).

At a fundamental level Shah and Chandra (89) simply regard the attacking species as water while Barrick specifically considers hydroxyl ion attack (29, 106). Using thermodynamic considerations Cook and Haque (109, 112) suggested that the adsorption of water dilates the gel structure of the cement paste, and hence reduces the surface energy. Using similar arguments, Wittman (245) also predicted a strength decrease as the moisture content increases, due to a combination of a decrease in surface energy and an increase of disjoining pressure at higher relative humidities of surfaces held together by Van der Waals forces. (The author questions the validity of this latter aspect, however.)

The most comprehensive application of SCC to cement mortar and concrete (after perhaps Barrick) is the work of Shah and Chandra (89), who were, in fact, the first to suggest the stress corrosion mechanism for cement

materials. These authors observed much faster crack growth rates for wet (as opposed to dry) specimens under sustained as well as cyclic loading. Their plot of normalised stress against damage rate (Fig. 8.4) is qualitatively comparable to the author's own V-K data. It shows that the rate of crack growth, when normalised, for both cyclic and sustained loading, increases exponentially. The interpretation is that the mechanism of failure is similar in both cases.

It is also interesting to note that Shah and Chandra regard the nature of the water incorporated in the cement as important. At a stress level of 90%, cement paste specimens with a water-cement ratio of 0.54 failed in 2 minutes, while 0.4 water-cement ratio specimens, identically loaded, did not fail after 4 hours. (All specimens were sealed in an asphalt compound after casting). The interesting implication, as seen by the present author, is that intrinsic water in the paste itself can act as the stress corrosion agent, albeit that the crack growth rate is slower than if environmental water were abundantly available.

8.2.5 Summary

This section has examined the characteristics of crack development and fracture of cement materials as reported in the literature. Mechanisms of stable microcracking including crack tip stress field interaction and stress redistribution, creep and stress corrosion cracking have been examined. The process zone phenomenon at the tip of a propagating crack has been discussed but it is still unclear why a crack takes a certain path or why it has an associated process zone at all. In an effort to try to understand these microcracking characteristics more clearly, the SEM fracture study described below was undertaken.

8.3 Microstructural Investigations of Crack Propagation

8.3.1 Introduction

Of the methods available for obtaining information about the microstructural mechanisms of fracture in cement paste and mortar, (and indeed any material), high magnification observations have probably been the most widely utilised. Both optical microscopy as well as scanning electron microscopy (SEM) have been extensively used (see Chapters 2 and

5). Generally, however, the surfaces examined have been post fracture surfaces (39, 41, 288, 377). In the case of cement-based materials, unfortunately, the amount of information about crack initiation and propagation under static or fatigue conditions, obtainable from such SEM micrographs, is limited.

Greater understanding of the nature of fracture, and its initiation and propagation characteristics should presumably be obtainable from "live", in situ observations of a slow, controllably-propagating crack. This section, 8.3, deals with an experimental investigation of such in situ controlled cracking observations, conducted inside the specimen chamber of a conventional SEM.

8.3.2 Previous Studies

Observations of cracking in concrete, made using visual techniques (75, 83, 89, 281), photo-elastic techniques (107, 141, 257) and X-ray methods (83, 196), are all limited in resolution to cracks larger than about 25 microns.

Greater resolution is obtainable by going to SEM examination but methods of in situ fracturing of specimens have only relatively recently been developed (74, 75, 345, 363, 364, 378-380). Normally this technique implies that specimens (for SEM) are tested in a high vacuum, totally dry environment, although recently 'wet cell' loading systems have also been developed (4, 380). It is convenient, in SEM in situ testing, to consider two categories: "dry" and "wet" test conditions, with the former using conventional methods and the latter, wet cell techniques.

The requirements of an experimental system to evaluate in situ - "live" - fracture in cement materials thus needs high resolution (and magnification - e.g. using a SEM), careful control of load application, ideally stable crack propagation, operation in a vacuum environment, and preferably, sufficient translational and rotational freedom of a specimen loading stage to facilitate easy 'following' and photographing of a propagating crack.

Early investigations of in situ fracture of cement paste were undertaken by Higgins and Bailey (75). They examined small cement specimens opened

by wedge loading under completely wet conditions, using conventional optical microscopy. They utilised diffuse illumination of (partially translucent) cement to reveal the crack, as discussed in section 7.2.5.3 for underwater crack tip observations. Because of its restriction to underwater conditions and optical microscopy this technique, although elegant, was limited in resolving power to cracks at least several microns wide. No fine detail of the crack tip or cracking mechanisms was really obtainable although tortuosity of the cracking path was evident.

Real time, in situ, SEM fracture observations of tungsten carbide cobalt composites have been made by Pyo Hong and Gurland (379) by wedge opening loading of polymer encased specimens (similar to conventional mounted andpolished "micro" specimems). Similar in situ fracture studies by Manning and Goodhew (381) using hydraulically-applied pure tension methods and by Kobayashi and Ohr (382, 383) using a TEM specimen disc loaded in bending at its polished hole, both suffered from the limitation that cracking was not controllable. The cracking tended to be fast and non-uniform. This also appeared to be the case for the more sophisticated in situ SEM fracture studies of cement paste and mortar performed by Mindess and Diamond and co-workers (345, 363, 364) on wedge opening loaded compact tension specimens. Similar fast fracture behaviour was observed by the author for asbestos cement in flexure, (378). Mindess and Diamond's results and micrographs (345, 363), while graphically illustrating the tortuosity of the fracture path and other characterisitics of cracking, discussed subsequently, were made with rather limited fine control of slow cracking and crack advance. This is presumably related to the brittle characteristic of the wedge opening loading compact tension system where the stress intensity increases with crack length, thus promoting fast fracture. The brittle nature of the specimen and stored strain energy at fracture also do not assist in slow stable crack growth.

Mindess and Diamond's early studies (345, 363) employed relatively large CT specimens (32 X 25 X 13 mm) of cement paste and mortar; the mortar had a water cement ratio of 0.4 or 0.5 and approximately equal proportions of 300 micron sand and cement. Initially, Mindess and Diamond did not polish and coat their specimens (345) but subsequently did so to improve discrimination between cement and sand and to minimise charging effects.

The cracking process in mortars is complicated, resulting in topologically complex, 3D cracking. It was evident that simple fracture mechanics models of a "single crack" greatly oversimplify the geometric features of the crack extension process. Cracks are tortuous and predominantly, but not exclusively, follow interfaces between sand grains. Such observations have also been reported by Tait and Bohm (74). This inter particle cracking tended to follow pre-existing or incipient shrinkage cracks at sand interfaces and could lead to debonding of the sand from more than one surface. Crack branching was extensively observed together with "crack jumping" or crack discontinuities. Allied to this latter observation was that of extensive fine cracking adjacent to the main crack, consistent with a passing process zone. The resolution obtained (or at least reported) by Mindess and Diamond (345, 363) was insufficient to obtain identification of the tip of a crack, which tended to diffuse into process zone type of microcracking. The control of progressive cracking in their earlier studies was also somewhat coarse, indicating discrete crack width increments of only about 10 microns.

Subsequent, pure compression studies by Mindess and Diamond (364) with Lovell (380) were, however, able to obtain greater resolution for observation of cracking processes, for cracks as narrow as 2 to 5 microns. These latter tests and observations were also conducted on 6 X 6 X 20 mm prisms in a high humidity environment using a special chamber and water saturated air inflow. This recent work by Mindess and Diamond (364, 380) is seen as particularly important, especially in view of their ability to observe cracking under moist conditions, and thus free from normal drying shrinkage of drying microcracks, as well as microcracks caused by evacuation.

In the following section a double torsion technique of observing crack propagation in cement and mortar in situ in an SEM is described. This technique has the advantage of slow, totally controlled crack propagation and arrest and, coupled with special freeze drying techniques, evacuation cracking is minimised, and thus high resolution of crack propagation is obtainable. This is the first time a double torsion loading rig has been used inside an SEM and crack growth control, with increments in crack length of less than a micron, is at least an order of magnitude better than other work. Such a system also facilitates observation of the crack tip which has not been reported before.

8.3.3 In Situ SEM Double Torsion Fracture : Experimental Systems

8.3.3.1 In Situ Loading Rig

For the in-situ SEM studies discussed here the double torsion loading system was used. As discussed in detail in Chapters 6 and 7, the DT system provides a constant stress intensity regime with crack length, for at least the central third of the specimen.

The loading system was required to be small and light, so that it could not only conveniently fit into the specimen chamber of the SEM, but also be readily manipulated.

A conventional three point bend loading stage of the Cambridge Stereoscan 180 provided the foundation of the in situ DT loading rig. This was particularly versatile as five degrees of translational and rotational freedom (in all) of the goniometer could be utilised to optimise specimen observation and to follow controllable crack propagation in the specimen. The standard three point bend system of the Cambridge 180 utilised a retracting double pin system fitted between two clevises (Fig. 8.5). The method of retraction of these two clevises consisted of the rotation of a helix against a concentric key or pin. The standard form of this three point bend system, virtually as supplied, is apparent in the plan view in Fig. 8.6(a). Here the outer loading pins have been replaced by specially machined screws (item 7 of Fig. 8.5), but otherwise the three point loading nature of the system is clear, particularly the central (3 point bend) loading pin.

Onto this lower conventional test surface the other specially machined units were located. These were, sequentially, the base plate (containing locating pins, (item 9), and 1.5 mm ball bearing load points, (item 6); the specimen itself (item 5); the upper loading plate, (item 2), (of low magnetic susceptibility brass and containing the loading (item 4) and pivot (item 3) points, and tapered aperture to facilitate secondary electron collection over a wide range of tilt angle); and finally the upper locking nuts, (item 1), which tightened onto the retracting screws, (item 7). Views of the sequential placement of these units is shown in Fig. 8.6 (a to d).

The location and securing of both the specimen and the loading plate was critical. Great care was employed to ensure good alignment and proper seating of the lower and upper load points (items 6 and 4) against the DT specimen, as well as both the remote pivot points.

Once a specimen was located and the loading plate lightly secured, a very fine copper wire was attached from the upper surface of the coated specimen to the base plate chassis by means of conventional SEM "silver dag" conducting paint. This went some way to earthing the specimen and thus minimised charging effects during subsequent cracking and fracture. This earthing procedure could only be carried out after the loading plate was secure, since the DT specimen location and alignment was so delicate that merely touching with the wire or silver dag paint could upset such alignment. A small recess was hence machined in the loading plate at the remote end to facilitate this earthing wire attachment (see e.g. Fig. 8.6 (d). A photograph (in plan) of the specimen and test system ready for insertion into the Scanner (except for the earthing wire) is shown in Fig. 8.6 (d).

The mode of operation at this stage was that by symmetrically retracting the clevis units of the retracting load system (item 7), the loading plate (item 2) would pivot on the rounded pivot points (item 3), applying load to the DT specimen through the loading points (item 4). With practice it was relatively straightforward to grow nearly straight cracks in the DT specimen in a totally controllable way. Views of the in situ DT loading system in its goniometer stage prior to adding the loading plate, are shown in Fig. 8.7 (a,b,c) and with this loading plate on the stage in Fig. 8.7(d).

The loading of the DT specimen was applied by micrometer rotation of an external screw connected to an articulated arm. Such linkages are clearly apparent in Figs. 8.6 and 8.7 and similar ones were used for goniometer translation and rotation. All these rotations of linkages were applied through vacuum seals, standard to the Cambridge S180. Since the pitch of the micrometer drum was very fine and the loading linkage connected to a worm screw onto a cog on the loading helix, extremely delicate and gradual control of loading could be achieved. With practice it was possible to grow the cracks in increments smaller than could be

resolved in the scanner (and in any case, to certainly less than one tenth of a micron) In this aspect the in situ DT loading system for the SEM is superior to other methods.

8.3.3.2 Specimen Fabrication and Preparation

Two specimen types were investigated. These included the high strength mortar mentioned earlier as well as a specimen series made as a mortar from RHPC cement and coarse ground clinker. Tests on an ordinary cement paste yielded limited information because of the difficulty in distinguishing in the fine cement grains. The specimens were cut with a diamond saw from larger castings that had previously been prepared and cured under various regimes. The rich mortar specimens were prepared as described earlier (Chapters 3 and 7). The mortar specimens were moist cured for 50 to 56 days then air cured before testing at an age of approximately six months.

To try to obtain a greater understanding of the cracking in cement paste itself, a special mix was made up of coarse cement from crushed clinker, with grain sizes less than 500 microns. These coarse cement grains were mixed with orindary RHPC, (with typical grain size of 3 to 8 microns) in equal proportions and hydrated in the usual way. In this manner it was readily possible to distinguish individual cement grains in the DT specimen during SEM observation and relate cracking behaviour to these grains.

The specimens were all cut to size (33 X 11 X 1.1 mm) using a diamond saw under a copious water flow. A thin (200 micron) slit was centrally cut in one end of the specimen and tapered off in a wedge fashion to the central third (constant K region) of the specimen (See, for example, Fig. 8.6 (c,d)). No full length grooves were cut in the specimen (as it was already only 1.1 mm thick).

The specimens were polished with alumina paste to manifest the various phases in the specimen (e.g. cement matrix with either sand or clinker grains) and also to provide a flat surface to facilitate crack observation (364). Early studies with unpolished specimens gave less information as the grains were often covered with a thin film of cement paste hydration product.

8.3.3.3 Freeze Drying

Initially, the specimens were prepared for testing by simply gradually drying them out (air drying for several days, followed by desiccator storage), before coating for evaluation. It was found, however, that this drying process led to several microcracks in the surface which could prejudice testing and performance, as noted by Mindess and Diamond, (345, 363). It has been suggested (371), that significant shrinkage cracking does not develop in specimens which are less than about 1 mm thick, but this contention is not universally supported, (384). Hence, a process of freeze drying was used on all subsequent specimens which markedly improved matters and significantly reduced surface microcracking.

The concept of freeze drying is reasonably well accepted in some fields, particularly the life sciences, (385), and soils (386) but its use and application for cement paste and mortar is not well documented (387, 388). Freeze drying involves rapid freezing of the specimen, with its inherent water, followed by vacuum sublimation of this "water" so that the specimen dries out with minimal damage to the structure or fabric. The cooling needs to be very rapid (less than 10 seconds) to at least $-130^{o}C$ (below which ice crystal growth is inhibited), and usually temperatures of $-150^{o}C$ to $-180^{o}C$ are used (386). In this situation the water freezes into an amorphous glassy or vitreous state without forming damaging conventional ice crystals. It is this vitreous form of frozen water which is sublimated off, also at sufficiently rapid rates so that water does not form.

The cooling can be done in liquid nitrogen itself, but this can form a surrounding - and thus insulating - layer of gas bubbles around the specimen, which would delay the cooling rate. Preferable cooling liquids are propane, isopentane or freon ($CHClF_2$) (down to $-150^{o}C$ at which temperature freon solidifies), usually cooled with liquid nitrogen.

The drying is then promptly conducted in a vacuum system where sublimated moisture, which is drawn off, is trapped in a moisture trap. The sublimation is carried out under cold conditions, but not below $-130^{o}C$.

In the system employed here the specimens were freeze dried by simply immersing the specimen in a small glass phial of liquid nitrogren. Because the specimens were so thin ($\simeq$1 mm) the cooling was very rapid - of the order of a few seconds - before the boiling action stopped, and thus no special fluids were used. The specimens were then transferred to the freeze drying unit's vacuum system where the 'ice' was sublimated off and trapped in a moisture trap. The drying was usually conducted overnight and the specimens cunningly sealed and stored under vacuum condition in their phials until required for coating prior to SEM observation.

The phials were opened under vacuum and the specimen located on the coating platform to be coated with layers of carbon and 60/40 gold/palladium on the tension surface of the DT specimen. Coated specimens were stored in a desiccator before being examined in the SEM.

The benefits of freeze drying, over conventional desiccator drying and evacuation, of specimens for SEM were investigated. Figs. 8.8 (a) and (b) indicate the surfaces of (a) freeze dried and cooled and (b) desiccator dried and coated, paste specimens at the same magnification (x310). The freeze dried surface exhibits significantly less microcracking than conventionally dried specimens. In an attempt to quantify this advantage in reducing microcracks by freeze drying, counts of the number of microcracks on a mapping matrix were recorded. No special areas were selected. On each consecutive field of view (at a magnification of 310 times) a sketch of the microcracks was made. Typical photographic sequences of such scans are shown in Figs. 8.9 (a) and (b) for freeze dried and desiccator dried samples respectively, which indicate the greater preponderance of microcracks on non freeze dried specimens.

Actual scans of more extensive areas (of different specimens) (still at magnification of 310 times) are shown in Figs. 8.10(a) and (b). If the numbers of cracked to uncracked map area elements are considered, then the normal desiccator drying process results in about twice as much microcracking as freeze dried specimens. If the actual number of microcracks is considered, then the benefit of freeze drying is an approximate 3 times reduction in microcracking. In view of this benefit of freeze drying in reducing the degree of microcracking, it was employed for all subsequent in situ studies for mortar and cement clinker.

Results of in situ fracture observations are given in the following section.

8.3.4 In Situ SEM Fracture Results

8.3.4.1 Mortar Studies

Since the double torsion specimen had a conductive coating, which was connected to the loading chassis by means of the fine copper wire, macroscopic charging effects were minimal. However, at high magnification local cracks, initiated by the loading system, frequently revealed localised charging as electrons were not conducted away from the freshly exposed non-conducting fracture surface. This phenomenon, rather than proving a hindrance, was utilised as a means of identifying the freshly developed and propagating cracks and distinguishing them from (rare) pre-existing shrinkage cracks. These latter would have been coated and thus not exhibit charging effects.

In mortar, the major crack (approximately 1 to 4 microns wide), could easily be followed as it propagated, and was arrested at any stage simply by stopping the micrometer screw loading. A sequence of micrographs delineating the progress of a crack in mortar can be seen in the composite 'collage' sequence, Fig. 8.11(a). The crack initiated in the vicinity of the end of the starter slit (in the lowest frame of Fig. 8.11 (a)) and propagated "upwards" as seen in this sequence.

Various characteristics of the cracking are apparent, which are consistent with Mindess and Diamond's observations (345, 363, 364, 380) mentioned earlier. The crack is very tortuous and meanders considerably and is certainly not a single straight crack. Crack branching is also apparent, for example see Fig. 8.11(b), which represents an enlarged version of the area shown in the frame of Fig. 8.11(a). Allied to this is so-called "crack jumping" (363, 345) or discontinuous cracking, where a crack appears to terminate and an adjacent crack, often parallel to the first, opens up and proceeds in the original general direction (Fig. 8.11(b)).

A certain amount of debonding of the aggregate particles is observed with the crack often skirting around, or close to, the edge of a sand

particle, (Fig. 8.11(a)). This is not always the case, however, as can be seen from the crack and the sand particle at the top of Fig. 8.11(a). This sand particle is shown enlarged in Figs. 8.11(c) and (d). Here the crack preferentially propagates through the sand grain, rather than around it, even though the sand/cement interface would appear not to be far from the crack's intended direction. No debonding of the sand is seen at all in Fig. 8.11(d) and it appears energetically preferable for the crack to go approximately straight, irrespective of the grains in its path. The interpretation suggested is that the stress intensity field at the crack tip plays a significant role in "selecting" the crack path, at least for fully hydrated(6 month old) mortars. It can be argued, however, that the crack path observed on the surface, (i.e. through the aggregate, as opposed to around it), may be governed more by, perhaps large, sub surface aggregate particles and hence be considered as an "iceberg" problem, where 90% of the structure is hidden. It is nonetheless an interesting observation that aggregate fracture with no debonding is not an uncommon occurrence.

Similar crack debonding of aggregate particles, followed by cracking through the aggregate, is shown in Fig. 8.11 (e) and (f). In both cases the general crack direction is from bottom to top. In (e) the propagating crack encounters an aggregate particle and starts to debond, but after a little way propagates through the corner of the aggregate, causing a discontinuous crack, or crack jump, to continue the crack. In Fig. 8.11 (f) the propagating crack initially skirts the lower aggregate, then goes through it (exhibiting crack branching as well) before continuing, diagonally left, to debond the next adjacent aggregate particle.

Often when crack branching occurs, e.g. Figs. 8.11 (f, e, a), one branch predominates and the other becomes relatively inactive, a finding also observed by Mindess (345, 363).

A measure of the fine control of the loading system, and an attempt to watch an actual crack tip grow, is evident from Figs. 8.12 (a) to (c). In this sequence a propagating crack in an aggregate particle is seen to approach an existing (diagonal) shrinkage crack. The propagating crack also exhibits significantly more charging. On slightly increasing the load applied to the DT specimen, a parallel crack from a separate branch

appears, which on further loading approaches the shrinkage crack. This shrinkage crack also widens and exhibits more charging as uncoated material is exposed.

Further evidence of crack branching and crack discontinuity (for cracks growing from top to bottom) and the process zone mentioned earlier (Fig. 8.1) are shown in Figs. 8.13(a) and (b). A regime of cracking is observed which is often parallel and adjacent to the main crack direction. Discontinuity of cracks, cracking around and through aggregates, aggregate debonding and crack jumping all indicate the existence of a zone of high stress intensity near the macrocrack tip, which zone becomes microcracked as the macrocrack passes. Efforts to measure the size of this process zone in mortar depended on the size limitation of cracks which were to be included in the evaluation. Strictly a quantitative computer-based method is required to quantify the process zone size, but for the mortar used here and evaluated in this way, indications were that this zone size was approximately 1 to 4 mm across.

8.3.4.2 Cement Clinker Studies

In an attempt to understanding microcracking of cement paste itself, unencumbered with sand aggregate debonding features an artificial cement "mortar" was made using cement clinker, crushed to provide large grains (20-500 μm) of clinker "aggregate".

Experiments on clinker cement paste specimens gave similar fracture results to mortar material. Individual grains, of clinker in this case, were somewhat more difficult to distinguish on the SEM screen, as the grains and matrix were both cement and had essentially the same composition. The grains can, however, be seen in Figs. 8.14(a) and (b) as the more glossy, polished areas, and the crack appears to go predominantly around the grains. This is especially the case in Fig. 8.14 (a) which was only 3 days old, and less so for clinker paste shown in (b) where the clinker paste was 14 days old. In this latter case there appeared to be more evidence of cracking through clinker grains and not only around them.

This evidence is broadly consistent with the work of Walsh et al. (41) who reported a change in fracture path for cement paste from intergranular at short hydration times (41) to transgranular after 21 days of hydration. Such behaviour is reasonable since at young hydration ages the weakest regions of a hydrating cement paste would presumably be the interparticle spaces, with the hard grains providing more crack resistance. At longer curing times the intergrain matrix is more consolidated and more fully hydrated thus providing more resistance to cracking. Thus a crack would tend to run approximately straight, irrespective of grains in its path. Such evidence of transgranular fracture is clear, particularly in the upper frame of Fig. 8.14 (b) where the crack runs immediately to the left of (glossy) clinker grains. Figures 8.14 (a) and (b) also illustrate the tortuous nature of the crack path, crack branching and crack jumping, in a manner not dissimilar from cracking in mortar.

Observation of the progress of a crack tip and an associated process zone are illustrated in the figure sequences of Fig. 8.15. The composite photograph (a) shows the "tip" of a propagating crack at the top right hand corner. The process zone of cracking ahead is quite extensive (over all four frames) and is fortuitously shown up by the charging effects, which is not the case for pre-existing coated shrinkage or drying cracks. After application of a small increment of load the crack has propagated diagonally downwards, and the tip moved outside the field of view, resulting in a slight relaxation of cracks in the (previously existing) process zone, Fig. 8.15(b).

The best evidence of gradual crack tip extension obtained to date is shown in Fig. 8.16. The crack tip is propagating diagonally from top left to bottom right and each micrograph was taken after a small increment of load. The tip was actually observed to move in real time (under constant load) in a manner consistent with load or stress relaxation mechanisms mentioned in Chapters 6 and 7. The crack duly arrested after propagating about a micron. This arrest was fortuitous as it facilitated the taking of the scanning photograph, which itself takes about 40 seconds to expose the film in a scanning mode. The sequence of crack propagation was thus as follows. After a small load increment the crack propagated a small amount but only after a slight delay (of a

second or two) and continued to propagate in a manner similar to the load relaxation tests for a further period of up to half a minute. In due course it arrested and no further propagation occurred in the times observed up to 30 minutes.

(Incidentally, observations of the rate of this crack propagation rate, and other similar cracks, across the screen was typically between one tenth of a micron and one micron per second, which is consistent with the lower end of the crack propagation rates observed in Chapter 7 on macro scale DT specimens, see for example Figs. 7.12 to 7.15. Of course it is acknowledged that the environments and stress intensities are totally different (and indeed unknown) but it was an interesting observation that crack propagation can still occur in such a dry environment at realistic growth rates). This slow crack propagation was also not absolutely smooth and continuous (i.e. the rate was non linear) but propagated in a series of discrete jumps, each of the order of a fraction of a micron. This is an interesting area of research for further study.

Examination of the sequence of micrographs in Fig. 8.16 shows quite graphically the slow progress of the crack of the fine control of the in situ DT loading system. At this fine level, i.e. high magnification, local process zone effects appear to be absent. This would then seem to suggest that it may be reasonable to put at least a lower bound on the spacing of cracks in the process zone of about 10 to 20 microns.

Further evidence of process zone microcracking in freeze dried clinker cement paste is shown in Figs. 8.17 (a) and (b) for 14 day old and 3 day old specimens respectively.

The transgranular nature of the cracking in 8.17 (a) is again apparent together with crack branching (near the slit tip at the top) and crack jumping (near the bottom of Fig. 8.17(a)).

Similar strong evidence on a macro scale for a process zone (at low magnification) is apparent in Fig. 8.17(b). In addition to the main crack from the slit tip small "veins" of microcracking showing extensive branching are apparent : one from the slit tip and just to the right of the main crack and another from the main crack at about 45^{o} to it and about 400 microns from the slit. Once again it would appear that

microcracking as a result of high stress concentrations near the crack tip of a small DT specimen results in a "process zone" of damage, and that this strongly influences subsequent fracture behaviour.

8.3.5 Discussion and Conclusions

The nature of microcracking of cement and mortar has been investigated by means of the in situ fracture studies in the scanning electron microscope. While the environment inside the microscope (high vacuum, absolutely dry) is somewhat unrealistic, certain characteristics of the fracture can still be evaluated.

The cracking is very tortuous, and topologically complex as has been noted by other observers (41, 281, 345, 363). There also appears to be a process zone of microcracking in the high stress intensity area in the vicinity of the crack tip. For the high strength mortar and cement paste investigated here this process zone size seems to be of the order of 1 to 4 mm, more in keeping with the estimated process zone size suggested by Swamy (281) and very much smaller than the 100 to 200 mm mentioned by Sok (301) and others (276, 325).

In view of this tortuosity and process zone, not to mention crack branching and crack discontinuity or jumping, extensive energy is absorbed in growing a crack in cement systems. Hence single crack fracture mechanics models greatly over-simplify the fracture process and any fracture toughness measurement based simply on visually-observed crack length is sure to give an underestimate of the intrinsic toughness of the material. This is because the actual fracture surface areas generated are far larger than would be expected from a single crack. The implication is that the true intrinsic strength of the cement material may well be significantly greater than has been measured to date.

From the in situ studies mentioned here it would appear that at young hydration ages, (up to 3 days at least), the fracture path is predominantly intergranular and becomes progressively transgranular with time. Such observations have been suggested before by Walsh et al. (41) and Dalgleish, Pratt and Moss (14), but only from post fracture observations. The crack path appears to become straighter with hydration age as well, as evidenced from the clinker studies, and more dependent on

the stress intensity at the crack tip rather than the grains in its path (14). Walsh et al. (41) report that the fracture path is predominantly through (weaker) calcium hydroxide platelets, followed by interfaces between these and the surrounding C-S-H matrix and lastly (most seldom) through the C-S-H fibre matrix itself.

In the case of mortar fracture, cracking was mostly along debonded aggregate interfaces, and it has been suggested (141, 387) that cement paste hydrated near an aggregate particle does not necessarily generate the same microstructure. Pre-existing microcracks at such interfaces are considered major sources of flaws which extend under load (257). However, substantial evidence of cracking through aggregate particles, sometimes with no debonding, was obtained, especially for well-hydrated (6 month) specimens. This again suggests that, for well-cured specimens, the stress intensity at "the" crack tip governs fracture path almost as much as aggregate particles in its way.

The SEM in situ DT fracture system described here was very suitable for obtaining and controlling very fine crack tip growth, as might be expected from a double torsion technique, which is ideal for brittle materials. Mindess and Diamond (345, 363) and Swamy (281) report great difficulty in observing crack tips. Such difficulties were also experienced here, as the crack appears to diffuse into a general microcrack process zone. It was possible in the present case, however, to identify crack tips and to monitor their progressive growth - often a fraction of a micron at a time - by careful loading of the DT system. Such controlled slow growth did not appear to be possible with Mindess' compact tension (345, 363) or compression specimens (364, 380).

It is interesting to note that an increase in the measured toughness is often obtained with increasing slit depth for slow crack growth toughness evaluation methods for mortar and concrete. Conversely, fracture methods which relied on a rapidly propagating crack due to fast montonic loading as used by earlier workers (26, 127, 137, 252), gave a reduced measure of fracture toughness with increasing crack depth. Such contrasting behaviour in these cases may be interpreted in terms of a process zone effect where increases in crack length cause greater energy to be absorbed in process zone effects for a slowly propagating crack, rather than for a rapidly propagating one, where process zone cracks do not have time to develop.

In summary, it is probably true to say that the behaviour of the cement microstructure during fracture is the key to an improved understanding of the mode of failure of the material, and may suggest ways in which the strength and toughness may be increased (14). The present technique seems appropriate for investigations to further this knowledge. Any fracture model must, however, take into account the extensive energy dissipative processes, in the generation of the crack process zone, crack branching and general multiple cracking as observed and described above.

The present scope of this in situ DT fracture technique may be extended, for both cement pastes and mortars, to distinguish between intergranular and transgranular fracture of cement grains, and interfaces as a function of, for example, age (4, 39, 41, 278), curing history (95, 113, 365), water cement ratio (307) width of the propagating stable crack (75, 365), and cement grain size. Extensive testing could be undertaken to compare the effects of different types and relative sizes of aggregates (and their bonding (39, 278), since the macroscopic strength and toughness of concrete is related to these factors (278, 377). This SEM technique promises to be a useful tool in the understanding of fracture in concrete and other brittle, multiphase materials.

8.4 Correlation of Double Torsion and Compression Results

8.4.1 Introduction

It was mentioned in Section 7.1 that one of the principal reasons for undertaking the DT test programmes was to obtain a better understanding of "single" crack propagation rates. These were described in Chapter 4 as "damage accumulation rates" but are not readily amenable to fracture mechanics-type interpretation. The damage, as monitored in the compression tests, measured the cumulative or integral effect of a three dimensional series of microcracks, while the DT studies effectively monitored single crack behaviour. In reality, as is apparent from the previous sections, a propagating "single" crack actually has a microcracking process zone of questionable size associated with it. It is, however, still meaningful to talk about propagation rate of a "single" crack in a DT system. The test conditions in many of the

compression and DT test programmes were similar and it is now in order, in this section, to discuss the similarities and differences between the results and the ensuing interpretations.

8.4.2 Damage/Single Microcrack Correspondence

The equivalence of "damage" with microcracking in compression tests has been mentioned previously (section 3.5.1, and references 89, 92, 179-183). Microcracking damage was readily detected in both static loading and fatigue, by means of ultrasonic strain and acoustic emission techniques. The rate of such damage accumulation is presumably closely allied to DT single crack growth velocity, determined statically by load relaxation, $\left(\frac{\delta P}{\delta t}\right)_y$, or constant ramp rate, $\left(\frac{\delta y}{\delta t}\right)_P$, or simply under fatigue conditions by observations of the crack tip. This follows since the macroscopic damage can only be the integral or summed effect of a whole series of individual cracks. Differences could also presumably arise due to possible interacting (synergistic) effects. It is also reasonable to suppose that the compressive damage results give a more "average" effect of behaviour since individual crack effects, for example, intermittent crack arrest, would be masked by the effect of all the other cracks. Such similarity and differences, under comparable testing conditions, are examined in more detail in the following section.

8.4.3 Differences between Compression and DT Results

It was considered advantageous, firstly, to discuss the differences in damage/microcrack growth rate results between compression and DT test methods as this highlights the subsequent large degree of similarity between the results of the two techniques.

There is no real analogue in the DT system of the SN curve for compression fatigue, or indeed of fatigue life. In both test situations the rate of damage accumulation depends on the maximum cyclic stress level and stress amplitude (or more strictly, maximum stress intensity and stress intensity amplitude). The double torsion system, however, conveniently measures crack growth rates, or velocities, V, where the duration of the test obviously depends on (i) the length of the initial starter crack and (ii) the maximum and cyclic applied stresses. In such a system fatigue life has little useful meaning.

In the double torsion case, since single crack growth rate is measured there is no analogue of compression fatigue's residual and elastic strain or recovery (see for example, Fig. 4.5 (b,c)) which really arises due to the effect of several microcracks. The DT system is also able to be modelled theoretically to obtain the meaningful fracture mechanics parameters of stress intensity, K, and crack velocity. This is not readily achievable with the compression prism system.

The DT system has the advantage that V-K curves are obtainable from both static and fatigue testing modes whereas for the compression prism system (as used here) damage rate data has only been obtained in fatigue. (It is worth noting, however, that sustained compression load tests can be undertaken, and associated microcrack damage monitored, as undertaken, for example, by Awad and Hilsdorf (89). The time for damage to develop under sustained load tests is, however, relatively large and such tests were not conducted in the present programme.)

The development of damage due to microcracking in compression fatigue tests was observed to be sigmoidal in form (Figs. 4.1, 4.3, 4.9), apparently because of the need for inherent flaws to develop into stable, growing cracks in the initial part of the fatigue life. Subsequently, the rate becomes approximately linear and this stage is comparable to fatigue in the DT system under constant cyclic loading conditions, which results in linear crack length, a, versus number of cycles, N, curves (Figs. 7.19-7.21).

The extent or 'degree' of damage, which is greater in fatigue than in static compression tests (as reported, for example, in Chapter 5 and Figs. 4.6, 5.5 and 5.8) is not a useful parameter in DT testing. In the latter, rate of crack growth and associated stress intensity, leading to V-K curves, are the principal parameters that are obtained.

It is not feasible to record or obtain meaningful acoustic emission data from the DT tests because of the relatively greater grinding noise from the loading points and lower AE from cracking events. The source of such load point noise was not easily mechanically filtered since specimen alignment in the DT system was critical. This is one area, i.e. the AE PIP system, where the compression results reveal extra microcracking information and complement the DT system results.

Although it would have been possible, fast loading and fast unloading waveform type tests were not undertaken on the DT specimens because of the lack of useful information from the compression results.

The particularly interesting aspect of the g parameter V-K curve predictions of Evans and Fuller (235), from static to fatigue crack growth rates, does not have an analogue in the compression studies. Scatter in V-K data is generally significantly less (Figs. 7.14-7.17) than corresponding time to failure and damage rate data (Figs. 2.28, 4.1, 4.22-4.29) since single crack growth rates under known load conditions are more indicative of intrinsic material behaviour. Time (or number of cycles) to failure tends to fluctuate significantly with initial flaw conditions and localised material variability in the compression prisms.

As described in Chapter 7, the closeness of fit of actual fatigue V-K data with the predicted V-K fatigue line from statically derived V-K data, suggests that the mechanism of fracture in both cases is of the same form. The crack velocities are, however, distinctly faster in the fatigue case compared to the static case for a given stress intensity. This may be due to additional dislocation pile up, or extra stresses created in the cement bonds in the vicinity of the crack tip under fatigue conditions, which are then more susceptible to environmental attack. A mechanism of stress corrosion cracking is consistent with this concept and is discussed further in section 8.5.

8.4.4 Similarities in Compression/DT Results

The most distinctive similarities in the results of the damage monitoring of compression series and the V-K behaviour of the double torsion technique are in their response to (i) frequency (and elapsed fatigue test duration), (ii) environmental moisture and (iii) temperature. These are discussed in turn, as follows.

(i) Frequency and Time Dependence

It was shown in Chapter 4 that compression tests at three frequencies (0.1, 1 and 10 Hz) resulted in (UPTT and strain) damage accumulation

curves that separated into three regimes, apparently dependent on frequency (Figs. 4.22-4.24). The rate of damage accumulation per cycle, $\frac{d(\text{Damage})}{dn}$, initially appeared to be frequency dependent (Fig. 4.25), but when plotted as a function of time was simply found to be time dependent (Figs. 4.27, 4.28). This was the case for both wet and dry test conditions (Fig. 4.26).

DT V-K curves show an exactly analogous behaviour (Fig. 7.21), where crack growth rate per cycle was apparently greater the lower the frequency (Fig. 7.22). This latter figure is directly comparable with Fig. 4.25 for compression specimens, and Figs. 7.23 (b) with Fig. 4.27 (c). Similar analogies exist for dry specimens : Fig. 7.25 (b) compared to Fig. 4.28. The implication is that the results of both systems are valid and self consistent. The damage monitoring rate of compression specimens is comparable to V-K data obtained from DT specimen at least as far as the effect of elapsed fatiguing time is concerned, (and also, as will be seen later, with respect to moisture and temperature effects). Thus it seems in order to consider the same mechanisms of fatigue and fracture as being applicable in both compression and DT fatigue, under similar test conditions.

The DT frequency series did, however, reveal an additional aspect of fracture not apparent in compression damage monitoring. Fig. 7.26 indicates the intermittent characteristic of 'a' versus 'N' curves consistent with sporadic crack arrest. Similar behaviour was also observed in the in situ SEM studies, but on a much smaller scale and under nominally dry and static conditions. Such behaviour is consistent with the crack encountering periodic crack stoppers, like aggregate or strong cement grains, that effectively arrest the crack for a short period. In due course the crack tip (or its process zone which probably amounts to the same thing) works its way around, or through, the obstacle and crack growth again proceeds at the uniform rate.

(ii) Environmental Moisture Dependence

The similarity in the results of time dependence studies, as outlined above, between DT and compression conditions carries over for both wet and dry testing environments. Further examination of comparative wet and

dry damage accumulation rate results and V-K curve results further substantiate the similarities. The relative amount of separation in (compression) damage rate in Fig. 4.26 is consistent with the separation or "shift" between wet and dry (DT based) V-K lines of Fig. 7.17(a) and (b). This is so for both fatigue (Fig. 7.17) as well as static (Fig. 7.14) wet versus dry tests.

(iii) Temperature Dependence

The microcracking rate results of tests at increased temperatures under water are again comparable in the compression and double torsion tests. Damage accumulation results were more difficult to obtain experimentally in the compression case, but the trend indicated in Figs. 4.41(a) and (b) is that the damage rate is greater at the higher temperature and also that the amount of microcracking damage is also greater at the higher temperature, as indicated by the AE pseudo isometric plot results (Fig. 4.42).

In the case of the double torsion tests the crack growth rate results are more readily noticeable. DT changeover tests from 25°C to 55°C immediately revealed accelerated crack growth rates (Figs. 7.20 (a) and 7.28) even though with time at temperature the rate subsequently appeared to decrease (Figs. 7.28 and 7.29). It is quite clear, however, that the crack growth rate, $\frac{da}{dt}$ (or V), accelerates by about 20 to 30 times with water temperature changes from 25°C to 55°C, for both static (Fig. 7.15) and fatigue (Fig. 7.16) cases. Such behaviour is consistent with a thermally-activated cracking mechanism, such as stress corrosion, for which an activation energy was meaningful. Its evaluation and some discussion on activation energy were covered in Chapter 7.

8.4.5 Summary

This section has established the strong correlation between damage accumulation results, obtained in compression, with V-K single crack growth data obtained from DT specimens, for the major testing conditions of variable frequency, time duration, environmental moisture and temperature. The equivalence of microcracking damage and single crack growth is clearly apparent and it thus appears in order to examine the microcracking mechanism of each case together. Such a mechanism would

apparently depend on elapsed time, amplitude of fatigue (from the g factor studies of Evans and Fuller (235)), availability of moisture (a strong dependence) and temperature (in a thermally activated manner consistent with Arrhenius behaviour.) The mechanism or model would also need to accommodate the phenomenological observations of no true strain rate; decreased life and increased AE PIP for high dwell load fatigue tests; the intermittent characteristic of crack growth rate (as observed in section 8.3.4.2 and Fig. 7.26); the sigmoidal (3 regime) behaviour of damage development and a deceleration in crack growth rate with time for DT specimens subjected to sustained high temperature (Fig. 7.28). A form of microcrack interaction of the crack tip coupled with stress corrosion cracking is consistent with these requirements and this is discussed, together with microcracking and crack propagation for the present material, in more detail in the following section.

8.5. Discussion of Microcracking and a Model for Crack Propagation

8.5.1 Introduction

The previous section has shown that double torsion and compression specimens of mortar respond in very similar ways to cyclic fatigue. The equivalence of microcracking, on the one hand as damage in compression prisms, and on the other ahead of a 'single' crack has been highlighted. It is now appropriate to examine the mechanistic details of such microcracking in greater depth and also to consider models to describe the fatigue fracture of the material used in this study. These topics are discussed in this section.

8.5.2 Microcracking and Mechanistic Models of Fracture

It is appropriate firstly to put forward a mechanistic explanation of the sigmoidal (3 phase) damage development behaviour so frequently observed. The form of the damage development in compression fatigue has been shown (at 80% maximum stress level at least) to be of a sigmoidal form (Figs. 4.3, 4.5, 4.9, 4.22 to 4.24). It is quite apparent that, when fatigue loading is first initiated, there is an early rapid change in both the transit time (for example, Fig. 4.5) and the measured surface strain (e.g. Fig. 4.10(c)). After this initial change the rate of increase diminishes until damage development rates become virtually linear.

The interpretation of this behaviour lies in the interaction of stress and strain fields associated with the crack tips of pre-existing microcracks, as outlined in section 8.2.4.1. During the first fatigue load cycle, stress fields and associated strain fields increase at pre-existing flaws or microcracks. In certain cases (for the larger of these microcracks) the local increase in stress intensity will be sufficient to propagate the flaw slightly and some of the stored strain energy will be absorbed in generation of the new fracture surfaces. In so doing there will be a reduction in the stored strain energy to levels below that required to propagate the microcrack. In addition the microcrack may encounter locally more crack resistant (tougher)regions like cement or sand grains, and this microcrack will arrest.

Other microcracks in the vicinity of the first may, however, be smaller, and hence have a smaller stress field and stored strain energy field associated with it. Thus on first fatigue loading such (smaller) microcracks may not propagate. On subsequent fatigue loadings, however, the zone of microcracking and stored strain energy field of the first flaw (now slightly propagated) could now interact with the strain energy field of these secondary smaller flaws to the extent that one or more of them could propagate.

Such a process is expected to develop rapidly in the first few fatigue load cycles as almost all such readily achievable microcrack interactions and slight crack propagations take place and stable local stress conditions are achieved. In a sense all the "susceptible" microcracks have been 'unzipped', and further fatigue load applications do not in themselves cause significant further microcracking or damage, and the damage rate slows down, as observed, i.e. the start of stage II. This process of "unzipping" as mentioned in section 8.2.4.1 requires typically between 10 and 20 cycles at low frequencies (0.1 Hz) and approximately 100 cycles at high frequencies (10 Hz). Careful observation of non PIP acoustic emission results, e.g. Fig. 3.24, indicates substantial AE on first loading which rapidly dies away when equilibrium is achieved. Unfortuately the PIP recording system precluded the detection of such noise in the first few cycles. The local microcrack situation is now regarded as in relatively stable equilibrium and susceptible to the stress corrosion attack mechanism mentioned early. Bonds at microcrack

tips are highly stressed due to the large stress concentration causing a high stress intensity and are more readily attacked by corrosive ions from the water (e.g. hydroxyl or hydrogen ions). The microcrack can then propagate further and relax the stored strain energy.

This process is interpreted as continuing steadily and uniformly as indicated by the linear (stage II) portion of the damage accumulation curves. It takes a finite time for the corrosive attack to occur and thus individual cracks propagate in an intermittent manner. This is observed in the 'single' crack DT trace of crack length versus number of cycles, of (for example) Fig. 7.26, and indeed in the in situ SEM cracking (Fig. 7.16, sectin 8.3.4.2), albeit at a much smaller rate because of the much reduced moisture content, in the clinker specimen in the SEM. This intermittent microcracking behaviour is also consistent with the intermittent or sporadic nature of the acoustic emission PIP observations.

The third regime of the sigmoidal damage development curves is interpreted as the stage at which any further microcrack propagation can only occur by microcracks interconnecting. The structure becomes effectively full of microcracks and the stage is reached where they interconnect to form macrocracks. It has already been noted (in Chapter 5) that there is more microcracking under fatigue than static conditions. The energy absorbed from fresh surfaces is now not sufficient to accommodate all the crack tip strain energy due to stress concentrations of the (larger) crack and the system becomes unstable. More macrocracks rapidly develop and interlink and final fracture soon follows.

This model seems to be consistent with the observation that at <u>low</u> fatigue stress levels the degree of damage changes very little after first loading. The first few load cycles cause the material to take up the stress slightly, propagate all the potentially susceptible cracks (by the above mechanism) within its load capabilities, and thus relieve the stresses and reduce the strain energy. Subsequent fatigue loadings do not, however, because they are low, increase the local stress intensity sufficiently to cause either significant additional crack propagation or associated stress corrosion cracking attack and thus the damage traces

remain virtually unchanged with time (or number of cycles). Very gradually there may indeed be very slow crack propagation and associated reduction of stored strain energy with resultant microcrack interaction but the process is very much slower than at higher stress levels.

Conversely, it also follows that fatigue at high stress levels leads to 'steep' sigmoidal damage curves because of the relatively large degree of localised cracking occuring (because applied loads are so much closer to ultimate) with a greater associated stress corrosion cracking component since the stresses are higher.

Such discussion would appear to explain the form and shape of the sigmoidal damage curves, as well as their relative steepness. Similar models have been inferred by Stroeven (309) and Kotsovos (488). It is in order to examine the double torsion microcracking case for a moment to evaluate why it does not also exhibit similar sigmoidal rate behaviour. The answer really lies in the fact that for at least the middle third of the DT specimen and probably as much as the central fifty percent, the applied stress intensity is effectively constant, despite increasing single crack length (Section 6.4.5 and Fig. 6.15). Hence the observed fatigue crack propagation rate is also effectively constant (e.g. Fig. 7.19 and 7.21), except perhaps for very localised sporadic arrests (Fig. 7.26). In the compression case, however, as a microcrack develops (even into a macrocrack) the stress intensity increases with crack length (for the same applied load conditions) thus providing the increased driving force to crack it further.

It is also interesting to note that the above concept of microcracking in fatigue is consistent with observed changes in modulus, or more strictly, stress-strain behaviour. The increased degree or extent of microcracking as fatigue progresses would result in a more compliant structure and this is indeed the situation as shown in Figs. 2.29 (143), and Fig. 2.31 (a) (from the present study). Because the structure is more microcracked as a result of fatigue it becomes softer, or more compliant, as fatigue progresses.

It has been suggested (e.g. 46, 269, 374) that fatigue failure is associated with a limiting or critical strain criterion but no evidence

of this was found by the author in the present tests. Such a critical strain concept may also be at odds with the above microcracking model, since the stage at which final failure occurs depends on the degree of microcracking in the structure and also on the fatigue test conditions.

The model of microcracking and crack tip strain energy field-microcrack interaction would be in accordance with the temperature test results as well. It is reasonable to suppose that the microcracking process under wet and heated conditions is thermally activated. This is seen to be the case with the rate of microcracking damage accumulation being greater under both wet and hot conditions in accordance with an Arrhenius behaviour (Figs. 4.26, 4.41, 4.42, 7.14 to 7.17, and Fig. 7.20). A moisture dependent thermally activated mechanism of microcracking attack is therefore suggested. Indeed, Terrien, (225) from acoustic emission studies of concrete, regards the presence of water as accelerating the microcracking and thus enhancing the relaxation of applied stresses. The means of microcrack acceleration under wet conditions may even be due to reductions in the C-S-H solid surface tension in underwater environments.

The results of the waveform tests (fast loading versus fast unloading) indicated that there did not appear to be any true strain rate fracture mechanism and that elapsed fatiguing time (from the frequency effect studies) appears of more importance. The fatigue tests incorporating a dwell period at either the maximum or minimum load (section 4.4.4) further indicated the likelihood of a stress dependent moisture enhanced fracture mechanism, since the average lives at high level dwell compared to low level dwell were 270 and 1005 cycles respectively.

The acoustic emission results add further insight to the nature of the cracking mechanism. The normal AE behaviour, as is evident from almost any of the AE PIP traces shown in this thesis, was that noise (and cracking) was intermittent or sporadic. There was always a lot of noise on first loading in fatigue (often unfortunately lost as the PIP and load thresholds were set) but subsequently the fatigue process was not in itself very noisy. The applied loads in fatigue were identical and so it is to be expected from the Kaiser effect studies (section 3.5.4.5 and Fig. 3.23) that noise would be very limited unless the previously experienced local stress intensity level was exceeded. This "stress

intensity level" does indeed become exceeded, but only for a localised regime as crack tip strain field interaction and cracking take place (assisted by moisture dependent mechanisms). Thus the AE PIP behaviour also seems to be in line with this microcracking model.

With regard to the fatigue dwell tests recently mentioned it was clearly apparent that fatigue lives were shorter at the greater sustained stress level. The damage accumulation behaviour was seemingly similar from the AE PIP viewpoint (except for the shorter life) Fig. 4.40,. Closer examination of the PIP trace, Fig. 4.40, however, revealed there was more AE noise close to the maximum stress level in the short life (high stress level) case. Exactly such behaviour might be expected from a sustained stress dependent failure mechanism, such as stress corrosion, since the microcracking - and AE - would be greatest at the largest stresses, which in this case is longer lasting.

8.5.3 Fundamental Mechanistic Models of Fatigue Microcracking

The microcracking models discussed in section 8.2.4 were concerned with evaluation at a microscopic level and the subsequent strain energy field-microcrack interaction model developed. This section is concerned with cracking mechanisms at an even greater magnification on a more fundamental level.

The cracking mechanism would need to be compatible with the observations that microcracking increases with (and fatigue is hastened by) : larger cyclic stress amplitude, increased maximum stress, longer fatigue durations, presence of water and increases in temperature. (This is evident at least for the high fatigue stress levels investigated in this thesis.) The mechanism of a form of stress corrosion has been mentioned on various occasions and seems to be a viable mechanism. Before this is discussed in more detail, however, other mechanisms are examined.

Cuthrell (205, 359) has suggested that a form of Rebinder-Westwood attack may be responsbile (for certain ceramic materials at least), based on acoustic emission studies. Cuthrell suggests that hydrogen from the surrounding liquid may diffuse into highly stressed crack tip regions since it (the hydrogen atom) is so small. This could then cause

subsequent embrittlement and microcracking, as observed by AE techniques. Cuthrell's work pertains particularly to wear and abrasion, but it is reasonable to apply a similar type of argument to this case of weakening at the cement crack tips. If such a mechanism were to apply the diffusion rates would presumably be temperature dependent, and the observations of sections 4.5 and 7.4 indicate that microcracking growth rate does indeed increase with temperature. Further work needs to be undertaken, however, in different environments, particularly of variable pH and zeta potential, to test this mechanism (205, 359).

The concept of plasticity at a crack tip has also to be evaluated, and while this has been considered for various ceramic materials (234, 235), its application to cement materials is questionable. In such cement materials there does not appear to be any localised crack tip plasticity on a micro level (see, for example, the lack of any such evidence in the high magnification observations of section 8.3). In addition, the absence of a cyclic crack propagation effect (e.g. due to frequency or strain rate variations), tends to discount the existence of cyclic crack propagation mechanisms. It has been suggested by Krohn and Hasselman (375), that localised crack tip heating may occur (due to irreversible elastic extension and contraction of the bonds in the non linear region) which leads to an increased rate of slow crack growth, because the crack tip region attains a temperature that exceeds the ambient temperature. This heating phenomenon is expected to become more prominent as the frequency increases and hence, the heat dissipation rate increases. However, no such effect of increased cracking at the higher frequencies was observed. Evans and Linzer conducted similar high frequency fatigue studies on tungsten carbide cobalt, where localised crack tip plasticity does occur, and also observed the existence of a cyclic crack propagation effect (234). They conclude that crack tip plasticity may be a necessary but not sufficient condition for the onset of a cyclic crack propagation effect in ceramics.

For fatigue in ceramics Evans (389) considers various fundamental fatigue mechanisms that do not rely on crack tip plasticity. Two of these appear noteworthy in the context of cement mortar. One of these, consists of localised shear stresses and stress intensities developing at an inclined pre-existing microcrack to levels above the localised shear toughness,

K_{II}. Evans gives some involved mathematical justification (389) which is beyond the scope of the present thesis. Such a mechanism would appear to be independent of local moisture and temperature, however.

The other useful fatigue mechanism mentioned by Evans for ceramics pertains more to an established macrocrack. Such a macrocrack incorporates contacting asperities that form because of small displacements from stress relaxation of strain energy fields(Fig. 8.18). Very large stresses develop at the asperities during the compression half cycle and could lead to the formation of lateral cracks, from the highly stressed localised zone, (Fig. 8.18).

Such a mechanism seems viable for cement mortar as asperities and associated process zone cracking are indeed observed (Figs. 8.1, 8.13(b), 8.15 and 8.17(b)). Such a mechanism could also explain the AE PIP noise observed on unloading near the minimum load, as noted in Chapter 4 (e.g. Figs. 4.8, 4.13). However, such a noise source may be expected to occur on <u>every</u> unloading cycle and this was not observed. Thus the realistic application of this type of fatigue mechanism to cement mortar is again questionable and a return is made to the stress corrosion concept.

The g factor analysis due to Evans (234, 389), and Evans and Fuller (235) indicates that the acceleration in crack growth rate over and above static test rates, due to cycling, is merely a cyclic manifestation of stress corrosion cracking (for glass and porcelain (389)). In other words, for such materials, 'true' fatigue effects involing localised crack tip plasticity mechanisms, appear to be of minor significance, since there is good correlation between the fatigue data and the statically based g factor V-K line prediction. Parallel conclusions may be drawn here from cement mortar since the g factor prediction approach also appears valid (see Chapter 7 and Figs. 7.14 to 7.17). The mechanism of failure appears to be of the same form for both static and cyclic fatigue.

A type of stress corrosion mechanism, due possibly to hydroxyl ion attack of stressed silicate bonds in the vicintiy of the crack tip, is attractive since it appears to cover a large proportion of the observed phenomenology. For example, microcracking rate is faster in wet than dry

conditions and increases with temperature (Figs. 4.26, 7.14 to 7.17). However, the question of why fatigue still occurs in ostensibly dry environments still needs to be answered. The crack growth rate is significantly slower (Figs. 4.26, 7.14, 7.16, 7.17) and is postulated still to be due to a form of SCC since the relative humidities were only approximately 10 to 25% and not absolutely zero. Thus water was not entirely absent and SCC could still occur since, for example, Wiederhorn has observed SCC attack of silicate bonds (in glass) at humidities as low as 0.02% (Fig. 7.27). In addition there is a substantial amount of water intrinsic to hydrated mortar which is trapped in capillary pores, interlayer spaces or even as water of hydration (which exists even in dry specimens) and which could become available for SCC attack under appropriate high stress circumstances.

Finally, it is worth mentioning the hydrowedge mechanism of fatigue that was postulated in Chapter 7 and shown at least to be plausible and may explain the AE on unloading in the AE PIP traces for moist and wet specimens. However, the extent of its contribution to cracking may well be minor because of the absence of any waveform effect on crack growth rate.

8.6 Summary

(1) This chapter has examined the mechanisms and models of microcrack development and fatigue fracture by first reviewing existing literature and examining the process zone of microcracking near a crack tip. Models of stable microcracking have also been examined at a microcrack level.

(2) An in situ SEM study has been undertaken using small DT specimens which could be loaded inside the chamber of an SEM. The DT loading system coupled with specimen freeze drying enabled high resolution observations of crack growth to be undertaken. Cracking was controllable so that increments in crack length a fraction of a micron at a time could be made, for both cement mortar and a clinker type mortar. The in situ SEM observations indicated that cracking was tortuous and meandering and that there was an associated small process zone of up to a few

millimetres across in the vicinity of the crack tip. Cracking occurred not only around sand and clinker grains but also through them (especially with increasing hydration age in the latter case). Such observations of the multiple nature of microcracking indicate that fracture mechanics evaluations of toughness based on the concept of a single crack will be in error as the cracking area is very much larger than is superficially observed. Significant amounts of energy go into the creation of the process zone.

(3) Correspondence between compression microcrack damage and single crack growth from double torsion specimens is good and the rates of their development correlate very well for the parameters of moisture condition, elapsed testing time (or frequency) and temperature. Such differences as existed between the two testing techniques (compression and DT) arose more from experimental peculiarities rather than from intrinsic material differences. Generally the DT based V-K curves were more useful (than compression damage results) as they are amenable to a fracture mechanics interpretation. The compression fatigue studies did, however, yield valuable data, particularly from the AE pseudo isometric plot technique results.

(4) Microcracking models and mechanisms, appropriate to the material used here, were discussed, including creep, shear microcracking and crack tip plasticity. It was concluded that the probable process of microcracking in fatigue depended on a form of stress corrosion cracking. Such cracking could produce strain energy field interactions or microcrack interactions in the vicinity of propagating micro-flaws and microcracks in a manner consistent with observed sigmoidal damage development. A stress corrosion cracking mechanism is also regarded as compatible with the observations of increased rate of crack growth (i) in abundant moisture environments and (ii) at increased temperatures.

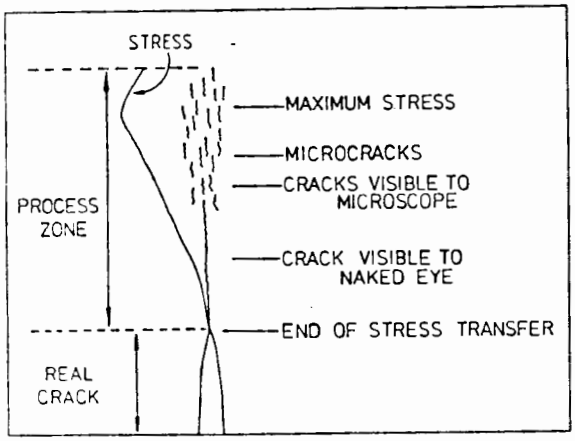

Fig. 8.1(a) The crack tip and process zone according to Hilleborg (393). The crack tip is not well defined.

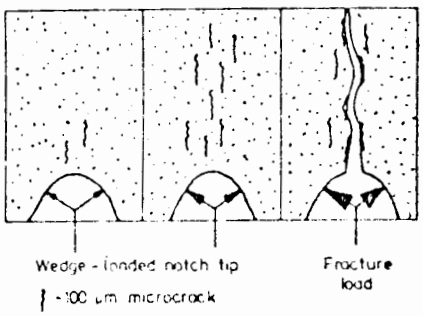

Fig. 8.1(b) Development of a propagating zone of microcracks in cement paste upon increasing tensile stress, (according to Higgins and Bailey (75).

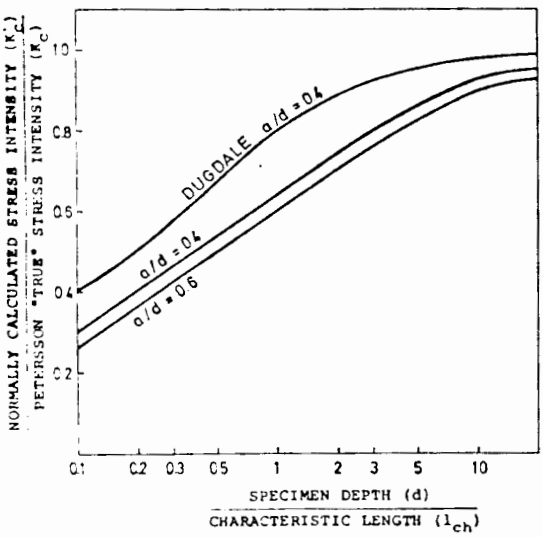

Fig. 8.2 Petersson's estimation (129) of the degree to which small specimens under - estimate the true toughness.

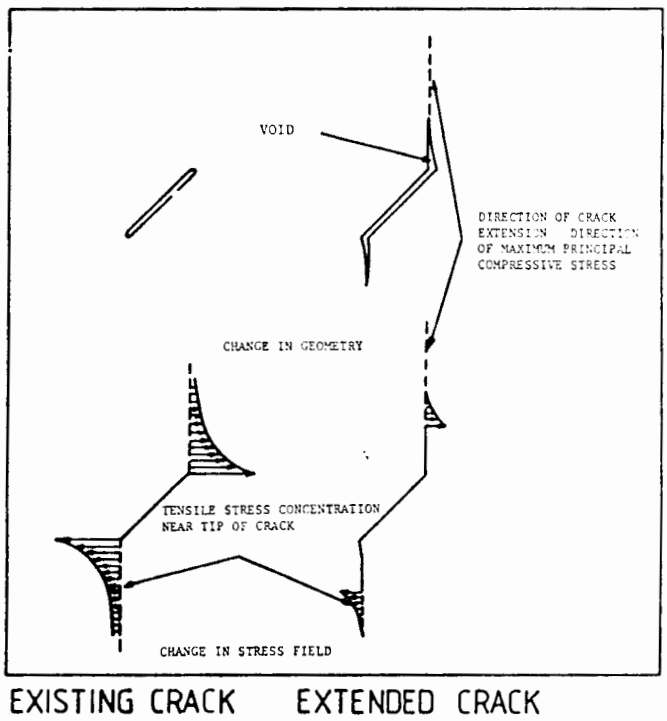

Fig. 8.3 Schematic representation of changes in crack geometry of stress field associated with crack extension. (after Kotsovos and Newman (367)).

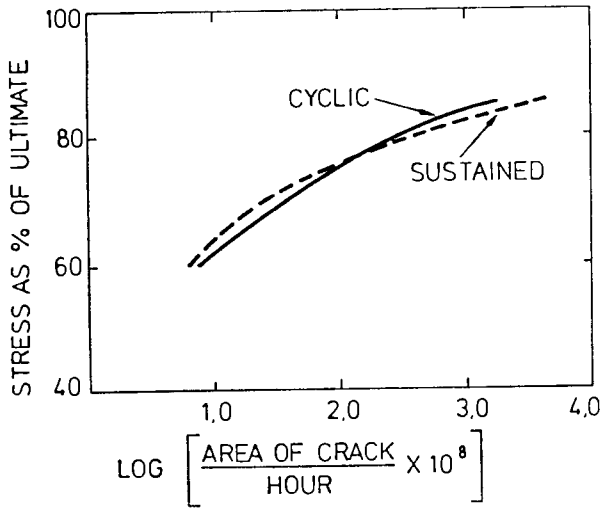

Fig. 8.4 Crack propagation rate under cyclic and sustained loading as estimated from crack areas. (After Shah and Chandra (89).

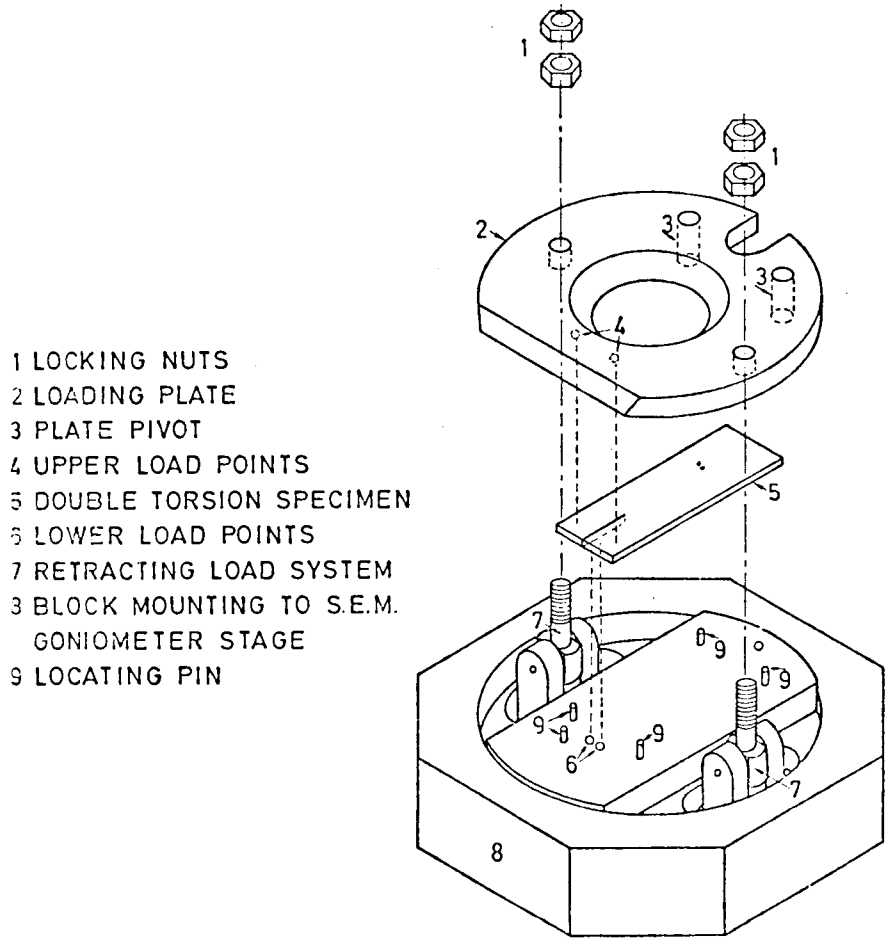

Fig. 8.5 Expanded view of the in situ scanning electron microscopes double torsion loading system.

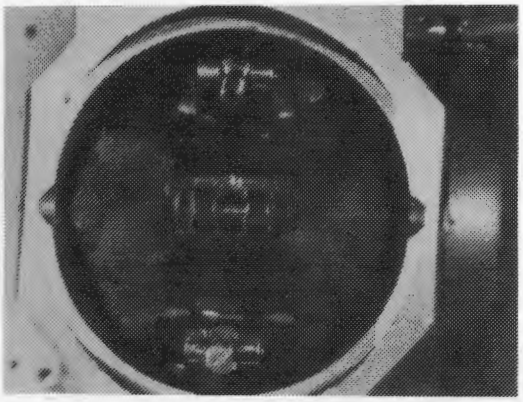

(a)

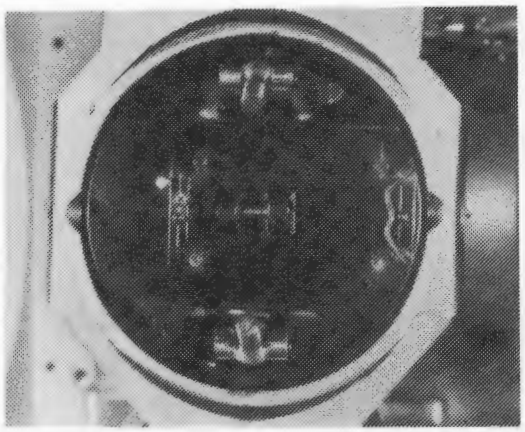

(b)

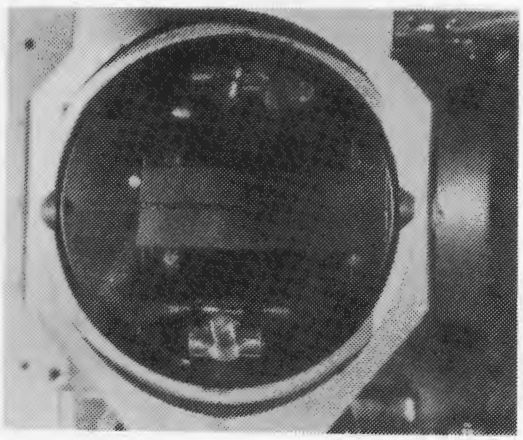

(c)

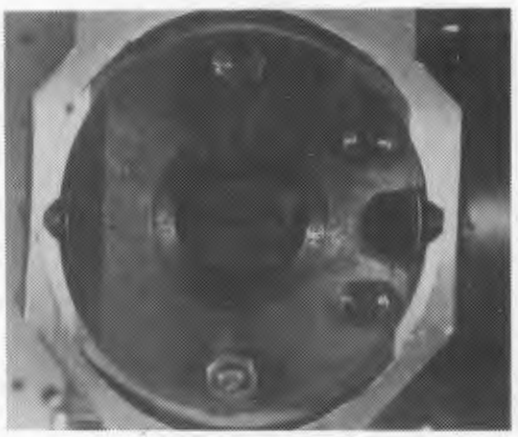

(d)

Fig. 8.6 Plan view photographs of the in situ DT loading rig. the original 3 point bend rig (a) has the central bend roller ocvered by the base plate in (b) which includes the lower (inner) DT specimenloading points and locating pins. The DT specimen is shown located in (c) with the loading plate secured in (d).

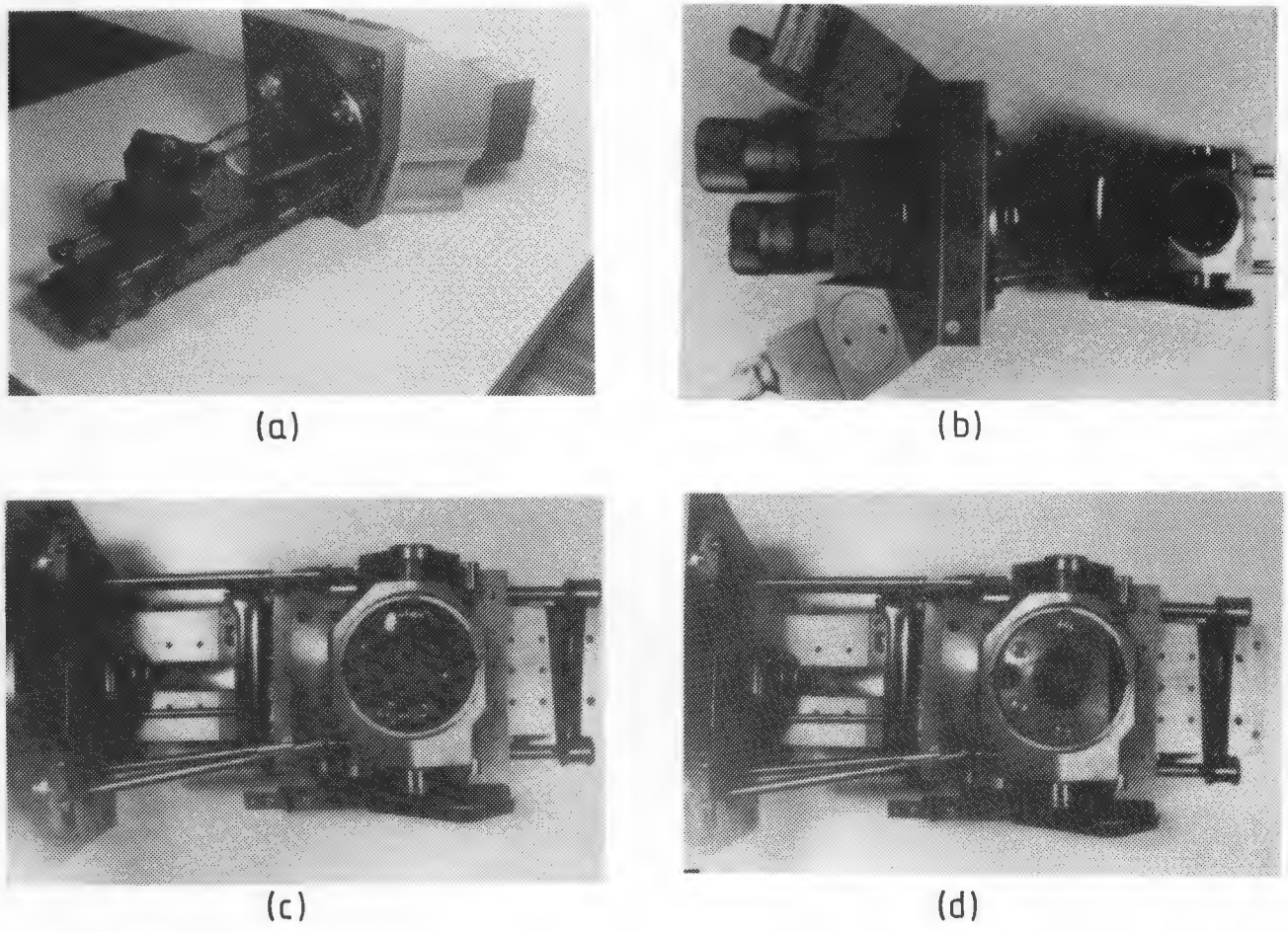

Fig. 8.7 The in situ loading system in its goniometer stage. Views a, b and c show the specimen without the loading plate while view d includes the loading plate. The vernier screw drives and articulation system for loading as well as conventional specimen translation and rotation are clearly apparent.

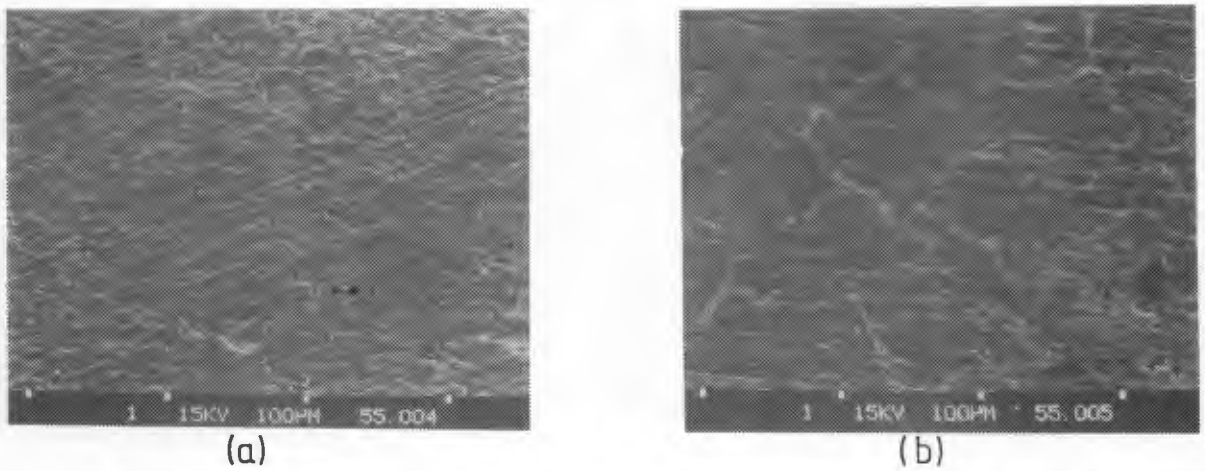

Fig. 8.8 Polished DT specimens at the same magnification (310x) showing the microcracking contrast from preparation by (a) freeze drying and (b) desiccator drying. There is generally substantially less microcracking using the freeze drying preparation technique.

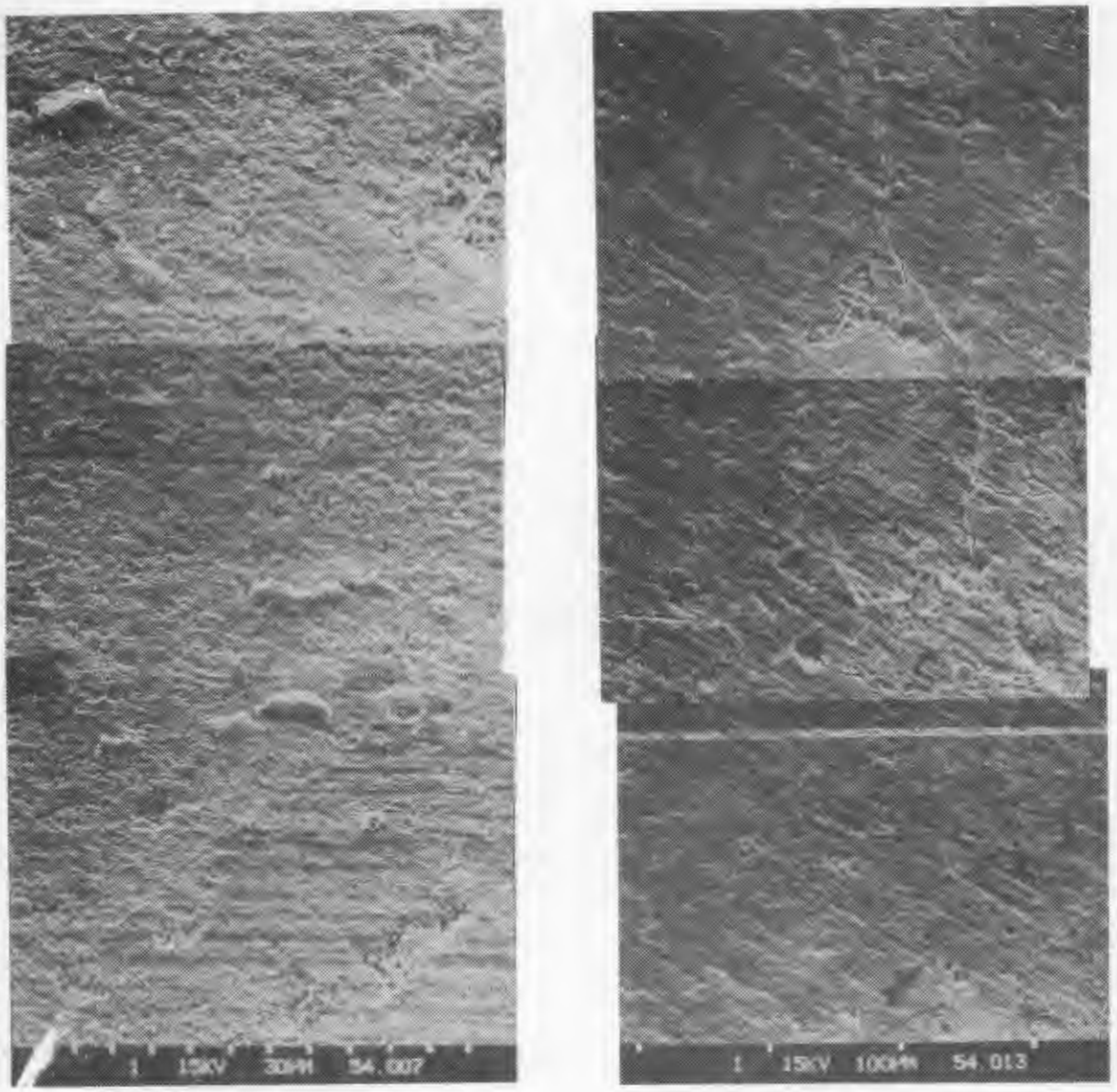

Fig. 8.9 Freeze dried (a) and desiccator dried (b) DT samples illustrating the reduction in surface microcracking with freeze drying.

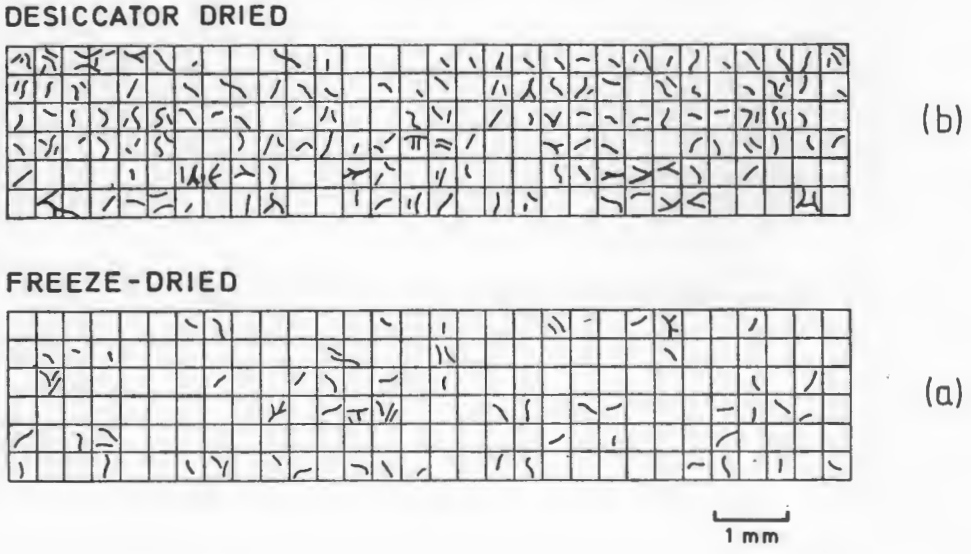

Fig. 8.10 Microcrack scan maps from (a) freeze dried and (b) desiccator dried DT specimens.

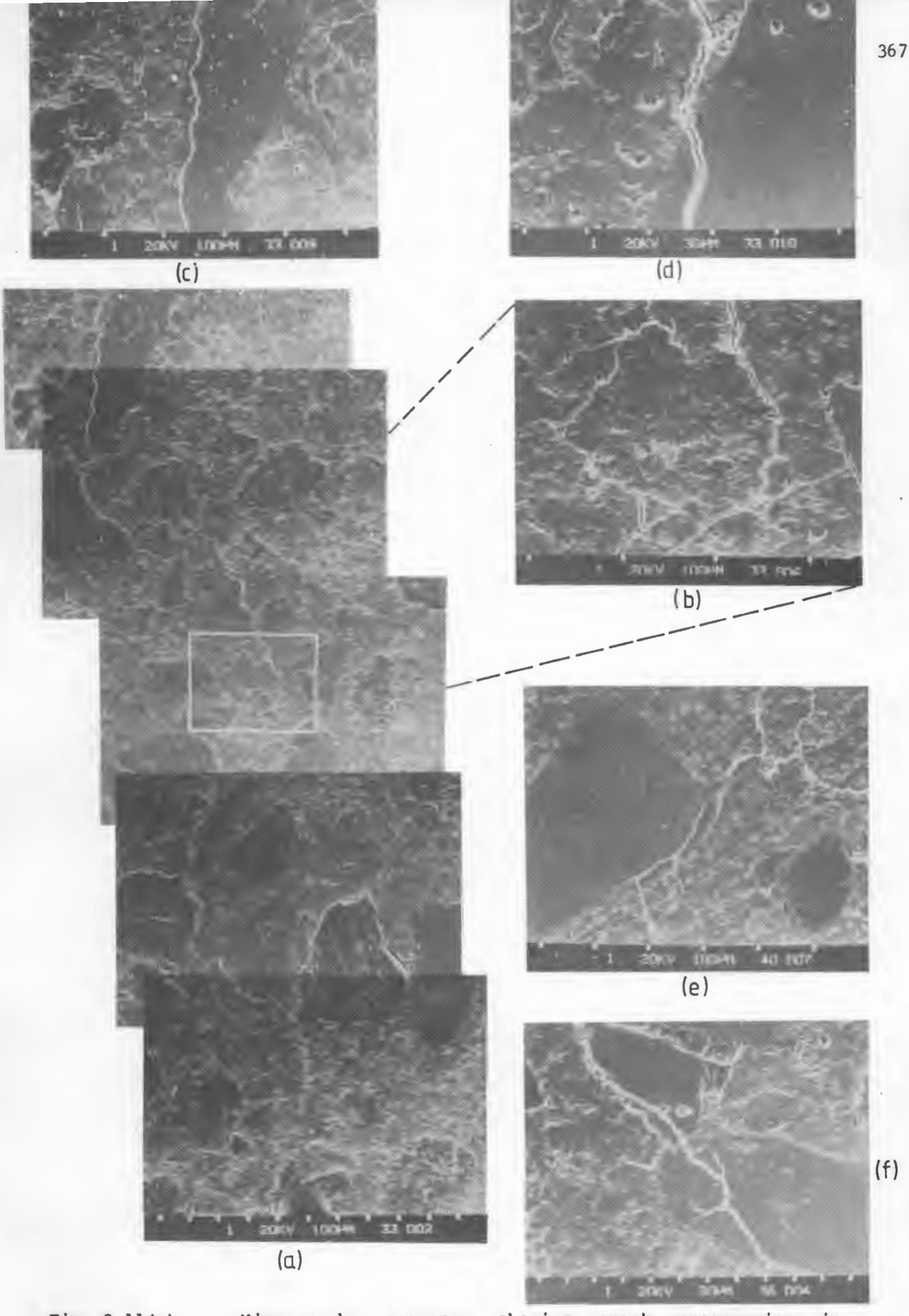

Fig. 8.11(a) Micrography sequence showing crack progression in mortar. The crack path is tortuous and meandering often exhibiting crack branching and crack jumping (b). (This micrograph is an enlargement of the box in (a)). The crack travels mostly around sand grains (a) but some cracking through them also occurs, (c) and (d), both with associated debonding (e) and (f) without. Fig. (f) also shows crack branching.

(a)

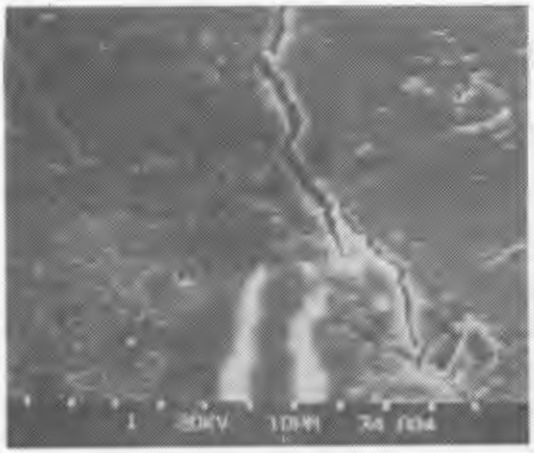

(b)

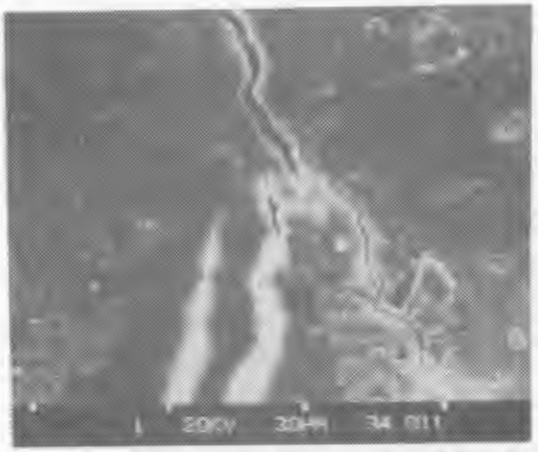

(c)

Fig. 8.12 (a,b,c) Sequential micrographas of the tip of a microcrack in a sand grain approaching a macrocrack following small successive load increments.

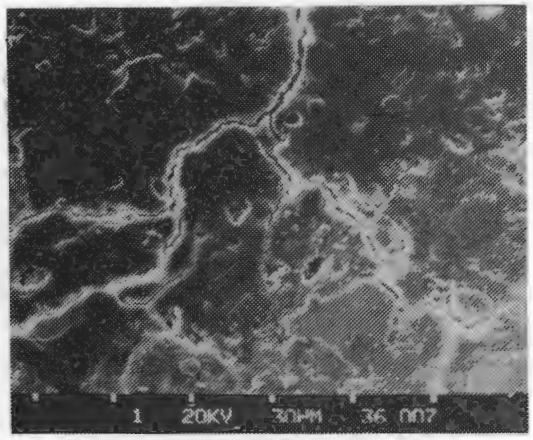

(a)

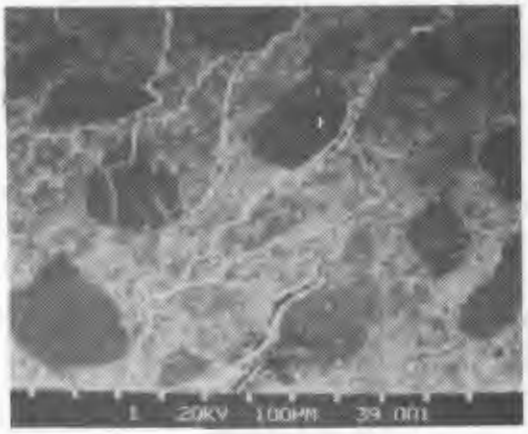

(b)

Fig. 8.13 Evidence of (a) crack branching and (b) crack discontinuity or "jumping". An impression of the process zone can also be obtained from these micrographs.

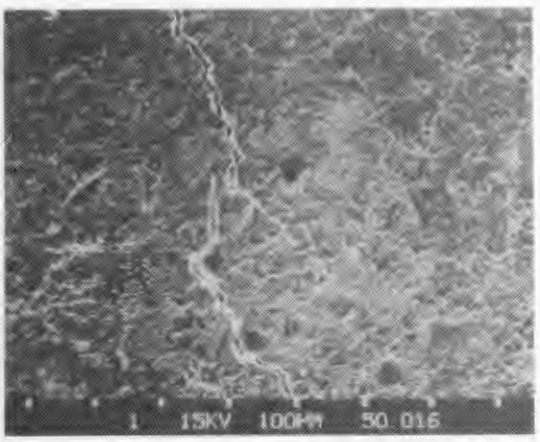

(b)

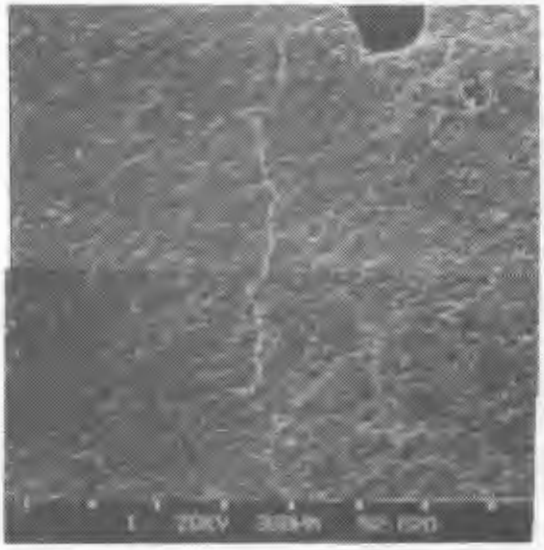

(a)

Fig. 8.14 Evidence of cracks going (a) mostly around clinker grains (in 3 day old cement) and (b) both around and through clinker grains (in 14 day old specimens). Fig. (b) also shows crack jumping (i.e. crack discontinuity).

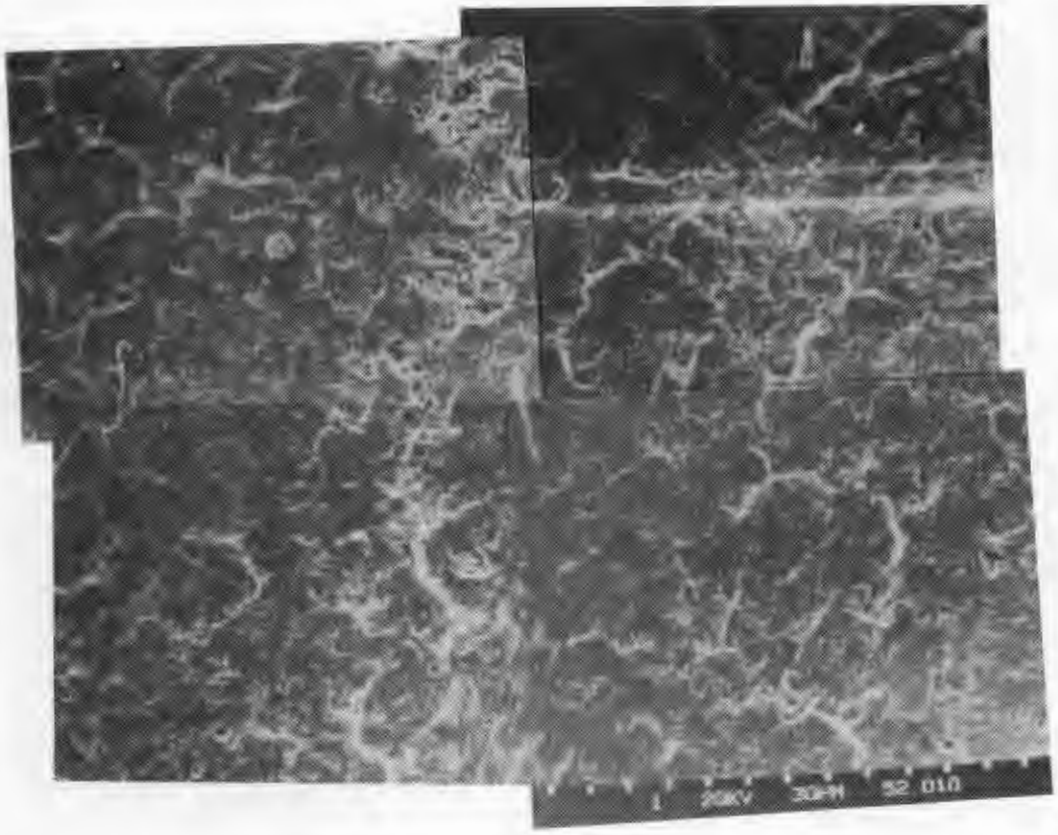

(a)

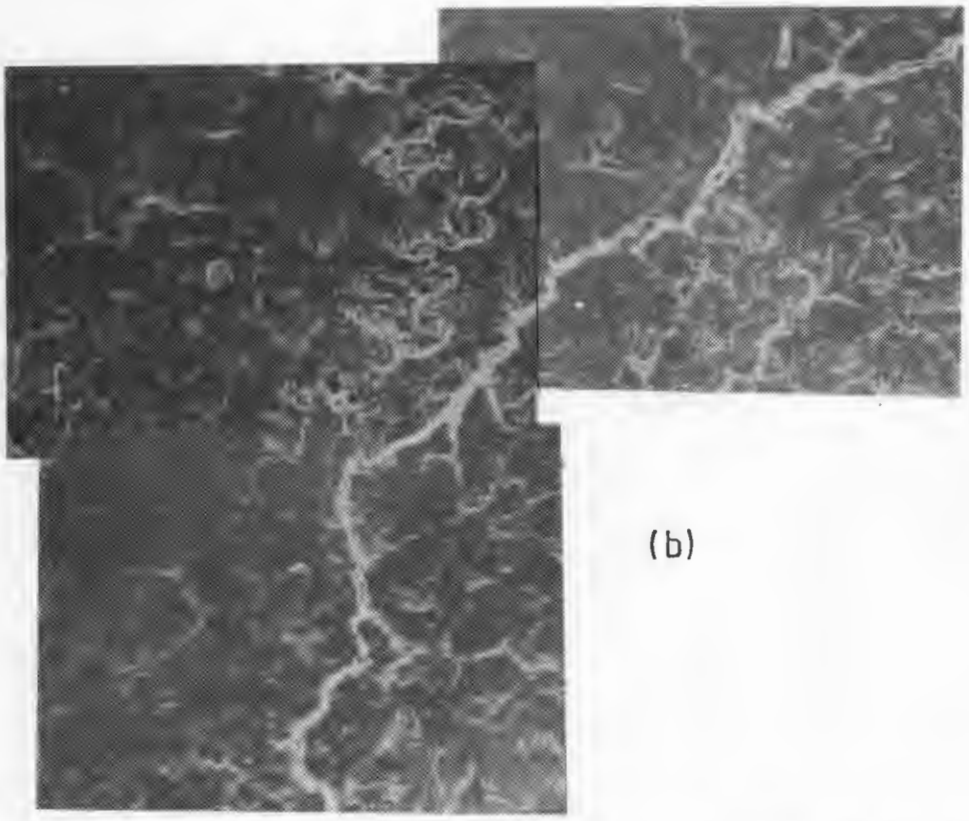

(b)

Fig. 8.15 Composite micrographs illustrating (a) the form of the process zone in the vicinity of the crack tip (major crack occurring from the top right hand corner). In (b) the macrocrack has passed and there is some relaxation of the process zone cracking.

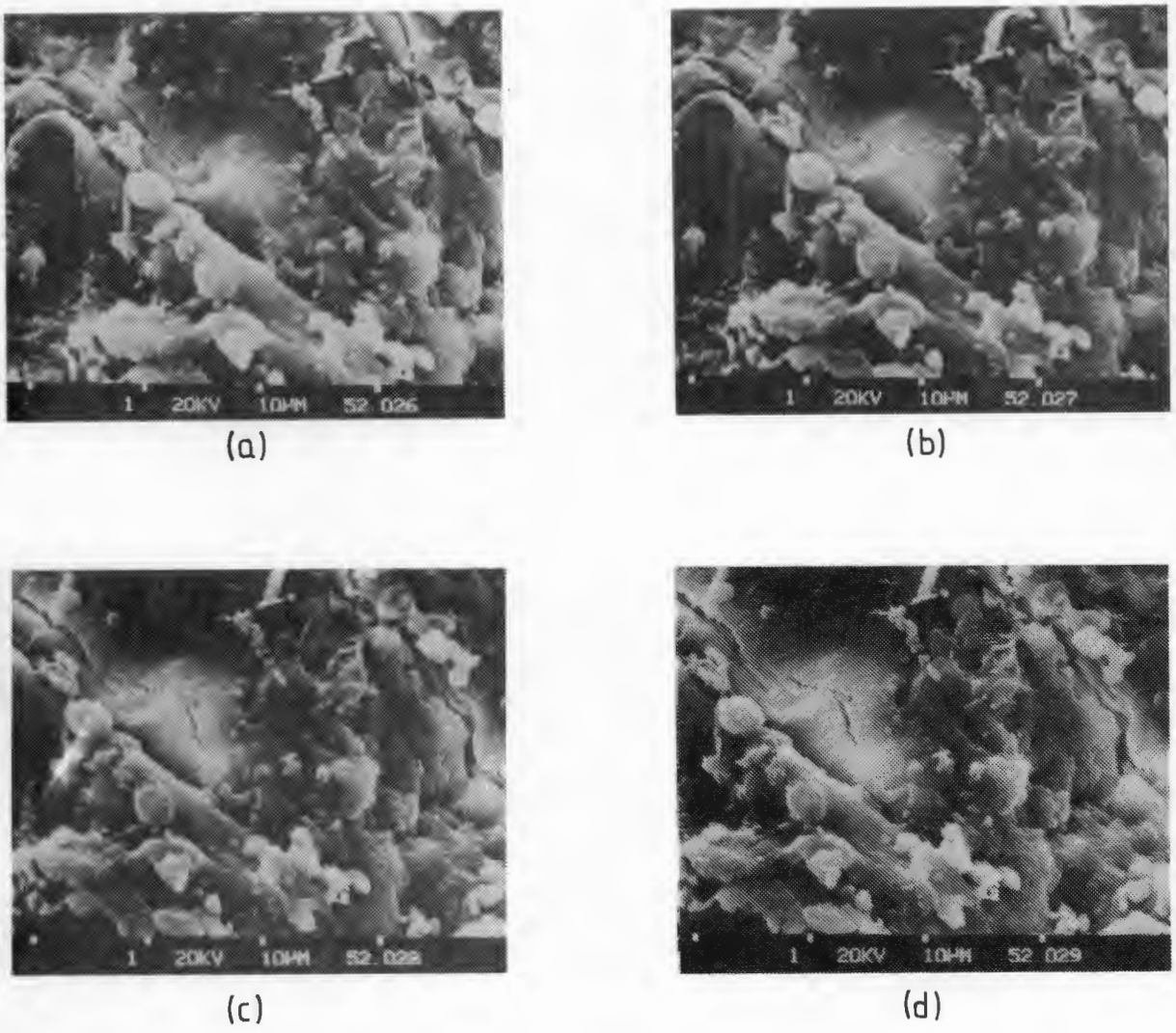

Fig. 8.16 Microcracking sequence of crack tip propagation in cement clinker (with the crack travelling from top left corner towards the bottom right corner). The slow increase in the growth of the crack following small load increments as seen in (a) to (d) illustrates the fine control of the in situ DT loading system.

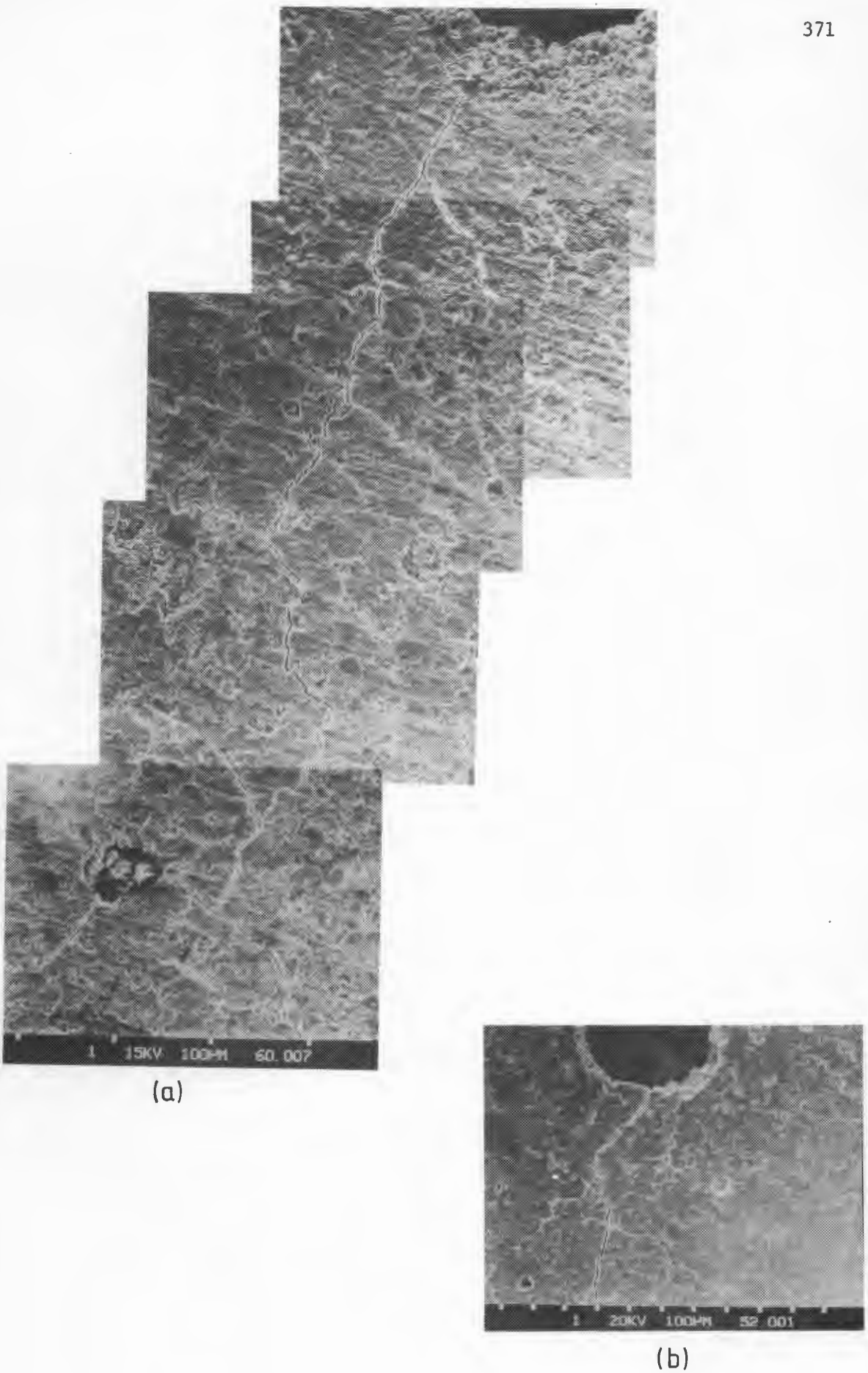

Fig. 8.17 Evidence of process zone microcracking in (a) 14 day old clinker cement and (b) 3 day old clinker cement. Small "veins" of microcracking showing extensive branching are also apparent in addition to the main crack (b).

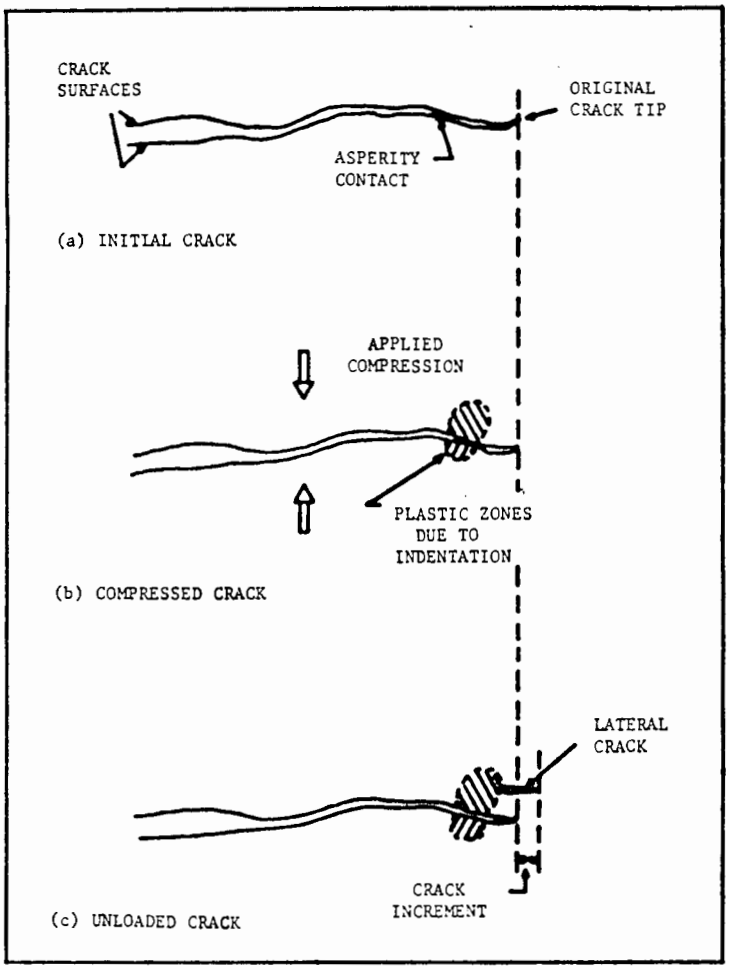

Fig. 8.18 The model for formation of lateral cracks at crack surface asperities (after Evans (389).

"Of that there is no manner of doubt
No probable, possible shadow of doubt -
No possible doubt whatever."!

W.S. Gilbert - The Gondaliers

CHAPTER NINE : SUMMARY, CONCLUSIONS AND FUTURE WORK

9.1 Introduction

The thesis set out to contribute to the understanding of fatigue and subsequent fracture of cement mortar. From a review of the literature it appeared that there were certain questions about the behaviour of mortar and concrete in fatigue which remained unanswered despite some substantial research efforts. Such questions included: what factors control the mechanical performance of concrete under service (e.g. fatigue) load conditions? what part do environmental and time-dependent aspects play in fatigue? how do cracks develop and propagate, at a microscopic level? how does microcracking damage intitiate and subsequent fracture occur? and what mechanistic models can be employed to describe the phenomenology?

Consequently an experimental fatigue testing programme was undertaken on cement mortar to try to answer these and related questions. Cement mortar was chosen as it is representative of concrete on a small scale, without the handling difficulties of cement paste or the aggregate consistency problems of concrete. The conclusions, as they have been developed through the thesis, are listed below.

9.2 Summary and Conclusions

1. An extensive review of the background to this work was undertaken in Chapter 2, covering cement hydration and the development of strength. Such a review of static strength development, including the importance of flaws was seen as a pre-requisite for the discussion of cement materials subject to fatigue loading. Specific shortcomings in the state of knowledge were identified and included the effect, on fatigue behaviour

and the associated development of damage due to microcracking, of cycling frequency, loading rate and waveform, environmental moisture condition, and temperature. Improved measurements of how damage develops and the ability to detect and subsequently track a crack were considered necessary, together with an assessment of whether fracture mechanics could meaningfully be applied to cement materials subject to fatigue as has been the case in metallic, polymeric and some other composite material systems.

2. Experimental details of compression fatigue testing were described in Chapter 3 and included details of ultrasonic pulse transit time (UPTT), strain and acoustic emission (AE) damage monitoring techniques, suitable for both static and fatigue tests. A novel pseudo-isometric plot (PIP) AE technique was developed for detecting where, on the load cycle, microcracking damage occurred during fatigue.

3. Compression fatigue studies on mortar prisms were undertaken (Chapter 4) to supplement the existing understanding that fatigue life is principally controlled by cyclic stress range and maximum cyclic stress level, assuming that other test conditions are constant. Fatigue of mortar can be adequately described in terms of the SN or Wohler curve approach.

4. Microcracking damage develops continuously during fatigue and the methods of measuring such damage accumulation in this thesis were particularly successful. Good correlation of general cracking behaviour, as well as macrocrack events, (Chapter 4) was obtained between the UPTT and AE (particularly PIP) methods, as well as surface strain monitoring (but to a lesser extent, as it was the least sensitive of the damage monitoring techniques.) Reliable mortar AE microcracking data was obtained in the frequency range 45 to 200 kHZ, by simple filtering to remove the (lower frequency) fatigue machine noise (Chapters 3 and 4).

5. Such AE was discrete and sporadic or intermittent and unquestionably associated with fatigue microcracking. Knowing the AE PIP noise characteristics it was possible to predict a macrocracking event or impending failure (Chapter 4).

6. The development with respect to time, of fatigue damage in compression occurred in three, fairly clearly delineated regimes (Chapters 3 and 4). There was an initial, rapid increase in microcracking following first application of the fatiguing load followed in stage II by an almost linear increase in the accumulation of damage. This led ultimately to a third, rapid damage accumulation stage, where cracks coalesced and final failure followed shortly afterwards.

7. Under constant compression fatigue conditions (i.e. constant cyclic load range and maximum stress level) other parameters become life controlling, for example, the duration of a fatigue test. This was inferred from fatigue frequency effect studies at 0.1, 1 and 10 Hz (Chapter 4). An initial distinction of microcracking damage accumulation rates into three (frequency) regimes was found to reduce to a simple fatigue duration time dependence.

8. Such independence from a true strain rate effect was further supported by the results of waveform tests which compared a fast loading sawtooth with a fast unloading sawtooth waveform (Chapter 4). There appeared to be no difference in fatigue lives or damage accumulation behaviour, suggesting that there was no rate dependence, and that elapsed test duration was of more importance.

9. Limited fatigue tests incorporating dwell periods at either a high compressive stress level or low stress level yielded shorter and longer lives respectively (Chapter 4). More AE PIP damage was also observed in the high dwell, short life tests at maximum load. Such behaviour is again consistent with a time dependent failure mechanism.

10. Compression fatigue tests on specimens dried to below 25% RH (and probably closer to 10%) yielded a higher fatigue strength (64% as compared to 54% for moist and wet specimens) (Chapter 4). Fatigue lifetimes also increased by about an order of magnitude. Damage accumulation rates were also similarly reduced for dry specimens.

11. Despite experimental difficulties, it was clear that underwater fatigue tests at $60^{o}C$ had shorter lives and sustained more damage than similar fatigue tests at the lower temperatures of $45^{o}C$ and $25^{o}C$ (Chapter 4).

12. A brief study of the effect of strength increases of up to 20% observed after prefatiguing in compression was described in Chapter 5. A model was proposed to explain the phenomenon, which relied on the initial exposure of unhydrated cement during fatigue (through process zone microcracking, or possibly, attrition). This was followed subsequently by rehydration of this exposed cement by available water. Dried specimens, free of uncombined moisture, did not exhibit any fatigue strengthening.

13. The damage monitoring studies of compression prisms in fatigue can not readily be interpreted in terms of actual flaw sizes or areas and hence, to provide some insight as to the value of a fracture mechanics approach, the project was extended to evaluate nominally "single" crack growth using double torsion (DT) specimens under similar test conditions to those used in compression fatigue tests.

14. A review of the application of fracture mechanics to cement materials was first required, particularly with regard to fatigue crack propagation, although aspects of the generation and application of static fracture toughness (K_{Ic}) values for concrete, mortar and cement paste were also briefly considered (Chapter 6). It would appear that, despite extensive literature on the subject, excessive "pseudo-plastic" behaviour invalidates the applicability of LEFM in its conventional usage. It may be concluded that either (a) the stress intensity factor is not a valid index for concrete fracture; or (b) fracture mechanics may only be applicable if the crack tip deformation/microcracking zone is either (i) relatively small, or (ii) accounted for by some means (e.g. Petersson's size correction); or (c) the mechanism of failure is independent of the geometry (and other factors mentioned earlier) and thus stress intensity is a valid index.

15. Fracture toughness and fatigue crack propagation testing techniques that yield stress intensities that are independent of crack length were examined in Chapter 6 - particularly the double cantilever beam (DCB) and double torsion (DT) methods. The experimental practicalities of the latter (DT) technique were considered in detail because of its extensive application in this thesis, expecially with respect to obtaining valid crack velocity-stress intensity, or V-K,

curves. It was considered that the stress intensity parameter, K, was meaningful for use in fatigue crack propagation studies if the material, which in reality is severely microcracked, is considered as a continuum.

16. An extensive experimental programme was undertaken to study 'single' crack fatigue crack propagation using the DT system, as described in Chapter 7, and techniques for observing the crack 'tip' under dry, moist and underwater conditions have been developed.

17. Crack growth data was processed in the form of V-K, curves to facilitate quantitative evaluation of the influence of the experimental variables studied. 'Static' V-K curves were also obtained using load relaxation at constant position and also (to a lesser extent) constant ramp rate/constant load methods and all these methods were found to give similar results.

18. Damage accumulation results obtained in compression fatigue under a variety of test conditions correlate very well with "single" crack growth rates obtained from DT tests under similar test conditions (Chapter 7 and 8). For example, the relative rates of microcrcking damage development (in compression tests) and single crack growth (in DT tests) exhibit very similar behaviour with respect to the effect of cycling frequency, environmental moisture and temperature.

19. Cyclic fatigue tests were undertaken for a variety of parameters including frequency (0.1 to 10 Hz), moisture environment (RH from 10% through to underwater tests), temperature ($25^{o}C$ to $55^{o}C$) and curing history (seven day old to 18 month old specimens). The DT fatigue method was particularly powerful as "changeover" tests could be undertaken. Here changing only one parameter during fatigue readily revealed any changes in crack growth rate, due to that parameter, without suffering from any experimental variability problems due to material or test system, etc., since the whole test was performed on the very same specimen.

20. Both static and fatigue V-K curve results reported in Chapter 7 showed that :

(i) changing from a dry to a wet condition resulted in a crack growth increase of about 4.5 orders of magnitude.

(ii) temperature increases (underwater) from 25°C to 55°C resulted in a crack growth rate increase of about 1.4 orders of magnitude (i.e. about 25 times). The crack growth rate was also reduced by increased curing.

21. The crack growth rates could be described by an Arrhenius type of equation (Chapter 7):-

$$\frac{da}{dt} = V = V_o \; K_I^n \exp\left(\frac{-\Delta H}{RT}\right)$$

The activation energy for crack propagation, ΔH, was approximately 83 to 99 kJ/mol. The so-called "stress corrosion index", n, was approximately 26 ± 4.

22. An in situ SEM system employing a miniature DT specimen loading rig and small (1mm thick) freeze dried specimens of mortar and clinker has been developed, as described in Chapter 8. Very fine control of cracking, to less than a micron, was obtainable, and facilitated careful observation of the character of cracking (under static loading). The crack path observed was tortuous and often, but interestingly, not always, around aggregate and cement grains. There was significant evidence of cracking through sand and cement grains, which seemed to increase with hydration age. The evidence of an extensively cracked process zone at the crack tip suggests that any fracture mechanics toughness measurements based on a measured crack length may be too low because of the substantial energy going into creating these cracked surfaces.

23. The microcracking behaviour in mortar, when viewed as a 'single' crack, was of a stepped or intermittent nature at both a microscopic level (in the in situ DT SEM studies) and in DT fatigue studies (Fig. 7.26).

24. DT changeover tests underwater, with temperature as the variable parameter, indicated that a temperature increase from 25°C to 55°C resulted in an immediate increase in crack growth rate. However, with time at this higher temperature the crack growth rate decelerated even to

levels below the initial growth rate. This latter phenomenon may possibly be attributable to the propagating crack encountering areas which had (by then experienced some accelerated curing.

25. Discussion of the development of microcracking and mechanisms of fracture has been given in Chapter 8. The process zone of microcracking in the vicinity of a crack tip has been reviewed in some detail, together with various models of microcracking.

26. Fatigue crack rate behaviour in the form of V-K curves can be predicted from static crack growth rates from an analysis due to Evans and Fuller (235). The implication is that the cracking mechanism is of the same form and in this case probably one of stress-assisted (in situ) environmental attack, or stress corrosion cracking. Evans and Fuller (235) regard such static and fatigue correspondence (in other materials) as merely the "cyclic manifestation of stress corrosion cracking."

27. A model of microcracking was proposed, involving localised stress corrosion cracking at crack tips, possibly involving hydroxyl ion attack of silicate bonds. This was followed by crack tip microcrack interaction and strain energy field interaction resulting in stress relaxation and appears to explain both the three phase sigmoidal damage accumulation behaviour and the single crack growth behaviour under all the test conditions and environments. The three phase sigmoidal behaviour of microcracking damage in fatigue is consistent with this model if microcracking is considered to stabilise and reach local equilibrium conditions only after 10 to 50 fatigue cycles. This is due to interaction of the microcracking zone of a propagating flaw with the strain energy field of the tip of a non propagating microcrack as discussed in section 8.5. Stage II corresponds with linear microcrack growth governed by the SCC mechanism. Stage III, of rapid fast fracture, is interpreted as the interconnecting of microcracks to form macrocracks without the capacity to absorb all the stored strain energy, with fast fracture soon following.

28. An additional mechanism of microcracking involving "hydrowedging" - trapping of water or debris in a closing crack - was considered, in view of the AE PIP noise observed close to the lowest load on unloading, and shown to be, at least, plausible. Its contribution may, however, be

relatively small in comparison to the more general microcracking, because of the absence of any strain rate dependence and because such AE PIP noise was only observed intermittently and not on every load cycle.

9.3 Future Work

This section lists future research work that should be undertaken following on from the studies described here, and is divided into (i) compression fatigue studies (ii) Double torsion studies (iii) In situ SEM fractographic studies and (iv) mechanistic studies. This list is by no means exhaustive but rather lists the more important future research areas in priority order, within each section.

9.3.1 Compression Fatigue Studies

- From the typical sigmoidal damage accumulation traces it was evident that significant amounts of microcracking occurred in the first few cycles. Techniques should be developed to monitor this damage in the first few cycles more carefully, particularly from an AE viewpoint. Unfortunately the requirements of the AE and PIP setting up system precluded the acquisition of such early AE PIP data. The solution to this problem could possibly lie in the presetting of the fatigue mean stress level and cyclic amplitude on the fatigue machine. The evaluation of the relative importance of the damage developed in the first few cycles could be considered in this way.

- It would be of particular interest to conduct compression fatigue test programmes (e.g. the frequency programme) on very dry specimens (i.e. with RH less than 0.01%). Since the suggested mechanism of microcracking was one of SCC it is conceivable that tests in an extremely dry environment would exhibit very little damage or very slow damage rates in fatigue, if this model is correct.

- With regard to the Kaiser effect in the AE studies it would be of interest to see to what extent specimens recovered (and therefore could again exhibit the Kaiser effect) after first loading, and how such recovery depended on elapsed time. Such studies would supplement the understanding of the microcracking interaction and stress relaxation model, as well as the rehydration concept described in Chapter 5.

- The variable load programme described by Hilsdorf and Kesler (157) and Bennett and Jinawath (156) involving, in effect, a constant cyclic stress but a change in mean level (Fig. 2.34(a)), needs further investigation. These authors' results are contradctory and reliable results of such tests, including both fatigue life and damage accumulation behaviour, would indicate the relative importance of cyclic stress amplitude and maximum stress level.

9.3.2 Double Torsion Studies

- Parallel, very dry (RH 0.01%) fatigue tests should be undertaken on DT specimens, again to evaluate whether fatigue crack growth rates are very much lower and whether the proposed SCC mechanism is indeed fully appropriate. It would be interesting to see if frequency effect changeover tests in such a regime would yield crack growth results which are still dependent on elapsed testing time.

- The deceleration of the crack growth rate at sustained high ($55^{o}C$) temperature after an initial increase in crack velocity (Fig. 7.28) is a particularly interesting phenomenon. An attempt to ascertain if it is indeed due to accelerated curing (as suggested in Chapter 7) could be made for both mortar and concrete specimens by comparing the crack growth rates of specimens which had had half the DT specimen (either the first half, or the second half) subject to an underwater preheating procedure at $60^{o}C$. At the boundary between the preheated to the non preheated material (in either direction) on the very same specimen, a change in crack growth rate would presumably be seen. Variations in preheat temperature and time would serve to quantify the significance of the effect.

- The periodic arrest characteristic of crack length 'a' versus number of cycles, N, for DT specimens needs to be investigated further to see whether the arrest phenomenon is more pronounced under wet than in dry conditions.

9.3.3 In Situ SEM DT Fractographic Studies

- A rigorous study of the crack path as a function of hydration age (intergranular versus transgranular) should be undertaken on cement clinker specimens using the powerful SEM in situ DT equipment. A further variable could be water-cement ratio and its effect on interparticle cracking (in both cement clinker and mortar) as a function of hydration age.

9.3.4 Mechanistic Studies

- In view of the proposed SCC mechanism, electrochemical corrosion studies of cracking in cement should be undertaken. Coupled with this is the effect of pH on the cracking behaviour and of ions in solution in the vicinity of the crack tip. For example, tests on specimens soaked in methanol could be undertaken. Such studies could serve to identify if hydroxyl ion attack of silicate bonds really does occur or whether hydrogen atoms play any significant role.

REFERENCES

1. D.D. Double "Cement - a respectable material?" Nature, Vol. 289, pp. 348,349, January 1981.

2. J.D. Birchall "Special report on the hydration of cement", Cem. and Conc. Res., Vol. 10, pp. 869-873, 1980.

3. J.D. Birchall, A.J. Howard and D.D. Double, Cem. Conc. Res. Vol. 10, pp. 145, 1980.

4. D.D. Double, A. Hellawell and S.J. Perry, Proc. Roy. Soc., London A 359, p.435, 1978.

5. D.D. Double and A. Hellawell "The solidification of cement" Scientific American, Vol. 237 (1) pp. 82-90, 1977.

6. H.M. Jennings and P.L. Pratt "On the hydration of cement" Proc. Brit. Ceramic Soc. No. 28. Special Edition Conf. Mineralogy of Ceramics, Edit. Taylor and Rogers, pp. 179-193, June 1979.

7. H.M. Jennings and P.L. Pratt "On the reactions leading to CSH, CH and ettringite during the hydration of cement" private communication, 1979.

8. S. Diamond and E.E. Lachowski "On the morphology of type III C-S-H gel" Cem. and Con. Res. Vol. 10 pp. 703-705, 1980.

9. S. Diamond "Proc of the conf. on hydraulic cement pastes; their structure and properties" Sheffield 8-9 April pp. 2-30, Cem. and Conc. Assoc. 1976.

10. P.L. Pratt and H.M. Jennings "The microchemistry and microstructure of portland cement" Ann. Rev. Mater. Sci. Vol. II pp. 723-49, 1981.

11. B.J. Dalgleish, A. Ghose, H.M. Jennings and P.L. Pratt "The early reaction between portland cement and water." Dept. Met. and Mat. Sci., Imperial College, Research Report, 1981.

12. J. Skalny, I. Jawed and H.F.W. Taylor "Studies on the hydration of cement - recent developments" World Cement Technology, Vol. 183, Sept. 1978.

13. A. Ghose, H.M. Jennings, P.L. Pratt and P. Barnes. "Fibrous growth products in the hydration of portland cement and related systems" private communication, 1981.

14. B.J. Dalgleish, P.L. Pratt and R.I. Moss. "Preparation techniques and the microscopical examination of portland cement paste and C_3S" Cement and Concrete Research, Vol. 10, pp. 665-676, 1980.

15. J.D. Birchall, A.J. Howard and K. Kendall, Nature, Vol. 292, July, 1981.

16. A. Kelly, F.R.S. Editorial of "Materials in Engineering Applications" Vol. 1, April 1979.

17. J.B. Martin, "Plasticity" MIT Press, 1975.

18. I.C. review "Economic Concrete" International Consturction, June 1982.

19. J.D. Birchall, J. Howard and K. Kendall "A concrete approach to the energy crisis" The Metallurgist and Materials Technology, pp. 35-38 January 1983.

20. A. Kelly, F.R.S. "Saving energy with organic solids" Physics Bulletin, p. 250, June 1977.

21. W.O. Alexander "Economics of energy and materials", J. Materials Science and Engineering, pp. 195-203, Vol. 29, 1977.

22. D.D. Double and A. Hellawell "The hydration of portland cement" Nature, Vol. 261, No. 5560, pp. 486-488, June 1976.

23. J.D. Birchall, A.J. Howard and K. Kendall "A cement spring" J. Material Science Letters, Vol. 1, pp.125-126, 1982.

24. R.B. Tait and S.S. Willmott, "Impact fracture of Dolosse" Fracture Research Report FRP 82/34, Metallurgy Dept. University of the Witwatersrand, Dec. 1982.

25. T.T.C. Hsu, "Fatigue of plain concrete" A.C.I. Journals pp. 292-305, July/Aug., 1981.

26. C.E. Kesler "Effect of speed of testing on the flexural strength of plain concrete", Proc. of Highway Research Board 32, pp. 251-258, 1953.

27. M.E. Awad and H.K. Hilsdorf, "Strength and deformation characteristics of plain concrete subject to high repeated and structural loads." Report No. 372, Civil. Eng. Dept., University of Illinois, Urbana, Feb. 1971.

28. P.R. Sparks and J.B. Menzies, "The effect of rate of loading upon the static and fatigue strength of plain concrete in compression" Mag. Conc. Res., Vol. 25, No. 83, pp. 73-80, June 1973.

29. J.E. Barrick and E.M. Krokosky, "The effects of temperature and relative humidity on static strength of hydrated portland cement." Journal of Testing and Evaluation, JTEVA, Vol. 4, No. 1, pp. 61-73, Jan. 1976.

30. A. Husak and E.M. Krokosky, "Static fatigue of hydrated cement concrete." American Conc. Inst. Journal, Vol. 68, No. 4, pp. 263-271, 1971.

31. B.C. Gerwick, "The role of FIP in research in concrete" Cement XXIX, No. 12, 1977.

32. F.M. Lea, "The chemistry of cement and concrete." 3rd Edn., Edward Arnold, 1970.

33. A.M. Neville, "Properties of concrete." Pitman Publishing Co., 1977.

34. C.V.Y. Chong, "Properties of Materials", M. and E. Handbook Pub. MacDonald and Evans, U.K., 1977.

35. F.S. Fulton, "Concrete Technology", Portland Cement Institute, Johannesburg, 1969.

36. S. Brunauer "Tobermorite gel - The heart of concrete", American Scientist (50), pp. 210-229, 1962.

37. H.F.W. Taylor "Mineralogy, microstructure and mechanical properties of cements", pp. 147-163, 1978.

38. J.D. Birchall, A.J. Howard and J.E. Bailey "On the hydration of portland cement" Proc. Roy. Soc. London, A Vol. 360, pp. 445-453, 1978.

39. R.B. Williamson, "Solidification of portland cement", Prg. Mat. Sci., Vol. 15, pp. 189-286, 1973.

40. R.H. Bogue and W. Lerch, "Hydration of portland cement compounds" Indust. Engineering Chem., Vol. 26, p. 837, 1934.

41. D. Walsh, M.A. Otooni, M.E. Taylor Jr. and Marcinkowski, J. Mat. Sci., Vol. 9, p. 423, 1974.

42. E. Brevel, Cement and Conc. Res., Vol. 6, p. 129, 1976.

43. A. Traetteberg and V.S. Ramachandran, J. Appl. Chem. and Biotech., Vol. 24, p. 157, 1974.

44. H.G. Midgely, "Electron microscopy of set portland cement Structure, Solid mechanics and engineering design. Ed. M. Te'eni, Wiley-Interscience, pp. 275-287, 1971.

45. J.A. Gard, J.W. Howison and H.F.W. Taylor, Mag. Corc. Res. 11 (33), pp.151-158, 1959.

46. D.H. Taylor, Jou. Testing and Evaluation, Vol. 5, No. 2, p. 102, 1977.

47. V.S. Ramachandran, Cement and Conc. Res., Vol. 6, p. 623, 1976.

48. V.S. Ramachandran and R.F. Feldman, J. Appl. Chem. and Biotech., Vol. 23 p. 625, 1973.

49. T.C. Powers, Proc. Int. Conf. on Struct. Conc. London 3rd 1965.

50. P. Barnes, A. Ghose and A.L. McKay "Cement tubules another look" Cement and Conc., Res. Vol. 10, p. 639, 1980.

51. J.D. Birchall "Discussion of paper 'Cement tubules another look' by P. Barnes, A. Ghose and A.L. McKay." Cement and Conc. Res. Vol. II, pp. 299-300, 1981.

52. J.E. Bailey and D. Chescoe "Microstructure development during the hydration of portland cement." Proc. Brit. Ceram. Soc. No. 28. Special edition Conf. Mineralogy of Ceramics, Edit. Taylor and Rogers, pp. 165-177, June 1979.

53. T.C. Powers and T.L. Brownyard, "Studies of the physical properties of hardened portland cement paste", Bull. 22, Portland Cement Assoc., Chicago, 1948.

54. D.D. Double, "A discussion of the paper 'Cement tubules another look' by P. Barnes, A. Ghose and A.L. McKay", Cem. and Conc. Res., Vol. 11, pp. 303-304, 1981.

55. N.L. Thomas, D.A. Jameson and D.D. Double "The effect of lead nitrate on the early hydration of portland cement" Cem. and Conc. Res., Vol. 11 pp. 143-153, 1981.

56. O.A. Kayyali, C.L. Page, A.G.B. Ritchie, "Frost action on immature cement paste - microstructural features" A.C. Journal, pp. 264-268, July/August, 1980.

57. T.C. Powers, J. Res. Dev. Labs., Portland Cement Assoc., 3(1) 47, 1961.

58. R.D. Coatman, N.L. Thomas and D.D. Double, "Studies on the growth of 'silicate gardens' and related phenomena J Mat . Sci., Vol. 15, pp. 2017-2026, 1980.

59. D.L. Kantro, S. Brunauer and C. Weise, J. Phys. Chem. 66 pp. 1804-9, 1962.

60. R.L. Berger, F.V. Lawrence Jr. and J.F. Young, "Studies on the hydration of tricalcium silicate pastes II. Strength development and fracture characteristics" Cem. and Conc. Res., 3 [5] pp. 497-508, 1973.

61. R.L. Berger, J.F. Young and F.V. Lawrence, Cem. and Conc. Res., 2633-36, 1972.

62. H.M. Jennings and P.L. Pratt, "An experimental argument for the existence of a protective membrane surrounding portland cement during the induction period", Cem. and Conc. Res., Vol. 9, pp. 501-506, 1979.

63. N.L. Thomas and D.D. Double, "Calcium and silicon concentrations in solution during the early hydration of portland cement and tricalcium silicate", Cem. and Conc. Res., Vol. 11, pp. 675-687, 1981.

64. A.A. Rahman and D.D. Double "Dilation of portland cement grains during early hydration and the effect of applied hydrostatic pressure on hydration", Cem. and Conc. Res., Vol. 12, pp. 33-38, 1982.

65. G.W. Groves, "Portland cement clinker viewed by T.E.M.", J. Mat. Sci., Vol. 16, pp. 1063-1070, 1981.

66. C.J. Goodbrake, J.F. Young and R.L. Berger, "Reaction of hydraulic calcium silicates with carbon dioxide and water", J. Amer. Ceram. Soc., Vol. 62, 9-10, pp. 488-491, Sept/Oct 1979.

67. J. Jambor, "Hydraulic cement pastes : their structure and properties" Cem. and Conc. Res., Assoc. (U.K.) p. 175, 1975.

68. R.F. Feldman and J.J. Beaudoin, "Microstructure and strength of hydrated cement", Cem. and Conc. Res., 76, p. 389, 1976.

69. R.F. Feldman and J.J. Beaudoin, "Structure and properties of porous cement systems and their modification by impregnants" Hydraulic Cement Pastes: their structure and properties. Proc. Conf. Sheffield, pp. 150-165, Cement and Concrete Assoc., 8,9 April 1976.

70. N. McN. Alford, Amer. Conc. Inst. Vol. 11 (4), p. 605, 1981.

71. N. McN. Alford and A.A. Rahman, "An assessment of porosity and pore sizes in hardened cement pastes", J. Mat. Sci., Vol. 16, pp. 3105-3114, 1981.

72. D.D. Higgins and J.E. Bailey, "Fracture measurements on cement paste", Jou. Mater. Sci., Vol. 11, pp. 1995-2003, 1976.

73. M. Wecharatana and S.P. Shah, "Double torsion tests for studying slow crack growth of portland cement mortar", Cem. and Conc. Res., Vol. 10, pp. 833-844, 1980.

74. R.B. Tait and H. Bohm, "In situ SEM examinations of double torsion fracture of concrete", Proc. of E.M. Soc. of S.A., p.29, Dec. 1980.

75. D.D. Higgins and J.F. Bailey, "Proceedings of the conference on hydraulic cement pastes : their structure and properties", Cem. and Conc. Assoc., pp. 283-296, Sheffield, April, 1976.

76. J.D. Birchall, A.J. Howard and K. Kendall, Nature, Vol. 289, No. 5796, p. 388, 1981.

77. N. McN. Alford, G.W. Groves and D.D. Double, "Physical properties of high strength cement pastes" Cem. and Conc. Res., Vol. 12, pp. 349-358, 1982.

78. S. Walker and D.L. Bloem, "Effects of aggregate size on properties of concrete" J. Amer. Conc. Inst., Vol. 57, pp. 283-298, Sept. 1960.

79. Duff A. Abrams, "Design of concrete mixtures" Bulletin No. 1 Structural Materials Research Laboratory, Lewis Institute, Chicago, Dec. 1918.

80. S. Popovics, "Generalization of the Abrams Law - prediction of strength development of concrete from cement properties" ACI Journal , pp. 123-129, March/April, 1981.

81. A. Hummel, Das Beton - ABC (Berlin W. Ernst, 1959).

82. R. Jones and M.F. Kaplan, "The effects of coarse aggregates on the mode of failure of concrete in compression and flexure" Mag. Conc. Res., Vol. 9, No. 26, pp. 89-94, August 1957.

83. T.T.C. Hsu, F.O. Slate, G.M. Sturman and G. Winter, "Microcracking of plain concrete and shape of the stress strain curve", J. Amer. Conc. Inst., Vol. 60 [2], pp. 209-224, 1963.

84. A. Liu, A. Nilson and F. Slate, A.C.I. Journals, Proc., 69, pp. 291-295, 1972.

85. K. Krishnaswamy, A.C.I. Journal, Proc. 65, pp. 856-862, 1968.

86. K. Alexander and J. Wardlow, Nature, Vol. 187, pp. 230-231, 1960.

87. H. Gilkey, A.C.I. Journal, Proc. 57, pp. 1287-1312, 1961.

88. D. Ravina, A.C.I. Journal, Proc. 70, pp. 582-588, 1973.

89. S.P. Shah and S. Chandra, J. Amer. Conc. Inst. Vol. 67, p. 816, 1970.

90. M.F. Kaplan, A.C.I. Journal, Proc. 55, pp. 1193-1208, 1959.

91. H.C. Entroy and Shacklock, "Design of high strength concrete mixes", Proc. Symposium on mix Design and Quality Control of Concrete, London, C and CA, pp. 55-73, May 1954.

92. J. Wastiels "Behaviour of concrete under multiaxial stresses - a review", Cem. and Conc. Res., Vol. 9, pp. 35-44, 1979.

93. S.P. Shah and G. Winter, "Inelastic behaviour and fracture of concrete: Causes, mechanisms and control of cracking in concrete" Amer. Conc. Inst. Sp. Publication No. 20 pp. S-28 1968.

94. A. Jensen, Acta Polytechnica Scandinavica, Civ. Eng. and Building Constr. Series, No. CI 66, p. 59, 1970.

95. E.W. Bennett, "Fatigue in Concrete", Concrete Vol. 8, No. 5, p. 43, May 1974.

96. E.W. Bennett and S.E. St. J. Muir, Mag. Conc. Res., Vol. 19, No. 59, p. 113, 1967.

97. H.A. Kormeling, A.J. Zielinski and H.W. Reinhardt, "Experiments on concrete under single and repeated uniaxial impact tensile loading", Delft University of Technology, Report 5-80-3, May 1980.

98. D. McHenry and J.J. Shideler, "Review of data on effect of speed in mechanical testing of concrete", ASTM, STP, No. 185 pp. 72-82, 1956.

99. D.C. Spooner "Stress strain time relationships for concrete", Mag. of Conc. Res., Vol. 23, No. 75-76, pp. 127, June 1971.

100. K. Komlos, "Investigation of rheological properties of concrete in uniaxial tension", Materialsprufing 12, 1970.

101. D.L. Birkimer and R. Linderman, "Dynamic tensile strength of concrete materials." Jou. A.C.I., Title 68-8, Jan. 1971.

102. B. Zech and F.J. Wittman, "Variability and mean value of strength of concrete as a function of load", A.C.I. Journal, pp. 358-362, Sept/Oct. 1980.

103. E.K. Schrader, "Impact resistance and test procedure for concrete", A.C.I. Journal, pp. 141-146, March/April 1981.

104. S. Mindess, J.S. Nadeau, "Effects of loading rate on the flexural strength of concrete mortar", Bull. Amer. Ceram. Soc., 56[4], 429-430, 1977.

105. S. Mindess, J.S. Nadeau and J.M. Hay, Cem. and Conc. Res., 4, (953), 1974.

106. J.E. Barrick, "The effect of temperature and relative humidity on static fatigue of hydrated portland cement", Ph.D. Thesis Carnegie Mellon University, USA., 1972.

107. D.R. McCreath, J.B. Newman and K. Newman, "The influence of aggregate particles on the local strain distrubtion and fracture mechanism of cement paste during drying shrinkage and loading to failure", Materiaux et Constructions Vol. 2, No. 7, pp. 73-84, 1969.

108. A.D. Morris, M. Sc. Thesis, University of Cape Town, 1978.

109. D.J. Cook and M.N. Haque, "Strength reduction and length changes in concrete and mortar on water and methanol sorption", Cem. and Conc. Res., 4(5), 735-744 (1974).

110. M.N. Haque, "Influences on flexural strength", Concrete, p.26 Feb. 1981.

111. S. Walker and D.L. Bloem, "Studies of flexural strength of concrete, Part 3, Effect of variation in testing procedures, ASTM, Proc. 57 pp. 1122, 1957.

112. D.J. Cook and M.N. Haque, "The effect of sorption on the tensile creep and strength reduction of dessicated concrete", Cem. and Conc. Res., 4, 3, 367-379, 1974.

113. P.W. Keene, "An unsolved mystery in concrete technology", Concrete p.31, November 1979.

114. J.C. Saeman and G.W. Washa, "Variation of mortar and concrete properties with temperature", J. Amer. Conc. Inst. Vol. 54, pp. 385-395, Nov. 1957.

115. G.J. Verbeck and R.H. Helmuth, "Structure and physical properties of cement paste", Proc. 5th Int. Symp. on the Chemistry of Cement. Part III pp 1-32, Tokyo, 1968.

116. P. Kleiger, "Effect of mixing and curing temperature on concrete strength, J. Amer. Conc. Inst. Vol. 54 pp. 1063-1081, June 1958.

117. N.G. Zolders, "Effect of high temperatures on concretes incorporating different aggregates", Mines Branch Research Report R64, Dept. of Mines, Ottowa, May 1960.

118. H.S. Lew and T.W. Reichard, "Mechanical properties of concrete at early ages", A.C.I. Journal pp. 533-542, October 1978.

119. H. Mihashi and M. Izumi, "A stochastic theory for concrete fracture", Cem. and Conc. Res., Vol. 7, No. 4, pp. 411-422, 1977.

120. A.M. Neville, "Properties of hardened concrete", Reinforced Concrete Engineering Vol. 1, Materials Structural Elements and Safety, Ed. by B. Bresler, Pub. Wiley, 1973.

121. T.Z. Harmathy and J.E. Berndt, "Hydrated cement and lightweight concrete at elevated temperatures" Journ. Amer. Conc. Inst. pp. 93-11, Jan. 1966.

122. H. Potgieter and R.B. Tait, Polymer impregnation of concrete", M. Sc. Thesis, (U.C.T.) 1980.

123. S. Walker and D.L. Bloem, "Effects of curing and moisture distribution on measured strength of concrete", Proc. Highway Research Board 36, pp. 334-346, 1957.

124. T.C. Hansen and L. Erikson, "Temperature Change effect on behaviour of cement paste mortar and concrete under load", Jour. Amer. Conc. Inst. pp. 489-503, April 1966.

125. British Standards Institute, Codes of Practice, CP110, CP114, 1972.

126. H. Green, "Impact strength of concrete", Proc. Inst. C.E. 28, pp. 383-396, London, July 1964.

127. D.J. Naus and J.L. Lott, "Fracture toughness of portland cement concretes", Jour. Amer. Conc. Inst. June 1969.

128. K.L. Watson, "The estimation of fracture surface energy as a measure of the toughness of hardened cement pastes", Cem. and Conc. Res., Vol. 8, No. 5, pp. 651-656, 1978.

129. P.E. Petersson, "Fracture energy of concrete : Method of determination" Cem. and Conc. Res., Vol. 10, pp. 78-89, 1980.

130. J.H. Brown and C.D. Pomeroy, "Fracture toughness of cement paste and mortars", Cem. and Conc. Res., Vol. 3, No. 4, pp. 475-480, 1973.

131. F. Moavenzadeh and R. Kuguel "Fracture of concrete", Journ. of Materials, JMLSA, Vol. 4, No. 3, pp. 497-519, Sept. 1969.

132. J.W. Murdock, "The mechanism of fatigue failure in concrete", Illinois, PhD. Thesis, 1960.

133. H.F. Clemmer, "Fatigue of concrete", Proc. ASTM , Vol. 22 II, 1922.

134. R.B. Crepps, "Fatigue of mortar", Proc. ASTM ,Vol. 23 II pp. 329-340, 1923.

135. J.W. Murdock, "A critical review of research on fatigue of plain concrete", University of Illinois, Engineering Bulletin. 1960

136. J.M. Hanson, "Considerations for design of concrete structures subject to fatigue loading", ACI Committee 215 Report, A.C.I. Journal, pp. 97-117, March 1974.

137. J.L. Van Ornum, Trans. Amer. Soc. Civ. Eng., Vol. 58, p. 190, 1903.

138. J. Antrim, Highway Res. Rec., 210, p. 95, 1968.

139. H.A. Williams, "Fatigue tests of lightweight aggregate concrete beams" Proc. A.C.I. Vol. 39, pp. 441-447, 1943.

140. J.A. Neal and C.E. Kesler, "Some aspects of the fatigue of concrete", T. and A.M. Report, No. 657, July 1963.

141. P. Stroeven, "Mechanics of microcracking in concrete subjected to fatigue loading", Mechanical behaviour of Materials Conference, Vol. 3, ICM 3, pp. 141-150, Cambridge, England, August 1979.

142. H.A.W. Cornelissen and G. Timmers, "Fatigue of plain concrete in uniaxial tension and alternating tension compression", Reports 5-81-7, Stevin Lab., Dept. Civ., Eng. Delft University of Technology, April 1981.

143. E.W. Bennet and N.K. Raju, "Structure, solid mechanics and engineering design", Ed. M. Te'eni, Wiley-Interscience, p.10, 1971.

144. C.E. Kessler, "Fatigue and fracture of concrete", Stanton Walker Lecture No. 8, Univ. of Maryland, 1970.

145. E. Probst, "The influence of rapidly alternating loading on concrete and reinforced concrete", The Structural Engineer, Vol. 9, pp. 410-429, December 1931.

146. J.W. Murdock and C.E. Kesler, The American Concrete Inst. 55, p. 221, 1958.

147. I.D.C. Imbert, "The effects of holes on tensile deformation in plain concrete" presented at Annual Conference, Highway Research Board, America, Jan. 1940.

148. J.T. McCall, "Probability of fatigue failure of plain concrete", Jour. Amer. Conc. Inst. Vol. 30, No. 2, pp. 233-245, August 1958.

149. G.L. Lott and C.E. Kesler, "Crack propagation in plain concrete", T.A.M. report 648, Illinois, Urbana, 1962.

150. J.A. Neal and C.E. Kessler, Proc. Int. Cong. on the Structure of Concrete, London, September, 1965.

151. K.O. Raithby and J.W. Galloway, "Effects of moisture condition, age and rate of loading on fatigue of plain concrete", S.P. 41, Abeles Symposium, pp. 15-33, 1971.

152. N.K. Raju, "Comparative study of the fatigue behaviour of concrete, mortar and paste in uniaxial compression", A.C.I. Journal, pp. 461-463, June 1970.

153. J. Glucklich, "Static and fatigue fracture of portland cement mortars in flexure", Proc. 1st Int. Conf. on Fracture, pp. 1343-1382, Sendai, Japan, V, 2, 1965.

154. J. Glucklich, "Fracture of plain concrete", Journal of the Engineering Mechanics Division, Proceedings, Amer. Soc. Div. Eng. Vol. 89, No. E.M.6, pp. 127-138, 1963.

155. J.H. Brown, "Measuring the fracture toughness of cement paste and mortar", Mag. Conc. Res., Vol. 24, No. 81, pp. 185-195, Dec. 1972.

156. E.W. Bennet and P. Jinawath, "Compressive strength of concrete under repeated loading of varying intensity" Leeds Univ.: Conf. on the service life of supporting structures in concrete and panel buildings, Brno, Czechoslovakia, Oct. 1975.

157. M.K. Hilsdorf and C.E. Kesler, "Fatigue strength of concrete under varying flexural stresses", Proc. A.C.I., pp. 1059-1075, 1966.

158. O. Graf and E. Brenner, "Experiments for investigating the resistance of concrete under often repeated compression loads", Bulletin No's 76 and 83, Deutscher Ausschus fur Eisenbeton, 1934 and 1936.

159. F.S. Ople and C.L. Hulsbos, "Probable fatigue life of plain concrete with a stress gradient", J. Amer. Conc. Inst., 63, pp. 59-81, Jan. 1966.

160. R.G. L'Hermite, "Volume Changes of Concrete", 4th Int. Symposium on Chem. of Cement, pp. 620-625, Washington D.C. Oct. 1960.

161. R.B. Tait and G.G. Garrett, "Mechanical behaviour and damage assessments in cement based materials", Research Report, Univ. of Cape Town, June 1978.

162. D.C. Spooner, Mag. Conc. Res., Vol. 24, No. 79, p. 85, 1972.

163. N. Venaut, Revue des Materiaux de Construction No. 550-551, p. 333, July-Aug. 1961; No. 552, p. 393, Sept. 61.

164. A. Neville, Civil Engineering, pp. 773-774, 1957.

165. A. de S. Jayatilaka and V.K.N. Nanayakkara, "Compression failures in brittle materials: relating observations to a theoretical model", J. Material Science 16, Letters, pp. 1726-1728, 1981.

166. ASTM - C - 42 - 68, 1968.

167. K. Newman and L. Lachance, Proc. of ASTM 64, pp. 1044-1067, 1964.

168. D.J. Cook and P. Chindaprasirt, "Influence of loading history upon the compressive properties of concrete", Mag. Conc. Res., Vol. 32, No. 111, pp. 89-100, June 1980.

169. H. Gonnerman, Structural materials Res. Lab., Bulletin 16, Lewis Institute, Chicago, 1952.

170. L. Mills and R. Zimmerman, A.C.I. Journal, Proc. 67 pp. 802-807, 1970.

171. H. Kupfer, H. Hilsdorf and H. Rusch, A.C.I. Journal, Proc. 66, pp. 656-666, 1969.

172. D. Hobbs, Cem. and Conc. Ass. Tech. Report. 42-484, 1973.

173. R.A. Ashbee, C.A.R. Heritage and R.W. Jordan, "The expanded hysteresis loop for measuring the damping properties of concrete", Mag. Conc. Res., Vol. 28, pp. 148, Sept. 1976.

174. British Standards Institution, B.S. 1881:1970, "Methods of testing Concrete".

175. R.P. Gerber and R.B. Tait, "Effects of the rate of loading on the fatigue of cement based materials", CSIR Research report, Aug. 1979.

176. R.W. Jordan, "The effect of stress, frequency, curing, mix and age upon the damping of concrete", Mag. Conc. Res., Vol. 32, No. 113, p. 195, Dec. 1980.

177. ASTM Code, C39-61, 1961.

178. H.W. Chung, "An appraisal of the ultrasonic pulse technique for detecting voids in concrete", Concrete, p. 25, Nov. 1978.

179. R. Jones, Brit., J. App. Phys., 3, 7 (p.229), 1952.

180. P. Desayi, "Fracture of Concrete in compression", Materials and structures : Research and Testing, Vol. 10, No. 57, pp. 139-144, June 1977.

181. F.E. Richart, A. Brandtzaeg and R.L. Brown, "A study of the failure of concrete under combined compressive stresses". Bulletin 185, Eng. Expt. station, University of Illinois, 1928.

182. M.F. Kaplan, "Strains and stresses of concrete at initiation of cracking near failure", A.C.I. Journal, p. 853, July 1963.

183. A.E. Cawkell, "Investigation of quality of thick concrete by ultrasonic pulse propagation", Mag. Conc. Res., Vol. 10, No. 28, pp. 23-26, March 1958.

184. A. Maher, D. Darwin, "Mortar constituent of concrete in compression", A.C.I. Journal, pp. 100-109, March 1982.

185. D.G. Spooner and J.W. Doughill, Mag. Conc. Res., 27, 9, p.151, 1975.

186. J. Glucklich, "The effect of microcracking on time dependent deformations and the long term strength of concrete", pp. 176-189, of the "Structure of Concrete", Eds. A.C., Brooks and K. Newman, Cem. and Conc. Ass., London, 1968.

187. A. Bentur, R.L. Berger, F.V. Lawrence, N.B. Milestone, S. Mindess and J.F. Young, "Creep and drying shrinkage of calcium silicate pastes - A hypothesis of irreversible strains", Cem. and Conc. Res., Vol. 9, pp. 83-96, 1979.

188. B.G. Long, H.J. Kurtz and T.A. Sandenaw , "An instrument and a technique for field determination of the modulus of elasticity and flexural strength of concrete pavements", Proc. A.C.I., PACIA, Vol. 41, p. 217, 1945.

189. D.A. Anderson and R.K. Seals, Pusle velocity as a prediction of 28 and 90 day strength, A.C.I. Journal, pp. 116, March, 1981.

190. M.F. Kaplan, "The effects of age and water cement ratio upon the relation between ultrasonic pulse velocity and compressive strength of concrete", Mag. of Conc. Res. (London), Vol. 11, No. 32, pp. 85-92; July, 1959.

191. M.F. Kaplan, "The relation between ultrasonic pulse velocity and the compressive strength of concretes having the same workability but different mix proportions", Mag. Conc. Res. (London), Vol. 12, No. 34, pp. 3-8, March 1960.

192. K. Newman and J.B. Newman, "Failure theories and design criteria for plain concrete" Imperial College, Research group report, Concrete materials, pp. 963-995, 1970.

193. N.K. Raju, "Small concrete specimens under repeated compressive loads by pulse velocity technique", Jour. of Matls JMLSA, Vol. 5, No. 2, p. 262, June 1970.

194. G.S. Robinson, "Methods of detecting the formation of an properties of microcracks in concrete", in AE Brooks and K. Newman (Eds) 'The Structure of Concrete", Cem. and Conc. Assoc. London pp. 131-145, 1968.

195. M. Russel, "N.D.T. System development unit, AERE Harwell, Type 3127-1, Instruction Manual", April 1975.

196. G.G. Garrett, R.D. Hoare, H.M. Jennings, A.D. Morris, D.J. Pitman and R.B. Tait, "Mechanical behaviour and damage assessment in cement based materials", C.S.I.R./A.E.B. Research Report, University of Cape Town, March, 1977.

197. G.G. Garrett, H.M. Jennings and R.B. Tait, "The fatigue hardening behaviour of cement based materials", Jou. Materials Sci. 14, p. 296,-306, 1979.

198. B.J. Dalgleish, P.L. Pratt and R.D. Rawlings, "The fracture toughness testing of ceramics and acoustic emission", Mat. Sci. and Engineering, 45, pp. 9-20, (1980).

199. A.S. Tetelman and A.G. Evans, "Failure prediction in brittle materials using fracture mechanics and acoustic emission", Fracture Mechanics of Ceramics, Plenum Press, pp. 895-924, 1974.

200. ASTM S.T.P. 505, "Acoustic emission testing", 1972.

201. H.N.G. Wadley, C.B. Scruby and J.H. Speake, "Acoustic emission for physical examination of metals" International Metals Review, No. 2, pp. 41-64, 1980.

202. B.J. Dalgleish, A. Fakhr, P.L. Pratt, and R.D. Rawlings, "The temperature dependence of the fracture toughness and acoustic emission of polycrystalline alumina." J. Mater Sci., 14, pp. 2605-2615, 1979.

203. A.G. Evans, M. Linzer and L.R. Russel, "Acoustic emission and crack propagation in polycrystalline alumina", Mat. Sci. and Engineering, 15, pp. 253-261, 1974.

204. J.M. Carlyle and W.R. Scott, "Acoustic emission fatigue analyser", Experimental Mechanics, pp. 269-378, Oct. 1976.

205. R.E. Cuthrell, "The role of ion aggregates in Rebinder Westwood environmental effects on wear as monitored by acoustic emision", J. Appl. Physics, Vol. 49, No. 1, p.432, Jan. 1978.

206. B.H. Schofield, "Acoustic emission under applied stress", Air force lab. tech. report, No. ASD-TDR-63-509, Part 1 1963, Part II 1964.

207. C.A. Tatro, "Some techniques in the detection of crystal slip in metals", Div. of Eng. Res., Eng. Dept., Michigan State University, 1959.

208. F.J. Guild, D. Walton, R.D. Adams and D. Short "The application of AE to fibre reinforced composite materials", Composites, p. 173, July 1976.

209. N.W. Ringshall, Ph.D. Thesis, Cambridge "Acoustic emission and fracture processes in metals", 1978.

210. H. Tanaka and R. Honiuchi, Scripta, Met. 9, (7) pp. 777, 1975.

211. T. Ingham, A.L. Stott and A. Cowan, Int. Jour. Pressure Vessels and Piping, 3, 1975.

212. M. Arii, H. Kashiwaya and T. Yanuki, Eng. Fracture Mech. 7, p. 551, 1975.

213. R.T. Sedgewick, J. Applied Phys, 39 (3) p. 1728, 1968.

214. G. Clark, "Acoustic emission monitoring and materials, tests: Review", Dept. Met. and Mat. Sci., Cambridge Univesity, 1977.

215. W.M. McCabe, R.M. Koerner and A.E. Lord, "A.E. behaviour of concrete lab. specimens", A.C.I. Jour. p.367, July 1976.

216. H. Dunegan, D. Harris and C. Tatro, "Fracture analysis by use of A.E." Eng. Fract. Mech. 1, p. 105, 1968.

217. L.J. Graham and G.A. Alers, "Microstructural aspects of A.E. in ceramics." ASTM STP 571, 1975.

218. T.R. Millshall and R. Rothwell, Nat. Phys. Sci., 229 (5) p.155, 1971.

219. S.A.S. Akers, Ph.D. Thesis, University of Witwatersrand, 1980.

220. J. Kaiser, "Knowledge and research on noise measurements during tensile stressing of metals." Arkiv. für Eisenhuttenvesen, Vol. 24, No. 43, 1953.

221. V.H. Rusch, "Physikalische Fragen derBeton prufung." Zement-Kalk-Gibs, Vol. 12, No. 1, Jan. 1956. (Cement and Conc. Assoc. Translation No. 80).

222. V.H. Rusch, "Research towards a general flexural theory for structural concrete", Jour. A.C.I. Proc. No. 57, pp.1-28, July 1960.

223. W. Ruetz, "Two different physical mechanisms of creep in concrete", in the 'Structure of Concrete' 1968, Cem. and Conc. Assoc. (Eds.) A.E. Brooks and K. Newman, pp. 146-153.

224. D. Wells, "An acoustic apparatus to record emissions from concrete under strain", Nuclear Engineering and Design, Vol. 12, p. 80, May 1970.

225. M. Terrien, "Emission acoustique et comportement mecanique post critique d'un beton sollicite en traction" Bull Liaison, Lab. P. et Ch., 105, 2398, Janu 1980.

226. A.T. Green, "Stress wave emission and fracture of prestressed concrete reactor vessel materials." 2nd Int. Am. Conf. on Mat. Ech., Ann. Soc. of Mech. Eng. Vol. 1, pp. 635-649, Aug. 1970.

227. J. Nielsen and D.T. Griffin "Acoustic emission of plain concrete" J.T.E.V.A., Vol. 5, No. 6, p. 476, Nov. 1977.

228. R.E. Goodman "Subaudible noise during compression of rock", Bull of Geological Soc. of America, Vol. 74, No. 487, 1963.

229. R.B. Tait, "The acoustic emission monitor for concrete and mortar: Construction and operating details". Research Report, University of Cape Town, Nov. 1980.

230. C.B. Scruby and H.N.G. Wadley "A calibrated capacitance transducer for detection of acoustic emission". J. Physics D. 11, (11), 1487-1494, 1978.

231. B.M. Assimacopoulos, R.F. Warner and C.E. Ekberg, "High speed fatigue tests on small specimens of plain concrete." J. Prestressed Conc. Inst., 4, pp. 53-70, Sept. 1959.

232. P.D. Arthur, J.C. Earl, T. Hodgkiss, "Fatigue of reinforced concrete in seawater", Concrete, p.26, May 1979.

233. D.J. Hannant, "An experimental investigation of the creep mechanisms in concrete", Proc. of Southampton Conf. Civil Eng. Materials, 1969. (Ed.) M. Te'eni, Part 1, 1969.

234. A.G. Evans and M. Linzer, "High frequency cyclic crack propagation in ceramic materials", Int. J. Fractrue, 12, pp. 217-222, 1976.

235. A.G. Evans and E.R. Fuller, "Crack propagation in ceramic materials under cyclic loading conditions", Met. Trans. Vol. 5, pp. 27-33, Jan. 1974.

236. R. Tepfers and T. Kutti, "Fatigue strength of plain, ordinary and lightweight concrete", A.C.I. Jour., p. 635, May 1979.

237. P.C. Paris and F. Erdogan, J. Basic Eng., ASME Trans., 85, 528-534, 1963.

238. J.A. Neal, "Some aspects of fatigue in concrete", Ph.D. Thesis, University of Illinois, 1965.

239. M. Mamillan, Ann. Inst. Tech. Batim., Vol 23, No. 267, April 1970.

240. K.R. Lauer and F.O. Slate "Autogenous healing of cement paste", A.C.I. Jou., Proc. Vol. 52, No. 10, pp. 1083-1098, June 1956.

241. G. Batson, C. Ball, L. Bailey, E. Landey and J. Hooks., Jou. A.C.I., 69, 673 1972.

242. G.A. Hirst and A.M. Neville, Cement and Conc. Res., 6, 5 p715, 1976.

243. C.P. Whaley and A.M. Neville, Mag. Conc. Res., 25, 84, p.145, 1973.

244. J.P. Romualdi, Int. Conf. on Structure of Concrete, London, Session D, p. 190, 1965.

245. F.H. Wittman, "The structure of hardened cement paste, a basis for a better understanding of the material properties", Hydraulic Cement Pastes: Their structure and Properties, Cement and Concrete Research Association, 1975.

246. J.R. Verna and T.E. Stelson "Repeated loading effect on ultimate static strength of concrete beams", Jour. A.C.I. p.743, June 1963.

247. H.M. Jennings "The developing microstructure in portland cement", Advances in cement technology (Ed. by S.N. Ghosh), Pergamon Press, p. 349, 1983.

248. G. Groves, Private Communication, 1981.

249. S. Mindess, "Application of fracture mechanics to cement and concrete," 81st Annual meeting of American Ceramic Soc., Cincinatti, Paper I, SII, 1979.

250. A.D. Husak, "Static fatigue of portland cement concrete" Ph.D. Thesis, Carnegie Mellon University, Pittsburg, 1969.

251. B. Hillemeir and H.K. Hilsdorf, "Fracture mechanics studies on concrete composites", Cem and Conc. Res., vol. 7, p. 523, 1977.

252. S.P. Shah and F.J. McGarry, "Griffith fracture criterion and concrete", Jour. Eng. Mech. Div., Proc. ASCE 47 [EM6] p.1663, 1971.

253. O.E. Gjorv., S.I. Sorensen and A. Arnesen "Notch sensitivity and fracture toughenss of concrete", Cem. and Conc. Res., Vol. 7 [3], p. 333, 1977.

254. C.E. Kesler, D.J. Naus and J.L. Lott, "Freacture mechanics: its applicability to concrete", Proc. 1971, Int. Conf. on Mech. Behaviour of Materials, Vol. IV, p. 113, Japanese Soc. of Matl., 1972.

255. D.J. Cook and G. Crookham, "Discussion on notch sensitivity and fracture toughness of concrete" by Gjorv et al., Cem. and Conc. Res., Vol. 8, p. 387, 1978.

256. P.C. Strange and A.H. Bryant "Experimental tests on concrete fracture", Proceedings, ASCE, J. Eng. Mech., Div. 105 [EM2], 337-343, 1979.

257. N. Swamy, "Aggregate-matrix interactions in concrete systems", pp.301-315 in structure, Solid Mechanics and Engineering Design, Proc. of Southampton Civ. Eng. Math. Conf., Wiley Interscience 1969.

258. A.A. Griffith, "Theory of rupture", Proc. of 1st Int. Congress of Applied Mechanics, Delft, pp.55, 1924.

259. R.J. Charles, "Static fatigue in glass", J. Applied Physics Vol. 29, No. 11, pp. 1549, 1958.

260. R.H. Mills, Fifth Int. Symp. Cement Chemistry III, 74, 1968.

261. R.B. Tait, "A review of the application of fracture mechanics to cement based materials", Research Report, University of Witwatersrand, Oct., 1983.

262. A.A. Griffith, "The phenomena of rupture and flow in solids", Philosophical Transactions, Royal Soc. of London, Vol. A221, 1921.

263. J.F. Knott, "Fundamentals of fracture mechanics", Butterworths, London, 1973.

264. D. Broek, "Fracture of Solids: Elementary Engineering Fracture Mechanics", Leyden Noordhof Int. Pub. 1974.

265. ISI Publication 121, "Fracture Toughness", 1968.

266. S.T. Rolfe and J.M. Barsom, "Fracture and fatigue control in structures: Application of fracture mechanics" Prentice Hall, 1977.

267. M.F. Kaplan, "Crack propagation and fracture of concrete, Jou. A.C.I., Title 58-28, p.591, Nov. 1961.

268. J.J. Beaudoin, "Effect of humidity and porosity on fracture of hardened portland cement". Cem. and Conc. Res., Vol. 12, p.705, 1982.

269. L. Javan and B.L. Dury, "Fracture toughness of fibre reinforced concrete", Concrete, Vol. 13, No. 12, p.31, Dec. 1979.

270. A.M. Neville, "Some aspects of the strength of concrete" Civ. Eng. (London) Part I, 54 [639], p. 153, Part II, 54 [640], 1308, Part III 54 [64], 1435, (1959).

271. G.T. Hahn, R.G. Hoagland, M.F. Kanninen, and A.R. Rosenfield, "A preliminary study of fast fracture and arrest in the DCB test specimen". Proc. Int. Conf. or Dynamic Crack Propagation, Noordhof Int. Pub. Co., p.649, 1973.

272. B. Barr and T. Bear, "Fracture toughness", Concrete, Vol. 11, No. 4, p.30, 1977.

273. G.B. Welch and B. Haisman "Application of fracture mechanics to concrete and measurement of fracture toughness", Materials and Structures, Research and Testing, Vol. 2, No. 9, p.171, may June 1969.

274. J.P. Romualdi and G.B. Batson, "Mechanics of crack arrest in concrete", J. Eng. Mech. Div., Proc. Ann. Soc. Civ. Eng., p.147, June 1963.

275. N. McN. Alford and A.B. Poole, "The effect of shape and surface texture on the fracture toughness of mortars", Cem. and Conc. Res., Vol. 9, p. 583, 1979.

276. A. Hilleborg, "Analysis of one single crack", Report to RILEM T.C. 50-FMC, Jan. 1981.

277. S. Ziegeldorf, H.S. Muller and H.K. Hilsdorf, "A model law for the notch sensitivity of brittle materials", Cem. and Conc. Res., Vol. 10, p.589, 1980.

278. P.E. Petersson, "Fracture energy of concrete: practical performance and experimental results", Cem. and Conc. Res., Vol. 10, p.91, 1980.

279. S. Mindess, F.V. Lawrence and C.E. Kesler, Cem. and Conc. Res., Vol. 7, 731, 1977.

280. K.L. Watson, N.B. Eden and J.R. Farrant, Precast Concrete, 8, 81, 1977.

281. R.N. Swamy, "Influence of slow crack growth on the fracture resistance of fibre cement composites", Cement composites, Vol. 2, No. 1, 1980.

282. G.T. Halvorsen "Toughness comparisons for some plain concretes", Int. J. of Cement composites, Vol. 2, No. 3, pp.143, 1980.

283. A.A. Khrapkov, L.P. Trapesnikov, G.S. Geinats, V.I. Paschenko and A.P. Pak. "The applicatin of fracture mechanics to the investigation of cracking in massive concrete construction elements of dams." p.1211 in Fracture 1977, Vol. 3, ICF 4, Waterloo, Canada, 1977.

284. J.S. Nadeau, S. Mindess and J.M. Hay, "Slow crack growth in cement paste", J. Amer. Ceramic Soc., Vol. 57, No. 2, p.51, Feb. 1974.

285. A.G. Evans, J.R. Clifton and E. Anderson, "The fracture mechanics of mortars", Cem. and Conc. Res., Vol. 6, p. 535, 1976.

286. A.N. Wyss, "Application of fracture mechanics to cracking of concrete beams", Ph.D. Thesis, University of Washington, 1971.

287. P.F. Walsh, "Crack initiation in plain concrete", Mag. Conc., Res., Vol. 28, No. 94, p.37, 1976.

288. A. Grudemo, "Microcracks, fracture mechanisms and strength of cement paste", Cem. and Conc. Res., Vol. 9, p. 19, 1979.

289. J. Mazars, "Existence of a critical strain energy release rate for concrete", Fracture Vol. 3, ICF 4, Waterloo, Canada, 1977.

290. H. Kitagawa, S. Kim and M. Suyama, "Determination of fracture toughness of concrete materials by diametral compression tests" p.160 in Proc. of 19th Japan Congress on Mat. Research, Tokyo, 1976.

291. T.T. Shih and J. Opoku, "Application of fracture mechanics to ceramics materials - a state of the art review", Eng. Fracture Mechanics, Vol. 12, pp.479-498, 1979.

292. G.R. Irwin and J.A. Kies, "Critical energy release rate analysis of fracture strength", Welding Journal, Vol. 33, p.193, April 1954.

293. J. Nakayama, "Direct measurement of fracture energies of brittle heterogeneous materials". J. Am. Ceramic Soc., Vol. 48, No. 11, p.583, Nov. 1965.

294. A.G. Evans, "Fracture mechanics determinations" from book 'Fracture mechanics of ceramics' Vol. 1 (Eds) R.C. Bradt, C.P.H. Hasselman and F.F. Lange, pp. 17-48, Plenum Press, 1974.

295. R.W. Davidge and G. Tappin, "The effective surface energy of brittle materials", J. Mater. Sci., 3, p.165, 1968.

296. H.G. Tattersall and G. Tappin, "The work of fracture and its measurement in metals, ceramics and other materials", J. Mater Sci, I, p.296, 1966.

297. R.B. Tait and G.G. Garrett, "Fracture and fatigue of cement mortar" presented at 'Fracture 79', Ed. by G.G. Garrett, 1979.

298. P.E. Petersson, "Comments on strength and fracture properties of asbestos cement mortar composites", J. Mater. Sci, 15 (Letters), p. 2387, 1980.

299. C.V.S. Kameswara Rao, "Effect of aggregate size on the minimum size of test specimen", Int. J. of Cement composites, Vol. 1, No. 3, p.177, 1979.

300. M. Modeer, "A fracture mechanics approach to the failure analysis of concrete materials", Report TVBM, 1001, University of Lund, Sweden, 1979.

301. C. Sok, J. Baron, and D. Francois, "Mechanique de la rupture appliquee au beton hydraulique" Com. Conc. Res. 9, 641-648, 1979.

302. D.J. Green, P.S. Nicholson, J.D. Embury, "Fracture of a brittle particulate composite, part I", J. Mater. Sci, 14, p.1413, 1979.

303. K. Togawa, T. Satoh and K. Araki, "Parameters on the fracture toughness of mortar and concrete", 27th General Meeting of Cement Assoc. of Japan, Toky, 1973.

304. F.H. Wittman, "Surface tension, shrinkage and strengh of hardened cement paste", Materiaux et Construction, 1 [6], p. 547, 1968.

305. J.O. Ontwater, M.C. Murphy, R.G. Kimble and J.T. Berry, "Double torsion technique as a universal fracture toughness test method", Fracture Toughness and Slow Stable Cracking ASTM STP 559, pp.127-138, 1974.

306. J.A. Kies and B.J. Clark, "Fracture 1969", Ed. P.L. Pratt, p.483, Chapman and Hall, London, 1969.

307. D.P. Williams and A.G. Evans, "A simple method for studying slow crack growth" Journal of Testing and Evaluatin, JTEVA Vol. 1, No. 4, pp. 264-270, July 1973.

308. R.W. Davidge and A.G. Evans, Mater. Sci., Eng., Vol. 6, p. 281, 1970.

309. A.G. Evans, "A method for evaluating the time dependent failure characteristics of brittle materials and its application to polycrystalline alumina", J. Mater. Sci. Vol. 7, p. 1137, 1972.

310. B.K. Atkinson, "Fracture toughness of Tennessee Sandstone and Carryn Marble using the D.T. testing method", Int. J. Rock Mech. Min. Sci. & Geomech. Abstract 16, pp. 49-53, 1979.

311. C.D. Beachem, J.A. Kies and B.F. Brown. "A constant K specimen for stress corrosion cracking tests", Materials research and Standards, MTRSA, Vol. 11, No. 4, p.30. April 1971.

312. R.W. Davidge, J.R. McLaren, and G. Tappin, "Strength probability time S.P.T. relationships in ceramics", J. Mater. Sci., Vol. 8, pp. 1699-1705, 1973.

313. A.G. Evans and M. Linzer, "High frequency cyclic crack propagation in ceramic materials", Internal Report NBS 1974 - Private Communication 1974.

314. M.C. Murphy, R.G. Kumble, J.T. Berry and J.O. Outwater, "Fracture toughness determination in cast metals", A.F.S. Transactions 30, pp. 158-162, 1973.

315. A.G. Evans and S.M. Wiederhorn, "Crack propagation and failure prediction in silicon nitride at elevated temperatures", J. Mater. Sci., Vol. 9, pp. 270-278, 1974.

316. A.G. Evans, L.R. Russel and D.W. Richerson, "Slow crack growth in ceramic materials at elevated temperatures", Metallurgical Transactions A, Vol 6A pp. 707-716, April 1975.

317. M.J. Murray and C.M. Perrott, "Fracture toughness of sintered carbide measured by the double torsion method", Proc. Int. Conf. Hard Mater. Tool Technology, p. 314, Carnegie Mellon Univ., Pittsburg, Penn. 1976.

318. J.S. Nadeau, "Subcritical crack growth in vitreous carbon at room temperature", J. Amer. Ceram. Soc., Vol. 57, No. 7 pp. 303-306, July 1974.

319. R.H. French and Rishi Raj, "Use of DT method to study crack propagation in an adhesive layer", Journ. Testing and Evaluation. JTEVA Vol. 7, No. 3, pp. 160-167, May 1979.

320. A.V. Virkar and R.S. Gordon, "Crack front profiles in D.T. Specs." J. Amer. Ceram. Soc. - Discussion and Notes, Vol. 58, No. 11-12, pp. 536-537, Nov/Dec 1975.

321. Li Shing Li, R.F. Pabst, "Subcritical crack growth in partially stablized zirconia (PSZ)", J. Mater. Sci, Vol. 15, pp. 2861-2866, 1980.

322. B.J. Pletka, E.R. Fuller and B.G. Koepke, "An evaluation of double torsion testing - Experimental", ASTM 678, "Fracture Mechanics applied to Brittle Materials", Ed. S.W. Freiman, Amer. Soc. for Testing and Materials, pp. 19-37, Aug. 1979.

323. E.R. Fuller Jr., "An evaluation of D.T. testing - Analysis", Fracture Mechanics Applied to Brittle Materials, ASTM, S.T.P., 678, Ed. S.W. Freiman, Amer. Soc. for Testing and Materials, pp. 3-18, 1979.

324. G.G. Trantina, "Stress analysis of the double torsion specimen", J. Amer. Ceram. Soc., Vol. 60, No. 7-8, pp. 338-341, July 1977.

325. A. Hillberborg, "Theoretical analysis of the double torsion test", Cem. and Conc. Res., Vol. 13, pp. 69-80, 1983.

326. B.K. Atkinson, "Stress corrosion and the rate dependent tensile, failure of a fine grained quartz rock." Tectonophysics, Vol. 65, pp. 281-290, June 1980.

327. J.G. Bruce, W.W. Gerberich and B.G. Koepka, "Subcritical crack growth in PZT", Vol. 4, (Eds.) R.C. Bradt, D.P.H. Hasselman and F.F. Lange, Plenum Press, New York, pp. 687-709, 1978.

328. A.G. Evans, Private Communication, 1980.

329. A.G. Evans, Int. J. Fracture, Vol. 9, No. 3, pp. 267-275, Sept. 1973.

330. C.G. Annis and J.S. Cargill, "Fracture mechanics of Ceramics", Vol. 4, Eds. R.C. Bradt, D.P.H. Hasselman and F.F. Lange, Plenum Press, New York, pp. 737-744, 1978.

331. P.S. Leevers, "Crack front shape effects in the double torsion test", J. Mat. Sci., Vol. 17, pp. 2469-2480, 1982.

332. K.R. McKinney and H.L. Smith, "Method of studying subcritical cracking of opaque materials", J. Amer. Ceram. Soc., Vol. 56, No. 1, pp. 30-32, January 1973.

333. B.J. Pletka and S.M. Wiederhorn. "A comparison of failure predictions by strength and fracture mechanics techniques" J. Mat. Sci., Vol. 17, 1247-1268, 1982.

334. A.S.T. Yam and S. Mindess, "The effects of fibre reinforcement on crack propagation in concrete", Int. J. Cement composites and lightweight Concrete, Vol. 4, No. 2, pp. 83-93, May 1982.

335. D.K. Shetty and A.V. Virkar, J. Amer. Ceram. Soc. Vol. 61, No. 1 - 2, pp. 93-94, Jan/Feb 1978.

336. P.R. Fry. M.Sc. Thesis. University of the Witwatersrand, Metallurgy Dept., 1982.

337. R.F. Pabst and J. Weick, J. Mat. Sci., Vol. 16, pp. 836-838, 1981.

338. B.J. Pletka and S.M. Wiederhorn, "Fracture Mechanics of Ceramics", Vol. 4, pp. 745-759, Plenum Press, N.Y., 1978

339. B.P. Hughes and J.E. Ash, "Short term loading and deformation of concrete in uniaxial tension and pure torsion", Mag. of Conc. Res. Vol. 20, No. 64, pp. 145-154, Sept. 1968.

340. S.M. Wiederhorn, "Influence of water vapour on crack propagation in soda lime glass", J. Amer. Ceram. Soc., Vol. 50, No. 8, pp. 407-414, Aug. 1967.

341. ASTM Standard E399-78, 1978.

342. A.G. Evans, "Slow crack growth in brittle materials under dynamic loading conditions", Int. J. of Fracture, Vol. 10, pp. 251-259, 1974.

343. R.B. Tait and G.G. Garrett, "Effect of time, frequency, moisture condition and temperature on V-K crack growth rates in cement mortar". To be published.

344. A.V. Virkar and R.S. Gordon, J. Amer. Ceram. Soc., Vol. 59, No. 1-2, pp. 68-71, Jan/Feb, 1976.

345. M.I. Hakeem and M.G. Phillips, J. of Mat. Sci., Vol. 14, pp. 2901-2905, 1979.

346. D. Watstein, "Effect of straining rate on the compressive strength and elastic properties of concrete", J. Am. Concr. Inst. Vol. 49, No. 8, pp.729-744, 1952.

347. J. Takeda and H. Tachikawa, "Deformation and fracture of concrete subjected to dynamic load", Mechanical Behaviour of materials, Vol. IV, Soc. of Mat. Sci., pp. 267-277, Japan, 1972.

348. K. Katsuta, Trans. Arch. Inst., Japan, 53, 1943-45.

349. P.G. Jones and E.E. Richart, "The effects of speed of testing on strength and elastic properties of concrete", ASTM Proc., 36 Part II, pp 380-392, 1936.

350. P.J.F. Wright, "The effect of the method of test on the flexural strength of concrete", Mag. Conc. Res., Vol. 4, pp. 67-76, 1952.

351. D.J. McNeely and S.D. Lash, "Tensile strength of concrete", J. Amer. Conc. Inst. Vol. 60, No. 6, pp. 751-760, 1963.

352. L.S. Williams, "Mechanical properties of engineering ceramics", Ed. W.W. Kriegel and H. Palmour, pub: Interscience, 1961.

353. S.M. Wiederhorn, "Mechanics of subcritical crack growth in glass", Presented at the 2nd Int. Symp. on fracture mechanics of ceramics Penn. State Univ. July 26, 1977.

354. F. Daniels and R.A. Alberty, "Physical Chemistry", Wiley 4th Ed. 1975.

355. G.A. Hirst and A.M. Neville, "Activation energy of creep of concrete under short term static and cyclic stresses", Mag. of Conc. Res., Vol. 29, No. 98, March, 1977.

356. J.P. Singh, K. Niihara and D.P.H. Hasselman", Analysis of thermal fatigue behaviour of brittle structural materials", J. Mat. Sci. Vol. 16, pp. 2789-2797, 1981.

357. B.R. Gamble and J.M. Illston, "Rate of deformation of cement paste and concrete during regimes of variable stress, moisture content and temperature", Hydraulic Cement Pastes: their structure and properties, Proc. of Conf. at Sheffield Univ., Cem. and Conc. Assoc., April 1976.

358. W.B. Hillig and R.J. Charles, "High Strength Materials", p. 682, Wiley, New York, 1965.

359. R.E. Cuthrell, "The influence of hydrogen on the deformation and fracture of the near surface region of solids: proposed origin of the Rebinder Westwood effect". Jour. Mat. Sci., Vol. 14, pp. 612-618, 1979.

360. S.H. White, "Electrical conductivity in quartz", Nature, London Physical Sci., No. 3, p. 233, 1964

361. W.J. Plumbridge, "Mechano-environmental effects in fatigue", Mat. Sci. and Engineering Vol. 27, pp. 197-208, 1977.

362. J.W. Ireland, "Mechanics of Fluids", Chapter 10, London, Butterworth, 1971.

363. S. Mindess and S. Diamond, "The cracking and fracture of mortar", accepted for publication in "Materials and Structures, RILEM" private communication, 1981.

364. S. Mindess and S. Diamond, "A device for direct observation of cracking of cement paste or mortar under compressive loading within a scanning electron microscope", Cem. and Conc. Res., Vol. 12, pp. 569-576, 1982.

365. M. Kawamura, "Internal Stresses and Microcrack formation caused by drying in hardened cement pastes", J. Amer. Ceram. Soc., Vol. 61, No. 7-8, Aug. 1978.

366. R.L. Carasquillo, F.O. Slate and A.H. Nilson, "Microcracking and bheaviour of high strength concrete subject to short term load", A.C.I. Journal, p. 179, May/June 1981.

367. M.D. Kotsovos and J.B. Newman, "Fracture mechanics and Concrete behaviour", Mag. of Conc. Res. Vol. 33, No. 115, pp. 103-112, June 1981.

368. Y.V. Zaitsev and F.H. Wittman, "Crack propagation in a two phase material such as concrete", Fracture 1977, Vol. 3, pp. 1197-1203, Proc. of 4th Int. Conf. on Fracture Waterloo, Canada, June 1977.

369. R.L. Berger, "Calcium hydroxide: its role in the fracture of C_3S paste", Science Vol. 175, No. 4022, pp. 626-629, 1972.

370. B. Marchese, "Microstructure of Mature Alite phases", J. Amer. Ceram. Soc., Vol. 61, No. 7-8, pp. 349-355, Aug. 1978.

371. Z.P. Bazant and W.J. Raftshal, "Effect of cracking in drying and shrinkage specimens", Cem. and Conc. Res. Vol. 12, pp. 209-226, 1982.

372. A. Hillerborg, M. Modeer and P.E. Petersson, Cem. and Conc. Res., No. 6, p. 773, 1976.

373. A.J. Zielinski and H.W. Reinhard, "Stress strain behaviour of concrete and mortar at high rate of loading" Cem. and Conc. Res. Vol. 12, pp. 309-319, 1982.

374. R. Adams and P.W. McMillan, J. Mat. Sci., Vol. 12, p. 643, 1977.

375. D.A. Krohn and D.P.H. Hasselman, "Static and cyclic fatigue behaviour of a polycrystalline alumina", J. Amer. Ceram. Soc., Vol. 55, No. 4, pp. 208-211, 1972.

376. J. Glucklich, "The strength of concrete as a composite material", Mech. Behaviour of Materials, Vol. IV, Soc. of Mat. Sci., pp. 104-112, Japan, 1972.

377. L. Struble, J. Skalny and S. Mindess, "A review of the cement aggregate bond", Cem. and Conc. Res., Vol. 10, pp. 277-286, 1980.

378. S.A.S. Akers, G.G. Garrett, and R.B. Tait, "In situ scanning electron microscope observations of flexural failure of asbestos cement", Proc. of EMSSA Vol. 7, p.57, 1977.

379. Joon Pyo Hong and J. Gurland: Dept. Metallurgy, Brown Univ., U.S.A. Private Communication, 1980.

380. S. Diamond, S. Mindess and J. Lovell, "Use of a Robinson backscatter detector and "wet cell" for examination of wet cement paste and mortar specimens under load", Cem. and Conc. Res., Vol. 13, 107-113, 1983.

381. M.I. Manning and D.J. Goodhew, "An hydraulic straining stage of use in scanning electron microscopes", J. Phys. E., Sci. Instruments, Vol. 12, p. 464, 1979.

382. S. Kobayashi and S.M. Ohr, "In situ fracture experiments in b.c.c. metals", Philosophical Magazine A, Vol. 42, No. 6, p. 763, 1980.

383. S. Kobayashi and S.M. Ohr, "In situ observations of the formation of a plastic zone ahead of a crack tip in copper." Scripta Met. Vol. 15, p. 343, 1981.

384. S. Chatterji, N. Thaulow and P. Christensen, "Formation of shrinkage cracks in thin specimens of cement paste", Cem. and Conc. Res., Vol. 11, p. 155, 1981.

385. P.R. Smith, "Freeze drying specimens for electron microscopy", J. of Ultrastructure Research, 72, p. 380, 1980.

386. J.E. Gillot, "Study of the fabric of fine grain sediments with the scanning electron microscope." J. Sedimentary Petrology, Vol. 39, No. 1, pp. 90-105, 1969.

387. B.D. Barnes, S. Diamond and W.L. Dolch, "Hollow shell hydration of cement particles in bulk cement paste". Cem. and Conc. Res., Vol. 8, p. 263, 1978.

388. D.M.F. Orr, "Application of the scanning electron microscope to the study of initial hydration of portland cement paste", Cem. and Conc. Res., Vol. 13, 146, 1983.

389. A.G. Evans, "Fatigue in Ceramics", Int. J. Fracture, Vol. 16, No. 6, p. 485, Dec. 1980.

390. J.D. Todd, "Structural Theory and Analysis", MacMillan Press, 1974

"Contrariwise" continued Tweedledee "if it was so, it might be; and if it were so, it would be; but as it isn't, it ain't. That's Logic."

Alice Through the Looking Glass
Lewis Carrol

APPENDIX A

Analysis of the Double Torsion System

The double torsion specimen can be considered as two elastic torsion bars each having a rectangular cross section and loaded as shown in Fig. 6.11 to a load of P/2. It is well known, (see, for example, Todds book ( )) that for small deflections, y, and for bars where width is much greater than specimen thickness, the torsional strain Θ, is given by the following expression. (See Fig. 6.11 for parameter identification).

$$\Theta \approx \frac{y}{w_m} \approx \frac{Ta}{I_p G} \qquad A.1$$

where
- T = Torsional moment $(P/2)\, w_m$
- $P/2$ = Total load applied to one bar
- G = shear modulus of the material
- a = crack length *
- I_p = polar moment of inertia of one torsion bar
- t = plate thickness
- t_n = plate thickness in plane of crack
- $W/2$ = bar width
- w_m = moment arm
- y = displacement of loading points.

* It should be noted that the crack front is not flat for this type of specimen and this point will be discussed later; however, the term "crack length" used herein refers to the longest portion of the crack, that is the length at the tension surface of the specimen in Fig. 6.11

Now the polar moment of inertia for one bar, I_p, is given by Outwater et al (305)(other analyses 323, 316 are similar) as

$$I_p = \frac{Wt^3}{32}\left(\frac{16}{3} - 6.72\,\frac{t}{W}\left(1 - \frac{4}{3}\left(\frac{t}{W}\right)^4\right)\right) \approx \frac{Wt^3}{6}\left(1 - \frac{5t}{4W}\right) \qquad \text{A.2}$$

if $\frac{t}{W}$ is small.

(Many analyses regard $\frac{t}{W}$ as so small that the term $\left(1 - \frac{5t}{4W}\right)$ is regarded as approximately equal to 1.0. However since $\frac{t}{W}$ is typically $\frac{1}{8}$ to $\frac{1}{16}$ this implies an error of approximately 8 to 16% which is often not acceptable (198)).

$$\text{Hence } \theta \approx \frac{y}{w_m} \approx \frac{3Pa\ w_m}{Wt^3 G\left(1-\frac{5}{4}\,\frac{t}{W}\right)} \qquad \text{A.3}$$

For convenience $\phi \equiv \left(1 - \frac{5}{4}\,\frac{t}{W}\right)$

Then rearranging

$$\frac{y}{P} \approx \frac{3\,w_m^2\,a}{Wt^3\,G\,\phi} \approx C \qquad \text{A.4}$$

where C is the elastic compliance.

The strain energy release rate $\mathcal{G}$ for crack extension is related to the specimen compliance by the expression (292)

$$\mathcal{G} = \frac{P^2}{2}\left(\frac{dC}{dA}\right) \qquad \text{A.5}$$

where A is the area of the crack.

If the shape of the crack front is independent of crack length (see discussion on crack profile in section 6.4.7) then

$$\mathcal{G} = \frac{P^2}{2t_n}\left(\frac{dC}{da}\right) \qquad A.6$$

For a double torsion specimen where deflections beyond the crack are negligible the strain energy release rate is obtained by differentiating equation A.4 with respect to a and substituting in equation A.6.

$$\mathcal{G} = \frac{P^2}{2t_n}\left(\frac{3w_m^2}{Wt^3 G \phi}\right) \qquad A.7$$

The stress intensity K is related to $\mathcal{G}$ by

$$K = (E\mathcal{G})^{\frac{1}{2}} \quad \text{for plane stress} \qquad A.8$$

$$\text{and} \quad K = \left(\frac{E\mathcal{G}}{1-\nu^2}\right)^{\frac{1}{2}} \quad \text{for plane strain} \qquad A.9$$

where E is Youngs Modulus. Hence

$$K = \left(\frac{3P^2 w_m^2 E}{\phi 2 t_n t^3 GW}\right)^{\frac{1}{2}} \qquad A.10$$

since the plane stress condition holds for this thin plate case. This point is, however, still debatable (275,276).

E and G are related by

$$G = \frac{E}{2(1+\nu)} \qquad A.11$$

where ν is Poissons ratio and equation A.10 reduces to

$$K = Pw_m \left(\frac{3\ (1+\nu)}{t^3 t_n\ W\psi}\right)^{\frac{1}{2}} \quad \text{for plane stress} \qquad \text{A.12(a)}$$

$$\text{or} \quad K = Pw_m \left(\frac{3}{t^3 t_n\ W\ (1-\nu)\psi}\right)^{\frac{1}{2}} \quad \text{for plane strain} \qquad \text{A.12(b)}$$

The stress intensity factor, K, is thus a function of applied load, specimen dimensions and Poissons ratio - it is independent of crack length. It is this feature which makes the specimen extremely useful for certain types of sub critical crack growth studies. For a rigorous analysis of the double torsion system the reader is referred to Fuller (323).

A slight modification to this (classical) theory and analysis of the double torsion system has been introduced by Wecharatana and Shah (73). They recognised that there are non linear inelastic deformations in the process zone, of double torsion tests on mortar, but assumed the torsion bars were otherwise elastic. This implies that elastic as well as inelastic energy is absorbed during slow crack growth and that equation A.6 needs to be modified slightly.

Wecharatana and Shah (73) considered four cases of strain energy release rate calculation, including the classical one. They found that an analysis incorporating both plastic deformations and changes in the unloading compliance was the most realistic (Fig. A.1). Using the notation of Fig. A.1(b) they proposed, in place of equation A.6, the following expression for strain energy release rate.

$$\mathcal{G}_1 = \frac{P_1 P_2}{2}\left[\frac{dC_R}{dA} + \left(\frac{P_1 + P_2}{P_1 P_2}\right)\frac{d\delta_p}{dA}\right] \qquad \text{A.13}$$

This equation could be rewritten as

$$\mathcal{G}_1 = \frac{P_1 P_2}{2}\ \frac{dC_m}{dA} \qquad \text{A.14}$$

where C_m is the "modified compliance", (73).

Their results, using this analysis, indicated that the classical analysis slightly overestimated the toughness at large crack lengths, but at small crack lengths the two approaches were very similar.

In this present project, because much of the work was completed prior to publication of this paper, and because the difference is not great, the original classical analysis was used.

Fig.A.1.: Schematic models for different fracture behaviour and corresponding strain energy release rates. (From Wecharatana and Shah, (73).)

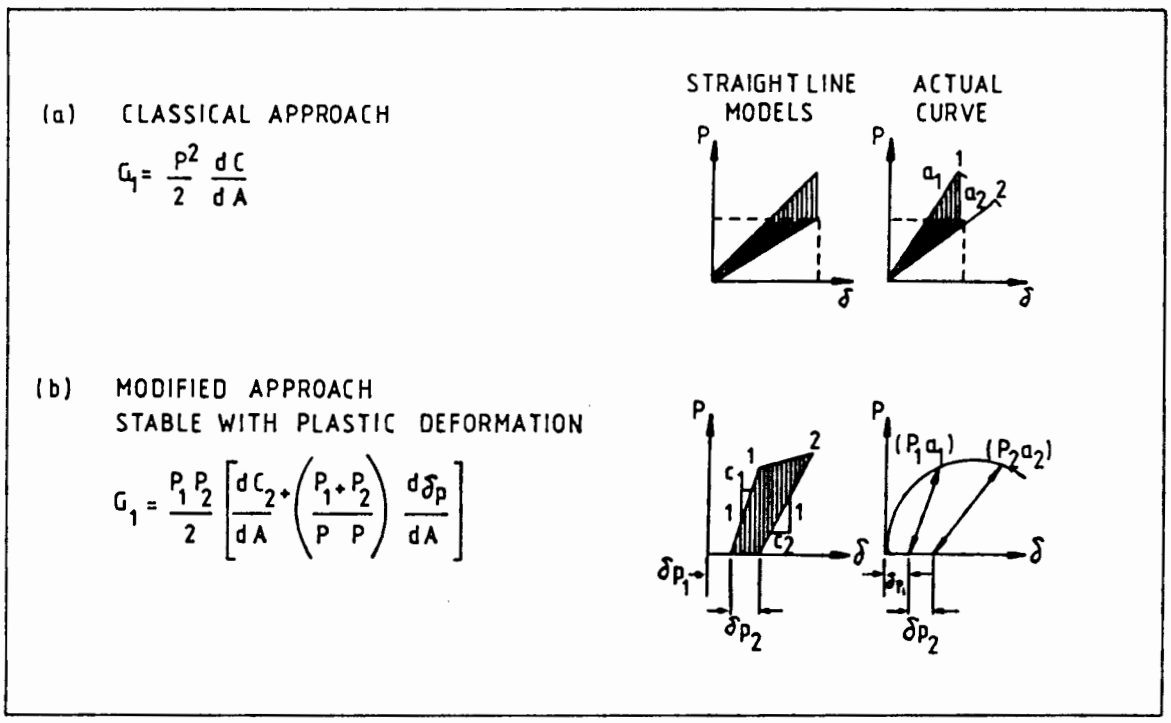

Appendix B1

Rate of change of load at fixed displacement for double torsion crack velocity determination

At a fixed displacement, (ie y = constant) differentiation of equation A.4, with respect to time, t, leads to

$$\left(\frac{da}{dt}\right)_y = -\frac{Wt_o^3 G\, y\, \phi}{3w_m^2 P^2} \cdot \left(\frac{dP}{dt}\right)_y \qquad B.1$$

(Note that the notation for thickness,"t", used in equation A.4 has been replaced with t_o, to avoid confusion with the time differential, dt.)

The crack growth rate at each load can thus be found directly from the rate of load relaxation at constant displacement, simply from the slope of the load relaxation curve, if the displacement and specimen dimensions are known. The corresponding stress intensity can be found from the load using equation 6.3 (or equations A.12(a) and (b) from Appendix A.)

An alternative method would be to determine the crack growth from the experimental compliance relationship, first proposed and used by McKinney and Smith(332), and illustrated in Fig 6.12.

The compliance C is generally expressed (307) as

$$C = \frac{y}{P} = (Ba + D) \qquad B.2$$

where B is the slope of the compliance curve and D is the intercept. Differentiating this with respect to time at constant displacement gives

$$\left(\frac{da}{dt}\right)_y = -\frac{(Ba + D)}{BP} \cdot \left(\frac{dP}{dt}\right)_y \qquad B.3$$

For constant displacement, from equation B.2 it can be seen that

$$P(Ba + D) = P_i(Ba_i + D) = P_f(Ba_f + D) \qquad B.4$$

where P_i and a_i are the initial load and crack length and P_f and a_f the final values after relaxation. Solving for (Ba +D) and substituting in B.3 gives

$$\left(\frac{da}{dt}\right)_y = - \frac{P_{i,f}}{P^2} \left[a_{i,f} + \frac{D}{B} \left(\frac{dP}{dt}\right)_y \right] \qquad B.5$$

In general, except for very low modulus materials (such as polymers), or for very small crack lengths, D/B is very much less than a_i, so that

$$\left(\frac{da}{dt}\right)_y \approx - \frac{P_{i,f}\ a_{i,f}}{P^2} \left(\frac{dP}{dt}\right)_y \qquad B.6$$

Thus, the crack growth rate can be found from the rate of load relaxation, if the crack length at the onset or completion of relaxation is also measured. Equations B.6 and B.1 can be used interchangeably, depending on which parameters are most easily measured. Both the techniques have been used most successfully by Evans (294,309) and co-workers (307,285,308) as well as other researchers at various times, (105,249,284,310,311,321,318,319,332).

Appendix B.2

Rate of change of displacement at fixed load for double torsion crack velocity determination

At constant load, differentiation of equation 6.4 leads to

$$\left(\frac{da}{dt}\right)_p = \frac{\psi W t_o^3 G}{3w_m^2 P} \cdot \left(\frac{dy}{dt}\right)_p \qquad B.7$$

(Once again the thickness of the DT specimen in equation 6.4 has been expressed as t_o to avoid confusion with the notation for time, t.)

Thus, if the rate of change of deflection is known (which is, essentially, the stroke control ramp rate) and if the load is constant, (which is approximately true for a slowly running crack, in a statically loaded DT test), then it is possible, using equation B.7 alone, to determine the crack growth rate.

An alternative method of determining crack velocity at constant load, from experimentally determined compliance relationships, is analogous to the situation for constant displacement. Using a similar analysis, differentiating equation B.2 with respect to time at constant load gives

$$\frac{1}{P}\left(\frac{dy}{dt}\right)_p = B\left(\frac{da}{dt}\right)_p \qquad B.8$$

At constant load

$$B\frac{y}{\left(a + \frac{D}{B}\right)} = \frac{y_i}{B\left(a_i + \frac{D}{B}\right)} = \frac{y_f}{B\left(a_f + \frac{D}{B}\right)} \qquad B.9$$

$$\text{or} \quad B = \frac{y_{i,f}}{\left(a_{i,f} + \frac{D}{B}\right) P} \qquad B.10$$

Therefore

$$\left(\frac{da}{dt}\right)_p = \frac{\left(a_{i,f} + \frac{D}{B}\right)}{y_{i,f}} \cdot \left(\frac{dy}{dt}\right)_p \qquad \text{B.11}$$

And, if $\frac{D}{B}$ is very much less than a_i, which is the usual case, the crack growth rate $\left(\frac{da}{dt}\right)_p$ can be determined from the ramp rate $\left(\frac{dy}{dt}\right)_p$ and the initial or final crack lengths and deflections. This latter analysis is included for completeness, since it is presumably easier to obtain values of the parameters in equation B.7, than for crack length or deflection from equation B.11. A full analysis is given by Evans, Russel and Richerson (294) in an appendix to that paper.

APPENDIX C

Fracture Mechanics Analysis of Slow Crack Growth of the Double Torsion Specimen Under Cyclic Fatigue Conditions

(Note : Some of the following analysis has been abstracted from Evans and Fuller (235))

The quasi-static slow crack growth in ceramic materials in a stress corroding medium can be given by (353)

$$V \equiv \left(\frac{da}{dt}\right) = AK^n \qquad C.1$$

Two control modes, displacement control and load control are considered.

(A) Displacement Control

Static Loading

Considering first the static condition, the crack velocity can be determined for constant displacement control, from the rate of load relaxation (309), (see also equation B.6)

$$\left(\frac{da}{dt}\right)_y = - \frac{a_i P_i}{P^2} \left(\frac{\delta P}{\delta t}\right)_y \qquad C.2$$

where P is the load, a_i and P_i are the initial values of the crack length and load respectively and y is the displacement.

The corresponding stress intensity factor is then obtained, for the plane strain condition, from Appendix A, equation A.12,

$$K_1 = P\, w_m \left[\frac{3}{Wt^3 t_n\, \phi\, (1-\nu)}\right]^{\frac{1}{2}} \equiv \beta P \qquad C.3$$

where W, w_m, t and t_n are specimen dimensions, ν is Poissons ratio and

$$\psi \equiv (1 - \frac{5}{4}\frac{t}{W}).$$

(B) Displacement Control
Cyclic Loading

Similarly, for cyclic loading it can be shown (235) that an equation analogous to C.2 describes the increment in crack length during one cycle, δa, as

$$\delta a = - \frac{a_i P_i (\delta P)}{P(P + \delta P)} \qquad C.4$$

where δP is the load decrement during a cycle measured between points of constant displacement y.

The average velocity per cycle can be calculated in terms of the slow crack growth parameters.

For the double torsion specimen the compliance is a function of the crack length, or

$$y = P(\alpha a + \gamma) \qquad C.5$$

where α is a constant and γ is approximately equal to zero for ceramic and cement materials (see, e.g. Fig. 6.12 of Chapter 6).

Substituting the static slow crack growth parameter from equation C.1 and eliminating P using equations C.3 and C.5 gives

$$\frac{da}{dt} = A\beta^n P^n = A\left(\frac{\beta}{\alpha}\right)^n \left(\frac{y}{a}\right)^n$$

$$\therefore \quad y^n dt = \frac{1}{A}\left(\frac{\alpha}{\beta}\right)^n a^n da \qquad C.6$$

Integration for a periodic displacement with a constant average displacement, y_a, and amplitude y_o ($= \zeta\ y_a$ where $0 \leqslant \zeta \leqslant 1$;
for example $y(t) = y_a + y_o \sin(\omega t)$)

gives

$$\int_o^t \left[\frac{y(t')}{y_a}\right]^n dt' = \frac{1}{(n+1)\ A\ y_a^n} \left(\frac{\alpha}{\beta}\right)^n \left[a^{n+1} - a_i^{n+1}\right] \qquad C.7$$

Defining $g(n,\xi) = \frac{1}{\lambda} \int_o^\lambda \left[\frac{\sigma(t)}{\sigma_a}\right]^n dt$ C.8

where λ is the period and σ_a the average stress and g depends on n and the cyclic amplitude ξ, it can be seen that the left hand side of equation C.7 is $g\lambda$. For one cycle, therefore,

$$g = \frac{1}{(n+1)\ A\ y_a^n} \left(\frac{\alpha}{\beta}\right)^n \frac{a_i^{n+1}}{\lambda} \left[\left(\frac{a_i + \delta a}{a_i}\right)^{n+1} - 1\right] \qquad C.9$$

If the crack length increment per cycle δa is small, the exponent can be expanded using the binomial theorem as

$$\left(1 + \frac{\delta a}{a_i}\right)^{n+1} \approx \left(1 + (n+1)\ \frac{\delta a}{a_i} + \ldots\ldots\right).$$

Hence,

$$g = \left(\frac{\alpha}{\beta}\right)^n \frac{\delta a}{A\lambda} \left(\frac{a_i}{y_a}\right)^n \qquad C.10$$

Also from equations C.3 and C.5

$$K_I \equiv \beta P \text{ and } y = P\alpha a$$
$$y_a = K_{Ia} \left(\frac{\alpha}{\beta}\right) a_i \qquad C.11$$

where K_{Ia} is the average stress intensity factor for a cycle.

Substituting for $\left(\frac{y_a}{a_i}\right)$ from C.11 into C.10.

$$g = \left(\frac{\alpha}{\beta}\right)^n \frac{\delta a}{A\lambda} \left(\frac{\beta}{\alpha}\right)^n \frac{1}{K_{Ia}{}^n}$$

$$\therefore \frac{\delta a}{\lambda} = gA\, K_{Ia}{}^n \qquad \text{C.12}$$

i.e. the average crack velocity per cycle for cyclic loading.

Comparing this with the static case equation C.1 shows that the ratio of crack velocities under cyclic and static loading will be given by

$$g \left(= \frac{gAK_{Ia}{}^n}{AK_I{}^n}\right) = \frac{V_c}{V_s} = \frac{\text{cyclic crack velocity}}{\text{static crack velocity}}$$

for the same K_I, if there is no enhanced effect of cycling on the rate of slow crack growth.

Experimentally one can undertake the tests in displacement control where $\frac{\Delta y}{y_{av}}$ is kept constant and measurements are performed for small increments in crack length. From equation C.7

$$g\lambda = \frac{1}{(n+1)Ay_a^n} \left(\frac{\alpha}{\beta}\right)^n \left[a^{n+1} - a_i{}^{n+1}\right] \qquad \text{C.7}$$

For convenience let $\left[\frac{1}{g\lambda(n+1)A\, ya^n} \left(\frac{\alpha}{\beta}\right)^n\right] \equiv x$

$$\therefore 1 = x\left[a^{n+1} - a_i{}^{n+1}\right]$$

$$\therefore a_i{}^{n+1} + \frac{1}{x} = a^{n+1} \qquad \text{but } a = \frac{y}{cP}$$

$$\therefore \quad \frac{y^{n+1}}{\alpha^{n+1} P_{av}^{n+1}} = \frac{xa_i^{n+1} + 1}{x}$$

$$\therefore \quad P_{av}^{n+1} = \frac{x\, y^{n+1}}{\alpha^{n+1}(xa_i^{n+1} + 1)} = \frac{x\, P_i^{n+1} a_i a^n}{(1 + xa^{n+1})}$$

$$\therefore \quad P_{av}^{n+1} = \frac{P_i^{n+1} a_i}{(\frac{1}{xa^n} + a_i)} = \frac{a_i P_i^{n+1}}{\left(a_i + g\lambda(n+1)A\, y_a^n \left(\frac{\beta}{\alpha}\right)^n \frac{\alpha^n P_i^n}{y^n}\right)}$$

$$P_{av}^{n+1} = \frac{a_i P_i^{n+1}}{\left[a_i + g\lambda(n+1)A\, \beta^n P_i^n\right]} \qquad \text{C.12}$$

(B) Load Control

Alternatively (and possibly preferably) the tests can be undertaken in load control at constant P and ΔP in which case the average displacement rate, $\dot{y}_{av}$, is determined.

From C.10 $\quad g = \left(\frac{\alpha}{\beta}\right)^n \frac{\delta a}{A\lambda} \left(\frac{a_i}{y_a}\right)^n$ C.10

But $y = a\alpha P$ and for load control P is constant, so

$$\delta a = \frac{\delta y}{\alpha P}$$

$$\therefore \quad \frac{\delta y}{\alpha P \lambda} = Ag\left(\frac{\beta}{\alpha}\right)^n \left(\frac{y_a}{a_i}\right)^n = g\left(\frac{\beta}{\alpha}\right)^n \frac{a_i^n}{a_i^n} \alpha^n P_{av}^n A$$

$$\therefore \quad \frac{\delta y}{\lambda} = A\, g\, \beta^n P_{av}^{n+1} \alpha \qquad \text{C.15}$$

This measurement of the rate of change of displacement under constant load control conditions at different frequencies will illustrate any cyclic slow crack growth effect. A similar analysis gives the average crack growth rate, again assuming a quasi static growth mechanism, as

$$\left(\frac{da}{dt}\right)_{av} = g\, A\, \beta^n P_{av}^n \qquad \text{C.16}$$

Evaluation of g

It remains only to evaluate the integral g.

This is undertaken explicitly in Evans and Fuller's paper (235) and the results only for sinusoidal, square wave and triangular loading are included. See Figs. C.1, C.2 and C.3. An extended version of Fig.C.1 for sinusoidal loading relevant to this Thesis is shown in Fig.C.4.

For completeness the relations from which these figures are drawn are respectively

$$g(n,\xi) = \int_{1=o}^{[n/2]_T} \left[\frac{n!}{(n-21)!\ (1!)^2}\right] \left(\frac{\xi}{2}\right)^{21}$$

for sinusoidal loading, where $[n/2]_T$ is truncated value of $\frac{n}{2}$.

The results for a square wave stress are

$$g\left(\begin{matrix} n \\ 1 \end{matrix} \xi\right) = \int_{1=o}^{[n/2]_T} \left[\frac{n!}{(n-21)!\ (21)!}\right] \xi^{21}$$

and for a saw tooth stress wave

$$g(n,\xi) = \int_{1=o}^{[n/2]_T} \left[\frac{n!}{(n-21)!\ (21+1)!}\right] \xi^{21}$$

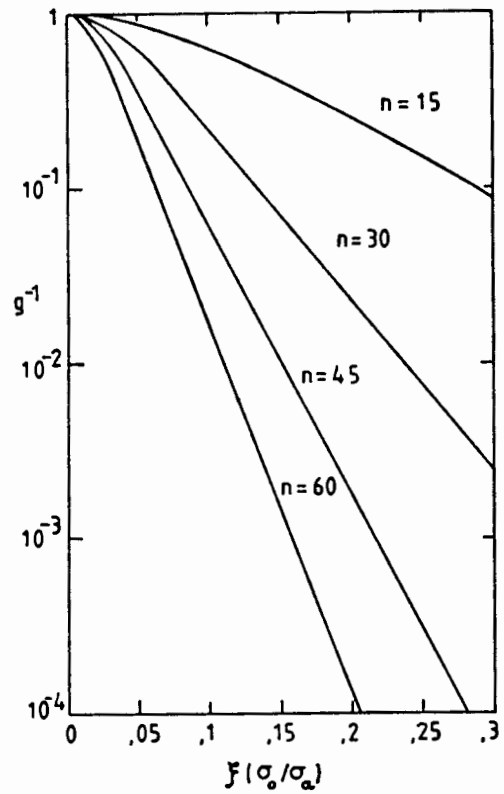

C.1

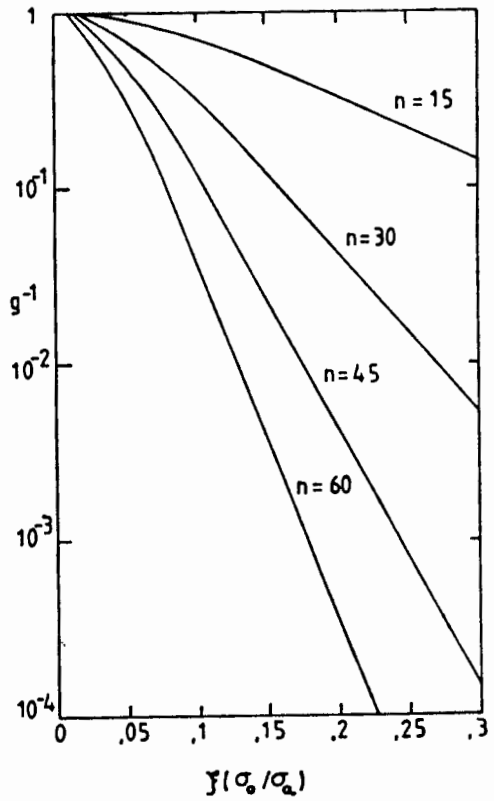

C.2

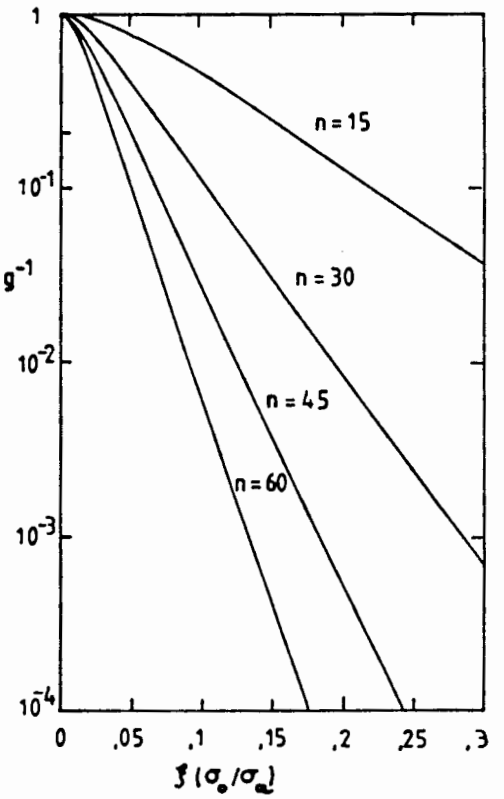

C.3

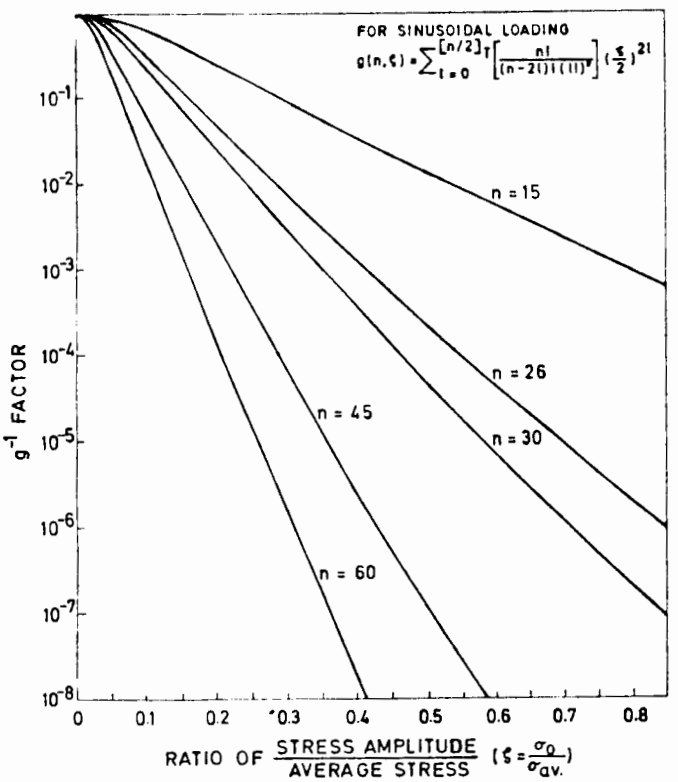

C.4

Figs. C.1,2,3 and 4: Evans and Fuller's g factor as a function of effective ratio(ζ) of stress amplitude to average stress(235). Figs. C1, C2 and C3 refer respectively to sinusoidal, square wave and triangular sawtooth waveforms. Fig. C4 is an extended version of C1 for sinusoidal loading to incorporate greater load ranges and also a line for n=26.

APPENDIX D

"Se non e vero, e molto bon trovato"
(If it is not true, it is a happy invention)

16th Century, Anon.

CALCULATION OF "HYDROWEDGE" PRESSURES IN A CLOSING CRACK

D.1 Introduction

The following analysis attempts to estimate the pressure developments due to a fluid trapped in a closing wedge.

It is assumed that the wedge surfaces are sufficiently large compared to the thickness of the fluid "film" that the flow is two dimensional. The velocity gradients normal to the directions of motion will be relatively large so that only viscous forces need to be considered. It follows therefore that the value of Reynolds number for the flow will be small. It is assumed that there is no turbulence and that inertial effects can be ignored.

D.2 General Equation for Laminar Flow Between Flat Surfaces

The situation of laminar flow between flat surfaces is first considered for simplicity, and to obtain a general equation.

Consider a small rectangular element of fluid at x, y as shown in Fig.D.1(a). This element is shown enlarged in Fig.D.1(b) together with the pressure and shear forces acting on its faces.

Hence $pdy + (\tau + d\tau)dx = (p + dp)dy + \tau\, dx$

$$\therefore \quad dpdy = d\tau dx$$

$$\therefore \quad \frac{dp}{dx} = \frac{d\tau}{dy}$$

Now $\tau = \mu\frac{du}{dy}$ (the general definition of dynamic viscosity, μ)

$$\therefore \quad \frac{d\tau}{dy} = \mu \frac{d^2u}{dy^2}$$

$$\therefore \quad \frac{dp}{dx} = \mu \frac{d^2u}{dy^2} \qquad \text{D.1}$$

Integrating twice with respect to y

$$\frac{dp}{dx}\ \frac{y^2}{2} = \mu u_y + A_y + B \qquad \text{D.2}$$

D.3 Velocity Between Stationary Plates

Consider now the wedge problem where the plates of the wedge are stationary.

The boundary conditions (from Fig.D.2) are that the velocity u = 0 when y = 0 and when y = h (= Θx) .

Hence when y = 0, u = 0 from equation D.2

then B = 0.

When y = h, u = 0

$$\frac{dp}{dx}\ \frac{h^2}{2} = \mu o + Ah$$

$$\therefore \quad A = \frac{dp}{dx}\ \frac{h}{2}$$

$$\therefore \quad \frac{dp}{dx}\ \frac{y^2}{2} = \mu\, u_y + \frac{dp}{dx}\ \frac{hy}{2}$$

$$\therefore \quad u_y = \frac{1}{2\mu}\ \frac{dp}{dx}\ (y^2 - hy) \qquad \text{D.3}$$

The velocity distribution is therefore parabolic and the mean velocity is two

thirds of the maximum.

D.4 Flow Equations for the Closing Wedge and Pressure Development

The flow conditions are shown in Fig.D.3.

Hence $Q_x - \dot{x}\Theta\Delta x = Q_x + \frac{dQ}{dx}\Delta x$

$$\therefore \quad Q_x = -\frac{x^2}{2}\dot{\Theta} \qquad \text{D.4}$$

But $Q_x = \int_o^h u\,dy$

i.e. the flow is the integral of the velocity over the front (pressure differences over the parabolic velocity front are ignored).

Using equation D.3

$$\therefore \quad Q_x = \frac{1}{2\mu}\frac{dp}{dx}\int_o^h (y^2 - hy)dy$$

$$= \frac{1}{2\mu}\frac{dP}{dx}\left[\frac{y^3}{3} - \frac{hy^2}{2}\right]_o^h = -\frac{1}{12\mu}\frac{dP}{dx}h^3$$

But this is identically equal to equation D.4 and using $h = \Theta x$.

$$-\frac{x^2}{2}\dot{\Theta} = -\frac{1}{12\mu}\frac{dP}{dx}h^3$$

$$\therefore \quad \frac{dP}{dx} = 6\mu\dot{\Theta}\frac{x^2}{x^3\Theta^3} = 6\mu\dot{\Theta}\Theta^{-3}x^{-1}$$

$$\therefore \int dP = 6\mu\dot{\Theta}\Theta^{-3} \int \frac{1}{x} dx$$

$$\Delta P = 6\mu\dot{\Theta}\Theta^{-3} \ln(x) + \text{constant.}$$

If we assume a boundary condition, P = 0 at x = a (where a is the crack length) then

$$\Delta P = 6\mu\dot{\Theta}\Theta^{-3} \ln\left(\frac{x}{a}\right) \qquad \text{D.5}$$

Unfortunately this expression (D.5) has a singularity at the crack tip where x = 0 but it may perhaps be overcome by assuming that the crack does not open and close purely as a linear wedge but rather as some asymptotic function, as shown in Fig.D.4, such that $\frac{dy}{dx}$ at the crack tip tends to zero, i.e. $\frac{dy}{dx} \rightarrow 0$.

The equation D.5 can then be used in calculating the pressure difference in the closing "wedge" crack by substituting appropriate values into the equation as follows -

D.4 Evaluation of Pressure Development in the Closing Wedge Crack

It is very difficult to choose appropriate values of the parameters for substitution into equation D.5 below

$$\Delta P = 6\mu\dot{\Theta}\Theta^{-3} \ln\left(\frac{x}{a}\right)$$

because of their wide range. Generally average values have been taken. Observation of cracks in mortar put the crack angle at between ten degrees at the most to probably 10^{-2} of a degree, and a value of one tenth of a degree (= 0.00175 radians) is used. At cycling frequencies of 1Hz (mid range between 10Hz and 0.1Hz) the angular velocity $\dot{\Theta}$ is then $\approx$ -0.002 rads/sec.

To avoid the singularity but still be close to the crack tip the pressure calculation is taken for x = 1 micron and crack lengths of the order of 1 millimetre.

The dynamic viscosity of water, μ , at $20^{o}C$ under presumably slight pressure conditions is taken as

$$\mu = 1.2 \times 10^{-2} \text{ N/ms.}$$

Substitution of the above values into equation D.5 above yields a pressure difference at one micron from the tip due to the closing wedge of

$$\Delta P = -6 \times 1.2 \times 10^{-2} \times \frac{0.002}{(.00175)^3} \times \ln\left(\frac{1}{1000}\right)$$

(Note that the pressure difference ΔP is positive as the angular velocity $\dot{\theta}$ is negative and so is the logarithmic expression).

$$\therefore \Delta P = 0.18 \text{ MPa}$$

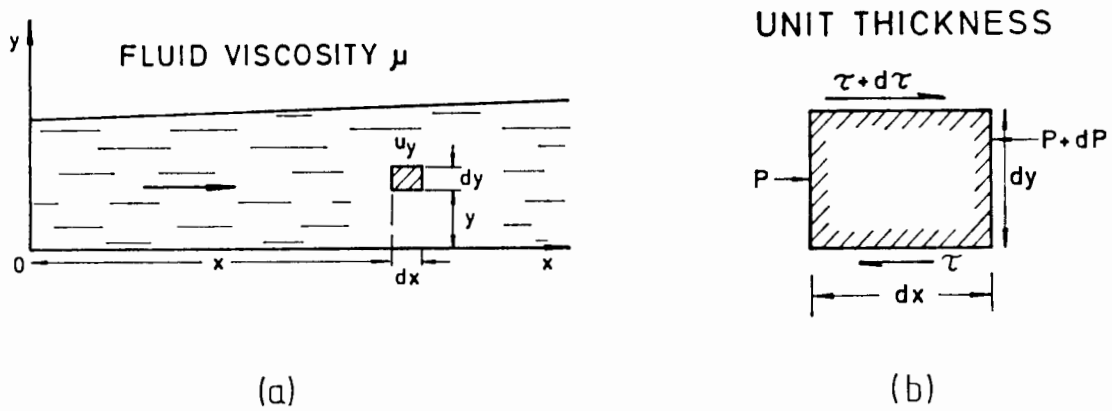

Fig. D.1. (a) Shows a small rectangular element of fluid at x,y, shown enlarged in (b) with the appropriate pressure and shear forces acting on it, to facilitate calculation of the hydrowedge mechanism.

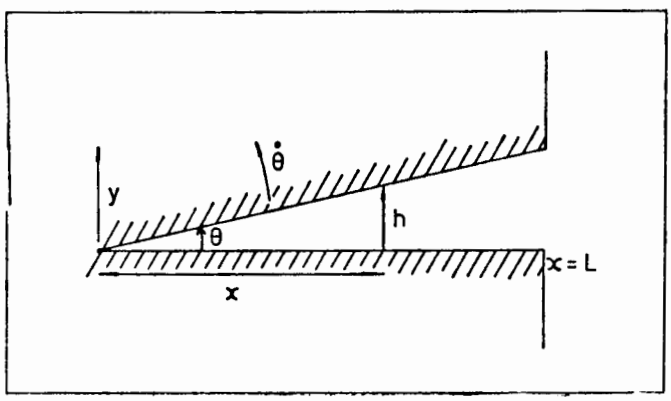

Fig. D.2. Stationary wedge plates used in the calculation of fluid flow velocity.

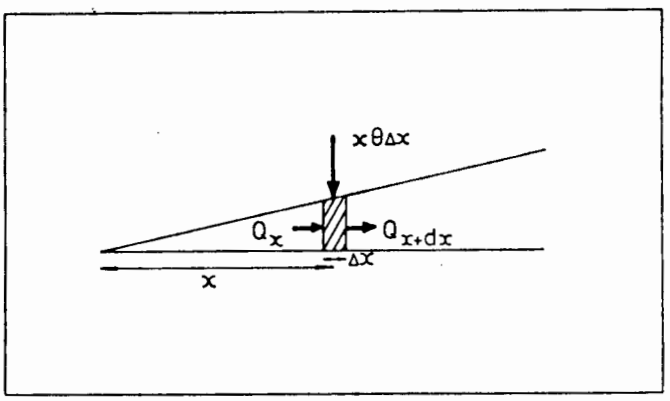

Fig. D.3. Showing flow conditions for a closing wedge.

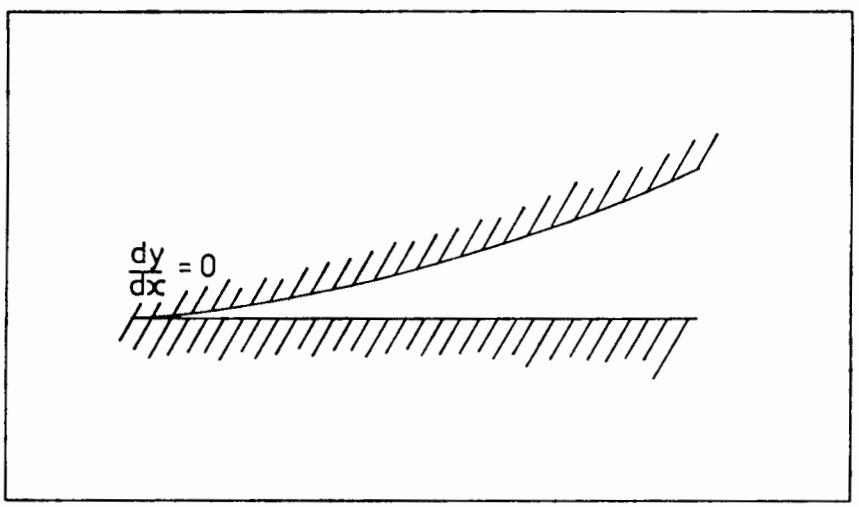

Fig. D.4. Probable more realistic approximation of a closing wedge where $\frac{dy}{dx} \to 0$ at the crack tip.